

10148/A

# Technology of turbine plant operating with wet steam

Proceedings of the international conference organized by the British Nuclear Energy Society in association with the Institution of Mechanical Engineers and the European Nuclear Society, and held in London on 11-13 October 1988

British Nuclear Energy Society, London



LOAN

Conference organized by the British Nuclear Energy Society in association with the Institution of Mechanical Engineers and the European Nuclear Society

Organizing Committee: J. M. Mitchell (Chairman), Dr F. Bakhtar, L. M. Dartnell, H. F. J. Hadrill, F. R. Harris and H. M. Whipp

621.165

British Library Cataloguing in Publication Data

Technology of turbine plant operating with wet steam.

1. Electricity supply. Generation. Fossil fuelled steam turbogenerators

I. British Nuclear Energy Society II. Institution of Mechanical Engineers III. European Nuclear Society

621.31'2132

ISBN 0 7277 1395 7

First published 1989

© British Nuclear Energy Society, 1988, 1989, unless otherwise stated

All rights, including translation, reserved. Except for fair copying, no part of this publication may be reproduced, stored in a retrieval system, or transmitted in any form or by any means electronic, mechanical, photocopying, recording or otherwise, without the prior written permission of the publisher. Requests should be directed to the Publications Manager, Thomas Telford Limited, Thomas Telford House, 1 Heron Quay, London E14 9XF.

Papers or other contributions and the statements made or the opinions expressed therein are published on the understanding that the author of the contribution is solely responsible for the opinions expressed in it and that its publication does not necessarily imply that such statements and or opinions are or reflect the views or opinions of the British Nuclear Energy Society.

Published for the British Nuclear Energy Society by Thomas Telford Limited, Thomas Telford House, 1 Heron Quay, London E14 9XF.

Printed in England by Inprint of Luton (Designers and Printers) Ltd.

# Contents

## Turbine design and operational experience

Keynote Address. G. A. W. BLACKMAN	1
1. Design, development and operating experience with wet steam turbines. J. R. BOLTER	3
2. Modern large 3000 rev/min steam turbines for pressurized water reactor power stations. J. MUSCROFT	15
3a. EDF experience with PWR turbine plant: crack-generating stress corrosion of low pressure rotors. C. MALHERBE and G. PAGES	25
3b. EDF experience with PWR turbine plant: corrosion-erosion with PWR secondary cycles. C. MALHERBE and J. MARCEAU	29
3c. EDF experience with PWR turbine plant: moisture-separator reheater thermal expansion faults. C. MALHERBE and J. MARCEAU	33
3d. EDF experience with PWR turbine plant: operation and maintenance of condensers. C. MALHERBE and B. VINCENT	35
4. Operating experience with 1100 MW wet steam turbines in a nuclear power plant. R. I. PAWLIGER	39
5. Operational experience with 1300 MW wet steam turbines. J. KEYSSELITZ and U. PETER	47
6. On the design limits of steam turbine last stages. G. GYARMATHY and W. SCHLACHTER	55
7. Advanced nuclear turbines for large output. T. HIRABAYASHI, A. OHJI, A. SUZUKI and S. NAGAO	65
8. Steam turbines for nuclear power stations in Czechoslovakia and their use for district heating. J. DRAHÝ	71
9. Reliability of LP steam turbines. J. E. BERTILSSON	77

## Ancillary plant and materials of construction

11. Development of designs for moisture separator reheaters. C. J. MONKS and J. P. PEYRELONGUE	87
12. Experience with centrifugal separators and vertical-tubed reheaters associated with large wet steam turbines. A. R. KERNAHAN and W. R. REID	99
13. Feedheating plants for wet steam cycles. C. J. MONKS	107

14.	<b>Main features of turbines for geothermal applications.</b> J. A. KUBIAK, J. F. PEREZ and A. GUTIERREZ	117
15.	<b>Design, materials and fabrication in NEI Parsons' large wet steam turbines.</b> A. J. SUMMERFIELD and M. LEES	123
16.	<b>Materials for turbine plant operating with wet steam.</b> D. V. THORNTON	131
17.	<b>The manufacturing development of LP rotors for large steam turbines.</b> G. A. HONEYMAN and R. D. CONROY	139
18.	<b>French experience of corrosion in nuclear turbines.</b> P. AUBRY and D. DUCHATEAU	145

## **Flow analysis and measurement**

19.	<b>The flow in last stages of large steam turbines at part load and low load.</b> W. RIESS, U. BLÖCKER and H.-G. OTTO	153
20.	<b>Wetness measurements in a model multistage low pressure steam turbine.</b> B. R. HALLER, R. G. UNSWORTH, P. T. WALTERS and M. J. LORD	161
21.	<b>A reconsideration of wetness loss in LP steam turbines.</b> S. A SKILLINGS, M. J. MOORE, P. T. WALTERS and R. JACKSON	171
22.	<b>A calculation and measurement of the flow field in a steam condenser external to the tube nest.</b> M. ŠŤASTNÝ and M. FEISTAUER	179
23.	<b>On-line measurement methods of single component velocities in two-phase flow systems.</b> D. BARSCHDORFF and D. WETZLAR	185
24.	<b>Effects of steam inlet conditions on behaviour of non-equilibrium flow in the primary wet steam turbine stage.</b> M. Z. YU, B. SUN and W. S. WANG	191
25.	<b>An examination of the effect of 'wake chopping' on droplet sizes in steam turbines.</b> F. BAKHTAR and A. V. HEATON	197
26.	<b>Fog droplet size measurement and calculation in wet steam turbines.</b> A. KLEITZ, A. R. LAALI and J. J. COURANT	201
27.	<b>Improving the accuracy of wetness measurements in generating turbines by using a new procedure for analysing optical transmission data.</b> P. T. WALTERS	207
28.	<b>Calculations of the nozzle coefficient of discharge of wet steam turbine stages.</b> Z. JINLING and C. YINIAN	217
29.	<b>Water drop sizing and the development of an off-line automatic drop image analysis system.</b> M. JINGRU and P. SHAOMIN	223
30.	<b>On the dissimilarities in wet steam behaviour in model and full-scale turbines.</b> F. BAKHTAR and A. V. HEATON	229

# Keynote Address

G. A. W. BLACKMAN, CBE, FEng, Central Electricity Generating Board

The technology of turbine plant operating with wet steam is a subject which is of immense and continuing interest in relation to nuclear power and the low pressure region of steam turbines for fossil-fired and geothermal power stations. It is a subject which is of special significance to the UK electricity supply industry, not only because we are embarking on a substantial programme of new nuclear and coal-fired power stations, but also because of its relevance to our existing large fossil-fired steam turbine plant.

The Conference Papers cover many issues relating to wet steam technology. These range from design and flow modelling studies, through development, materials specification and manufacturing techniques to operating experience and on-line measurement of actual physical parameters in turbine generators connected to their local power systems. The Authors of these Papers come from many different countries and, therefore, the conference seen as a whole reflects the state of the art world-wide.

The closing of the information feedback loop between realisation of a concept and the design stage is an essential step in improving our understanding of the behaviour of this type of plant and the fluid flows within it.

Figures published for the year ending March 1988, excluding all the Comecon countries with the exception of Hungary, show that 329 nuclear reactors were operational. These have a total design capacity of over 273 000 MW.

By any standards this is an enormous tranche of power station plant and it is noteworthy that three main reactor systems, namely the pressurised water reactor, the boiling water reactor and the pressurised heavy water reactor, or CANDU, alone account for almost 94% of it. It hardly needs stating that these nuclear steam supply systems have the important common feature that they all produce steam at saturation conditions.

In other words, utilities world-wide, from Finland to South Korea and to South America, have invested in over 250 000 MW of power station plant, relying on wet steam turbine technology to produce the energy they need to drive their economies.

This massive investment often represents a significant proportion of a country's gross domestic product and reflects both the status of electricity as an essential commodity and the confidence that decision-makers have that this type of plant will fulfil their needs for

reliable and economic supplies of electricity.

The CEBG shares this high level of confidence in wet steam technology. We have developed a strategy which proposes the construction of four large PWR power stations in order to help meet the growing demands for electricity in the United Kingdom.

An examination of the operating results for nuclear power stations illustrates how well placed the confidence in wet steam technology is. Plants with wet steam turbines are achieving annual load factors of well over 90%. Since first synchronisation, lifetime load factors of over 80% have been returned by many units world-wide.

These and other remarkable results are all the more creditable when it is recognised that these figures include downtime caused by both routine outages for reactor refuelling and maintenance, and breakdown of components completely divorced from the steam turbine plant.

Overall operating experience with wet steam technology is generally favourable; several factors contribute to this situation. Firstly, most wet steam turbine plant is associated with nuclear steam supply systems operating in a base load regime. Secondly, the operating temperatures are lower and change less with load. These two considerations lead to lower thermal fatigue and the absence of creep related failures. Thirdly, slow speed machines, into which category many wet steam turbines fall, generally exhibit lower stress levels and are subject to fewer cycles than high speed machines.

However, several areas of difficulty have arisen which require careful investigation to identify causal mechanisms and to enable solutions to be implemented, both at the design stage as part of operating feedback reviews, and as retrofits to maintain existing plant at the high levels of availability required by utilities.

One particular phenomenon encountered in many countries is stress corrosion cracking. The CEBG experienced this in a spectacular way at Hinkley Point 'A' in 1969, when a catastrophic failure of low pressure turbine discs occurred. The failure mechanism was quickly pinpointed, and the resulting information led to design revisions with reduced stress levels and incorporating fewer stress concentrating features. Plant under threat was guaranteed by detailed inspection procedures which allowed continued operation without the risk of more

## KEYNOTE ADDRESS

failures in service.

Also of special significance is wire drawing or worming erosion, which is the removal of metal from surfaces as a result of leakage of wet steam at high pressure through small clearances. This challenge has been met by the use of special materials and careful design features, and by the extraction of moisture from the path of blades in the high pressure region of the turbine. These and other issues will be described in detail at this Conference, leading, I am sure, to a wider and greater understanding of the processes involved.

Indeed, development and research aimed at refining the technology of turbine plant operating with wet steam is moving quickly on, as can be deduced from the number and quality of Papers to be presented at this Conference. Manufacturers, utilities and universities are all aiming at even higher levels of reliability and efficiency.

At present, the CEGB owns and operates 74 power stations, of which 55, the great majority, are fossil-fired or nuclear power stations. None of them employs wet cycles as would be found in, say, a CANDU plant.

However, the economy of this country is now more buoyant than it has been for some considerable time. As such, demand for electricity is rising. Our latest forecasts indicate that some 6000 MW of new capacity will be required by 1995, and 12000 MW by the year 2000. These estimates take into account not only the rise in demand but also the need to retire life expired plant and those nuclear stations which will no longer be able to make an economic contribution to our business.

The CEGB plans to meet this extra demand in three ways

- (a) by building new nuclear stations
- (b) by building new coal stations
- (c) by extending the life of our existing plant where this is technically feasible and economically attractive.

Following a thorough review of the nuclear plant available, we have concluded that the PWR offers the most economic method of generation able to meet the strict safety standards imposed by the licensing authority. Our proposed programme is based on the Westinghouse four loop design of PWR, known as the standardised nuclear unit power plant (SNUPP), which is already operating very successfully in the USA, namely at Calloway and Wolf Creek.

The CEGB proposes to build four single reactor stations with dual high speed wet steam turbines giving a net electrical output of 1175 MW. The first station is now under construction at Sizewell in Suffolk and will be commissioned in 1994. At the time of this Conference, the project is within budget and slightly ahead of schedule.

The public inquiry into our second station, at Hinkley Point in Somerset, opened a week ago, but it is likely to be some considerable time before the result is known.

The length of time required between the decision to build a nuclear station and the commissioning date is such that we must also

build new fossil-fired plant to meet the projected demands of the 1990s. We have developed a new reference design of coal-fired power station, using twin 900 MW units based on existing proven technology which utilises methods and materials that are well understood and where performance is completely predictable.

Many of the principles and techniques discussed at this Conference apply not only to wet steam plant but also to the wet region of turbines employing higher steam conditions. Much remains to be learnt of the behaviour of wet steam in a turbine blade path, and this is reflected in the significant proportion of Papers of a research or scientific nature.

Major advances in the efficiency of low pressure turbine blading have been made possible by the development of new analytical methods and the enormous increase in computing power that has become available in recent years.

While the raw formulae for these methods have been known for many years, they are being progressively updated and refined. They are also being validated by measuring the physical parameters involved on full-size units in commercial operation.

In this context, I am able to report that such work in the United Kingdom involves collaboration between British manufacturers and our own Central Electricity Research Laboratories. Two Papers included in the Conference give details of their findings.

The CEGB is already benefiting from developments in the efficiency of low pressure turbines. New, more highly twisted blades, have been retrofitted to several of our power stations, resulting in reductions in specific fuel requirements and direct cost savings.

We are actively evaluating the application of these techniques to other power stations, with a view to undertaking similar programmes where the gains in efficiency and reliability promise good returns on the investment required.

We are now finding that detailed design and development of LP blading and careful optimisation with the remainder of the plant have a significant bearing on the overall economics of generation from our proposed new coal-fired stations.

Furthermore, the work undertaken to improve the performance of low pressure turbines in fossil-fired power stations can readily be translated to plant operating with wet cycles.

In conclusion, the technology of turbine plant operating with wet steam is of fundamental importance to power systems world-wide, especially to those employing large amounts of nuclear plant that produce saturated steam. Great strides have been made in our understanding of the behaviour of such plant and further progress is an achievable goal.

The CEGB's statutory duty to provide a safe, secure and economic supply of electricity will be discharged by building plant operating with wet steam cycles and by continuing to adopt new technology as it becomes applicable to both new and existing conventional plant. The operating experience of plant of this type is second to none. The challenges that have arisen have been met successfully and this mature technology offers excellent prospects for the future.

# 1. Design, development and operating experience with wet steam turbines

J. R. BOLTER, BSc, FEng, FIMechE, NEI Parsons Ltd

The paper first describes the special characteristics of wet steam units. It then goes on to discuss the principal features of the units manufactured by the author's company, the considerations on which the designs were based, and the development work carried out to validate them. Some of the design features such as the separator/reheater units and the arrangements for water extraction in the HP turbine are unconventional. An important characteristic of all nuclear plant is the combination of high capital cost and low fuel cost, and the consequent emphasis placed on high availability. The paper describes some service problems experienced with wet steam plant and how these were overcome with minimum loss of generation. The paper also describes a number of the developments for future wet steam plant which have evolved from these experiences, and from research and development programmes aimed at increasing the efficiency and reliability of both conventional and wet steam units. Blading, rotor construction and separator/reheater units are considered.

## 1. INTRODUCTION

The development in the 1950's and 1960's of water cooled reactors producing steam at pressures between 40 bar and 70 bar, usually about one quarter percent wet, led to the development of designs of steam turbine which differ markedly from the fossil fired units which at that time had undergone continuous development for more than seventy years. Whilst in one sense the use of saturated steam represented a reversion to much older practice, it was coupled with an increase in steam pressure and a very large increase in size. It therefore presented some novel design problems.

NEI Parsons has manufactured the following units, all for operation on steam from CANDU reactors and all running at 1800 rpm.

Station	Customer	No. Units	Stop Valve Pressure bar	Commissioning dates
Pickering A	Ontario Hydro	4 x 540MW	40.3	1971-73
Bruce A	Ontario Hydro	4 x 800MW	42.4	1977-78
Point Lepreau	New Brunswick EPC	1 x 680MW	46.5	1982
Wolsung	Korea EPC	1 x 680MW	46.5	1982
Pickering B	Ontario Hydro	4 x 540MW	40.3	1982-85

Figure 1 is a cross section of the HP and one of the three LP turbine Bruce 800 MW units and is typical of all the units.

## 2. PRINCIPAL CHARACTERISTICS

The salient features of turbine plant for operating with wet steam are:-

2.1 Temperatures are low, eliminating all problems with creep and creep relaxation, and temper embrittlement. Thermal fatigue, although still a consideration, is less important than on fossil fired plant because:

- the temperature range is less
- the change in temperature with load is less
- nuclear power plant tends to operate at base load throughout its life

2.2 Because of the low pressure and temperature the steam mass flow per megawatt generated is increased. The increase in the volume flow of the steam, particularly at inlet to the high pressure turbine, is even more marked. Table 1 compares the volume flows at different points of the steam cycle on a fossil fired plant and a unit operating on steam conditions typical of a Candu reactor. The comparison between fossil fired plant and PWR steam conditions is very similar but the ratios are slightly smaller.

TABLE 1

	Fossil Fired Plant	CANDU Plant
Stop valve mass flow	1.0	1.69
Stop valve volume flow	1.0	3.43
LP turbine inlet mass flow	1.0	1.90
LP turbine inlet volume flow	1.0	1.07
Mass flow to condenser	1.0	1.79
Volume flow to condenser	1.0	1.72

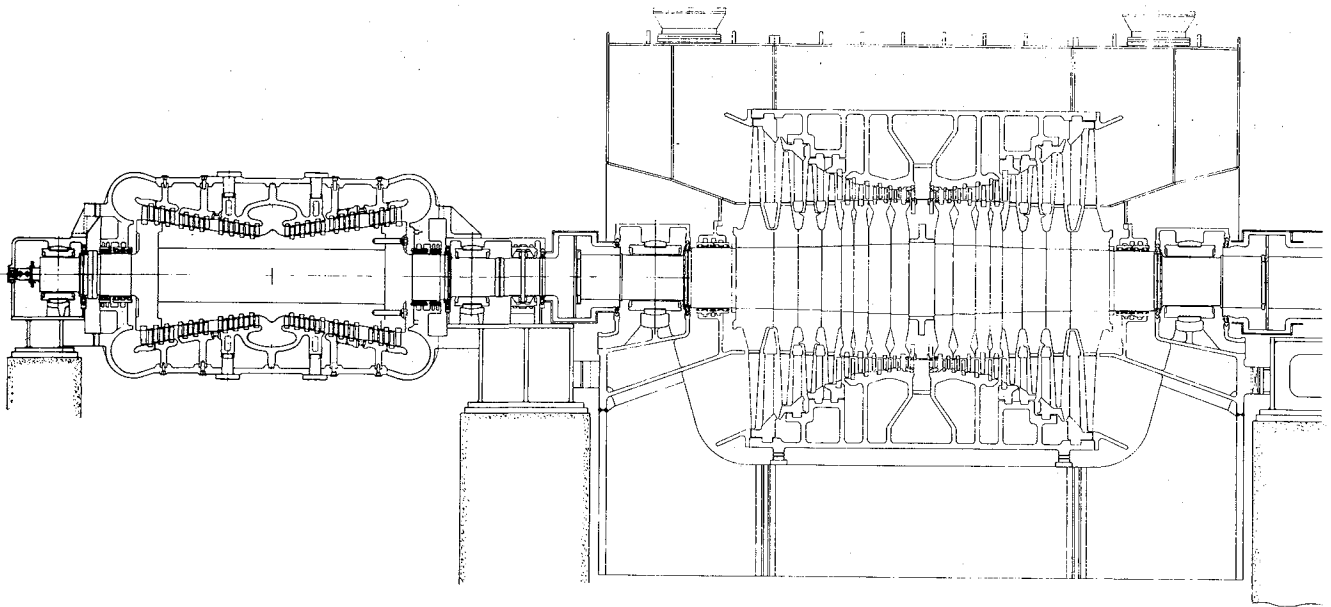


Fig. 1 - Turbine for Wet Steam Cycle. 800 MW, 1800 rev/min

2.3 The whole of the expansion in the HP turbine is wet so there is a potential risk of erosion damage, and a certainty of losses additional to those normal in HP turbines. Designers have therefore paid much attention to means of ensuring that as much as possible of the water formed during the expansion is removed and to assessing the losses caused by the water which remains.

2.4 To avoid excessive wetness in the LP turbine expansion, moisture removal and reheat are needed between HP and LP turbines. With water cooled reactors, reheat from the primary heat source is not practicable and reheat has to be by surface type heat exchangers supplied with live steam from the reactor. As this steam is condensed without doing useful work in the turbine, the reheating process is thermodynamically inefficient. To improve the heat rate an initial stage of reheating with steam extracted from an intermediate stage of the HP turbine expansion is often provided. Usually this heat exchanger is arranged within the same reheater shell. Even with this refinement, the reduction in wetness losses in the LP turbine only partially offset the thermodynamic losses in the reheater. So reheat improves the heat rate of wet steam plant much less than conventional fossil fired power plant. Indeed, some early wet steam turbines were constructed with water separation only, but water separation and reheat is now universal on large saturated steam turbine generators.

2.5 Although the energy of the steam in the separators and reheaters is less than in a conventional fossil fired reheater, it is sufficient to cause unacceptably high transient overspeed on full load rejection, and valves which close under governor action have to be provided at inlet to the LP turbines.

No special problems arise in the design of low pressure turbine blading, since with reheat the wetness at exhaust is not much higher than on fossil fired units. However, some special difficulties have arisen with the construction of turbine rotors. Indeed the low pressure turbine is the component which principally determines the choice of rotational speed.

The following sections discuss the considerations which have to be taken into account in the design of the turbine, and the solutions adopted by the author's Company for existing and future plant.

### 3. HIGH PRESSURE TURBINE BLADING

When the first Parsons wet steam units were designed, there was very little experience by which to judge the amount of erosion which would occur in the HP turbine. Although it was appreciated that the droplets would be small and blade and steam velocities low, the volume of water in relation to the volume of steam is very much higher than in low pressure turbines. Special features were therefore introduced to extract the maximum amount of water from the blade path. Parsons traditional 50% reaction design was retained, as this gives minimum steam velocities in relation to blade speed, but in addition:

- In order to facilitate the removal of water, the moving blades were of cantilever unshrouded construction with lacing wires on the longest blades only.
- The cylinder bore was made as smooth as possible so that water centrifuged outward would flow along the bore with the minimum risk of re-entrainment.
- Special extraction grooves were developed to ensure that the maximum amount of water was extracted from the blade path.

- Cylinders were cast in 2 1/4% chromium, 1% molybdenum steel with erosion resistant facings at points particularly vulnerable to erosion. No special measures were applied to the blade grooves, since it was felt that the use of Parsons well established segmental blading with tightly fitted stainless steel side locking strip would prevent any significant leakage.

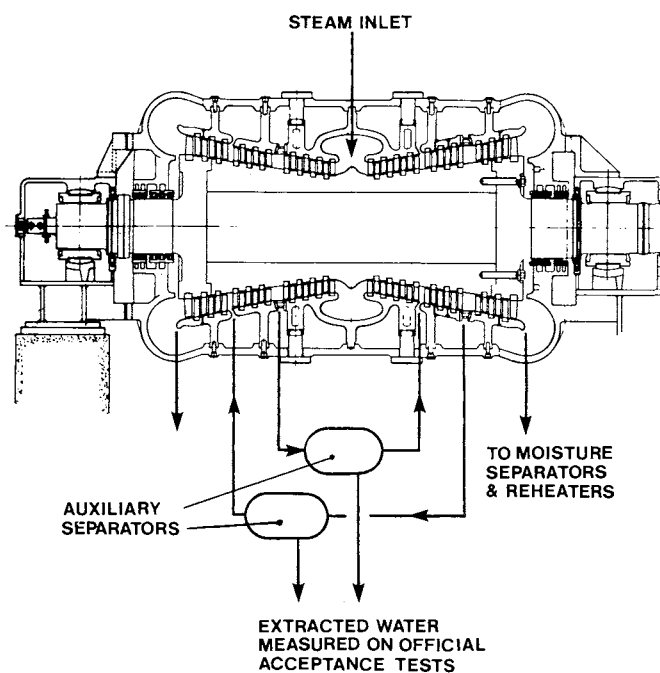


Fig. 2

The experimental work on which the design of Pickering and subsequent units were based is described in reference 1.

In the event, the service performance of the HP turbine blading confirmed the experimental predictions.

On all units the HP turbine blading has been completely reliable, predicted efficiencies have been achieved, and there has been no significant erosion. It has been general experience in the industry that the combination of 12% chromium blading steels with 2 1/4% chromium, 1% molybdenum turbine casings has given excellent resistance to erosion.

Measurements to determine the performance of individual components on wet steam turbines in service are notoriously difficult, since most of the expansion lies in the wet region, and it is particularly difficult to establish the amount of water extracted from the blade path. No conclusive results could be deduced from tests on the Pickering units, but on the later Bruce units, which have no feed heating or reheater extractions from the HP turbine blade path, a novel arrangement of auxiliary water separators was used (Reference 1). The amount of water extracted could be measured directly and the results for two different extraction belt geometries are shown in Fig. 3.

⊕ UNIT 1 TEST RESULTS (LOUVRED BELT)  
 ⊙ UNIT 4 TEST RESULTS (PERFORATED PLATE BELT)

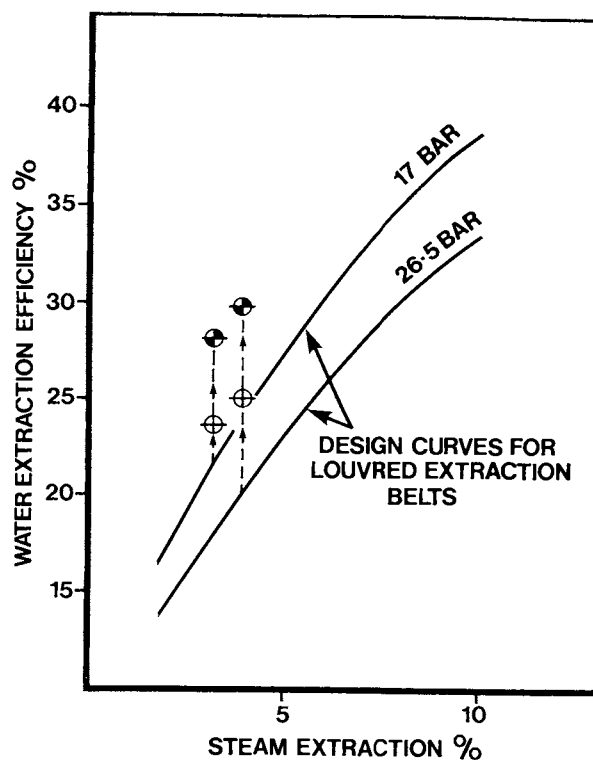


Fig. 3

During tests on a model turbine the amount of water removed from the blade path through a lowered extraction belt was measured at different steam pressures and with different amounts of steam passing through the louvres. The results of these tests were extrapolated into design curves, which plot drain efficiency (the percentage of water extracted divided by the total water present) against the steam extracted expressed as a percentage of the steam flowing through the turbine. As might be expected, the amount of water extracted increases the amount of steam extracted, and is greater at lower pressure.

Superimposed in these curves are test results on the full size units, where the amount of steam extracted is determined by the performance of the feed heater to which the extraction belt is connected.

Unit 1 was fitted with louvred extraction belts similar to those tested in the model : the extraction rate was higher than that predicted from the model, but less dependent on pressure than had been anticipated.

Unit 4 was fitted with a different type of extraction belt which gave a higher extraction rate, also comparatively unaffected by steam pressure.

On Parsons current designs for wet steam turbines, conventional shrouded moving blades with reduced tip leakage are used in the early stages, where wetness is low and reduction of steam leakage most important.

## TURBINE DESIGN AND OPERATIONAL EXPERIENCE

### 4. HP TURBINE ROTOR CONSTRUCTION

On all these 1800 rpm units, the HP turbine rotors were of Parsons' well established "hollow and stub" construction, wherein stub shafts are attached by a shrink fit to a hollow forging and thermally tightened tapbolts give additional security. This construction allowed the use of a relatively high chromium steel for the main body of the rotor without incurring the risk of lubrication problems at the bearings, and avoided the need for very large forgings which were not readily available at that time.

On one design of rotor, where the pitch circle diameter of the stub end tapbolts was smaller than the spigot (Figure 2), high eccentricity was experienced on cold starts. Steam leaking past the heads of the tapbolts condensed during shut down and re-evaporated during starting. Since the bore of the rotor body is not, in practice, absolutely concentric with the bearings, the water film on the rotor bore is not uniform and the rotor does not heat up evenly, causing a transient thermal bend. This was completely overcome by fitting spiral wound gaskets under the heads of the tapbolts.

A further problem encountered was stress corrosion cracking of the tapbolts. As the shrink fit is more than adequate to resist all the forces acting on the joint, even at overspeed, no service problems were experienced. The problem was traced to the practice of coating the bolt threads with molybdenum disulphide grease which, in the presence of moisture, initiated the cracking. It was eliminated by fitting bolts of improved geometry to closely controlled extensions and using a graphite based thread lubricant.

Now that they are widely available in high quality, one piece rotor forgings are more cost effective and reliable, and they are used on all current high speed and low speed designs.

### 5. LOW PRESSURE TURBINE BLADING

On the first units, the LP turbine blading was similar to that developed for cross compound fossil fired units and had open ended moving blades with brazed lacing wires. Whilst reliability has been good, with no forced outages, some braze cracking has been found. Occasionally such cracks have propagated into the blade.

On the later Bruce units, which have last stage blades 1057 mm long, shrouded moving blading was used in the early stages. In the remaining stages loose lacing wires were extensively used, comprising overlapped wires of semi-circular cross section or, in regions of higher centrifugal stress, round wires or tubes in long lengths. This construction is almost equivalent to continuous lacing and gives excellent control of vibration characteristics. On the Bruce units not a single blade crack has been discovered in 40 machine years of operation.

On current designs, both high and low speed, the use of coverbands or shrouding has been extended to all the blades, except the last one or two stages. This reduces steam leakage and the losses associated with lacing wires and stubs in the blade path.

On the last stage, and on some penultimate stages, a novel form of construction is used. The application of modern fluid dynamic computational techniques has led to the development of last stage moving blades with a rather higher degree of twist than earlier designs. Such blades have a pronounced tendency to untwist as they run up to speed: if this tendency is resisted by fitting lacing devices at the blade tip, high stresses are introduced both in the lacing and in the relatively thin blade sections near the tip.

One solution is to have no restraint: however such blades must be of large chord to give adequately high vibration frequency and to give sufficient stiffness to control tip flutter at low loads. Another solution is to have a restraint or restraints lower down the blade, but this is subject to the same objections as tip restraints, albeit to a lesser degree. Moreover the presence of obstructions in the main flow path lowers the blading efficiency.

The solution adopted by the author's company is shown in Figure 4: the blade is constructed with excess twist so that at speed its natural shape gives the desired blade stagger at all points. After assembly of the blades in the rotor, the sockets of the ball ended struts are screwed into place, producing a compression in the tip struts and rotating the blade tips into their normal running position.

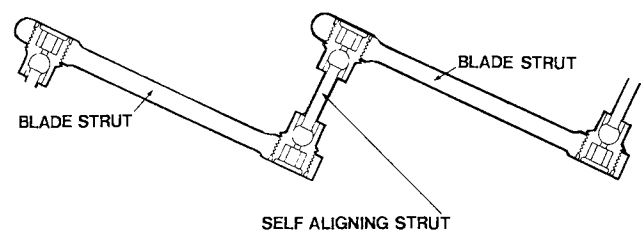


Fig. 4

The compression in the struts induces local torsional stresses in the blade sections, but in the absence of centrifugal or oscillatory stresses these are harmless. The compression in the struts produces a useful pre-load on the blade roots, which helps to prevent movement during barring. At normal operating speed the blades assume their natural shape and the compression in the struts and the torsional stresses in the blade fall almost to zero (in practice matters are arranged so that about 10% of the initial compression remains at normal operating speed).

Figure 5 illustrates a 3000 rpm test wheel with blades 1070 mm long giving an exhaust area of 9.54 sq. metres per flow. Similar blades 914 mm and 858 mm long have been developed and are in service in the U.K. and overseas. These have proved very satisfactory both in efficiency and reliability.



Fig. 5

A characteristic of all these blades is that because of the very simple construction, the measured vibration characteristics are very close to those predicted by calculation.

Large exhaust areas are therefore available even at 3000 rpm. The choice of turbine generator speed is discussed in section 9.

6. LP TURBINE ROTOR CONSTRUCTION

Until 1982 Parsons low speed wet steam turbines had low pressure rotors of shrunk disc construction. Although the merits of monobloc or one-piece LP rotor forgings were appreciated when the earlier units were designed and had been applied to high speed turbines, forgings of sufficient size for low speed units were not then available.

Accordingly the traditional construction which had been well proven on the low speed lines of cross compound fossil fired units was retained. The discs had keyways (Fig. 7a) to provide circumferential location in the unlikely event of an excessive overspeed.

In 1969 the attention of the industry was drawn to the possibility of stress corrosion cracking at the disc bores on non-reheat units, and to the much greater incidence of cracking at the crowns of keyways (references 7, 8 and 9).

The cracking appeared to correlate with the relationship between disc bore temperature and local saturation temperature : where the disc bore temperature is below the saturation temperature, condensation will take place and stress corrosion cracking may occur. There are many other factors such as the type of feedwater treatment and the rigour with which it is carried out, but rotor temperature distribution and disc bore/keyway stresses appear to be the principal factors which determine whether stress corrosion cracking occurs.

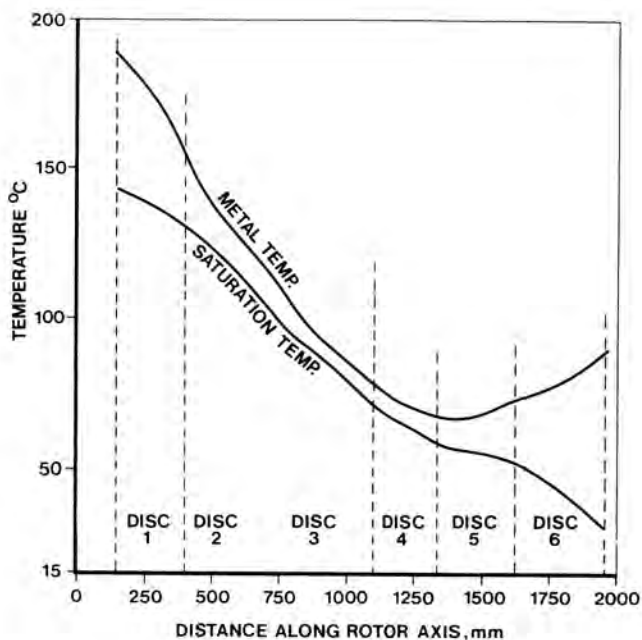


Fig. 6

The full load temperature distribution of the LP turbine rotors of the wet steam units, then under construction, was calculated (Fig. 6). This shows that the temperature of the disc bores is everywhere above the saturation temperature of the steam. The large temperature differences at the first and last discs are due respectively to the superheat in the steam at inlet, and to the warming effect of the steam leaking inwards from the shaft end glands.

It was concluded that the disc bores would remain dry whilst the units were on load and that stress corrosion cracking was unlikely, since disc bore stresses were moderate. Nevertheless it was considered prudent to eliminate keyways on all LP turbine rotors whose manufacture had not progressed too far, and a construction incorporating "driving pegs" was adopted (Fig. 7b). The four Pickering 'A' units and one unit at Bruce had keyways and the remainder had driving pegs.

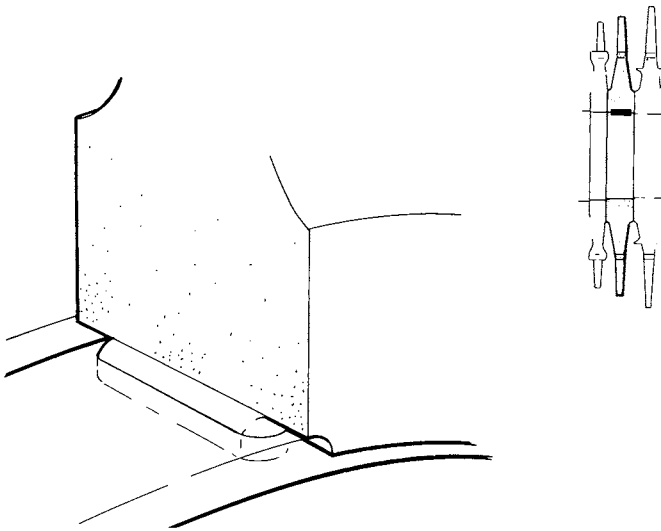


Fig. 7 (a)

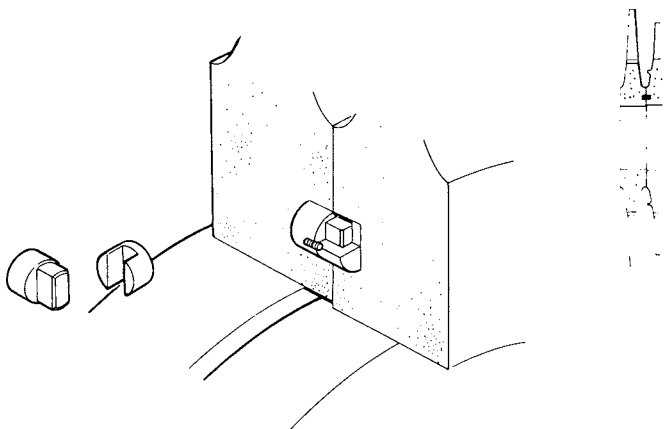


Fig. 7 (b)

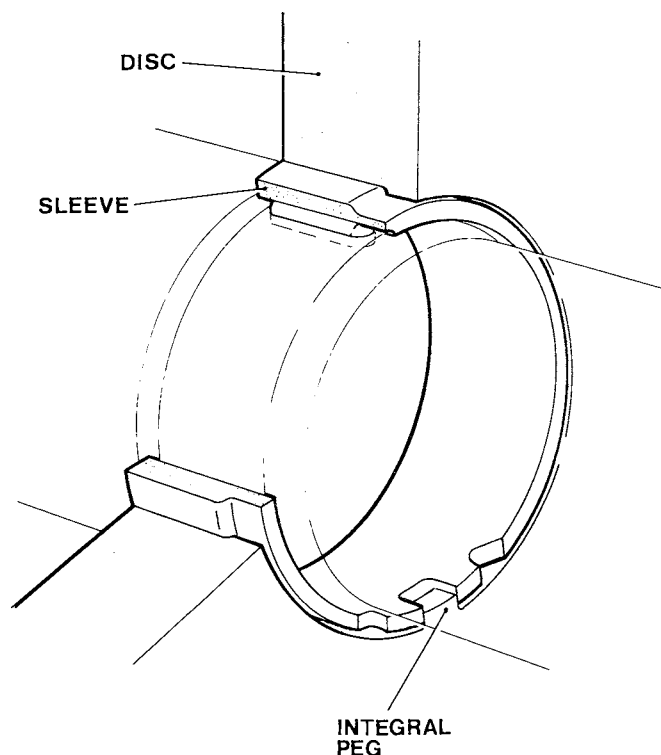


Fig. 7 (c)

In 1980 it became known that a number of units in the U.S.A. had suffered stress corrosion cracking at disc keyways. Whilst the Pickering units had a low crossover pressure, resulting in a relatively low wetness in the expansion and a small rotor diameter with relatively massive hubs to the discs, resulting in low centrifugal stresses, it was considered essential to determine whether cracking was present. As the customer had already ordered four more units and a train of spare rotors, the longest running rotors at Pickering 'A' were withdrawn from service for examination, firstly by an ultrasonic technique and subsequently by dismantling one train of rotors. No cracks were found by either technique, but subsequently ultrasonic techniques have indicated minor cracking of one disc at the crown of the keyways on each of two rotors. No cracking has been detected at disc bores.

In rebuilding the dismantled rotors, consideration was given to boring out the discs to eliminate the keyways and shrinking them on to a new, larger diameter shaft. However the profiles of some discs were such as to preclude the fitting of driving pegs, so an alternative "integral peg" construction was devised to allow the existing discs and shafts to be re-used with intermediate sleeves (Figure 7c).

One of the reasons for the variable incidence of stress corrosion cracking in disc keyways appears to be the inevitable variability in the fit of the key in the keyway. If for example there is a tighter fit at the downstream end, the keyway will be subjected to upstream steam pressure and condensation is more likely. Conversely, if the tight fit is at the upstream end the steam pressure in the keyway will be lower and condensation and stress corrosion cracking may be avoided.

More modern constructions such as the driving button or the integral peg are considered to be less susceptible, since there is no pressure gradient forcing steam and possible contaminants into the most highly stressed areas, where stress levels are in any case somewhat lower than with bore keyways.

Shrunk disc construction is no longer acceptable for new units and the alternative high integrity rotor constructions now available are discussed in reference 5 (this conference).

#### 7. STEAM VALVES

The low steam temperatures and pressures on wet steam turbines present few problems and the main consideration is the very large volume flows which have to be accommodated. Four sets of valves at inlet to the HP turbine and two sets at inlet to each LP turbine are virtually universal practice. Usually full arc admission is adopted for HP turbines so eliminating the need for external cross

connections to reduce the loss of load whilst exercising steam valves. However some units in the U.S. have sequential valve opening with partial admission and this will improve the heat rate at partial loads.

A potential problem associated with the HP throttle valves arises from the large amount of energy, particularly acoustic energy, dissipated at part loads. The steam chests are almost invariably cast. This dictates scantlings not too different to those of fossil fired units and there have been few problems with the chests themselves. On the other hand the low steam pressure and temperature allow the use of pipes which are an order less in thickness than pipes of the same diameter on fossil fired plant. In some cases, this has led to problems of pipe vibration and careful consideration is now given to the mechanisms by which this can be excited.

Reference 2 gives an account of a particular problem of this type which was overcome by modifications to the valve profile.

Some manufacturers (Reference 3) make special arrangements to reduce the forces acting on the valve plug itself and guided valve heads are widely used in wet steam turbines. This construction is used on the Bruce units which operate at 42.4 bar inlet pressure, have a steam inlet flow equivalent to a PWR turbine of about 1300MW rating and so have valves of comparable size. No problems attributable to forces acting on the valve plug have been experienced.

On reheat valve systems the use of butterfly valves has become almost universal because of their low pressure drop and reduced cost compared to the plug type valves often used in early units. Generally two identical valves in series are used, and on modern units are operated by quick acting relays powered by high pressure fluid under the control of the governor.

#### 8. MOISTURE SEPARATORS AND REHEATERS

In embarking on the design and development of moisture separator and reheater equipment, there was very little practical experience of large equipment of this type. The novel design adopted on all Parsons wet steam turbines derived from the following considerations.

The relative volumes of the live and reheated steam dictated that the live steam should be inside the tubes where it would condense. Condensation within tubes is not common and the extent to which the presence of condensate would affect heat transfer and lead to bi-phase flow problems was unknown. It was therefore felt to be prudent for the tubes to be vertical, and relatively short, so that the amount of condensate formed in each tube was small and would drain easily. In the Bruce reheaters the quantity of steam condensed in

one of the front tubes (20 mm bore, 5.8 metres long) is only 28 cc/sec at full load. These tubes are of course the most highly loaded in the reheater and the quantity will be less on the other rows of tubes.

With this arrangement the heat transfer inside the tubes will be very high and the heat exchange surface required is dictated entirely by the heat transfer coefficient on the outside of the tubes. External integral finning of the tubes was therefore adopted to reduce the total length of tube required.

These considerations led to the adoption of a matrix of vertical tubes, approximately square in plan view, and contained within a vertical cylindrical vessel. To avoid unacceptable thermal stresses, it was decided that the tubes and their top and bottom headers would be independent of the vessel and mounted within it.

To avoid excessively thick tube plates, the tubes were divided into several bundles, usually five, each with separate top and bottom headers, the reheated steam flow passing across each tube bundle in turn.

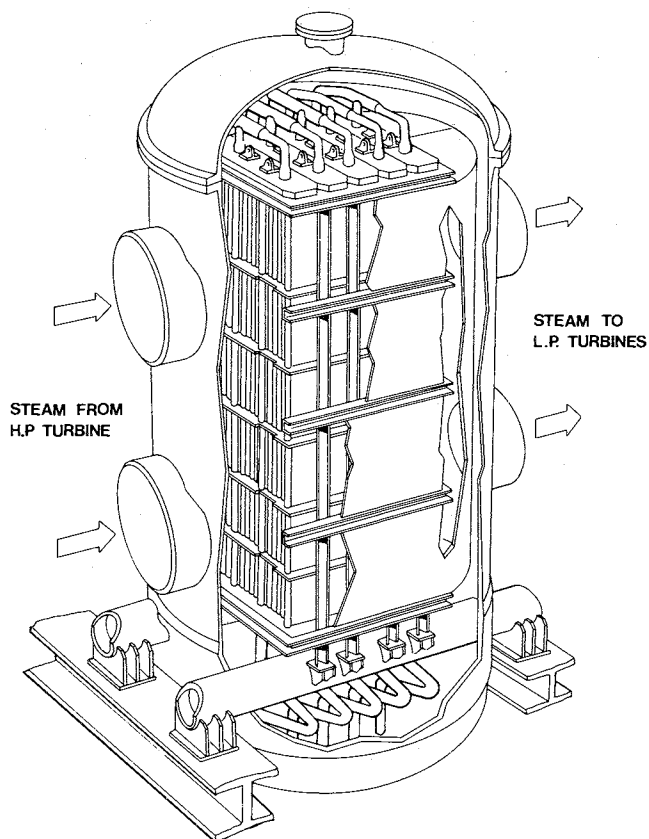
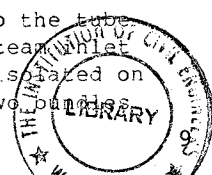


Fig. 8

The relatively narrow tube plates minimised the tube plate thickness and permitted a compact bolted joint for access to the tube ends. Each bundle has separate steam inlet and water drain pipes and can be isolated on load in case of leakage. Up to two bundles



## TURBINE DESIGN AND OPERATIONAL EXPERIENCE

can be isolated on one reheater without producing an unacceptable unbalance in LP turbine inlet temperature.

On units with two stage steam reheating all tube bundles are identical, the front bundles being connected to the bled steam supply and the rear bundles to the live steam supply.

The tubes are expanded and face welded into carbon steel tube plates. For most applications carbon steel tubes have been used and have proved entirely satisfactory. Stainless steel tubes have also been used, and in this case the tubeplates are faced with stainless steel to which the tubes are seal welded.

The weight of the bundles is transferred to the foundations by two large diameter steel tubes which penetrate a thickened strake of the pressure vessel, which thus serves only to contain the internal pressure. The vessel is maintained at constant temperature by an internal shield which directs the reheated steam into the outlet pipes. There is a large diameter top flange for access to the tube bundles.

The use of a "zig-zag" plate type water separator immediately upstream of the first tube bundle was considered, but was rejected on two counts.

1. The velocity head of the steam entering the bundle was relatively high.

2. It was known from experience on gas turbine inter-coolers that uniform velocity is crucial to the satisfactory performance of this type of separator. It was evident that this would not easily be achieved within the confines of an economical pressure vessel.

Parsons already had encouraging experience with centrifugal separators, which had been developed for removing ash from the working fluid of coal burning gas turbines, and it was decided to incorporate separators in the pipe lines between the HP turbine and the reheater.

An account of the development of the separators is given in reference (1). The design used on all the recent units is illustrated in Figure 9: the essential features are the flush louvres, extraction of steam through the louvre gaps, and the large diameter outlet pipe with straightening vanes, which minimise pressure drop and ensure an acceptable flow distribution in the reheater tube bundles. More details of the development, construction and service performance of the separator and reheaters are given in reference 4 (this conference).

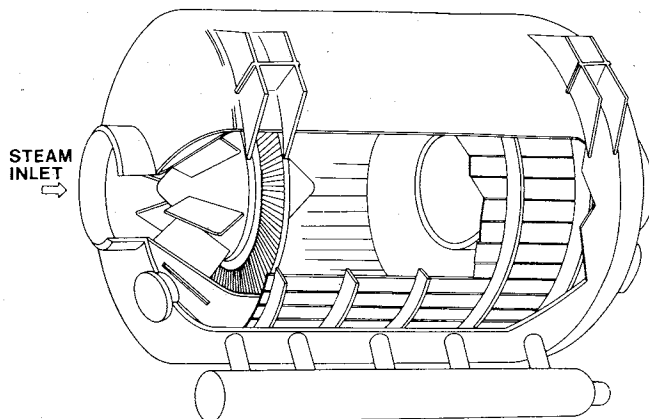


Fig. 9

### 9. CHOICE OF ROTATIONAL SPEED

Much has been written about the optimum rotational speed for wet steam turbine generators, whereas on tandem compound fossil fired plant there is generally little argument: high speed units are highly desirable so that the high temperature parts are compact and able to withstand rapid changes in temperature without being subjected to unacceptable thermal stresses.

On low temperature wet steam units which will operate at high loads throughout their lives, consideration of thermal stresses are much less important, and the choice can be made mainly on the basis of heat rate, reliability and capital cost.

Generally reactors are designed to give a definite thermal output, i.e. a fixed quantity of heat, so that a lower heat rate results in greater output at the generator terminals. Because reactors and their supporting services are expensive the value placed on extra output is high: £2,000/kW is a typical figure.

In comparing the heat rates of high speed and low speed units we need consider only HP and LP turbine efficiencies and leaving loss, since all other parameters are essentially independent of rotational speed.

#### 9.1 Turbine Efficiency

There is likely to be little difference in high pressure turbine efficiency between high speed and low speed designs because, as noted earlier, steam volume flows are large and the leakage losses will be small on both designs. There will probably be a slightly increased leakage loss on the low speed design but this will be offset by increased pressure losses at inlet and outlet to the casing on the high speed design.

In the past it has generally been found that low speed LP turbines have had higher efficiencies than high speed turbines of equal output. This is mainly because the low speed unit, with a smaller heat drop per stage, has

a lower flare in the blade annulus. Consequently the steam flow is closer to that predicted by the simple cylindrical flow calculations used at that time, and by which the blade geometries were then determined.

In recent years, mainly due to the application of modern fluid dynamic computational techniques, the efficiency of turbine blading has increased markedly and is now progressing asymptotically towards practical upper limits. Progress is being made on all aspects which contribute to efficiency:

- low loss profiles
- control of secondary losses
- control of steam leakage
- the prediction of steam velocities in highly divergent steam flows
- the maintenance of positive reaction at all blade heights

The application of these techniques, in both low and high speed units, will reduce the already small differences in blading efficiency between the two designs. It is true that the low speed design will have slightly higher leakage losses but the high speed design will have higher losses associated with higher steam velocities in the LP turbine. It may be expected, therefore modern high speed and low speed designs from the same stable will have the same blading efficiency and heat rate will depend almost entirely on leaving loss, i.e. on the exhaust area provided by the last stage LP blades.

## 9.2 Exhaust Area

In 50 Hz countries, the maximum exhaust area for service proven steel blades running at 3,000 rpm is approximately 9 to 10 sq. metres per flow and the corresponding areas at 60 Hz are 6 to 7 sq. metres/flow. Assuming that eight exhaust flows is the maximum which could reasonably be allowed, areas up to about 80 sq. metres and 56 sq. metres respectively can be provided.

At low speed, exhaust areas of 15 sq. metres per flow at 60 Hz and 20 sq. metres per flow at 50 Hz are readily available.

For outputs of 600 MW upwards, i.e. the majority of applications, 60 Hz plant operates exclusively at 1800 rpm. Indeed there are very few wet steam units operating at 3600 rpm.

At 50 Hz, both 3000 rpm and 1500 rpm units are practical over a wide range of outputs and the choice depends entirely on the balance between the value of extra kilowatts generated by a low speed design and the extra cost of its purchase and installation. Maintenance costs are not expected to be significantly different.

Economic consideration of the balance between kilowatts and costs is commonplace in the assessment of tenders for steam turbine plant and the value the customer places on heat rate or on extra kilowatts output is usually stated in tender specifications. With fossil fired

plant this value is much more dependent on anticipated but uncertain trends in fuel prices than in the case of nuclear plant where fuel represents a much lower proportion of the generating costs. It follows that whilst on fossil fired plant the evaluation figures are relatively uncertain and are not always followed strictly, on nuclear plant selection of the optimum design can be based on much more secure data. Thus extra exhaust area is more likely to be selected than would be the case on fossil fired plant.

It is to be expected that manufacturers will continue to develop longer high speed LP blades using titanium or more advanced steels, so long as increasing losses due to high relative steam velocities are not sufficient to offset the gains achieved by reducing the leaving loss. These developments will progressively increase the megawatt rating at which a low speed unit becomes the economic choice. On the other hand reactor outputs are also likely to increase, since the present limit appears to be purely a regulatory one and a corresponding increase in the output of turbine generators will be required. For low speed designs there would seem to be no difficulty in increasing output to 2000 MW using existing technology.

## 9.3 Reliability

Records show that the reliability of wet steam turbines is very high: life time load factors achieved by many reactors would not be feasible without very reliable turbine generators. Since many of the causes of outages are independent of rotational speed, it is not to be expected that there will be much difference in the reliability of high and low speed turbine generators.

Given that suitable rotor constructions are used there are a number of factors which seem to weigh in favour of the low speed unit, particularly if unit sizes increase.

### i) Lower Stress Levels

Whilst few failures in steam turbines are attributable to too high a stress level per se, and the absence of creep in wet steam turbines removes a constraint, a lower stress level will make any component more tolerant of mal-operation, material defects and unpredicted or unsuspected factors. This effect will be greater on those parts of the turbine which operate in wet steam. In this environment the fatigue properties of steels are lower than in air or dry steam: moreover the stress to failure continues to fall continuously as the number of cycles is increased, instead of reaching a limiting value. On balance therefore it is likely that there will be a small margin in favour of the lower speed unit.

### ii) HP Casing Design

On a half speed unit, the HP turbine casing is larger and inherently better able to resist the forces and moments exerted by large

## TURBINE DESIGN AND OPERATIONAL EXPERIENCE

diameter pipes. However this effect must not be exaggerated, as the pipes are relatively thin in relation to their diameter, and to the thickness of the turbine casings.

### iii) Generators

Half speed generators have inherent advantages over full speed designs, apart from the obvious one of generally lower stress levels. These are discussed in some detail in reference 6 and it would be inappropriate to repeat them all here. However two advantages of the half speed unit, due to its more symmetrical construction, should be mentioned.

a) Full speed generator rotors are inherently stiffer across the pole faces than across the winding slots. This asymmetry is a potential source of double frequency vibration, and material has to be removed from the pole face to equalise the stiffness without adversely affecting the magnetic properties or mechanical integrity of the rotor, or giving rise to unacceptable heating under fault conditions. This becomes more difficult as unit ratings increase.

On the other hand a four pole unit is inherently symmetrical and no such considerations arise.

b) The intense magnetic pull of the generator rotor distorts the stator core and the axes of the distortion rotate at the same speed as the rotor. The form of the distortion has four nodes on a full speed generator and eight on a half speed, resulting in deflections an order less in magnitude. In fact, because of the lower circumferential magnetic flux in the half speed unit, the core is usually made less deep in relation to its diameter, but deflections due to magnetic pull are still much less than on a full speed unit.

There are, in fact, few design considerations which do not favour the half speed generator. There are penalties in the size and cost, though these are much less than would at first be expected by a turbine designer versed in the laws of dynamic similarity.

For any given duty the choice between high speed and low speed wet steam turbine generators will depend mainly on the economic balance between cost and heat rate. Where the balance is close, other considerations, such as the manufacturers or operators perception of the likely reliability will influence the choice. With continuing turbine and generator development, the unit size at which the break-even point occurs will increase.

## 10. FUTURE PLANT

Future wet steam plant will incorporate many of the developments which have been completed for fossil fired plant, particularly in auxiliary systems and control. High speed units in particular will use blading, pedestals, LP turbine cylinders and generators identical to those of fossil fired units.

Only two developments are considered here, HP steam valves and the layout of reheaters and separators.

### 10.1 Steam Chests

On Parson's existing wet steam units, the four steam chests are arranged at the steam end of the HP turbine to which they are connected by loop pipes and the chests are free to move in a horizontal plane. Each chest contains an emergency stop valve and a governor valve, both valve spindle being vertical. The governor valves are operated through variable ratio levers which:

- give a high mechanical advantage at low valve lift when forces on the valve are high
- help to linearise the relationship between steam flow and actuator movement

- avoid the valve actuator being directly above the hot valve

The emergency valve is an inverted valve operated directly by the relay.

This arrangement has given very good service but:

- the loop pipes have a number of bends and therefore a high pressure drop
- there are large forces on the pivots of the variable ratio levers which can give rise to wear
- access to the inverted emergency valves is difficult

Figure 10 shows the new valve arrangement which is now incorporated in Parsons complete range of turbine generators.

For a 1200 MW wet steam unit the valves are virtually identical to the reheat valves of a 900 MW fossil fired unit, since the volume flows are very similar.

All valves are directly coupled to the actuators. The emergency stop valves are arranged horizontally alongside the turbine, and the governor valves are arranged at 30° to the horizontal with a 90° bend leading steam to the turbine cylinder.

This bend allows the turbine covers to be lifted without disturbing the valves and their operating relays. Apart from this bend almost every other change in direction of the steam is associated with a valve, where a bend is inevitable in any case. Thus there is a reduction in pressure drop, compared to the former arrangement, making a worthwhile contribution to improvement in heat rate.

Accessibility of the actuators for on-load or off-load maintenance is excellent, all being at or close to machine centreline.

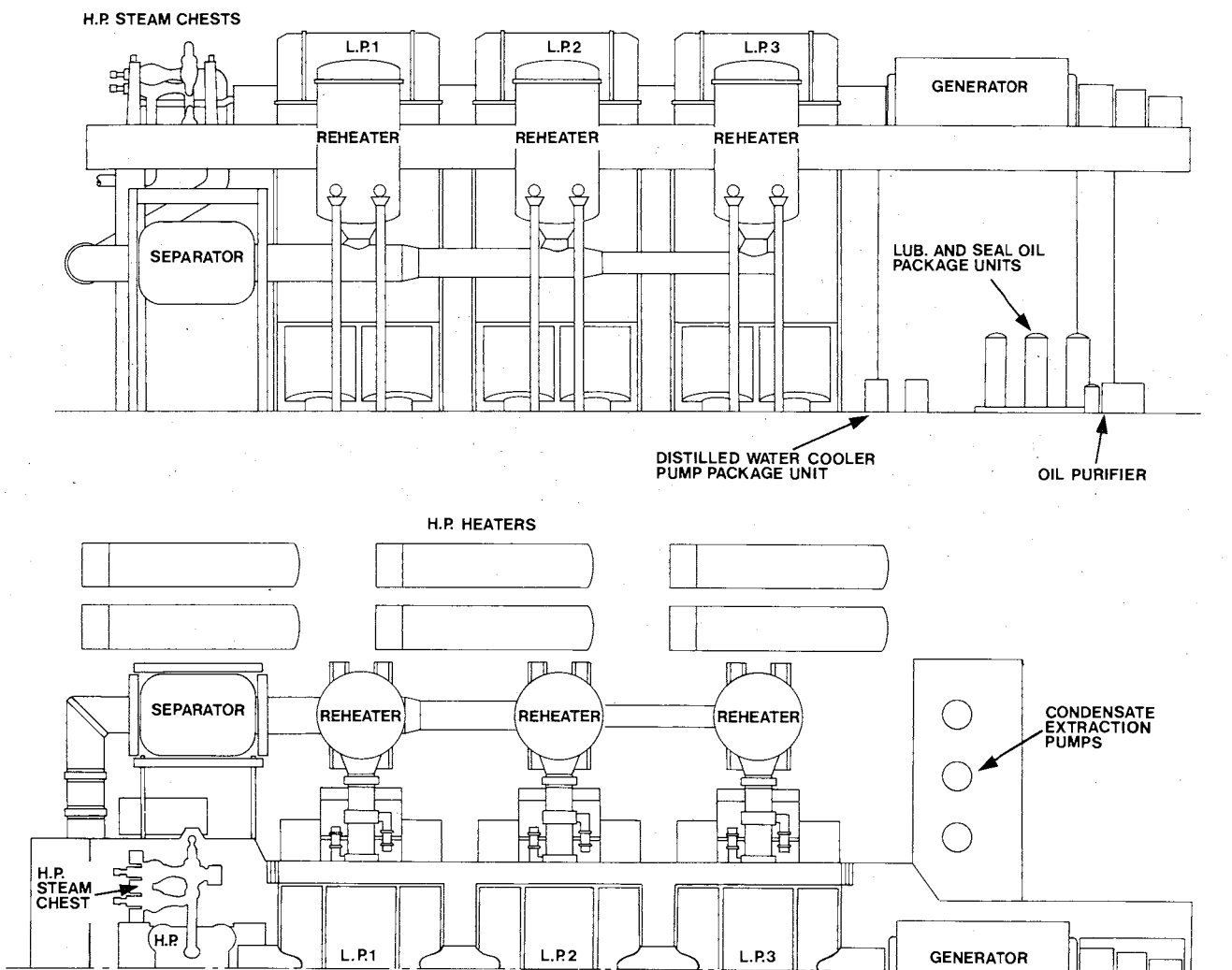


Fig. 10

## TURBINE DESIGN AND OPERATIONAL EXPERIENCE

The emergency stop valve and the governor valve bodies are similar but the former contains the steam strainer and the valve plug incorporates a pilot valve. The valve heads are balanced, minimising the force required from the actuator, and the only large force on the mechanism is the axial pull of the actuator against the spring and steam forces.

### 10.2 Reheaters and Separators

For a given steam cycle and terminal temperature difference, the reheater surface is almost exactly proportional to unit rating. However, the increasing value placed on heat rate, or additional kilowatts, has led to the introduction of two stage reheaters, wherein the first stage is fed with steam tapped from an intermediate stage in the HP turbine expansion. This in itself reduces the mean temperature difference in the reheater, but there is in addition a tendency to reduce the terminal temperature difference, i.e. to raise the reheater outlet temperature in relation to the live steam temperature. These developments demand a substantial increase in surface and thus in the size of the reheater vessels : to a point where the design of the main flanged joint becomes difficult.

For such applications the arrangement shown in Fig. 10 has been developed. Wet steam from the HP turbine passes to two centrifugal separators arranged at low level alongside the HP turbine. From the separators the dried steam passes along bus pipes arranged beneath separate reheater vessels, in this case six in number. Steam enters the reheaters from the bottom and passes upward across and into the front face of the reheater bundle. The construction of the reheaters is otherwise similar to that of earlier designs. The reheated steam passes through a single outlet to the LP turbine via the reheat emergency and intercept valves.

These developments give a compact plant which is easy to maintain. Pressure drops in the steam cycle are low, resulting in a low heat rate.

### 11. CONCLUSION

The industry is well placed to supply efficient and reliable turbine generators for operation on saturated steam up to the highest ratings at present envisaged, which are limited by the reactors rather than the turbine generators.

The high cost of reactors has led to a high value being placed on the heat rate and thus the output of the turbine generators. Many of

the developments which have been brought to a successful conclusion on fossil fired plant will be incorporated into saturated steam plant, together with some developments specific to such plant.

The choice of rotational speed will remain a matter for economic analysis, the additional output and potentially higher reliability of half speed units being weighed against additional cost. In 60 cycle countries half speed units are likely to dominate, whereas in 50 cycle countries both will find application in the foreseeable future.

### REFERENCES

1. PARSONS N.C. The Development of Large Wet-Steam Turbines. The Sir Charles Parsons Memorial Lecture 1972.
2. USHER J. Wet-Steam Turbine Operational Experience and Reliability. Institution of Mechanical Engineers Conference "Steam Turbines for the 1980's" October 1979.
3. MOINAUD C.H. and BRUNAR H.R.B. Recent developments in the field of Steam Turbines and their Application to PWR and fast breeder units ratio 1000 to 1500 MW<sub>e</sub>. Institution of Mechanical Engineers Conferences "Steam Plant for Pressurised Water Reactors". October 1983.
4. REID W.R. and KERNAHAN A.R. Experience with Centrifugal Separators and Vertical-Tubed Reheaters associated with Large Wet-Steam Turbines. This conference.
5. CONROY R.D. and HONEYMAN R.D. The Manufacture of LP Turbine Rotors for Large Steam Turbines. This conference.
6. TREECE D.R. The Effect of Operating Speed on Large Steam Turbine-Generator and Exciter Design. Beama Power Conference Singapore November 1979.
7. KALDERON D. Steam Turbine Failure at Hinkley Point 'A'. Proceedings Institution of Mechanical Engineers June 1972.
8. GRAY J.L. Investigation into the Consequences of the Failure of a Turbine Generator at Hinkley Point 'A' Power Station. Proceedings Institution of Mechanical Engineers June 1972.
9. HODGE J.M. and MOGFORD I.L. UK Experience of Stress Corrosion Cracking in Steam Turbine Discs. Proceedings Institution of Mechanical Engineers 1979.

## 2. Modern large 3000 rev/min steam turbines for pressurized water reactor power stations

J. MUSCROFT, MA, MIMechE, GEC Turbine Generators Ltd

**SYNOPSIS** The general thermodynamic cycle requirements applying to modern 3000 rpm steam turbines for pressurised water reactor power stations are reviewed. Consideration is given to factors affecting thermal efficiency, including the optimisation of cycle parameters and the use of moisture separation and steam reheating. Principles of mechanical design, based on a modular design concept for turbine cylinders, are discussed with reference to a range of 3000 rpm turbines with outputs up to 1300 MW. The most recent developments, involving machines of 630 MW and 985 MW output currently under construction, are described. The importance of service experience with nuclear steam turbines associated with a variety of types of water cooled reactor is emphasized, and its relevance to the design of modern 3000 rpm turbines for pressurised water reactor applications discussed.

### 1. INTRODUCTION

Significant service experience now exists with steam turbines for wet steam nuclear applications. The first such GEC machines entered service in 1965 and a number of machines have now achieved over 100,000 hours in service. The experience embraces machines associated with different types of water cooled reactors, some machines running at half speed (1800 RPM) on 60 Hz systems and some at full speed (3000 RPM) on 50 Hz systems. The most recent developments have involved pressurised water reactor applications on 50 Hz systems. 985 MW machines for the Guangdong Nuclear Power Station in the People's Republic of China and 630 MW machines for the first PWR application in the United Kingdom at Sizewell 'B' Power Station are now under construction. The general design features of the complete range of such 3000 RPM steam turbines for PWR applications are described below against the background of the earlier experience.

### 2. THERMODYNAMIC CYCLE PARAMETERS

#### 2.1 General Thermodynamic Requirements

The basic design of the turbine and associated plant for water cooled reactors is governed by thermodynamic requirements. Relatively low pressure steam, initially at saturated conditions or slightly wet, is expanded in the high pressure cylinder with increase in wetness during expansion. At a suitably selected HP cylinder exhaust pressure external water separation, by mechanical means, is used to produce virtually dry saturated steam. This is followed by steam-to-steam reheating using either live steam or live steam and bled steam to improve cycle efficiency and also to avoid excessive wetness in the low pressure expansion. Expansion of this superheated steam follows in the low pressure

cylinders. Suitable provision is made in the turbine feedheating system for acceptance of the water drained from the water separator and from the live and bled steam reheaters to maximise efficiency.

#### 2.2 Turbine Terminal Conditions

In modern PWR applications turbine stop valve pressures are typically 60-70 bar with steam wetness values at turbine inlet of the order 0.25-0.40%. Final feedwater temperatures demanded by the reactor are generally in the range 220-230°C in recent applications, requiring extraction pressures of about 25 to 30 bar for steam tapped to the final heater.

#### 2.3 Moisture Separator Reheater

Modern large turbines for use with wet steam cycles employ external moisture separation. This is followed by live steam reheating which results in performance improvement and in a low pressure expansion which, at the thermodynamically optimum levels of pressure chosen for water separation, leads to an expansion line close to that used in a typical high temperature reheat cycle as shown in Figure 1.

The additional use of a bled steam reheater is governed by economic factors. The low pressure expansion line is not affected and the issue is one of efficiency improvement, and therefore increased output, against additional cost, the degree of improvement being dependent on factors which can be selected by the turbine supplier. Principal factors are the HP cylinder exhaust pressure, the bled steam pressure from the appropriate stage of the HP cylinder, and the terminal temperature difference in the reheater. The bled steam reheater improves the cycle efficiency by reducing the amount of steam taken by the live



Table 1. Typical economic values of total exhaust area

CW temperature °C	15	22
Range of economically achievable backpressures (mbar)	70-45	95-65
600/700 MW	32-54m <sup>2</sup>	26-40m <sup>2</sup>
900/1000 MW	48-77m <sup>2</sup>	38-57m <sup>2</sup>
1200/1300 MW	66-101m <sup>2</sup>	50-75m <sup>2</sup>

Table 2. Typical required number of LP cylinders

CW temperature °C	15		22	
Last stage blade length	945mm blade	New longer blade	945mm blade	New longer blade
600/700 MW	3	2	2	2
900/1000 MW	4	3	3	2 or 3
1200/1300 MW	4*	3 or 4	4	3

\* without full utilization of the low cooling water temperature potential.

Table 1 summarises the typically economic values for total turbine exhaust area for a range of condenser cooling water temperatures, condenser pressures and outputs up to 1300 MW. For 3000 RPM turbines the numbers of low pressure cylinders typically required in GEC turbines to provide the economic exhaust area are given in Table 2. The maximum number of LP cylinders that can be practically employed in a tandem machine arrangement is considered to be four. It can be seen that the majority of applications, other than the highest outputs at low cooling water temperatures, can be met by using the 945mm blade. The development of a new LP cylinder with longer last stage blades, as discussed later, extends the range of application of 3000 rpm machines for 50 Hz generation to cover the complete output range at the lowest cooling water temperatures envisaged.

## 2.7 Other Factors Affecting Cycle Efficiency

In addition to the factors discussed above, many other internal parameters associated with the plant have an effect on the cycle efficiency. They include total number of

feedheating stages, terminal temperature differences for feedwater heaters and drain coolers, terminal temperature differences for bled steam and live steam reheaters and pressure drop through the moisture separator and reheater.

Each of these parameters can be modified so as to increase efficiency, but in each instance only at additional cost. Whether such improvements are worthwhile can only be determined by an economic assessment, and because in each application different evaluation factors apply, the optimised values of these parameters differ from case to case.

## 3. MODULAR CYLINDER DESIGN

### 3.1 Modular Design Concept

The organisation of the design of a series of machines covering a wide output range from a number of standard cylinder modules is discussed in detail for high temperature turbines at 3000 rpm in Reference 1. A similar approach is adopted to the design of cylinder modules for nuclear wet steam turbines for both 50 Hz and 60 Hz systems as discussed in Reference 2. Essentially a particular cylinder module has a fixed rotor geometry and fixed outer casing scantlings. Stationary and moving blade heights are varied, usually over only the early stages, to match the flow requirements over the range of output considered. In the case of LP cylinders adjustments to sizes of rotor journals and couplings are made to suit the transmitted machine torque.

### 3.2 High Pressure Cylinder Modules

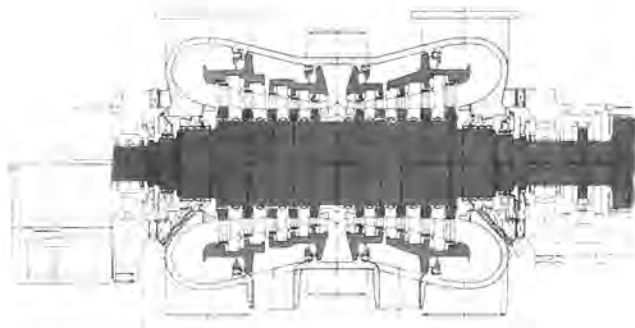
For 50 Hz application at 3000 rpm separate HP cylinder modules are designed to cover the output ranges 600-700 MW, 900-1000 MW and 1200-1300 MW. Similar principles of construction are used in each case and a typical cylinder module for a machine output of 900-1000 MW is shown in Figure 3a.

The cylinder consists of two flows, each with five stages of blading. Because the inlet pressure and temperature are only moderate the casing is essentially of single shell construction, with diaphragms mounted in diaphragm carriers to permit ease of extraction of bled steam. The four steam inlet pipes are attached directly to the casing. To ease the arrangement of external pipework on this cylinder supplying steam to two HP heaters, steam tapplings from two different stages are bled asymmetrically, one from each flow. Steam exhausts through eight exhaust pipes, located symmetrically in top and bottom halves, with four at each end of the casing.

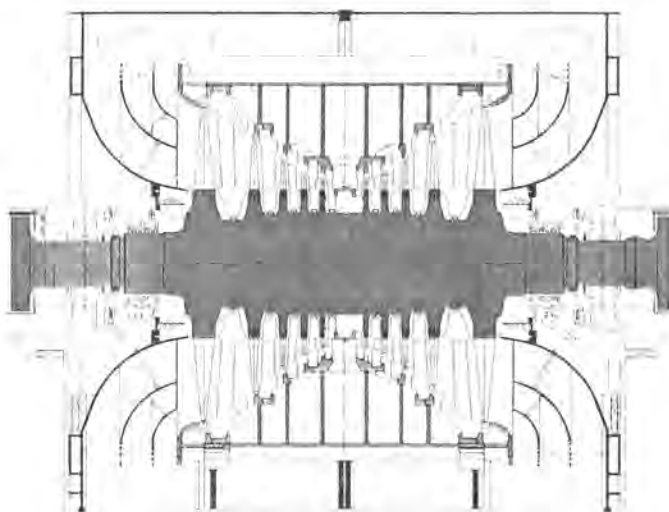
As on high temperature cylinders, disc and diaphragm type of construction is employed. The moving blades are shrouded and are attached to the monobloc rotor using pinned roots. The diaphragms, containing the fixed blades, are kinematically supported in the diaphragm carriers so as to remain concentric whilst permitting relative thermal expansion. The

diaphragms carry the rotor interstage spring-backed glands and also, on an extension ring, the tip seals, which co-operate with cylindrical projections on the moving blade shrouding. This type of construction ensures that small effective radial clearances are maintained over long periods of operation.

Arrangements are made for internal moisture extraction at each stage where this is not automatically effected at bled steam tapping points. An extension to the diaphragm mounted tip seal is appropriately slotted to permit extraction of water collecting on the outer flow boundary. This water is collected and passed through drilled passages in the casings to a stage at low pressure via an outlet flow swirler, thus avoiding any erosion problems at discharge.



a) 900-1000 MW HP cylinder module.



b) Standard LP cylinder module.

Fig.3. 3000 RPM turbine cylinder modules.

### 3.3 Low Pressure Cylinder Modules

The current design of the standard GEC 3000 rpm LP cylinder module with 945mm last row blades is shown in Figure 3b. This module is identical to that used on a large number of high temperature machines over a wide range of outputs. The five stages of blading in each flow are carried on a monobloc rotor. The diaphragms are mounted in a single shell inner casing supported in a fabricated outer casing. Steam is admitted through two inlets in the top half and steam exhausts downwards to an underslung condenser. The condenser may be floor mounted with a flexible connection to the turbine or spring mounted with a rigid connection to the turbine.

## 4. 3000 RPM MACHINES FOR PWR APPLICATIONS

### 4.1 Standard Machine Range

Machines covering the range 600 to 1300 MW include the appropriate HP cylinder module in tandem arrangement with two, three or four of the appropriate LP cylinder modules as indicated earlier in Table 2. Typical machines for this range of outputs for moderate cooling water temperatures are shown in Figure 4.

In all the machines the HP rotors are stiff, having their major critical speeds above the running speed, whilst each of the standard LP rotors has its first major critical speed below the running speed. Each rotor is supported on two bearings which are mounted in pedestals supported directly on the low tuned foundation block, which may be of either steel or concrete construction. The rotor thrust bearing is mounted in the bearing pedestal between the HP and the first LP cylinder.

The moisture separator and reheater vessels are normally mounted horizontally at turbine floor level on each side of the turbine alongside the low pressure cylinders. Detail design aspects of moisture separator reheaters are discussed in detail in Reference 3. A typical arrangement of a 1000 MW machine supported on a concrete foundation block with horizontally mounted moisture separator and reheater vessels is shown in Figure 5.

### 4.2 630 MW Turbines for Sizewell 'B' Power Station in the United Kingdom

For the first turbines for PWR application in the United Kingdom, 630 MW machines at Sizewell 'B' Power Station, the HP cylinder will be the smallest of the module range described earlier. With an inlet pressure of 66.8 bar and an optimised exhaust pressure of 5.9 bar, an economic assessment showed that three high pressure heaters could be justified, with bled steam taken after the second, third and fourth stages of blading. Bled steam for the reheater is also taken after the second stage. Bled steam quantities and general cylinder design considerations led to the bled steam being taken symmetrically from both flows after stage two but asymmetrically from the rear flow after stage three and from the front flow after stage four.

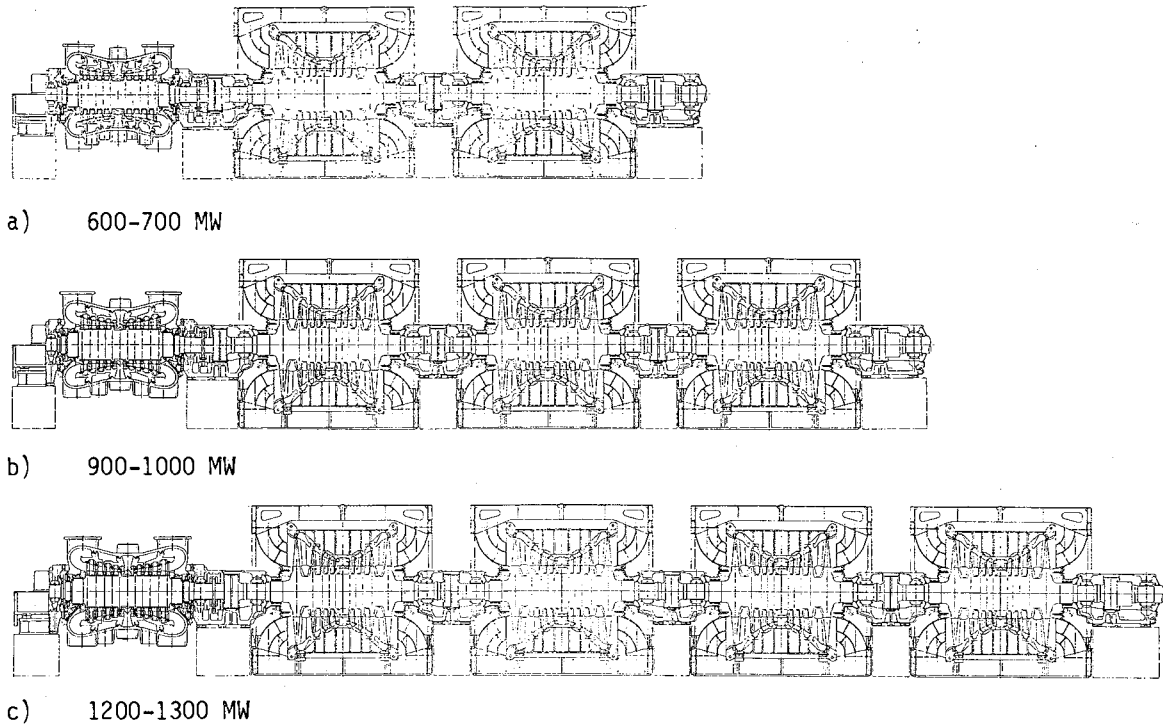


Fig. 4. Standard 3000 RPM turbines for 600-1300 MW PWR applications.

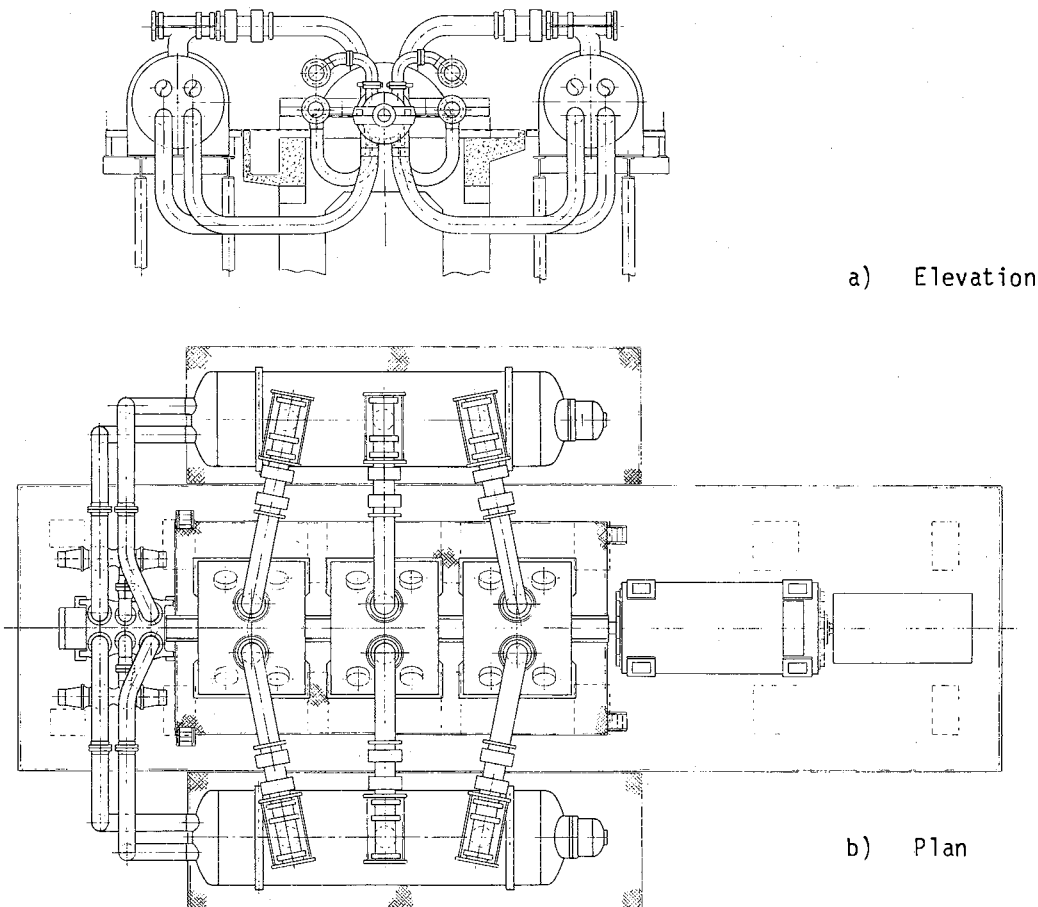
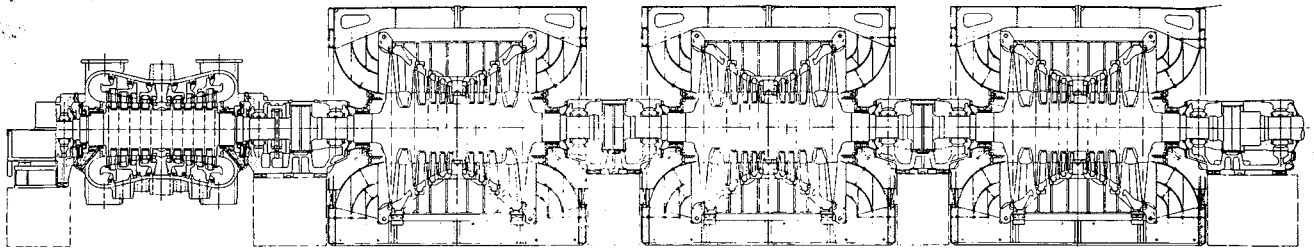
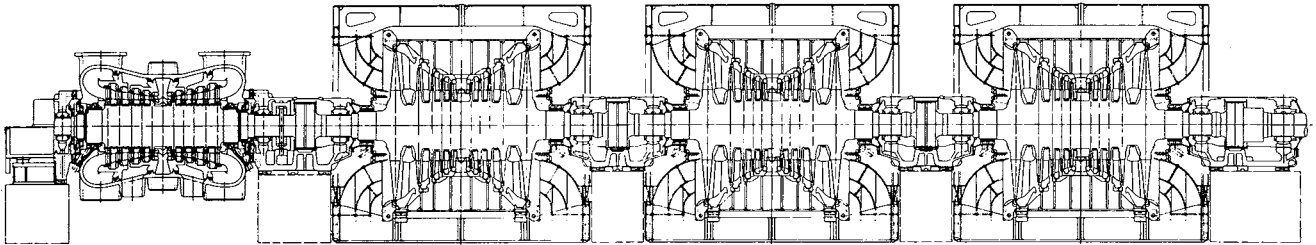


Fig. 5. General arrangement of PWR turbine and moisture separator and reheater vessels.



a) 630 MW turbine for Sizewell 'B' Power Station



b) 985 MW turbine for Guangdong Nuclear Power Station

Fig. 6. 3000 RPM PWR turbines.

The average cooling water temperature at Sizewell 'B' is 13°C and for an optimised back pressure of 43 mbar the economic exhaust area is provided by using three standard LP cylinders. A section through the machine is shown in Figure 6a.

#### 4.3 985 MW Turbines for Guangdong Nuclear Power Station in the People's Republic of China

For the 985 MW turbines for the Guangdong PWR Power Station in China the HP cylinder will be the intermediate module of the range described earlier. With an inlet pressure of 64.3 bar, slightly lower than that at Sizewell 'B', and an optimised exhaust pressure of 7.8 bar, higher than that at Sizewell 'B', two high pressure heaters are used taking bled steam after the second and third stages of blading. As on the turbines for Sizewell 'B' Power Station bled steam for the reheater is taken after stage two. The bled steam is taken asymmetrically from the rear flow after stage two and the front flow after stage three.

The average cooling water temperature at Guangdong Nuclear Power Station is 23°C and for an optimised back pressure of 75 mbar the economic exhaust area is provided by using three standard LP cylinders, the same as for the Sizewell 'B' turbine. The higher exhaust steam flow for the larger output Guangdong turbine is offset by the higher cooling water temperature and consequently higher optimised back pressure than at Sizewell 'B', so that similar exhaust areas are required. A section through the turbine for Guangdong Nuclear Power Station is shown in Figure 6b.

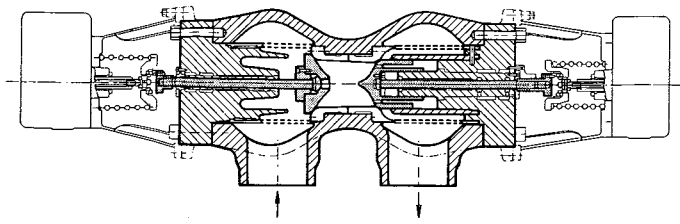
## 5. CONTROL REQUIREMENTS AND VALVE ARRANGEMENTS

### 5.1 Governing and Control

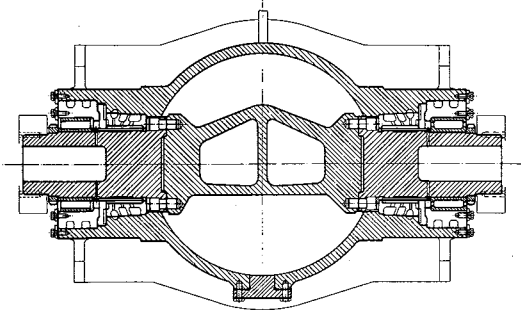
To provide the required fast response and high reliability an electro-hydraulic governing and control system, with two out of three channel logic, is used, employing high pressure fire resistant fluid in the valve hydraulic operating gear. Use of an electric governor facilitates interfacing of the turbine and reactor control systems and co-ordinated operation of the turbine bypass system. Since nuclear units generally operate at high levels of base load, throttle control is used in all cases, with four governing valves opening in unison. To prevent the large volumes of steam and flashing water stored in the reheaters from causing high machine overspeed under electrical load rejection, interceptor valves are required in the hot reheat pipes between the reheater outlets and LP cylinder inlets.

### 5.2 High Pressure Valves

The main stop and governing valves used for present PWR applications are similar in design to those used for reheat valves on high temperature turbines with appropriate material changes. Each machine employs four stop and four governing valves. A piloted stop valve, surrounded by a strainer, and a single seated balanced governing valve are arranged coaxially opposed in a single chest as shown in Figure 7a. These chests are mounted horizontally on flexible supports, two on each side of the HP cylinder, with short loop pipes connecting to the turbine inlets. The chests are stacked in pairs vertically as can be seen in Figure 5.



a) High pressure stop and governing valves.



b) Low pressure valves.

Fig. 7. Valve arrangements.

### 5.3 Low Pressure Valves

Because of the large volumetric flow at LP cylinder inlet the interceptor valves are of necessity of very large size, generally in the range 900 to 1050mm diameter. Butterfly valves as shown in Figure 7b are well suited to this application, having the advantage of providing very low pressure drop in the normal operating fully open position. They are used for both stop and governing valves, one stop and one governing valve being combined in a single chest located in each hot reheat pipe. Substantial operating experience now exists with valves of this design.

## 6. MATERIAL SELECTION & OPERATING EXPERIENCE

### 6.1 Wet Steam Erosion

As discussed earlier steam conditions in the LP cylinders of PWR turbines with moisture separation and live steam reheating are very similar to those in high temperature turbines. It is evident therefore that there are no special erosion problems.

However, in the HP cylinder conditions are completely different from those in high temperature turbines. The progressive increase in wetness through the cylinder at relatively high pressures has a powerful potential for causing erosion damage. With the velocities of the moisture droplets and main steam not differing significantly at the relatively high steam densities applying, coupled with the use of stainless steel for the whole steam path, blade path erosion is not a significant problem. Potential for erosion damage is highest in the casings and associated pipework and valves, either where there are changes in flow direction or across joint surfaces of pressure seals.

### 6.2 Operating Experience with Nuclear Wet Steam Turbines

It follows from the above that experience with nuclear wet steam turbines has greatest relevance to the design of the HP cylinder, valves and pipework, with particular reference to erosion problems due to the steam wetness. In considering these problems for full speed 3000 rpm PWR turbines experience with wet steam turbines running at both full speed and half speed and operating with different types of reactor is fully relevant. Service experience with 17 GEC turbines with ratings up to 1200 MW, including PWR, BWR, CANDU and SGHWR applications, amounts to more than 170 machine years, with individual machine operating times up to 150,000 hours.

Earliest experience was with a small machine of 22 MW rating running at 3600 rpm with a CANDU reactor. This was followed by two larger machines, a 100 MW machine running at 3000 rpm using SGHWR steam and a 220 MW machine running at 1800 rpm with a CANDU reactor. A number of erosion problems were initially encountered on these units, for which design solutions were evolved and changes made in material selection, and these were proved by subsequent service.

Later machines incorporating these features have now achieved considerable service experience. A machine of 54 MW rating at 3000 rpm for a BWR station in Holland has run for 130000 hours. At 3000 rpm two further machines for BWR application, of 400 MW output, have each been in operation for more than 70,000 hours. The HP cylinders of these 400 MW machines are of single flow type, so the experience is equivalent to that of a double flow cylinder on a machine of up to 800 MW output. The machines employ three LP cylinders, the LP rotors being of shrunk-on-disc type construction. Although not relevant to modern 3000 rpm turbine designs, it is of interest to note that inspection of these LP rotors after approximately 45,000 hours service demonstrated freedom from stress corrosion cracking at the disc bores and in the vicinity of the locating dowel holes in the disc hubs. These machines are in service at Ringhals Nuclear Power Station in Sweden, as shown in Fig. 8, where, to minimise radiation levels in the turbine hall for this BWR application, concrete shielding is provided around the HP cylinder and the moisture separator reheater vessels are located below floor level. At 1800 rpm a 600 MW turbine for PWR application in Korea has reached over 60,000 hours of operation. Inspection of the HP cylinders of all these machines have shown them to be in very good condition.

At the larger outputs two 1200 MW PWR turbines running at 1800 rpm are in service at San Onofre in the USA. A similar 1200 MW unit, but for a BWR application, is in service at Enrico Fermi Power Station, also in the USA. Two 1000 MW PWR turbines, also running at 1800 rpm but of later design, are in service in

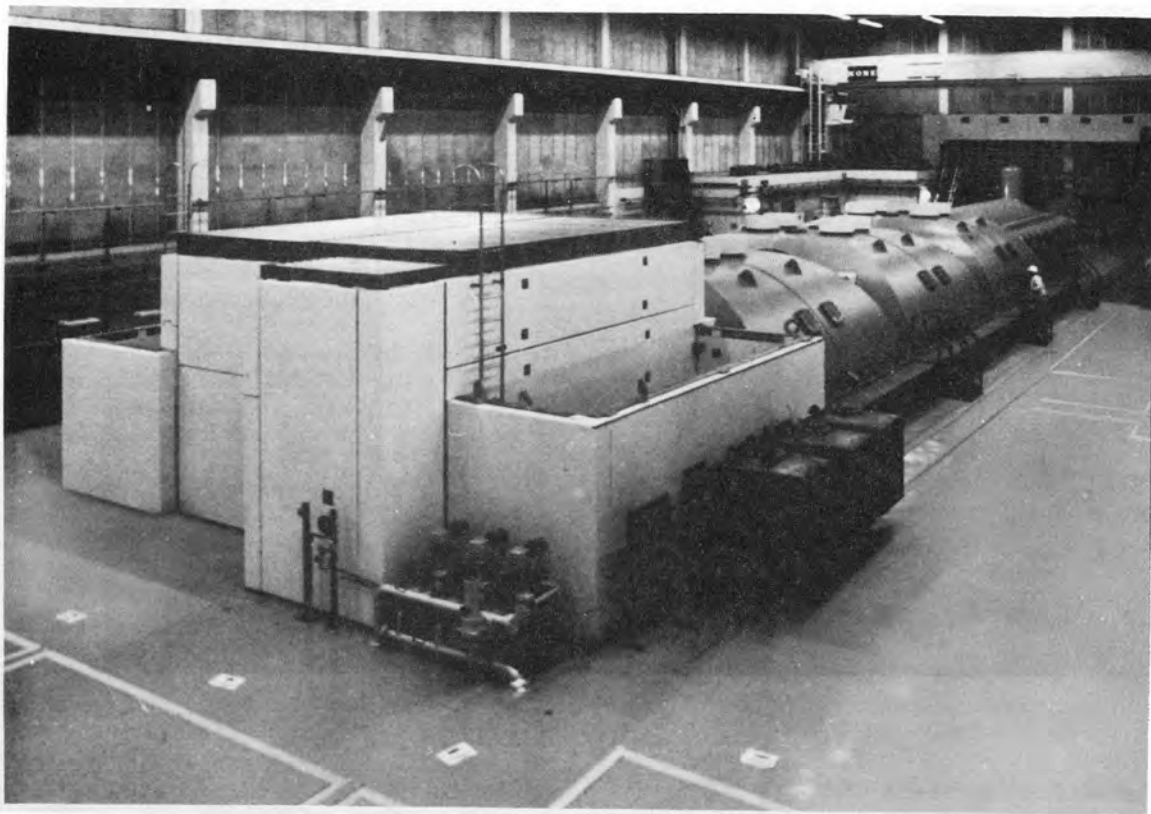


Fig. 8. 400 MW 3000 RPM turbine in BWR power station.

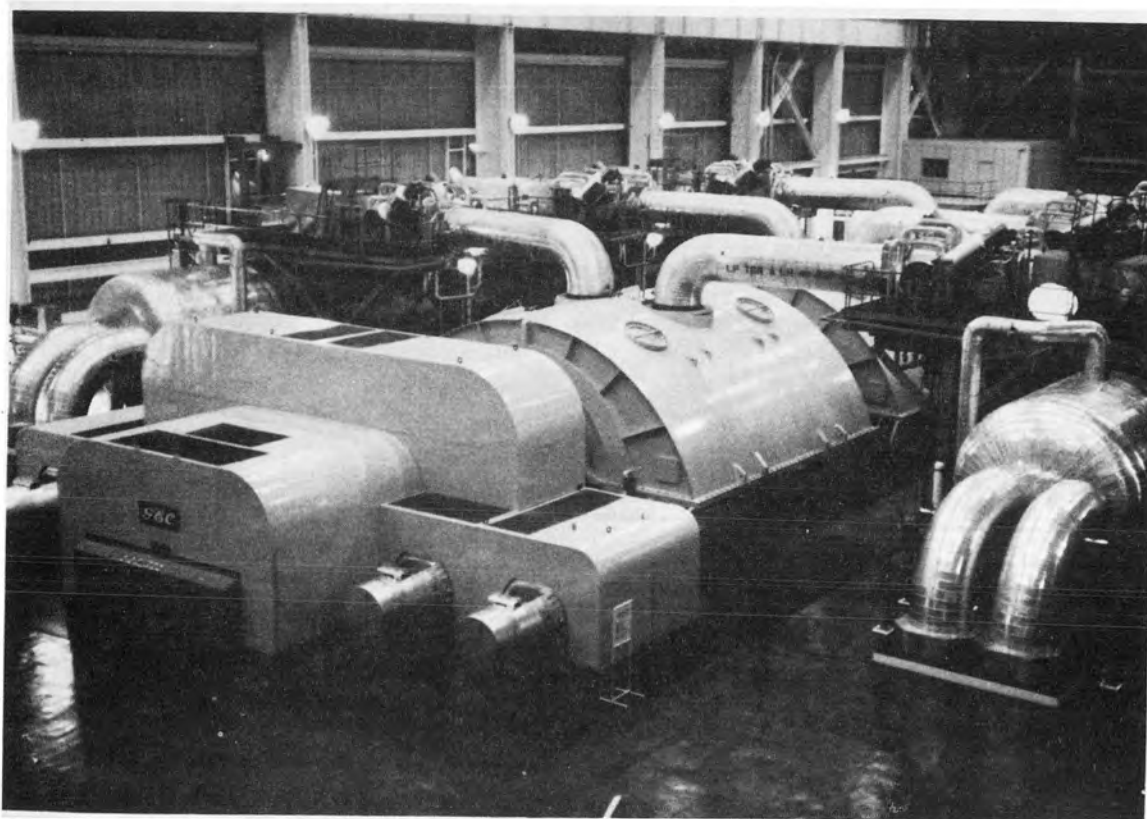


Fig. 9. 1000 MW 1800 RPM turbine in PWR power station.

Korea. The machine arrangement of these 1000 MW turbines is generally similar to that of large 3000 rpm turbines and is shown in Figure 9.

### 6.3 Material Selection

The above experience allows confident selection of materials for components in wet steam environments, as discussed in detail by Thornton (Reference 4) in a companion paper to this Conference. The selection depends on steam pressure and wetness and the nature of the steam flow associated with the particular design features of the components involved.

At the very low levels of wetness at turbine inlet carbon steel is used for steam pipework and valve chests. For the HP casings and diaphragm carriers, where the level of wetness is greater, a low chromium alloy steel is used. The same material is also used for cold reheat pipes.

For welded diaphragms a fully stainless steel blade path is employed, including the nozzle blades and spacer bands forming the nozzle annulus boundaries at inner and outer diameters. Low alloy steel is adequate for diaphragm inner and outer rings.

On the faces of all joints sustaining pressure differences a deposit of stainless steel cladding is applied to prevent any significant wire drawing erosion. Such faces include bolted joints between top and bottom half casings and diaphragm carriers, and axial contact surfaces at diaphragm carrier and diaphragm supports. In addition to the application of protective cladding on the horizontal joint faces of diaphragm inner and outer rings, the top and bottom half diaphragms are bolted together across the outer rings to assist in joint protection.

No special protection is applied to the body of the low alloy steel HP rotor, nor to the interstage gland regions. However, because of the high degree of exhaust wetness, the rotor end glands are packed with dry steam obtained by throttling live steam.

### 7. FUTURE DEVELOPMENT OF 3000 RPM NUCLEAR WET STEAM TURBINES

Increase in unit size of 3000 rpm nuclear wet steam turbines is limited only by the exhaust area of existing LP cylinders and the number of LP cylinders that can be deployed in a single unit. Against a background of likely increase of unit size of both fossil

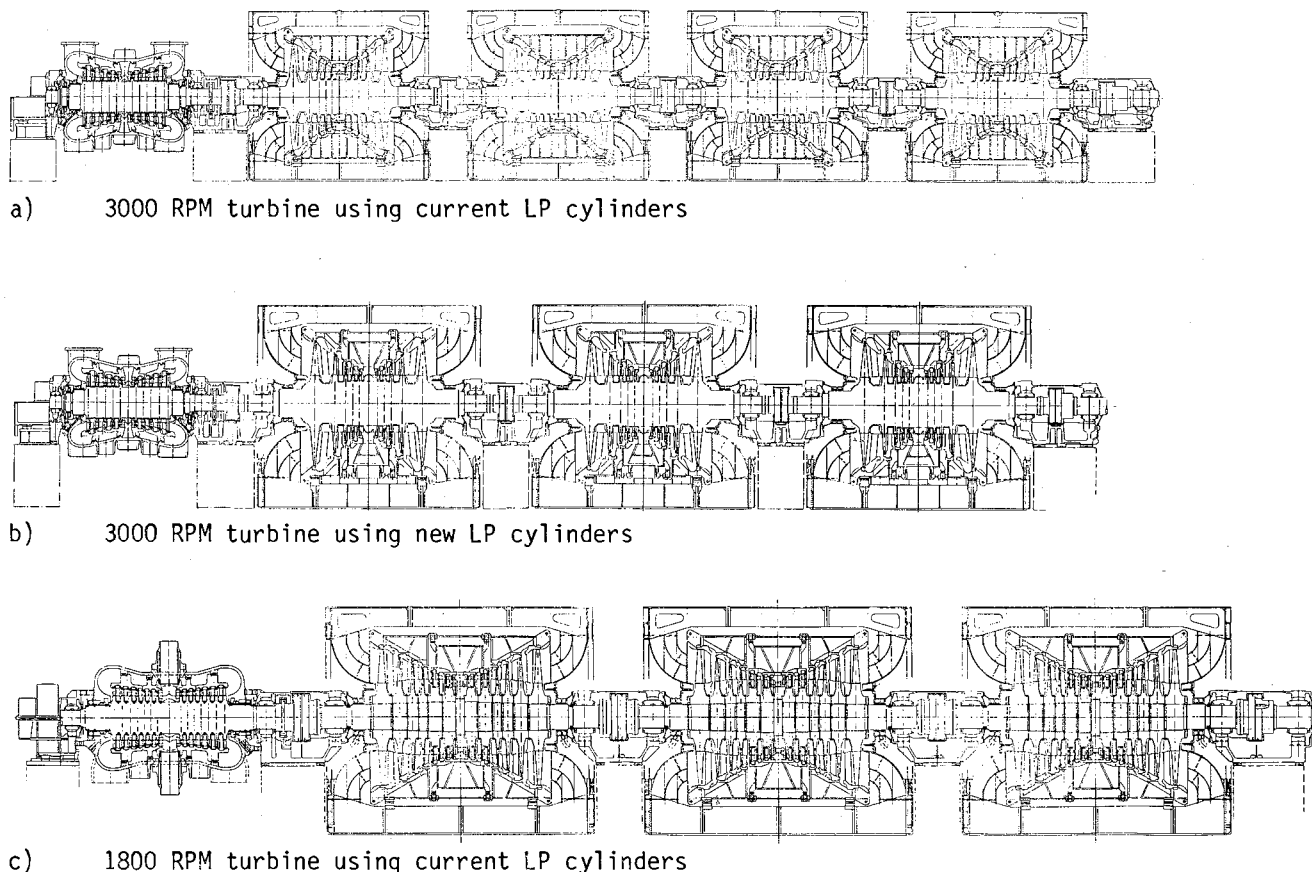


Fig. 10. Turbines for 1200-1300 MW PWR applications.

## TURBINE DESIGN AND OPERATIONAL EXPERIENCE

high temperature turbines and nuclear wet steam turbines a new LP cylinder has been developed utilising a new last row blade of length greater than the 945mm blade on which current large GEC turbine designs are based. The new blade provides an exhaust area significantly greater than the current blade and readily permits increase of unit size to 1200 -1300MW for the lowest likely cooling water temperatures.

For such a 1200-1300 MW machine the HP cylinder will be the largest of the module range described earlier. The LP cylinders will have similar basic design features to the smaller module described earlier. The LP rotor will be of monobloc construction, taking advantage of advances in steel making and rotor forging practices achieved in recent years. Rotors are now available of significantly increased size, having at the same time improved material strength and toughness properties, compared with those available at the time of initial design of the smaller LP rotor in current use. The design of the new last stage blade has taken advantage of the advances made in recent years in the understanding of the nature of the three dimensional flow structure in last stages of steam turbines using improved computational techniques supported by confirmatory flow tests.

Figure 10 shows an arrangement of a 1200-1300 MW machine using three of the new LP cylinders compared with a machine of the same output using four of the current LP cylinders. Although the new LP cylinders are individually larger, the use of three instead of four results in reduction in overall length of the new machine compared with that using the current LP cylinders. For the lowest likely cooling water temperatures a greater exhaust area could be provided by using four of the new LP cylinders. Also shown for comparison in Figure 10 is the arrangement of a half speed 1800 rpm machine for 60 Hz systems having the same output, similar to machines currently in service. The new 3000 rpm machine is substantially shorter than the existing lower speed machine.

## 8. CONCLUSIONS

For application in PWR power stations on 50 Hz electrical systems a range of modern 3000 rpm steam turbines has been designed covering the output range up to 1300 MW. The designs are based on substantial operating experience with machines associated with a variety of water cooled reactors. The machines have optimised thermodynamic cycle parameters with external moisture separation and steam reheating to provide high thermal efficiencies. They are formed from a small number of standard cylinder modules, the low pressure cylinder modules being identical to those used on large high temperature turbines.

Typical of machines from the lower and intermediate output ranges, 630 MW turbines for Sizewell 'B' Power Station in the United Kingdom and 985 MW turbines for Guangdong Nuclear Power Station in the People's Republic of China are currently under construction. Development of a new LP cylinder, significantly larger than that used on the Sizewell 'B' and Guangdong turbines and also on many high temperature turbines currently in service, ensures that highly efficient 3000 rpm turbine designs are now available for the higher output range with the lowest likely cooling water temperatures.

## REFERENCES

1. D. Kalderon - Design of large steam turbines for fossil and nuclear power stations. I.Mech.E. Conference 1979 "Steam turbines for the 1980's".
2. G. Hobson and J. Muscroft - Design of large steam turbines for pressurised water reactor power stations. I.Mech.E. Conference 1983 "Steam plant for pressurised water reactors".
3. C.J. Monks and J.P. Peyrelongue - Development of designs of moisture separator reheaters. B.N.E.S. Conference 1988 "Technology of turbine plant operating with wet steam."
4. D.V. Thornton - Materials for turbine plant operating with wet steam. B.N.E.S. Conference 1988 "Technology of turbine plant operating with wet steam."

### 3a. EDF experience with PWR turbine plant: crack-generating stress corrosion of low pressure rotors

C. MALHERBE and G. PAGES, Electricité de France

The first signs of stress corrosion were detected in 1986 on low pressure rotors with shrunk-on disks in the 900 MW turbogenerator sets of France's first contract program (known as "CP1"). The two affected rotors were subjected to expert investigations and various measures were taken to permit continued operation of the turbogenerator sets without significantly compromising availability or safety. A complementary program to renew a high percentage of all LP rotors over coming years is underway to counter this development of cracking.

#### INTRODUCTION

Electricité de France's PWR 900 MW nuclear power plants have 34 units equipped with two types of turbogenerator sets:

- 24 impulse turbogenerator sets in the first contract program "CP1" units,
- 10 reaction turbogenerator sets in the second contract program "CP2" units.

Two different techniques were employed in construction of their LP rotors:

- shrunk-on disks for type CP1 rotors,
- welded disks for type CP2 rotors.

Generally speaking, the operational behaviour of the turbines has been satisfactory as shown by the excellent availability statistics for EDF power plants. However, in 1986, crack-generating stress corrosion appeared on the LP rotor shrunk-on disks in the "CP1" sets. This phenomenon, internationally known through the number of cases encountered with sometimes disastrous results (as witnessed by several destructive failures), has been widely published.

This paper presents the results of examinations carried out during refuelling outages and also current trends for countering the development of cracking of LP rotor disks in the "CP1" series.

#### TECHNOLOGY OF "CP1" LP ROTORS

The lineshaft of "CP1" turbines consists of one HP rotor and three LP rotors rotating at 1500 r.p.m.

There are a limited number of technological solutions for LP rotor construction:

- a forged single-block rotor,
- a welded disk rotor,
- a shrunk-on disk rotor.

At the time of their construction, ALSTHOM BELFORT, the CP1 contractor could not use the single-block technique because of the excessive mass of forged parts, and naturally employed the shrunk-on disk technique that had been already used in the past.

Each "shrunk-on disk technology" LP rotor weighs 145000 kg and consists of the following main parts (cf. fig. 1):

- a forged shaft,
- a set of 12 disks shrunk-on the shaft, symmetrically disposed about a central spacer,
- coupling sleeves shrunk-on the shaft,
- blades.

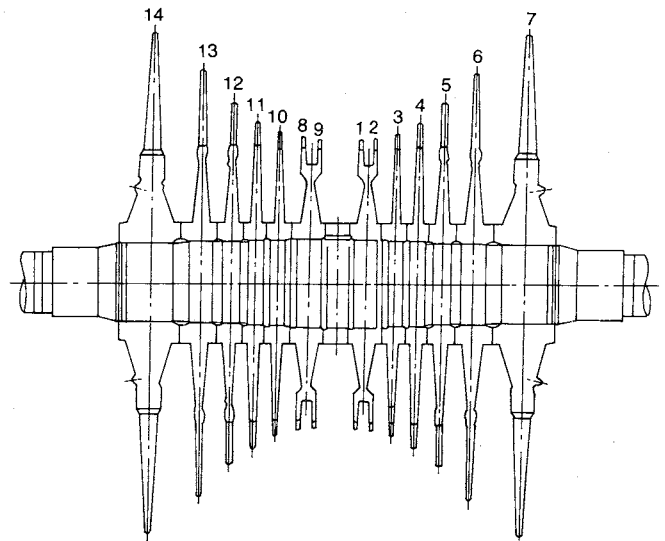


Fig. 1 - 900 MW Low Pressure Rotor

To make the disks one with the shaft, they are normally shrunk-on at bore level and, exceptionally, using a pin-keying system as shown in the appended drawing (figure nr. 1). The latter system only plays an effective role in the case of shrunk-on disks becoming loose due to centrifugal force at about 120% nominal rotating speed (1500 r.p.m.). In practice, such a situation only occurs during in-factory overspeed tests and only excessive overspeed in operation might result in such an incident (extremely rare, only a limited number of cases have occurred in past operations).

TURBINE DESIGN AND OPERATIONAL EXPERIENCE

The shrunk-on technique is similar to those used by some constructors (WESTINGHOUSE, GENERAL ELECTRIC, KWU, etc.) when confronted with the problem of making large scale LP turbine rotors, rotating at 1500 or 1800 r.p.m. because at the time, there were no technological solutions such as:

- forged single-block rotors,
- welded disk rotors.

BRIEF REVIEW OF PROBLEMS ENCOUNTERED WORLDWIDE

The main problem here is CRACK-GENERATING STRESS CORROSION OF PRESSURISED DISKS IN A WET ATMOSPHERE.

Since 1969, numerous cracks in shrunk-on LP rotor disks have been found in nuclear and fossil-fuel powered plants in GREAT BRITAIN, AUSTRALIA, SOUTH FRICA, SWEDEN, USSR and the USA.

All experts investigations on damaged machines have confirmed that cracking was due to stress corrosion.

From a total of almost 300 disk-constructed LP rotors inspected in the UK and the USA, this phenomenon was detected on 174 rotors, that is on more than one rotor out of two.

This very serious phenomenon led to:

1. Partial destruction of three machines when affected disks failed:

- in oil fired plant after 31 years' service,
- at HINKLEY POINT A in GREAT BRITAIN (1969) after 5 years' service,
- at YANKEE ROWE in the USA (1980) after 20 years' service.

2. Affected rotor failure during an in-pit overspeed test in GREAT BRITAIN (1969).

3. Admitting temporary deteriorated operating conditions:

- operating with cracked disks,
- removal of disks with unacceptable defects.

4. Launching of affected LP rotor renovation or replacement programs as in:

- GREAT BRITAIN, reconstruction of 93 low-power LP rotors after 1973 by procuring oversized shafts and disk reboring to remove bore keyways.
- USA, by replacing existing rotors with forged single-block rotors or welded disks. This currently involves forty of so rotors.

PROBLEMS ENCOUNTERED WITH EDF "CP1" ROTORS

"The bursting of disks at Hinkley Point "A" in 1969 took place prior to the construction of EDF machines. Information from Hinkley Point "A" thus enabled the EDF machines to be designed without stress concentrating features such as bore keyways and with lower levels of stress, thereby reducing risk of stress corrosion. Furthermore, inspection procedures were devised to enable condition of disk and shaft to be checked".

Until September 1986, no indications were detected during shrunk-on disk bore inspections. The inspection of rotors LP2 and LP3 at the BUGEY 4 unit during a refuelling outage, after 51500 operating hours, revealed major indications in the bores of 3 disks (two "11" disks and one "4" disks).

The nature of these indications, that is:

- localisation in hot disk area and at the beginning of condensation,
- high mechanical stress zone,

- development in the axial-radial direction,
  - multiple indications,
- led us to presume we were very probably confronted with the stress corrosion phenomenon encountered abroad.

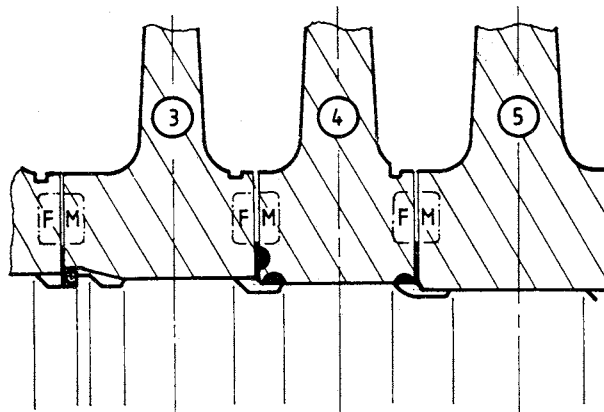


Fig. 2. Location of the Disc Cracks

As a result, an extensive in-depth inspection program was implemented during the 1987 refuelling outages.

Inspection results

The inspection covered almost half of the 75 LP rotors in service (including 3 replacement rotors). The oldest rotor inspected had 67000 hours of operation to its credit.

The following chart gives breakdown of rotors by unit age:

Age range				Total number of rotors
0	to	10000	h	2
10000	to	20000	h	6
20000	to	30000	h	5
	30000	to 40000	h	6
40000	to	50000	h	32
	50000	to 60000	h	18
60000	to	70000	h	6
Total .....				75

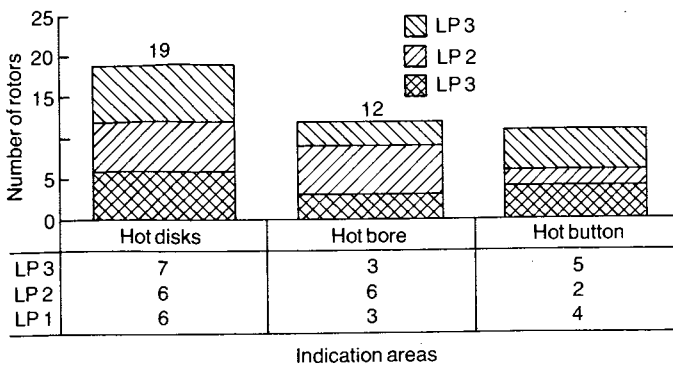
Indications attributed to stress corrosion were detected on twenty or so rotors, mainly on those with more than 40000 operating hours.

Most of the indications are located in the first interdisk gap downstream from the Wilson line.

Expert investigation of the rotors

Three rotors were withdrawn from operation during the 1987 series of inspection, to perform in-depth expert investigation of indications revealed by non-destructive tests.

Two of the three rotors have had the shrunk-on disks removed and one is under investigation, so it is a little early to draw conclusions. The results of these investigations are shown on Figure nr.3.



Hotdisks are number 1-2, 3, 4, 5 and symmetric disks

Fig. 3. Number of rotors with indications  
(Copyright: EDF/SPT/Div. MACBINES)

Two main locations of the cracks:

- the first location is the bore where we found large cracks, the deepest of them were 25 mm,
- the second location is the drive button where we found a lot of small cracks.

The critical crack size depends on the location and moreover on the combination of the location: we could admit a crack deepness of 40 mm in the bore but, if a bore crack is located in a button area, the crack size we can allow is only 30 mm.

One of the major problems we are facing is the velocity of the crack in time. Up to day, we have not enough datas to give a good figure of the velocity; so, we suppose a 10 mm/year velocity in order to adjust the periodicity of the controls.

Up to now, only one rotor has been unshrunk and two main features were confirmed from the analysis:

- the cracks were stress corrosion cracks,
- the non-destructive tests were pessimist, i.e. the actual size of the cracks were smaller than the control figures (- 20%).

#### Measures taken

The main measures taken to avoid compromising machine safety and availability are basically the following:

1. Precise determination of critical defect size and defects tolerable in operation.
2. Improvement of inspection techniques to refine localisation and sizing of defects,

indispensable in determining degree of rotor risk during operation.

3. Continuation of rotor inspection work in 1988, so as to:

- define defect evolution kinetics,
- adapt machine operating policy and repair scenarios in consequence.

4. Increase of number of replacement rotors to cover the repair of the most affected rotors. The number of spare rotors will be increased from 3 to 6 in 1988, and to 9 in 1989.

5. Studies for the rehabilitation of defect-affected rotors. Maximum advantage will be taken disk-removal operations to make improvements on shrunk-on disk technology in the face of stress corrosion phenomena (especially by protecting sensitive zones).

The main features of the design improvements are:

- nickel coating of the sensitive zones,
- increasing of the gap between discs,
- modification of steam flow through the inter-discs seals in order to avoid condensation.

Technical dispositions should be finalised by summer of 1988; process qualification, fabrication and perfecting of the necessary tools should be finished by the end of this year.

With a cost of about 14m FFrs per rotor, the operation will be started this year on the three rotors removed from operation.

#### Repair scenario envisaged

To date, the state of acquired knowledge, that is:

- number of rotors affected,
  - size of observed defects,
  - kinetics of estimated growth,
- and availability as of 1989 of 9 replacement rotors have allowed us to plan on a repair program for 6 rotors per year starting with the 1989 campaigns.

#### OUTLOOK FOR THE NEXT 2 OR 3 YEARS - CONCLUSIONS

Given the 1987 inspections, the state of health of all the LP rotors is not immediately critical; however, it is essential to:

- maintain our surveillance efforts over the next few years so as to take all measures necessary should the problem evolve differently,
- start repair operations immediately trying to spread these operations over the maximum period of time without significantly compromising machine safety or operating flexibility.



## 3b. EDF experience with PWR turbine plant: corrosion-erosion in PWR secondary cycles

C. MALHERBE and J. MARCEAU, Electricité de France

Significant corrosion-erosion damage has occurred on certain components of the first French 900 MW power plants. These components include: feedwater heaters, moisture-separator reheaters, valves, fittings and pipes.

Various corrective measures were therefore taken to avoid corrosion-erosion in the future. These measures are listed below:

- modification of steam generator feedwater conditioning,
- modifications in design criteria and choice of materials for new heaters,
- addition of water-separator tanks or high velocity separators (HVS) on the steam extractor pipe that supply the heaters in operation,
- installation of protective nozzles at the inlets of HP heater tubes,
- use of a different grade of steel for steam or condensate pipes and for casings of certain valves and fittings.

The cost of such modifications on a 900 MW power unit is 12 million French francs.

### INTRODUCTION

Secondary system equipment for French PWR power plants was designed according to the criteria used for fossil-fired power units (velocity of the fluids, design of equipment, etc.) while taking into account the theoretical moisture content deduced from the pressure reduction curve in the turbine. Moisture measurements recently carried out on high-pressure steam extractors revealed the presence of moisture far in excess of the theoretical value.

Since the commissioning of these installations, steam generator feedwater has been ammonia-treated (pH = 9).

The initial corrosion-erosion damage appeared after 10,000 hours of operation, first in the carbon steel pipes that connect the high-pressure cylinder of the turbine to the moisture-separator reheaters, and then in the steam extractor pipes and steam-filled vessels of high-pressure feedwater heaters R6, R5 and R4 (fig. 1 and 2).

This phenomenon was also observed during an inspection campaign conducted in several power plants to measure corrosion losses on sections of pipes conveying drain water, condensate and vent pipes, as well as on the associated valves and fittings.

For reasons of personnel safety, equipment availability and to reduce the iron content of the steam generator feedwater, EDF swiftly launched a series of actions to provide:

- a better understanding of the corrosion-erosion phenomenon and of the influence of the different parameters that govern it. This includes the creation of the water test loop "CIROCO", monitoring of the equipment in service, study of wet steam corrosion on several dozens of test-pieces taken from different materials,

- a change in method of feedwater conditioning (switch to morpholine pH = 9.1 to 9.3),
- for drying of the extraction steam and protection of the vessel walls by coverings and condensate expansion caissons of stainless steel to insure correct resistance to corrosion-erosion of the bundles and equipment secondary vessels,
- installation of stainless austenitic steel (grade 304L) protective nozzles at the inlets of the unalloyed steel tubes of the HP heaters,
- a different grade of steel for certain piping elements and associated valve casings,
- annual checking of feedwater piping thicknesses and of pressure boundaries which cannot be inspected using ultra-sonic means,
- for future equipment (feedheaters, moisture-separator reheaters, pipes, valves and fittings, etc.), use of corrosion-erosion resistant materials for secondary vessels subject to high-velocity flow and exchange bundles.

### SUMMARY DESCRIPTION OF THE SECONDARY SYSTEMS

French PWR power plants are equipped with two types of secondary systems:

a) 1st type: without deaerator feedwater tank (simplified diagram fig. 1) on the twenty-four 900 MW power plant units of the first program (called the "CP1" program),

b) 2nd type: with deaerator feedwater tank (simplified diagram fig. 2) on the ten 900 MW power plant units of the 2nd program (CP2) and the twenty 1300 MW power plant units of the 3rd program (the first one being known as P4 and the others as P'4).

The first type includes a low pressure (L.P.) feedwater plant with 4 heating levels and a high-pressure (H.P.) feedwater plant with 2 heating levels fitted on 2 feedwater lines.

## TURBINE DESIGN AND OPERATIONAL EXPERIENCE

Condensates from 4 superheater bundles flow into 2 phase-separator tanks adjoining the R6 heaters, as shown in fig. 3

Condensates from heaters 6, 5 and 4 and from the moisture-separators, flow into a drain tank where they are covered and re-injected into the feedwater upstream of the feedwater pumps.

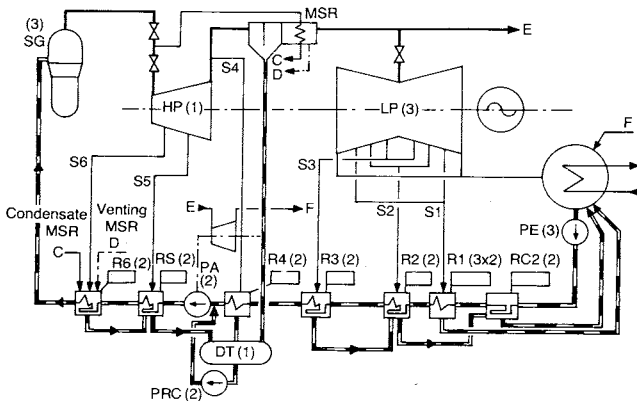


Fig. 1 - PWR 900 MW -P1  
Piping schematic secondary cycle

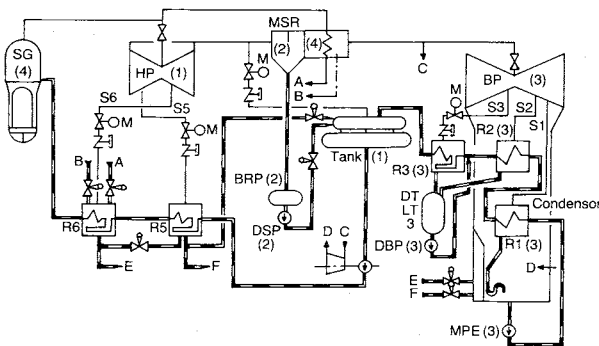


Fig. 2 - PWR 1300 MW - P4  
Piping schematic secondary cycle

The second type includes an L.P. water station with 3 heating levels arranged on 2 lines in the case of the 900 MW power plants and 3 lines in the case of the 1300 MW power plants, plus a deaerator feedtank and finally, an H.P. feedwater plant with 1 heating-level for the 900 MW power plants and 2 for the 1300 MW power plants. These H.P. heaters are fitted on 2 feedwater lines. In the case of the 1300 MW P'4 power plants, the reheater condensate enters the bottom of the steam-filled vessels of the R6 heaters.

The L.P. feedheaters are installed horizontally. The H.P. feedheaters are installed either:

- vertically with the water box in the bottom and a single steam extractor inlet on the upper extremity, in the case of the 900 MW P1 power plants, or
- horizontally with 2 steam extractor inlets for power units of the types 900 - P2 and 1300 - P4 and P'4.

The heat exchange bundles are composed of tubes made of the following materials:

Table 1. Exchange bundle materials

900 MW P1			900 MW P2			1300 P'4		
R1	R2 to R4	R5 to R6	R1 - R2	R3	R5	R1 - R2	R3	R5 - R6
Brass or 304 L	304 L	Carbon steel	Brass	304 L	Carbon steel	Brass or 304 L	304 L	Carbon steel

The vessels for heaters and deaerator tanks are made of carbon steel. The deflectors and energy dispersers on the condensate inlet are made of stainless steel.

### PROBLEMS ENCOUNTERED

During the first refuelling outage, a reduction in thickness was observed in the walls of the carbon steel pipes connecting the high-pressure turbine and the moisture-separator reheaters. Furthermore, the envelopes of the latter has sustained notable losses of material. Immediate action was taken which largely consisted of replacing the piping with 304L stainless steel, improving the flow through the wet steam inlet in the moisture-separator reheater circuit and protecting its envelope by means of a stainless steel plate covering laid according to the method used for tiles.

Regarding the L.P. turbine, the corrosion-erosion damage remained within the limits of the diaphragm seats in the internal casings. Local weld repair in stainless steel (309) was carried out accordingly.

EDF then considered the corrosion-erosion problem solved. However, five years after commissioning of the first 900 MW power plants, alarming signs began to appear: perforation of the carbon steel tubes on the R4 feedheaters at Bugey and perforation of the medium sized condensate flow pipes.

This situation which, if uncorrected, could lead to prolonged inoperability and high maintenance costs was analysed in collaboration with the equipment constructors.

The intake, distribution, sparging and wet steam ducts as well as the deaerator discs that equip the deaerator feedtanks are made of stainless steel.

The no. 4 steam extractor pipe and the connecting pipes between the H.P. cylinder of the turbine and the moisture-separator reheaters are made of 304L steel. Pipes related to steam extractors 5 and 6 and to condensate extraction are made of carbon steel as are the casings of the associated valves.

Large scale routine checks were then decided upon and carried out during plant outages; i.e.: visual inspection, and thickness measuring by ultra-sonic inspection. Significant losses of material were observed on certain heaters or associated tanks (R4, R5, R6) as well as on steam extraction pipes (S5, S6).

Locally, on certain apparatus, the minimum design thickness was reached, prompting the plant operator to establish two types of emergency measures:

- temporary replacement of certain equipment parts (envelope shells of feedheaters 4 and 5),

- a decrease in equipment test pressure to comply with the regulations governing steam pressure vessel (steam pressure reduction justified by the large margins assumed in the design).

These administrative measures made it possible to define a margin by comparison with the minimum required thickness, and to defer the overhaul or modification of the equipment concerned, as specified in the following section.

The main deteriorations recorded are described below:

- condensate recovery tanks of the reheaters adjoining the R6 feedheater (fig. 3):  
Little erosion on the bottom, heavy erosion the envelope in the condensate expansion areas, necessitating a change of tank pending the final modification of the system fig. 4).

- R6 feedheaters (fig. 3):  
Heavy corrosion-erosion on the bottom of the envelope near the first tube support plates and near to the inlet for condensates from the adjoining tank (even for apparatus of a service life of less than 20,000 hours). Certain apparatus were subject to test pressure reduction.

- R5 feedheaters (fig. 3):  
Heavy corrosion-erosion opposite the steam extraction inlet and at right angles to the first tube support plates. Certain envelope shells have already been replaced and shield in the form of stainless steel linings placed opposite the inlet of the steam extractors of the modified apparatus. A loss of thickness was also noted near the condensate return flow from

the R6 heater. R5 heater supply will subsequently be carried out via an adjoining water separator tank (as per fig. 4).

- R4 feedheaters:

It was on the envelopes of these heaters that the corrosion-erosion damage was the most rapid. Long before reaching 30,000 operating hours, heavy losses of thickness were recorded in the bottom of the envelope (near the inlet of steam extractor 4) and on the straight part, over a length of 5 to 6 m, notably at right angles to the tube support plates.

It was quickly decided to change the heater 4 envelopes on plant series 900 MW CP1. This change involved:

- . an increase in the envelope diameter in order to reduce fluid velocities,
- . introduction of a second steam extraction inlet and installation of an envelope in 304L steel.

- moisture-separator reheaters:

These items of equipment, on which corrosion-erosion was expected, have been, from outset, the subject of very stringent supervision. During the first years, a shield was installed in the apparatus on the wet steam inlet. But it became obvious that the corrosion-erosion area was progressively spreading over the entire envelope, well beyond the area protected by stainless steel cladding or by lining plates. The envelope protection will be extended to the bottom of the apparatus and will be ensured by the installation of free-expansion 304L steel tiles according to a system patented by the constructor.

About the tube bundle, the only corrosion-erosion attack was located on the U bend part of the tubes (CP1 design only). The remedy consisted in the installation of seal screen to avoid wet steam path along this part of the bundle.

- Steam extraction pipes 5 and 6:

Heavy losses of thickness were recorded, notably in the elbows. This required the partial replacement of certain sections pending the final modification. The pipes will shortly be replaced with 304L stainless steel.

- Other pipes and associated appertenances valves and fittings:

Heavy corrosion-erosion was detected on pipes carrying condensate and drain water and high-pressure vent pipes particularly downstream of the pressure reducing valves, and on associated tanks and valve casings. Certain pipe elements were changed temporarily and certain valves weld repaired pending the final modifications.

Also, after 40,000 hours of operation, corrosion-erosion appeared at tube inlets and on the tube plates of HP heaters R5 and R6 (corrosion-erosion on the feedwater side caused high velocities of water and turbulence).

**REMEDIAL MEASURES INTRODUCED TO AVOID CORROSION-EROSION DAMAGE**

The modification of steam generator feedwater conditioning constitutes a major step towards improving the resistance of carbon steels to corrosion-erosion phenomena. However it cannot guarantee, for a 30 year period, the protection of equipment operating in the temperature range between 100 and 250°C when such equipment is submitted to wet stream or high velocity water jets.

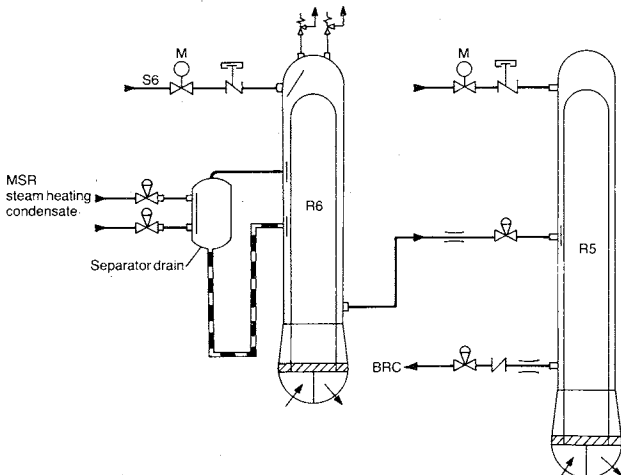


Fig. 3 - PWR 900 MW - P1  
HP5 and 6 Heaters initial Design

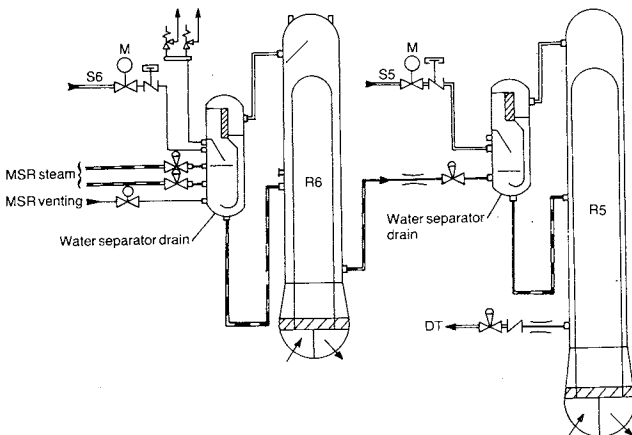


Fig. 4 - PWR 1300 MW - P1  
HP5 and 6 Heaters after modification

TURBINE DESIGN AND OPERATIONAL EXPERIENCE

For several years, EDF has been orienting equipment design and adopting appropriate materials, but underestimated the rate of corrosion-erosion at operating temperatures over 185°C, particularly with wet steam.

The modifications made on equipment were conducted in two stages, and dealt with the following points:

a) Prior to 1982:

- Reduction in the velocity of fluids by introduction of horizontal high pressure heaters with multiple bleed steam inlets.
- Introduction of 304L stainless steel for: low pressure heater heat exchange tubes, connection tubes between the high-pressure cylinder of the turbine and the moisture-separator reheaters, the piping of steam extractor 4, the wet steam ducts supplying the moisture-separator reheaters (installation of lining plates for 900 MW "CP1" units and 1300 MW units), the deaerators and separator units.

b) After 1982:

The modifications mainly involved the high-pressure feedwater plant and associated equipment. They included:

- Modifications to reduce the moisture content in the steam supply to the heater (value sought: 1% in mass) to avoid corrosion of the vessel and bundles:
  - . addition of a tank equipped with a water separator drum, adjoining each heater, and into which the bleed steam and condensates flow in the case of a vertical heater. Case of 900 MW CP1 power plants (as shown in fig. 4),
  - . addition of a high velocity moisture separator on the bleed steam pipe in the case of a horizontal heater (as shown in fig. 5).

- Modifications aimed at reducing fluid velocities, i.e.: addition of a second bleed steam inlet on the R4 heaters of power units 900 MW CP1.
  - Modifications to protect the vessels from the impact of water jets in areas of condensate return: installation of strainer-fitted pressure reducing valves made of 304L stainless steel for heaters on 1300 MW P'4 power plants.
  - Change of materials (choice of 304L):
    - . for the steam vessels of R4 heaters on the 900 MW CP1 power plants,
    - . for the piping of steam extractors 5 and 6, for pipe elements downstream of the control valves that drain off the condensates, and for ventilation pipes and associated valve and fittings - on all power plants.
  - Introduction of corrosion-erosion resistant material for vessels under steam (low alloy steel): 1 to 2% chrome) and for the tubes of heat exchanger bundles (439L) on the H.P. heaters and reheaters - on the new power plant series now under study.
  - To avoid the corrosion-erosion observed on the feedwater side at tube inlet and on the unalloyed steel tube plates of the HP heaters, special end-pieces have been installed. These end-pieces, made of stainless steel, have a collar or are tulip-shaped. They have been installed on all inlets of LP heater tubes at "CP1" and "CP2" units, and will be installed on P4 and P'4 units. For new units, the tube plates will be clad.
- Up to now, the behaviour of both systems, with and without deaerator, is similar from the corrosion-erosion point of view. Nevertheless, the standard for the new units is with deaerator in order to obtain the best oxygen rate control.

CONCLUSIONS

High levels of corrosion-erosion, occasionally unexpected and often involving a high rate of metal loss (1 mm in thickness per year), were observed in particular on high-pressure feedwater plants in PWR units. These occurrences of corrosion-erosion induced EDF to study and implement significant modifications, often at very short notice, in order to insure the continued operability of their plants and to comply with French regulations currently in force, relative to pressure vessels.

The results of the actions engaged to date have been satisfactory, with no notable outages or accidents attributable to these problems.

The final modifications should, in the future, insure good reliability of the equipment in operation, personnel safety and a reduction in the iron content of steam generator feedwater. Experience acquired in operating the initial PWR power plants will now be taken into account in the design of future equipment.

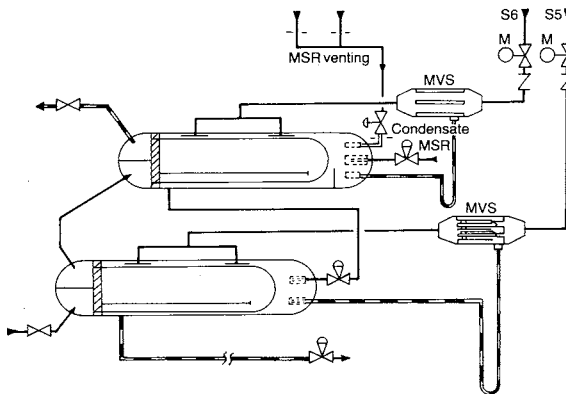


Fig. 5 - PWR 1300 MW - P4  
HP5 and 6 Heater with HVS

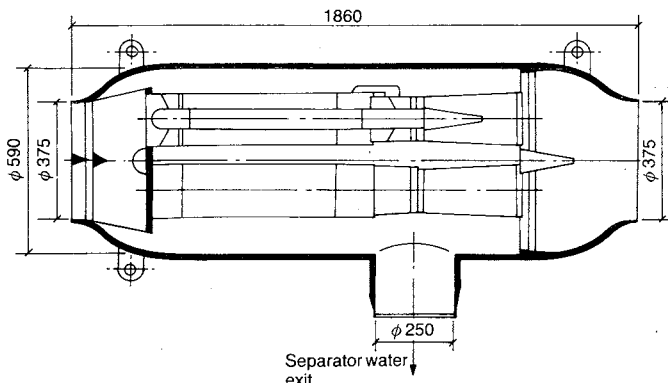


Fig. 6 - HVS Fur heater S6

## 3c. EDF experience with PWR turbine plant: moisture-separator reheater thermal expansion faults

C. MALHERBE and J. MARCEAU, Electricité de France

The bundles of the moisture-separator reheaters that equip 900 MW "CP2" PWR units and 1300 MW PWR units are composed of tubes made of austenitic stainless steel. Since the outset, there have been cases of tubes becoming wedged in their spacer plates, which causes excessive plate deformation. The spacer plates most affected by this problem are those located near the tube U-bends. This deformation - that can only increase with time - necessitates either bundle replacement or in-depth modifications on the tube-support structure, together with the use of specific operating procedure.

### INTRODUCTION

The bundles on reheaters at 900 MW "CP1" power plant units are composed of knurled unalloyed steel tubes. Their behaviour has been very satisfactory. The BBC-technology bundles on reheaters at 900 MW "CP2" power plant units are composed of smooth austenitic stainless steel (grade 304L) tubes. The supporting structure for these bundles is made of unalloyed steel.

When these 900 MW "CP2" series moisture-separator reheaters were started up - even before full power was attained - significant deformation was detected on the spacer plates located near bundle U-bends. This deformation had been caused by the thermal expansion difference between the hairpin-shaped tube (made of austenitic stainless steel) and the support structure (made of unalloyed steel).

### EXPLANATION OF THE INCIDENT

During bundle heating, very high friction forces appear to hinder the free longitudinal expansion of the tubes through their plates, particularly in the area near the U-bends. These friction forces therefore generate thrust forces which are unacceptable for the plates; the plates buckle and thus jam the tubes. This phenomenon can be amplified by the presence of oxides in the interstice between the tube and the spacer plate. The state of a bundle thus deformed can only deteriorate during successive temperature transients, and damage to the bundle progresses further and further towards the steam box.

### REMEDIES PERFORMED ON THE 900 MW "CP2" MOISTURE-SEPARATOR REHEATERS

Several modifications have been made to the bundles, depending on the point in manufacturing/installation progress, i.e.:

- on the first unit, after a few months' operation at a power load of up to 50%, the badly deformed bundles were scrapped and replaced by new bundles;
- on installed bundles, the tail plate were made no longer solid with the bearing structure, and the last spacer plates were reinforced on their

flanks by tubes connected to the beams that compose the bundle structure;

- subsequently, as these initial reinforcements were found to be insufficient, the manufacturer cut the bearing structure into 4 to 5 elements, thereby allowing each "block" of 2 or 3 plates (still solid with the tubes) to move under the effects of expansion.

To avoid the migration of these "blocks" towards the bundle tail, an anti-creep system was associated to each block. The behaviour of the devices has been effective and has allowed the bundles to be saved.

Moreover, so as to reduce the differential expansion due to the temperature difference between main steam and heating steam, a valve setting procedure has been implemented so that heating steam flow valve opening is a function of the unit's power.

New diaphragms have been installed at bundle tube inlet to secure greater uniformity of the heat exchanged in each tube, and thereby avoid the inadequate loading (and flooding) of certain tubes.

For the bundles that had not yet been manufactured (i.e., those for CHINON B4), and those to replace the two damaged bundles at CRUAS 3), another grade of steel was selected for the tubes. This material, ferritic stainless steel (grade 439L) has the same thermal expansion coefficient as the steel used for the support structure. The behaviour of these bundles is very satisfactory.

### INCIDENTS ENCOUNTERED AND REMEDIES USED FOR THE MSRs OF THE 1300 MW P4 AND P'4 PWR SERIES

The first seven units of the 1300 MW PWR series were also equipped with reheater bundles made of smooth austenitic stainless steel (grade 304L) tubes. The deterioration detected on the bundles of the 900 MW "CP2" series led the manufacturer to reinforce the bundle tail spacer plates on the equipment already manufactured. Nevertheless, after a year of operation, these reinforcements were found to be insufficient: deformations and tube blocking in their spacer plates were observed on almost all bundles with tubes made of 304L grade steel.

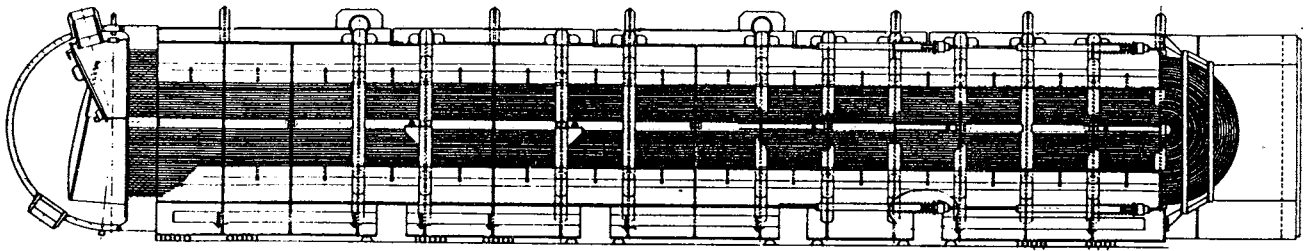


Fig. 1 - Section of the CP2 Moisture Separator Reheater

On the first two units of the series, the damaged bundles were replaced by new bundles with knurled tubes made of chromium ferritic steel (grade 439L). Later units put into operation were equipped with the same bundles from the outset. The standard for future tube material is 439L, used for new design and spare parts as well.

Five units are still operating with deformed tubes. Keeping them in service requires the respect of strict operating instructions and monitoring. Every three months, leak-detection inspections are performed during operation. On these units, a new valve-setting procedure has been established for the opening of the valve that adjusts the heating steam flow.

#### CONCLUSION

The use of austenitic stainless steel tubes for reheater bundles and of unalloyed steel support structure is the root cause of tubes becoming wedged in the support plates, and of significant unavailability of the 900 MW "CP2" series in particular.

These incidents have incurred high maintenance costs.

The behaviour of bundles composed of knurled or smooth tubes made of ferritic stainless steel (grade 439L) is very satisfactory.

### 3d. EDF experience with PWR turbine plant: operation and maintenance of condensers

C. MALHERBE and B. VINCENT, Electricité de France

Over recent years, the condensers at Electricité de France nuclear power plants have been subjected to increased surveillance. This is performed both during operation to detect water intake, and during unit outages to acquire precise knowledge on the general state of the heat exchanger, especially the tube bundle.

The main reason behind Electricité de France's work in this field is essentially due to the fact that switching to nuclear PWR technology has changed the qualitative importance of the condenser. In effect, the condenser can largely contribute to the long lifetime of steam generators by preserving the quality of extraction water chemistry.

Our policy for condenser surveillance is based on operating feedback and is part of the overall preventive maintenance program applicable to all our nuclear plants. It implies technico-economic choices regarding condenser renovation and design.

In this paper, we will first briefly describe the technology of the nuclear power plant condensers operated by EDF. Then, we will examine the main operating feedback data, and finally outline the surveillance performed on condensers.

#### 1. TECHNOLOGY OF NUCLEAR POWER PLANT CONDENSERS

##### 1.1 Materials used

Specific technical choices were made for the tube bundle-tube sheet assembly depending on the type of cooling water (fresh water or sea water), so as to guarantee complete condenser leaktightness. Tube sheet connections are expanded on all our condensers.

Most of the condensers at river-side sites have drawn brass tubes without welds. However, better knowledge of the "diseases" affecting brass has in recent years led EDF to use more exotic materials. The latest units of the 1300 MW series have tubes and tube sheets entirely made of stainless steel. At fresh-water sites, titanium has only been used in very isolated cases (in particular for partial retubing and, at a few 1300 MW units, in the air coolers).

Condensers at sea-shore sites were, as on the first 900 MW units, equipped with tube bundles made of titanium. The tube-sheet liners at the sea-water side are made of cupro-aluminium. Cupro-aluminium behaviour has not been completely satisfactory at all sites, and now the tendency is for tube sheets lined with titanium.

##### 1.2 Tube bundle design

The tube bundles of the first eighteen 900 MW units of fresh water sites, and also of a few 1300 MW units, are composed of straight bundles (BBC technique). All the other units have radiant type tube bundles (DELAS TECHNIQUE) which permits better steam penetration.

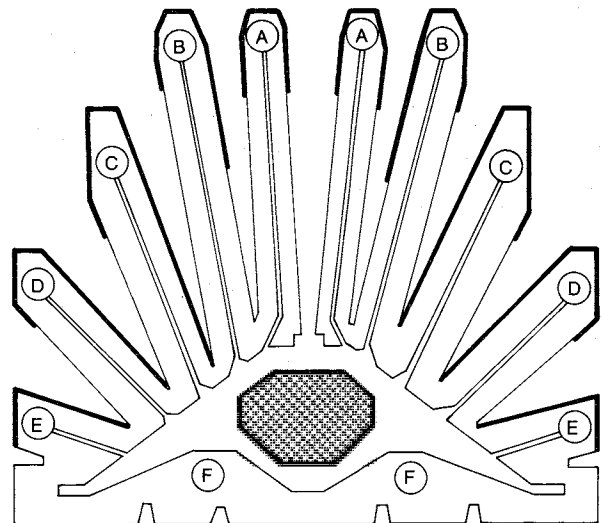


Fig. 1a - Radiant Tube Bundle

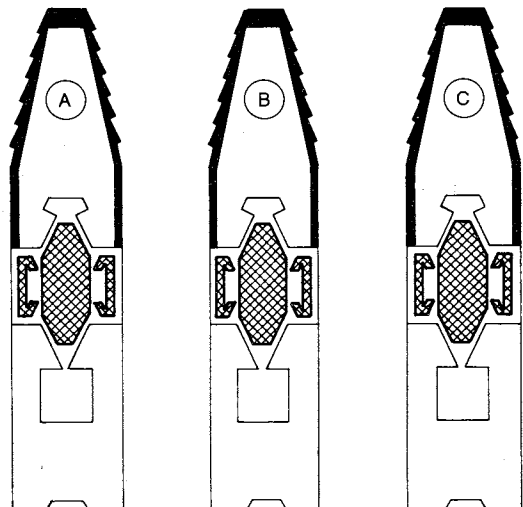


Fig. 1b - Straight Bundle

## TURBINE DESIGN AND OPERATIONAL EXPERIENCE

### 1.3 Condenser size

The increased unit power of PWRs, the poor steam characteristics, and the new role accorded to by-passing, have led to bigger condensers.

For example, a closed-circuit 1300 MW condenser has 128 000 tubes, 14 meters long, for a heat exchange surface of approximately 70 000 square meters. The housing is approximately 15 meters high, 18 meters wide, and more than 40 meters long. Such a condenser weighs 1900 metric tons when empty, and 3000 tons when in operation.

### 2. MAIN OPERATING FEEDBACK DATA: CONDENSER "DISEASES"

These "diseases" primarily concern the tube bundle. They are all generic in nature. Tube sheet corrosion has also been encountered, although only at a few sea-shore sites (on cupro-aluminium tube-sheets).

Among the PWR condenser tube sheet deteriorations observed, the following distinctions can be made:

#### a. Steam side:

- Erosion by wet steam.

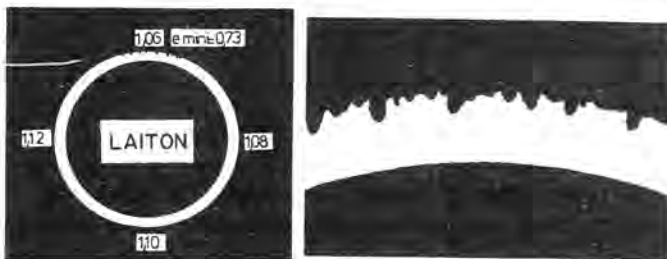


Fig. 2 - Erosion by wet steam

This is the removal of metal by the impact of the water droplets contained in the steam and ejected at high speed from turbine exhausts. Only the first and second rows of impact tubes are affected. Once metal has been removed, the tubes become rough and eventually holes appear.

All of the material used for tubes can be affected, however the kinetics are different. Of these materials, brass is the least resistant; under the same conditions of use, austenitic stainless steel and titanium appear to be the best.

The distribution of erosion on a condenser bundle depends on assembly design and structure given the turbine exhaust, the neck and associated devices, the bundle form and the condenser volume.

The kinetics of this phenomenon is specific to each unit. There is no direct relation, whether it be operating hours or equivalent number of hours at full power. We presume that erosion occurs on reaching a threshold over a certain load. Consequently, the brass impact tubes in the Bugey 2 and 3 condensers were replaced by titanium tubes after 15000 operating hours.

Under this heading, we find damage caused by bundle vibration due to the steam velocity effect on a given structure.

The most frequent wear is caused by mutual contact of tubes, markings at tube spacer plates

### - Degradation caused by vibration



Fig. 3 - Degradation by vibration

and, more rarely, fatigue rupture due to alternate flexural stress on the tube. The most damaging (mutual tube contact and fatigue rupture) are a result of vibrating tubes.

Sea-shore sites operating in winter with seawater at very low temperatures are subject to this type of deterioration. The risk is increased when the condenser operates at 100% load with only one pump on operation.

The tubes at the bundle tip are the most exposed. It also happens that some tubes at the bottom of the lobes are the home of major vibrations.

An efficient response to bundle instability consists of reducing the movement range of the tubes, which means increasing their rigidity and frequency. We use the lathing technique where tube range is most exposed. The lathes can either be hard (propylene or nylon) or soft (Rilsan). All PWR condensers are now lathed. Condensers under construction will be better protected by a greater number of support plates.

- Ammonia corrosion



Fig. 4 - Ammonia corrosion

This well-known phenomenon is limited to copper alloys, and so to EDF condensers in fresh water. It is distinguished by tube wall dissolution due to ammonia liquors running down the tube spacer plates. This phenomenon occurs in the air coolers and even in the dead layers near the air coolers.

Chronologically, this type of corrosion can happen at any time in the life of a condenser. It appeared during commissioning in most condensers of the 900 MW CP2 series (CHINON B, ST-LAURENT B and CRUAS). It was only in 1986, after 40 000 operating hours, that it became manifest at TRICASTIN 1.

Preventive measures must be taken right from the design stage: a detailed study on cold points and extraction of non-condensable gas has to be effected. Material insensitive to ammonia corrosion (stainless steels, titanium) should be selected for these specific zones.

On existing condensers, this "disease" requires retubing of the affected zone in a more or less short period of time. Three condensers in the 900 MW series have already been retubed in

the air cooler zones.

b. Raw water side:

- Regular abrasion of copper-alloy tubes.

This degradation consists of a regular loss of metal from the whole circumference and length of the inside surface of the tube.

First detected at the BUGEY plant in the Rhône valley, ten other 900 MW plants are now affected. Thickness losses can reach 0.4 to 0.5 mm for an initial thickness of 1 mm after 60 000 hours of operation.

The current explanation that is most consistent with the observations made involves a continuous mechanical action of the continuous cleaning device balls in the presence of abrasive solid particles. Regular abrasion and corrosion-erosion are two very different "diseases" that do not generally occur together. Corrosion-erosion, as such, does not exist in French nuclear power plant condensers at this time. Electricité de France will, in all likelihood, have to completely retube some of its river-side condensers in years to come.

### 3. CONDENSER SURVEILLANCE BASIC PREVENTIVE MAINTENANCE PROGRAM

Apart from monitoring the condenser in operation, which basically consist of detecting raw or sea water intake using the installed instrumentation, particular care is taken when inspecting the entire condenser during unit outages.

#### 3.1 Non-destructive tests

Electricité de France has over the last few years applied, so as to gain maximum benefit from the series effect, a basic prevention maintenance program on the condensers. With this program, instructions for all inspection operations and their associated corrective measures are provided for each type of bundle. In this way, the apparatus are analysed every year and the results enable comparative analyses between units on the same site or on different sites.

Essentially, as already stated, inspections are carried out on the tube bundle to detect and quantify existing "diseases". Inspections are visual, mostly using eddy currents. The latter have been considerably developed and nowadays afford great accuracy in detecting and quantifying size of attacks. Nevertheless, it is sometimes necessary to extract tubes, for example to determine the cause of a new signal.

Visual examinations of the tube bundle are

made on the steam side to define erosion area on the bundle. Results are recorded in the form of charts showing blast marks and rough areas, and also holes. All rough tubes are plugged. Moreover, comparative reading of the results for condensers of the same design is an excellent source of information and enables solutions for bundle protection to be evolved.

Eddy current tests are performed according to standard grids and as a function of the "diseases" being sought. For a brass tube condenser, the program calls for the examination of approximately 3% of the tubes; in a titanium tube condenser, the extent reduces to 0,5%. If bundle tightness during the following cycle is likely to be impaired by thinning of walls, the affected tubes are plugged.

All the other sub-assemblies in the condenser are also subject to examination, most often visual (tubular plates and chanel heads, internal structure of the condenser, by-pass containment, flexible seals for turbine connection).

#### 3.2 Leaktightness examinations

Industrial practice shows that it is worthwhile to check tube bundle leaktightness at the end of each outage period.

Electricité de France recommends its systematic implementation after each refuelling outage, preferably using helium. This type of test has to be performed with the condenser under vacuum, and is more accurate than the so-called "water weight" test. With helium test, several tens of cubic centimeters are detected per hour. The helium method also enables differentiation between leaks in the tubes and expansion leaks.

### CONCLUSION

French nuclear plants had more than two million brass tubes and 1.5 million titanium tubes at the beginning of 1988. In 1992, there will be about 2.7 million brass and 2 million titanium tubes.

The condenser inspection program that EDF has already undertaken will therefore continue in the future in order to maintain at a low level and even reduce forced outages caused by the condensers. In 1987, these forced outages represented less than 0.05 percent of the energy potential of our nuclear plants overall.



# 4. Operating experience with 1100 MW wet steam turbines in a nuclear power plant

R. I. PAWLIGER, BME, PE, MASME, American Electric Power Service Corporation

The American Electric Power Company, one of the largest U.S. electric utilities, has over ten years of experience in the successful operation of two 1100-MW wet steam turbines. The two machines, each designed by a different manufacturer, are in base-load service in a Pressurized Water Reactor nuclear power plant. This paper presents the highlights of that experience, covering turbine reliability, performance, inspection and operation. The results of a full-scale ASME code performance test of one of the turbines are discussed. Moisture erosion, typical in wet steam cycles, has been found in the turbine steam path and piping systems. Problems that occurred early in the life of the external moisture separators and reheaters, and how these problems were resolved, are discussed. The more recent industry-wide problem of disc cracking of built-up rotors and the mitigation of that problem through periodic inspections and a change in rotor design are also covered.

## THE AMERICAN ELECTRIC POWER COMPANY

1. The American Electric Power Co. (AEP) is one of the largest electric utility companies in the United States. AEP's generating capacity is approximately 23-GW, of which 85% is coal fired. An in-house group -- the AEP Service Corporation -- provides central management and professional services, principally engineering, and has earned the reputation of being a technological leader in the U.S. utility industry.

## COOK NUCLEAR PLANT

2. In mid-1967, AEP ordered two Pressurized Water Reactors (PWR) of the 1100-MW class

from the Westinghouse Electric Company. These were erected at the Donald C. Cook Nuclear Plant on the southeastern shore of Lake Michigan. Unit 1, with a General Electric (U.S. made) turbine-generator, was put into commercial service in August 1975. Unit 2, with a Brown Boveri (Swiss made) machine, was commissioned in July 1978.

## Heat Cycle

3. The heat cycles of both units are very similar (see Fig. 1) and have a single-stage reheater, six stages of regenerative feedwater heating and two 65% capacity feed pumps -- each driven by an auxiliary turbine.

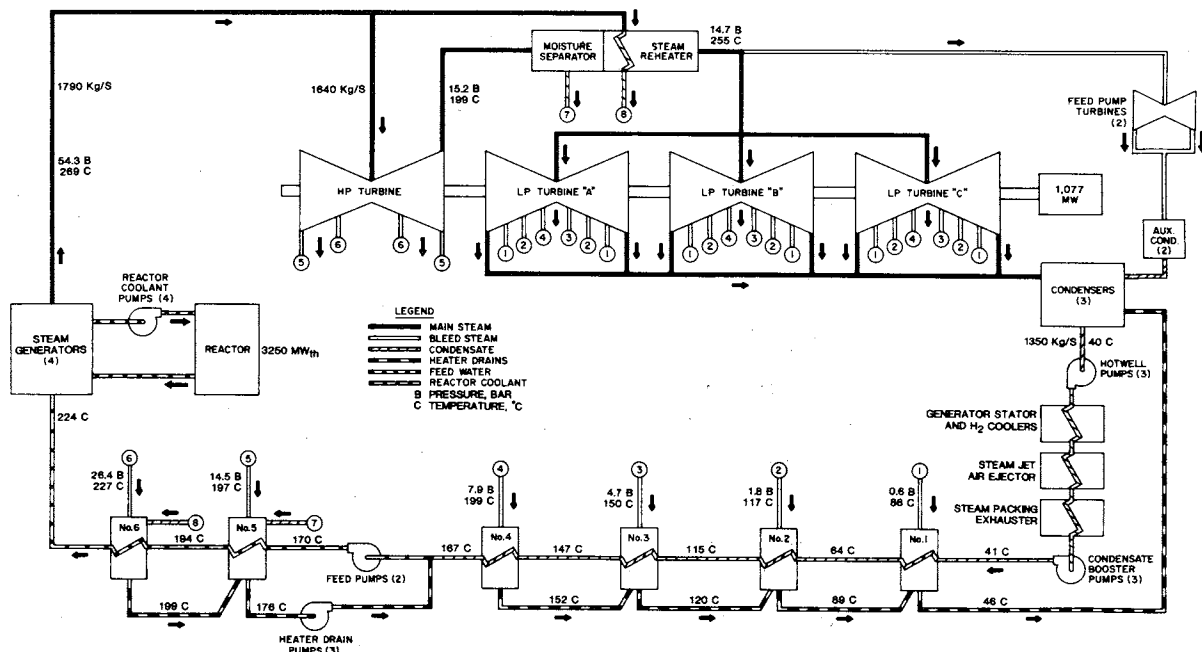


Fig. 1. Heat cycle diagram of Unit 1 at full load

## TURBINE DESIGN AND OPERATIONAL EXPERIENCE

A once-through cooling water system is used for the steam condensers, taking water from and returning it to Lake Michigan. Deaeration is accomplished in the condenser and with hydrazine injection. Saturated steam at 54 bar (full load) is supplied to the turbines. Steam pressure increases with decreasing load. Expansion of the steam through the machine results in the accumulation of significant moisture as depicted by the turbine expansion lines shown on the Mollier Diagram, Fig. 2. For comparison, the expansion line of a modern, single-reheat fossil unit is also shown.

### Turbine Description

4. The turbine-generator of each unit consists of a tandem-compound, six-flow, 1800 rpm turbine, driving a 4-pole generator. Compounding is arranged in a double-flow, high-pressure (h-p) turbine and three identical double-flow low-pressure (l-p) turbines. A comparison of the principal design features of the two machines is given in Table 1. An engineering model of Unit 2 was made to help layout the turbine piping (Fig. 3). Further details of the design may be found in Ref. 1, 2, and 3.

5. The relatively low operating temperatures allow the use of high-strength low-alloy steel in the turbine's construction. With most of the expansion taking place in the wet region, parts of the inner surfaces of the casings directly in the steam path are lined with stainless steel to

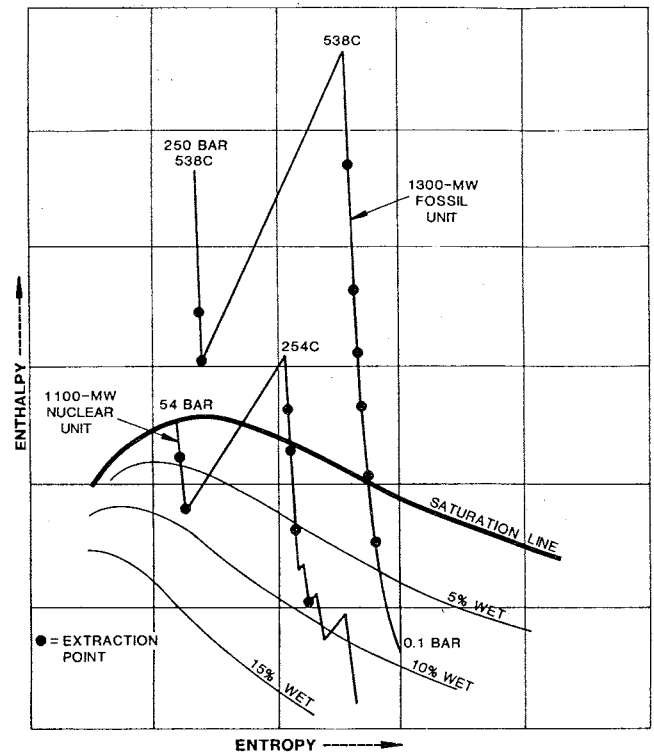


Fig. 2. Expansion Lines at full load. Jogs in wet region are from internal moisture separation

protect against water erosion. The outer portion of the leading edge of the last-stage blades is protected against erosion by stellite shields on Unit 1 and by induction hardening on Unit 2.

Table 1. Principal Design Features of the Cook Nuclear Plant Turbines.

Feature	Unit 1 - GE	Unit 2 - BBC
Net Maximum Capacity	1030-MW	1100-MW
Turbine Arrangement	Tandem compound 6-flow 1800-rpm, 1090 mm LSB	Tandem compound 6-flow 1800-rpm, 1320 mm LSB
Overall Length	68.3 M	75.4 M
Steam Conditions (full load)	54 bar, 0.25% wet, 1795 Kg/s	54 bar, 0.25% wet, 1853 Kg/s
Net Heat-Rate (full load)	3.14 J/W-s (10,700 Btu/Kwh)	3.12 J/W-s (10,630 Btu/Kwh)
Valves	4 stop, 4 control 6 combined stop and intercept	4 combined stop and control 6 reheat stop, 6 intercept
Control	Electrohydraulic, Governing stage, Full arc admission (originally partial arc).	Mechanical hydraulic, No governing stage, Full arc admission
Rotors	Forged shaft, integral h-p discs Shrunk-on l-p discs, 1 stage/disc	Forged low-alloy discs, Welded construction
Casings h-p l-p	Low-alloy cast steel Fabricated steel hoods, Cast steel inner casings centerline supported in exhaust hood	Low-alloy cast steel Fabricated steel hoods, Cast steel inner casings supported on steel beams cantilevered from foundation
Main Journal Bearings	10; largest 760 x 710 mm	6; largest 900 x 900 mm
Moisture Separators	Two vessels, chevrons	Two vessels, wire mesh
Reheaters	2, 90/10 Cu-Ni tubes	8, 321 stainless steel tubes

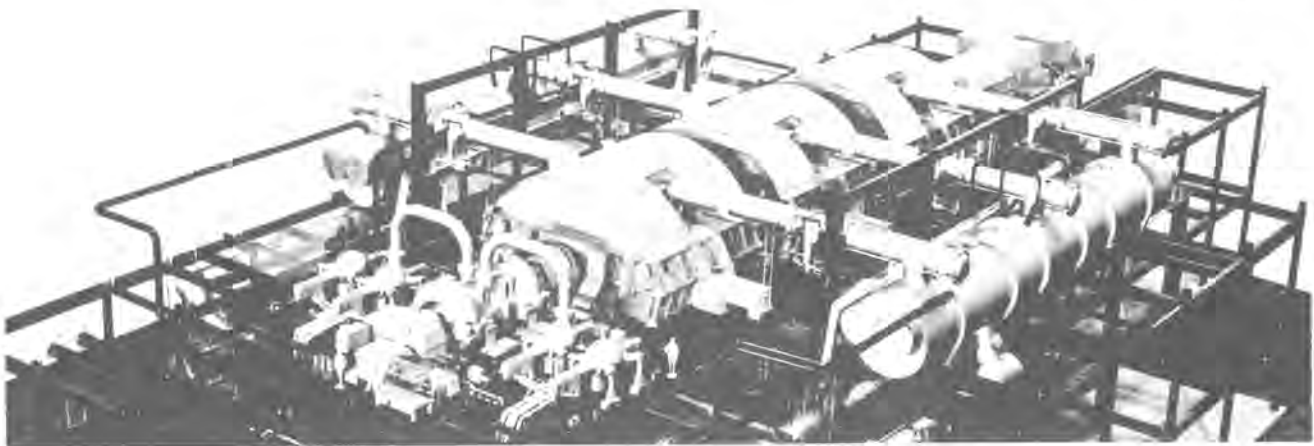


Fig. 3. Scale model (1:25) of Unit 2 turbine-generator

6. If the steam expanded without the removal of moisture as it is formed, the exhaust steam would be more than 20% wet. Such high moisture content would be detrimental to the machine's efficiency and would result in unacceptably high erosion rates. Therefore, external moisture separators, supplied by the turbine manufacturer, are interposed in the steam path between the h-p turbine exhaust and the l-p turbine inlet. Both units are fitted with single-stage reheaters in the same vessel with the moisture separators. Provisions are also made for collection and removal of some of the moisture as it forms inside the turbine. The rotating blades of three l-p stages of Unit 1 are equipped with moisture removal grooves; separated water is drained either at special drain points or along with steam at the next extraction point.

7. The designers believed that the problems associated with moisture in a wet steam turbine are a trade-off for problems associated with high temperatures and pressures in a typical fossil machine. Experience at the Cook Nuclear Plant and AEP fossil plants supports that belief.

#### Reliability

8. Both units' turbines have a very low forced outage rate. The main contributing factors to this excellent record are operation as base load units and performance of normal and preventive maintenance during the refueling outages. These shut-downs provide opportunities to inspect and perform maintenance on the turbines and, consequently, the unplanned (forced) outage time of these machines is minimized. Overall reliability has been as good as or slightly better than comparably sized fossil turbines.

9. The majority of the routine problems encountered are similar to those encountered on fossil steam turbines. One exception has been the absence of balancing difficulties on the nuclear turbines. Essentially no in situ balancing has been required, and these half-speed machines show a low sensitivity to vibration stimuli.

10. Each turbine-generator has had only one major forced outage during their lifetime. These were caused by first-stage blade failures on Unit 1 and a generator stator bar problem on Unit 2. The major equipment reliability problem has been reheater tube leaks on both units, but this has had no effect on the availability of either unit since they can and do operate without the reheaters in service.

11. The reliability of the feed pump turbines has also been very good. There have been no reliability problems attributable to operation with wet steam.

#### Performance

12. The low cost of nuclear fuel compared with coal, coupled with the higher capital cost of nuclear power plants, mandate that the nuclear units be base loaded. Table 2 shows the performance of both units.

Table 2. Lifetime Performance Statistics

Through end of 1987	Unit 1	Unit 2
Service time, hours	80,406	59,662
Gross Generation, 10 <sup>6</sup> KWH	75,498	58,479
Auxiliary Power, %	3.83	3.47
*Net Output Factor, %	87.7	86.0
*Net Capacity Factor, %	61.8	60.0
Longest continuous run, days	174	226

\* Definition per Ref. 4.

#### Thermal Performance

13. These cycles are designed for a net thermal efficiency of approximately 31.9% at full load. Performance of these units is monitored daily by comparing the actual output with the expected output, allowing for circulating water temperature, alternate draining of feedwater heaters, blowing down steam generators, and so forth. Thermal input to the cycle is measured continuously, permitting monitoring of the unit's heat-rate. The trend of this monitoring indicates that the actual output and heat-rate remains within 1.5% of the expected value, and there is no discernible degradation with time.

## TURBINE DESIGN AND OPERATIONAL EXPERIENCE

14. Unit 2 was subject to a full-scale code acceptance test in early 1979, eight months after the unit was put into commercial service. The testing required precision measurement of some 140 temperatures, 115 pressures, 5 major water flows throughout the cycle and electric power output. Because much of the steam in the cycle is in the wet region, the steam's quality was determined by the use of radioactive sodium as a tracer. A central device was developed by BBC to inject the water soluble tracer into 25 injection points and collect samples from 65 other points throughout the cycle. Results of the tests (Ref. 5,6) indicate that the turbine's heat-rate, under idealized steady-state test conditions, was 1% better than guaranteed.

15. Some important results from this test and from Unit 1 component tests are:

- o Isolating the cycle for testing results in a gain in output of up to 0.7%. This promotes constant vigilance in minimizing leaks, both internal and external to the cycle.
- o Reheat operation improves the heat-rate by approximately 1.0% compared to non-reheat.
- o The turbine flow passing capability was too great for the reactor's licensed rating, leading to reblading of Unit 2 inlet stages to allow greater valve opening and concomitant lower throttling loss.
- o A modest decrease in steam pressure does not adversely effect performance. Pressure reduction is currently being evaluated to reduce risk of stress corrosion cracking of steam generator tubes.

### Inspections

16. Internal inspections of the turbines are performed during refueling outages at approximately 18-month intervals. Only one of the four turbines on each shaft is inspected during an outage unless there are reasons to do otherwise. Thus, upwards of 30,000 hours of service have elapsed between major inspections of a particular turbine. Fig. 4 depicts the inspection history of the Unit 1 turbines.

17. The MSRs, several of the principal steam valves, and the cross-under pipe are also inspected during each refueling outage. These inspections are conducted to determine the extent of water erosion, deposits of foreign material, cracking, misalignment and to make necessary repairs. For the most part, the findings are quite similar to what is found when inspecting a dry steam turbine. The notable difference in the wet steam turbine is the absence of solid particle erosion and the presence of water erosion. A summary of erosion experienced by these two units is given in Table 3, progressing through the machine in the direction of steam flow.

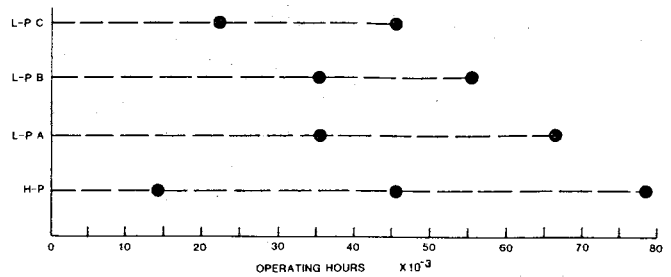


Fig. 4. Major inspections of Unit 1 turbines

18. Very stringent secondary system water chemistry criteria is imposed on the nuclear cycle, primarily for the benefit of the steam generators. Normal values (parts per 10<sup>9</sup>) are Sodium < 5; Chlorides < 10; Dissolved Oxygen < 5; Iron < 20; and Silica < 100. A pH of 8.8-9.2 is maintained. As a result, there is very little carryover of solids in the steam and there is no accumulation of deposits on the turbine blades. Any deposits that might tend to accumulate are washed off by the wet steam.

19. The last stage blades, which operate at the highest velocity (tip speed of 419 and 498 m/s) and in the wettest environment, are resisting erosion very well. There is no significant difference in erosion resistance between the stellite shielded blades of Unit 1 and the hardened blades of Unit 2. Studies and developments by the manufacturers have resulted in a satisfactory last stage blade design to resist erosion (Ref. 7, 8).

20. Where erosion does exist, it poses little threat to the integrity of the turbine unless the erosion is undetected. This has been the case in some of the steam piping, where pipe walls have eroded completely through, resulting in steam leaks. Pipe erosion has also been experienced in other PWR power plants in the U.S. Reports of pipe failures surfaced in the industry in early 1982. These reports prompted extensive research and investigation into the phenomenon and the development of mitigation strategies. Ref. 9, 10, and 11 provide further details.

21. In response to this concern, AEP initiated an inspection program in late 1982 at the Cook Nuclear Plant. The pipe wall thickness at key locations on extraction lines and the cross-under pipe are periodically measured using ultrasonic examination. All of these systems were originally constructed with carbon steel pipe and fittings. Where erosion required action, the pipe or fittings were replaced with austenitic stainless steel, type 304. Replacements have mainly been in 90° elbows, although some straight lengths have been replaced or pad welded. The largest components replaced have been the 1.5 M diameter mitered elbows in Unit 2 cross-under pipes. Unit 2 h-p turbine expands steam to 7 bar, compared with 15 bar in Unit 1, resulting in a wetter cross-under for Unit 2.

Table 3. Summary of Water Erosion Inspections

<u>Location</u>	<u>Unit 1</u>	<u>Unit 2</u>
Main Steam Valves	No problems	No problems
Inlet Nozzles/Vanes	Slight trailing edge thinning	No problems
1st Stage Blading	Minimal erosion	No problems
h-p Casing	No problems	Caulking eroded in interstage seal strips
Cross-Under	Localized erosion	Through-wall erosion at elbows, "Tiger Striping" on straight length (Fig. 5)
Extraction Pipes	Major erosion on some extractions	Major erosion on some extractions
Moisture Separator	Medium (heavy at inlet)	Extreme erosion with original design, no problems with new design
Reheaters	No problems	Extreme erosion with original design, minimal problems with new design and modified separator
Cross-Over Pipe	No problems	No problems
1-p Turbine Inlet	No problems	Heavy erosion on stationary blade spacers
1-p Inner Casing	Erosion on horizontal joint of diaphragms and inner casings	Heavy erosion on blade carrier fits and seals
1-p Blading (including last stage blades)	Minimal	Minimal (Fig. 6)
Exhaust Hoods	No problems	No problems

#### Turbine Operation and Maintenance

22. Interviews were held with some of the plant staff responsible for the daily operation and periodic maintenance of these turbines. Personnel who had prior experience in similar roles in a fossil-fired power plant were selected so that a direct comparison between a "wet" and "dry" steam turbine could be made. The consensus was that there is little difference between the operation of the two types of turbines. The controls and response of the turbines were similar. The wet steam turbines presented far fewer concerns with differential expansion between the casings and rotor. This can be attributed to the lower temperature and slower loading rate of the nuclear turbine. The latter is a requirement of the reactor.

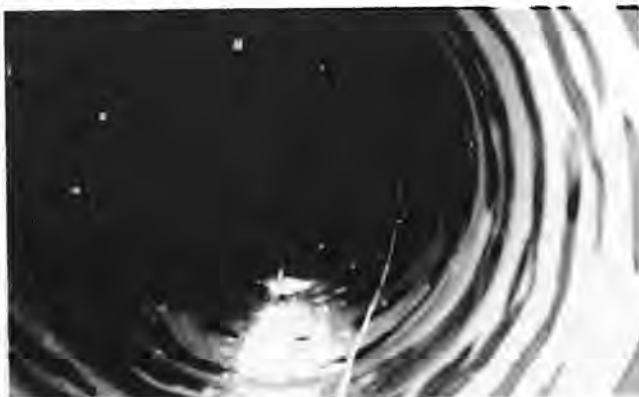


Fig. 5. "Tiger Striping" in Unit 2 cross-under pipe after 49,100 hours of operation

23. Because of higher erosion rates in the piping systems, wet steam plants experience many more steam leaks, especially on small drain lines. That problem ought to be mitigated as more of the piping susceptible to erosion is replaced with erosion-resistant material.

24. Keeping air in-leakage to an absolute minimum is extremely important in PWR units to keep the feedwater free of dissolved oxygen. Despite the huge size of the turbines and other components subject to vacuum, constant vigilance by the operating staff has been successful in keeping air in-leakage under 300 std liters/min.



Fig. 6. Last stage blades of Unit 2 after 49,100 hours of operation

## TURBINE DESIGN AND OPERATIONAL EXPERIENCE

25. From a maintenance viewpoint, the wet steam turbines are far easier to disassemble and assemble despite being larger than high-temperature fossil turbines. Joint bolts are more easily removed in the nuclear turbines, and there are fewer parts to handle as a result of single-shell vs. double-shell construction of the h-p turbine.

26. The steam valves of the nuclear turbine are not subject to oxide build-up on the stems, thus allowing longer intervals between valve overhauls. Maintenance effort is required to repair erosion damage in wet steam turbines but that is offset by not having to contend with solid particle erosion, the principal wear agent in fossil-fueled steam turbines. Even though there is no significant deposit build-up in wet steam turbines, the parts are blast cleaned prior to nondestructive examination, the same as for fossil machines.

27. Experience with the feedwater heaters upstream of the feed-pumps has been good, despite the high moisture content of the extraction steam. Early problems in the high-pressure heaters immediately downstream of the feed-pumps were traced to flow-induced vibration of the tubes in the drain cooler section. This was corrected by staking the tubes in that area and enlarging the opening to the drain cooler. There have been relatively few tube leaks in the high-pressure or low-pressure feedwater heaters, all tubed with 304 stainless steel material.

28. The main steam condensers -- one per l-p turbine -- were installed with arsenical copper tubes. Tube leaks occurred frequently, primarily as a result of steam side erosion, tube vibration, and corrosion due to ammonia attack. The high moisture content of the exhaust steam led to heavy erosion of the upper peripheral condenser tubes. Energy absorbing grating and protective baffling were added to protect these tubes. In 1984-1985, all condensers were retubed and design improvements were made in the tube support system to eliminate the frequent tube leaks and the resultant contamination of the condensate/feedwater system. Stainless steel was selected for its better erosion resistance and to eliminate a major source of copper in the cycle.

### Major Problems and Their Resolution

29. The two wet steam turbines described in this paper are both early-vintage machines of their class and, as such, were subject to "growing pains". Nonetheless, some of the major problems with these machines and how they were, or are, being resolved is worthy of discussion. This experience and the resolution of problems will benefit the design of future wet steam turbines.

30. Moisture Separator/Reheaters. The external moisture separators and reheaters of both units were, by far, the biggest concern.

The two moisture separators were designed by different firms, using different separation concepts. Neither separator performed up to expectations. Unit 2 moisture separation was so bad -- an estimated 35% effectiveness vs. 97.9% design because of mal-distribution -- that localized water carryover seriously damaged the carbon-steel tubes of the reheaters in short order. Extensive revisions, guided by air model testing, produced a more uniform distribution of the water over the entire length of the moisture separator. These revisions resulted in an effectiveness approaching the expected 97.9%. The badly damaged reheaters were replaced in 1980 with a new design incorporating a multi-pass arrangement and tubes of stainless steel. Multi-pass design provides for a continuous flow of excess steam through the tubes, thus ensuring stable operation without penalizing performance. In the interim, the unit operated at less than full reheat temperatures for long periods without suffering extensive erosion in the l-p turbines.

31. Unit 1 moisture separator also did not perform up to expectations; installation of flow guides improved that situation. Of more concern, were frequent tube-to-tubesheet weld cracking and tube bundle and support plate distortion brought on by thermal stresses resulting from unsteady plug flow within the tubes. The installation of orifices at the inlets of the "U" tubes promoted more uniform steam flow and thus solved that problem. The original reheaters of 90/10 Cu/Ni finned tubes are still in operation after 13 years, with only 4.1% of the tubes plugged because of leaks. Typical reheater life in the industry has averaged between 8 and 10 years. AEP plans to replace Unit 1 reheaters in 1990. The new reheaters will be tubed with stainless steel because of an increasing trend in tube leaks over the last few years, and to eliminate the copper in the cycle.

32. Blades. There have been minimal problems with the stationary and rotating blades. Only one major blade failure occurred and that was on the governing stage of Unit 1 in early 1982 after nearly 46,000 hours of operation. Several blades cracked at the base with cracking attributed to high-cycle fatigue. Fretting damage was observed on the root surfaces between adjacent blades.

33. The immediate corrective action was to replace the first stage blades with identical spares and to change to a full arc admission mode to remove the stimulus from the buckets. This caused a derating from 1050-MW to 1030-MW since the turbine was no longer operating at a valve point. Long-term corrective action includes obtaining an interference fit for the first stage blades by using liquid N<sub>2</sub> for assembly, nozzle set-back of approximately 25 mm to reduce the stimuli caused by the blade passing between

active and inactive arcs, and a modification to the radius on the root hook. These corrections will allow the turbine to return to the partial arc mode and recover the 20-MW.

34. Disc Cracking. In 1982, cracks were found in the keyways of several of the shrunk-on discs of one Unit 1 1-p rotor. Reports of similar cracks in many other wet steam turbines utilizing the shrunk-on disc design emerged at that time (Ref. 12). These reports attracted much attention in the utility industry because of concern for the risk of a rotor or disc fracture such as occurred at Ridgeland Unit 4 in Chicago in 1954 and at Hinkley Point "A" No. 5 in England in 1969.

35. These cracks, it was later determined, were caused by stress corrosion and the manufacturer identified the mechanism that allowed the corrodent to form and concentrate. Stress analysis and fracture analysis determined that it was acceptable and safe to continue in operation, even with the cracks, provided that the cracks did not exceed a pre-determined maximum size (Ref. 13).

36. Consequently, a program was undertaken to periodically ultrasonically inspect the rotors to see if new cracks had developed and to monitor the propagation of previously detected cracks. To date, 10 of the 48 discs have developed cracks. Cracks are confined to the 4th, 5th, and 6th stages (of the 8 stage 1-p rotor) with a maximum crack depth of 15 mm. The manufacturer recommends re-inspection of these particular rotors at six-year intervals. This recommendation considers such parameters as crack size and growth rate, actual material properties, wheel operating temperature, and a probabilistic evaluation of generating an external missile in the event of a disc burst. AEP purchased a bladed spare rotor to minimize outage time if a future inspection reveals that a rotor is unacceptable for continued operation. This spare is a monoblock rotor (i.e. single piece forging) with no shrunk-on discs.

37. The Unit 2 rotors use the standard BBC welded rotor construction and, therefore, are not subject to this cracking problem.

#### CONCLUSION

38. The operating experience of these two wet steam turbines, with total service approaching 150,000 hours, has, for the most part, met AEP's expectations. Being early vintage machines of their size class, they were not free of problems. None of these problems have been insurmountable nor have they detracted from the good operation and performance records established. More important to the industry, is that their

operating experience provided valuable input to the design of future wet steam turbines.

#### REFERENCES

1. SPENCER, R. C. and BOOTH, J. A. Heat Rate Performance of Nuclear Steam Turbine-Generators (General Electric Company). American Power Conference, April 1968.
2. MILLER, E. H. and SCHOFIELD, P. The Performance of Large Steam Turbine-Generators with Water Reactors (General Electric Company). ASME Winter Annual Meeting, November 1972.
3. HOSSLI, W. The 1160 MW Turbine for Donald C. Cook Nuclear Power Plant of AEP. Brown Boveri Review, January 1972.
4. Generating Availability Data System (GADS). North American Electric Reliability Council (NERC), 1986.
5. Cook Nuclear Plant - Unit 2 Initial Performance Test Report, AEPSC (internal), January 1980. Initial Performance Tests - Cook 2 Test Report, BBC (internal) August 1980.
6. PAWLIGER, R. I. et.al. Experience in Heat-Rate Acceptance Tests of Steam Turbine-Generators. American Power Conference, April 1982.
7. MILLER, E. H. (General Electric Company) Modern Nuclear Turbine Design. American Power Conference, April 1964.
8. SOMM, E. A Means of Estimating the Erosion Hazard in Low-Pressure Steam Turbines. Brown Boveri Review, October 1971, p.458 et.seq.
9. Erosion/Corrosion in Nuclear Plant Steam Piping: Causes and Inspection Program Guidelines. Electric Power Research Institute (EPRI). Report NP-3944, April 1985.
10. Erosion/Corrosion in PWR Secondary Circuits. Central Electricity Generating Board (CEGB), TPRD/L/3114/R87, March 1987.
11. Prediction and Mitigation of Erosion-Corrosion Wear in Secondary Piping Systems of Nuclear Power Plants. U.S. Nuclear Regulatory Commission, NUREG/CR-5007, September 1987.
12. Steam Turbine Disc Cracking Experience. Report NP-2429, Electric Power Research Institute (EPRI), Volumes 1-7, June 1982.
13. Stress and Fracture Analysis of Shrunk-On Steam Turbine Discs. Electric Power Research Institute (EPRI), Report NP-3340, January 1984.



## 5. Operational experience with 1300 MW wet steam turbines

Dipl. Ing. J. KEYSSELITZ and Dr Rer. NAT. U. PETER, Rheinisch - Westfälisches Elektrizitätswerk, Essen

Following a brief summary of the thermodynamic design, the authors go into special features of design and control engineering with particular emphasis on erosion protection and overspeed behaviour. This is followed by a description of the operating behaviour. All the units are attested smooth running, also at load changes and part-load operation. The specific heat consumption, determined by acceptance tests, was lower than guaranteed. The intercepting tests also revealed that in the case of load shedding from rated load to station supply with  $n_{\max} = 180 \text{ min}^{-1}$  there is a good margin of shutdown safety. This shutdown safety is checked every three to four years unless such tests are required by network failures. Information is given on initial teething troubles which could all be remedied. Practical test methods are described for detection and analysis of cracks and rate of crack growth due to stress corrosion of large built-up type rotors. The favourable operating experience shows that the overall concept is correct in its thermodynamic, structural and control engineering design and permits safe operation.

### INTRODUCTION

1. Today the 1300 MW turbogenerator set is the standard rating for operation with nuclear steam supply in the Federal Republic of Germany (see Fig. 1).
2. On 24 August 1974 the first 1300 MW wet steam turbine was synchronised. When, in February 1975, all initial start-up tests required for a nuclear power station had finally been carried out, the turbine was put into continuous operation. A total of fourteen wet steam turbines of this design and rating are currently in service; altogether they have accumulated nearly 66 years of operation.

### DESCRIPTION OF THE 1300 MW WET STEAM TURBINE

3. A brief summary of the thermodynamic design and the structural as well as control engineering characteristics of the 1300 MW wet steam turbine is given to provide a better understanding of the operating experience described later.

#### Thermodynamic Design

4. The main steam with a pressure of approx. 70 bar, a temperature of 286 °C and a steam moisture content of 0.25 % is fed to the double-flow HP cylinder by way of four combined emergency trip and control valves, and is expanded down to the transfer pressure of some 11 bar (see Fig. 2).
5. After being dried and superheated in a combined moisture separator/reheater, where the heating is by main steam, the steam is admitted to the double-flow, 8 stage LP cylinders - two or three in number, depending on the temperature of the cooling water - at a pressure of approx. 10.5 bar and a temperature of 220 °C. In case of river water cooling the

condenser pressure is about 0.04 - 0.045 bar; in case of closed-circuit cooling using wet cooling towers, it is about 0.08 - 0.09 bar.

#### Structural and Control Engineering Characteristics

6. In the structural and control engineering areas of the design of wet steam turbines, the following two points have to be given special attention
7. - control of erosion and erosion-corrosion
8. - control of overspeed behaviour.
9. Erosion. Erosion is caused by water drops hitting the blade surface at a high relative speed near the tip section of the last LP stages (see Fig. 3). To reduce this attack the following measures were taken
10. - adequate dimensioning of the axial gap between fixed and rotating blades, so as to atomise and accelerate the large water drops.
11. - use of fixed blades with sharp trailing edges, to avoid formation of large water drops.
12. - hardening of the endangered leading edges of the rotating blades.
13. Erosion-Corrosion. Erosion-corrosion is a chemical-mechanical surface degradation. It is caused by the protective oxide layer, which forms at the surface of low-alloy steels, being continuously worn away by water drops or water streaks pulled along at high steam velocity and with high turbulence. The following counter-measures were taken
14. - chrome steel was used as material for endangered structural members (e.g. gland segments, HP inner casings)
15. - surfaces were spray-coated with protective layers based on chromium and nickel (e.g. inner surfaces of HP outer casings).

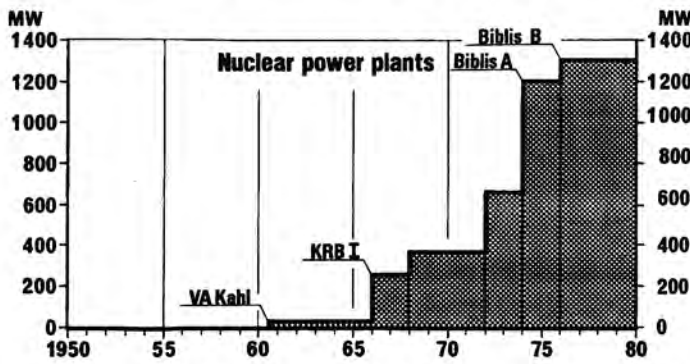


Fig. 1. Development of unit power of thermal power plants (Federal Republic of Germany)

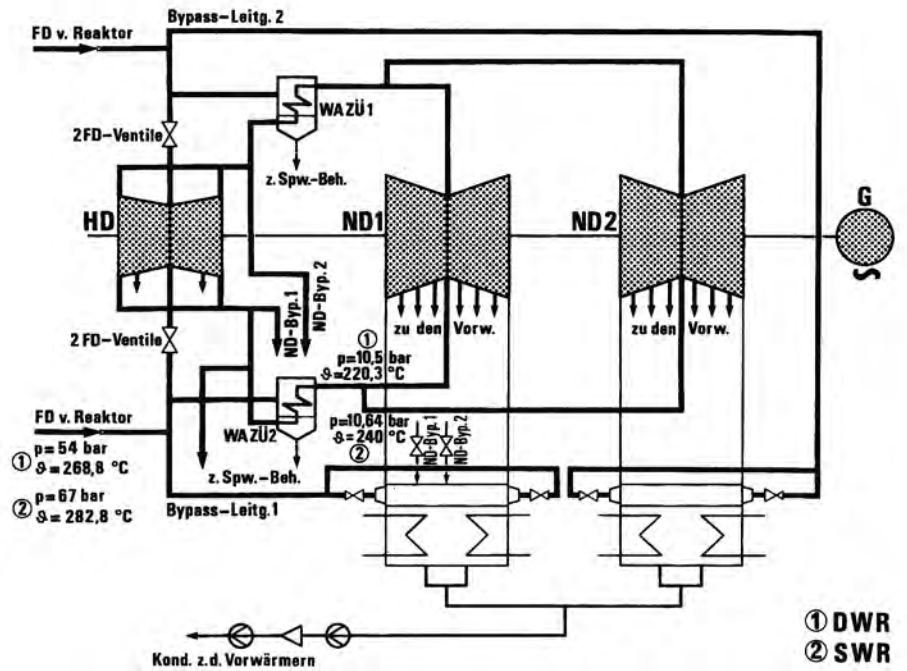


Fig. 2. Steam flow diagram of 1300 MW turbine of PWR - i.e. BWR - nuclear power plant



Fig. 3. Drop impact erosion between shroudings in inner casing of LP-part of Biblis turbines

16. Overspeed Behaviour. A large quantity of water is always present inside the HP turbine cylinder (a water film is present over the entire steam pressurized surface) and in the interstage moisture separators. When load is rejected, the drop in pressure results in the water film flashing to steam, which considerably influences the speed which the turbine attains. If the load were rejected to the auxiliary load, the transient speed rise would reach approx. 15 %, if it were fully rejected to no-load, it would reach approx. 35 %, greatly exceeding the overspeed trip setting (see Fig. 4).

17. To keep the speed rise within acceptable limits (1.5 % below trip speed) after load rejection, some or all of the following measures are taken

18. - intercepting flap valves in front of the LP cylinders.

19. - by-pass valves conducting the flashed steam from the HP cylinder around the LP cylinders and into the condenser.

20. - overspeed governor - anticipatory action. At an overspeed of 6 % it checks the control valves for being closed and the wheel chamber pressure for corresponding to the no-load running condition, so that in case of failure the tripping mechanism is released.

21. These measures are completed by the use of vacuum breakers (in PWR plants only); by the use of extraction check valves and valves isolating the reheater condensate tank and the water separator collecting tank.

#### OPERATING BEHAVIOUR

22. Nevertheless, the 1300 MW wet steam turbines also had their "teething troubles". That they were just initial problems has been proven by the course of events. They were found with the first turbines to be built, as well as with machines which had not yet been strengthened, but did not occur with machines where the necessary modifications could be incorporated during production (see Fig. 5).

23. These weak points, which mainly concerned the HP blading, seal strips, the pipes in the HP turbine section, and the moisture separator/reheater, are dealt with in more detail in the following sections.

#### HP-Fixed Blading

24. The fixed blade failure of unit Biblis A as a prototype turbine and the same problem in unit B were reported in 1976.

25. The reason of these failures was a kind of blade fixing construction (pronged root and effect of brittling of rivets of the rivetted shroudings).

26. This construction was replaced back in 1976 by blading with integrated shrouding, i.e. blade and cover plate of the blade milled of one piece, and inverted T-root.

27. The problems have therefore been remedied since 1976.

#### HP Rotor Blading

28. We knew that there had been problems with 600 MW reheated steam turbines of the manufacturer who also produced the 1300 MW wet

steam turbines, as to the fixing of the HP rotor blading. Due to an unfavourable blade root design and insufficient prestressing upon installation of the blades, several rotating blades had loosened. Some had broken shrouding as a result of reduced damping.

29. During a refuelling outage, the turbine at Biblis was examined by means of an endoscope and a blade fracture in the first HP rotating stage was discovered.

30. During scheduled unit outages this machine, as well as the others, was modified:

31. - improvement of details in the blade root within the limits of the shaft geometry, for example

32. grinding correction of the angles of the diamond shaped top plate and bottom plate of each blade in order to guarantee a definite prestressing.

33. reinforcement of the projecting bottom plate by increase of thickness.

34. - ensuring the correct prestress upon installation.

35. - checking the blade installation condition by measurement.

36. All HP blading has shown perfect performance in operation since these modifications, thus confirming the success of the measures taken.

#### LP Rotor Blading

37. Early in 1985 we had a defect in stage 6 of the moving blading at a LP rotor in Gundremmingen C after only 1.400 operating hours. 3 blades of LP2/GE were broken in the upper blade bottom and 6 other blades had incipient cracks. This case concerned the first row of freestanding blades of the LP rotor, the length of this blade is 825 mm.

38. Investigation indicated fatigue fractures, starting at the inlet side of the pressure face. Vibrations of the flutter type were identified.

39. Such flutter vibration may be the result of enhancement of the actual blade vibration by additional aerodynamic forces due to varying of unsteady flow characteristics, so that this is a stability problem.

40. For improved damping in the failed stage at Gundremmingen C as well as in unit B and at Grafenrheinfeld, a 5 mm diameter damping wire was installed. All these units were considered to be equally threatened, having the same mass-flow per casing.

41. Investigations meanwhile carried out by the manufacturer came to the conclusion that damping by Z-lacing near the blade tip (88 mm) and a 10 mm diameter longitudinal splitted wire at an intermediate height (312 mm from tip) would be recommended as the best solution (see Fig. 6).

42. This double lacing suppresses other forms of vibrations which is considered to be a great advantage.

43. For the time being no long term solution has been found. At the moment several turbines are being retrofitted with Z-lacing. The more expensive way would be a stronger disk and a stronger blade, this solution is already offered by the manufacturer.

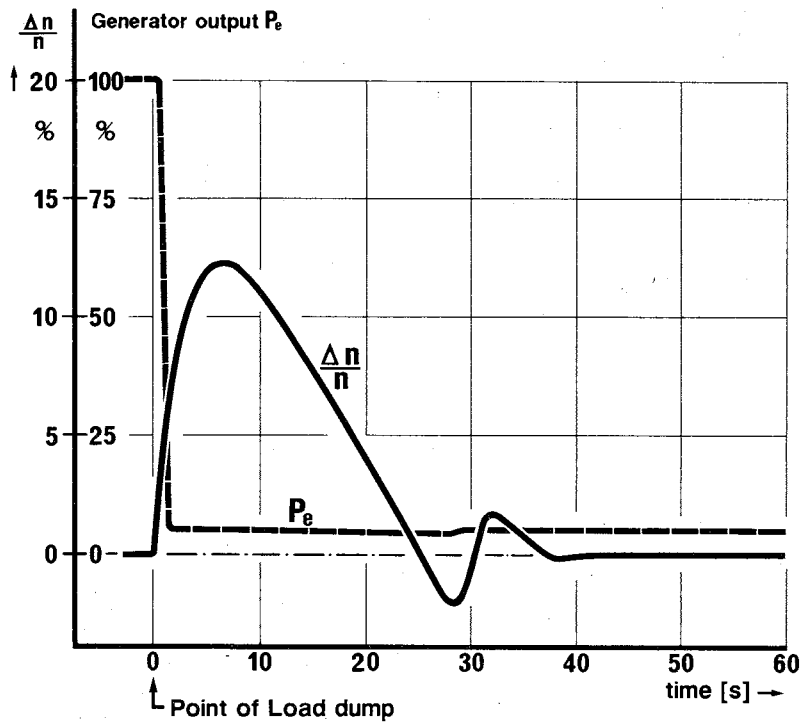


Fig. 4. Load dump from 100% power to internal power ( $55 \text{ MW}_e$ )

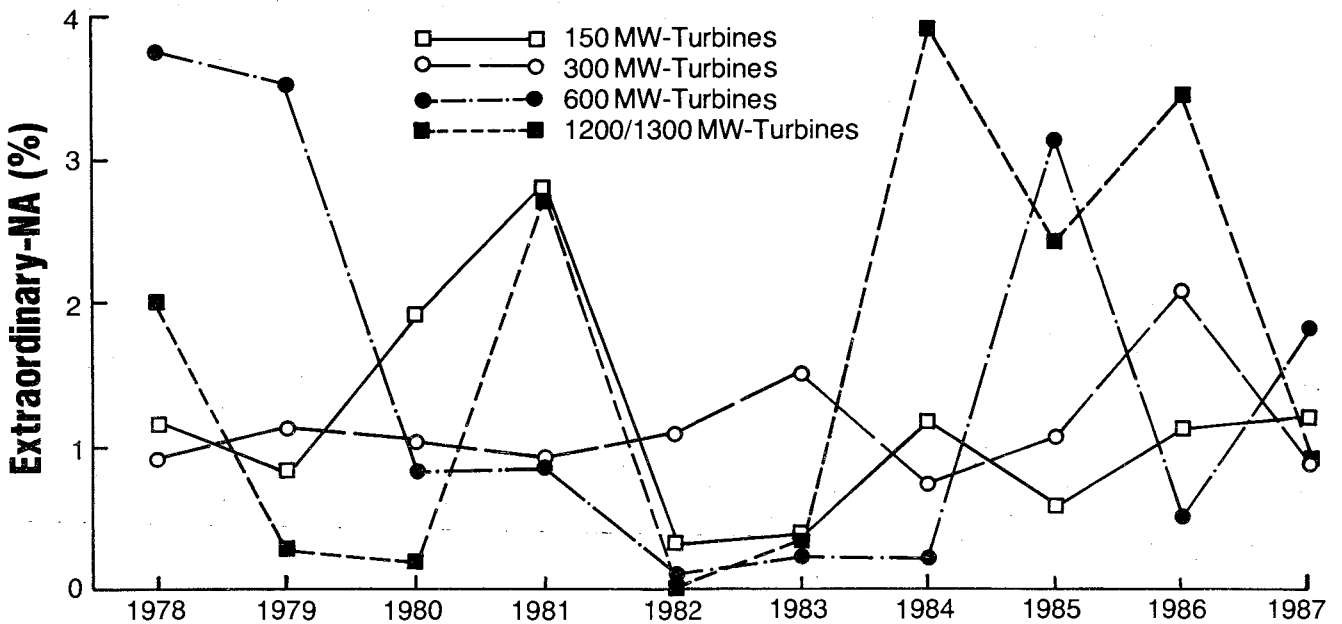


Fig. 5. Extraordinary part of non-availability of turbines

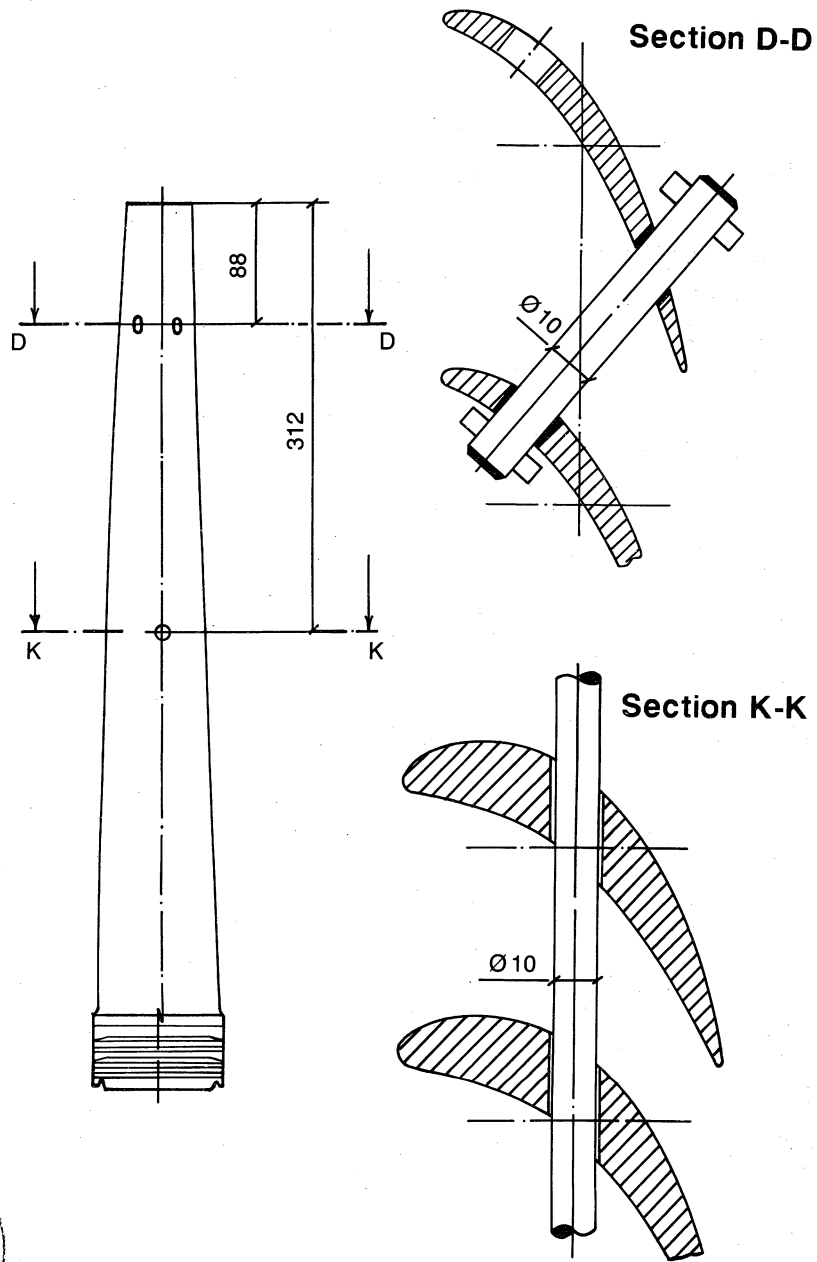


Fig. 6. Z-lacing and damper wire of stage of LP-blading 1300 MW wet steam turbine

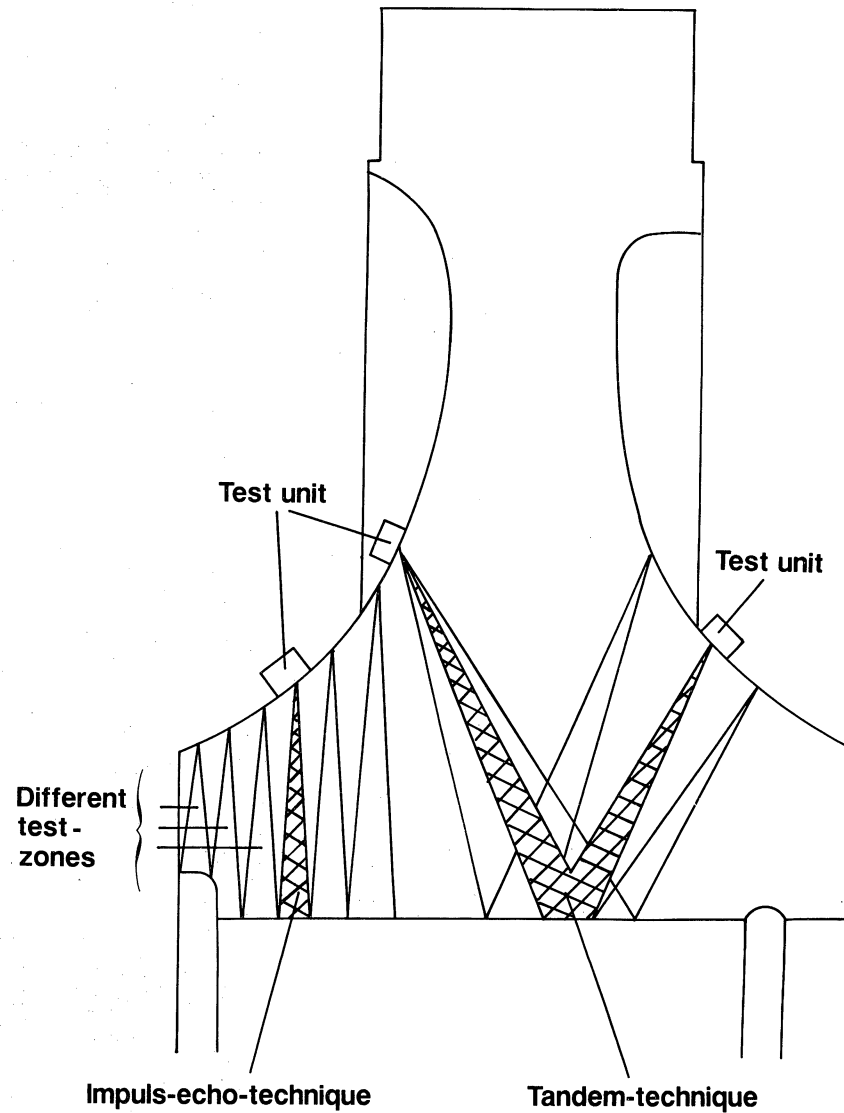


Fig. 7. US examination of built-up rotor discs



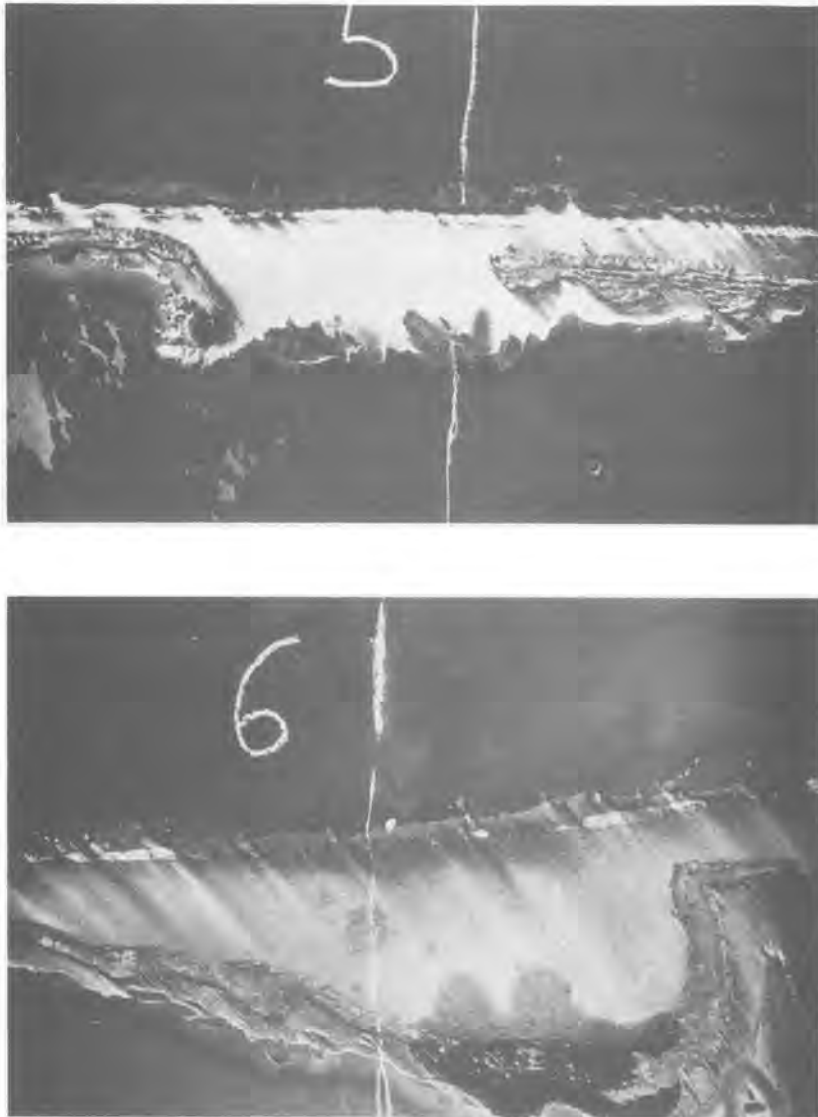


Fig. 8. Corrosion erosion in the extraction steam pipes of a 1300 MW wet steam turbine

#### BUILT-UP LP ROTOR INSPECTION

44. In recent years several defects have occurred in the hub area of built-up LP rotors in the US and in France. Experience indicates that the defects are due to stress corrosion.

45. In the Federal Republic of Germany this kind of damage has been experienced only rarely in older conventional units, usually under special chemical conditions.

46. In spite of these comparatively very good operating results non-destructive-test methods to acquire early knowledge of incipient cracking have been developed in Germany. For large built-up rotors these methods are practised periodically.

47. In contrast to the USA, where these examinations are prescribed by the supervisory authorities, in Germany this problem is implemented in cooperation between the customer, the manufacturer and the insurance company.

48. The stress corrosion may be the result of

49. - impurities in the feedwater, with decrease of pH-values and increase of CO<sub>2</sub>-values

50. - service stress

51. - detail design (notch effect).

52. Non-destructive-tests deliver early knowledge of smallest findings that might possibly become crack starters. Therefore before the initial start up a reference measuring is recommended to facilitate the interpretation of later indications in the range of < 10 mm (see Fig. 7).

53. Our strategy departs from the assumption that, considering the toughness of material a rate of crack growth is to be assumed, which leads to a critical crack size which could threaten the component part after a total operating time 50.000 hours. This calculation of crack growth is based on conservative assumptions.

54. If a reference measurement was not performed, it has to be accomplished after a time of operation of 40.000 to 60.000 hours. In case of a negative result a further test is recommended after further operation of 50.000 hours.

55. For the built-up rotors of RWE, all the checked rotors showed negative results.

56. Above all, suitable chemical control with constantly high pH-values, high steam purity, and low conductance, are the reasons for the satisfactory operating behaviour of our units.

#### PIPES IN THE HP TURBINE SECTION

57. Although, on account of the knowledge acquired about the potential damage by erosion-corrosion, endangered parts such as bends were already protected with spray coatings, inspections of HP exhaust steam and extraction pipes made of St 35 or St 37 respectively revealed unacceptable wall erosion, even on the straight pipe lengths - mainly in the area of welding joints. With a design wall thickness of 15 mm for the HP exhaust steam pipes and approx. 8 - 11 mm for the extraction pipes, the attack amounted to about 1 - 2 mm per year over large areas. For some points, however, values of up to 4 mm were measured (see Fig. 8).

58. In order to guarantee long term safe operation it was advisable to change the pipe material. Pipes made of 10 CrMo 910 were used, which had been proven to be resistant to erosion-corrosion.

#### MOISTURE SEPARATOR/REHEATER

59. In the reheat part of a moisture separator/reheater, damage was found at the spacer brackets of the tube nest. The mounting brackets had partly come loose, had slipped, or had even partially broken.

60. The result was movement and vibration in the tube nests concerned, which in turn led to tube fractures.

61. It was recognized that the damage was caused by a fault which had occurred during the repair of previous damage.

62. In order to prevent subsequent damage, the tube nests of both reheaters were withdrawn since it was impossible to repair the damaged nests.

63. New nests with stronger mounting brackets had been installed.

64. Since 1980 a new type of complete moisture separator/reheater has been applied in all new power plants. In this case four single nests were mounted in the reheater.

#### SUMMARY

65. We draw the following conclusion from what has been said so far:

66. - After a couple of initial start-up difficulties the 1300 MW wet steam turbines have stood their test.

67. - An almost undisturbed service record for the last few years has proved the reliability of these turbines, so that similar good operating experience is also to be expected for the future.



## 6. On the design limits of steam turbine last stages

Professor Dr G. GYARMATHY, Swiss Federal Institute of Technology, and Dr W. SCHLACHTER, ASEA Brown Boveri Ltd, Switzerland

The economic benefits resulting from an increased exhaust flow annulus area in large steam turbines have led the manufacturers to pay attention to the optimization of their last-stage designs. Interestingly, all manufacturers have realized blades of closely similar overall geometric proportions. In this paper, the reasons for this uniformity are analysed. By considering design criteria like the stress level in the rotor, the stress level and the vibration frequency of the blades, the aerodynamic quality of the near-hub and near-tip cascades and the level of erosion danger, it is shown that the designer has very little freedom to deviate from an optimum tip-to-hub diameter ratio. The value of this ratio is determined by the annulus area to be achieved, the shaft speed and the materials to be used. The results indicate the possibilities and the promise of further developments.

### INTRODUCTION

1. For a number of reasons, the design of the last LP (low-pressure) turbine stage is one of the most intriguing problems of steam turbine technology. To mention a few

- the very large steam volume flow rate calls for a large flow annulus area, i.e., long, highly stressed blades rotating with very high tip speed;
- the steam reaches supersonic speeds in several regions of the blading
- steam wetness complicates the design problem and causes damage by erosion;
- blade vibration problems may easily arise.

2. For any given plant and site, the LP exit volume flow rate  $Q$  and the network frequency are prescribed. The manufacturer has some freedom in choosing the shaft speed  $\omega_n$  by providing a standard 2-pole or a "half-speed" (4-pole) generator, in determining the number  $i$  of parallel LP flows and in selecting their exit annulus area  $S$ .

3. Since the exit kinetic energy constitutes a significant loss, the magnitude of which is proportional to the square of  $Q/iS$ , the product  $iS$  is to be kept high. The increase of  $i$  involves design complications and a considerable increase of overall shaft length with further consequences regarding plant and building size. Cost considerations will therefore urge the designer to try to make  $S$  as high as possible before deciding to make a step increase in the number of flows.

4. Thus, the achievement of a high LP exit-annulus surface area  $S$  was, and continues to be, of paramount interest.

5. A straightforward but expensive method involves the reduction of shaft speed by the use of a 4-pole generator. While this allows the designer to increase  $S$  considerably and keep the number of LP flows low (say  $i = 4$  instead of  $i = 6$ ), the weight of each component becomes multiplied and the costs increase accordingly. Thus, a smaller full-speed machine with its annulus area  $S$  pushed to the limits remains an interesting option even if its number of flows has to be higher than that of a half speed unit.

6. We see that the design of the LP last stage centers around two questions:

a. By what means can the exit annulus area of a full-speed LP turbine be pushed to its utmost limits without sacrifices in reliability and stage efficiency?

b. How should the last stage be designed in cases where the exit area size needs not to be at its extremes?

7. The answer to these questions will be sought by investigating the physical factors influencing the design of the last stage.

8. If  $\omega_n$  is the given nominal angular speed of rotation and  $2r_H$  is the diameter of the rotor at the exit cross section ("hub" diameter), then  $u_H = \omega_n r_H$  is the peripheral velocity of the rotor. The exit-annulus surface area is given by

$$S = \pi r_H^2 (X^2 - 1) = \pi \frac{u_H^2}{\omega_n^2} (X^2 - 1) \quad (1)$$

where  $X = r_T/r_H$  is the tip-to-hub radius ratio (or diameter ratio) of the last-stage rotor blading. It is seen that any given value of  $S$  can be realized with an infinite variety of combinations of  $u_H$  and  $X$ . The corresponding peripheral speed at the tip is

$$u_T = \omega_n r_T = u_H X \quad (2)$$

9. In Figure 1 the values of the velocities  $u_T$ ,  $u_H$  and diameters  $2r_T$ ,  $2r_H$  are independently plotted in the  $X$ ,  $S$  plane for the case of 50 Hertz full-speed machines ( $\omega_n = 314.2$  rad/s). Low  $X$  values lead to large rotors with short blades and high  $X$  values to small rotors with long blades, as illustrated by the sketches referring to cases A and B.

### LIMITING FACTORS IN DESIGN

10. With respect to static mechanical stresses, the critical problem areas are the rotor disc, the blade roots and the blades themselves. Critical dynamic stresses can arise in free-standing blades if their fundamental bending-mode frequency is low. From the aerody-

## TURBINE DESIGN AND OPERATIONAL EXPERIENCE

dynamic point of view, boundary layer disbehaviour, shock losses due to high Mach numbers, wetness losses and erosion have to be kept in acceptable bounds. By varying  $X$  at any  $S$ , some

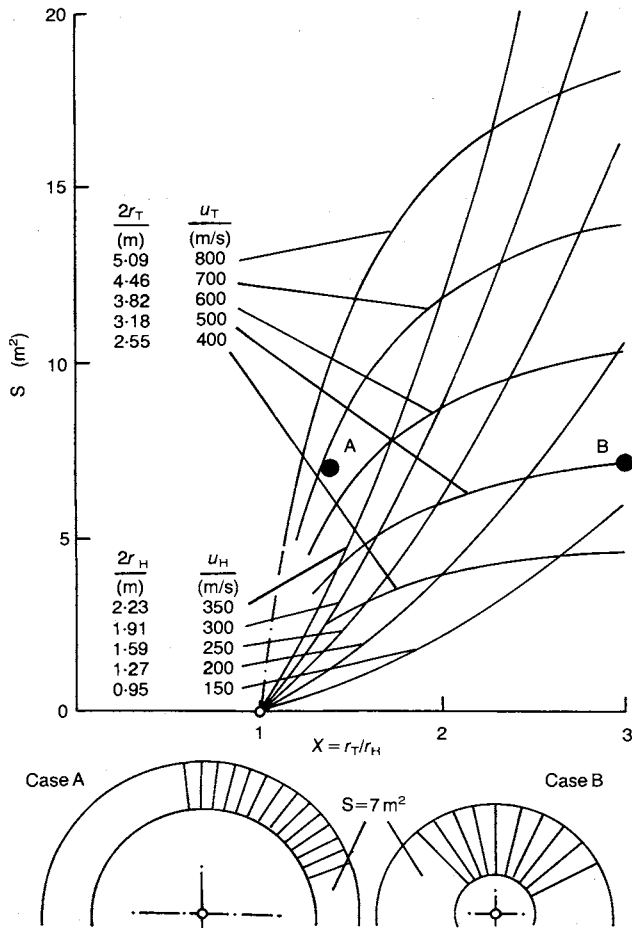


Fig. 1 Tip and hub diameter and peripheral velocity in function of the annulus area  $S$  and diameter ratio  $X$ , for 50-cycle full-speed turbines.

of these factors are eased while others are aggravated, and a compromise has to be sought.

### Mechanical Limits

#### •Rotor disc stress

11. From the many existing varieties of steam turbine rotors we base our analysis on the solid (non-perforated) disc, Figure 2, as used in welded multiple-disc rotors, because they are suitable for a simplified analysis and have become known as particularly suited for large-size LP units. We are interested in the influence of the design parameters  $S$  and  $X$  on the peak stress in the rotor,  $\sigma_R^{\max}$ , at given shaft speed. The basic equations will be derived from simple two-dimensional analysis of a single disc having uniform temperature. The centrifugal forces caused by the blading will be represented by a uniform mean radial stress

$$\bar{\sigma}_{rD}$$

acting at the radius  $r_D$  of the disc / blade-root transition.

12. According to standard textbooks, like e.g. Traupel's [1], the radial distribution of the tangential and radial stress components in a rotating disc of radius  $r_D$  and density  $\rho_D$  is given by

$$\sigma_r(r) = A_r(r) \bar{\sigma}_{rD} + B_r(r) \rho_D \omega_n^2 r_D^2 \quad (3)$$

$$\sigma_t(r) = A_t(r) \bar{\sigma}_{rD} + B_t(r) \rho_D \omega_n^2 r_D^2 \quad (4)$$

where the analytical form of the functions  $A_r$ ,  $A_t$ ,  $B_r$  and  $B_t$  is dependent on the disc thickness distribution  $y(r)$ . For a disc of constant thickness  $y_D$

$$A_r(r) = A_t(r) = 1$$

$$B_r(r) = \frac{3+\nu}{8} \left(1 - \frac{r^2}{r_D^2}\right) \quad (5)$$

$$B_t(r) = \frac{3+\nu}{8} - \frac{1+3\nu}{8} \frac{r^2}{r_D^2}$$

where  $\nu$  is Poisson's ratio of the disc material. The maximum stress occurs at the axis and has the value

$$\sigma_D^{\max} = \sigma_r(0) = \sigma_t(0) = \bar{\sigma}_{rD} + \frac{3+\nu}{8} \rho_D \omega_n^2 r_D^2 \quad (6)$$

13. The value of  $\bar{\sigma}_{rD}$  can be obtained from the radial forces arising from the presence of the blades and of the blade root structure. If  $\bar{\sigma}_B(r_H)$  denotes the mean radial stress in each blade at the hub radius where the blade profiles have a cross section  $f_H$ , and if the root structure is composed of roughly equal volumes of blade and disc material, we have

$$\bar{\sigma}_{rD} = \frac{\bar{\sigma}_B(r_H) f_H}{f_D y_D} + \frac{\rho_B + \rho_D}{2} (1 - X_D) \omega_n^2 r_H^2 \quad (7)$$

where  $X_D = r_D/r_H = t_D/t_H$  characterizes the radial extent of the root structure,  $t_D$  and  $t_H$  is the blade pitch at  $r_D$  and  $r_H$ , respectively,  $\rho_B$  is the density of the blade material and  $y_D = y(r_D)$  is the disc thickness.

Expressing  $f_H$  as

$$f_H = \alpha_H t_H y_H \quad (8)$$

where the coefficient  $\alpha_H$  is a measure for the "compactness" of the blade cascade at the hub radius, and inserting (7) into (6) we get

$$\sigma_D^{\max} = \bar{\sigma}_B(r_H) \frac{\alpha_H y_H}{X_D y_D} + \frac{\rho_B + \rho_D}{2} (1 - X_D) \omega_n^2 r_H^2 + \frac{3+\nu}{8} \rho_D \omega_n^2 r_H^2 X_D^2 \quad (9)$$

14. If the permissible stress level  $\sigma_D^{\max}$  and the blade radial stress  $\sigma_B$  are given, the maximum permissible hub speed,  $u_H^{\max} = \omega_n r_H (\sigma_D^{\max})$ , can be calculated from the geometric shape as

$$(u_H^{\max})^2 = \frac{1}{\rho_D} \frac{\sigma_D^{\max} - \bar{\sigma}_B(r_H) \frac{\alpha_H y_H}{X_D y_D}}{(1 - X_D) + \frac{3+\nu}{8} X_D^2 - \left(1 - \frac{\rho_B}{\rho_D}\right) \frac{1 - X_D}{2}} \quad (10)$$

15. Typically, for chromium steel blades and disc,  $\rho_D = \rho_B = 7.8 \cdot 10^3 \text{ kg/m}^3$ ,  $\nu = 0.3$ ,  $\sigma_D^{\max} = 300 \cdot 10^6 \text{ N/m}^2$  and  $\sigma_B(r_H) = 500 \cdot 10^6 \text{ N/m}^2$ . The root structure may typically have  $X_D = 0.92$  and  $y_H = y_D$ . Reasons discussed further below lead to

highly compact hub cascades, typically corresponding to  $\alpha_H = 0.25$ . These values give

$$\bar{\sigma}_{rD} = 167 \cdot 10^6 \text{ N/m}^2$$

and

$$u_H^{\max} = \sqrt{\frac{10^6}{7.8 \cdot 10^3} \frac{300 - 136}{0.08 + 0.349}} = 223 \text{ m/s} \quad (11)$$

giving a rotor diameter of  $2r_H^{\max} = 1.42 \text{ m}$ .

16. If a disc of variable thickness is used,  $u_H^{\max}$  values around 300 m/s or slightly above can be achieved with the same materials. It appears from Eq. (10) that the value of  $u_H^{\max}$  is independent of the annulus area  $S$ . In the  $X, S$  plot, Fig. 1, any condition  $u_H < u_H^{\max}$  is seen to set a lower limit on  $X$  at a given  $S$  or an upper limit on  $S$  at a given  $X$ .

17. By using titanium blades on steel rotors,  $\rho_B/\rho_D \approx 0.6$  is achieved, and  $u_H^{\max}$  increases by a small amount (from 223 to 227 m/s in the above example).

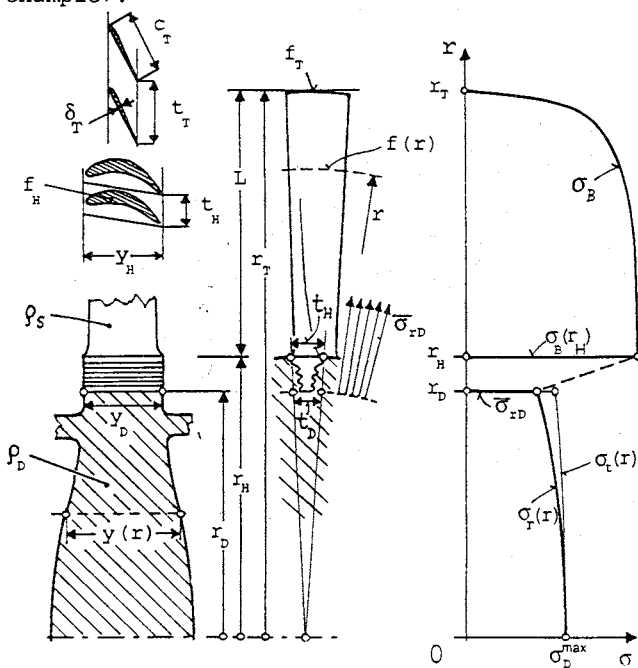


Fig. 2 Disc and blade geometry and stress distributions.

#### Rotor blade stress

18. Since the radial stresses caused by the centrifugal forces are predominant in LP turbine blading, bending and torsional stresses will be disregarded. The blade radial stress  $\bar{\sigma}_B(r)$  shall be assumed to be uniform within any cross section of the blade. The case of free-standing (unlaced) blades will be considered.

19. For a given hub speed  $u_H$  and hub mean stress level  $\bar{\sigma}_B(r_H)$ , the longest blades (i.e., the largest annulus area) are obtained if the blade is tapered for constant nominal stress  $\sigma_B^*$ .

20. This is achieved if the blade cross section  $f(r)$  decreases with  $r$  according to the law [1]

$$f(r) = f_H \exp\left[-\frac{\rho_B u_H^2}{2\sigma_B^*} \left(\frac{r^2}{r_H^2} - 1\right)\right] \quad (12)$$

giving a hub-to-tip taper ratio of

$$\frac{f_T}{f_H} = \exp\left[-\frac{\rho_B u_H^2}{2\sigma_B^*} (X^2 - 1)\right] = \exp\left(-\frac{\rho_B \omega_n^2}{2\pi\sigma_B^*} S\right) \quad (13)$$

21. The second equation was obtained by using Eq. (1). The important conclusion is found that the taper of constant-stress blades only depends on the annulus area size but not on  $X$ .

22. It can be shown that the blade mean stress at the hub is related to  $\sigma_B^*$  by

$$\bar{\sigma}_B(r_H) = \sigma_B^* \left(1 - \frac{f_T}{f_H}\right) \quad (14)$$

Eq. (13) can now be written as

$$\frac{\ln(f_T/f_H)}{1 - f_T/f_H} = -\frac{S}{S^*} \quad (15)$$

where

$$S^* = \frac{2\pi \bar{\sigma}_B(r_H)}{\rho_B \omega_n^2} \quad (16)$$

is a reference area expressing the influence of blade materials.

23. If  $\bar{\sigma}_B(r_H) = 500 \cdot 10^6 \text{ N/m}^2$ ,  $\rho_B = 7.8 \cdot 10^3 \text{ kg/m}^3$  and  $\omega_n = 314.2 \text{ rad/s}$ , we have  $S^* = 4.05 \text{ m}^2$ , giving the values shown in Table 1. With titanium blades ( $\rho_B = 4.6 \cdot 10^3 \text{ kg/m}^3$ ) we have  $S^* = 6.9 \text{ m}^2$ . With titanium,  $6.9/4.05 = 1.7$  times larger areas  $S$  can be achieved at any given taper ratio.

Table 1. Blade taper for constant nominal blade stress

$S(\text{m}^2)$	steel	18.84	16.17	12.77	11.12	10.36	9.04	8.15	6.97
titanium	32.10	27.55	21.76	18.94	17.63	15.40	13.89	11.87	
$f_T/f_H$	0.01	0.02	0.05	0.08	0.10	0.15	0.20	0.30	

24. Blade taper means that the compactness of the cascade rapidly diminishes along the span of the blade. The combination of low  $f_T/f_H$  ratios with high diameter ratios necessarily leads to aerodynamic problems which will be treated further below. By the use of hollow rotor blades the possibility theoretically exists to decouple the mechanical stressing and aerodynamic contouring problems.

25. Slow-turning, large-diameter, single-exhaust, vertical-axis low-pressure turbines, as envisaged in an old patent by C. Seippel [2], might alleviate the centrifugal stress problems if combined with light-weight, high-strength plastic blade materials. Modern composites, like e.g. Kevlar 49, have  $\sigma_B/\rho_B$  ratios of the order of  $500 \cdot 10^3 \text{ m}^2/\text{s}^2$ , giving  $S^* \approx 30 \text{ m}$  for full-speed rotors.

At slower speeds, very high areas would become feasible without the need of excessive blade taper.

#### Blade root structure

26. In the region between  $r_D$  and  $r_H$  the stresses have a complex pattern both in the blade root and in the disc rim shown in Figure 3. The aim of the root design must be, regardless of the particular geometry used (grooves, pins, etc.), to keep  $\sigma_{rD}$  close to  $\sigma_D^{\max}$  without locally exceeding the latter limit. Local stress concentrations in notches of the blade root structure put a limit on the

compactness of the hub cascade,  $\alpha_H$ , and require careful harmonization of the blade and disc stress levels. The blade root problem is accounted for in the present treatment by the use of realistic (optimized) geometric and stress data in Eq. (9).

Vibrational Limits

27. It is a classical design rule that the lowest vibrational frequency of a blade should exceed the double of the shaft rotation frequency. The lowest eigenfrequency  $\omega_e$  is that of the first bending mode. Neglecting the influence of rotation at first, following estimate can be made for  $\omega_e$  by using the theory of a slender beam of length  $L$  rigidly fixed at one end and free at the other [1].

$$\omega_{e0} = \frac{K_e}{L^2} \sqrt{\frac{EJ_H}{\rho_B f_H}} \quad (17)$$

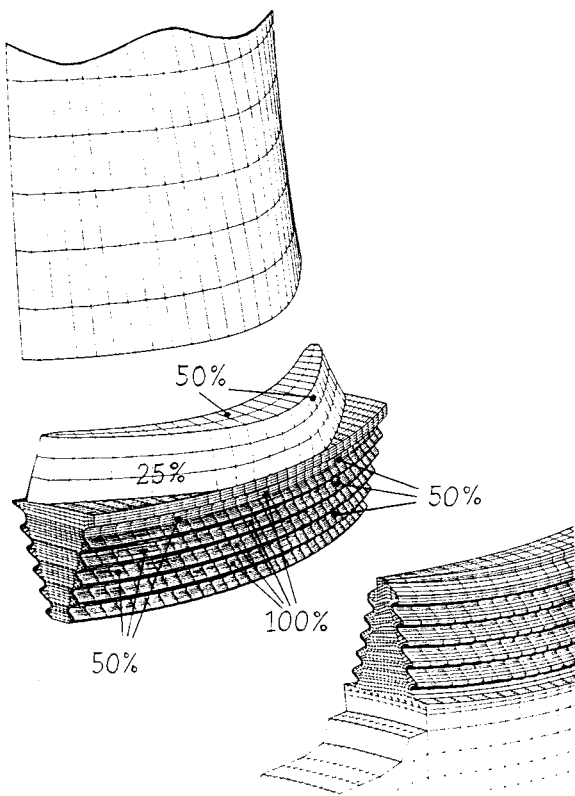


Fig. 3 Calculated stress patterns in the blade root region.

28. Here  $E$  is Young's modulus,  $J_H$  is the smallest moment of inertia of the hub profile section and  $K_e$  is a numerical coefficient resulting from theory. The value of  $K_e$  depends on the taper and shape of the beam,  $K_e \approx 5.0$  being a realistic value for strongly tapered blades and e.g.  $K_e = 3.5$  pertaining to prismatic beams. The blade length  $L$  can be written, using Eq. (1), as

$$L = r_T - r_H = (X-1)r_H = \frac{X-1}{\sqrt{X^2-1}} \sqrt{\frac{S}{\pi}} \quad (18)$$

$J_H/f_H$  is conveniently non-dimensionalized by  $t_H^2 = (2\pi r_H/N_B)^2$  where  $t_H$  is the blade pitch at the hub and  $N_B$  is the number of rotor blades.

Inserting these into Eq. (17) and eliminating  $r_H$  by  $S$  with help of Eq. (1), one obtains

$$\omega_{e0} = \frac{K_e}{N_B} \sqrt{\frac{E}{\rho_B}} \sqrt{\frac{J_H}{t_H^2}} \sqrt{\frac{4\pi^3(X+1)}{S(X-1)^3}} \quad (19)$$

29. The above vibration frequency pertains to the blade at stand-still ( $\omega = 0$ ). At the nominal rotor speed  $\omega_n$ , the stiffening effect of the centrifugal forces raises  $\omega_e$  to the value

$$\omega_e \approx \sqrt{\omega_{e0}^2 + \omega_n^2 \left[ \left( \frac{1}{X-1} + \frac{3}{4} \right) K_\omega - \cos^2 \beta \right]} \quad (20)$$

where the numerical coefficient [1] pertaining to the first bending mode is  $K_\omega = 1.61$ . The angle  $\beta$  characterizes the vibrational direction of the blade's center of gravity with respect to the peripheral direction and is of little influence.

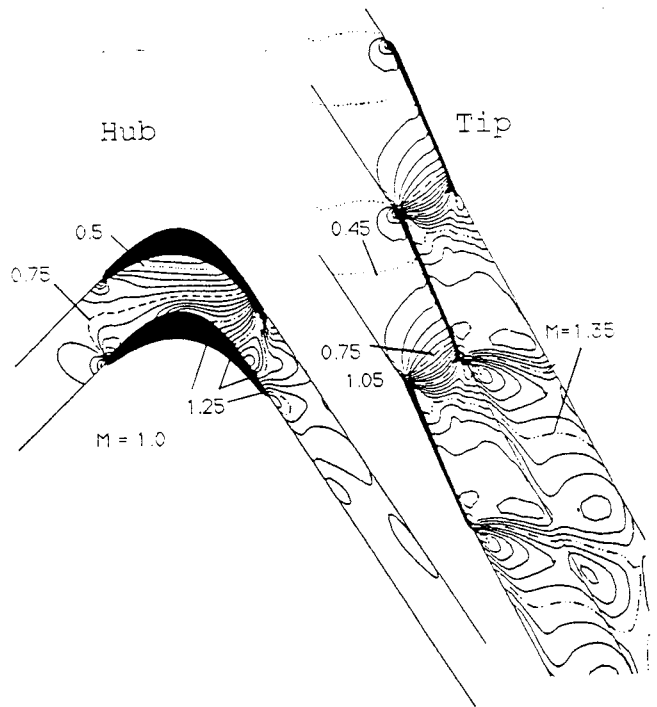


Fig. 4 Relative-flow Mach number contours in typical last-stage hub and tip cascades.

The classical design rule mentioned above requires the blade to be stiff enough to fulfill the condition

$$\omega_e > 2\omega_n \quad (21)$$

30. Since  $\omega_{e0}$  and  $\omega_e$  decrease with increasing blade length, this vibration frequency condition puts an upper limit on the annulus area. Setting e.g.  $\omega_e = 2.2\omega_n$  and expressing  $S$  from Eqs. (19) and (20), one gets

$$S_{max} = \left( \frac{G}{N_B} \right)^2 V(X) \quad (22)$$

where

$$G = \sqrt{K_e^2 \frac{E \pi^3}{\rho_B \omega_n^2} \frac{J_H}{t_H^2}} \quad (23)$$

and

$$V(X) = \frac{4(X+1)/(X-1)^3}{2.2^2 - \left( \frac{1}{X-1} + \frac{3}{4} \right) K_\omega + \cos^2 \beta} \quad (24)$$

31. This vibration limit depends strongly on the tip-to-hub ratio X and on the blade number  $N_B$ . Since steel and titanium have very similar  $E/r_B$  values, the materials choice has little effect on  $S_{max}$ .

32. The blade shape influence, represented by  $(J_H/t_H 2f_H)$ ,  $K_e$ ,  $K_w$  and  $\beta$ , is of moderate importance. Aerodynamic considerations will anyway prevent the effective use of blade shape as an instrument to achieve stiffer blades.

33. Typical data like  $E/\rho_B = 2.5 \cdot 10^7 \text{ m}^2/\text{s}^2$ ,  $\omega_n = 314.2 \text{ rad/s}$ ,  $J_H/t_H 2f_H = 0.11$ ,  $K_e = 5$ ,  $K_w = 1.61$  and  $\beta = 40^\circ$  yield  $G \approx 150 \text{ m}$  and values of  $V(X)$  as listed below.

Table 2. Vibration frequency limit function

X	1.0	2.0	2.2	2.5	2.8	3.0
V(X)	$\infty$	4.59	2.57	1.31	0.78	0.58

34. Composite plastics would allow to build slightly stiffer blades. Typically, they have  $E/\rho \geq 4 \cdot 10^7 \text{ m}^2/\text{s}^2$ , giving  $G \approx 180 \text{ m}$ . This means an increase of  $S_{max}$  by about 50 percent at constant X and  $N_B$ .

35. Another vibrational limit, due to the occurrence of aeroelastically induced blade flutter in certain operating points, may be of significance for certain designs and can be eliminated by using part-span shrouds. No general quantification of this limit appears to be feasible on the basis of our present knowledge.

Aerodynamic Limits

• Cascade Geometry

36. In blades designed for constant radial stress the blade profile cross section  $f(r)$  decreases exponentially with radius, as discussed in Sect. 3.1.2. The taper ratio  $f_T/f_H$  appeared to be a function of the exit annulus area S only, and not of the tip-to-hub ratio X, cf. Eq. (13).

37. Along the blade, concurrently with the decrease of  $f(r)$ , the cascade pitch  $t = 2\pi r/N_B$  increases. The aerodynamicist is confronted at the hub with the task of accommodating closely spaced bulky profiles without obstructing the flow and causing high losses. At the tip the blades have to be thin, still the cascade ought to give sufficient guidance to the flow. Typical designs for the hub and tip cascades are shown in Figure 4. The Mach number level in both cascades is high. Supersonic values occur at the nozzle outlet near the hub and at the rotor outlet near the tip, see also Wallon [3].

38. The hub profile cross sectional area  $f_H$  is expressed by Eq. (8) as

$$f_H = \alpha_H y_H t_H = \alpha_H \frac{y_H}{t_H} t_H^2 \quad (25)$$

where  $\alpha_H$  characterizes the compactness of the hub cascade. Aerodynamically feasible maximum values of  $\alpha_H$  seem to lie about 0.25 to 0.30, and those of  $y_H/t_H$  about 4 to 5.

39. At the tip, a well-guided acceleration of the flow to supersonic speeds relative to the blade requires the blade chord  $c_T$  to be comparable to or larger than the blade pitch  $t_T$ , giving  $(c_T/t_T)_{min} = 1$ . For a prescribed small area  $f_T$ , the mean blade thickness  $\delta_T = f_T/c_T$  will therefore have to be small.

40. On the other hand, the necessity to avoid

plate-type vibration of the blade extremity and manufacturing considerations require sufficiently thick tip profiles. A practical rule of thumb is expressed as  $(\delta_T/c_T)_{min} \approx 0.025$ .

41. The blade cross sectional area at the tip can also be written as

$$f_T = \delta_T c_T = \left(\frac{\delta_T}{c_T}\right) \left(\frac{c_T}{t_T}\right)^2 t_H^2 X^2 \quad (26)$$

Combining Eqs. (25) and (26) and expressing X we have

$$X = \sqrt{C \frac{f_T}{f_H}} \quad (27)$$

where

$$C = \frac{(y_H/t_H) \alpha_H}{(\delta_T/c_T) (c_T/t_T)^2} \quad (28)$$

42. For the maximum acceptable value of C we obtain, using the above criteria,

$$C_{max} \approx \frac{5 \cdot 0.03}{0.025 \cdot 1^2} \approx 60$$

43. With this value for C, Eq. (27) assigns to each value of  $f_T/f_H$  a maximum aerodynamically feasible radius ratio X. Since  $f_T/f_H$  is directly coupled to the annulus area S by Eq. (15), Eq. (27) results in a single limit curve in the X, S plane. This limit will depend on the value assumed for C and on the blade material used, because this has a great effect on the  $f_T/f_S$  vs. S relationship.

Reaction grade distribution

44. In order to keep flow losses within acceptable limits, the reaction grade of the stage, R, has to fulfill the condition

$$R_{min} < R < R_{max} \quad (29)$$

along the whole blade span. Typical limiting values are  $R_{min} \approx 0.05 \dots 0.10$  and  $R_{max} \approx 0.70 \dots 0.90$ . The reaction grade is defined as

$$R = \frac{\Delta h_{rotor}}{\Delta h} \quad (30)$$

where  $\Delta h = \Delta h_{stator} + \Delta h_{rotor}$  is the stage enthalpy drop. The variation of R (from a low value at the hub to a high value at the tip) is mainly due to the variation of the peripheral velocity along the blade span. This influence can be quantified in a rough way by a simple analysis based on following approximations:

- $\Delta h$  is constant from hub to tip
- the flow has no swirl ahead of and behind the stage
- the meridional through flow velocity at any stream surface stays constant.

45. These approximations result in a straightforward relationship between R and the rotor-inlet peripheral velocity  $u_1$  at the stream surface in question:

$$1 - R \approx \frac{\Delta h}{2u_1^2} \quad (31)$$

46. If the conicity of the inner and outer duct walls in the rotor cascade domain is expressed by the radius ratios  $(r_1/r_2)_H$  and  $(r_1/r_2)_T$ , we can set  $u_{1H} = (r_1/r_2)_H u_H$ ,  $u_{1T} = (r_1/r_2)_T X u_H$  and obtain

$$\frac{1 - R_T}{1 - R_H} = \frac{U_{1H}^2}{U_{1T}^2} = \frac{(r_1/r_2)_H^2}{(r_1/r_2)_T^2 X^2} \quad (32)$$

47. By setting  $R_H = R_{min}$ ,  $R_T = R_{max}$ , we may calculate an estimate for the highest diameter ratio compatible with these reaction grade limits:

$$X_{max} = \frac{(r_1/r_2)_H}{(r_1/r_2)_T} \sqrt{\frac{1 - R_{min}}{1 - R_{max}}} \quad (33)$$

48. The numerical values for typical current design practice are  $R_{min} = 0.1$ ,  $R_{max} = 0.8$ ,  $(r_1/r_2)_H = 1$ ,  $(r_1/r_2)_T = 0.9$ , yielding  $X_{max} = 2.36$ .

49. It is seen that the clue to making  $X_{max}$  large is a high reaction at the tip (say,  $R_{max} > 0.9$ ), while  $R_{min}$  may stay as high as 0.2...0.3 without affecting  $X_{max}$  too much. Therefore the root reaction need not be made too low. An inward conicity of the rotor,  $(r_1/r_2)_H > 1$ , helps to increase  $X_{max}$ .

50. A more comprehensive treatment of the hub-to-tip reaction distribution based on radial equilibrium of flow and including swirl and meridional acceleration and variation of  $\Delta h$  shows that higher  $X_{max}$  limits can be attained for given  $R_{min}$  and  $R_{max}$ . However, the limit stays independent of area  $S$ . For  $R_{max} \approx 0.8$  it is realistic to set

$$X_{max} = 2.6 \text{ to } 2.8 \quad (34)$$

and  $X_{max} \geq 3.0$  if tip reaction is made to approach or exceed 0.9.

•Mach number problems

51. In order to avoid high losses, the aerodynamic design has to ensure that the hub-inlet relative Mach number to the rotor blade row,  $M_{w1H}$ , stays clearly subsonic (especially if the hub cascade is highly compact), and that the rotor-exit relative Mach number at the tip,  $M_{w2T}$ , obtains the high value needed for providing swirl-free outflow toward the diffuser. By considering actual designs, like the one illustrated in Figure 4, it appears that the limits imposed on  $u_H$  and  $u_T$  by mechanical reasons are such that the Mach number levels in steam flow can be handled with acceptable losses.

•Blade Erosion

52. Beside fluid dynamic and metallurgical factors not directly influenced by the exit annulus geometry, the main parameter affecting the blade erosion rate is the tip speed  $u_T$  of the rotor blades. Experience has shown that tip speeds well beyond  $u_T = 600$  m/s are feasible in LP turbines. A tentative limit due to blade erosion of appropriately protected blades shall be represented by the condition

$$u_T = \text{constant} = 700 \dots 750 \text{ m/s} \quad (35)$$

53. More refined limiting conditions could be obtained for particular cases if the amount of wetness and its impact on the blades were considered in detail, as e.g. demonstrated by Krzyzanowski and co-workers [4].

Design Boundaries

•Feasibility domain

54. Each limit condition discussed above can be represented by a curve in the  $X, S$  plane. These limits have been calculated for  $\omega_n = 314.2$  rad/s (i.e., for full-speed turbines in 50 cycles networks). The results are plotted in Figure 5.

55. Following critical values, as representative of current technology, have been used

- a) Rotor stress limit, Eq. (10):  
 $u_H^{max} = 250; 300; 320$  m/s
- b) Blade stress limit, Eq. (15):  
 $S^* = 4.05 \text{ m}^2$  (steel blades stressed 500 N/mm<sup>2</sup>)  
 $S^* = 6.90 \text{ m}^2$  (titanium blades stressed 500 N/mm<sup>2</sup>)
- c) Blade frequency limit, Eqs. (22) and (24) for metals (steel, titanium):  
 $G = 150$  m,  $K_\omega = 1, 61$ ,  $\beta = 40^\circ$   
 $N_B = 50; 60; 75$  blades
- d) Cascade geometry limit, Eq. (27):  
 $C = 60$
- e) Reaction distribution limit, Eq. (34):  
 $X_{max} = 2.6; 2.8$
- f) Blade erosion limit, Eq. (35):  
 $u_T = 700; 750$  m/s

56. For composite plastics ( $S^* \approx 30 \text{ m}^2$ ), limit b lies far outside the field shown in the figure, and limit c is raised by a factor 1.5.

57. The domain in which feasible designs can be made is seen to be a wedge-shaped area positioned in the neighbourhood of  $X = 2$ .

58. It should be noted that all boundaries obtained are rigorously valid for machines running at any other nominal shaft speed  $\omega_n^*$ , if the  $S$  values are corrected according to

$$S_{corr} = \left(\frac{314 \text{ rad/s}}{\omega_n}\right)^2 S \quad (36)$$

59. This is evident from the fact that, in all equations,  $S$  and  $\omega_n$  only and exclusively occur in the combination  $\omega_n^2 S$ , i.e., limits are set for the value of the product  $\omega_n^2 S$  only, rather than for  $S$  alone.

•Design for maximum exit annulus area

60. It appears from Figure 5 that large annuli can only be achieved in a narrow range of tip-to-hub diameter ratio values around  $X = 2.2$ .

61. With steel blades the maximum achievable annulus area on full-speed rotors is about  $S \approx 11 \text{ m}^2$  for 50-cycle networks and  $S_{60} = (50/60)^2 11 = 7.6 \text{ m}^2$  for 60 cycles.

61. This limit size of about  $S = 10 \dots 12 \text{ m}^2$  is seen to be imposed by several physically independent factors. Therefore an increase in area cannot be achieved by relaxing one of the constraints only.

63. By use of titanium blades instead of steel, the cascade geometry limit is seen to be very efficiently relaxed. This change leaves the rotor stress and blade frequency limits unaffected, however, preventing any significant increase in area. If the blade frequency is simultaneously raised (e.g. by reducing the number of blades and increasing the profile dimensions accordingly),  $S$  can be further increased up to the erosion limit which then is likely to become the next problem. If the high limits offered by titanium cannot be fully utilized, the titanium blades may be designed for a lower stress level, bringing some benefits

in terms of rotor stresses and of aerodynamic quality (hub and/or tip cascade geometry).

64. Full profit from titanium blades, permitting an area of about  $S = 16 \text{ m}^2$  (or  $S_{60} = 11 \text{ m}^2$ ) to be realized, can only be obtained if tip speeds above 750 m/s can be accepted with regard to erosion and transonic flow and, simultaneously, the vibrational constraints are markedly relaxed. Low blade numbers (around or below  $N_B = 40$ ) or the transition from "stiff" ( $\omega_e > 2\omega_n$ ) to "flexible" ( $\omega_e < 2\omega_n$ ) blades may be two alternative answers. Stiffening by part-span obstructions has disadvantages due to increased losses but may be imperative by vibrational reasons. The remarkable Alsthom design now being tested [3] for 3000 rpm (with  $S = 14.6 \text{ m}^2$ ,  $L = 1360 \text{ mm}$ ,  $X = 2.32$ , tip speed 750 m/s, titanium blades) has two stiffening shrouds, one at the tip and one at 70 % span.

- the blade stresses may be relieved without causing aerodynamic problems, and
- the tip speed and tip diameter will tend to be high, resulting in a larger overall diameter and higher materials costs than in case of high X.

68. By choosing a high X (say  $X > 2.2$ ) for a given area:

- the rotor becomes less loaded (as beneficial especially for shrunk-on rotor designs),
- slightly smaller overall diameters are obtained, but
- the aerodynamic design problems associated with high tip-to-hub ratios tend to remain important, and
- the rotor diameter is reduced, making rotor dynamics problems more acute.

69. It appears that the choice of X values on the low side will be the better compromise in most cases, especially if solid-disc rotors are used.

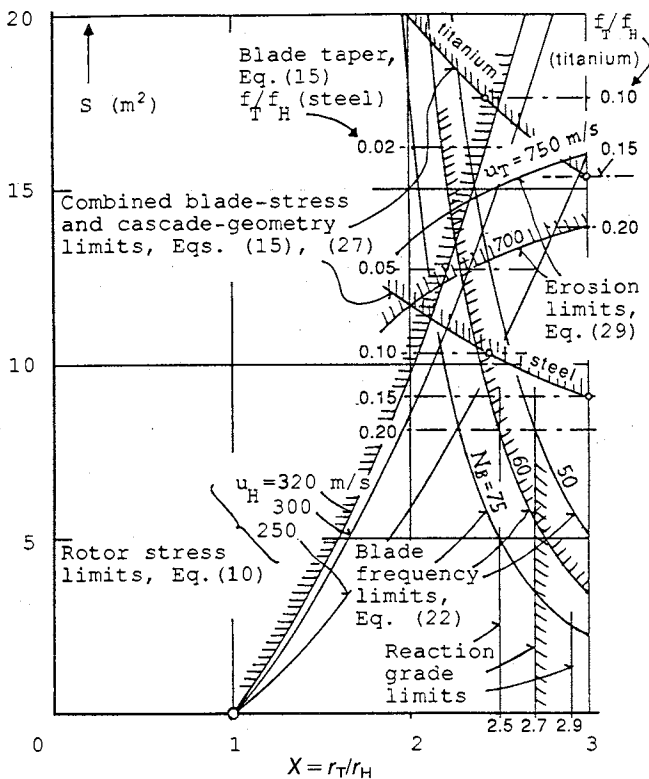


Fig. 5 Calculated design limits in the X, S plane (parameter values as given in text) with representative design limits

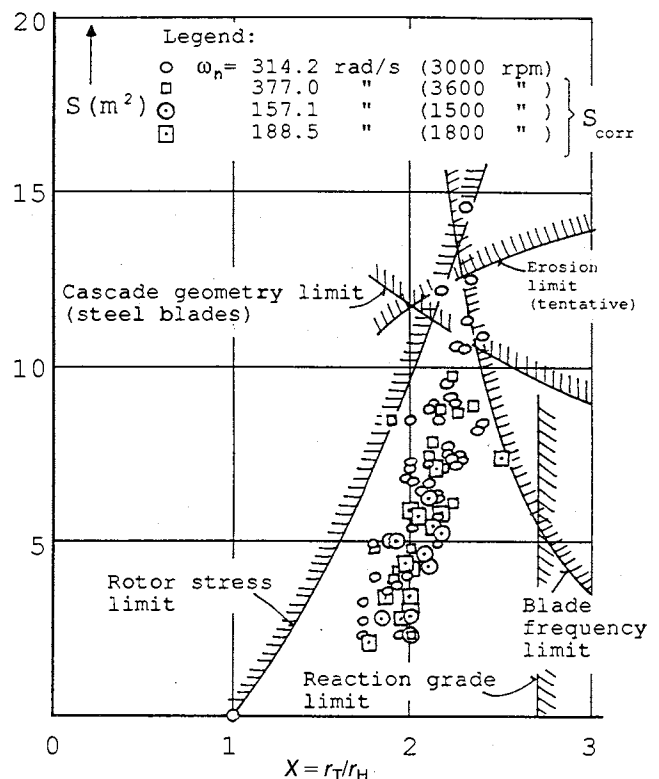


Fig. 6 Compilation of actual last-stage parameters of various manufacturers

65. Composite plastic blades offer very large S values but have to be protected against erosion which is likely to be the limiting factor in this case.

•Optimization within the conservative range

66. If the largest possible area per LP flow is not imperatively needed, more conservative designs with lower S values can be adopted. At low S values, X can be selected in a wide range between the limits imposed by rotor stresses and vibration frequencies. The selection of the proper X is a matter of design optimization. The criteria affecting it will be discussed below.

67. By choosing a low X (say  $X < 2$ ) for a given area:

- the rotor diameter and the rotor stresses are relatively high,
- the blade frequencies are high,

•Comparison with existing stage designs

70. It is interesting to confront the boundaries shown in Figure 5 with existing LP last-stage designs. For this purpose, the S, X data of all LP stages of known manufacturers have been compiled in Figure 6. An early compilation of this type was published in [5]. The small circles refer to 50-cycle, full-speed machines. For other types, the corrected area  $S_{corr}$  has been plotted. Open circles indicate 50-cycle half-speed machines. Square symbols pertain to 60-cycle full-speed or half-speed units.

71. It is seen that all stages fall into the narrow domain left free by the various limits. Several 50-cycles designs feature area values above  $10 \text{ m}^2$  with the above-mentioned Alsthom 7

titanium design of 14.6 m<sup>2</sup> at the top. Most half-speed LP turbines are of conservative design (S<sub>corr</sub> < 6 m<sup>2</sup>). The tendency is clearly seen to reduce the diameter ratio X when S is moderate.

FLEXIBLE BLADES

72. In the attainment of large annulus areas, as offered by titanium blades, the first-mode blade-vibration frequency was shown to be a severe limit. This raises the question whether the requirement of "stiff" blades can be abandoned, and the eigenfrequency ω<sub>e</sub> can be allowed to lie below the second speed harmonic, 2ω.

73. Such "flexible" blades inherently display a strong resonance during start-up and run-out when the momentary shaft speed ω becomes equal to ω<sub>e</sub>/2. The excitation is due, as pointed out by Kellenberger [6], to the combined effect of the shaft unbalance and the anisotropy of the bearings, causing the blade roots to move along elliptic paths rather than pure circles around the axis.

74. For the analysis it suffices to consider the first bending mode and to model the blade by a single-mass oscillator as shown in Figure 7. The mass m is positioned at the extremity of a flexible beam of length l and shall have, at rotor speed ω, the eigenfrequency ω<sub>e</sub>. The blade damping shall be proportional to deflection velocity and characterized by the logarithmic decrement D.

75. During each revolution, the rotor center completes an ellipse characterized by two half-axis a and b (where a > b), usually moving in the same sense as the rotation.

76. If the blade deflections are small and the angle φ is used to describe the motion of the blade, cf. Figure 7, the vibration was shown to obey an inhomogeneous differential equation of the Mathieu type

$$\ddot{\phi} + 2\omega_e D \dot{\phi} + [\omega_e^2 + \omega_n^2 \frac{a-b}{2l} \cos(2\omega_n t + \psi - \phi_2)] \phi = \omega_n^2 [\frac{a+b}{2l} \sin(\phi_1 - \psi) - \frac{a-b}{2l} \sin(2\omega_n t + \psi - \phi_2)] \quad (37)$$

with ψ defining the position of the blade with respect to a reference point on the rotor periphery. φ<sub>1</sub> and φ<sub>2</sub> are constants related to the inclination of the ellipse.

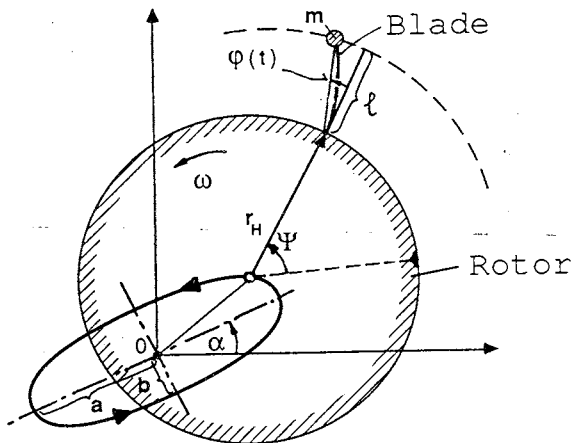


Fig. 7 Blade root excitation by elliptic vibration of rotor center. Stability plot [6] of Eq. (37).

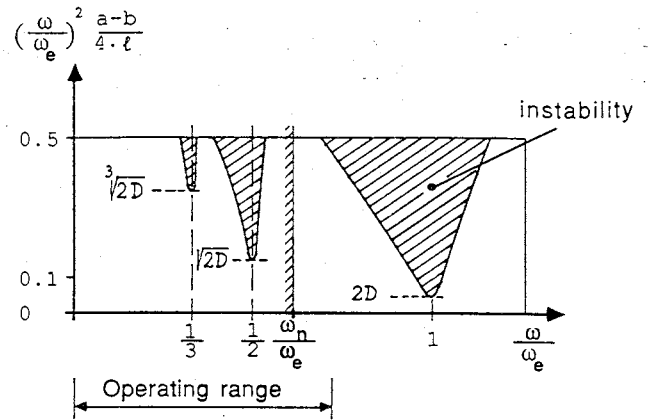


Fig. 8 Stability plot [6] of Equation (37)

77. The stability of the system depends on the combined effect of root excitation and blade damping. Solution of Eq. (37) leads to the stability chart given in Figure 8 [6] where the abscissa is proportional to rotor speed and the ordinate to the excitation amplitude.

78. It is seen that the most dangerous instability occurs around ω = ω<sub>e</sub> and therefore lies outside the range of operation (0 < ω < 1.15 ω<sub>n</sub>). Further instabilities occur at ω = ω<sub>e</sub>/2 and ω = ω<sub>e</sub>/3, provided the damping is sufficiently small. The critical damping at ω = ω<sub>e</sub>/2 is given by

$$D_{crit} = \frac{1}{2} \left( \frac{a-b}{8l} \right)^2 \quad (38)$$

yielding D<sub>crit</sub> ≈ 2 · 10<sup>-9</sup> for pessimistic values like a - b = 0.2 mm and l = 400 mm. The actual damping of free-standing blades is of the order of D = 0.001 to 0.010. Therefore instabilities within the range of operation can be clearly outruled.

79. There remains to be considered the amplitude of quasi-steady resonance vibration during start-up and run-out when ω<sub>n</sub> = ω<sub>e</sub>/2 is crossed. The center-of-gravity linear vibration amplitude lφ<sub>0</sub> is found to be

$$l\phi_0 \approx \frac{a-b}{16D} \quad (39)$$

80. It appears that in case of low damping and large unbalance significant amplitudes can arise while the rotor is accelerated through the neighbourhood of the resonance speed. With D = 0.005 and a - b = 0.1 mm, which are realistic values, the amplitudes are of the order of 1.2 mm, by no ways negligible. A minimum safety requirement would be a rapid crossing of the resonance range in order to avoid damage by blade fatigue.

81. One can conclude that "flexible" free-standing blades of first bending frequencies (ω<sub>e</sub>/2π) below the two-fold rotation frequency 2(ω<sub>n</sub>/2π), if combined with sufficient damping, are a promising option in extending the flow capacity of LP last stages.

82. In the X vs S diagram, Figure 5, this has the effect of moving the blade frequency limit to higher X values. The limit line for steel or titanium has been calculated by lowering the minimum permissible eigenfrequency ω<sub>e</sub> from 2.2 ω<sub>n</sub> to 1.4 ω<sub>n</sub>. Even for the highest blade number considered, N<sub>B</sub> = 75 t, the limit is found to be

virtually removed from the field shown in Figure 5. (At  $X = 2.9$  the limit is  $S = 18.5 \text{ m}^2$  and at  $X = 3.0$  it is  $S = 15.0 \text{ m}^2$ .)

CONCLUSIONS

83. The maximum last-stage surface area compatible with any given nominal shaft speed has been shown to be limited by a number of mechanical and aerodynamic considerations. For full-speed 50-cycle turbines about  $S = 11 \text{ m}^2$  can be achieved with steel rotor blades and about 12 to 16  $\text{m}^2$  with titanium blades. In the steel case, the most severe limit is an aerodynamic one. In the titanium case blade frequency and erosion are the main restrictions.

84. At current technology, the maximum area can be achieved with tip-to-hub diameter ratios about 2.1 to 2.3.

85. In order to increase the area limit further, several constraints have to be eased simultaneously. In order to fully benefit from the aerodynamic improvements offered by titanium or plastic composites, the erosion and blade-vibration problems require severe attention.

86. The vibration limits can be eased by decreasing the number of rotor blades (and increasing their profile chord accordingly) or by admitting "flexible" blades which have a first bending-mode frequency below twice the running speed, or by using part-span shrouds.

87. Sandwich-type fabricated hollow steel blades could bring about the same effect as solid titanium blades. In case of titanium, the higher stiffness of hollow blades brings no further advantages.

87. In view of the other limitations, a further increase of rotor disc stress levels has comparatively little effect on the achievable maximum area.

88. With titanium blades and greatly eased vibrational and erosional restrictions the optimum tip-to-hub diameter ratio would slightly increase (to about 2.3 to 2.5 for an area in the range of 14 to 16  $\text{m}^2$ ). Simultaneously, alternative designs of large diameter ratios (of about 3) would become mechanically feasible.

89. Composite plastic blades, if not erosion resistant, are not attractive for full-speed machines. On very slow shafts (1/3 or 1/4 speed) they offer the chance of very large areas in a single exhaust. Such high-X designs would require an important aerodynamic development aimed at high reaction in the tip cascade and a generally high Mach number level.

90. All limit conditions define the area  $S$  in terms of the product  $\omega^2 S$ . Therefore the conclusions can be fully transferred from 50-cycle to 60-cycle machines or to units running at half speed or less, by scaling all linear dimensions inversely to shaft speed.

REFERENCES

[1] Traupel, W.: "Thermische Turbomaschinen", Vol. II, 3rd Ed. Springer, Berlin-Heidelberg-New York, 1982

[2] Seippel, C.: Dampfturbinengruppe für grosse Leistungen, Swiss Patent No. 424 810 (Appl. 8. Sept. 1964)

[3] Wallon, M.: Last-Stage Blading: A Key Factor in Steam Turbine Development Alsthom Review Nr. 9, Dec. 1987, pp. 3-16.

[4] Krzyzanowski, J. & Weigle B.: Toward the Criterion of Erosion Threat of Steam Turbine Blading through the Structure of the Droplet Stream, Trans. of IFFM, Nr. 71/72, Gdansk, 1976

[5] Deych, M.E., and Troianowski, B.M.: "Untersuchung und Berechnung axialer Turbinenstufen". VEB Verlag Technik, Berlin, 1973

[6] Kellenberger, W: Double-frequency forced vibration of turbine blades due to an elliptical orbit of the rotor. Mech E Conf. Publ. 1984-10, London (1984)

NOTATION

a	major half axis of rotor-path ellipse
A	disc shape influence function
b	minor half axis of rotor-path ellipse
B	disc shape influence function
c	blade chord
C	constant of the cascade geometry criterion Eq. (25)
D	damping decrement
E	Young's modulus of elasticity
f	cross sectional area of blade profile or shaft
G	constant of the blade vibration criterion, Eq. (23)
$\Delta h$	static enthalpy drop (no index: of entire stage)
i	number of parallel LP flows
J	section moment of inertia
$K_e, K_\omega$	numerical constants of the beam eigenfrequency equation
l	equivalent beam length of single-mass system
L	blade length (span)
m	equivalent blade mass
M	Mach number
$N_B$	number of rotor blades per row
Q	exit volume flow rate
r	radius
R	reaction grade
S	annular exit-surface area
t	blade pitch
u	peripheral speed
V	function of the blade vibration criterion
X	hub-to-tip radius (and diameter) ratio
Y	disc thickness
$\alpha$	cascade compactness ratio, Eq. (8)
$\beta$	angle of blade vibration direction with respect to rotor periphery
$\delta$	blade profile thickness
$\nu$	elastic contraction coefficient
$\rho$	density
$\sigma$	tensile stress
$\varphi$	deflection angle of vibrating mass
$\omega, \omega_n$	rotor angular speed (arbitrary and nominal)
$\omega_e, \omega_{eo}$	circular eigenfrequency of blade vibration (with and without rotor rotation)

INDICES

B	blade material
corr	corrected to $\omega_n = 314.2 \text{ rad/s}$
D	disc material or disc periphery
H	hub (rotor periphery)
r	radial component
t	tangential component
T	blade tip
-	mean value
0,1,2	planes upstream, between and downstream of stator and rotor blade row



## 7. Advanced nuclear turbines for large output

T. HIRABAYASHI, BSc(Eng), A. OHJI, BSc(Eng), A. SUZUKI, MSc(Eng) and S. NAGAO, BSc(Eng),  
Toshiba Corporation, Japan

An advanced large nuclear turbine suitable for 1,300-1,500 MW has been successfully developed for use in the 1990's and beyond. The last stage blade is 52-inch long, with efficient transonic profiles. Monobloc low-pressure rotors will bring higher reliability and maintainability compared with conventional shrunk-on rotors. Various countermeasures against water droplet attack are also applied to the new turbine for reduction of blade erosion and improvement in reliability.

### INTRODUCTION

Since the introduction of light-water reactors, remarkable progress has been achieved with nuclear power generation systems, realizing high levels both of security and availability. Based on the accumulation of technological experience, the next steps of development have been started, not only for reactors but also for turbine plant, aiming at further improvements in efficiency, reliability, operational flexibility and maintainability. To meet the above requirements, Toshiba has recently developed a large-capacity nuclear turbine with a power output of 1,300-1,500MW, incorporating various advanced technologies. Fig.1 shows a cross-section of the new turbine, which consists of a double-flow HP cylinder and 3 double-flow LP cylinders arranged in tandem.

The last stage blade (LSB) is one of the key-parts of a steam turbine from the viewpoint of both unit capacity and thermal efficiency. A newly developed 52-inch LSB is one of the longest in the world, and has efficient transonic blade profiles, bringing an improvement in unit thermal performance. Aerodynamic and mechanical characteristics have been fully checked, using a model turbine and a full-scale rotating test wheel.

The low-pressure rotor of the new turbine weighs about 280 tons. By using monobloc rotors instead of those using shrunk-on discs,

significant improvements in reliability and maintainability can be obtained, because the stress levels in the rotor are decreased, stress corrosion cracking at the key way, sometimes found with shrunk-on discs, are eliminated, and the rotor vibration level is considerably reduced.

Various countermeasures against droplet erosion of the LSBs are incorporated in the new turbine. Elaborate experiments have been made in the model turbine both to investigate the wet steam flows in a nuclear turbine and to verify several protection systems such as drain extractions. The application of a reheat cycle, with moisture separator reheaters installed upstream of the LP cylinders also contributes to the reduction of droplet erosion.

This paper gives details of the development of the above techniques, applied to the new turbine.

### 52-INCH LAST STAGE BLADE

#### (a) Principal features of the 52-inch blade

The last stage of a nuclear turbine contributes more than 10 percent of the overall turbine output, and the exhaust annulus area of a LSB determines the maximum steam flow rate. The exhaust area also controls the magnitude of the exhaust losses, which have a considerable

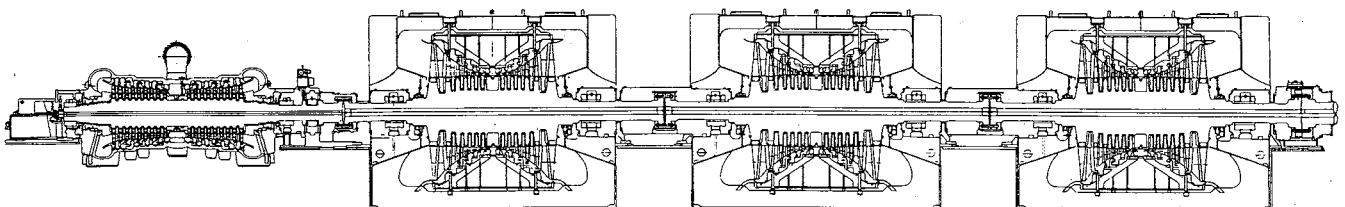


Fig.1 Cross Section of 1300-1500MW Nuclear Turbine



Fig.2 52-inch LSB Test Wheel

effect on plant efficiency. For these reasons, it becomes essential, for increasing the unit capacity and improving the thermal efficiency of power plants, to develop a LSB with larger exhaust area and higher efficiency. To cater for this requirement, Toshiba has developed a 52-inch last stage blade with high efficiency and reliability for 4-pole units (Fig. 2). This LSB is one of the largest in the world with respect to blade length and exhaust area. The table below shows the main particulars of the 52-inch LSB in comparison with current 41-inch and 43-inch Toshiba LSBs.

Blade, in.	52	41	43
Speed, rpm	1500/1800	1500	1800
Length, mm	1320	1041	1092
Ann.Area, m <sup>2</sup>	16.7	11.5	11.5

Owing to its large exhaust annulus area, which is approximately 1.5 times that of current 1,500 rpm 41-inch or 1,800 rpm 43-inch LSB, the 52-inch blade provides several important benefits, as follows:-

-Increase in unit capacity

Applying the 52-inch LSB to the TC6F (tandem compound 6 flows) type of turbine, which is one of the standard configurations for large nuclear power plants, the unit power can be increased by more than 30 percent compared with the TC6F turbine using 41-inch or 43-inch LSB, permitting the economical construction of nuclear power turbines of capacity 1,300 1,500 MW, and even up to 1,800 MW.

-Improvement in turbine efficiency

A distinct improvement in plant heat rate

is attainable, as the large annulus area decreases the exhaust steam velocity, resulting in a reduction of exhaust energy losses. In addition, a significant increase in turbine internal efficiency is expected owing to the better efficiency of the 52-inch last stage brought about by improved blade profiles. The overall gain in unit efficiency compared with a TC6F-41-inch turbine exceeds 3 percent.

During the development of the 52-inch LSB, updated technologies for numerical analysis and verification tests were fully utilized. The key items of the development processes are described below.

(b) Aerodynamic performance

The first step of the aerodynamic design is to analyse the three-dimensional flow pattern, which specifies flow conditions such as steam velocity and flow angle at the inlet and outlet of the LSB. The blade profile at each section of the 52-inch LSB has been designed to meet those flow conditions. The profile design must satisfy, at the same time, the mechanical requirements of stress caused by the centrifugal force, and the vibration characteristics, so that optimization of the design has to be done iteratively.

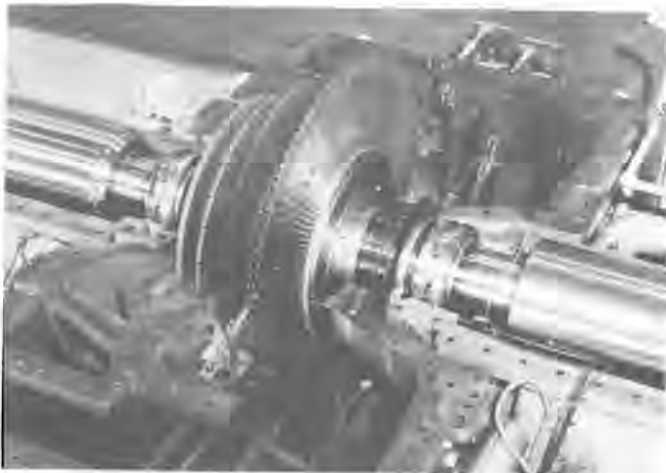
The flow characteristics around the 52-inch LSB are typical of those for large LSBs, for instance, subsonic inlet and supersonic outlet relative velocities at each cross section. To achieve these transonic flows with minimum aerodynamic losses, blade profiles have been carefully optimized. Of particular note is the form of the blade near the tip section, where the outlet Mach number exceeds 1.5. A transonic profile is employed, with a convergent-divergent flow passage, having an essentially flat form with reverse curvature of the suction surface, so that only weak edge shocks are produced, and maximum profile efficiency is achieved.

The advantages of the developed profile have been verified in a two-dimensional cascade tunnel designed to operate with steam as the working fluid. Extensive use is made of Schlieren photography to establish the shock wave patterns under supersonic conditions.

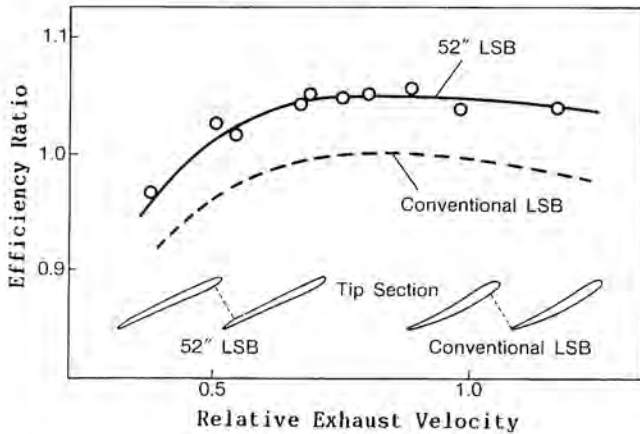
The final proving of the overall efficiency of the 52-inch last stage has been carried out by the use of an accurately scaled model low pressure turbine (Fig. 3 (a)). The similarity of aerodynamic and thermodynamic conditions between the model and the actual machine is accurately maintained by operating the model at the same blade peripheral speed as the full-size turbine. The stage efficiency of the new 52-inch blade has been verified to exceed conventional LSBs by more than 5 percent, owing to the transonic profiles and the advanced design methods (Fig. 3 (b)).

(c) Mechanical Reliability

Because of the large blade length and the high rotational speed, large centrifugal forces act on LSBs. The first step in the structural



(a) Model Turbine



(b) Measured Efficiency

Fig.3 Test Performance of 52-inch Last Stage

design is to check the mean centrifugal stress to be sufficiently low compared with the material strength. Stress analyses are then performed, using a three-dimensional finite element method to confirm that the local stresses do not exceed those permissible at any point. The strength of the fork type fastening is also theoretically and experimentally checked.

In addition to the centrifugal stresses, the LSB experiences alternating stresses caused by blade vibration during operation. Excitation forces of the flow increase, especially under low load or high exhaust pressure, as the aerodynamic conditions around the blades deviate significantly from design point. Vibration stresses acting on the blades over a wide operating range have been investigated in the low pressure model turbine of Fig. 3 (a). In Fig. 4 measured vibration stresses of the blades are plotted against exhaust Mach number, which is dependent on load, for both loosely-connected and rigidly-connected blades, with two lacing wires. The vibration stresses of blades with both types of connection increase in the low load region below Mach numbers of 0.2-0.3, due to the turbulent flow around the blades. Even in such conditions, the maximum stress of the loosely-connected blades is observed to be

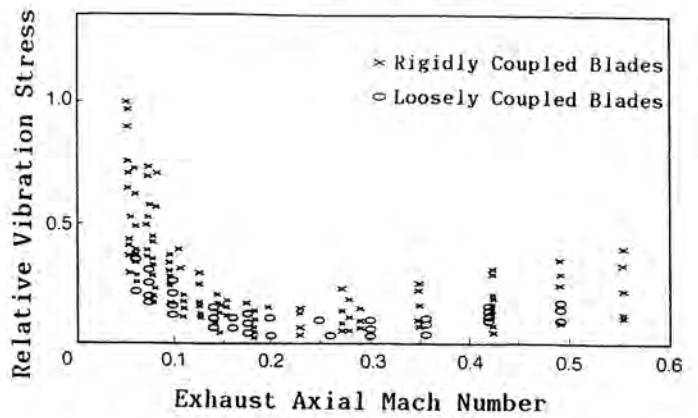


Fig.4 Measured Vibration Stresses at Different Loads

significantly lower than that of the rigidly-connected blades, owing to the enhanced mechanical damping. For the structural design of the 52-inch LSB, the loose connection with two lacing wires is adopted, to minimize the flow-induced vibration under low load or high exhaust pressure operation.

To verify the overall reliability of the 52-inch LSB, a rotational vibration test was finally conducted using full-size blades mounted on a test wheel (Fig. 2). It has been confirmed that the blade is appropriately tuned to avoid resonance at the both operating speeds of 25 rps (1,500 rpm) and 30 rps (1,800 rpm), as shown in Campbell diagram in Fig. 5.

MONOBLOC LP ROTOR

The low-pressure rotors of the new turbine have a body diameter of 2,800 mm and a weight of approximately 280 tons. Though such large rotors had traditionally been built by

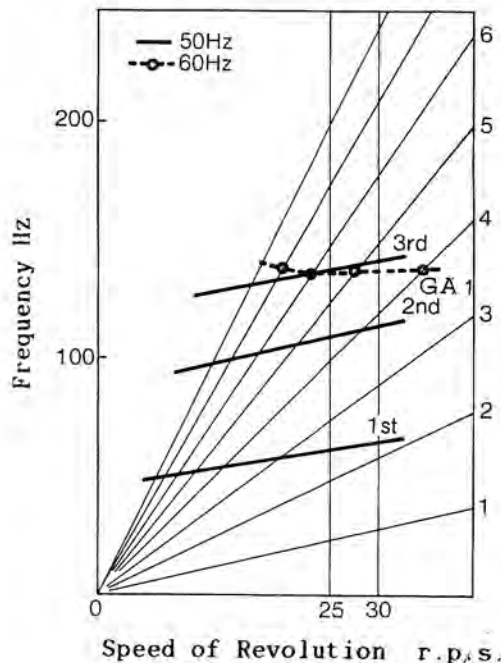


Fig.5 Campbell Diagram of 52-inch LSB



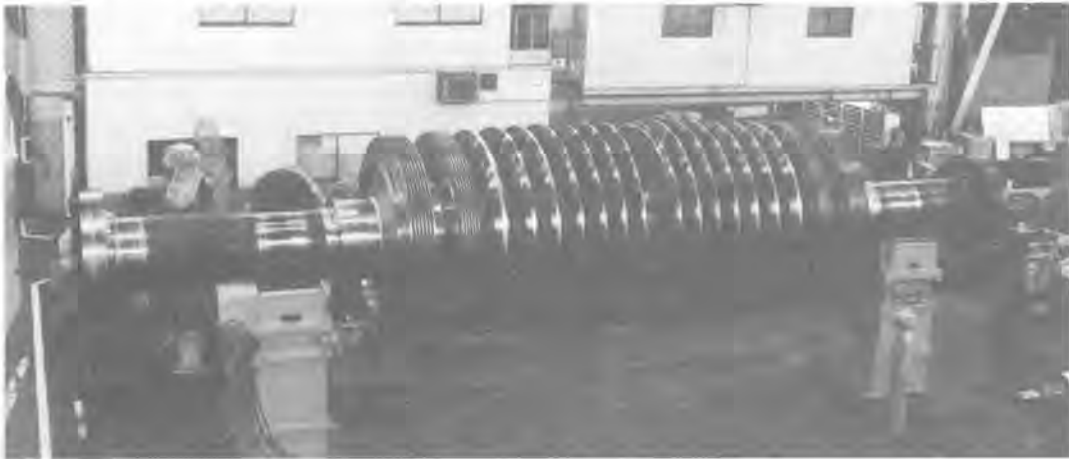


Fig.6 Monobloc Rotor for 1100MW Turbine

shrinking wheels on to shafts, recent progress in the steel making process has enabled the manufacture of very large monobloc rotors. Toshiba has experience of more than 10 monobloc rotors for LP cylinders of large half-speed turbine units. Fig. 6 shows, as an example, a manufactured monobloc rotor for a 1,100 MW nuclear turbine, with a body diameter of 2,600 mm, overall length of 12,000 mm, and weight of 270 tons.

(a) Advantages of Monobloc Rotors

The application of monobloc LP rotors for a large nuclear unit brings the following important benefits of reliability and maintainability, compared with built-up rotors:-

-Simple structure

A complex structure composed of a shaft with many wheels, and keys and couplings can be

simplified to comprise only one component. There is then no possibility of relative displacement between adjacent parts, such as a rotational displacement between a coupling and the shaft due to an impact torque.

-Reduction of stress levels

The maximum stress in the rotor is reduced in the monobloc rotor, since the high stress at the wheel bore of a built-up rotor is avoided. Stress concentration at the keyways is also eliminated.

-Elimination of keyway cracking

Stress corrosion cracking has been found at the keyways of shrunk-on wheels under certain combinations of stress level, material and steam conditions. The monobloc rotor avoids this problem because it has no keyways.

-Improvement of rotor vibration

Rotor vibration levels are considerably reduced by replacing a built-up rotor with one of monobloc construction. Fig. 7 compares field data of vibration levels of the two types of LP rotor of a 1,100 MW unit at full load, and clearly shows this improvement.

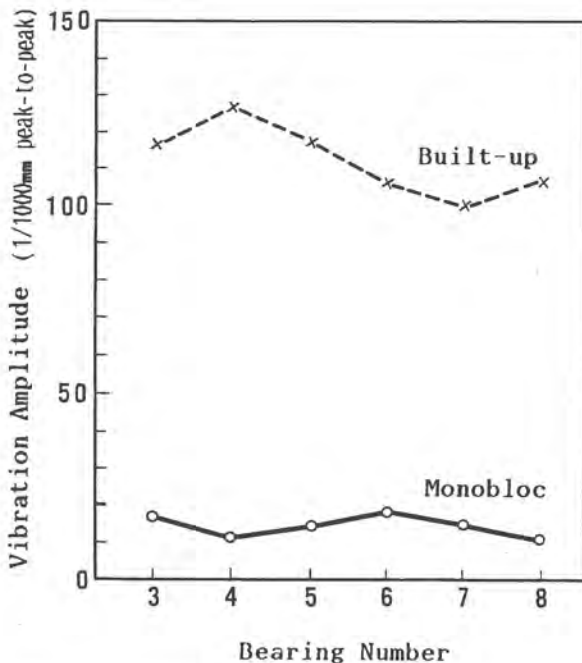


Fig.7 Shaft Vibration of Monobloc and Built-up Rotors

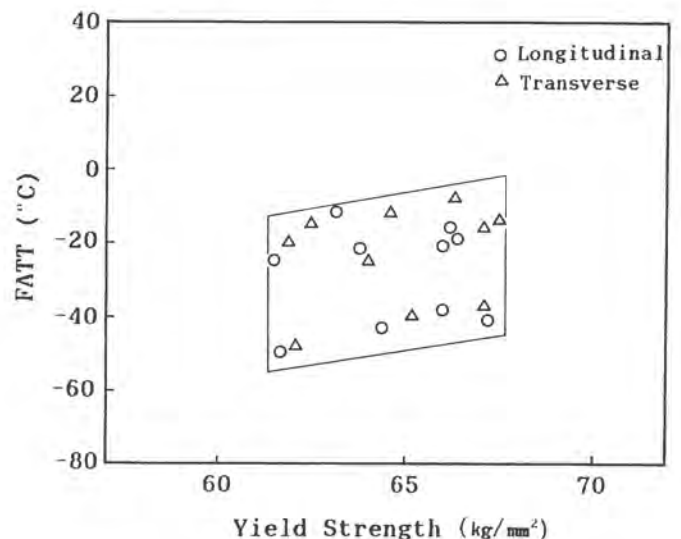


Fig.8 Yield Strength vs FATT at the Bore of Monobloc Rotors

-Improvement in maintainability

The low vibration level of the monobloc rotor has not necessitated any field balancing. Inspection of keyways is also unnecessary.

(b) Development of the monobloc rotor

Toshiba has since 1975 developed manufacturing techniques of very large monobloc rotors with steel makers. Advanced technologies at each step of the steel-making process have led to success in producing these large rotors. These techniques are briefly reviewed:-

-Melting process

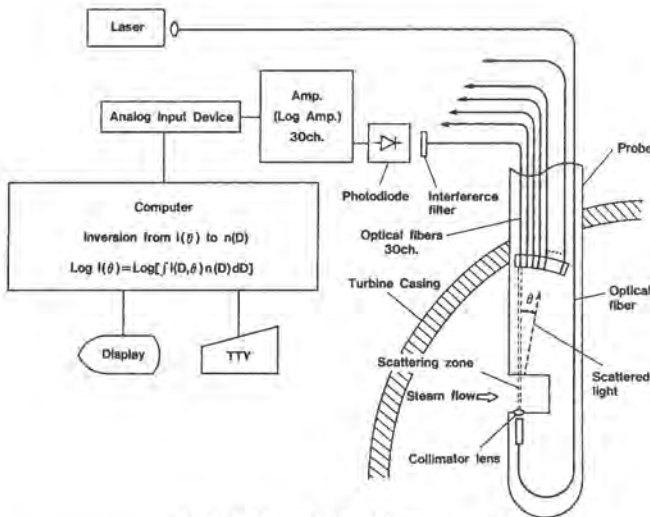
To make large ingots of over 500 tons, multiple charges of steel or ladle refining furnaces are utilized.

-Pouring process

A high quality ingot with fine microstructure and low Si-content is obtained by adopting a vacuum carbon deoxidization.

-Forging process

A high power press with a capacity up to 10,000 tons is effective for ensuring homogeneous mechanical properties throughout the ingot.



(a) Schematic Diagram



(b) Probe in Model Turbine

-Heat treatment

By multiple annealing and water-spray quenching, a fine microstructure and high toughness are obtained.

-Inspection

Developments in inspection methods, such as ultrasonic inspection from the center bore and outer surface, also contribute to the improvement in rotor quality.

The monobloc rotors manufactured show homogeneity in their metallurgical structures and mechanical properties throughout the large body. Fig. 8 illustrates the yield strength vs. FATT of the material obtained from the bore of the 3-3.5NiCrMoV monobloc rotors for 1,100 MW turbines.

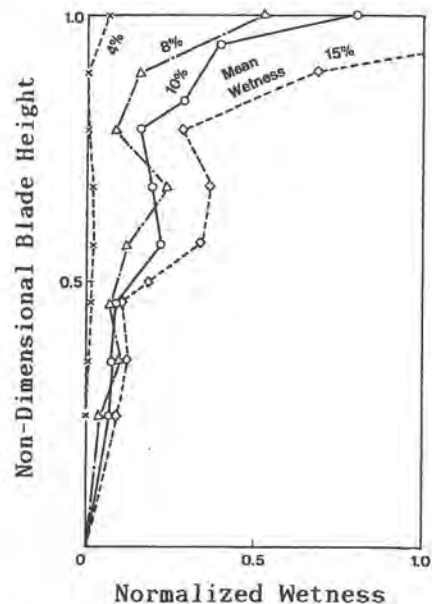
The low pressure rotor of the present 1,300-1,500 MW turbine has a weight of 280 tons, which is approximately the same as the 1,100 MW rotor of Fig. 6, and is therefore well within the feasible range.

COUNTERMEASURES AGAINST EROSION

(a) Investigation of wet steam flow

For the large LSBs, especially of nuclear-power turbines, adequate protection against droplet erosion is required because of the high peripheral speed and the relatively high value of steam wetness. Investigations were made firstly of the behaviour of wet steam flow in a turbine stage, using the model turbine of Fig. 3 (a).

An optical device has been introduced for measurements of droplet size and mass distribution utilizing a laser beam and a light scattering theory. Fig. 9 (a) shows the principle of this device, where a parallel laser beam is directed through the wet steam



(c) Measured Wetness Distribution

Fig.9 Droplet Measurement with an Optical Probe



## 8. Steam turbines for nuclear power stations in Czechoslovakia and their use for district heating

J. DRAHÝ, ME, CSc, ŠKODA-Works, Plzeň, Czechoslovakia

The first generation of nuclear power stations is equipped with 440 MW<sub>e</sub> pressurized water reactors. Each reactor supplies two 220 MW, 3000 rpm condensing type turbosets operating with saturated steam. After the completion of heating water piping systems, all of the 24 units of 220 MW in Czechoslovak nuclear power stations will be operated as double-purpose units, delivering both electricity and heat.

At present time, second-generation nuclear power stations, with 1000 MW<sub>e</sub> PWRs, are being built. Each such plant is equipped with one 1000 MW full-speed saturated steam turbine. The turbine is so designed as to pursue the extraction of steam corresponding to the following quantities of heat:

- 893 MJ/s with three-stage water heating (150/60 °C)
- 570 MJ/s with two-stage water heating (120/60 °C),

the steam being taken from uncontrolled steam extraction points.

### INTRODUCTION

1. The construction of power stations with condensing turbines in Czechoslovakia after World War II was characterized by two typical features. Firstly, the utilization of the rich resources of low-grade brown coal, and secondly the use of standardized unit ratings. To cater for the over-increasing total output required, fossil-fuelled power stations have been built with the following unit ratings:

- 6x 55 MW, non-reheat
- 6 x 110 MW and 4x 200 MW with reheat, using sub-critical initial steam conditions.

2. The development of thermal power engineering culminated (and was simultaneously terminated, toward the end of the seventies), in the entry into operation of a 500 MW power unit with steam conditions of 162 bar and 535/535 °C, operating with sliding pressure. Since that time no fossil-fuelled power stations have been built in Czechoslovakia.

3. In the early eighties, in consequence of some new requirements (enhanced utilization of primary fuel, and due account of ecological factors), interest in extending centralized long-distance delivery of heating water for the purposes of district heating was markedly increased.

4. While some 55 MW condensing units were decommissioned, the majority of them were reconstructed to serve as dual-purpose units, delivering both electricity and heat in conformity with local requirements. The modifications necessary were carried out after reaching the lifespan of the principal turbine components, that is after an average of 180 000 working hours.

5. Presently undergoing reconstruction are 110 MW steam turbines, which have reached the expiration of their operational lifespan. All of the turbines are being renovated, and are modified to provide better thermodynamic

efficiency and to allow of extracting heat for centralized district heating up to an output of 162 MJ/s with three-stage heating to 150 °C of the district heating water.

6. The urgent need large amounts of heat in some locations also necessitated reconstruction of the 200 MW turbines, which have not exhausted their design life, in order to allow of their use for combined production of electricity and heat. The first of such reconstructions, expected to supply heat extractions up to 260 MJ/s with three-stage heating of the district heating water, are to be in service in the early nineties.

7. The construction of further power stations in Czechoslovakia is based on the use of nuclear fuel. The first generation of nuclear power stations is equipped with 440 MW<sub>e</sub> pressurised water reactors produced in Skoda Concern Enterprise in conformity with Soviet designs. Eight such reactors are in operation and another four are under construction. Each reactor supplies two 220 MW, 3 000 rpm condensing-type turbosets operating with saturated steam. Since 1981 there have been brought into operation successively sixteen 220 MW units in two power stations; the last of the 220 MW series of turbines will be delivered for the third power station in 1991. Extraction of heat for district heating has been stipulated as an additional requirement.

8. At present time, second-generation nuclear power stations, with 1000 MW<sub>e</sub> PWRs, are being built. Each such plant is equipped with one 1000 MW full-speed saturated steam turbine. Again, one of the important requirements imposed is four the maximum possible heat extraction for district heating purposes. The locations for these nuclear power stations are chosen with due account of the possibility of utilizing the extracted heat.

Table 1

<u>Turbine</u>	
Power output at generator terminals (MW)	220
Admission steam pressure (bar abs.)	43,2
Temperature of saturated admission steam (°C)	256
Steam mass flow into HP cylinder ( t/hr)	1 356
Reheat temperature into LP cylinders ( °C)	216
Inlet pressure to the LP cylinders (bar abs.)	4,6
LP cylinders exhaust pressure at a cooling water temperature of 20 °C (mbar abs.)	53,5 / 68,4
Number of cylinders (1 HP + 2 LP)	3
Last stage blade length (mm)	840
Final feedwater temperature ( °C)	222
Rotational speed (rpm)	3000
<u>Feedheating plant</u>	
Number of LP heating stages	6
Number of HP heating stages	2

The delivery of the 1000 MW steam turbine for Temelín nuclear power station in Southern Bohemia will be completed in 1990. Subsequent installation of 12 steam turbines of this rating for Czechoslovak power station is programmed to proceed until 2010, the time intervals between individual turbines ranging from 18 to 24 months.

9. Greater details concerning both types of saturated-steam 3000 rpm turbines are given in the following sections.

#### 220 MW saturated-steam turbine

10. The principal parameters of this turbine are shown in table 1, together with leading particulars of the thermal layout (1).

11. The three-cylinder turbine consists of one double-flow HP cylinder and two double-flow LP cylinders. Setional view of the turbine is shown in fig. 1. Inlet steam control is achieved by two assemblies of valves, arranged symmetrically one on each side of the HP cylinder, each assembly consisting of one quick-closing stop valve and two governing valves.

12. The double-flow HP cylinder contains six impulse-type stages in each flow and, compared with the alternative single-flow arrangement, its design is more advantageous from the viewpoint of symmetrical steam outlet into the moisture separators: At outlet from the HP cylinder the steam pressure is 4,9 bar and the wetness is 12 %. The moisture separator reheaters reduce the steam wetness to 0,5 %. Followed by reheating of the steam in two stages, first by steam tapped from extraction point VII and secondary from extraction point VIII (see fig. 3) to temperature of 216 °C.

13. In order guard against adverse effects of the wet steam at relatively high pressure, the following measures have been adopted in the HP cylinder:

- welding of stainless-steel sealing strips at the horizontal points of both halves of the cylinder and of the diaphragms
- bolting together of both halves of the diaphragms to increase the contact pressure at the horizontal joint
- bolting of the diaphragms together in pairs, increase the contact pressure on the face sealing surface

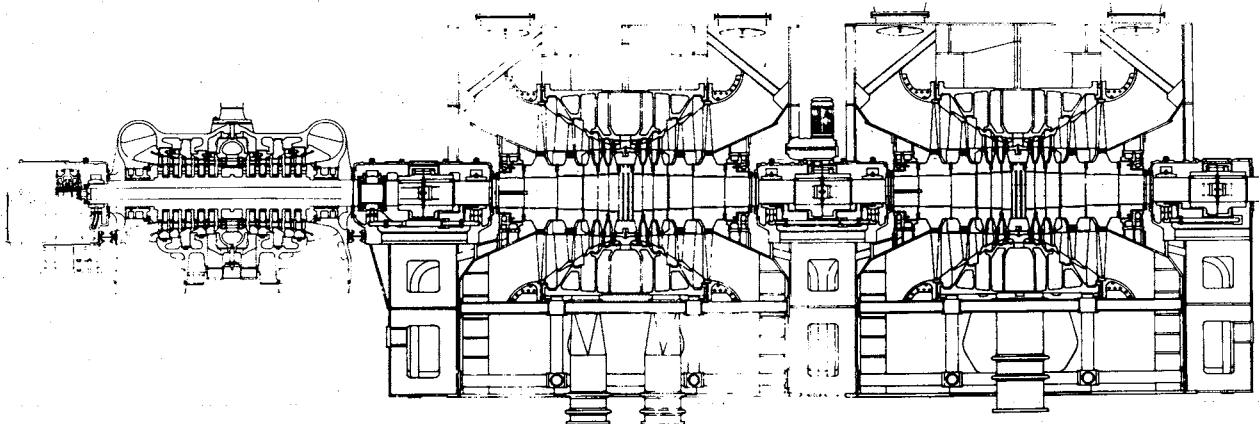


Fig. 1. 220 MW saturated steam turbine

Table 2.

Power station	Number of heating stages	Heat output MJ/s	Heating water temperature °C	Extraction point			
				III.	IV.	V.	VI.
I. Jaslovske Bohunice 8x 220 MW	2	60	70/150	-	-	yes	yes
II. Dukovany 8x 220 MW	3	85	70/144	yes	yes	yes	-
III. Mochovce 8x 220 MW	2	90	70/130	yes	-	yes	-
	3	120	70/150	yes	-	yes	yes

- removing the separated water by providing drain slots in the diaphragms.

14. The two double-flow LP cylinders with five stages in each flow, are almost identical, considered from the viewpoint of steam parameters and design, to the LP cylinders of a 500 MW condensing-type steam turbine designed for a fossil-fuelled power station. The built-up LP rotor consists of a shaft and discs with moving blades, the discs being shrunk on to the shaft after induction heating. In order to reduce the notch effect in torque transmission between discs and shaft, radial keys are provided.

15. The last stage blade with a length of 840 mm has undergone extensive experimental investigation in both - design and off - design - operating conditions and is in service in almost 30 units of output 200 MW in fossil-fuelled plant. Two rows of titanium-alloy dumping wire ensure circumferential binding of all the blades to form one assembly the blades. The blades of the penultimate are of very rugged design. These blades are free, without binding wire and are designed with tuned resonant frequencies, in order to withstand safety corrosion fatigue when operating near the Wilson line.

16. Fig. 2 shows the blading of 220 MW LP turbine rotor



Fig. 2. The blading of a 220 MW LP turbine rotor

#### Steam extraction from 220 MW turbines

17. In conformity with the customer's technical specification, the 220 MW turbine has been designed as a purely condensing unit, with uncontrolled steam extraction for the purpose of feed water heating.

18. The requirements for additional heat extraction for district heating purposes have been conceived when the first 16 turbines were in service or in an advanced stage of manufacture. A diagram of possible arrangements for steam extraction, for retrofitting of water heaters, is shown in fig. 3. The particular steam extraction points being tabulated below.

19. In determining extraction heat outputs and heating water temperature, both the requirements imposed by customers, and the limiting criteria have been taken into account. These include:

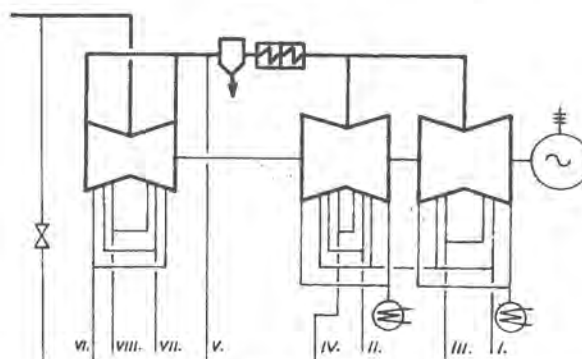


Fig. 3. Diagram of arrangement of uncontrolled steam extraction points for the 220 MW turbine

TURBINE DESIGN AND OPERATIONAL EXPERIENCE

- a) steam velocity in the extraction piping
- b) loading of the diaphragm and of the moving blades in the vicinity of the steam extraction point
- c) volumetric rate of flow through the last LP stage considered from a viewpoint of preventing windage and back-flow.

20. In power stations denoted by I and II in table 2, an additional requirement for heat extraction has been considered that is without any changes being made to the turbine.

21. The heating water piping from power station I to the town of Trnava situated 18 km away, is completed.

21. Power station II will deliver heat to the town of Brno (45 km away); the design of the district heating water system is in progress.

22. The ratio of the extracted heat to the lost electricity ranges between 5,88 and 7,14, depending on the extraction points and the uniformity of the water temperature rises in the individual heating stages.

23. After the completion of the heating water piping systems all of the 24 units of 220 MW in Czechoslovak nuclear power stations will be operated as double - purpose units, delivering both electricity and heat.

1000 MW saturated - steam turbine

24. The following table 3. presents the principal technical parameters of the 1000 MW full-speed saturated - steam turbine and its thermal cycle. (2)

Table 3.

<u>Turbine</u>		
Nominal power output at generator terminals	(MW)	1000
Admission steam pressure	(bar abs)	56
Temperature of saturated admission steam	(°C)	273,3
Admission steam wetness	(%)	0,5
Steam mass flow from steam generators	(t/hr)	6060
Steam mass flow into HP cylinder	(t/hr)	5495
Reheat temperature into HP cylinder	(°C)	251
Reheater outlet pressure	(bar abs.)	7,9
LP cylinder exhaust pressure at a cooling water temperature of 21° C	(mbar abs.)	71
Number of cylinders	(1 HP + 3 LP)	4
Last stage blade length	(mm)	1085
Final feedwater temperature	(°C)	221
Rotational speed	(rpm)	3000
<u>Feedheating plant</u>		
Number of LP heating stages		4
Number of HP heating stages		1
Number of parallel LP regenerating lines		3
Number of parallel HP regenerating lines		2
<u>Condensing plant</u>		
Number of condensers		3

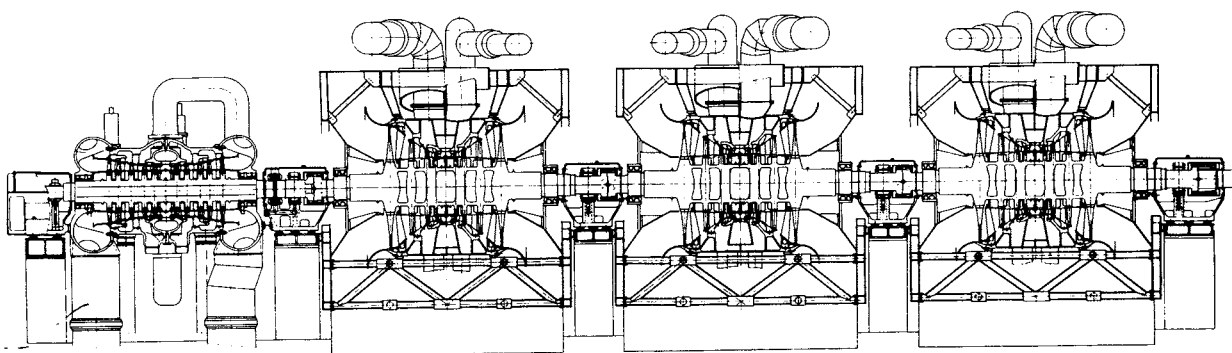


Fig. 4. 1000 MW, 3000 rpm saturated steam turbine

25. Fig. 4 shows a longitudinal sectional view of the steam turbine, consisting of one double-flow HP cylinder and three double-flow LP cylinders. The turbine is throttle-controlled. Each of the four valve assemblies, situated symmetrically two on either side of the HP cylinder, consists of one quick-closing stop valve and one governing valve. The electro-hydraulic control system uses mineral oil at a pressure of 48 bar, but the design allows a changeover to a fire - resistant fluid.

26. Each flows in the HP cylinder consists of 5 stages, using the same blade profile. Diaphragms, and the outer and inner cylinder castings, are made of 13 %-Cr stainless steel. The moving blades of all HP stages are derived from a reference blade, i.e. from the last HP stage having a length of 330 mm, which is for earlier stages successively shortened down to a length of 120 mm for the first HP stage. Each row of the HP cylinder develops an output of 41 MW, and the robust moving blades are electron-beam welded into packets and are carried on the rotor by means of finger-type roots. Welded shrouds are machined to provide labyrinths which function as effective circumferential seals.

27. From the HP cylinder the steam enters two horizontal separator reheaters situated at engine room floor level on each side of the LP cylinders. Single-stage reheat, using live steam 56 bar, is employed.

28. The double-flow LP cylinders have rotors welded from discs of constant - strenght profile, and shaft ends. There are 4 stages in each flow, with root diameter decreasing from 1850 mm for the first stage to 1750 mm for the last stage. The welded joint connecting the discs has an outside diameter of 1200 mm. The moving blades of the first two stages are fastened to the discs using finger-type roots, while these of the third and fourth LP stages use circular side-entry fir-tree roots.

29. The moving blades of the last LP stage have been designed in two alternative configurations, the base profile being the same in each case:

- as a free-standing blade with a length of 1085 mm
- with all blades connected into one assembly, using riveted connecting bridges; the blade length being 1050 mm.

30. The secondary circuit feed pumps are driven by condensing steam turbines, taking steam from the reheater outlet, with provision for the use of live steam, if required.

31. Leading particulars of the feed pump turbines are: nominal output 7,9 MW at 4500 rpm, maximum output 9,24 MW at 4700 rpm.

32. Two turbo-feed pumps are in operation under normal conditions, the third serving as a stand-by.

Steam extraction from 1000 MW turbine

33. One of the main technical requirements imposed on the turbine by the customer has been the possibility of attaining the highest feasible heat extraction in order to heat water for a centralised district heating system. The

turbine is so designed at to permit the extraction of steam corresponding to the following quantities of heat:

- 893 MJ/s with three - stage water heating (150/60°C)
- 570 MS/s with two - stage water heating (120/60°C),

the steam being taken from uncontrolled steam extraction points in conformity with the schema shown in diagram 5.

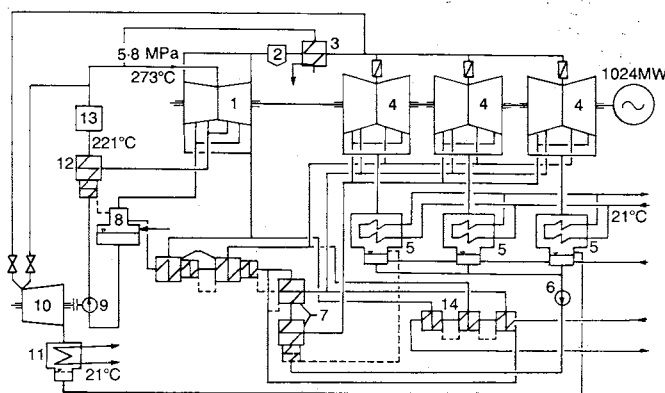


Fig. 5. Diagram of steam extraction from the 1000 MW turboset

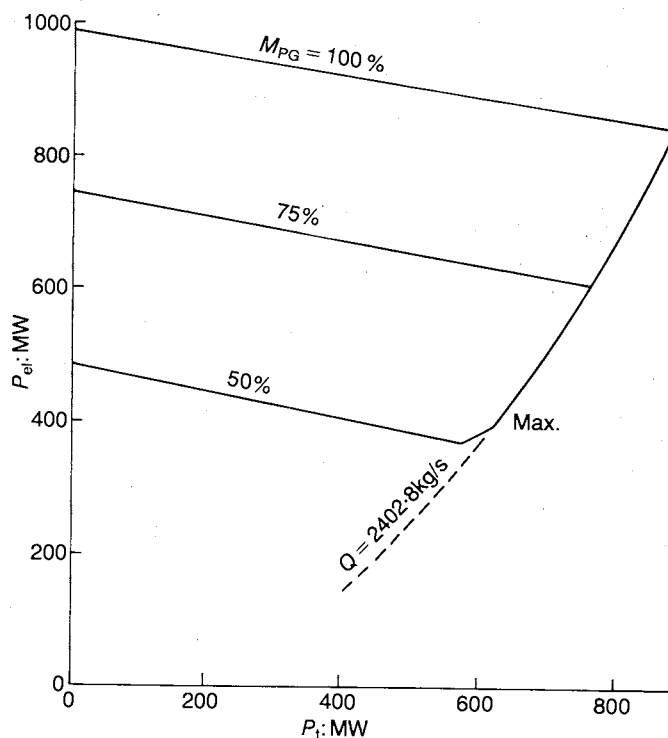


Fig. 6. Simplified diagram of electrical ( $P_{el}$ ) and heat ( $P_t$ ) outputs for the 1000 MW turbine

## TURBINE DESIGN AND OPERATIONAL EXPERIENCE

34. In addition, the design of the HP cylinder permits further uncontrolled steam extraction at a higher steam pressure, thereby ensuring the heating of water in the fourth or fifth heating stage up to 180 ... 200° C for possible future generation of the heating steam conveyed to the point of consumption using turbocompressors.

35. Fig. 6 shows a simplified steam extraction diagram, both for the highest heat extraction (MAX), and for the situation of extracting heat from the first units of Temelín nuclear power station, where the required heat output is 306 MJ/s in three-stage heating of water (65/150° C). The diagram shows the relationship between the electrical output of the units

and the heat output intended for district heating, for three different outputs of the steam generators (100%, 75%, 50%).

36. The sites for further 1000 MW nuclear power stations will be selected, duly taking into account the need for the highest possible extraction of heat for district heating.

### REFERENCES

1. Drahý J.: 220 MW saturated steam turbines for nuclear power stations. - Škoda Review 1976, No 2, p. 20 - 26
2. Drahý J.: 1000 MW saturated steam turbines for nuclear power stations. - Škoda Review 1987, No 1, p. 2 - 10.

## 9. Reliability of LP steam turbines

J. E. BERTILSSON and U. WILD, ASEA Brown Boveri Ltd, Switzerland

The design of LP-steam turbines is continuously being advanced to meet market demands. Along the efficiency improvement of the last blading stages result in an overall unit heat rate improvement of 0.6 % and this without any reduction of reliability and ease of maintainance. The paper describes the various boundary conditions, particularly in the wet steam area, taken into consideration in the design of to-days LP-turbines, the design methods used and how these methods are being verified to ensure reliable performance. The paper also discusses the specific problems encountered by other manufacturer's design in respect of stress corrosion cracking and how such problems can be resolved by retrofitting such units with the well proven Asea Brown Boveri design. Such an approach has been successfully implemented for quite a number of units.

### INTRODUCTION

Large low pressure turbine rotors for nuclear application of the shrunk-on disk type suffer from stress corrosion cracking (SCC) at the keyway and bore area.

The majority of the stress corrosion cracks have been observed by inspection before the cracks grew to critical size and thus, catastrophic failure was avoided in nearly all cases. Altogether, only three catastrophic failures of low pressure turbine disks have been reported for nuclear power plants and some disks have also burst due to SCC in fossil fired power stations.

Because of more demanding safety requirements, SCC of turbines in nuclear power plants is closely watched and regulated by government regulatory commissions.

The U.S. Nuclear Regulatory Commission (NRC), for example, request a turbine missile generation analysis which accounts for the SCC phenomena. In this missile analysis, the probability of unacceptable damage resulting from turbine missiles has to be demonstrated. The calculated probability figures determine the necessary inspection intervals of the low pressure turbine rotors.

The second major source of non-availability of low pressure turbines is the blading. The highest failure rate has been observed in the transition zone from superheated steam to wet steam, i.e. the Wilson Line. In order to increase the reliability of the LP-blading measures have to be taken to ensure a proper dynamic lay out of the blading and a reasonable level of the static blade stresses. The paper describes the design of modern blading for high efficiency and reliable LP-turbines.

The rotordynamic behaviour is also of importance and has to be considered during the design phase. The methods used will be discussed.

### RELIABLE ROTOR DESIGN

The quality of the rotating part of a turbine (rotor and blading) is of great importance to the availability of the entire power station because:

- o It is continuously subjected to both static and dynamic loads during service.
- o A spare is not generally supplied, so the loss of availability of the rotating part means outage of the entire installation.

Whereas failures in the blading can generally be overcome, or at least minimized, in a 'short' time, i.e. within a few weeks, problems with the rotor are of a much more troublesome variety. As a rule, they result in considerable limitations and interruptions to operation and require radical measures for their solution.

The different possibilities used by various manufacturers for the construction of steam turbine rotors are illustrated in Fig. 1.

There is no scientific explanation for the fact that the manufacturers employ different designs. Since the design is always a compromise, and is influenced by so many factors, the design chosen depends to a large extent on the relative importance attached to particular risks.

For example, Brown Boveri, had already decided to construct compact steam turbine rotors by welding together solid discs at the start of the 1930s. In the last 50 years, this manufacturing technique has been fully automated and has reached such a high standard that the risk of any manufacturing or operating error can be totally excluded.

Thanks this and the positive operating experience gained with both small and very large machines in the 1000 MW range as well as

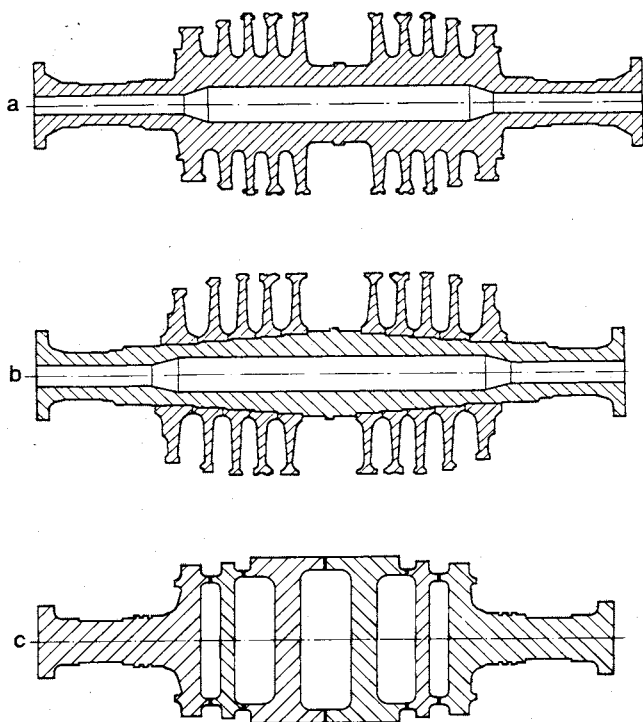


Fig. 1. Designs of steam turbine rotors

- a: Solid rotor
- b: Rotor with shrunk-on discs
- c: Welded rotor acc. to ABB design

the improvement in the steel making methods, this technology can now be applied completely without risk to large turbomachinery for conventional and nuclear power stations.

Serious operating difficulties caused by disc explosions, major cracks or SCC of the rotors are unknown to ABB customers.

Table 1 attempts to evaluate the most important factors responsible for the availability of low-pressure rotors.

Table 1. Evaluation of the most important factors determining the availability of LP-rotors

	Shrunk-on-discs	Solid rotor	Welded rotor
Loading at the critical locations in the rotor	High	Medium	Low
Yield strength of the material	High	Low	Low
Access of corrosive environment to highly loaded locations	Yes	Yes	No
Susceptibility to stress corrosion cracking	High	Medium	Low
Fracture toughness	High	Medium	High
Operating experience	Poor	None <sup>*)</sup>	Good
Lifetime	Short	Unknown	Long

<sup>\*)</sup> for large and half-speed units.

The evaluation of these factors demonstrates that the welded rotor has distinct advantages over the design with shrunk-on discs. Table 1 also shows just as clearly the technical lead which the welded rotor has over the monoblock rotor. The superiority of the welded steam turbine rotor has been described in several publications.

The characteristics of the most important rotor concepts are summarized in the following:

Turbine rotors with shrunk-on discs

A rotating disc having a central bore, considered as a component of a rotor, exhibits a much higher stress level at the most highly loaded location than a solid disc. For the bored disc, this is at the position of the shrink fit. The stress level at this location may be twice as high as in the solid disc, see Fig. 2.

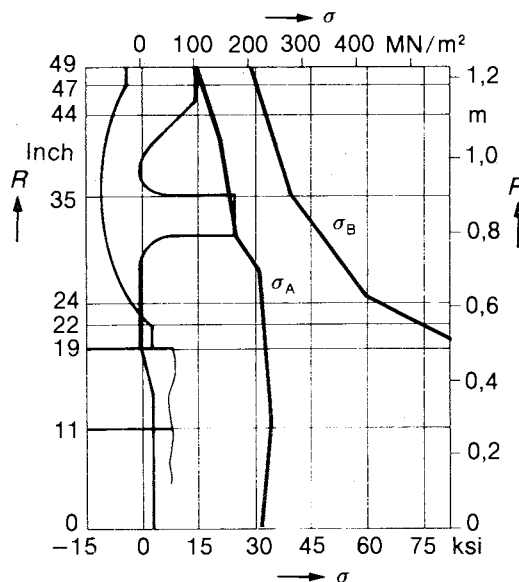


Fig. 2. Comparison of stresses in solid disc/axially bored disc

- $\sigma_A$  = Stress in welded rotor
- $\sigma_B$  = Stress in rotor with central shaft and shrunk-on disc
- $\sigma$  = Stress
- R = Rotor

The rotor shafts of steam turbomachinery are subjected to centrifugal forces which reduce the amount of shrink in the case of the shrunk-on disc design. Also disturbances from the power system (torsional vibrations) can cause the discs to 'slip' on the central shaft. For this reason, certain manufacturers have attempted to improve the rigidity of the connection between the disc and the central shaft by incorporating keys (Fig. 3).

However, this measure results in a considerable increase in the stresses at the corners of the keyways of the shrunk-on discs since the tangential stresses, which are already very high at these locations, are concentrated.

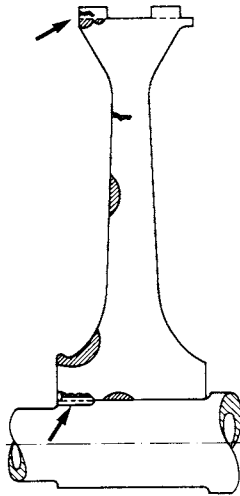


Fig. 3. Crack formation in low-pressure turbines of 700/900 MW nuclear power stations in the USA

Some designers have attempted to find a way out of this dilemma by adopting a radial orientation of the keys (Fig. 4).

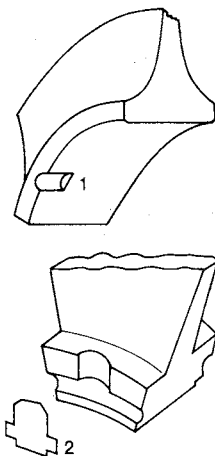


Fig. 4. Shrunken-on disc: key design

- 1 = Keyway
- 2 = Radial key

Although, this is an effective way of reducing the stress around the key, the basic problem of the increased disc loading at the position of the shrink fit still remains.

Solid Rotors

It is a logical step to consider the solid rotor in the quest for a solution to the problems posed by the rotor with shrunk-on discs. This solution does reduce risks in operation since the rotor itself comprises a single piece, just as in the case of the welded rotor; there are no longer any components which can become loosened during service (shrunk-on discs). The shrink-fit location has been eliminated and with it the potential of stress

corrosion cracking at the highly loaded shrink fit. Particularly for full-speed machines (3000 or 3600 rev/min), many manufacturers have successfully used the concept of the solid rotor even in the low-pressure region.

If the designer of half-speed steam turbine (1500 or 1800 rev/min) wishes to use the solid rotor for the low-pressure section of his turbine, then he must consider the several disadvantages including:

- o Low-pressure rotors of large half-speed steam turbines have a finished weight of 100 to 200 t and a body diameter of about 2 to 3 m. In order for a rotor of such large diameter to be manufactured, the steel manufacturer must be able to produce a forging of exceptional size; the final weights mentioned require ingots sizes of 200 to 400 t. This limits the possibilities of purchasing the starting material, and in principle only a single source exists. As a result, there is only a very limited international exchange of technical information - a situation hardly conducive to the achievement of high quality in the product.
- o A further disadvantage of the large monoblock rotors lies in the greater difficulty of testing compared with smaller forgings. Although considerable progress has been made in ultrasonic testing in recent years, the fact remains that the defect resolution capability is reduced as the size of the testpiece increases, i.e. the quality of the test is not as high. Such solid rotors are often provided with a central bore to avoid this difficulty. However, this leads in turn to a higher stress level at the central bore.

This serves to illustrate the technological limitations of the solid rotor. The technology of the large solid rotor provides a new situation which can only be proven by successful operation in the coming decade.

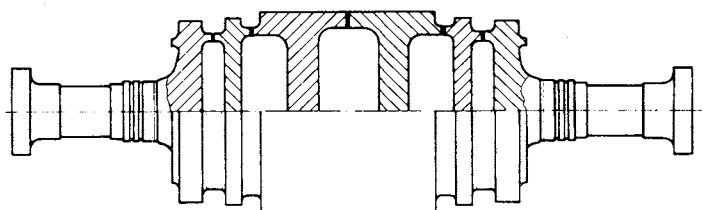


Fig. 5. Welded steam turbine rotor of ABB design with the following advantages:

- Low stress (no central bore, no keyways)
- No shrink-fit, i.e. no fretting fatigue
- Centres of the discs are in an inert atmosphere
- Low yield strength, i.e. low susceptibility to stress corrosion cracking

## TURBINE DESIGN AND OPERATIONAL EXPERIENCE

### Welded steam turbine rotors

The previously-mentioned disadvantages, both of the solid rotor and of the rotor built up with shrunk-on discs, do not apply to low-pressure rotors manufactured by welding together solid discs. Fig. 5 indicates the specific advantages of this solution.

It is of interest that the limits of development of this technique are not reached until well after the solid rotor has lost its viability. This is because the individual rotor elements (discs) can be supplied in excellent quality by a large number of steel manufacturers.

The welding technique itself has a 50-year tradition at Brown Boveri and is now fully automated. The essential experience (learning curve) had already been accumulated decades ago from relatively small rotors.

Table 2 provides a summary of ABB experience with welded rotors.

Table 2. ABB experience with welded rotors

Total built (including licensees)	> 4000 welded rotors
Experience since	1930
Range of application	- Steam turbines (high-pressure, intermediate-pressure and low-pressure turbine sections) - Gas turbines
Output range	2 to 1300 MW

### DESIGN OF LP-TURBINE BLADES

The flow conditions in the last LP stages have an extremely three-dimensional character. When developing the "old" LP turbines in the early seventies, the computer codes for the fluid-mechanical design of the LP last stage were capable to an only limited degree to consider these very complex flow conditions with adequate accuracy. This means that in the range of the greatest expansion the energy conversion takes place with low efficiency due to insufficient adaptation of the blading. After improving the program quality of the meridional flow design in the last 10 to 15 years, the last stages of today's turbines have an efficiency which is 2.5 to 3.5 % higher. Given the actual fuel prices, the resultant heat rate improvement of about 0.6 % is of economic interest so that the investment costs will pay off in some years.

Long outages of a turboset reduce the economic success and cannot be compensated by an even outstandingly high efficiency. This applies particularly to plants with high unit ratings and thus high availability has usually a higher priority than high efficiency..

The authors' company continuously developed the turbine family of the 1990s which is characterized by

- o compact construction (small dimensions in axial and radial direction)

- o good accessibility and serviceability
- o high reliability and availability, using proven materials and improved design methods
- o high efficiency of all turbine cylinders, improved primarily in the LP section by employing the most updated fluid-mechanical design methods.

The following chapters describes the special boundary conditions for the LP turbine design, the calculation methods used, the test equipment required for design verification and its specific operating characteristics.

### BOUNDARY CONDITIONS FOR LP-TURBINE DESIGN

With a given number of LP-turbine types, the most favourable design of exhaust area (in terms of efficiency) is chosen based on the outlet energy curves.

The selected staggering of the various type sizes and specified  $h/D_M$  values ( $h$  = blade height,  $D_M$  = mean outlet diameter), define the last stage dimensions, i.e. hub diameter, tip diameter and blade height.

To obtain a design as compact as possible, the  $h/D_M$  values were slightly increased compared with those of older LP turbines and are now  $h/D_{ME} = 0.33 \div 0.37$ .

For standard feedheater arrangements the extractions in the LP-turbine part vary in comparatively narrow limits with respect to the condensate flow, i.e. with the LP-turbine outlet flow the inlet flow is also known with sufficient accuracy. The inlet volume flow upstream of the LP turbine is determined by selecting the LP inlet pressure. The inlet volume flow of each LP-turbine type is varied in 3 steps.

The last two blade rows of all LP turbine types have twisted blades. Optimization parameters for selecting the twisting and the blade profile are the aerodynamic parameters and especially the outlet losses. In order to keep these losses within narrow limits over the possible volume flow range of a specific LP turbine, the geometry of the last stage stationary and rotating blades is adjusted stepwise as a function of the outlet volume flow.

### DESIGN OF A LP-TURBINE

A survey of the various steps and iterative loops required for the design of a LP turbine is given in Fig. 6. Before starting the design procedure, the definite extraction pressures and flow rates are calculated from the specified boundary conditions like exhaust flow rate and LP inlet pressure.

The calculation of the differential expansion of the shaft line relative to the LP inner casing has to be based on the roughly known expansion steam data in the individual turbine cylinders and the gland steam data. The differential expansion is important when selecting the shroud configuration because not all shroud designs are suitable for turbines with great differential expansions.

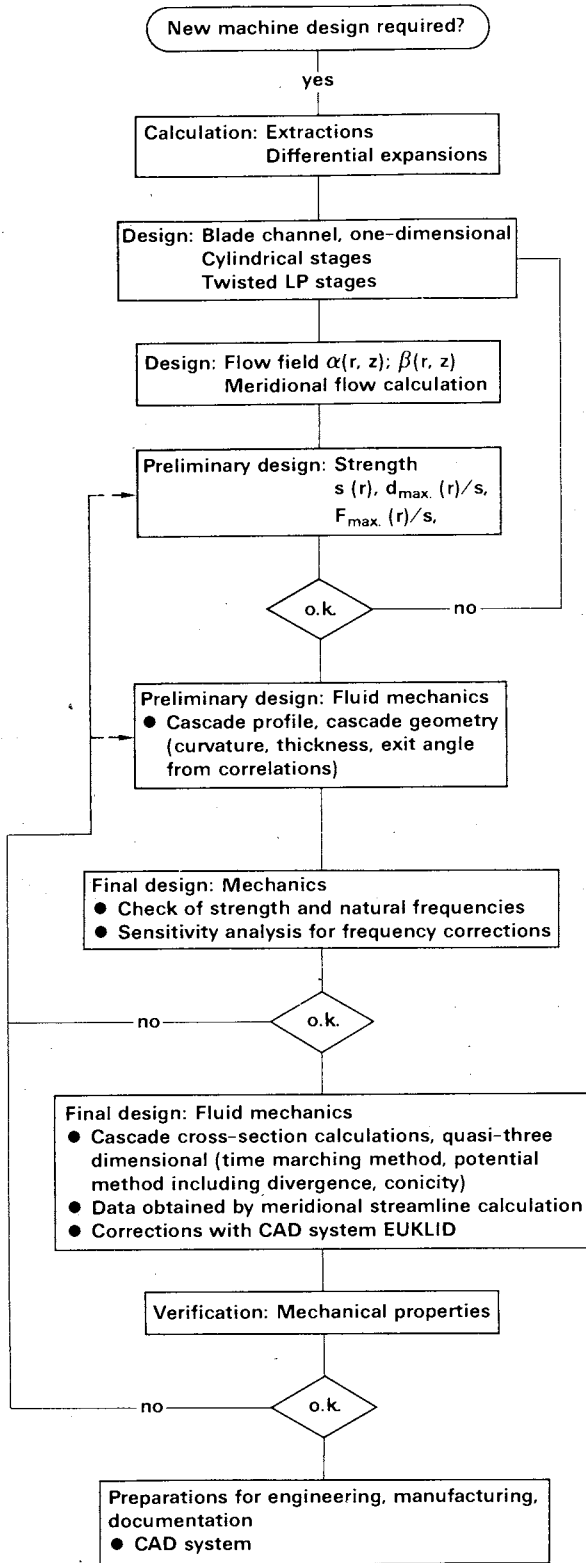


Fig. 6. LP-turbine design flow diagram

Once this preliminary work is done, the first design phase comprises the one-dimensional layout of the steam path with a more accurate specification of the blading in the area of the untwisted front stages including the inlet casing with inlet scroll and radial-axial stage, and a rough specification of the blade geometry at mean blade height for the last two twisted blade rows.

The design of the twisted last stages is done with repeatedly nested iterative loops.

The meridional flow calculation, the blade-to-blade calculation and the verification of blading strength and natural frequencies are included in the iteration.

The design process is completed with the CAD-preparation of manufacturing drawings and documents.

The following subsections describe in more detail the various steps of the iteration.

One-dimensional design

Inlet scroll and radial-axial stage. The introduction of the inlet scroll with following radial-axial stage, replacing the torodial inlet casing with a conventional first axial stage, is a typical example of the technical progress in small and controlled steps.

The first tests with a 2 x 180° LP inlet scroll with following radial-axial stage were made more than 10 years ago. Measurements taken on the test configuration, Fig. 7, proved conclusively that the stage efficiency in the usual design range could be increased by almost 3 % compared with the conventional configuration.

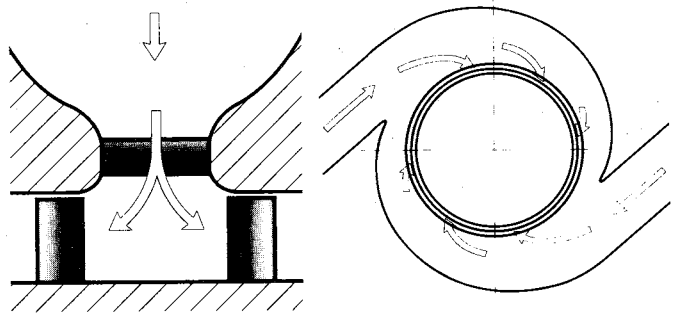


Fig. 7. Flow in turbine scroll with radial-axial first stage

The principle to generate a usable vortex already in the inlet casing and to correct it only slightly in the subsequent radial stationary blade row for ensuring an optimal flow admission to the first rotating blade row has meanwhile been applied successfully in all partial turbines (HP, IP and LP).

Meridional channel and untwisted blading. The calculation of the efficiency is based on extensive studies on a 5-stage test turbine where the geometries of the cascade and channel were varied systematically.

The profile 8000, developed in the 1970s was first used in a 600 MW plant in 1979. Since then more than 70 machines have been equipped with this type of profile. The reliability proved to be excellent.

From the fluid mechanics point of view the following advantages of this profile are worth mentioning:

- o the extremely high insensitivity to changes of the angle of incidence
- great operating range without substantial profile loss changes

## TURBINE DESIGN AND OPERATIONAL EXPERIENCE

- o controlled delay on the profile suction side
  - small momentum loss thickness
  - low loss level
- o thin profile trailing edge
  - low trailing edge losses
  - lower nozzle passing excitation of the following blade rows.

The design calculation includes a check of the static and dynamic strength properties of the blading. The calculation of the dynamic stress is based on test results obtained from a 2-stage test turbine, which was equipped with 50 % reaction stages of profile 8000.

The result of this study are empirical functions which describe the size of the transient blade forces as a function of the distance between the cascades and of the cascade load.

### Meridional flow design

The design of the two last stages takes into account the following criteria:

- o Uniform divergence of the streamlines over the blade height and smallest possible divergence especially in the hub area in order to simplify the profile design.
- o Relative inlet Mach numbers at hub and tip  $Ma_{w1} < 0.75$ .
- o Relative exit Mach numbers at the tip  $Ma_{w2} < 1.3$ .
- o Degree of reaction at the hub  $R \geq 20\%$ .
- o Manufacturing costs.

### Profile design

The meridional flow calculation yields the angle and Mach number distribution at the inlet and outlet of the individual stationary and rotating blade cascades of the two last stages. A special correction of angle was made in the boundary zones of the stationary and rotating blade rows in order to allow for the effects of gap and secondary flows.

For cascade cross-sections where the exit Mach numbers are  $Ma_2 < 1.0$  or  $Ma_{w2} < 1.0$  an inverse design method is used; cascade cross-sections with greater Mach numbers are designed iteratively, using a Q3D time marching procedure. For final design both methods can be coupled with a boundary layer procedure which is employed primarily to quantify the relative differences between the various design methods and to check the profile.

Q3D Time marching method The recalculation method is used for cascade cross-sections with exit Mach numbers  $Ma_2$  or  $Ma_{w2} > 1$ . For given cascade cross-sections, whose profiles can, if necessary, be modified comparatively easy using CAD-systems, the Mach number distributions are calculated along the profile contour and the position of the shocks checked and corrected, if required, using plots with constant Mach lines.

It is endeavoured to optimize the last stage geometry of the transonic and supersonic profiles like that of subsonic profiles, not

only for one operating point but for a comparatively great operating range. This calls for:

- o relatively low exit Mach numbers in the tip area of the last rotating blade row, i.e.  $Ma_{w2} = 1.2 \div 1.3$
- o tip cross-sections, which are insensitive to Mach number variations, i.e. the profile suction sides are not concave but straight.

Thus last stage geometry permits a substantial efficiency increase especially in the lower volume flow range of a turbine type.

### Vibrational design of the last stage rotating blades

As shown in the design flow diagram, Fig. 8, the design of the last stage rotating blades is by iteration taking into account the aerodynamic, vibrational and strength aspects.

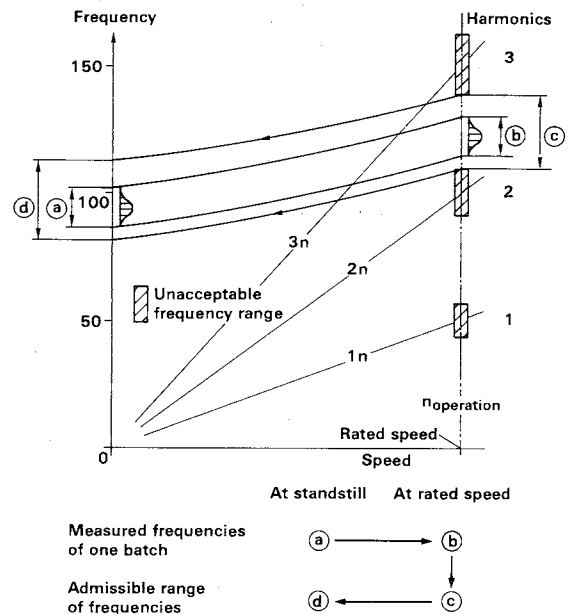


Fig. 8. Establishing admissible ranges for blade natural frequencies

It is a requirement for the vibrational design that all blades can be operated resonance-free at operating speed. Based on theoretical considerations and taking into account long-term operating experience with freestanding last stage blades, permissible natural frequency ranges were specified. Only blades whose natural frequency lies within the permissible frequency range according to calculation and measurement are used.

Finite-element programs are employed as auxiliary means for calculating the natural frequencies.

The location of the natural frequencies is specified definitely after taking zero-speed frequency measurements on each blade and measurements at operating speed on a definite number of blades for determining the frequency

increase due to the influence of centrifugal force, see Fig. 8.

Blade stresses

When assessing the stresses in the airfoil, static and dynamic forces are considered. Static stresses are stresses due to centrifugal force or caused by deformation and untwisting of the airfoil under the influence of centrifugal force.

Also considered is the bending stress due to steam forces exerted on the airfoil, although this stress is normally very small. An important factor for evaluating the total static stress is the Mises reference stress, Fig. 9.

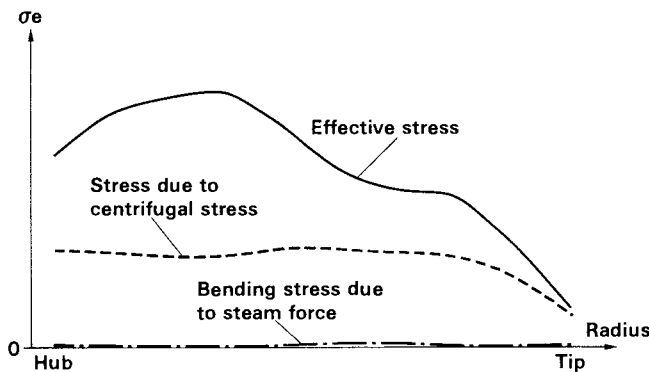


Fig. 9. Maximal static stresses of a last stage rotating blade at rated speed

All disturbances of the steady-state flow field cause a dynamic stress on the blade. If a machine is operated under rated conditions, the result, in the ultimate case, can be a complete relief of the steam forces, i.e. the alternating bending stress could be as high as the bending stress due to steam force. The recalculation of the design configuration is based on this case which is the most unfavourable. The actually existing stresses are considerably lower.

Markably higher alternating stresses can occur during operation with very small volume flows because the backflow from the exhaust chamber causes stochastic excitations of the airfoil. If the back pressure is high, as for example in turbines with air condensers, these excitations yield high stress amplitudes. Such conditions are taken into account with a special design of the last stage rotating blade, particularly in the airfoil-root area.

**EXPERIMENTAL STUDIES ON THE LOW-PRESSURE TEST TURBINE**

Investigations on test turbines have usually the following goals:

- o Verification of the calculation methods used for determining the distribution and absolute size of flow parameters in selected planes.
- o Adjustment of empiric correlations for exit angle and losses.

- o Optimization of components or geometric details which are not or not completely computable.

In the last few years the above goals were pursued by performing systematic tests on a LP test turbine.

**SUMMARY**

The use of the most updated calculation methods and the consistent application of the experimental results have produced a LP turbine, redesigned in details, which is shown in Fig. 10. The special features of this turbine are:

- o compact design
- o favourable, low-excitation flow
- o optimized blading with respect to efficiency and operating range
- o conically cut last stage rotating blade allowing an optimal diffusor desing.

During the design phase special attention was paid to the fact that the ranges of experience established for strength and vibrations were not exceeded. Performance testing of turbines built shows no significant deviations from the values established in the model tests.

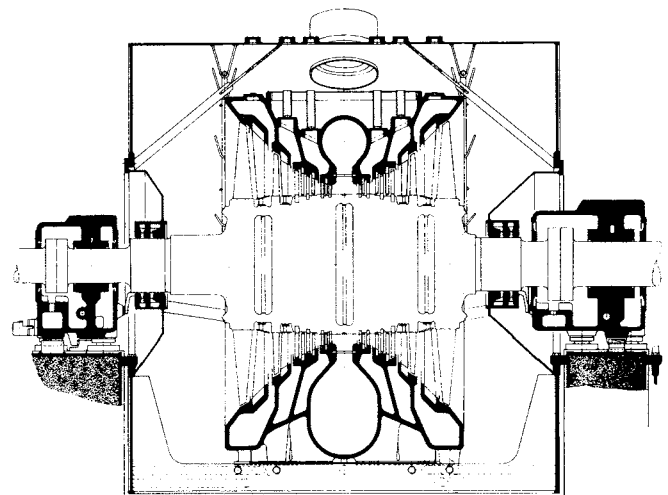


Fig. 10. LP-turbine

**DYNAMIC LAY OUT OF RETROFITTED STEAM TURBINES**

Welded LP-rotors have somewhat different mass and flexibility distribution than their non-welded counterparts. Consequently, even though the exchange of welded for non-welded rotors is made only in the LP-cylinder, the entire shaft line has to be analyzed as a total 'new' system. This is especially true with regard to the static bending line, bearing loads, critical speeds, unbalance sensitivity as well as torsional natural frequencies. An application of the proper design analyses for such a retrofit case is described in the following chapters.

## TURBINE DESIGN AND OPERATIONAL EXPERIENCE

### MODELLING OF THE SHAFT LINE

For the dynamic considerations of a turbine generator the most important influence is by the mass and stiffness distribution of the shaft line. The rotors are usually modelled by elements of constant mass and stiffness along the axis.

When the retrofit rotors are to be supplied by a manufacturer other than the original equipment manufacturer (OEM), all important dimensions have to be taken by measurements on site. These extensive measurements give the necessary information for the correct interface dimensions for new rotors as well as the dimensions of the specific rotors to be replaced. The whole shaft line can then accurately be modelled with up to 400 elements. For comparison, two models are established. One model is for the original shaft line and one for the new shaft line comprised of the original HP and generator rotors with the new LP-rotors.

### Critical speeds

An important step in the layout procedure is the calculation of the critical speeds (natural frequencies) of the system of coupled shafts as a function of the overall support-structure stiffness. The results are typically represented in graphs with speed versus support flexibility (inverse of the stiffness). These overview calculations are done for symmetrical stiffness and without damping.

Fig. 11 gives the example comparison of the critical speeds for a nuclear machine with three retrofitted LP-rotors. Because of the higher stiffness of the retrofit rotors, the three critical speeds of the new LP's, (solid lines in Fig. 11), are higher than of the original LP-rotors, (dashed lines in Fig. 11).

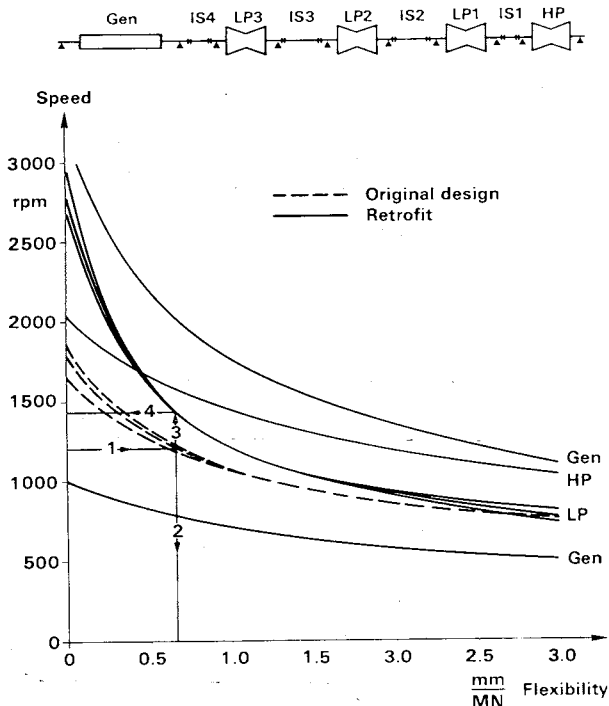


Fig. 11. Critical speeds as function of support flexibility

The critical speeds of the retrofit rotors are practically not influenced by the retained HP and generator rotors, mainly due to the realtive flexible connections (jack shafts) and the two bearings between the main rotors, inherent in the original unit layout.

### Unbalance shaft response

The assessment of running smoothness of a turbine generator is done not only by checking the critical speeds, but also by checking unbalance response, using calculations with all important parameters appropriately taken into consideration. For such calculations a finite-element code including a substructuring approach is used, and including all important properties of the rotors, bearings and pedestals together with existing experience.

Using various specified unbalance distributions, all natural frequencies are successively excited. As an example, results for an excitation of the first harmonic mode of LP 2 of a large nuclear turbine generator with three retrofitted LP's are given in Fig. 12.

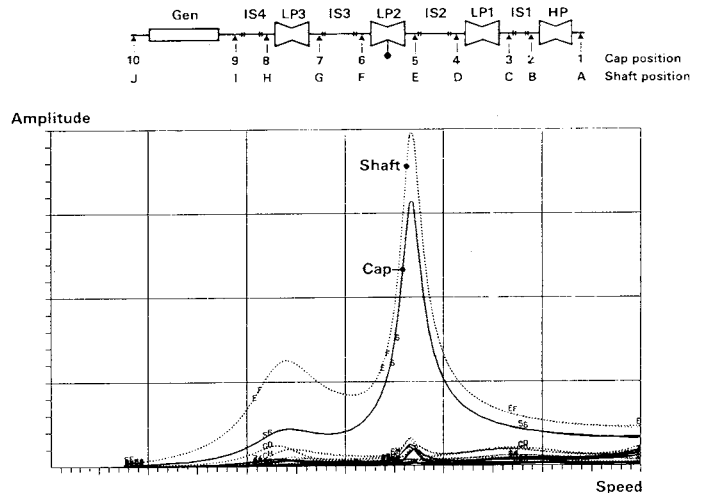


Fig. 12. Unbalance calculation for a retrofitted nuclear machine with an unbalance set in the LP 2 rotor

The amplitude peaks of the larger axis of the vibration ellipse characterizes the natural frequencies in horizontal and vertical direction, and the height of the amplitude is a measure of the unbalance sensitivity. To assess the amplitudes, criteria established during many years of manufacturing and operation of turbine generators are employed.

### Torsional vibrations

Similar to the lateral vibrations, the torsional vibration behaviour of the shaft line (and in special cases also the coupled system of rotor and last stage blades) has to be investigated to insure proper design, life and reliability. For these calculations the shaft-line is modelled by discrete masses.

A comparison of the calculated torsional natural frequencies of a nuclear machine with three retrofitted LP's shows that the new design with welded rotors has somewhat smaller

natural frequencies than the original configuration because of the higher inertia of the retrofitted welded LP rotor bodies. The natural frequencies were calculated to be considerably removed from the nominal and twice the nominal grid frequency. This is, of course, an indication that torsional vibration problems associated with resonances are unlikely.

**FIELD EXPERIENCE AND CONCLUSIONS**

One of the retrofitted units went into operation in early 1986 within the scheduled time. In Fig. 13 the retrofitted parts i.e. rotor, rotating and stationary blades and the inner casing together with the retained parts are shown.

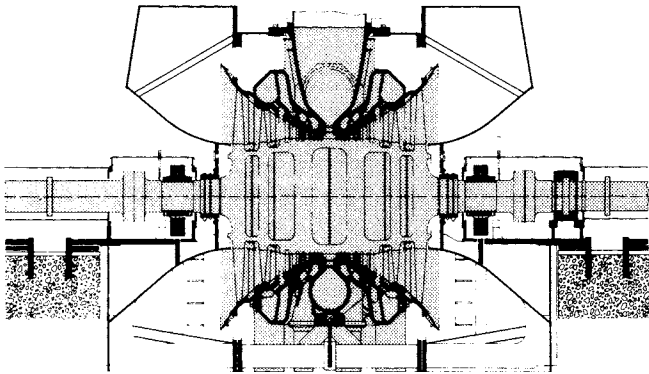


Fig. 13. ABB solution for the low-pressure turbines of nuclear power stations endangered by stress corrosion cracking

Even without having to perform field balancing the vibration behaviour is slightly improved over the original configuration. The critical speeds of the LP-rotors were observed at 1300-1370 rpm during the run-up on January 30, 1986, with maximum shaft vibrations of 7 mils (peak-to peak) at bearings nos. 3 and 4.

This is just one of many examples showing that partial replacement of existing components (retrofit) is a viable, cost efficient method to overcome inherent design deficiencies and mostly at the same time improving the plant performance considerably. It is however a prerequisite that such retrofit are designed with the same care as for the experienced manufacturer's own units.

**MISSILE ANALYSIS**

The U.S. Nuclear Regulatory Commission (NRC) request a turbine missile generation analysis which accounts for the SCC phenomena. In this missile analysis, the probability of unacceptable damage resulting from turbine missiles has to be demonstrated. The calculated probability figures determine the necessary inspection intervals of the low pressure turbine rotors.

Failures of large steam turbines have the potential to eject large high energy missiles which can damage other main components like the reactor. The probability  $P_4$  of unacceptable

damage resulting from turbine missiles is generally expressed as the product of:

- (1) the probability of turbine failure resulting in the ejection of turbine disk fragments through the turbine casing,  $P_1$ .
  - (2) the probability of ejected missiles striking main components,  $P_2$ .
  - (3) the probability of struck main components to fail,  $P_3$ .
- $P_4 = P_1 \cdot P_2 \cdot P_3 \leq 10^{-7}$  per year

Because of the uncertainties involved in calculating  $P_2$  and  $P_3$ , the NRC have defined the product  $P_2 \cdot P_3$  depending on the arrangement of the power plant, see Fig. 14.

Favorable		Unfavorable	
Turbine	Reactor	Turbine	Reactor
$P_2 \times P_3 \leq 10^{-3}$		$P_2 \times P_3 \leq 10^{-2}$	
$P_1 < 10^{-4}$		$P_1 < 10^{-5}$	

Fig. 14. Arrangement of power plant and NRC requirements

The NRC safety objective with regard to turbine missiles can be summarized in terms of two sets of criteria as shown in Fig. 15.

Case	Probability $P_1$		Required licensee action
	Turbine - Generator Set		
	Favorably oriented	Unfavorably oriented	
A	$< 10^{-4}$	$< 10^{-5}$	Loading turbine
B	$10^{-4} < P_1 < 10^{-3}$	$10^{-5} < P_1 < 10^{-4}$	Turbine may be kept in service until next scheduled outage
C	$10^{-3} < P_1 < 10^{-2}$	$10^{-4} < P_1 < 10^{-3}$	Turbine is to be isolated from steam supply within 60 days
D	$10^{-2} < P_1$	$10^{-3} < P_1$	Turbine is to be isolated from steam supply within 6 days

Fig. 15. New NRC-proposal; reliability criteria

## TURBINE DESIGN AND OPERATIONAL EXPERIENCE

For a given arrangement the procedure is reduced to the determination of the turbine missile generation probability  $P_1$  as a function of time.

Mathematical model for  $P_1$  - The probability of producing a disk fragment can be determined by means of fracture mechanics using crack growth rates and critical crack sizes.

### Resulting inspection intervals, conclusions

The probabilities of rotor fragment generation for the welded rotor are orders of magnitudes lower than those for the shrunk-on disk rotor.

Applying the NRC requirements listed in Fig. 15 the following inspection intervals have to be introduced assuming that in both units only one disk is affected by SCC and that the fragment will perforate the casing:

	<u>Favourably</u>	<u>Unfavourably</u>
	Oriented	
Welded Rotor:	35 years	22 years
Shrunk-on Disk:	~ 2,5 years	~ 1,5 years

The reasons for the superior results of the welded rotor are:

- (1) The lower net stress, leading to a critical crack size which is eight times greater than that one of the shrunk-on disk type.
- (2) The lower yield strength of the employed material leads to a calculated crack growth rate which is only one half of that for the shrunk-on disk rotor material.

It must be noted that these results are obtained with simplifying assumptions. The probability of crack initiation and the probability of perforating the casing may, in an actual case lower the probability of missile generation for both designs. On the other hand the number of disks or rotors in the actual power plant will increase the probability of missile generation. In any case, however, the analysis for the welded rotor will reveal much lower probabilities and therefore longer inspection intervals.

ABB have performed missile analysis on all of their LP rotor types in nuclear power plants. The results show that the usual inspection recommendation are in all cases much more stringent than the NRC requirements.

# 11. Development of designs for moisture separator reheaters

C. J. MONKS, GEC Turbine Generators Limited, and J. P. PEYRELONGUE, Stein Industrie

## SYNOPSIS

The general requirements and the specific solutions incorporated in current designs of moisture separator reheaters supplied by the author's companies for PWR projects in France, China and the UK are presented. The background development and experience gained from 200 operating units is reviewed.

### 1 INTRODUCTION

The authors' companies have separately been involved in many power station projects utilising wet steam from a variety of nuclear steam generators and have accumulated considerable service experience of moisture separator reheaters.

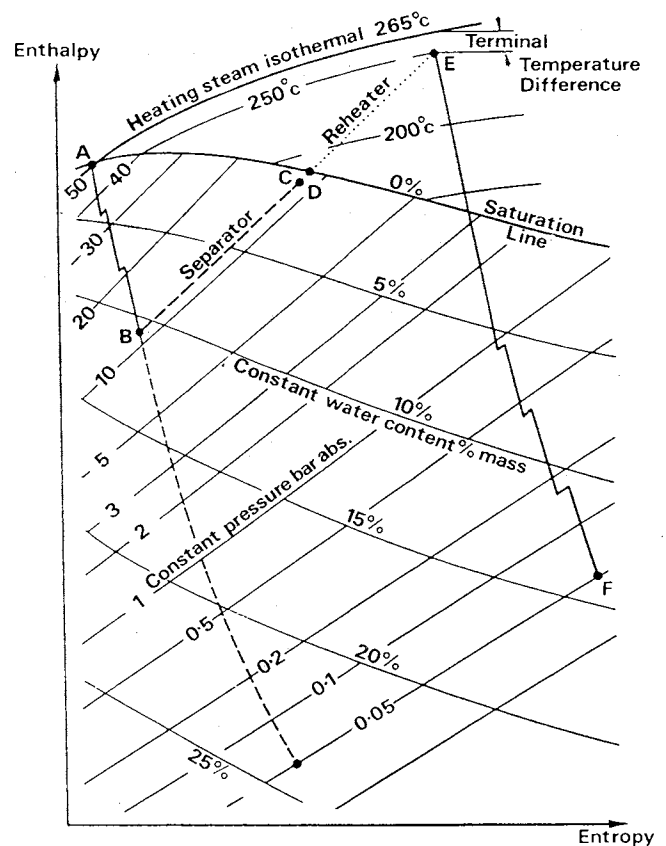
The extensive programme of pressurised water reactor PWR nuclear stations undertaken in France resulted in Stein Industrie completing a comprehensive development programme for moisture separator reheaters which has culminated in the latest design for the 1500 MW CHOOZ power plant being built by Electricite de France.

Since 1976 GEC Turbine Generators have had a technical agreement with Stein Industrie which has enabled the incorporation, in their moisture separator reheater designs, of basic features researched by Stein Industrie and which have proved successful in French PWR power plants.

The paper presents the principal features and latest designs of moisture separator reheaters adopted by Stein Industrie for the 1500MW PWR units at Chooz in France, and by GEC Turbine Generators for the 985MW PWR units at Daya Bay, Guangdong province, China, and the 2 x 630 MW PWR units at Sizewell B in the UK.

### 2. THE FUNCTIONS OF SEPARATION AND REHEAT

A Mollier diagram of a typical moisture separator reheater function is illustrated in Fig.1.



- A to B : HP cylinder expansion
- B to C : Water separation
- C to D : Residual water evaporation
- D to E : Steam superheating
- E to F : LP cylinders expansion

Fig.1 Mollier diagram of typical MSR function

## ANCILLARY PLANT AND MATERIALS OF CONSTRUCTION

### 2.1 Separation

In PWR power plants the turbine is supplied with saturated steam. After expansion in the high-pressure (HP) cylinder the steam contains 10 to 15% water. The majority of this must be removed before expansion can continue in the low-pressure (LP) cylinder. Moisture separators located between the HP and LP cylinders are therefore included in the cycle.

The separator must be effective over a wide range of droplet sizes, dynamic pressures and local water concentrations. It can be of the wire mesh, centrifugal or the chevron type. Only the chevron type is used in current combined moisture separator reheaters designed and built by the authors' companies.

The separator performance directly affects the reheater performance in that 1% residual water at the separator outlet increases the consumption of heating steam by 10%.

### 2.2 Reheat

In addition to the provision of separators it is now standard practice to provide reheating to further reduce wetness in the turbine low pressure cylinder and to improve cycle efficiency.

After separation, the steam passes through one or more reheater tube bundles which initially evaporate the residual water and then reheat the steam to a level sufficient to prevent the generation of an excessive amount of moisture in the later stages of expansion. In single stage reheaters the necessary heat comes from the condensation of about 10% of the live steam flow generated by the reactor.

In two stage reheaters an additional primary source of heating steam is provided by bleeding from the high pressure turbine cylinders after partial expansion of the live steam.

The outlet temperature differential between the reheated and the heating steam largely determines the size and cost of the reheater(s). For example to reduce the differential from 15 to 14°C requires an increase in heat exchange surface of 4%.

A single stage reheater reduces the steam consumption per KW generated by 1.5% to 2% and by a further 0.4% to 0.6% where a second stage of reheat is added.

### 2.3 Erosion-corrosion

In light water reactor systems there is a potential for damage to plant and piping due to the existence of increasing moisture during expansion of steam through the turbine. The loss of material thickness observed is the result of both mechanical and chemical influences.

This type of attack is known as erosion-corrosion and is strongly dependent on the chemical treatment of the water.

Erosion-corrosion usually occurs in wet steam flows on carbon-steel components and may result in a local metal loss of several millimetres a year. The mechanical integrity of the components can be rapidly jeopardized.

The rate of metal loss depends on the pH of the liquid phase, on temperatures, fluid velocity, water content, and the geometry of the obstacles.

It is significant between 40°C and 260°C and maximum at 180°C, which often corresponds to the temperature of the wet cycle steam at the HP turbine outlet.

Without the use of separation and reheat the resulting wet steam flow through parts of the LP turbine and associated plant would result in unacceptable erosion-corrosion of carbon steel components. The adoption of the moisture separator reheater minimizes or entirely eliminates this risk.

## 3. GENERAL REQUIREMENTS OF A MOISTURE SEPARATOR REHEATER

It is essential to the power plant that the moisture separator reheater has high reliability and achieves its performance. This must be achieved in a cost effective manner. Moisture separator reheaters are therefore subject to an economic evaluation to determine optimum performance which results in the following typical parameters:

- (a) Separating efficiency to be high enough to reduce the water content at the separator outlet to a maximum of 0.5%.
- (b) Outlet temperature differential between reheated steam and heating steam of about 15°C.
- (c) Two stage reheat, using for the first stage bled steam from the HP cylinder and for the second stage live steam.
- (d) Pressure drop of the main steam flow through the moisture separator reheater unit of the order of 3% of the inlet pressure.
- (e) The space occupied by the moisture separator reheater units in the turbine hall needs to be minimised. Whereas multiple smaller vessels could be used, the use of two vessels per turbine is ideal in that it minimises the amount of interconnecting pipework and the overall space required.

These requirements need to be

incorporated in designs which avoid, for the complete range of possible operating conditions, the problems that have been encountered world wide in many earlier moisture separator reheater designs.

4. GENERAL DESIGN ARRANGEMENT

As illustrated in Fig. 2, the combined moisture separator reheater is a complex unit requiring the accommodation of the main steam flow initially through a separator and then through two stages of reheater to the steam outlet connections.

The reheated steam has to be segregated from the cold wet steam by baffles incorporating seals to cater for differential expansions. There has to be good distribution of steam through the separator and reheater elements to ensure efficient separation and heat transfer. The flow of heating steam, condensed in the tubes, has to be controlled to avoid flow instability whilst maintaining efficient heat exchange. The steam headers must have effective sealing to achieve segregation of steam and condensate and avoid any risk of tube flooding.

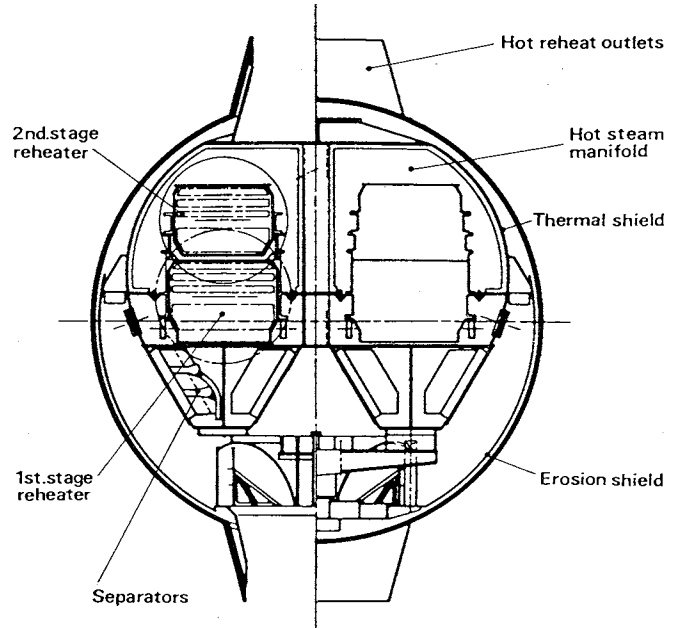


Fig.3 Cross section of M.S.R. Chooz B N.P.S.

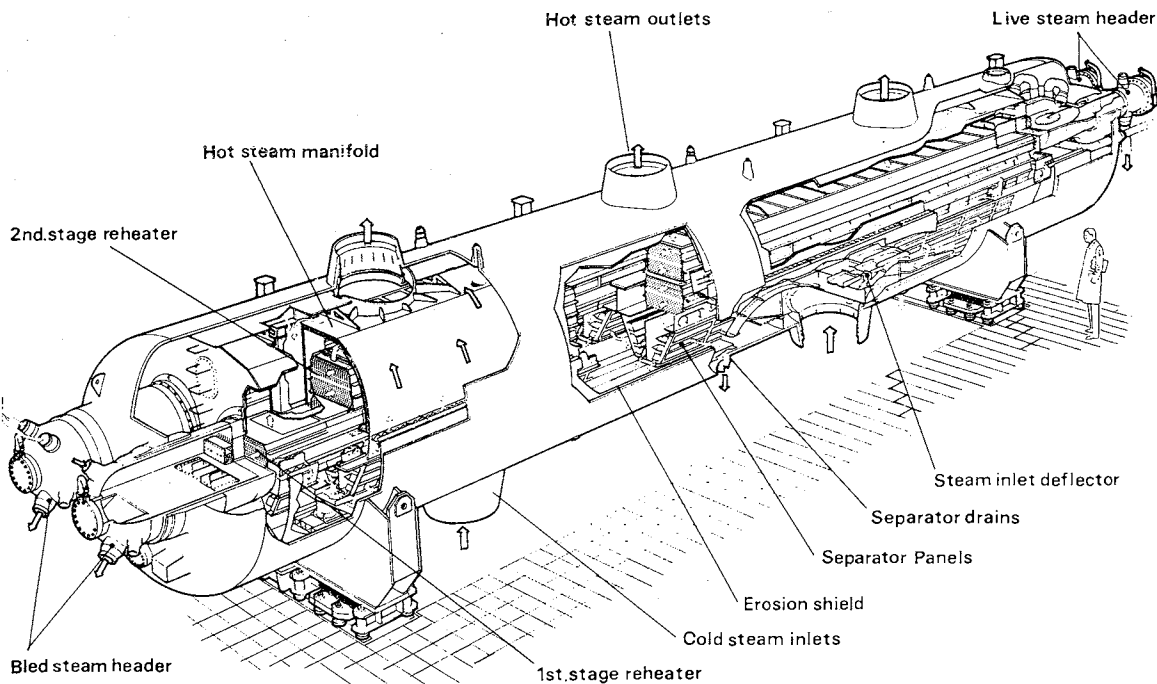


Fig.2 Moisture separator reheater Chooz B N.P.S.

## ANCILLARY PLANT AND MATERIALS OF CONSTRUCTION

In the moisture separator reheater designs illustrated this is accomplished by:-

- (a) an inlet chamber enabling the even distribution of wet steam flow upstream of the separators.
- (b) separator elements and their associated water drainage systems.
- (c) two reheater tube bundles.
- (d) a chamber to collect and channel the reheated steam to the outlet nozzles
- (e) an internal structure required to support the complement of separator elements and reheater tubenests. The support structure must facilitate all the differential expansions that occur during all possible modes of operation.
- (f) bypass prevention devices inside and around the reheater tube bundles.
- (g) internal baffles to channel the main steam and protect the pressure parts from thermal shocks during rapid load changes and also from risks of erosion-corrosion.

For large reheater units where several sets of separators and bundles are incorporated in the same vessel, a side-by-side arrangement, Fig. 3 provides a compact arrangement and minimises the space requirement on the turbine floor.

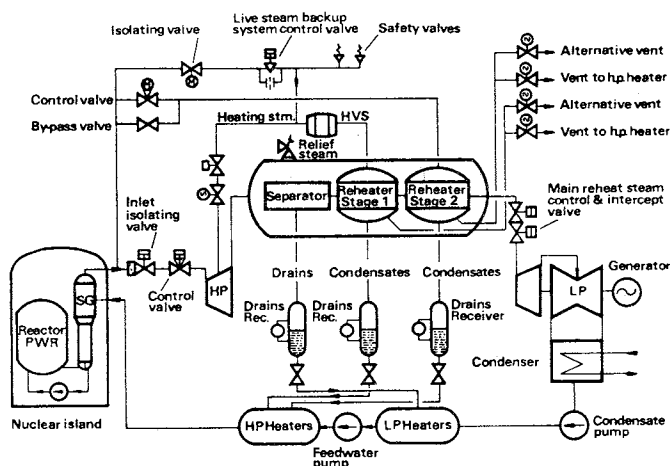


Fig. 4 Illustration of an M.S.R. in a PWR power cycle

The moisture separator reheater is incorporated in the power cycle as shown in Fig. 4 and is provided with the following auxiliary systems:-

- (a) heating steam supply systems.

- (b) heating steam condensate drainage systems (recovery tanks and piping).
- (c) reheater vent systems.
- (d) separator drainage systems (recovery tanks and piping).
- (e) moisture separator reheater relief system.

## 5. EXPERIENCE AND DEVELOPMENT

The authors' companies have over 75 years experience in the design and manufacture of heat exchange equipment and 20 years experience in the supply and operation of moisture separator reheaters.

Since 1970 an extensive programme of development to achieve high performance and reliable moisture separator reheater designs has been undertaken to meet the requirements of the French nuclear power programme.

Both the general principles and the specific details of design have been the subject of continuous experimental development in the authors' companies test facilities and in collaboration with Electricite de France. Information gained from extensive inspection and tests on operating plant has enabled design improvements resulting in improved thermal efficiency.

Detailed tests have been conducted on the following:

- (a) prepreparation and distribution of water at the inlet to the moisture separator reheater.
- (b) distribution of steam and water in the separators.
- (c) efficiency of separators in air/water mixtures and in wet steam.
- (d) heat exchange coefficients and pressure drops of finned tube bundles.
- (e) steam condensation conditions in long, horizontal U-tubes.
- (f) vibration of tubes.
- (g) wear of finned tubes and their supports.
- (h) behaviour of tube bundle during differential expansion between bundle and support structure.
- (i) operation of seal strips.
- (j) distribution of steam through moisture separator reheater vessels under various possible operating modes.

Finally, the experience acquired from some 200 operating moisture separator reheaters substantiates and complements the expertise of the authors' companies and has been incorporated in the current designs of moisture separator reheaters.

6. MOISTURE SEPARATOR REHEATERS FOR CHOOZ "B" (FRANCE)

6.1 General description

The first moisture separator reheaters of this class, Fig. 2, to be installed at CHOOZ B1 which will go critical in 1992.

The associated turbogenerator includes a combined high and intermediate pressure cylinder and 3 low pressure cylinders. The two horizontal moisture separator reheaters are installed on the floor of the turbine hall, on either side of the combined high and intermediate pressure cylinder, Fig. 5.

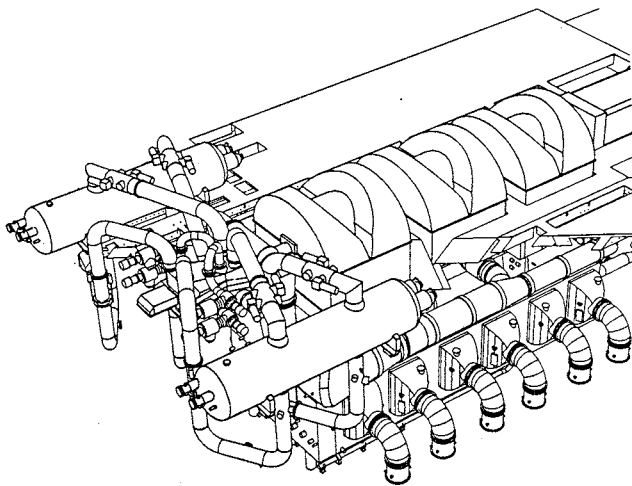


Fig. 5 Illustration of plant arrangement Chooz 'B' N.P.S.

The principal features of the design are detailed below. (The description follows the main flow through the moisture separator steam reheater).

6.2 Preseparation at inlet

The cold main steam is admitted to the lower part of the moisture separator reheaters via two nozzles. Opposite these, two deflectors partially separate the water from the steam and also protect the main separator from direct impingement by high velocity water droplets. They are shaped to promote uniform steam flow along the length of the moisture separator reheater assembly.

6.3 Steam distribution

Even distribution of the steam through the separators and reheaters is essential. The high pressure drop through the reheaters is sufficient to ensure the required uniformity of steam distribution through them.

However, the lower pressure drop of the separators is insufficient to ensure a local even steam flow into each element. To solve this problem the design takes advantage of the resistance of the reheaters by dividing the separators into several parallel cells.

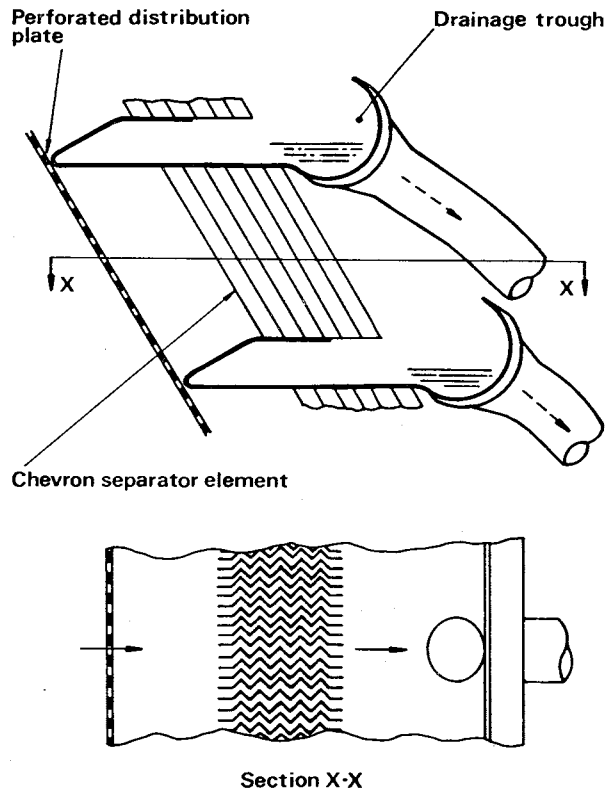
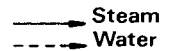


Fig. 6 'Stein' separator element

In each of these a separator panel and a dedicated reheater section are arranged in series.

Thus, the good longitudinal distribution imposed by the reheaters is utilized to induce an even flow through the separator panels. Even distribution across each separator panel is further assisted by upstream perforated plates built into the separator element, Fig. 6. Details of the perforated plate are established in flow tests conducted on scale models of the moisture separator reheater. The necessary flow distribution takes place in the large space provided upstream of the separators.

6.4 Protection from erosion-corrosion

Components in contact with wet steam are made of austenitic or ferritic stainless steel and are provided with a smooth profile.

The containing vessels are fabricated in

## ANCILLARY PLANT AND MATERIALS OF CONSTRUCTION

carbon steel and are protected by stainless steel liner plates.

### 6.5 Separators

Separation of the entrained water is achieved by the multiple changes in direction that the steam undergoes as it passes between a series of austenitic stainless steel corrugated plates, Fig. 6.

The water droplets hitting the walls form a film which is removed by a combination of gravity and the downward flow of the steam due to the inclination of the corrugations.

The plates have smooth convolutions without water collection pockets and therefore avoid the risk of water entrainment by local turbulence. The depth of each element is limited to 165mm, to avoid water inundation, and the width is approximately one metre and is chosen to align with alternate reheater tube support plates. The complete separator comprises a bank of such elements welded in to the support structure, as shown in Fig. 3.

### 6.6 Separator drainage

As illustrated in Fig. 6, the water entrained by the corrugated plates is efficiently removed by the drainage trough and an individual drain pipe fitted to each separator element. The pipes discharge into a system of drainage channels in the bottom of the containing vessel. Separated water finally combines with water collected from upstream of the separator in a drainage pot which incorporates a manometric seal to prevent steam leakage.

The drainage system is designed to limit the volume of water present in the vessel, thus reducing the consequences of drains flashing in the event of depressurisation following a plant load reduction.

### 6.7 Horizontal reheater bundles

The tube bundles consist of a nest of integrally finned tubes welded into circular tubeplates and headers. The headers have a tight fitting partition plate to segregate the incoming steam from condensate leaving the tubes.

The tubes are supported in a series of drilled plates positioned such that damaging vibrations are avoided. The bundle support system enables the free expansion of the tubes with any distortion at the bends being accommodated by hour glass drilling of the last support plate.

The bends, which are incorporated in the heat exchange surface, are subjected to cross tube steam flow and have supplementary supports to suppress potential vibration.

Leakage between the tubes and the vertical side walls of the bundle is prevented by a series of restrictions which protrude into the tubenest. This feature is necessary to achieve high thermal performance and also to prevent undercooling of the side tubes.

The tubes are made from type 439 ferritic stainless steel, which is similar to the American specification ASME Sd. 268 TP XM8. This material avoids the erosion-corrosion problems experienced in the carbon steel tubes of earlier moisture separator reheaters and has the advantage that, unlike austenitic stainless steel, its coefficient of expansion is similar to the carbon steel used in the remainder of the tube bundle.

The tube material has been used in the construction of reheater tube bundles since 1979. Combined with the other design features described it has given trouble free service in 30 tube bundles operating in French plants since 1984.

### 6.8 Flow of the heating steam and of the condensate

The design of horizontal reheater bundles is made difficult by the phenomenon of condensate undercooling. This arises mainly from the fact that the temperature difference between the heating steam and the steam being reheated varies for each row of tubes. As shown in Fig. 7(a) the inner rows of the tubenest operate without complete condensation of all the steam entering the tube whilst in the outer rows condensation is complete before the tube outlet.

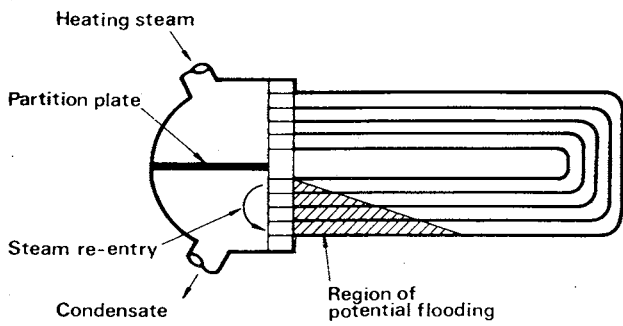
This results in potential flooding of the lower tubes and the risk of intermittent flooding of individual tubes.

As the heat transfer coefficient of the flooded section is much lower than that in the remainder of the tube, in which condensation takes place, the flooded section is cooled by the external cold steam flow.

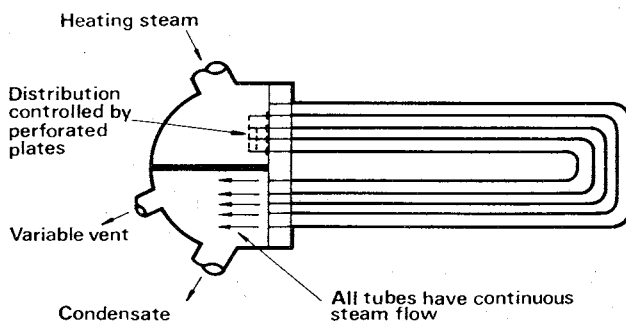
The resultant temperature differential causes distortion of the U tube resulting in friction between the tubes and their support plates and increased stresses. It is also possible for the water/steam interface in the tube to be unstable, giving rise to thermal cycling of the tube-to-tubesheet connections, and a risk of fatigue cracking.

The measures successfully adopted to solve the problem, illustrated in Fig. 7(b), are:

- (a) achieving gravity drainage by arranging the U-tubes in a vertical plane with downward circulation of the heating steam.



(a) Reheater tube flooding with uncontrolled condensation



(b) System for controlling condensation to prevent flooding and unacceptable undercooling

**Fig. 7 Illustration of reheader tubenest operation**

- (b) equalising the resistance of the tube rows by means of distribution plates fitted at the inlet of the tubes.
- (c) increasing the rate of steam flow in the tubes over that to be condensed in them by venting the outlet section of the header to a feedwater heater at a lower pressure. This vent flow represents 2 to 3% of the heating steam flow at full load and may be increased at part load.

Successful operation of over 200 dual-pass bundles have demonstrated the validity of these design principles.

**6.9 Operating conditions of the containing vessel**

Unless particular precautions are taken the vessel may be subject to a high thermal

gradient as a result of the temperature difference between the incoming cold steam and the outgoing reheated steam. The resulting overall thermal distortion would subject the vessel to thermal stresses. Furthermore, the vessel internals must achieve, for all operating conditions and particularly houseload operation, the following:

- (a) a good seal between wet steam, dry steam and reheated steam (in spite of thermal deflection).
- (b) free relative movement of the various sub-assemblies as a result of differential expansion during operation.

These requirements are not easily achievable in large units. The design solves this problem by maintaining the complete containing vessel at the cold steam temperature with an inner insulated chamber channelling the reheated main steam to the outlet nozzles, see Figs. 2 and 3.

The fixed points of contact between the vessel and the whole internal structure are limited to the outlet nozzles. The internals are therefore free to expand relative to the vessel.

**6.10 Limitation of leaks**

Experience of operating plant is that even slight bypassing of the separators or reheaters by wet steam significantly down grades the reheat temperature.

The arrangements for reheader bundle support and sealing are separate. With the dual bundle arrangement both of the second stages are supported via skates on the associated first stage bundles. These are supported within the frame by a series of wheels located on a track running the length of the tubenest. Sealing between the first stage reheader and the internal structure and between the two reheader stages is provided by flexible metal strips. The following precautions are taken to prevent bypassing without restricting thermal expansion of the components:-

- (a) the fully welded construction of the separator panels prevents any water bypassing.
- (b) flexible sealing strips ensure a sliding seal between the reheader bundles and the internal baffles.
- (c) the reheader tubenest headers are equipped with sliding packed glands where they pass through the chamber.

**7. MOISTURE SEPARATOR REHEADER DESIGNS FOR THE 985MW TURBINE GENERATORS FOR GUANGDONG NPS (CHINA) AND FOR THE 630MW TURBINE GENERATORS FOR SIZWELL 'B' NPS (UK)**

## ANCILLARY PLANT AND MATERIALS OF CONSTRUCTION

### 7.1 Basic design features

The basic design principles and features of moisture separator reheaters for these projects are the same as those adopted for the Chooz B1 station, described in preceding paragraphs. These include:

- (a) steam distribution between the parallel banks of separators.
- (b) protection from erosion-corrosion (including selection of material).
- (c) separators (design and material).
- (d) separator drainage.
- (e) horizontal reheaters bundles (design and material).
- (f) control of flow of heating steam and of the condensate.
- (g) control of operating conditions in the containing vessel and limitation of leakage between internal components.

### 7.2 Plant arrangement

The two vessels per turbine are located on either side of the three low pressure cylinders at turbine floor level, Fig. 8.

This results in a compact plant arrangement with symmetrical and minimum lengths of 2 $\frac{1}{4}$ % chrome steel cold reheat pipework and carbon steel hot reheat pipework. The latter, which discharge into the top of the turbine LP cylinders, also incorporate the butterfly type turbine interceptor valves. Condensate from each separator and reheater drains, by gravity, to the individual receivers located directly below the moisture separator reheaters.

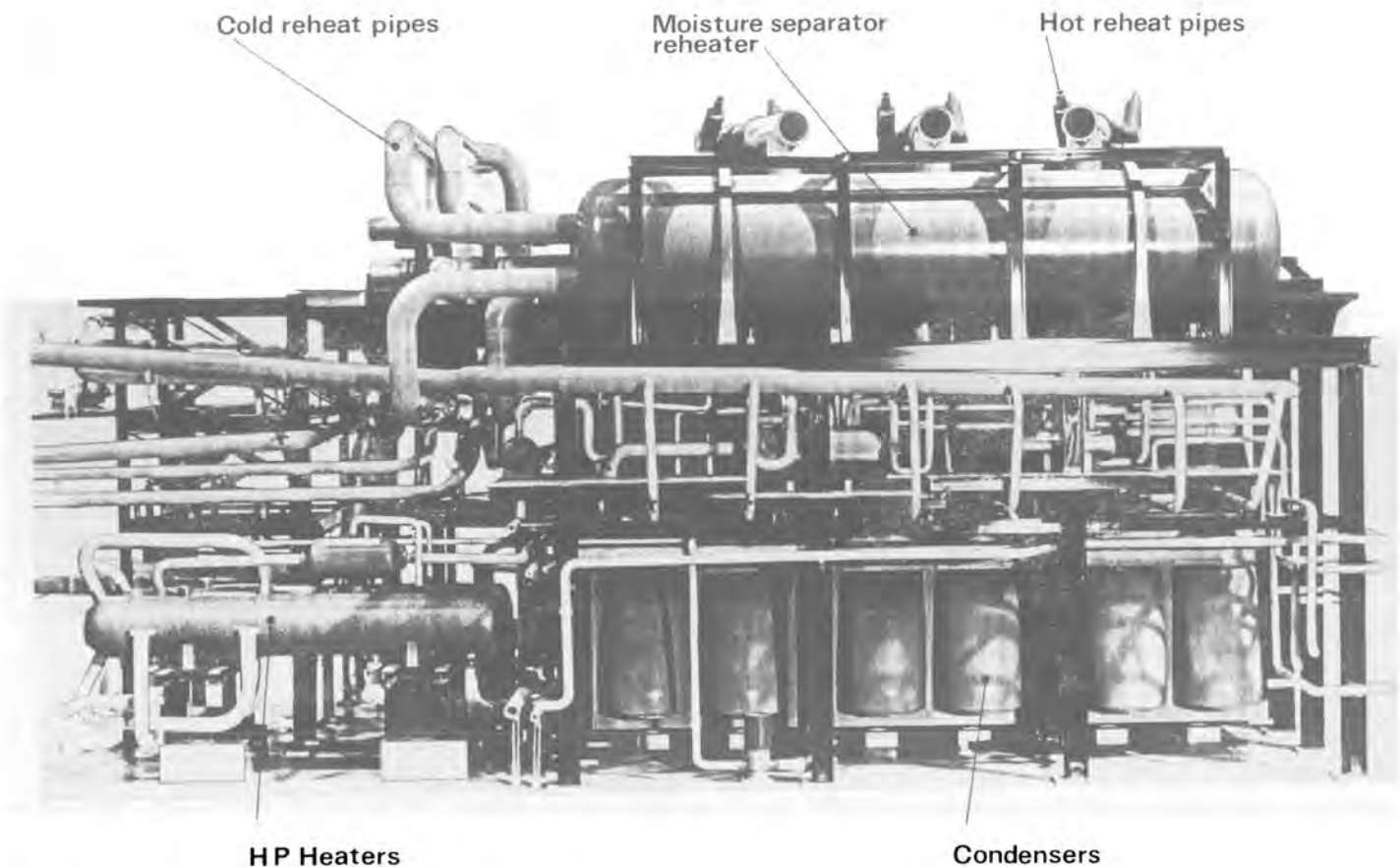


**Fig. 8 Plant arrangement incorporating MSR Sizewell B N.P.S.**

The MSR drainage system is described in more detail in a separate paper to this conference (Ref. 1).

7.3 General MSR description

As shown in Fig. 9 the units have one bled steam first stage and one live steam second stage reheater bundle located directly above the separators which are arranged in a V formation in the lower half of the vessel. The main wet steam is admitted to one end of the moisture separator reheater vessel through four inlet nozzles, Fig. 10. It then flows along the vessel in the ample space provided upstream of the separators.

Consequently the header of the first stage reheater is also within the vessel. A central tube passes through the end of the vessel to provide bled steam to the tube bundle and also facilitate personnel access to the headers to enable inspection and maintenance. The header of the second stage, live steam, reheater bundle is welded into the opposite end of the vessel.

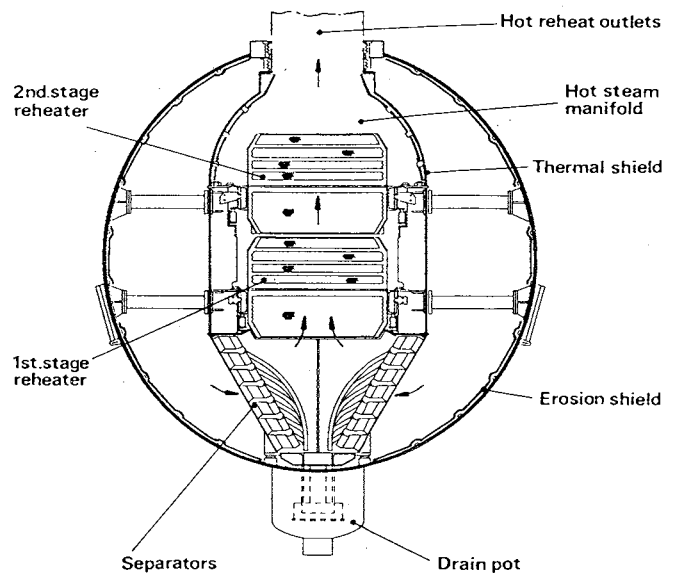


Fig. 9 Cross section of M.S.R. Guangdong/Sizewell N.P.S.

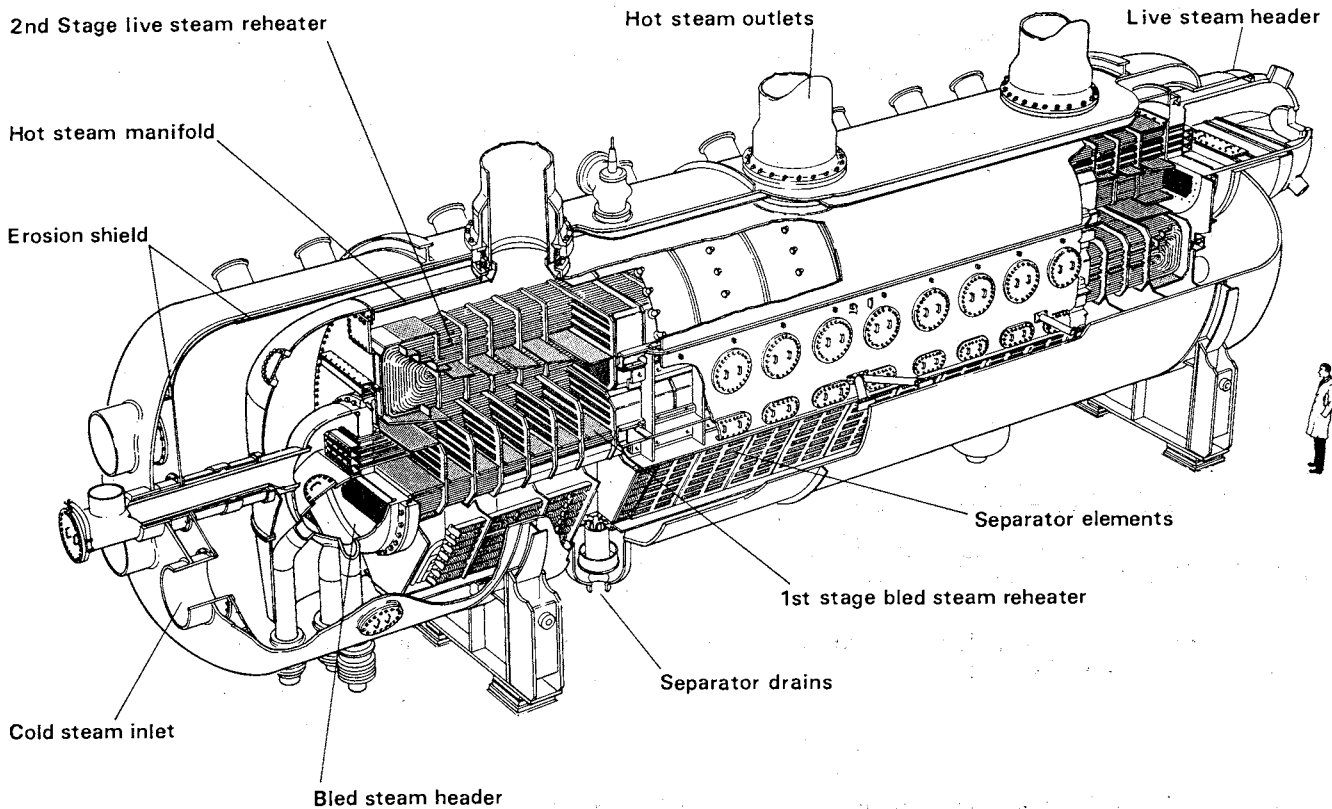
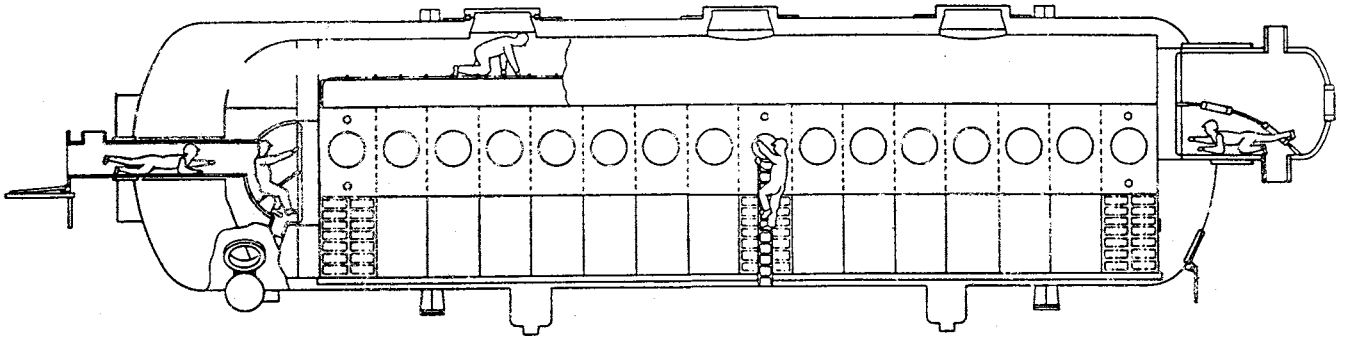
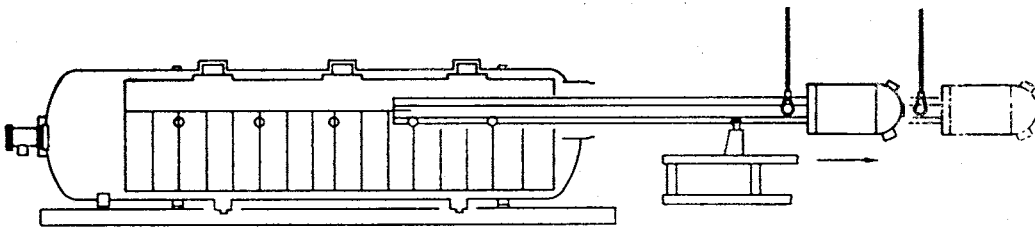


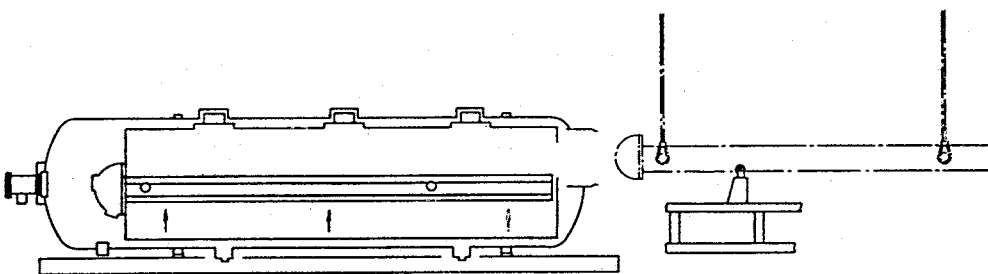
Fig.10 Moisture separator reheater Guangdong Sizewell N.P.S.



(a) Access to MSR for inspection and maintenance



(b) Withdrawal of live steam tube bundle using temporary steelwork as support and then crane used for final withdrawal and lift.



(c) First jack bled steam bundle up and then withdraw using same procedure as for live steam bundle.

Fig.11 Provision for inspection and maintenance of MSR.

After separation of the majority of the entrained water the main steam rises through the first and second stage reheater tube bundles. The reheated steam is contained and channelled to the three outlet connections by a manifold which has two skins. The inner skin is subjected to the hot steam temperature and acts as a thermal shield to the leak tight outer skin. This is maintained at the cold steam temperature by the substantial flow of cold reheat steam. The stagnant space between the inner and outer skins provides the necessary thermal insulation.

The complete containing vessel, the whole of the internal support structure, the separators and the the outer skin of the hot steam manifold normally operate at the cold reheat temperature thereby minimising differential expansions.

#### 7.4 Moisture separator reheater inspection and maintenance

Access routes in the moisture separator reheater for inspection and maintenance are shown on Fig. 11(a) and are similar to those provided in the French designs. Access to the reheater header internals is achieved independently of the moisture separator reheater containment vessel; to the first stage reheat by the bled steam inlet duct and the second stage by the header manway opening. Entry to the main vessel is gained through one of three manway doors.

For inspection of the area above the tubenests and the tubenest seals, entry is made

through removable inspection doors in the tubenest support structure.

All important components of the moisture separator reheater are accessible for inspection during planned shutdowns. Tube and seal weld integrity can be checked by testing inside the header for leakage of gas admitted to the containing vessel.

If it is ever necessary or advantageous to undertake complete tubenest removal this can be carried out as illustrated on Figs. 11(b) and 11(c), without removing the ends of the containment vessel.

#### 8. SUMMARY

The accumulated experience of the authors' companies since 1970 covers some 200 moisture separator reheater units operating in a range of steam cycles in many locations.

The combination of this extensive experience and the result of a comprehensive development programme, originally undertaken to meet the requirements of the large French nuclear PWR programme, has resulted in the latest moisture separator reheater designs as described in this paper.

#### REFERENCES

1. C.J. Monks "Feedheating Plant for Wet Steam Cycles". BNES 1988 Conf. Technology of Turbine Plant Operating on Wet Steam.



## 12. Experience with centrifugal separators and vertical-tubed reheaters associated with large wet steam turbines

A. R. KERNAHAN, BSc, MIMechE, and W. R. REID, BSc, MIMechE, NEI Parsons Ltd

The paper deals with the unique separators and reheaters developed by the authors' company. A total of 56 separators and 28 reheaters have been built and are successfully operating with turbine units ranging in size from 540MW to 800MW. The steam for these turbines is supplied from CANDU reactors. The original design concept is explained and brief reference is made to the supporting experimental work. Operational experience covering manufacture, plant arrangement, operational procedures, performance, reliability and maintenance is discussed, and some recent developments for incorporation in modern wet-steam projects are described.

### INTRODUCTION

1. The separation of moisture from the very wet steam exhausting from the HP turbines in wet cycle plant, together with reheating of the dried steam prior to the LP turbine inlets, constitute two distinct physical processes. Early consideration of the fundamental principles involved led NEI Parsons to adopt novel designs of equipment to accomplish these processes, and in particular to the decision that moisture separation and steam reheating should take place in separate vessels. Some account of these early considerations has been given by Bolter (ref. 1). The present paper gives details of the development and design work which followed, describes the separators and reheaters in more detail, and gives an account of experience with the 56 separators and 28 reheaters which have been supplied and installed.

2. These separators and reheaters have been extremely successful, and the basic concepts of the design have remained unchanged. The principal details of the separators and reheaters supplied are given in Table 1, and the service record of the associated turbine generator units is given in Table 2.

### GENERAL DESCRIPTION

#### Separators

3. Parsons separators are of the horizontal in-line centrifugal type (see Fig. 1) in which a swirl velocity is imparted to the 13% wet incoming steam by a complete ring of blades. These blades are similar to those used in a turbine. The steam-borne water droplets are therefore centrifuged outwards on to the surface of an internal cylindrical louvred cage. The cage is formed from separate louvre plates with full length axial drainage slots between the plates.

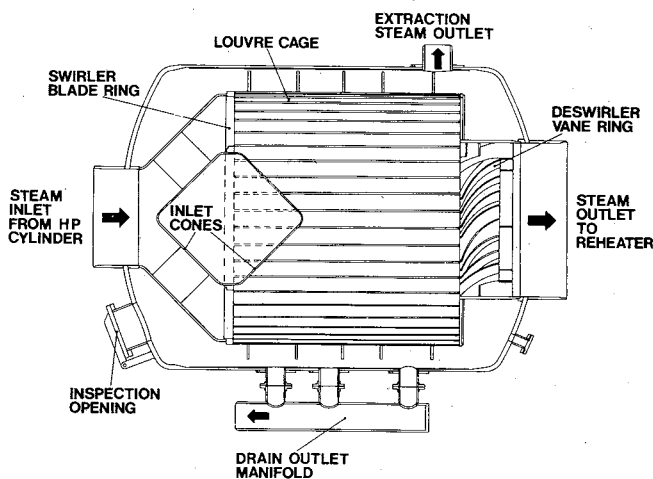


Fig. 1 Section through separator

4. The separated water passes through the drainage slots into the annular space between the louvre cage and the outer shell, its passage being assisted by a flow of extraction steam bled off to an appropriate stage of the feedheating plant. The water removed is collected below the separator in an external drains manifold and is also returned to the feedheating system.

5. The main outgoing steam, which is now only about 0.5% wet, flows through an axially located transfer pipe direct to the reheater. A ring of de-swirler vanes (see Fig. 2) is located at the entry to the transfer pipe to remove any swirl velocity component remaining in the outgoing steam flow. Four identical separators are used for each turbo-generator and are arranged two on each side of the machine.

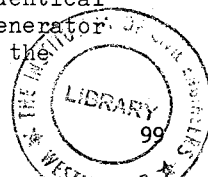




Fig. 2 Deswirl vane ring

**Reheaters**

6. The Parsons design of reheater consists of a number of vertical straight-tubed bundles, usually five, which are contained within a large vertical cylindrical vessel (see Fig. 3). The bundles are identical, and each consists of a bank of externally finned tubes which are end welded into a top inlet header and a bottom drain header. The bundles are further contained within a common inner housing which connects the bundle matrix to the vessel outlet pipes. Each bundle is independent and is free standing on two lower transverse tubular support struts which also support the inner housing. In most designs, the tubular struts are extended and incorporate the supporting feet for the main vessel.

7. Two identical reheaters are used for each turbo-generator and are arranged one on each side of the machine. The incoming steam from the two associated separators is heated in a single pass as it flows through the shell side of the tube bundle matrix. Each bundle is individually supplied with heating steam, either live steam direct from the nuclear boiler, or bled steam from an intermediate point on the HP turbine. The heating steam condenses as it flows downwards inside the tubes, thereby reheating the shell side steam flow to a superheated condition. The condensate is piped to an external collecting tank for return to the boiler or to the feed-heating plant. The steam supply pipes and condensate drain pipes are arranged with sufficient flexibility to accommodate thermal expansion.

8. The shell side outlet superheated steam flow then passes through piped connections to the LP turbines. Early designs incorporated a single outlet pipe which was manifolded to supply three LP turbines. Later arrangements include separate outlet pipes to each LP turbine to improve the shellside flow distribution through the tube bundle matrix.

Table 1. Principal details of NEIP separators and reheaters

	Units	Pickering 'A'	Pickering 'B'	Bruce 'A'	Pt. Lepreau Wolsung
<b>For one separator:-</b>					
Inlet pressure	kPa(a)	493	911	612	
Inlet wetness	%	10.7/12.1	8.7	11.8	
Mass flowrate	kg/s	174.8/177	265.9	219.6	
Efficiency	%	95/97	95	95	
Outlet wetness	%	0.6/0.4	0.45	0.6	
Outer diameter	m	3.505			
Overall length	m	5.258			
Working weight	tonnes	28	31	31	
<b>For one reheater:-</b>					
Heat load	MW	52.6	73.1	75.0	
T/S inlet press.	kPa(a)	4033	4240	4551	
T/S flowrate	kg/s	30.8	43.2	45.0	
Outlet TTD	°C	27.8	16.7		
S/S temp. rise	°C	73.3	61.7	83.4	
S/S outlet temp.	°C	223.9	237.2	242.6	
Outer diameter	m	3.962	4.648		
Overall height	m	8.788	11.176		
Tube diameter	m	0.019	0.029		
Bundle LBTP	m	4.801	5.791		
Working weight	tonnes	100	163		

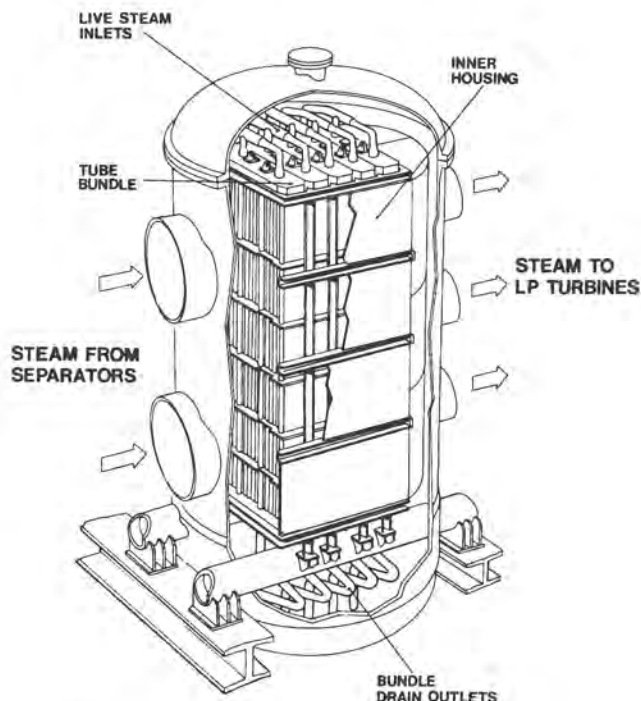


Fig. 3 Reheater assembly

DEVELOPMENT AND MATERIALS  
Separators

9. The early development work on Parsons separators was performed using approximately 1/5 scale model separators. These models were supplied with wet steam from the exhaust of an experimental turbine rather than from an artificially created wet steam supply. It was only by using turbine exhaust wet steam that the necessary thermal equilibrium between the steam and water phases was obtained, and a realistic distribution of wet steam droplet diameters produced which was appropriate to the intended separator duty.

10. Stairmand (ref. 2) had recommended a maximum design value of  $1340 \text{ kg m}^{-1}\text{s}^{-2}$  for the steam shear force parameter ( $Qv^2$ ) to avoid re-atomisation of the separated water film at a cyclone wall surface. It was established during the development work however, that a high separator efficiency could be obtained at the required steam flowrates with shear force parameters 2 to 3 times Stairmand's limit only when a concentric inner louvred cage was fitted. This allowed the centrifuged water to drain quickly into the quiescent annular chamber without risk of re-atomisation or re-entrainment in the outgoing steam flow.

11. Subsequent model work investigated water droplet formation and behaviour, steam and water loading on the louvres and through the louvre drainage slots, pressure drop and the effect of variations in geometrical features and extraction steam quantity. In particular, it was found that, contrary to expectation, flush louvres achieved a much higher separation efficiency - between 95 and 98% - than did overlapped louvres with raised leading edges. Moreover, this high efficiency could be maintained over a considerable range of louvre chord widths, drainage slot widths, steam flowrates and louvre water loading.

12. Water droplet formation and behaviour was studied by fitting observation windows in one of the model separators and in the test loop pipework. A theoretical analysis, ignoring considerations of steam purity and electrical charge on the water droplets, based on the work of Gyarmathy (ref. 3) and Gardner (ref. 4), was largely substantiated during these investigations of swirler blade geometry. It was known from previous work that a high proportion of the water contained in wet steam from a turbine exhaust flowed along the walls of the exhaust pipes. This important aspect was included in a study of separator inlet annulus and swirler blade ring geometry to optimise both the agglomeration and re-atomisation of the incoming water phase. The result of this study was to ensure that the range of droplet sizes produced at entry to the louvre cage could subsequently be centrifuged with a high separation efficiency.

Table 2. Operating statistics for NEIP wet steam turbine generator

Station and Unit	Unit Size (MW)	Operation from	Running hours to 31.12.87
<u>Pickering 'A'</u>			
Unit 1	540	25. 2.71	* 91152
2	540	15. 2.71	** 86278
3	540	24. 4.72	107588
4	540	26. 5.73	105701
<u>Bruce 'A'</u>			
Unit 1	800	14. 1.77	79362
2	800	7. 9.76	75639
3	800	14.12.77	78710
4	800	21.12.78	68366
<u>Pickering 'B'</u>			
Unit 1	540	19.12.82	34531
2	540	8.11.83	28831
3	540	17.11.84	23950
4	540	21. 1.86	15257
<u>Point Lepreau</u>	680	11. 9.82	43150
<u>Wolsung</u>	680	30.12.82	37012

\* Out of service from December 1983 to September 1987 for replacement of reactor pressure tubes.

\*\* Out of service August 1983 for replacement of reactor pressure tubes.

13. Tests were also performed to establish the relevant scaling criteria to confirm the applicability of model test results to the proposed full size separators. The correctness of the findings of this work has been established by the success of all of the full size separators which have been built.

14. These separators are designed for robust operation in the wet steam environment and are essentially maintenance-free. The inner parts are of erosion-resistant ferritic stainless steel (12Cr 1A1) and 2.1/4Cr-1Mo low alloy steel. The outer pressure vessel is of carbon steel with an internal cladding layer of ferritic stainless steel on the cylindrical section. The two dished end sections are unclad since they are in contact only with comparatively harmless flow velocities. Care is obviously required during manufacture to ensure adherence to the geometrical details established in the test programme.

15. The major influence on the overall pressure drop through the separator was found to be the degree of residual swirl present in the main outlet steam. Early experiments were performed using both steam and air models with outlet pipe diameters approximately one third that of the louvre

cage. Later results showed that the overall pressure drop could be reduced by almost 40% by nearly doubling the outlet pipe diameter. The provision of de-swirler vanes at the entry to the outlet pipe was also shown to result in further pressure recovery.

Reheaters

16. The reheaters are essentially a single-pass pure cross-flow heat exchanger. The initial thermal design, on the basis of low integrally-finned carbon steel tubes, was derived from the published correlations for such tubing developed by Briggs and Young (ref. 5). The practicality was influenced by the need to produce a matrix arrangement essentially square in plan view to minimise the diameter of the containing pressure vessel shell, and also to divide the matrix into a number of identical and interchangeable tube bundles. One bundle is shown in the horizontal position in Fig. 4.

17. Five tube bundles was found to be convenient; with fewer, the loss of one bundle would significantly affect the reheater performance and tubeplate thickness requirements, and with more, the increased shell diameter and number of bundle headers would incur higher total costs. In addition, the reduced number of axial tube rows in each bundle would result in excessive bundle flexibility making them liable to distortion during manufacture and maintenance, unless special precautions were taken.

18. Carbon steel has been used for all components in both the main shell and the tube bundles. The low maximum steam velocity, and stable condensate drainage process inside the vertical tubes, obviated the need for more erosion-resistant alloy steel tube material. Owing to the relatively high ductility of carbon steel, integral fins can be formed in tubes of this material with comparative ease. Suitable carbon steel finned tubing with a significantly enhanced external- to-internal surface area ratio was readily available so it was not necessary to consider the use of more expensive non-ferrous tubing. Also, the requirement to seal weld the ends of the tubes into the carbon steel tubeplate was achieved without the need for special surface preparations on the tubeplate weld face.

19. Bolted covers are used in the nominally identical top and bottom headers. The upper cover incorporates two baffled connections to aid distribution of the inlet steam, with the lower cover incorporating a single drain outlet connection. The tubes, and hence the top header, are free to expand upwards from the bottom header. Vibration of the tubes is prevented by a support structure, suspended from the top header and guided in the bottom header, which incorporates horizontal tube support plates. A number of the tube support plates are carefully adjusted to ensure adequate contact between the tubes and each support plate. The contact must be sufficient to preclude multiple spanning but must not inhibit vertical differential movement. Two vertical flow splitter plates are also incorporated in the support structure and these, together with the bundle side walls, avoid the establishment of an acoustic resonance.

PLANT LAYOUT

20. The layout of one reheater shell in the longitudinal pipework on each side of the turbine is shown in Fig. 5 which is a photograph of one of the 800MW Bruce 'A' turbine generators at Site. The domed top cover of one of the reheaters can be seen near the lower left hand corner of the photograph. Easy access is thus available for removal of the top cover for maintenance. The water separators are located beneath the turbine floor. At Pickering 'A', the separators were placed transversely in the horizontal loops of the HP exhaust pipes beyond the steam end of the machine, whereas on all later units they have been placed longitudinally and comparatively close to the reheaters.

21. In combination with the use of LP turbine steam inlets below the machine centreline, the arrangement at Bruce 'A' results in a clean and uncluttered turbine floor and facilitates accessibility to the turbines during maintenance. The 540MW units at Pickering, and the 680MW units at Point Lepreau and Wolsung, however, use a different design of inlet valve to the LP turbine and this results in the steam inlets being above the machine centreline. Fig. 6 shows a side elevation depicting the arrangement of the separators and reheaters on one of the 680MW units.



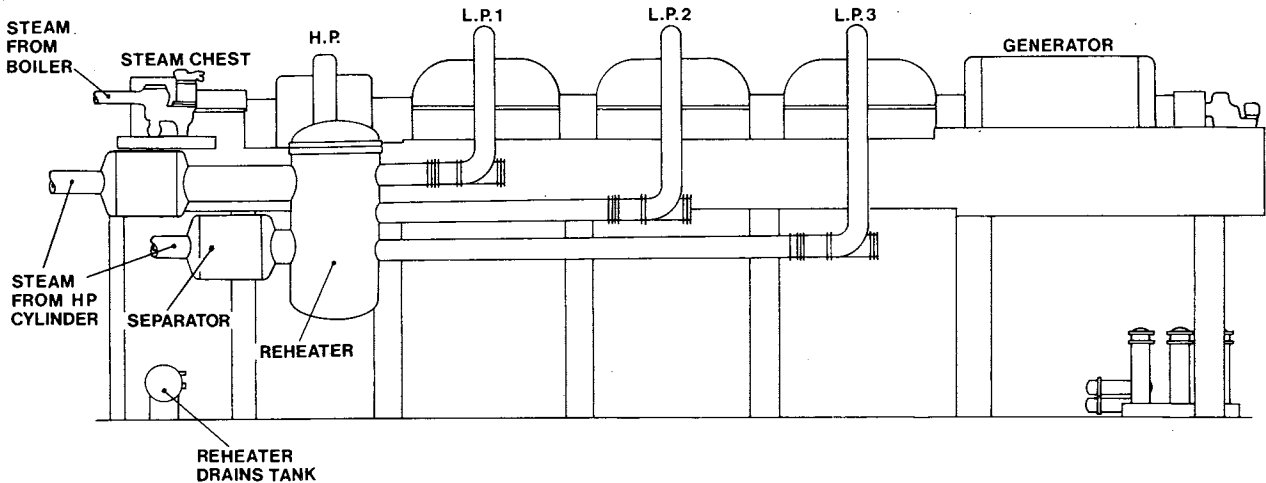


Fig. 6 Arrangement of separators and reheaters in a 680MW unit

22. Additional separators are required for any HP turbine which does not incorporate steam and water extraction belts supplying the feedheating system. In such turbines, the maximum steam wetness levels through the blade path is limited to acceptable values by passing extracted steam and water through external auxiliary separators at a number of stages along the turbine, as depicted diagrammatically in Fig. 7. The flow capacities of the appropriate HP turbine stages are designed to establish the necessary steam and water flows. These auxiliary separators are designed on the same principles as the main steam separators, but naturally are somewhat smaller.

**OPERATING EXPERIENCE**  
Mechanical reliability

23. Whilst it is true to say that the Parsons separators and reheaters have been extremely successful, a number of minor problems have occurred. In general, these have been overcome without difficulty.

24. Early in the life of the first Pickering machine, inspection revealed tube damage at the inlet of the front bundle in each reheater shell. The damage was adjacent to the steam inlet pipes and was caused by excessively high incoming steam flow velocity which resulted in fluidelastic excitation of the inadequately supported tubes. The tube bundles were therefore staked, thereby raising the tube natural frequency from 40Hz to an acceptable 90Hz. All subsequent units were provided with sufficient support plates in the reheater bundles to avoid all possible modes of tube vibration.

25. A pressure pulsation had also been present in the pipework between the water separators and reheaters at Pickering A. This was eliminated by fitting internal fairings to manhole inspection covers in the pipework.

26. On the Bruce reheaters, the outer tube rows were damaged as a result of differential vertical thermal expansion between the finned tubes and the tube bundle support frames. This was due to jamming of the tubes in the outer edges of the support plates which had been subject to weld distortion during manufacture adjacent to the bundle welded side plates. These difficulties were overcome by improved manufacturing standards together with a later change to an unwelded side wall construction. Subsequent service experience has been entirely satisfactory.

27. Some joint leakage has been experienced both on the bolted covers of reheater outer shells and on the covers of tube bundle headers. The former difficulties have been overcome by using improved gaskets while the latter have been alleviated by minimising the degree of thermal shock imposed on the bundle during the machine loading sequence.

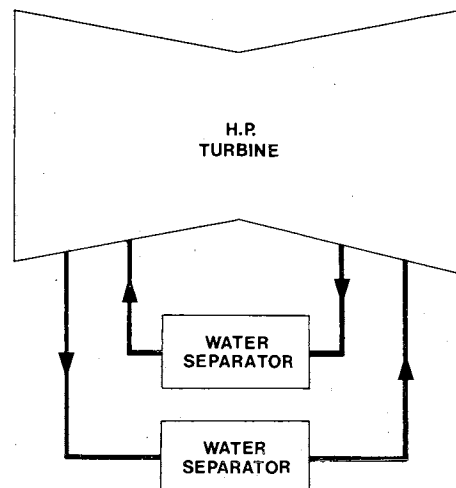


Fig. 7 Diagram of auxiliary separators

Erosion

28. There has not been a single case of reheater tube erosion emanating from flow conditions inside the tubes. The decision taken at the outset to use vertical tubes with condensation taking place in downflow in an orderly manner, and the consequent decision to use carbon steel for the tube material, has been entirely vindicated. It will be remembered that at the time of these developments, many reheaters installed elsewhere employed horizontal bundles of non-ferrous tubes with the result that severe tube erosion occurred under the highly turbulent 2-phase slug and plug flow regime present in such designs.

29. External erosion of reheater tubes has recently been discovered at Point Lepreau. Detailed investigation has indicated that steam-borne magnetite particles were present in the separator/reheater steam system and that these, together with excessive water carryover from the separators resulted in the tube bundle erosion damage. Some erosion of the separator to reheater transfer pipes, and of the separator extraction steam pipes, has also occurred.

30. A number of detailed manufacturing discrepancies were found in the separator construction and these corrected. A replacement front bundle employing erosion resistant stainless steel tube and support plate materials has also been installed in both reheaters. In addition, the feedwater chemical treatment method is being converted from ammonia pH control to morpholine pH control which should result in more stable and extensive surface oxide protective films on components throughout the steam and water cycle. The morpholine pH control method has continuously been used at Pickering 'A' and 'B', Bruce 'A' and Wolsung (see Table 2) where no such magnetite contamination problems have been countered.

Performance

31. Subject only to the exceptional and unsatisfactory case at Point Lepreau, separator performance has been excellent. No significant erosion or deterioration in surface finish has been noted during routine inspection of separators, and there is therefore no reason to suppose that performance will deteriorate during the life of the plant.

32. With regard to the reheaters, again it is true to say that thermal performance has been excellent. In all cases, the average reheated steam outlet temperature has been close to the design value. However, the tube-side distribution of the un-regulated steam supply to each identical bundle has resulted in a degree of condensate under-cooling occurring within the tubes, especially in the front bundle where the steam loading is greatest. The effect on the overall unit heat rate is small. The resulting vertical variation in shell side outlet temperature is preserved by the use of individual outlet pipes to each LP turbine,

the LP turbine fed from the lowest outlet pipe experiencing a lower inlet steam temperature than the other two LP turbines. The temperature difference can be up to 12°C, though again the effect on the overall unit heat rate is small.

33. The balance between the separators and reheaters on the left and right hand sides of the turbine has normally been quite close. Operation with different numbers of bundles isolated in the two reheater shells is permissible to ensure continuity of load generation, but the resulting loss of reheat and the need to limit the LP turbine exhaust wetness levels may require a restriction to be placed on the unit output.

Inspection and maintenance

34. The reheater design provides comparatively easy access for internal inspection and maintenance via top and bottom access openings in the main shell. Bundle removal is achieved by removing the bolted flanged cover from the main vessel, cutting the steam supply and drain pipes, and raising the bundle on the main station crane. It is advantageous to have a handling frame available on which to place the bundle for further inspection and repair if necessary.

35. Access to the inlet section of the separators (up to the swirler blade ring) is available through manhole openings in the HP turbine exhaust steam pipework. Access to the inside of the louvre cage section is normally through the reheater main shell top inspection opening or through a manhole opening in the separator to reheater outlet pipe.

36. The reheater main shell flanges originally used a segmented CAF and PTFE envelope type of gasket but these proved less than satisfactory. It is now the practice to employ a large single spiral wound gasket which can either be supplied complete or can be made up on site. Leakage from the bundle header cover joints which have a solid rectangular type of Nickel Silver gasket does still occur from time to time and some stations hold standby spare bundles to avoid the necessity for a repair operation during planned outage periods.

37. Apart from routine inspection, no maintenance of the separators is required.

Operation

38. Facilities are provided to allow individual reheater tube bundles to be fully isolated from the steam supply. This also allows on-load leakage testing to be carried out by isolating a bundle and monitoring the initial rate of decay of the internal pressure, together with the final equilibrium pressure level inside the bundle. The decay rates and equilibrium pressures for non-leaking bundles are dependent upon the bundle position within the reheater shell.

39. Operation with one bundle isolated in a reheater has only a minor effect on the reheated steam outlet temperature. However, more than two bundles isolated in one

reheater shell will result in a temperature imbalance in relation to the other reheater, and may necessitate the isolation of a bundle in the other reheater shell to restore temperature equilibrium across the machine. The resulting loss of reheat temperature to the LP turbines may then require a load reduction as already mentioned.

40. It is usual to provide a pre-warming control valve to allow the reheater bundles to be placed in service without experiencing excessive thermal shock. The carbon steel surfaces in both the reheaters and separators are protected against rusting during a prolonged unit outage by continuously blowing warmed air through the reheater/separator circuit. This protection is especially important in new machines to prevent rust bridging between the fins on carbon steel finned tube bundles, since this could result in a difficult cleaning operation or long term shortfall in reheater performance. The internal surfaces of the tube bundles are also protected during a prolonged outage by a dry-out process followed by nitrogen packing.

#### Associated systems

41. The normal principles governing the design of turbine drainage systems apply equally to separator and reheater drainage. The drain pipes should be of adequate size, and should slope continuously to the disposal point. Commoning of drains is not recommended. The steam trap which is normally fitted in the reheater shell drain pipe should be provided with an automatic motor operated bypass valve, activated by a level switch in the reheater shell to prevent the possibility of shell flooding rising into the lower steam outlet pipe to one of the LP turbines. Facilities for detecting blockage of the separator drain lines are also recommended.

#### RECENT DEVELOPMENTS

42. It is now common for power authorities to specify the use of stainless steel finned tubing in reheater bundles, and in keeping with this requirement, designs using stainless steel type 439L ferritic tube material and stainless steel support plates have been developed. As already described, two such bundles have been installed at Point Lepreau. This tube material requires an Inconel 625 cladding layer to be weld-deposited on the internal tubeplate face to which the tube ends are seal welded. The cladding process necessitates a design change in the tubeplate shape from the original hollow forging incorporating the header side walls, to a flat forging. The bolted header cover is correspondingly altered from a flat forging to a hollow forging. At the same time, the bundle header sealing arrangement has been improved to incorporate a reactive type of metal 'O' ring which is internally vented and silver coated on its sealing surface.

43. The good experience with the original carbon steel tubing, now strengthened by the

introduction of stainless steel tubing, means that bundle removal for tube leakage repair is almost unknown. In fact, the sole cause of bundle leakage in recent years has been gasket failure and this situation should be improved by the new design bundle header gasket. However, in order to eliminate fully the risk of gasket leakage, a further new design of bundle header is being developed in which the bolted joint arrangement is replaced by a semi-cylindrical cover welded directly to the tubeplate. Should a tube leak occur with this all-welded header design, it will be necessary to cut off the welded cover to obtain access for tube plugging, but the anticipated rarity of such occurrences makes this an acceptable risk.

#### CONCLUSION

44. The need for water separation and reheating of large flowrates of wet steam first arose with the introduction of wet steam power cycles. Willingness to contemplate novel solutions to these problems, coupled with thorough practical investigation in the laboratory, has contributed to the success of the separators and reheaters described in this paper. The practical experience gained during manufacture and in operation has emphasised the additional need for care and attention to detail in preparing the designs and during manufacture.

#### REFERENCES

- 1 Bolter, J.R. Design, development and operating experience with wet steam turbines. Brit. Nuc. En. Soc., Conference on technology of steam plant operating on wet steam. October, 1988.
- 2 Stairmand, C.J. The design and performance of cyclone separators. Trans. Inst. Chem. Engrs. 29,356, 1951.
- 3 Gyarmarthy, G. Basis for a theory for wet steam turbines. Bulletin No. 6, Institute of Thermal Turbo Machines. Fed. Tech. University of Zurich, 1963.
- 4 Gardner, G.C. Events leading to erosion in steam turbines. Proc.Inst.Mech.Eng., Vol.178, (Part 1), Page 23, 1963-4.
- 5 Briggs, D.E. & Young, E.H., Convection heat transfer and pressure drop of air flowing across triangular pitch banks of finned tubes. Chemical Engineering Symposium Series, Vol.59, No.41, pp 1-10, 1963.



# 13. Feedheating plant for wet steam cycles

C. J. MONKS, GEC Turbine Generators Limited

**SYNOPSIS** The design of feedwater heating plant for wet steam cycles must take account of the relatively high feedwater flow rates resulting from the combination of large turbine generator ratings and low initial steam conditions, the erosion potential due to the operation of the deaerator and HP feed heaters on wet steam and the need to accommodate substantial quantities of condensate from the moisture separator and reheaters involved in the cycle. The feed heater, deaerator and associated system designs adopted on 630 MW and 985 MW plant currently under construction are presented.

## 1. INTRODUCTION

The design of feedheating plant for turbines operating with wet steam generated by nuclear reactors is not fundamentally different from that normally used in fossil-fired power stations having turbines of large unit output. Nevertheless, as a direct result of different feedwater design quantities and bled steam conditions, significant differences exist in constructional details of components, in the choice of materials and in the design of various systems, particularly of those dealing with condensate or separated water.

This paper describes the design of the plant adopted by GEC Turbine Generators Limited for the 985 MW wet steam turbines for the Guangdong Nuclear Power Station (NPS) at Daya Bay in China and for the 630 MW wet steam turbine for the first PWR Station in the UK at Sizewell B. In this manner major significant features of the feedheating plant components and systems, typical of up to date design practice for a wet steam PWR power cycle, will be covered.

## 2. THE STEAM AND FEED CYCLE

The cycles were chosen to operate economically in conjunction with the GEC turbines as described in a separate paper to this conference (Ref. 1) and to produce a final feedwater temperature of 220-230°C. The possible variables considered in making the relevant choices were:

- (a) the number of feedheater stages
- (b) the surface of each feedheater and as a consequence the terminal temperature difference achieved
- (c) the provision of drain cooling
- (d) the provision of forward pumping of condensate

- (e) the sizing of bled steam lines
- (f) the routing of water separated in the moisture separator
- (g) the routing of live steam and bled steam condensates from respective tubenests of the reheaters

The chosen cycle for each project provides an economic balance between the installation, the operating costs and the evaluation of change in kW generated for each variation.

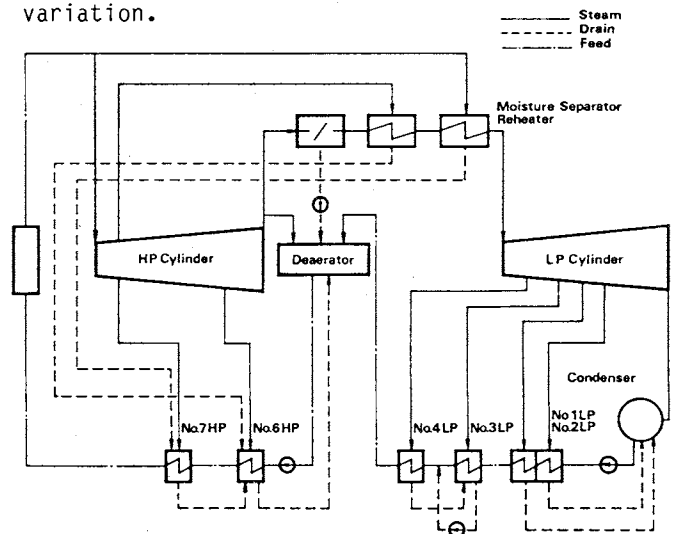


**Fig.1 Steam/Feed cycle for 985 M.W. turbine Guangdong N.P.S.**

The cycle adopted for the 985 MW Guangdong plant, Fig. 1, has four low pressure, one deaerating and two high pressure feedheating stages. The moisture separator drains, the reheater bled steam drains and the live steam drains are normally returned to the deaerator, the sixth and seventh feedheating stages respectively.

## ANCILLARY PLANT AND MATERIALS OF CONSTRUCTION

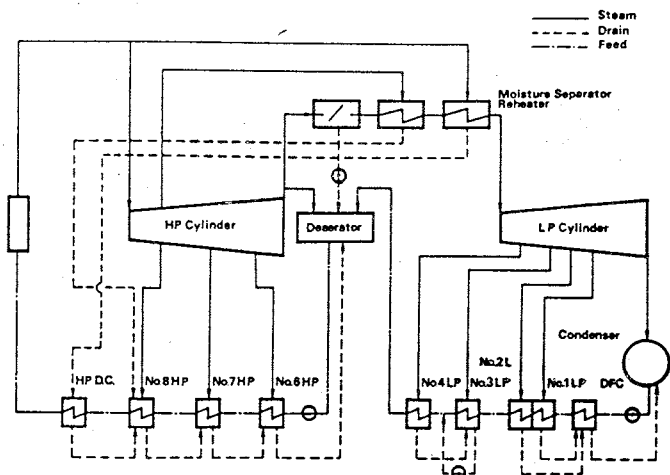


Fig. 2 Steam Feed cycle for 630 M.W. turbine Sizewell N.P.S.

For the Sizewell 630MW plant, Fig. 2, the different turbine stage pressures and a different economic evaluation of thermal performance justified the following changes:

- (a) An additional high pressure heater stage
- (b) The incorporation of a moisture separator reheater live steam drains cooler located in the high pressure feed line downstream of the last HP heater
- (c) The cooling of the No. 1 and 2 low pressure feedheater drains in a drain flash condenser prior to discharge of the condenser.

### 3. PLANT COMPONENTS

#### 3.1 Feedheaters - General

The authors company's designs of wet steam cycle feedheaters are in many respects similar to those established on superheated steam plant. Common to both cycles is the use of horizontal vessels located below the turbine and having naturally draining bled steam pipes so as to minimise the risk of water ingress to the turbine.

The proven design of horizontal feedheater incorporates a nest of 'U' tubes with a tubeplate and waterbox divided to provide two passes of feedwater per stage. To ensure low steam side pressure drops and the general avoidance of erosion by wet steam it is essential that the feedheaters operate with low velocity, uncomplicated steam flows. The low pressure drop is essential for high thermal efficiency, especially in feedheaters designed to achieve temperature differentials between the discharged feedwater and steam within the shell as low as 1°C and also to prevent any significant variation of water level within the feedheater shell which could result in submergence of some of the tubes and consequent loss of performance.

To achieve this the heater shells, Fig. 3, have large diameter steam inlets, so that the steam enters at low velocity, and are sized to provide a large annulus between tubes and shell which enables unobstructed steam distribution along the shell. The condensation process induces a radial steam flow into the tubenest which has a central vent to remove incondensable gases.

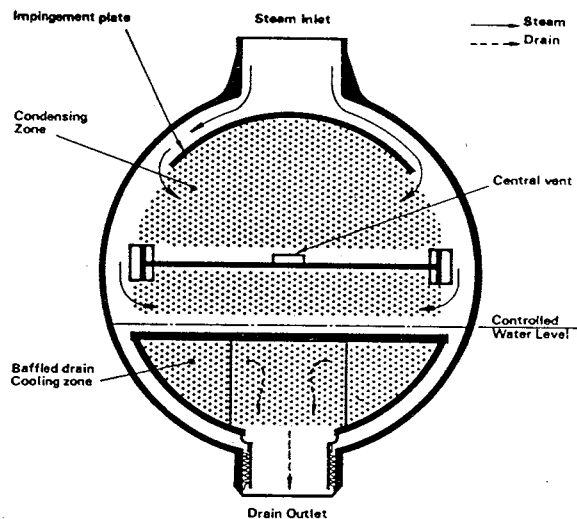


Fig. 3 Illustration of horizontal heater with integral drain cooler

Feedheaters having an integral drain cooler are arranged with partial flow of feedwater through a totally submerged section as shown in Fig. 3. As the section operates below a maintained water level any risk of erosion damage, or loss of performance, due to leakage of steam into the drain cooler is totally avoided and any loss of performance due to reheating of the drain by condensation of steam on the drain cooler enclosure is eliminated.

The ideal contraflow of drain and feedwater enables highly efficient drain cooling with temperature differentials between cooled drain and inlet feedwater as low as 3°C. The drain cooler enclosure is mounted independently of the main tubenest to facilitate differential expansion.

The feedheaters are designed and manufactured compliant with the pressure vessel code BS5500 and in order to minimise the risk of any joint leakage, are generally of all-welded construction.

Access for waterside inspection and maintenance is facilitated by the waterbox manway door and removable inner division

plates, and inspection of the steam side by suitably located openings in the shell which have bolted on covers.

### 3.2 Low Pressure Feedheaters

By comparison with fossil fired stations incorporating large reheat steam turbines, the LP feedwater flow, per kW generated, in typical PWR wet steam cycles is 70% larger. Furthermore a unit output of 985 MW is larger than on any fossil fired station for which GEC feedheating plant has been supplied. Consequently larger diameter feedheaters and increased sizes of pipes, valves and pumps are required.

Since the pressure and temperature of steam extracted from the LP cylinders of turbines for both wet and superheated steam cycles are similar there is little difference in the selection of materials or in general design features.

To conserve space the first and second stage low pressure feedheater stages are combined in single shells which are located in the low pressure turbine exhaust ducts below the low pressure cylinders from which they extract steam. The turbines for both the Guangdong and the Sizewell projects have three low pressure cylinders and consequently require three individual two stage feedheater shells.

The two stage feedheater design, Fig. 4 has four flows of feedwater arranged such that the lower pressure steam is condensed on the first and second passes and the higher pressure steam is condensed on the third and fourth passes. The second stage is contained within an inner shell which has independent steam and drain connections provided with inconel expansion pieces to facilitate differential expansion. The two stage heaters have condensing zones only, but, for the Sizewell project drains from both stages are cooled in a separate drain flash condenser. This unit is a condensing feedheater, similar to stages three and four, but incorporates drain inlet diffusers in a section of the shell baffled to facilitate flashing of the drains into steam without risk of damage to the tubenest.

The third and fourth stage low pressure feedheaters, Fig. 5, operate as individual vessels and are conveniently located alongside the turbine. The units operate in a single 100% flow line on the 630 MW plant for the Sizewell project and in double 50% flow lines for the larger feed flows of the 985 MW plant for the Guangdong project. The fourth stage feedheater on the Guangdong project also has an integral drain cooler.

In common with those on many operating fossil fuelled plants the low pressure feedheaters have 304L austenitic stainless steel tubes expanded into carbon steel tubeplates.

The tubenest supports, main shells and waterboxes are fabricated in carbon steel. The steam inlets are provided with stainless steel impingement plates to avoid damage to the tubenest.

The LP feedheaters have lengths up to 16.0m and outside diameters up to 2.1m, with a maximum dry weight approaching 50 tonnes.

### 3.3 Deaerating Feedheaters and High Level Storage Tanks

In both plants a spray type deaerating heater incorporated in a feedwater storage tank at an elevated position has been adopted.

By comparison with deaerators in fossil fired power stations the wet cycle units operate with considerably increased flows. The inflow of LP feedwater is up to 70% larger per kW generated and additional condensate returned to the storage tank comprises water extracted in the moisture separator together with the accumulated drains from the two stage reheater and the HP feedheaters. Steam generated by the returned drains combines with that bled from the cold reheat line to heat the incoming condensate to saturation temperature.

The flow rate of feedwater leaving the deaerator storage tank is, by comparison with deaerators in fossil fired stations about 100% larger per kW generated. With a unit output of 985 MW the feedwater flow and therefore, the corresponding size of storage tank are very large i.e. tanks of 4.3m diameter and 50m long.

Both plants have a simple and compact spray type deaerator, Fig. 6, in which the heating and deaeration is achieved by a combination of Stork spray devices, located within the storage tank and a system for introducing the heating steam into the stored water via a submerged steam rake.

Each spray device has a capacity of up to 1300 tonnes/hr. It comprises a series of stainless steel discs which, under the influence of internal water pressure, separate to discharge a fine spray of condensate onto a system of splash baffles, above the stored water.

The heating steam is distributed along the length of the tank by a manifold that feeds a large number of vertical pipes having perforated outlets at their lower end. Steam initially enters the stored water at a low level within the tank and rises to the surface where the majority is condensed on the cold water discharged by the spray devices. A small vent flow adjacent to each spray device conveys incondensable gases to the condenser.

Introduction of the steam into the stored water ensures that throughout the length and depth of the tank the contents are

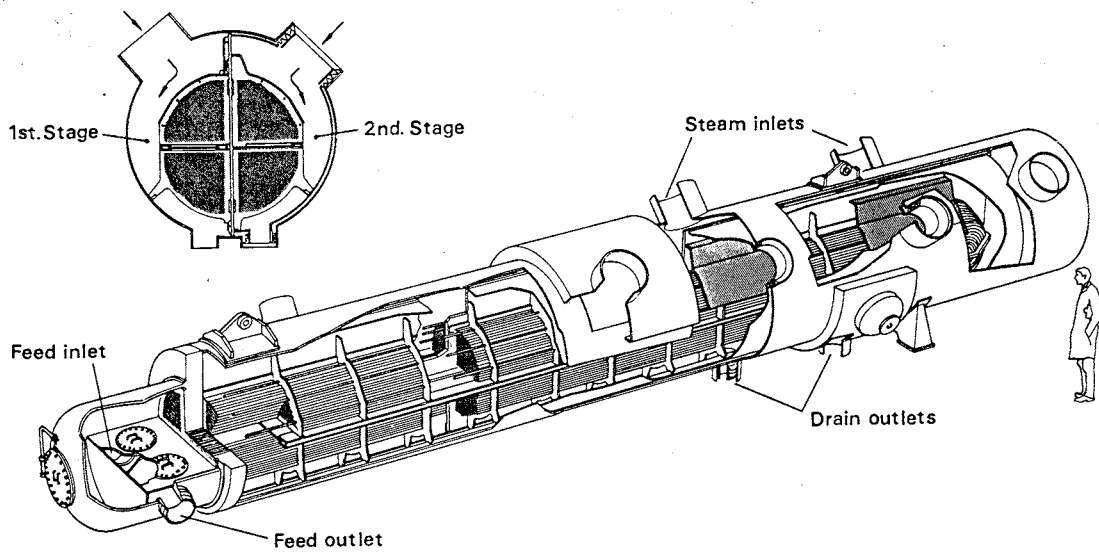


Fig. 4 Illustration of two stage LP feedheater

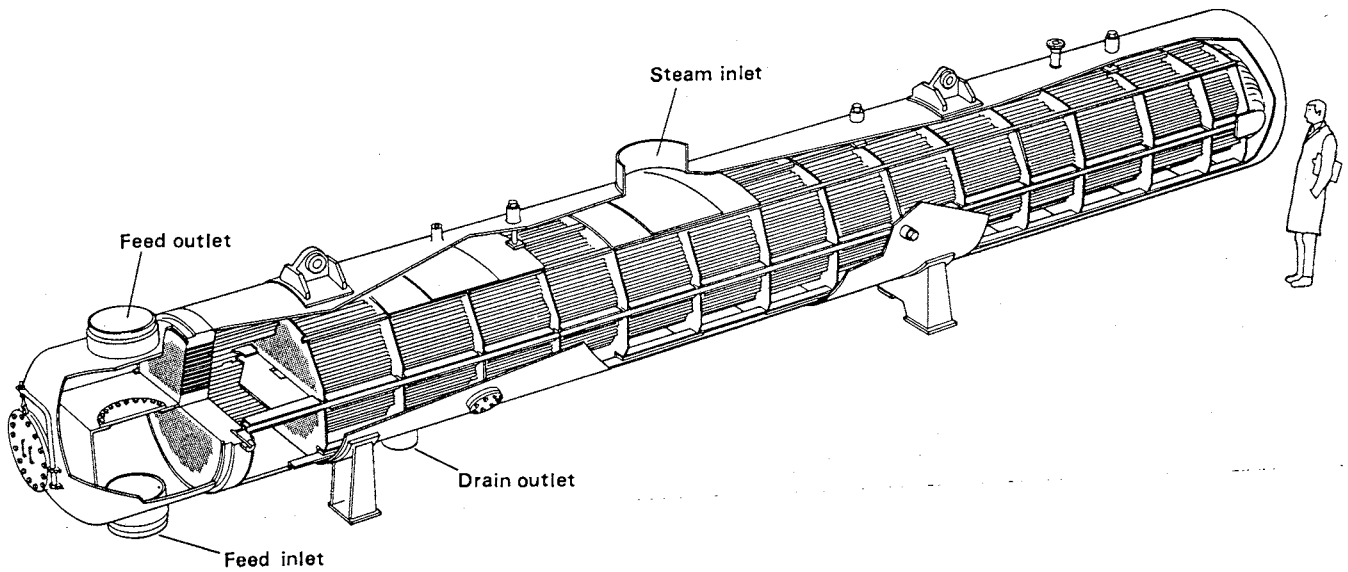


Fig. 5 Illustration of single stage LP feedheater.

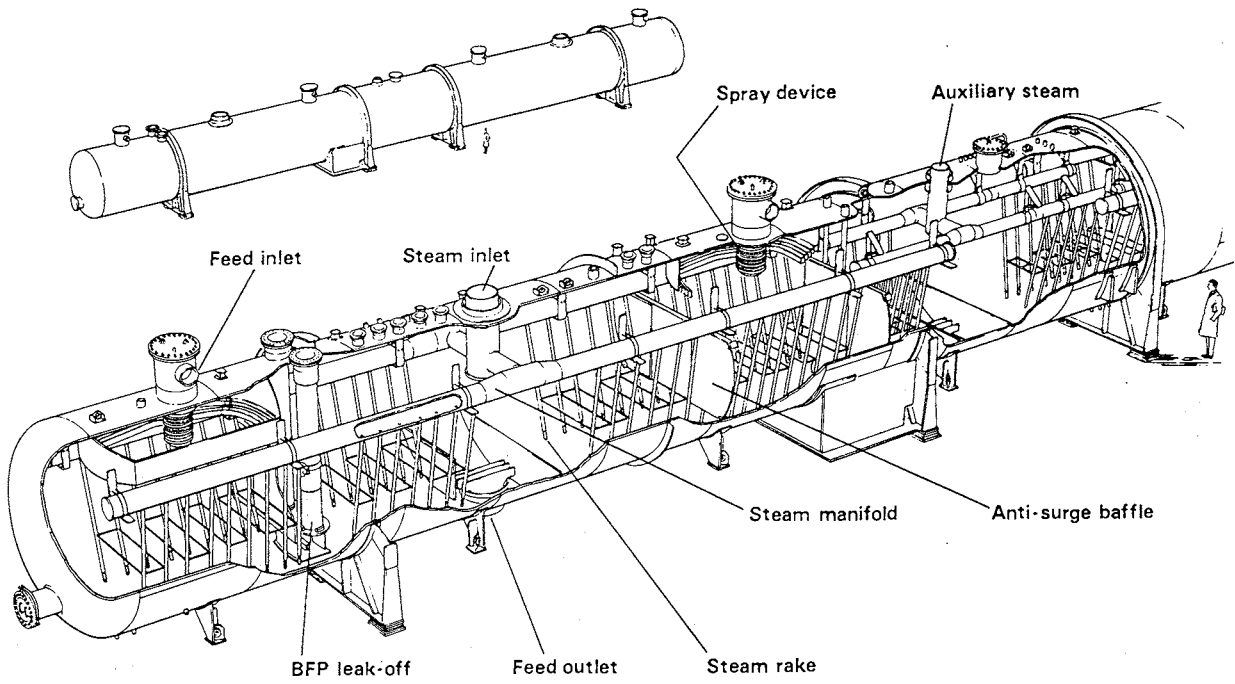


Fig.6 Illustration of deaerator

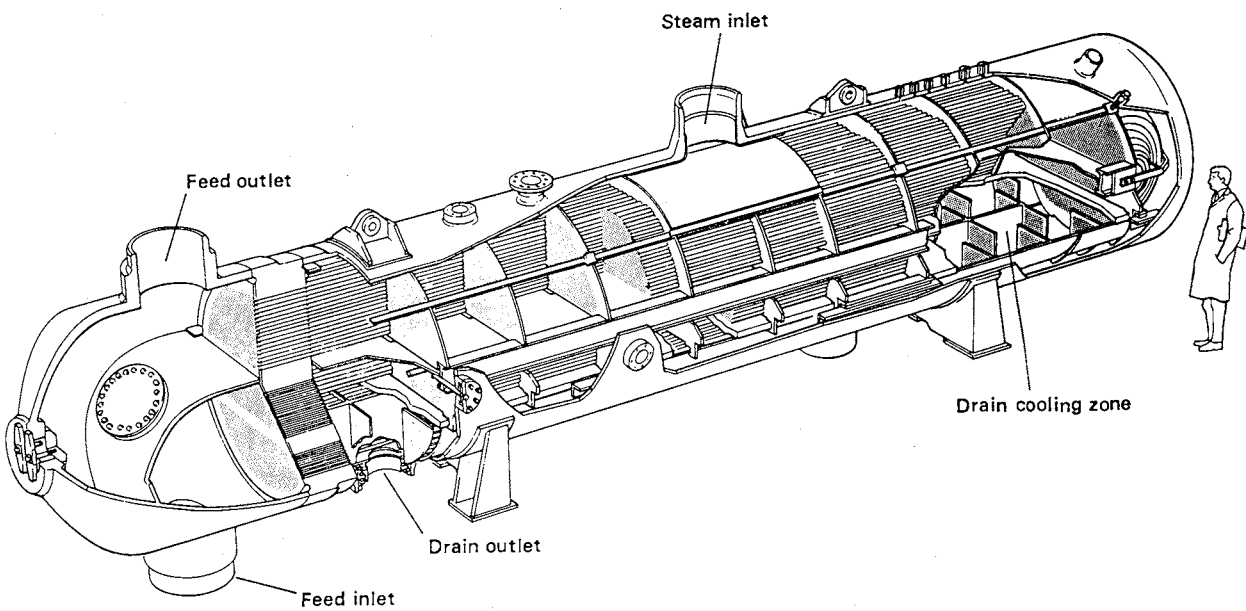


Fig.7 Illustration of wet steam HP feedheater

## ANCILLARY PLANT AND MATERIALS OF CONSTRUCTION

maintained at the saturation temperature corresponding to the local pressure. This ensures that a high level of deaeration is always maintained and also enables a reliable prediction of the pressure decay and of the available feed pump NPSH following a load rejection and other adverse operating conditions.

The distribution of steam along the shell minimises the rate of axial steam flow above the water level and the consequential potential for wave formation and harmful surges. The combination of low axial steam velocities and the anti surge baffles below the water level prevent any such surges.

The large quantities of incoming condensate from the moisture separator reheater, the high pressure feedheaters and also the occasional feed pump leak off flows are all discharged below the stored water level via a series of vertical diffusers distributed along the length of the storage tank.

The combination of the storage tank capacity and its elevation, together with the associated system controls, ensures that the required reactor feed pump NPSH is maintained during operational transients.

Following prior practice the deaerator storage tank and general internal fittings are fabricated in carbon steel. The spray devices, the incoming condensate and feed pump leak off diffusers are stainless steel. The use of wet steam requires the steam distribution system, within the tank, to be stainless steel in order to avoid erosion damage.

### 3.4 High Pressure Feedheaters

By comparison with the equivalent feedheaters in modern fossil fired subcritical steam power plant the wet cycle feedwater pressure is considerably lower, typically 120 bar rather than 220 bar. The feed flow is some 100% greater, per kW generated, which combined with the larger unit rating results in increased diameter tubeplates and vessels. The steam conditions are very different from those derived from modern high temperature reheat turbines. Instead of the steam being superheated it has a high moisture content.

The high pressure feedheaters, Fig. 7, have both condensing and integral drain cooling zones, and are provided in two 50% flow lines.

Whereas the condensing and drain cooling zones of wet cycle high pressure feedheaters generally operate in conditions similar to those for the superheated cycle and can therefore utilise established design solutions, the wet steam admission does require special consideration if erosion and impingement damage are to be avoided.

The feedheaters for these projects therefore have enlarged steam inlets to reduce the steam velocities and are provided with an austenitic stainless steel lining of the inlet connections and of the adjacent shell which, in conjunction with stainless steel impingement baffles, ensures that damage is avoided.

Steam velocities in the remainder of the vessel are sufficiently low to avoid erosion enabling the use of carbon steel. On the Guangdong project the customer chose to have the HP feedheater shell and internals manufactured in a low chrome steel.

The lower feed pressure facilitates the use of a fabricated carbon steel barrel design of waterbox rather than the cast steel hemispherical design commonly used for higher pressures. The modified shape facilitates the local stress relief of the waterbox closing weld and avoids the risk of embrittlement of the ferritic stainless steel tubing that could result from a total stress relief.

The 439 type ferritic stainless steel tubes are seal welded into inconel clad carbon steel tubeplates followed by an expansion to seal the crevice between tube and tubeplate.

The feedheaters have outside diameters up to 2.4 m and lengths of up to 13.5 m, with maximum dry weights in excess of 100 tonnes.

### 3.5 Pumps

It is important that when selecting and specifying the pumps for the feed system one not only establishes the required flow characteristics and chooses a pump design of high integrity, but also establishes the prevailing suction conditions during normal and transient modes of operation and ensures that the pumps are capable of operating in an acceptable manner during these conditions.

### 3.6 Feedwater Chemistry

Both stations employ titanium tubed condensers which enables the feed systems to operate with a high pH range of 9.2 - 9.6. This reduces the potential for erosion and corrosion of the system and influences the choice of materials as described in a separate paper to this conference (Ref. 2).

The feedwater system for the Sizewell NPS incorporates a condensate polishing plant which operates in a loop in the low pressure condensate system and is provided with its own booster pump.

The feedwater system for Guangdong NPS has no condensate polishing plant. To enable removal of debris from the system, especially a problem during plant commissioning and low load operation, a combination of magnetic filters in the condenser and mechanical filters in the low pressure condensate system is provided.

#### 4. FEEDHEATING PLANT SYSTEMS

The following system descriptions are for the plant as supplied for the Guangdong project. Although the different plant complement for the Sizewell 'B' NPS results in some modification to these systems they are generally similar.

##### 4.1 Bled Steam System

The bled steam pipes and valves operate with steam velocities that avoid significant erosion. The system, Fig. 8, operates to prevent the reverse flow of steam and in conjunction with other systems, the ingress of water to the turbine. It also enables isolation of the feedheaters from the turbine.

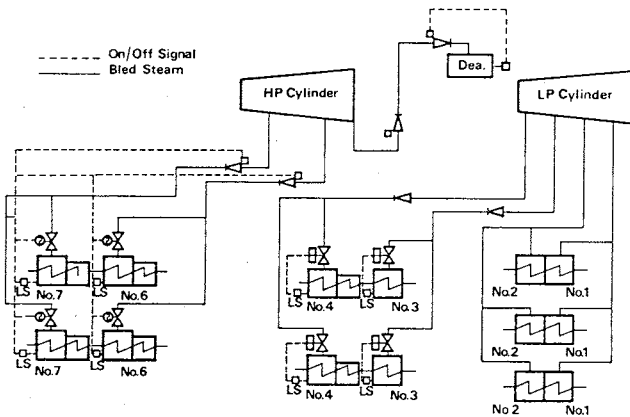


**Fig. 8 Bled steam system  
Guangdong N.P.S.**

Location of the two stage low pressure feedheaters in the turbine exhausts minimises the length of the associated large diameter bled steam pipes and enables the omission of bled steam isolating and non return valves. Water ingress to the turbine is prevented by a combination of primary and emergency manometrically sealed drains fitted to both sections of the feedheater and sized to prevent flooding.

All other feedheaters are provided with bled steam non return valves, mounted near to the turbines to prevent the reverse flow of steam or condensate. An isolating valve, mounted near to the feedheater, prevents condensate from the heater entering the bled steam pipe.

With the exception of the line to the high level deaerator, all feedheater bled steam lines fall continuously from the turbine to the feedheater and are therefore self draining whilst the feedheaters are operating. To remove condensate accumulating in the line, when either the bled steam isolating or non return valves are shut, a drain is provided upstream of each valve.

The bled steam line to the high level deaerator, which is taken from the cold reheat line, rises continuously. Under normal operation any condensate in the line will either be carried forward, into the deaerator, or back drain into the cold reheat line which has continuously operating drains. The valves in the deaerator steam line are also provided with an individual upstream drain.

Live steam at a reduced pressure is used to maintain the deaerator at a minimum pressure of approximately 1.5 bar during low load operation. During steam dumping direct to the condenser, following a turbine load rejection, live steam is also used to peg the deaerator pressure. This maintains the required feedwater temperature to the steam generator and also minimizes the reduction of feed pump NPSH.

The types of valve used in the wet steam cycle bled steam lines are similar to those used on superheated cycles. Non return valves are the inclined seat swinging disc type. Low pressure feedheater isolators are butterfly valves and high pressure feedheater isolators are parallel slide valves.

Following a turbine load rejection or a high water level in an associated feedheater the bled steam isolating valves are automatically closed and the power assisted closing of the non return valves in the lines to the deaerator and the high pressure heaters is activated.

Each feedheater is provided with an individual vent line, direct to the condenser and incorporating a control orifice.

The high pressure feedheater and deaerator heater bled steam piping and valves are in 2 $\frac{1}{4}$ % Cr 1% Mo steel which is resistant to erosion by the wet steam at the prevailing conditions. The low pressure feedheater bled steam pipework and valves operate with a steam velocity that enables the use of carbon steel.

##### 4.2 Feedwater Heater Drain System

The principles of the drainage system adopted are shown on Fig. 9, (for the sake of simplification only a single moisture separator reheater and single line of feedheaters is shown).

In order to minimise the disturbance to the system following either isolation of reheater tubenests or of feedheaters the individual drains from each of the two moisture separator reheater vessels discharge to only one line of high pressure feedheaters. Typically, during the on load testing of valves on one line of heaters, the diversion of drains to the condenser would be from only one moisture separator reheater vessel.

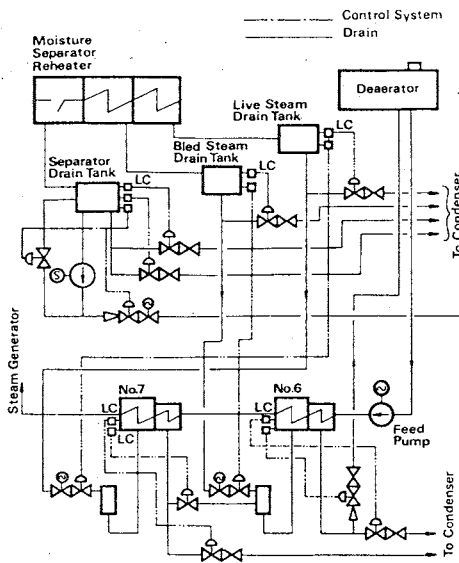


Fig 9(a) H.P. Feedheater drainage system  
Guangdong N.P.S.

As shown in Fig.9a each of the moisture separator and reheater drains is initially collected in an individual drains collecting vessel conveniently located below the moisture separator reheaters. The separator drains are then pumped to the elevated deaerator which operates at the same pressure. The bled steam and live steam reheater drains are discharged via a flashbox to the lower pressure sixth and seventh stage feedheaters respectively.

The combined drains from each seventh stage feedheater normally cascade via a flashbox to the sixth stage feedheater. Drains accumulated in the sixth stage feedheater normally discharge to the elevated deaerator but at low load, when there is insufficient pressure differential, are automatically diverted to the condenser.

All the reheater and HP feedheater drains are controlled by a modulating valve operated from a dedicated condensate level controller on the associated vessel.

As shown in Fig.9b the low pressure fourth stage feedheater drains cascade to a drains receiver where they combine with third stage drains and are then pumped into the feed line downstream of the third stage.

The combined first and second stage feedheaters normally drain independently to the condenser and are provided with alternative emergency drains to prevent flooding of the feedheater. All the two stage heater drains pass through unobstructed lines incorporating manometric seal loops and therefore avoid the risk of any isolation due to valve maloperation or malfunction.

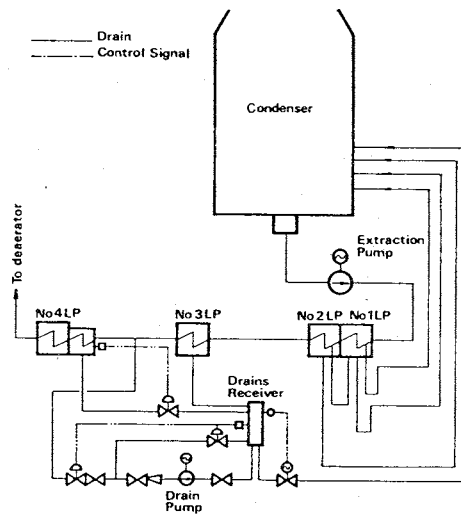


Fig 9(b) L.P. Feedheater drainage system  
Guangdong N.P.S.

Under fault conditions, or during on load testing of the system, the drains from the various vessels are automatically diverted to the condenser under the control of an emergency high condensate level controller on the associated vessel. The drainage system is also interlocked with the feedheater isolation so that all drains are automatically diverted in the event of the associated feedheater isolation.

All drain lines operating with saturated water are sized to operate at low velocity and are routed so as to prevent flashing prior to the control valves. Control valves are chosen to operate in a stable manner under flashing conditions.

Drain lines upstream of the control valves are carbon steel. The design and the materials of the control valves and of the pipework and diffusers downstream are chosen to avoid erosion damage.

#### 4.3 Feedwater Isolation

As shown in Fig.10 all of the feed heaters are provided with automatic feedwater isolation operated by a high condensate level switch on the heater shell. The valve closing time is sufficient to prevent flooding of the heater as required by ASME design standards.

The first two feedheater stages, in the form of three two stage feedheaters operating in parallel, have common butterfly type isolating valves which close automatically in the event of a high condensate level in any of the three vessels. Forward flow is maintained by a spring actuated bypass valve. Each of the individual feedheater shells is provided with hand operated isolating valves.

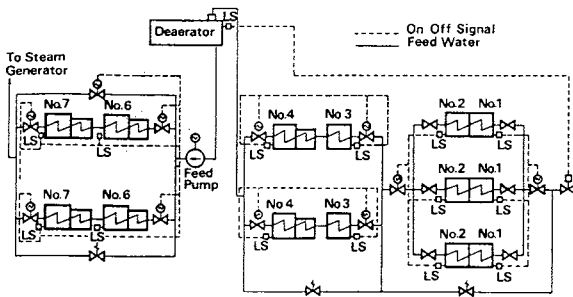


**Fig.10 Feedwater isolation  
Guangdong N.P.S.**

The third and fourth low pressure feedheaters are arranged in 50% lines with each line having butterfly isolating valves actuated by a high condensate level in either feedheater. Each line has a spring actuated bypass valve.

The sixth and seventh stage high pressure feedheaters are arranged in two 50% lines, each line having parallel slide isolating valves actuated by a high condensate level in either feedheater stage. In order to limit the reduction in final feedwater temperature when one bank of feedheaters is isolated, 65% of the feedwater flow passes through the operating bank and 35% through a bypass line incorporating an automatically opened motorised parallel slide valve and a metering orifice. A second spring actuated bypass valve operates in parallel and is provided to ensure a flow of feedwater to the steam generator in the event of failure of the motorised bypass valve.

**4.4 Feedwater Control and Inventory**

The control of the HP feedwater leaving the feed system has to meet the specific requirements of the steam generator designer.

As shown in Fig.11, the low pressure feedwater control is achieved by the combination of a maintained condensate level in the deaerator storage tank by feed flow control valves, and a maintained minimum condensate level in the condenser, by the controlled admission of demineralised make-up water.

The feed flow to the deaerator is controlled by two identical valves operating in parallel. The valves normally operate in unison, but to ensure stable operation at low condensate flow rates a single valve is used .

The provision of two valves enables, in the event of a single valve failure, the continued normal operation of the plant at full load.

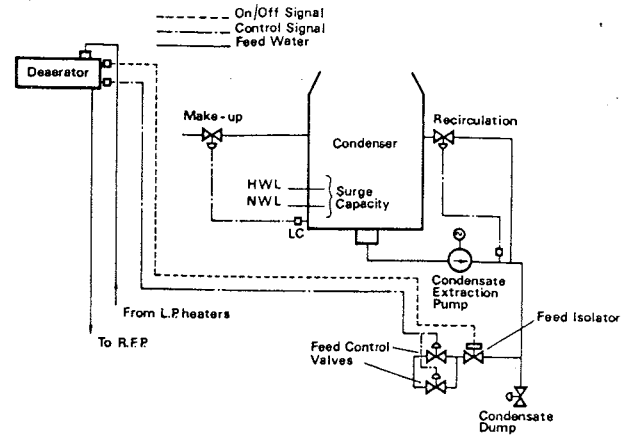


**Fig.11 L.P. Feedwater control  
Guangdong N.P.S.**

The valves have to provide the pressure differential between the system pressure and that generated by the pump under all conditions of operation involving an energy dissipation of up to 1 MW. They are the caged trim globe type which has a high resistance to plug vibration and cavitation and also operates with a low noise level.

The plant must be capable of storing sufficient water to handle steam generator water inventory changes and the feedwater expansion due to heating over the 0-100% power range. This is met by the provision of a total storage capacity in the condenser hotwells of 150 tonnes. There is, therefore, no requirement for a surplus condensate system.

At low load, when there is insufficient feed flow, an automatic recirculation from the LP feed system to the condenser maintains sufficient flow through the condenser extraction pumps and the turbine gland steam condenser to ensure their satisfactory operation.

**5. PLANT ARRANGEMENT**

The plant arrangements for large turbine generator projects are often developed using scale models or three dimensional computer models. The illustrations of plant arrangements included in this paper are photographs of the Sizewell plant model produced by the National Nuclear Corporation.

The low pressure feed system is arranged along one side of the turbine generator, see Fig. 12.

The location of the two stage low pressure feedheaters in the condenser neck, together with their extensive bled steam and drain pipework, considerably simplifies the plant arrangement inside the turbine hall.



**Fig.12 Location of L.P. Feedheaters Sizewell N.P.S.**

The feedheater shell is positioned so that steam flow between the turbine exhaust and the condenser tubenest is not impeded.

The third and fourth stage low pressure feedheaters are located adjacent to the low pressure cylinders from which they extract steam and the condenser extraction pumps, thereby enabling a compact arrangement of low pressure feed pipework. They are elevated so as to provide the required NPSH at the drain pump.

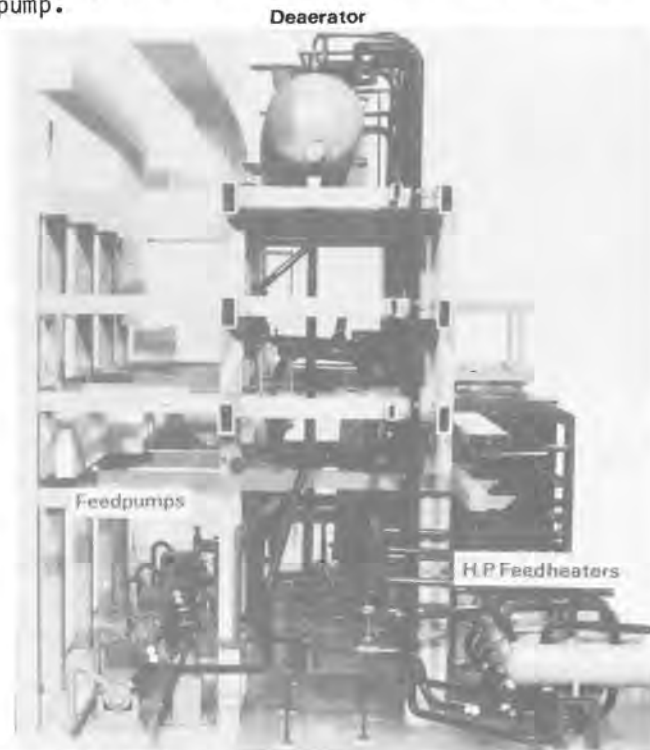


**Fig.13 Location of Deaerator Sizewell N.P.S.**

Fig. 13, shows the deaerator and its associated pipework which is located in an annexe alongside the turbine hall and conveniently above the reactor feed pumps so as to enable direct feed pump suction lines.

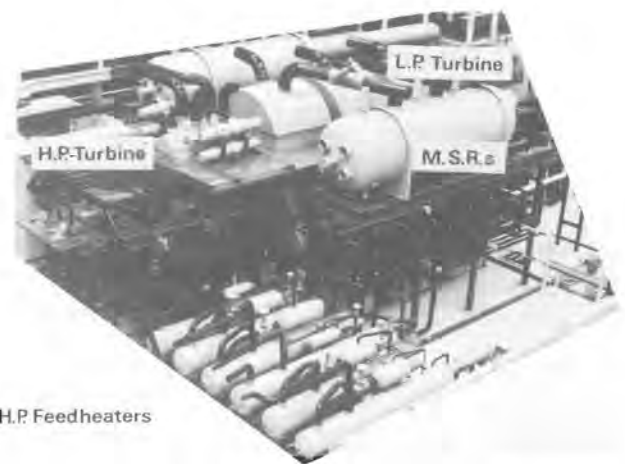


**Fig. 14 Location of H.P. Feedheaters Sizewell N.P.S.**

Fig. 14, shows the high pressure feedheaters located alongside the high pressure cylinder so as to minimise the lengths of bled steam pipework and in close proximity to the reactor feed pumps and the feed lines to the steam generator. The high pressure feedheaters are on a platform which enables accommodation of the drainage system below the feedheaters and facilitates, on plant shutdown, complete drainage of the high pressure feedheaters back to the condenser.

Platforms are provided to enable operation, inspection and maintenance of the feedheaters and the associated valves, controls and instruments. In the unlikely event that the feedheaters should require any major maintenance, it is considered preferable to remove them from the turbine hall to a suitable workplace. Should it be more convenient, it would be possible to retube in situ the two stage heaters located in the condenser neck.

## 6. FUTURE DEVELOPMENT

Whilst the feedheating plant being supplied for the 985MW Guangdong project requires relatively large components the same designs together with the available facilities for manufacture, shipping and erection would enable contracts for much larger plant ratings to be undertaken without the need for any significant further development.

## REFERENCES

1. J. Muscroft "Modern Large Steam Turbines for Pressurised Water Reactor Power Stations". B.N.E.S. 1988 Conf. Technology of Turbine Plant Operating and Wet Steam.
2. D.V. Thornton "Materials for Turbine Plant Operating and Wet Steam". B.N.E.S. 1988 Conf. Technology of Turbine Plant Operating and Wet Steam.

## 14. Main features of turbines for geothermal applications

J. A. KUBIAK, MSc, J. F. PEREZ, BSc, MPhil and A. GUTIERREZ, MSc, Instituto de Investigaciones Eléctricas, Cuernavaca, Mexico

Geothermal steam contains moisture, impurities and non-condensable gases which impose additional requirements for design, operation and maintenance of the turbine. The main design features of the turbines and supply vapour system are discussed together with means for avoiding major problems in operation especially those caused by erosion and corrosion of the blading system. Guidelines for maintenance are also presented.

### INTRODUCTION

1. Geothermal steam is extracted from a geothermal well. Generally the well may be a vapour or a liquid dominated reservoir from which the fluid is utilized, directly or indirectly, to drive a turbine (1). The geothermal fluid is a high-pressure, high temperature aqueous solution of salts and gases in varying proportions. The steam carries salts such as  $SiO_2$ ,  $CaCO_3$ , gases like  $H_2S$  and  $CO_2$  and also solid particles.

2. Noncondensable gases include hydrogen sulphide ( $H_2S$ ), carbon dioxide ( $CO_2$ ) hydrogen ions ( $H^+$ ), chloride ions ( $Cl^-$ ), ammonium ( $NH_4^+$ ), sulphide ions ( $SO_4^{2-}$ ) and others. The presence of the gases promotes corrosion, pitting, crevice corrosion, fatigue and stress corrosion.

3. The solid particles vary from silica, calcium carbonate and iron to small rock particles and are carried by the steam, causing erosion and scaling of steam flow path components. The deposits induce corrosion, diminish flow path area and cause unbalance of the rotor.

4. The moisture contained in the steam causes erosion of the blades which is one of the most serious problems of geothermal turbines. It also reduces turbine efficiency in proportion to the steam wetness. The scaling occurs mostly at the first or second stages of the turbine, whilst erosion takes place in the last stages.

5. To diminish or to avoid the above mentioned problems the piping system which supplies steam to the turbine must be carefully designed and equipped with facilities to remove moisture and contaminants from steam (2).

6. The special features of geothermal steam impose additional requirements on the design, operation and maintenance of geothermal turbines, and these are discussed in the present paper.

Problems arising from geothermal steam

7. Three major problems associated with the peculiar characteristics of geothermal steam are: scaling, corrosion and erosion which in turn reduce the lifetime of the turbine. The dimensions of geothermal turbines are large compared to those of conventional turbines for the same output and operating speed. The piping system and valves are in general larger than those of conventional machines due to low steam parameters, which are usually about 4-8 bar and 180 – 200 °C.

8. To provide protection against scaling, corrosion and erosion special design features should be adopted for piping system and turbine. (1)

9. As steam expands following the expansion line in the turbine there is a decrease of salt concentration in the dry steam. Though the steam expands across the saturation line, see Fig. 1, into the wet zone, such impurities as sodium chloride (NaCl), calcium chloride (KCl) and others deposit themselves at the first stage blades. Furthermore the steam at this point is submitted to wet-dry cycling during start-ups and shut-downs of the turbine.

10. On the other hand steam expands in the seals according to Fanno line and in the section where it is dry, the impurities deposit on the components of the seals. Also, during cold starts, steam condenses on metallic surfaces, and then evaporates when the turbine is heated-up (3).

11. The characteristics (impurities) of geothermal steam are quite complex and vary from field to field. A broad range of steam chloride contents and pH values depends on environment. In particular, steam condensate tends to be especially corrosive because of its low temperature and pH values and high concentration of acidic gases. The effects of the most corrosive chemicals presented in the geothermal fluids are given below. (3)

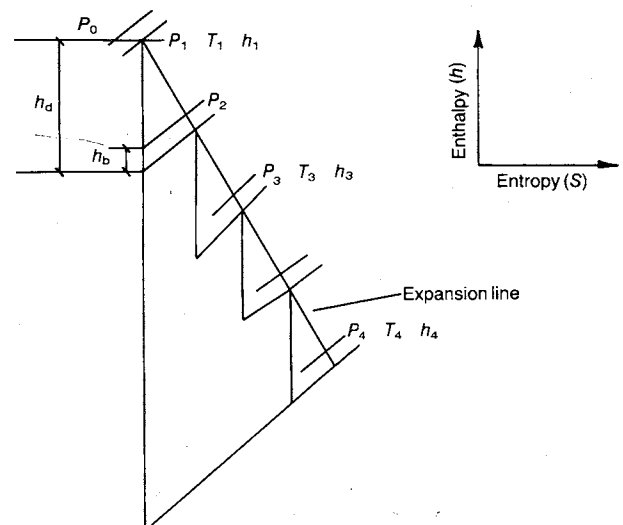


Fig. 1. Four-stage turbine expansion line

ANCILLARY PLANT AND MATERIALS OF CONSTRUCTION

12. Chlorine ions causes breakdown of the hard film of magnetite ( $Fe_3 O_4$ ) that protects base material and then precipitates pitting, crevice corrosion and stress corrosion. Hydrogen sulfide ( $H_2S$ ) causes pitting of stainless steel and corrosion of low-alloy steel. The presence of oxygen ( $O_2$ ) generally accelerates corrosion of mild steel. In turn, carbon dioxide ( $CO_2$ ) increases the uniform corrosion rate of mild steel in acidic solutions.

13. The effect of corrosive chemicals contained in the geothermal steam is specially serious on parts of the rotating equipment where the blades, rotors, valves and seals are affected. Corrosion causes breaking of blades, sticking of the valves, damage to seals, cracking of rotors and damage to the material of all components of geothermal power plants. Also, scaling reduces the load of the units.

Piping System

14. For successful operation of a geothermal power plant, the main steam supply system must be carefully designed, including items such as moisture separators, flashers, dehumidifiers, condensing traps, drains and a correct configuration of the pipe line. This is especially important in the case of double flash systems (2) and wellhead units (4) (Figs 2-3).

15. Excessive scaling in the piping system and in the auxiliary equipment, is entrained by the steam and then accumulates on turbine components. The piping system must therefore be checked periodically in order to observe the progress of scaling. Based on this inspection, the period of cleaning may be determined. This can vary depending upon the site of the geothermal plant.

16. In the design of piping systems many trivial errors can often be found which considerably increase scaling and erosion of the turbine. For example, scaling of the dehumidifier reduces its efficiency and in turn increases moisture in the steam. Deposits are then entrained by wet steam and travel to the turbine causing scaling, corrosion and erosion, see Fig. 4.

17. In the case of double flash systems the lack of adequate drains increases the erosion effect at last stages of the turbine, mainly at L-0 and L-1 rows, see Fig. 5.

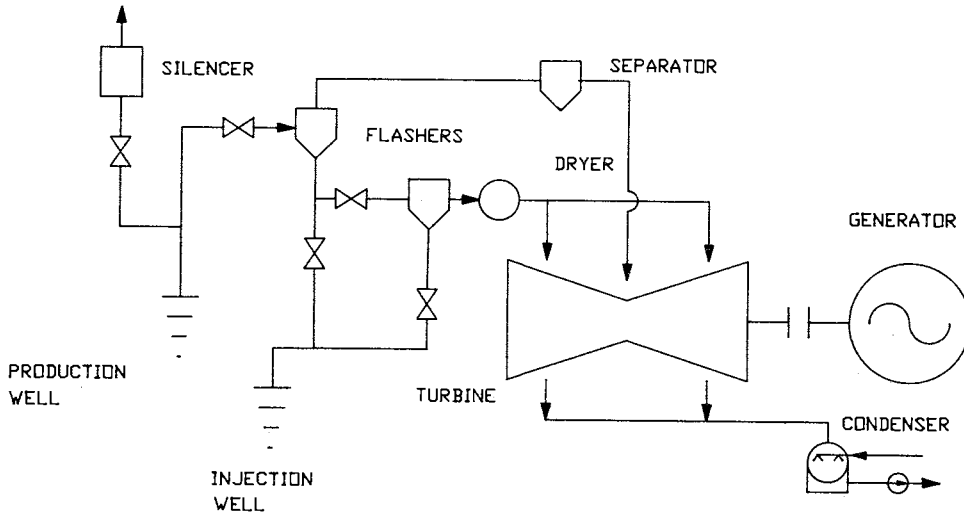


Fig. 2. Geothermal power plant piping system-double flash type

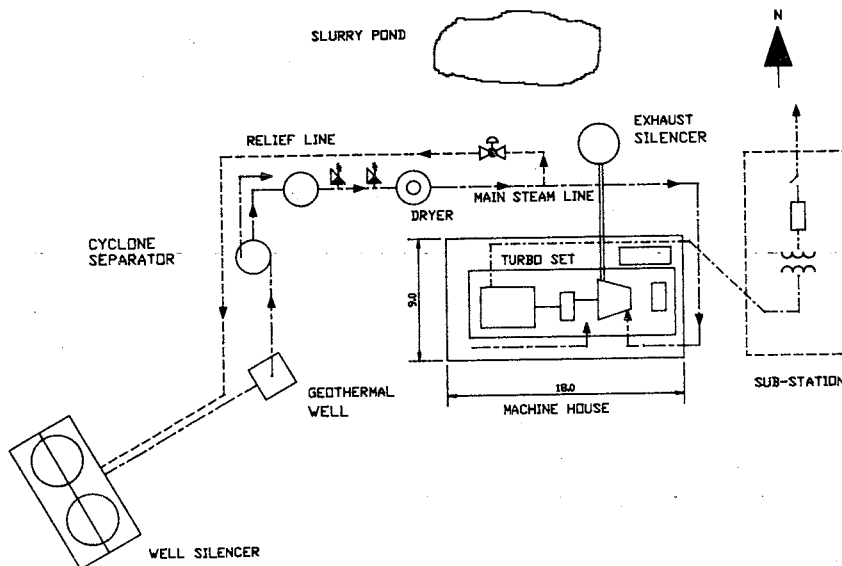


Fig. 3. Wellhead turboset back pressure type



Fig. 4. Heavy chemical deposits on diaphragm

18. Long pipe lines should be equipped with a sufficient number of condensing traps (5), and drains; particularly in the close vicinity of the turbine, Fig. 6. Each valve should be equipped with a drain. It is very important to provide adequate insulation for pipes, valves and the turbine itself. The drains should be located in the lowest point of each section and also in such a manner that effective heating of the piping and valve system can be carried out before start-up of the turbine. The drains must be placed in a suitable position in order to avoid mistakes such as the one illustrated in Fig. 7.

#### Design feature of geothermal turbines

19. Based on past experiences, the avoidance of the hazards which result from the inherent quality of steam containing moisture, corrosive gases and salts does not rely on choosing exotic materials different from those used in conventional industrial turbines. The usual materials such as cast steel for inlet valves, low alloys for rotors, 12% chrome steel for blades and gray cast iron or carbon steel for casings can be used. However, it is necessary to ensure good quality of the materials and a low stress design, avoiding stress concentrations. It is also required a control of metallurgical properties of the material to maintain a fully annealed condition, which tends to inhibit stress corrosion cracking.

20. The distance between nozzles and blades should be increased in order to reduce erosion of the rotor blades. This will cause a loss in efficiency so a compromise solution should be sought. The blade tip velocity in most cases should be no greater than 275 m/sec. to avoid severe erosion, though for modern materials is allowed up to 325 m/sec. A wide-pitch nozzle arrangement must be provided in the first stages to ensure a wide flow path preventing plugging and rubbing in the blading system caused by scale deposits. Special corrosion allowance factors should be added to the material thickness of the components. The gas content must be taken into account in the flow path thermodynamic calculations. The small heat drop available implies a low number of stages, hence for small and medium size turbines four or five stages are enough in a single cylinder. The blades of the first stage are sufficiently high to give a reasonable efficiency with full arc admission. The occurrence of steam wetness must be considered at the beginning of the expansion line. In case of geothermal turbines, reliability is a more important factor than efficiency.

#### Turbine construction and control system

21. Geothermal turbines are generally single casing and may be single or double flow with or without mixed pressure, depending on whether a single or double flash system is employed. They can be condensing or back-pressure types and no bled steam extractions are used.

22. Moisture extraction systems play an important role in geothermal steam turbines. These include drains at each stage, moisture catchers at the exit from each stage, (Fig. 8) grooved blades, and water separators after partway expansion. Preferably the first and second stages should be of impulse type to prevent scaling of the moving blades with consequent vibration due to unbalance.

23. Blade root design is not critical although a straddle type is recommended since it will protect the rotor dovetail, Fig. 9. The assembly of the turbine should be simple to facilitate maintenance and inspection with adequate man-holes, lifting devices and access for endscopes.

24. The turbine control system differs from that of conventional turbines. High steam volumes and steam impurities require butterfly or spool control valves to prevent sticking of the rods. These types of valves are of proved design in geothermal applications. Plug and seat valves are used for the main stop valves, working counterflow and energized to open. The valves must be checked at least twice a day to ensure that they are not stuck. Also, stellite coatings have to be used on the valve seats. In case of wide variations in the line steam pressure a turbine power output control or a pressure controller are recommended, otherwise a frequency control system will be sufficient.

25. For small turbines, a mechano-hydraulic control system is generally adequate but is not sufficient when the turbine control system includes several steam admissions or receives frequency and power control signals. In these cases an electrohydraulic control system will be required.



Fig. 5. Blade inlet edge erosion at tips and base of L-O blade row

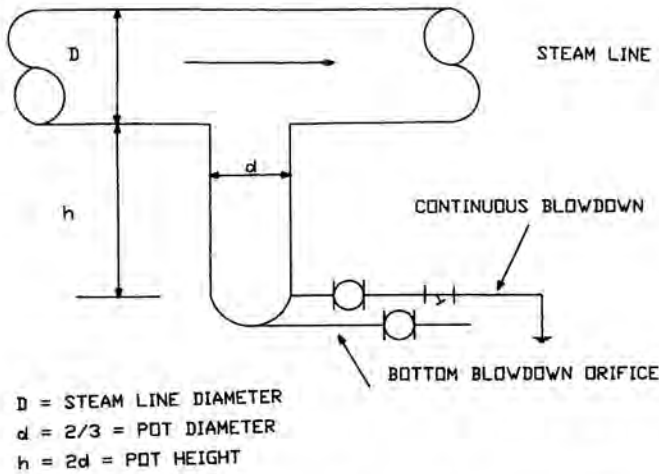


Fig. 6. Condensate pot design for long pipe steam lines

Operation - How to avoid problems

26. The starting-up curves should ensure that the turbine is heated in a manner that will diminish salt deposits as much as possible. All parameters should be recorded and carefully analyzed.

27. During prolonged operation scale deposits accumulate on the nozzles and moving blades. This causes reduction of turbine output and excessive axial forces affecting the thrust bearing. These effects can be detected by measuring the pressure in the steam chest or after the first stage and then relating it to the steam flow. In case of deposits, the relation between the flow and pressure is no longer a straight line. Any increase in bearing vibration may indicate excessive deposits on the moving blades.

28. A fibre-optic device can also be used for periodical inspection of the turbine. The periodical analysis of the steam parameters, (pressure and flow) at each point equipped with instrumentation, vibration analysis (amplitude, phase angle, spectrum), and axial position of the rotor, are key factors in safe operation of a geothermal turbine.

29. All drains should be open slightly during normal operation even at full load. Any anomalies in indication of the instruments should be carefully studied to avoid damage to the turbine.

30. Special procedures can be applied for washing operation at full or partial load to save maintenance expenditures. Comprehensive recording in the log-books will help to establish trends and gradual changes in the turbine performance which in turn will help to determine necessary intervals between overhauls.

Maintenance

31. The intervals between the overhauls should be determined according to:

- Analysis of operation records
- Preventive diagnostic tools (expert systems)
- Analysis of vibration
- Analysis of turbine performance
- Analysis of the erosion and corrosion progress carried out at each overhaul.

32. To determine a maintenance interval of a new unit installed in the new geothermal field, the following timing for the first 3 inspections are recommended:

- After 6 months
- After 1 year
- After 1.5 - 2 years

33. Analysis of each recorded data and findings during inspections will allow the determination proper of maintenance timing for the future successful operation of the plant. Also, the analysis will help to indicate desirable modification of the piping system (drains, condensing traps) since all characteristics of the geothermal field are not always known at the design stage. Sometimes inexpensive modifications can reduce considerably the scaling and erosion effects on the turbine.

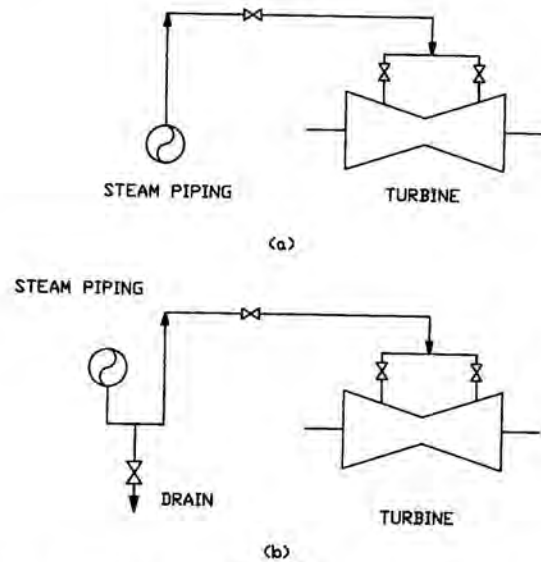


Fig. 7. Correct design of steam line with proper location of drain



Fig. 8. Grooved blades and moisture catchers at exit of each stage

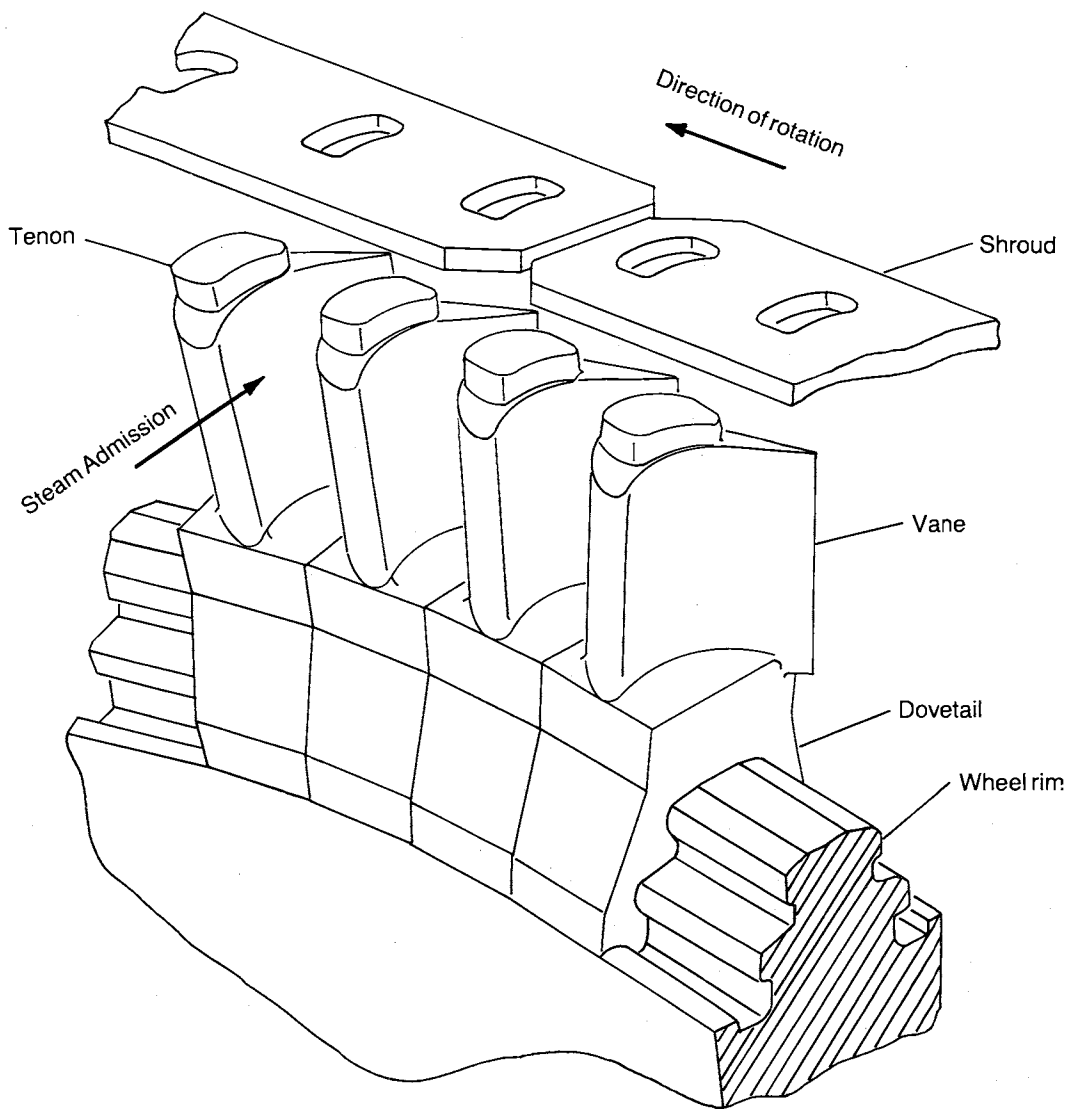


Fig. 9. Blading-rotor assembly, showing outside straddle blade root

**ACKNOWLEDGEMENTS**

The authors would like to thank the Electrical Research Institute (IRE) for permission of publishing this paper and the Federal Electric Utility Commission (CFE) for the access to their facilities.

The authors gratefully acknowledge the assistance given by colleagues in the preparation of this paper.

**REFERENCES**

1. GUTIERREZ A. and KUBIAK J.A. Differences between Geothermal and Conventional Steam Turbines, Heat Recovery System CMP, Vol. 7, No. 5, 453-462, Pergamon Journal, Great Britain, 1987.
2. KUBIAK J.A. and PEREZ J. Asesoría para revisión, diagnóstico y recomendaciones de la turbina

geotérmica, Internal Report of IIE, November 1987, El Salvador, C.A..  
No IIE/34/2250/I/007/F.

3. HIBARA Y. and HOMOSKI T. How to maintain Geothermal Steam Turbines, ASME Paper No. 80-JPCC-P -17
4. KUBIAK J.A., GUTIERREZ A. and PEREZ J. Technical Advantages and disadvantages of Geothermal wellhead Units, Heat Recovery System CMP Pergamon Journal, Great Britain (to be published).
5. GOUFREY D. J. A Solution to Severe Turbine Scaling at the Blundell Geothermal Plant, Utah Power & Light Company, Salt Lake City, Utah 89103.



# 15. Design, materials and fabrication in NEI Parsons' large wet steam turbines

A. J. SUMMERFIELD, MSc, MIM, MWeldI, and M. LEES, BSc, NEI Parsons

This paper outlines the elements involved in the design of NEI Parsons' wet steam turbines to combat the problems caused by erosion and describes the materials used in the manufacture of the principal components in those turbines, such as the High and Low Pressure turbine casings and blades. General explanations of the functions of the water separators and steam reheaters are followed by detailed descriptions of the materials and manufacturing procedures used for those NEI Parsons equipments in service in Canada. The paper also summarises manufacturing procedures that are being used for reheater tube bundles employing ferritic stainless steel tubes.

## INTRODUCTION

1. The steam generated in nuclear boilers, such as the CANDU, PWR and BWR types is supplied at relatively low pressures and temperatures compared with modern fossil fired plant. This "wet steam" condition means that erosion and corrosion are the main difficulties encountered in the choice of materials for the turbine and associated plant. As stated in the paper by Bolter (1), these steam conditions mean that creep, creep relaxation and temper embrittlement are eliminated.

2. NEI Parsons' wet steam turbines are designed to incorporate features and materials that are specifically chosen to prevent damage by water droplet erosion.

## THE INFLUENCE OF EROSION ON THE DESIGN OF LARGE WET STEAM TURBINES

### HP Turbines

3. In High Pressure turbines 50% reaction blading is employed. Typically, the steam enters the turbine in a virtually dry saturated condition and leaves with a wetness of some 12, or 13%. Thus, in the early stages, wetness does not pose a significant problem and thermodynamic efficiency is the dominant design requirement. For this reason, the early stages are conventional, shrouded blades. As the wetness increases, water droplets are formed, particularly along the outer boundary, disturbances in the contour of the outer boundary can cause these droplets to be re-entrained in the steam flow where their high momentum can cause pitting on the blade profile inlet edges. Water extraction becomes an essential feature of the design. Thus, the later stages consist of unshrouded blades with a smooth outer boundary to give relatively orderly flow near the blade tips. The natural tendency for water to concentrate in this region under the influence of centrifugal force is thus encouraged.

The water droplets are enabled to flow freely along the outer boundary and steam, which is extracted from this region through small drain ports adjacent to the blade tips, thus contains a high proportion of water.

4. At the feedheating extraction points, a specially designed porting, using perforated plates, results in the removal of a significant proportion of the total water present in the steam flow. This porting has been the subject of a research programme to define the optimum geometry for water extraction. At reheater extraction points the porting is not employed, as the presence of significant quantities of water in reheater tube bundles is not desirable.

5. By the above means, the wetness is maintained at a relatively low level throughout the HP turbine.

6. A new type of erosion damage was identified in wet steam turbines, particularly where a high pressure drop was experienced across a fixed element in the casing. It was found that diaphragms and casings could be cut across their horizontal joints and around the periphery of location grooves in the casing bore. This type of damage has become known as "worming" erosion, or "wire drawing".

7. HP turbine casings and blade rings are manufactured from cast 2.25% chromium 1% molybdenum alloy steel. The very tenacious oxide films formed by the chromium content have proved it to be very resistant to the normal types of erosion, but special attention has to be given, when engineering the turbines, to protect areas of the casing potentially vulnerable to worming erosion damage.

## ANCILLARY PLANT AND MATERIALS OF CONSTRUCTION

8. The horizontal joint of the blade carrier rings and outer casing are clad with an austenitic stainless steel weld deposit, which prevents water droplets, driven by high pressure differentials, from cutting a leakage path. Seating grooves, which locate blade rings into the outer casing, are also protected by similar weld deposits and this feature, together with the careful selection of materials for the fixed elements in the turbine, has prevented erosion damage.

9. NEI Parsons' standard form of fastening for 50% reaction blading is the serrated groove with side locking strip. This construction provides a tight seal leakage and, when combined with the low pressure drops across 50% reaction blade rows, worming erosion due to leakage through small clearances in the blade path, is avoided.

10. Blading material is standard 12-13% chromium martensitic wrought alloy steel, with the same material being employed for the side locking strips. This has proved to be entirely satisfactory in service with erosion and corrosion being minimised.

11. Erosion damage on the HP turbine rotors has also been prevented by the utilisation of 2.25% chromium 1% molybdenum alloy steel for the forgings.

### Water Separators and Steam Reheaters

12. In NEI Parsons' design of wet steam turbines, moisture separation and steam reheating are accomplished in separate vessels. Separators are provided in the transfer pipes between the HP and LP turbines to extract the moisture from the primary steam flow leaving the HP turbine before entry into the steam reheaters. There are four separators operating in parallel on a turbine generator unit, one located in the horizontal section of each of the four transfer pipes. Over 95% of the water in the steam is removed in the separators.

13. Erosion damage on water separators and steam reheaters has been found to be minimal, except on a machine where magnetite was present in the steam flow. In this case, the magnetite has acted as an added abrasive medium in conjunction with the water droplets in the steam.

### LP Turbines

14. The early stages of Low Pressure turbines consist of 50% reaction blading, which is similar to that used in the HP turbines; later stages being of variable reaction tapered and twisted design. LP blade path design is regularly updated using currently available fluid dynamic analysis to ensure optimum thermodynamic performance.

15. In wet steam turbines, turbine exhaust area is of particular importance because of the high specific steam consumption when compared with conventional cycles. NEI Parsons' LP turbine modules are, therefore, designed for use in multi cylinder applications with either 4, or 6 exhausts.

16. Usher<sup>(2)</sup> has indicated that erosion has been known for many years in LP turbines which have high blade tip speeds and operate in the wet region of the Mollier chart. The result of this is that the last two stages of moving blades become pitted on the profile inlet edges, near to the steam path outer boundary. In order to counteract this tendency for erosion, it has become the practice within the turbine generator industry to either harden the blade inlet edges, or to attach strips of hard steel, or "Stellite" for protection.

17. The LP turbine casings, rotors and blades are manufactured from conventional materials. An extensive account of the materials and fabrication processes involved in the manufacture of the rotors is given in the paper by Honeyman and Conroy<sup>(3)</sup>. LP turbine inner casings are manufactured from Spheroidal Graphite iron castings. Outer casings and turbine exhausts are manufactured from fabrication quality carbon steel. Blades are manufactured from the same group of 12-13% chromium martensitic wrought alloy steels as used in the HP turbine.

18. Erosion/corrosion in pipework carrying high velocity wet steam can cause wall thinning, especially in areas such as bends. This has led to the use of 2.25% chromium 1% molybdenum alloy steel tubing. Service experience with this material has been excellent.

## WATER SEPARATORS

### General Description

19. NEI Parsons separators are of the centrifugal type operating on the "cyclone" principle. Wet steam entering each separator passes through a diverging conical channel to a complete row of steam swirler blades. The swirler blade ring, comprising of a stationary row of reaction blades (50% reaction profile), imparts tangential velocity (swirl) to the steam and also acts as a water agglomerator.

20. The water films forming on the aerofoil surfaces of the swirler blades are subsequently detached as coarse droplets by the main steam flow.

21. The droplets are then centrifuged by the steam flow and deposited on to the inner surfaces of the louvered liner.

22. The cylindrical louvered liner, which is an essential feature of the separator design, removes and partitions the centrifuged free water from the main steam flow. The louvered arrangement provides a series of narrow axial apertures uniformly distributed around the periphery of the liner, which readily entrains the water droplets deposited. Separated water films then cascade around the outer surface of the louvered liner. To encourage the separated water to flow over to the louvers, extraction steam is taken off the separator vessel. The separated water finally passes from the vessel via drain pipes and a manifold directly below the vessel.

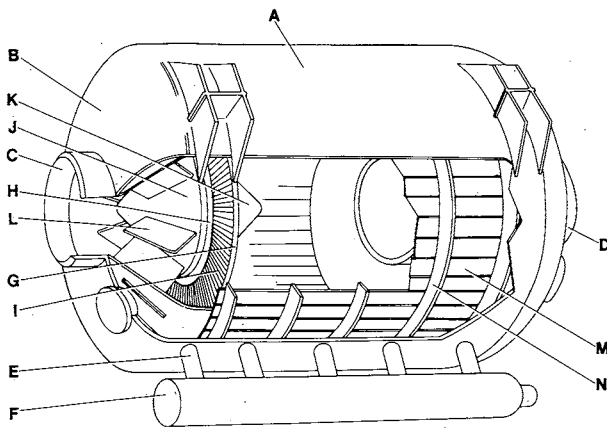


Fig. 1: Component parts of moisture separator (Refer to Table 1 for key to components).

23. Dried steam is transferred to the reheater via the central outlet nozzle from the separator vessel. Since the steam approaching the outlet has considerable swirl, there is a potential risk of subjecting the reheater tube bundles to unnecessary disturbances. To eliminate the undesirable tangential velocity component, anti swirl vanes are fitted into the outlet nozzle. These vanes ensure that an orderly low energy axial steam flow is presented to the reheater.

24. A cross sectional view of a water separator is shown in Fig. 1.

#### Materials and Fabrication

25. The separators are designed to eliminate, as far as possible, routine maintenance and inspection. To this end, the separator is an all welded construction, utilising materials intended to last the entire life of the plant without replacement. Materials have been selected to ensure that erosion and corrosion attack, by the working fluid, will be negligible over the specified operating life.

26. The separators consist of two basic parts:

An outer pressure containing shell which meets the requirements of a national pressure vessel code.

An inner cylindrical louvred assembly which furnishes the function of separating the water from the steam.

27. Whereas the outer shell is a relatively simple vessel, the inner assembly is a complicated fabrication requiring close attention to the tight design tolerances during fabrication.

28. Attention to these tolerances during manufacture of the two components means that, when they are assembled together, the gaps between the two meet the design requirements and thus, the efficiency of the separator can be guaranteed.

29. Materials used in the design of the separators have been selected on the basis of providing good erosion and corrosion resistance, coupled with ease of fabrication and good weldability.

Table 1  
Materials for the Major Components of the moisture separator

Component	Material	Component	Material
A Shell Plate	1&2 H	I Inner Blade Ring	2
B Dished Ends	1	J Blades	2
C Inlet Pipe	3	K Inlet Cone	3
D Outlet Pipe	2	L Outlet Cone	3
E Drain Pipework	2	M Vanes	3
F Drain Manifold	2	N Louvres	2
G Outer Blade Ring	2	O Louvre Support Rings	4

- 1 Pressure vessel quality carbon steel plate.
- 2 Type 405 ferritic stainless steel.
- 3 2.25% chromium 1% molybdenum alloy steel.
- 4 Fabrication quality carbon steel plate.

#### The Outer Shell

30. The outer shell is designed and manufactured to a national pressure vessel code. For those separators supplied for those NEI Parsons turbines installed in Canada, that code was the ASME Boiler and Pressure Vessel Code, Section VIII, Division I. As stated earlier, the materials were chosen to provide good erosion and corrosion resistance. The various parts of the shell are shown in Fig. 1 and the materials from which they are manufactured are described in Table 1.

31. The shell plate is manufactured from pressure vessel quality carbon steel plate to which Type 405 ferritic stainless steel plate has been roll bonded. The stainless steel takes the impact of the moisture passing through the louvred liner and, therefore prevents erosion of the shell. The composition and mechanical properties of the Type 405 stainless steel are given in Table 2.

32. The dished ends do not require cladding with an erosion resistant material as the steam is moving at relatively low velocities in these regions.

33. The shell is manufactured by rolling the clad plates and joining them together by welding. In order to facilitate welding of the carbon steel seam welds, the cladding is removed locally and then replaced by manual weld cladding after completion of the seam welds.

#### The Inner Cylindrical Louvred Assembly

34. With reference to Fig. 1 and Table 1, it can be seen that this assembly is a complicated fabrication involving dissimilar metal joints. In order that distortion is reduced to a minimum during the manufacture of this fabrication, it is necessary that a carefully controlled assembly sequence is used. The design and construction of these internal separator elements are not subject to any pressure vessel code requirements, as they are not primary pressure containing components.

## ANCILLARY PLANT AND MATERIALS OF CONSTRUCTION

Table 2  
Composition and Mechanical Properties of  
A Typical Type 405 Ferritic Stainless Steel

Chemical Composition			
Carbon	0.08% max.	Sulphur	0.03% max.
Silicon	0.80% max.	Chromium	12.00-14.00%
Manganese	1.00% max.	Nickel	0.05% max
Phosphorus	0.04% max.	Aluminium	0.10-0.30%

### Mechanical Properties

Tensile Strength, MPa	420 min.
0.2% Proof Stress, MPa	245 min.
Elongation, %	22 min.
Hardness, HB	192 max.



Fig. 2 : Welding of swirler blade ring.

35. The high velocity wet steam from the HP turbine exhaust enters the separators through the inlet pipe and passes through into the divergent annulus formed by the inlet and outlet cones.

36. This assembly, along with its vanes, is fabricated from 2.25% chromium 1% molybdenum steel plate, because of the high erosion potential of the steam flow.

37. The inlet cone channels the steam flow into the swirler blade ring where it has imparted a tangential velocity and the water droplets are agglomerated.

38. The swirler blade ring, as shown in Fig. 2, comprises a rolled and welded outer ring and a forged inner ring, both manufactured from Type 405 steel.

The swirler blades are made from rolled section Type 405 steel and they are fillet welded to the outer and inner rings using the Manual Metal Arc welding process and 18% chromium 10% nickel 2% molybdenum austenitic stainless steel electrodes.

39. The only real manufacturing problem that has occurred in the fabrication of the swirler rings was when the welds joining the blades to the rings were started and stopped at the leading, or trailing edges of the blades. The notches formed led to extensive weld cracking in those positions. It became necessary therefore, to initiate and finish welds along the faces of the blades and have continuous welds around the leading and trailing edges.

40. From the swirler ring, the steam is centrifuged out to the inner surfaces of the louvered liner. As shown in Fig. 3, the louvered liner consists of a number of Type 405 steel strips welded to carbon steel rings. It is important, when welding the louver strips to the rings to, to ensure that the strips remain straight and undistorted. Also, it must be ensured that the louvers remain flush, as overlapped louvers, or those with raised edges, lead to drops in water extraction efficiency. The water extracted at the louvers then passes into the separator drains.

41. The dried steam then passes through into the Type 405 steel outlet anti swirl vanes into the reheaters.

## STEAM REHEATERS

### General Description

42. The steam reheating plant associated with each turbine generator comprises two vertical cylindrical reheater vessels, one on each side of the turbine, each containing five identical tube elements, or tube bundles. Each tube element contains several hundred straight externally finned tubes welded into similar upper and lower rectangular header tubeplates.

43. The HP exhaust steam, which is to be reheated, flows across the shell side of the five tube elements in series in a single pass. The reheating steam is supplied to the upper header of each tube element and condenses on the inside of the tubes, the condensate being returned to the feed system.

44. The five tube elements are positioned within an inner support frame which locates them inside the shell and ensures that the shell side steam does not bypass the tube elements.

45. The vertical arrangement of the tubes eliminates problems associated with slug flow of the condensate within the tubes that can occur with horizontal configurations and ensures good drainage during unit shut down, or element isolation. Externally finned tubing is used to enhance the heat transfer capability on the shell side and hence reduce the total number of tubes, reheater size and shell side pressure loss compared with an unfinned tube arrangement.

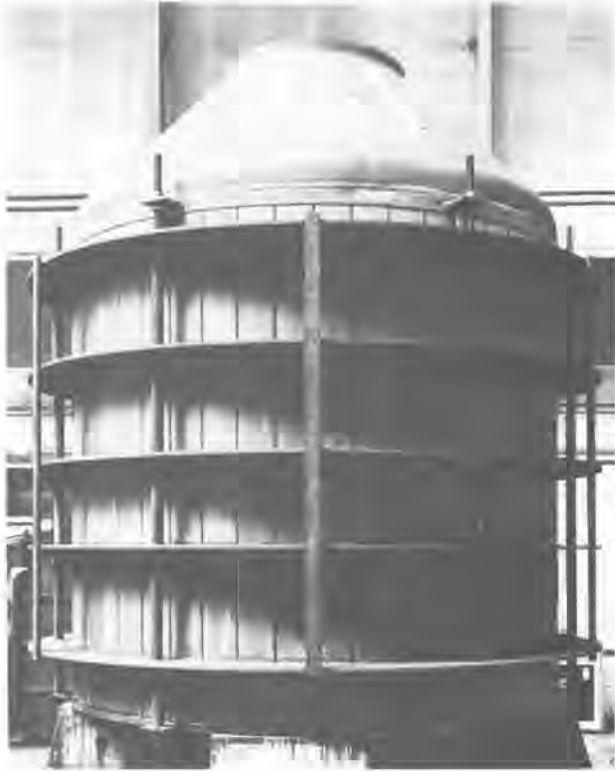


Fig. 3 : The inner louvered liner.

46. The tubes in each element are arranged in a narrow rectangular pattern with the long span being perpendicular to the direction of shell side steam flow. This results in a minimum shell diameter and facilitates element interchangeability and ease of manufacture, erection, leak detection and replacement of elements, if necessary.

47. The tube ends are seal welded into channel section headers, which incorporate bolted covers and a metal gasket.

48. Tube elements are free standing within the common support structure and are guided to allow free vertical expansion from the lower header cover. The tube support arrangement within in each tube element is fixed to the upper header and is allowed to expand downwards relative to the tubes. A sliding linkage arrangement between the tube support structure and lower header maintains the element shape during handling and under expansion conditions.

49. A cross section view of a reheater is shown in Fig. 4.

Materials and Fabrication

50. Similar to the separators, the reheaters are comprised of two main types of assembly:

An outer pressure containing shell which meets the design and manufacturing requirements of a national pressure vessel code, eg. the ASME Boiler and Pressure Vessel Code, Section VIII, Division I.

The five tube elements and their associated pipework and support structures. The tube elements are also subject to the same code design and manufacturing requirements as the shell.

51. The shell is manufactured from pressure vessel quality carbon steel. Although large, the reheater shells are manufactured as normal pressure vessels. The shell flanges are machined prior to welding. Jacking points are fitted to enable any distortion to be removed after welding. On completion, the shells are hydrostatically pressure tested in the vertical position, either on their own support feet, or on support rings.

52. The tube bundles, or elements are manufactured from the materials listed in Table 3.

53. Manufacture of the bundles is performed in the following sequence:

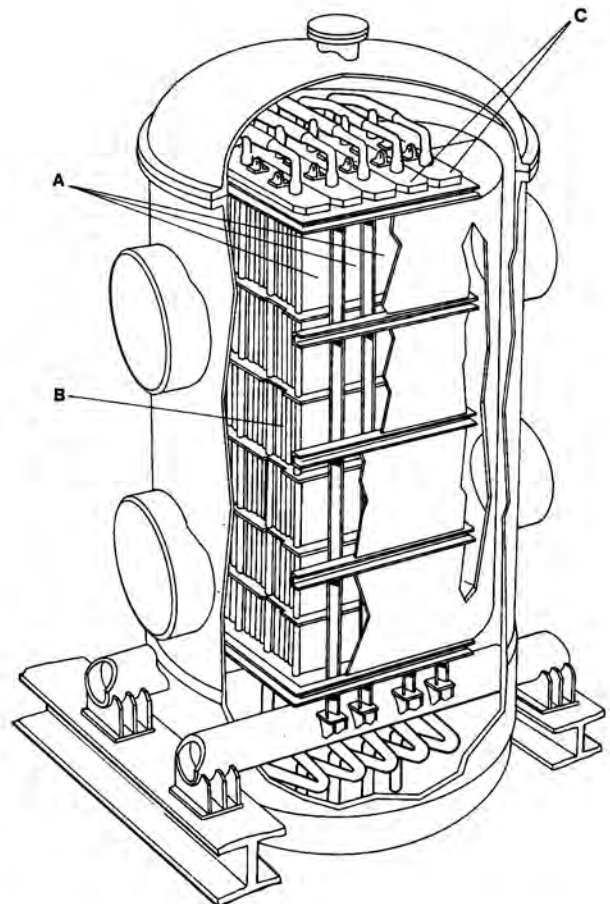


Fig. 4 : Cross section view of a reheater.

- A - Tube elements/bundles
- B - Tubes
- C - Tube element headers

## ANCILLARY PLANT AND MATERIALS OF CONSTRUCTION

Table 3

### Tube Bundle Component Materials

Headers, header covers - carbon steel forgings  
Tubes - carbon steel integrally finned tubing\*  
Support plates, support tubes, sealing strips and stiffeners - carbon steel

\* The sections of the tubes that pass through the headers and support plates are left plain, with no fins. The finning is made in a continuous, close pitched, helical pattern, similar to a screw thread.

#### 54. (1) Machining and Drilling of Headers, Covers and Support Plates

All machining and drilling is carried out on CNC machines. The headers are first machined all over and the cover stud holes are then drilled and tapped. At this stage, the recess for the header gasket is not machined out. Next, the tubeplate holes are drilled. The support plates are stack drilled; first undersize and then core drilled to drawing size. In the case of plates that are split, the split is made using a double band saw. The header covers are first rough machined on each side and then finally machined and drilled.

#### 55. (2) Manufacture of Side Plate Assemblies

Each side plate assembly consists of two support tubes and a joining plate, together with end sealing strips and stiffeners. The tubes and plates are set up in a jig, tack welded and then turned over. The welding is completed on the other side, following which, the assembly is returned to its former position to allow completion of the welds. The welds are ground clean and the sealing strips and stiffeners are then welded into position. These welds are also cleaned, following which the assembly is stress relieved, shot blasted and straightened, if required. The welds are then magnetic particle crack detected. Great importance is attached to the achievement of the necessary accuracy in the machining of these support tube and side plates.

#### 56. (3) Bundle Assembly

Throughout the assembly process, much attention is paid to the cleanliness of the tubes and the tubeplate holes. The procedure evolved has resulted in the minimal rejection of welds and in an overall saving in production time and cost. The bundle assembly is carried out on a large flat-bed building jig. The top header box is set up square on the jig and secured in position by welding on diagonal ties at the ends. The bundle cage is then built up using the distance tubes, end plates and tie rods. A visual and dimensional inspection is carried out to ensure that the structure is square and of the correct length.

#### 57. (4) Insertion of Tubes

It has been found that the tubes pass through the support plate holes more easily in one direction than in the other and it is important to ensure that when the tubes are lifted from the box, they will pass through the structure in the preferred direction. The tubes are removed from the box and the ends are cleaned with emery cloth and cleaning fluid.

They are then inserted through the support structure. Just prior to insertion into the top header box, the ends are again cleaned, as are the top header box holes. The tubes are then inserted through the top header box until they project by about 125 mm. The bottom header box, which has also been cleaned, is set up in position, squared and secured. The bottom header box holes are again cleaned and the tubes are pushed back into the holes.

#### 58. (5) Welding of Tubes

The top header is welded first. Preheat is applied around the periphery of the header box using electrical resistance heating elements and the header is covered in a heat retaining blanket. The tubeplate face and tube ends are thoroughly cleaned and dried out, prior to welding. Welding is done using automatic orbital Tungsten Inert Gas (T.I.G.) pulsed arc welding machines. On completion, the welds are cleaned and subjected to dye penetrant inspection. When the top header box welds are complete, the bottom tube ends are faced flush with the tubeplate face and then welded using the same procedure as before. On completion of the tube welding, the bundle is helium leak tested.

#### 59. (6) Stress Relieving

The tube to tubeplate welds at both ends are stress relieved together by the application of electrical resistance heating elements to the face of each tubeplate. On completion of the stress relieving process, the heat treatment equipment is removed and the bundle is cleaned to remove any scale. The tubes are then roller expanded into the tubeplates using controlled torque units.

#### 60. (7) Machining of the Gasket Faces

Since the welding of the tubes may result in slight distortion of the header boxes, machining of the gasket faces is not done until welding and stress relieving have been completed. The header cover is also machined at this time.

#### 61. (8) Fitting of Covers and Hydrostatic Testing

Following the machining of the header boxes, the covers are bolted on and the whole of the tube bundle is hydrostatically pressure tested. On completion, the bundle is drained and dried ready for despatch and fitting into the reheater shell.

Table 4  
Composition and Mechanical Properties of  
Type 439 Ferritic Stainless Steel  
Integrally Finned Tubes  
Chemical Composition

Carbon	0.02% max.	Chromium	17.00-18.75%
Manganese	1.00% max.	Aluminium	0.15% max.
Silicon	0.75% max.	Copper	0.15% max.
Phosphorus	0.03% max.	Nitrogen	0.025% max.
Sulphur	0.02% max.	Titanium	12 x sum of
Nickel	0.50% max.	C & N and	0.80% max.

#### Mechanical Properties

Tensile strength, MPa	415 min.
0.2% Proof Stress, MPa	205 min.
Elongation, %	20 min.
Hardness, HV	185 max.

#### Future Developments

62. The machine in which there has been erosion damage caused by magnetite in the steam flow, is having the first tube bundle in each reheater replaced by new bundles tubed with Type 439 ferritic stainless steel integrally finned tubing. The composition of Type 439 tubing is shown in Table 4.

63. Although the NEI Parsons' design of reheater tube bundle with its vertical, self draining tubes (and tube drying during outage periods) has not been susceptible to erosion, or corrosion damage, the use of stainless steel tubing is expected to become commonplace in the future. Figures 5 and 6 show respectively the tube to tubeplate welds joining the steel tubes to an Inconel weld clad tubeplate and the completed tube bundle. In order that the header can be weld clad, it has been made from a flat carbon manganese steel forging and the cover has been dished instead.



Fig. 5 : Automatic orbital T.I.G. tube to tubeplate welds between Type 439 finned tubes and Inconel weld clad reheater tube bundle header.



Fig. 6 : Finished reheater tube bundle with Type 439 finned tubes.

#### CONCLUSIONS

64. 1. Erosion damage, identified at the design stage as the main potential problem with the steam cycle, has been shown to be minimal. Features engineered into the design and materials chosen to prevent erosion damage have been found to be successful.

65. 2. The only circumstance where erosion in the separators and reheaters has been a problem is on a machine where magnetite has been found in the steam flow. In this case, the magnetite has acted as an added abrasive medium in conjunction with the water droplets in the steam.

66. 3. In the future it appears that stainless steel tubing will be required for at least the first tube bundle in a reheater, to prevent any erosion by incoming steam, or by preference of customers.

#### REFERENCES

- (1) Bolter J.R. - Design, development and operating experience with wet steam turbines (this conference).
- (2) Usher J. - Wet steam turbine operational experience Institution of Mechanical Engineers Conference "Steam turbines for the 1980's" London 9-12 Oct. 1979, Paper C200/79.
- (3) Honeyman G.A. and Conroy R.D. - The manufacture of LP rotors for large steam turbines (this conference).



## 16. Materials for turbine plant operating with wet steam

D. V. THORNTON, FIM, GEC Turbine Generators Ltd

**SYNOPSIS** The wet steam cycle associated with turbines for water cooled reactors imposes special requirements on the materials for certain components which are not met in the turbine plant of high temperature, fossil fuelled power stations. The selection of materials for such components operating with steam generated by water cooled reactors is reviewed.

In the high pressure cylinder the high velocity wet steam can cause significant surface wear and materials with resistance to damage by this erosion/corrosion mechanism are employed. The low pressure cylinder receives reheated steam and there are no special material requirements. For the feedheating and condensing plant, in addition to guarding against erosion/corrosion in the pipework and heater vessels, material selection must also address the special requirements of water cooled reactors for the feedwater chemistry. Materials containing copper are not acceptable and iron corrosion products, which may form during off load periods, must be minimised to restrict their transport to the reactor. These factors are also relevant to material selection for the moisture separator reheater which is a special item of plant for wet steam cycles.

### 1. INTRODUCTION

The selection of materials for turbine plant where the steam is generated from a water cooled reactor can now be based on a significant body of service experience. The first such machine designed and built by GEC Turbine Generator Company was commissioned in 1962, being a 22 MW turbine operating with a CANDU reactor. Since this time over twenty further nuclear wet steam turbines of up to 1200 MW rating have been designed to operate in conjunction with both direct and indirect cycle water cooled reactors. The total operating experience accumulated by GEC now exceeds 800,000 turbine running hours for plant associated with CANDU, SGHWR, BWR and PWR water cooled nuclear reactors. The design features of current large turbines and associated plant have been reviewed in references 1, 2 and 3.

Turbines operating with water cooled reactors receive steam at relatively low temperature and pressure as compared to plant for fossil fired stations. The effect of this steam cycle is that the HP turbine and HP heaters are required to operate in a high density wet steam environment and a special item of plant, a moisture separator reheater, is employed to deliver dry steam to the LP turbine. High velocity wet steam can cause erosion/corrosion attack of the surface of components which demands specific attention in design and materials selection.

The amount of entrained water in the HP turbine can be minimised by design of interstage water extraction arrangements and

precautions can be taken to limit the velocity and turbulence of the wet steam in the design of heater and reheater vessels. Chosen materials and surface protection measures to current standards have now operated for times in excess of 130,000 hours, and confirm that causes of damage due to erosion/corrosion by high velocity wet steam experienced on the first few machines have now been fully overcome. This is further supported by the good condition of larger 400-600 MW machines associated with both BWR and PWR reactors after 60,000 to 75,000 hours' service.

This paper describes the special conditions imposed on turbine plant operating in association with water cooled nuclear reactors, namely, erosion/corrosion due to wet steam and corrosion considerations arising from their feedwater chemistry requirements. The impact of these factors on material selection is reviewed for components in the HP turbine, moisture separator reheater, condenser and feedheaters.

### 2. EROSION/CORROSION DAMAGE

#### 2.1 Types of Damage

Various types of damage due to erosion/corrosion can occur in wet steam turbine plant as indicated in the following examples from early machines in which standard turbine materials were used.

If a leak path develops at a joint surface across which there is a pressure drop

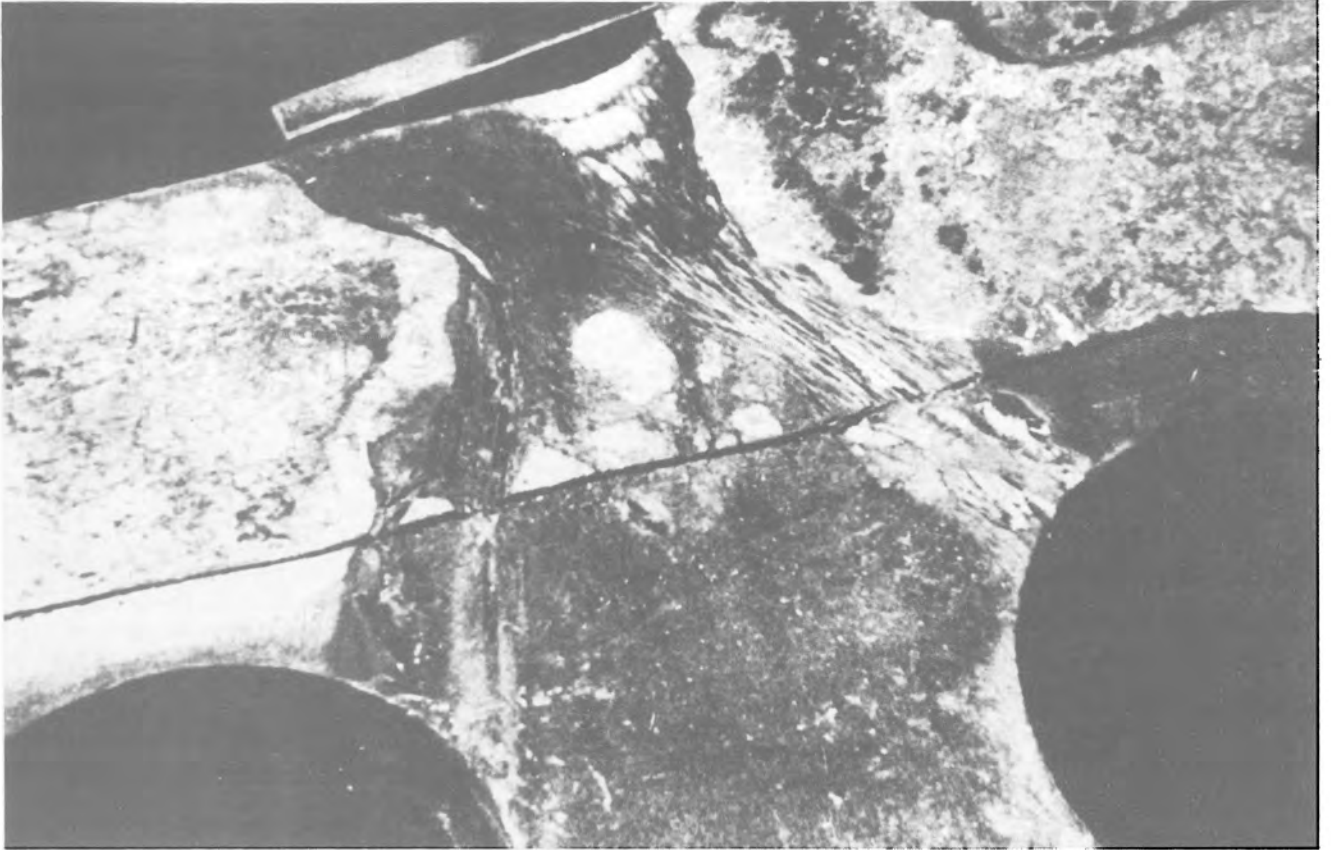


Fig. 1 - Wire-drawing attack on horizontal joint of carbon steel HP Cylinder.

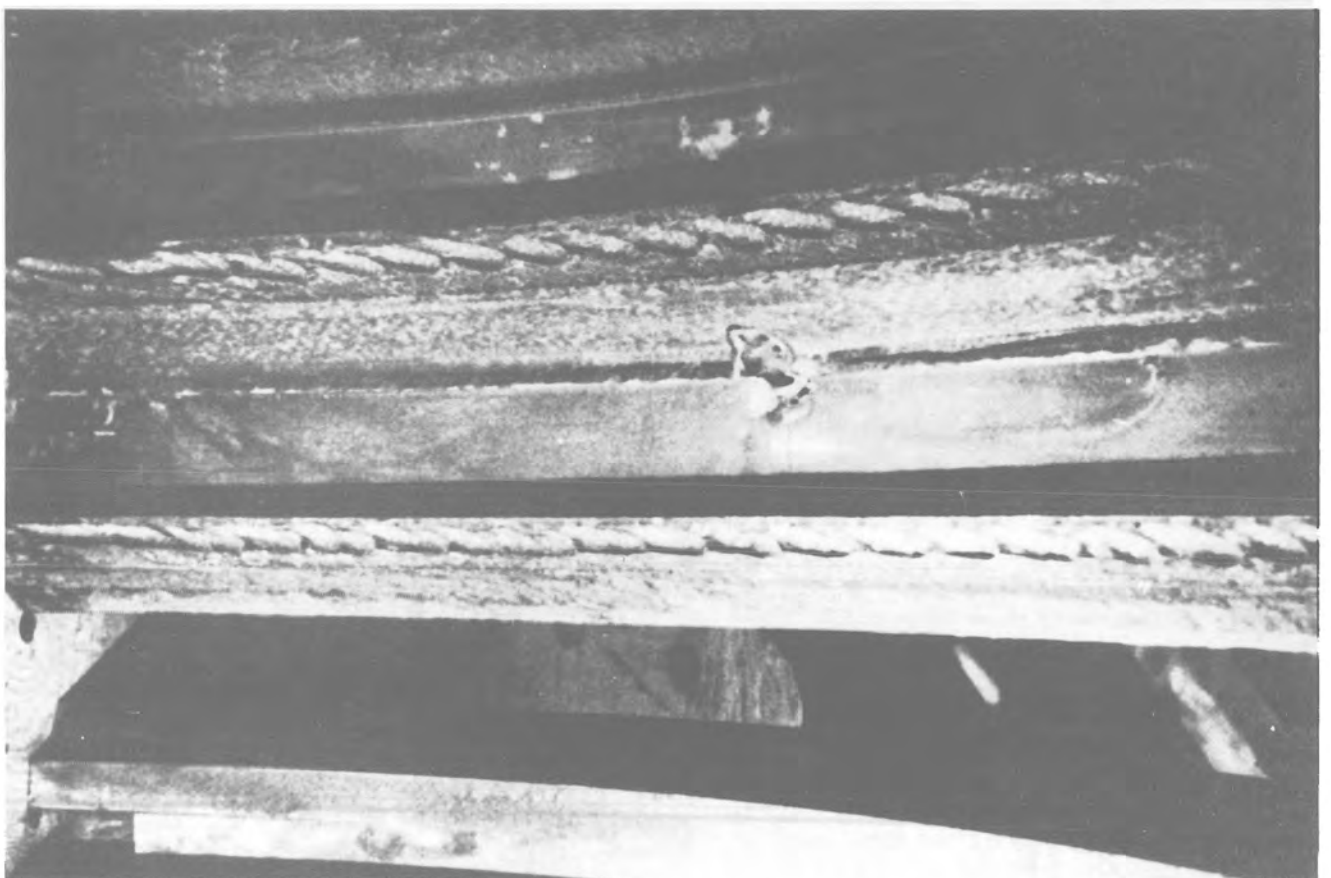


Fig. 2 - Cast iron cylinder liner showing impingement erosion damage.

the washing action of the high velocity steam can remove the surface oxide and produce cutting of the surface. This form of attack, called wire-drawing, is illustrated in Figure 1 where severe attack has occurred in the horizontal joint of a carbon steel cylinder. Typical components susceptible to wire-drawing attack are the horizontal joint surfaces of diaphragm, diaphragm carriers and casings.

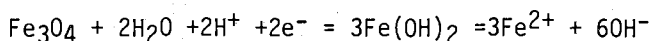
Figure 2 shows impingement erosion due to water droplets from the wet steam centrifuged by the rotating blades onto the adjacent stationary component. In this case the grey cast iron cylinder liner shows severe impingement damage opposite the moving blade tips.

Scouring damage has been experienced on the end-wall of carbon steel outer casings by wet steam swept into the cylinder exhaust. Similar attack is also experienced on carbon steel pipework, Figure 3, which shows erosion/corrosion damage at a bled steam pipe bend. In pipework systems carrying high velocity wet steam this form of erosion/corrosion can cause severe wall thinning which, in the extreme, may lead to penetration of the pipe wall at such features as elbows where there is a change in flow direction.

At the steam inlet to feedheater vessels it is necessary to protect the vessel internals from the effects of direct impingement by high velocity wet steam by means of a plate. Where carbon steel was used wastage of this impingement plate has been experienced. In the inlet region the steam flow may be turbulent and the carbon steel shell has been observed to suffer erosion/corrosion attack due to splashback of the wet steam from the impingement plate as illustrated in Figure 4.

## 2.2 Prediction of Damage

Erosion/corrosion is a mechanical-chemical process whereby the protective oxide layer on the metal surface is removed. This results from the dissolution of  $\text{Fe}^{2+}$  ions from the oxide:-



Equilibrium may be achieved between the protective oxide film on the metal surface and the ion concentration in the fluid in contact with the oxide. However, if this fluid layer is continuously replaced with water of low ion concentration equilibrium is not achieved and the dissolution process continues. High pressure, wet steam flowing at high velocity causes disturbance in this boundary layer, particularly at locations where there is a change in direction of flow, resulting in erosion/corrosion damage.

Test coupons were installed in one of the early machines to assess the erosion/corrosion behaviour of materials with a range of compositions. These samples were examined at

intervals over a period of 50,000 hours. At the test location the steam conditions, in terms of pressure, velocity, wetness (pvx) product ( $\text{psia} \times \text{ft}/\text{sec} \times \%$ ), was of the order of  $1 \times 10^5$  and it was observed that mild steel and cast iron suffered severe damage whereas 1CrMo, 2CrMo, 12Cr and austenitic stainless steel were not attacked.

Observation of actual component performance in the machine confirmed that an increase in the alloy content of steel, even of the residual elements in mild steel, improved the erosion/corrosion resistance. Chromium appeared particularly effective and other elements such as copper and molybdenum were also beneficial. This is considered to result from the formation of a more stable, less soluble surface oxide. In times up to 50,000 hours it was observed that materials containing more than 0.5% chromium did not exhibit damage in wet steam conditions with a pvx product up to  $1.0 \times 10^6$ . 12Cr ferritic stainless and 18Cr austenitic stainless steels were shown to be virtually immune to erosion/corrosion attack.

In addition to the parameters related to the local steam conditions the geometric configuration, by its effect on the steam flow, also has a strong influence on the rate of attack. Cumulative experience has led to recognition of the principal factors that affect erosion/corrosion damage and the relationships developed within the Company have been substantiated by service performance.

## 3. CORROSION

An additional constraint on material selection arises from the special requirements for the feedwater chemistry in water cooled reactors. The system chemistry is designed to protect the steam generator from corrosion and other problems arising from deposition of corrosion products transported from the materials of the turbine and, more importantly, the associated condenser, feedheaters and moisture separator reheater. In order to minimise these effects high purity feedwater chemistry has been adopted which influences the design and material selection for the condensing and feedheating plant and of the reheater tube nests in the MSR.

Steam generators of pressurised water reactors have suffered damage in the form of tube corrosion and more recently "denting" of the Inconel tubing. In early plants co-ordinated phosphate treatment was used leading to both stress corrosion and corrosion wastage of the tubes. Subsequently an all volatile treatment using ammonia and hydrazine dosing has been adopted. This reduced the tube corrosion problems but gave rise to corrosion in the crevice between tube and the carbon steel tube support sheet. Impurities concentrate in the crevice and provide conditions in which growth of a non-

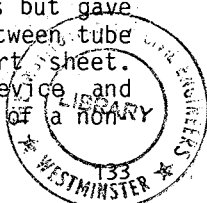




Fig. 3 - Erosion/corrosion of carbon steel bled steam pipe.

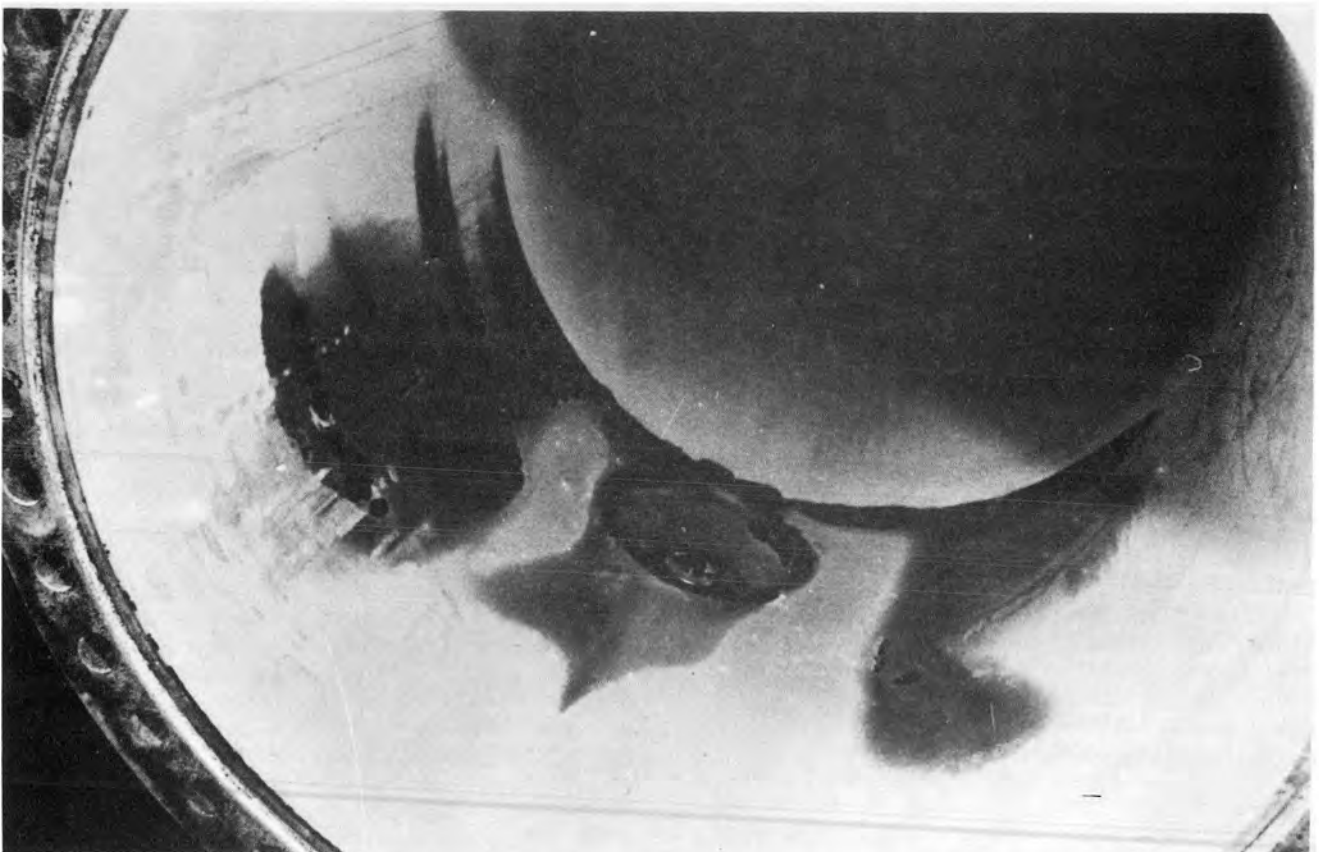


Fig. 4 - Splashback erosion/corrosion of carbon steel heater shell adjacent to bled steam inlet.

protective magnetite oxide occurs. The oxide has an increased volume relative to the parent material from which it formed resulting in deformation, "denting", of the tubes. The phenomenon is associated with the presence of acid chlorides and transported corrosion products (copper oxide or nickel oxide).

In the case of direct cycle water cooled reactors deposition of iron and copper oxides from the feedwater onto the fuel elements will alter the local heat transfer properties, leading to local hot spots and the associated risk of damage to the fuel element. In any event deposits on the fuel elements become radioactive and a minor proportion is carried over in the steam to the turbine and pipework which will extend maintenance periods if decontamination becomes necessary. The level of cobalt in materials of construction is limited to minimise the release to the system of this element with long half-life.

As with conventional fossil fired boiler systems the water treatment practice is optimised to minimise problems with the steam generating plant and in particular the transport of corrosion products from the secondary system. In direct cycle machines a high oxygen, neutral pH system is normally adopted. For early PWR plant, which included copper alloy heat exchanger materials, a pH range of 8.8-9.2 was chosen to limit dissolution of copper. More recently copper free systems have been adopted which enables the pH to be increased to 9.2-9.6, the optimum for minimising release of iron corrosion products.

The occurrence of corrosion under aerated conditions during shutdown can result in high transient levels of transported corrosion products on start-up. This can be minimised by provision of a steam or nitrogen blanket during off load periods or by the selection of materials resistant to atmospheric corrosion as discussed further in Sections 4.2 and 4.3.

#### 4. MATERIAL SELECTION

##### 4.1 HP Turbine

The steam conditions in the HP cylinder of turbines operating with water cooled reactors are significantly different from the superheated steam of high temperature machines. Marginal wetness at inlet increases to some 10% or more as the steam expands through the cylinder. Experience with the early wet machines quickly showed that at locations where the steam flow direction changed, and across joint surfaces where there is a pressure drop and some leakage is present, the components may suffer severe erosion/corrosion damage.

Stationary blades/diaphragm assemblies in early machines were manufactured in materials previously successfully used in high temperature machines. In certain diaphragms the rim and centre were in carbon steel in order to establish whether additional

protection or better materials were necessary. Significant wire drawing erosion occurred across the horizontal joint pressure faces. This damage was temporarily repaired with an austenitic steel weld deposit to restore the joint. Subsequent service showed no damage on the austenitic weld build-up but further attack had occurred to the base materials. Replacement diaphragms in  $2\frac{1}{4}$ CrMo steel with stainless steel inlaid on the horizontal joint faces have proved fully resistant to attack. This material combination has given excellent service for times in excess of  $10^5$  hours in turbines for direct cycle reactors.

Another potential area of attack on diaphragms is the pressure face of the rim where it bears against the carrier ring. This face can be fully protected by weld inlay of erosion resistant material.

HP outer casings on early machines were cast carbon steel and their service performance was satisfactory on certain turbines whereas on others significant wire drawing attack occurred on the half joint and there was also erosion/corrosion damage on the end wall where the wet steam was sweeping out of the casing. On later machines where cast  $2\frac{1}{4}$ CrMo casings were used, both with and without horizontal joint inlay, no sign of joint attack or surface scouring was evident.

The only problem experienced on the low alloy steel bolting was on one  $2\frac{1}{4}$ CrMo outer casing. The flange itself showed no evidence of damage due to steam leakage, whereas slight cutting at the joint location was observed in the 1CrMo bolts (see Fig. 5). Short stainless steel inserts fitted around the bolts at the horizontal joint can be employed as a precaution against this form of damage.

Modern machines therefore employ  $2\frac{1}{4}$ CrMo steel for the HP casing, for diaphragm carriers and for the rims and centres of fabricated diaphragms. Pressure surfaces which may possibly develop gaps during transient operation are inlaid with a weld deposit of stainless steel. This combination has now been fully proven to afford complete protection against wire drawing erosion. A typical example of the inlay on horizontal joint surfaces is shown in Fig. 6.

The steam path is constructed entirely of 12% chromium stainless steel for the moving and stationary blades and the steam passage walls at the inner and outer periphery. Stainless steel extension rings are fitted to the diaphragms outboard of the rotating blades to protect the diaphragm carriers and/or the turbine casing itself from erosion attack by the impact of water droplets flying off the shrouding of the rotating blades.

The low steam inlet temperature on wet nuclear turbines, typically 260°C, does not

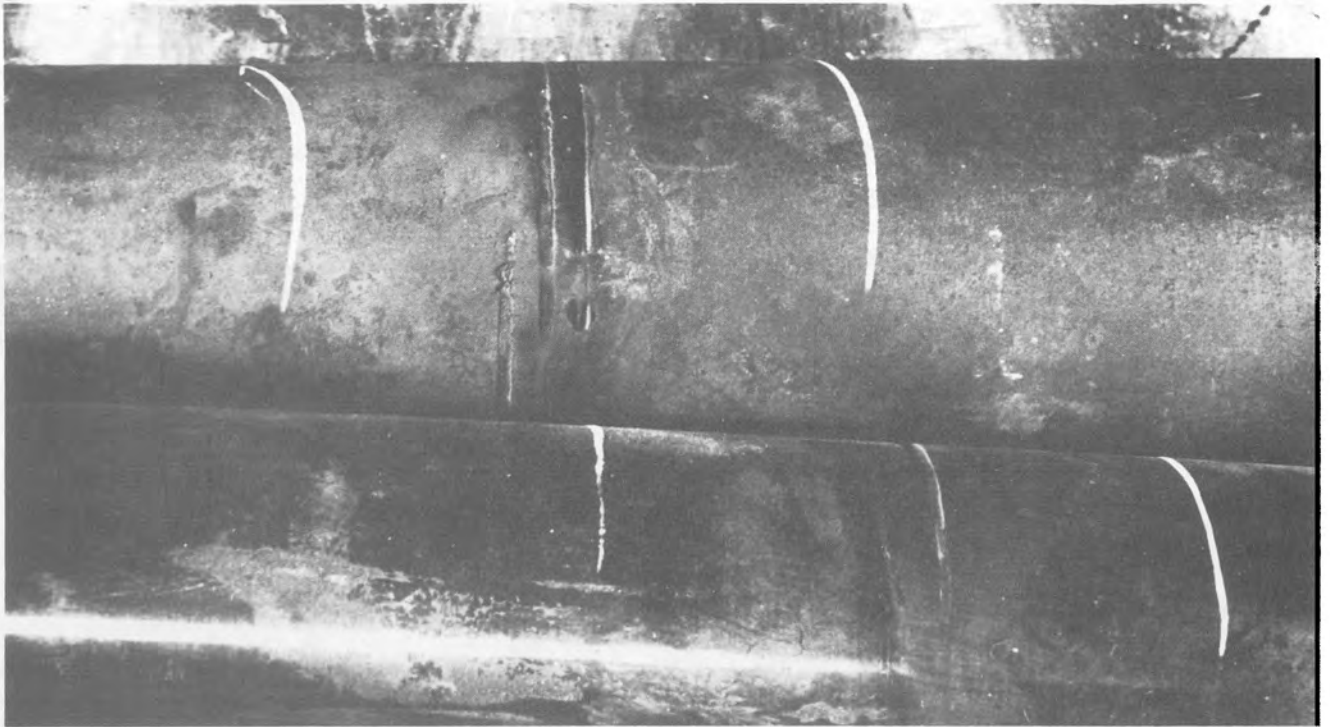


Fig. 5 - Cutting of 1%CrMo bolting of an HP cylinder horizontal joint.

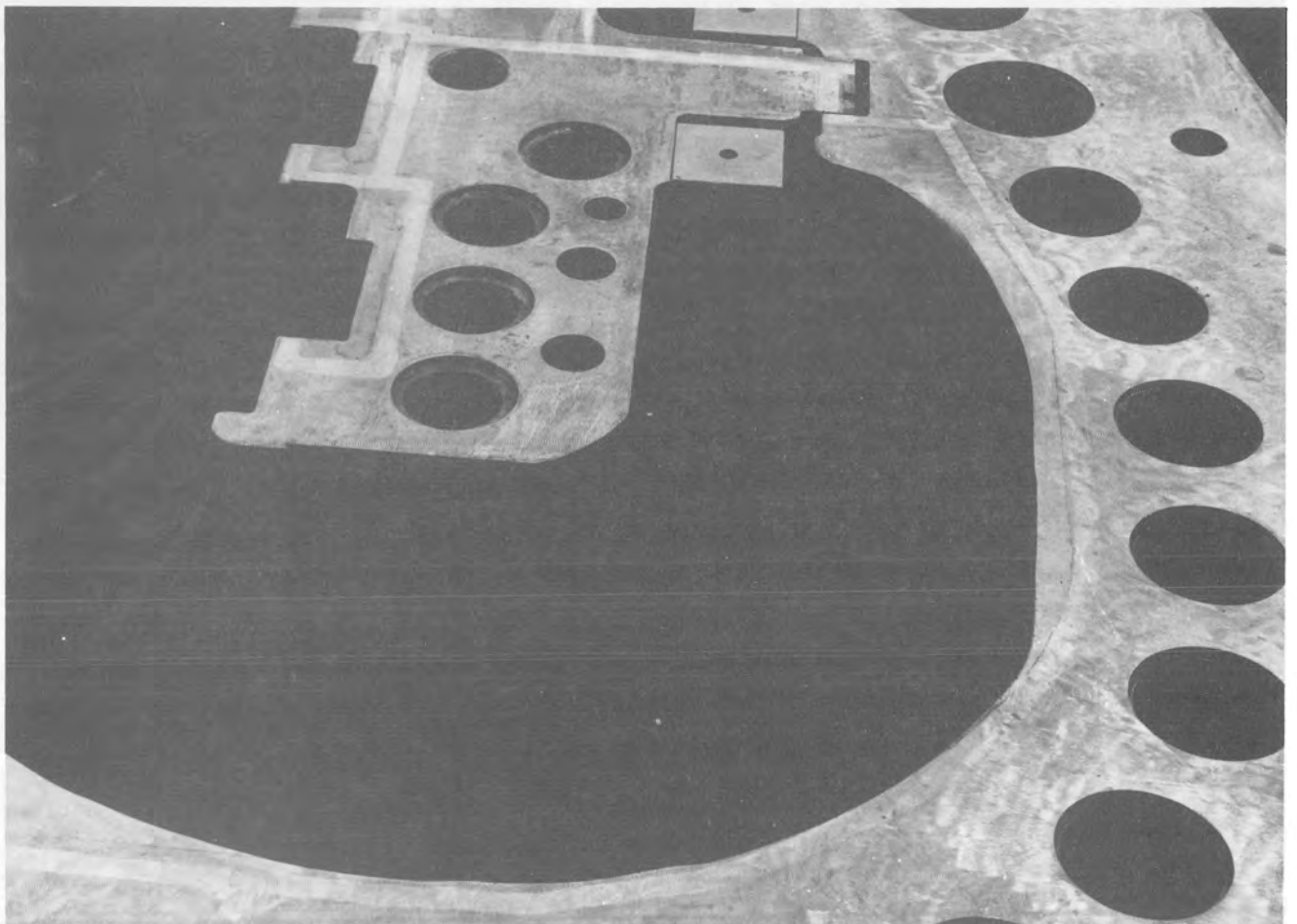


Fig. 6 - Stainless steel weld inlay on typical HP cylinder horizontal joint.

require a creep resisting rotor material as used in high temperature (565°C inlet) turbines. The steam inlet temperature is in fact similar to those normally encountered in low pressure cylinders of reheat turbines and the established NiCrMoV steel of high toughness is used for the HP rotor. This material has not exhibited attack of any sort due to the high velocity wet steam environment.

Other HP components such as the steam chests and inlet steam pipes which operate with steam of negligible wetness are manufactured in carbon steel and no problems have been encountered. However, pipework carrying substantially wet steam such as the HP exhaust cold reheat, bled steam and drains piping is manufactured from 2½CrMo.

#### 4.2 Moisture Separator and Reheater (MSR)

This special item of plant for wet steam cycles receives the HP exhaust steam from which the moisture is separated prior to being reheated through live steam and occasionally also bled steam tube nests to provide superheated steam to the LP turbines. The development of MSRs for wet steam turbines is described in reference 4. The steam from the MSR provides conditions in the LP cylinders which are very similar to those in turbines for fossil fired plant and hence there are no special requirements for the materials of the low pressure turbines.

A major consideration is the choice of material for the tubing of the MSR where a number of factors are involved. The material has to be compatible with the system chemistry requirements in terms of release of corrosion products formed both during operation and shutdown. In the reheater the steam is dried and impurities in the steam may deposit on the external surfaces of the tubes which therefore need to be resistant to pitting and stress corrosion attack. Externally finned tubes offer advantages in heat transfer to the design of the reheater and the selected material must be capable of withstanding the severe deformation of the finning process.

Copper based tubing was used in early designs and has the advantage of not requiring special lay up procedures to prevent atmospheric corrosion. However concern over copper contamination of the feedwater and its association with the steam generator tube denting problem in PWRs and hot spots on the fuel elements in BWRs has led to copper based tubing materials no longer being considered acceptable. Mild steel has also been employed but the externally finned tube surfaces experience significant rusting, leading to high iron loss to the system and deterioration in heat transfer performance, unless suitable protection from atmospheric corrosion is provided during shutdown. Austenitic stainless steel tubing is reported to have suffered stress corrosion cracking in MSR applications although with suitable precautions GEC experience has been fully satisfactory. To

avoid this form of attack a vent element in Incolloy was incorporated in the GEC design to dry out any residual moisture present after the separation process prior to the steam entering the austenitic steel tube nests.

A steel has now been developed and optimised to meet these special requirements of MSR tubing. Type 439 is an 18% chromium steel containing low levels of carbon and nitrogen which are balanced by titanium for ferrite stabilisation. The structure remains fully ferritic at all temperatures thus avoiding the need for post weld heat treatment of tube to tubeplate welds. The problems initially encountered during production of finned tubing, due to abrasive wear of the finning tools by hard particles of titanium carbonitride, have now been overcome by reduction in carbon, nitrogen and titanium levels. The material has excellent corrosion and stress corrosion resistance eliminating concern over salt deposits and shutdown corrosion. This combination of properties has recently led to GEC's adoption of this 18% chromium ferritic stainless steel for MSR tubing.

The design of the MSR avoids high velocity wet steam within the shell. In spite of this the inlet region is protected by internal stainless steel liners which continue for some length down the vessel until the inlet turbulence is dissipated. The separator elements by which the water droplets are removed from the wet HP exhaust steam are also manufactured from erosion resistant stainless steel. The structure supporting the tube nests and the shroud which collects the reheated steam are constructed from stainless steel on the external surface where they are in contact with wet steam.

#### 4.3 Condenser and Feedheaters

The feedwater chemistry requirements for nuclear wet steam turbines impose additional restraints in material selection. Release of metal ions to the feed system by corrosion has to be minimised, particularly in terms of iron and copper corrosion products.

For condensers in conventional fossil fired plant either copper-based or titanium tubing is used depending on the cooling water, the latter material being employed more recently for coastal sites. In this case maximum protection against sea-water ingress is afforded by the immunity of titanium to corrosion attack and the use of either a double tubeplate in the case of expanded tube/tubeplate construction or a single titanium clad mild steel tubeplate for seal welded tube/tubeplate construction. For nuclear wet steam turbines a titanium tubed condenser provides maximum protection from ingress of cooling water and eliminates the condenser as a source of copper contamination

of the feedwater.

Elimination of copper alloys from the feedwater system enables the pH range to be increased from 8.8-9.2 to 9.2-9.6 with the advantage of minimising the release of iron corrosion products to the feedwater system during base-load operation. However, release of corrosion products caused by atmospheric corrosion during shutdown must also be safeguarded. Austenitic stainless steel LP heater tubes as employed for fossil fired plant provide the necessary corrosion resistance but the carbon steel HP heater tubes used for such plant are susceptible to atmospheric corrosion during outages. Although austenitic stainless steel has been used for HP heater tube it has low thermal conductivity and thereby a significantly larger surface area is needed to provide similar heat transfer capacity. The 18% chromium ferritic stainless steel, which is being employed as extended surface tube for MSR application, has fifty per cent greater thermal conductivity than austenitic stainless steel and equivalent atmospheric corrosion resistance and has virtual immunity to chloride stress corrosion cracking. This material is now being used by GEC for the HP heater tubing.

Erosion/corrosion is a potential problem in feedheating plant in nuclear stations with water cooled reactors. Early turbines employing materials typical of those used on contemporary conventional plant suffered early in life erosion/corrosion damage to the HP heaters (see 2.1) in the steam inlet region. Modifications were undertaken whereby the carbon steel impingement plate was replaced in stainless steel and local weld deposition of stainless steel cladding was applied to protect the steam inlet from splashback of entrained water from the impingement plate. These heaters have now been in service for over twenty years and periodic internal inspections have shown that there is no further damage to the carbon steel shell and support frames and the stainless steel is fully effective in resisting erosion/corrosion attack. This is substantiated by satisfactory experience of feedheating plant on other machines.

The design of modern HP heaters provides a large annulus between the periphery of the tube nest and the containment vessel to provide a large unrestricted flow path along the shell and to maintain low steam velocity. Where higher steam velocities arise, at the steam inlet and at the support plates, the potential for erosion/corrosion attack is assessed by the relevant Company's criteria to guide material

selection and the extent of protection. In most areas carbon steel is satisfactory, however the steam inlet connection and the inlet region of the shell are lined with austenitic stainless steel. The inlet impingement plate and the tube support plates are manufactured from stainless steel.

## 5. CONCLUSION

GEC turbine plant operating with wet steam cycles in nuclear stations with water cooled reactors has been in commercial operation for over twenty years. The special problems associated with erosion/corrosion in these turbines caused by high velocity wet steam have been solved by substitution of higher alloy steels and the incorporation of special design features to remove moisture.

Steam generator damage has been observed which has called for additional attention to feedwater chemistry and for suitable material selection in the turbine heat exchangers. In particular, the elimination of copper and the use of stainless steel heat exchanger tubing result in a significant reduction in the transport of corrosion products to the reactor.

GEC now have adequate long term experience, demonstrated by periodic internal inspection of plant, to select with confidence materials to withstand the onerous duty of turbine plant operating with wet steam.

## REFERENCES

1. J. Muscroft - Modern large 3000 rpm steam turbines for pressurised water reactor power stations. Paper 2 to this Conference.
2. G. Hobson and J. Muscroft - Design of large steam turbines for pressurised water reactor power stations. I.Mech.E. Conference 1983 "Steam plant for pressurised water reactors".
3. D. Kalderon - Turbines, generators, separator/reheaters, condensers and feedheaters for the first PWR in the UK. University of Birmingham Conference 1985 "The pressurised water reactor and the United Kingdom".
4. C.J. Monks and J.P. Peyrelongue - Development of designs of moisture separator reheaters. Paper 11 to this Conference.

# 17. The manufacturing development of LP rotors for large steam turbines

G. A. HONEYMAN, BSc, MSc, PhD, MIM, Engineering Metallurgy, and R. D. CONROY, BSc, MSc, MWeldI, NEI Parsons Ltd

Three methods of low pressure rotor construction for steam turbine power plant have been available to the turbine generator manufacturer for many years:- shrunk-on disc, welded and monobloc. This paper appraises the steelmaking, forging and fabrication developments over the last few decades which have permitted these designs to progress to the high standards achieved today. The advantages and disadvantages of each type of rotor construction is discussed, concluding that the problems associated with the stress corrosion cracking of LP turbine discs has largely precluded this particular design from current steam turbine machines.

## INTRODUCTION

1. One of the largest and most critical components in the steam turbine is the low pressure (LP) rotor which has to withstand substantial centrifugal stresses whilst being resistant to corrosive media as the steam crosses the condensation line, normally in the last few stages of a fossil-fired LP turbine. The low speed, wet steam nuclear machines, of course, require corrosion resistance throughout the majority of the stages of all turbine rotors. The NiCrMoV steels have found acceptance throughout the whole Power Industry as being adequate for these specific requirements, having excellent toughness properties and reasonable resistance to the corrosion media. CrNiMo steels have developed independently for those rotors that have been constructed by welding.

2. The increase in rated output of turbine generators over the last 30 years with associated increases in size of all components has initiated extensive alloy development programmes coupled with major advances in steelmaking (1) and forging technology (2) enabling TG manufacturers to keep pace with the requirements of their customers. The progress towards larger machines operating with a conventional reheat cycle, has slowed somewhat in the last few years (Table 1) allowing an optimisation of existing technology and a greater understanding of materials in relation to their specific applications. The same cannot be said for the half-speed nuclear machines where the major emphasis has been the development of larger unit sizes (Table 2) resulting in components substantially greater in size than their fossil-fired counterparts.

Rating (MW)	Weight (Tonnes)	Diameter (mm)	Year in Operation
60	13.1	1220	1950
120	24.4	1525	1958
200	29.6	1550	1963
500	35.7	1625	1966
660	47.0	1625	1973

Table 1 : Progress of unbladed LP rotor weights and diameters for 3000 rpm units

Rating (MW)	Weight (Tonnes)	Diameter (mm)	Year in Operation
540	79.0	1980	1971
680	103.3	1980	1983
840	125.4	2285	1977
1300	150.0	2285	Future

Table 2 : Progress of unbladed LP rotor weights and diameters for 1800 rpm units

3. This paper sets out to describe the historical development of the LP turbine rotor over the last few decades for both high and low speed turbines incorporating the progress made by the forgemasters. They have worked in close collaboration with the TG manufacturers to produce high quality rotor forgings fit for purpose in the arduous conditions of the low pressure stages in a steam turbine.

METHODS OF ROTOR CONSTRUCTION

4. There are three methods of rotor construction generally available to the TG manufacturer:- shrunk-on disc, welded and monobloc (Fig. 1). All are used in the field of steam turbine technology, the tendency to favour a particular design being mainly one of historical development within each individual company.

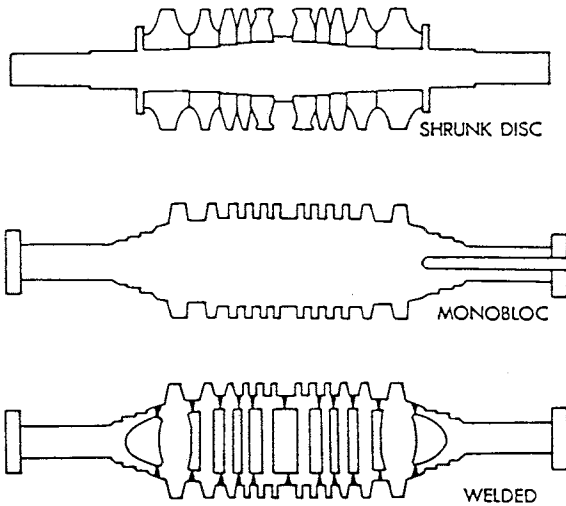


Fig 1 : Methods of rotor construction

Shrunk-on Discs

5. In the early years, most turbine builders including NEI Parsons used a shrunk-on disc construction for LP turbine as single piece forgings of the required size and integrity were not available. Disc construction gives a flexible rotor and introduces relatively high self weight bending and disc bore stresses. At 3000 rpm, it is difficult to design disc construction rotors with ratings greater than 500MW, while satisfying these parameters and the needs of the blade path. For low speed machines, however, the shrunk-on disc construction can be used for much larger units.

6. In the 1920's and 30's, the steels used for disc forgings in the U.K. were governed by the British Electrical and Allied Manufacturers Association Purchase Specification (3). There were four grades of steel with tensile strengths ranging from 460-740 MPa, however, their chemical compositions were never specified. At that time it was not considered advisable to stipulate the chemical properties of each grade, although it was understood that the lower strength steels would be manufactured from normalised carbon manganese grades whereas the high strength version would be an alloy steel, oil hardened and tempered. Steelmaking was not highly advanced in those early years and most discs were produced by the acid open hearth (AOH) process, which gave much dirtier steels because the slag had a lesser tendency to float out and because this method lacked the ability to lower phosphorus and sulphur levels during refining.

Consequently S and P contents up to 0.05% were permitted giving non-homogenous mechanical properties. This effect was exacerbated by the forging method which included an upsetting process, the relatively large forging reductions resulting in flatter more elongated inclusions. Ductility was therefore variable depending on the direction that measurements were taken and the specifications were written accordingly.

7. With the increase in unit sizes of the steam turbine and the demand for higher strength steels came a major development in material technology. By the late 1940's and early 1950's, the Cr-Mo steels were becoming increasingly used for turbine discs and the improvement in steelmaking afforded by the introduction of the Basic Electric Arc (BEA) process permitted the use of discs with much greater section thicknesses. Improved steel cleanliness gave more homogenous mechanical properties with increased toughness and a further refinement in the composition by the introduction of the water quenched NiCrMo and NiCrMoV steels in the 1960's produced discs which were both strong and extremely tough.

8. Non-metallic inclusions cannot be completely removed from steel, and the high forging reduction ratios associated with the manufacture of the disc has always resulted in defects which are much more responsive to ultrasonic inspection from the disc face with consequent high rejection rates. However, a recent invention, the Electroslag Remelt (ESR) process which refines the BEA ingot even further has produced superclean steels, ideal for the production of LP turbine discs.

9. One of the main advantages of the shrunk disc construction is that higher toughnesses can be obtained in each individual disc compared to a monobloc rotor of the same size. During manufacture, discs are always bored prior to quenching in water and the resultant fast cooling at the surface gives a refined lower bainite microstructure consistent with a high fracture toughness. The production of a number of smaller forgings for the disc construction rather than a large monobloc forging increases the number of suppliers available to the turbine maker and allows machining operations to be conducted in parallel. Another advantage is the interchangeability of the discs. Those requiring replacement can be shrunk-off the shaft and new ones shrunk on, a more economic method than replacing a whole monobloc rotor. Removal of the discs is facilitated by having a bored centre shaft. Liquid nitrogen can be pumped into the bore as the discs are heated up and the resultant contraction of the shaft as the bore of the disc expands permits easy withdrawal of the discs. Ultrasonic inspection of the individual components which make up the disc construction rotor is a much simpler and more accurate method than the inspection involved with a monobloc. The minimum detectable defect size is inversely proportional to the section thickness, hence much smaller defects can be detected in an LP disc than in a monobloc rotor.

10. A major disadvantage of a disc construction LP spindle is the susceptibility of the disc to stress corrosion cracking at disc bores especially at the keyway. The catastrophic failure of LP discs in Hinkley Point Power Station in 1969 has led to a major appraisal of this form of construction as a contender for the LP rotor design. Following this failure, a national survey of disced rotors was made by the CEGB (4) which identified those non-reheat machines as being the most susceptible [i.e. stress corrosion cracking was associated with wet steam conditions. Cracks were observed predominantly at the keyway which concentrates the stress by a factor of approximately 3:1.

11. A major rehabilitation programme with the objective of rebuilding rotors without keyways was initiated and existing support discs were machined to remove the keyways and shrunk on to shafts of larger diameters. Alternative forms of construction for these rotors were not sought at the time since alignment changes would have been necessary because of different rotor deflection characteristics. Since the Hinkley Point failure, a number of investigations have taken place (4,5,6) to consider more fully what factors affect the susceptibility of LP discs to stress corrosion cracking. Paradoxically, Hodge and Mogford (4) found that the incidence of disc cracking was not related to material composition, the NiCrMoV steels being as susceptible as the CrMo steels. Nevertheless, the superior fracture toughness properties of the NiCrMoV steels ensured more resistance to catastrophic brittle fracture. An analysis of field and laboratory data by Eason et al (5) considered that the tempering temperature (and hence the yield strength) of the material was a dominant feature whereas composition and operating temperatures have less effect on crack initiation. In contrast, the discussion of Hodge and Mogford's paper (6) realised a significant influence of operating temperature on stress corrosion crack growth rates with the 3CrMo, AOH steels showing the highest values.

12. A further disadvantage of the disc construction is that the manufacturing sequence can be more complex. Additional operations may include the shrinking on and the removal of discs associated with two overspeed tests.

13. Despite the problems of stress corrosion cracking in LP discs, the shrunk-on construction continues to operate in many units worldwide and some of the largest rotors (7,8) found in low speed nuclear machines under wet steam conditions have shown adequate service over many years.

#### Welded Construction

14. A long established method of turbine rotor construction is the welded disc or polybloc pioneered by Brown Boveri et Cie (9) some sixty years ago. Doubts about the ability of the forging industry to maintain its development of the monobloc forging in line with the turbine-makers requirements provided the incentive to further develop the fabricated design to a position where it offered both superior engineering and an economic alternative to the shrunk disc design. In the U.K., a similar response was first taken in the 1960's by the then GEC (Erith) turbine-generator manufacturer who installed a total of eight welded LP turbine rotors in 500MW units. A 2CrNiMo material was selected for the discs and stub end forgings which were fabricated by Richardson Westgarth (10). These rotors have been operating trouble free for over fifteen years.

15. The development of the welded rotor has also been undertaken by NEI Parsons where initial work examined the weldability of a high carbon NiCrMoV steel and low carbon 2CrNiMo steel. The adoption of the higher strength NiCrMoV steel for development purposes was considered necessary to achieve the required strength levels. However, following the acquisition of the GEC (Erith) turbine-generator business by Parsons in 1965 and because of difficulties with the welding of the higher carbon NiCrMoV steel, research was concentrated on the establishment of designs and manufacturing methods for a 660MW LP turbine utilising the weldable 2CrNiMo steel. Fabrication equipment was purchased and welding, heat treatment and NDT procedures were developed. The work programme included fracture toughness testing, fatigue testing, stress relaxation data evaluation, and NDT characterisation as well as the conventional testing programme required for welded components. This work culminated in the building of three LP turbine rotors for a 660MW unit at Drax Power Station working alongside turbines of the same size operating with monobloc LP rotor forgings, all of which have operated satisfactorily for over thirteen years.

16. In parallel with this development and because it was considered that even larger higher strength forgings would be required, which may not have been achieved with the development of the monobloc forging, the decision was taken to develop a high strength weldable steel. The requirement was for a steel with a minimum 0.2% proof strength of 770 MPa for a last stage disc of some 1800mm diameter and 800mm hub thickness. The selection of a 5NiCrMoV steel stems from its well established use in plate form for submarines. One of the major advantages of this steel was its known resistance to weld heat affected zone (HAZ) cracking and its potential for good hardenability and toughness. A collaborative project (11) between Parsons and BSC River Don (currently Forgemasters Engineering) resulted in the development of a steel and weldment that met the target requirements.

17. Other research projects at the time were being established by forgemasters who foresaw a widening gap between their melting and forging capabilities and the turbine makers requirements. Terni Forgemasters undertook a novel method which was to utilise existing high strength 3.5 NiCrMoV disc forgings and to butter (weld clad) the proposed weld preparation area on the disc face, before reforging and heat treatment. Two other European forgemasters, Creusot Loire and BSC River Don, approached the problem in another way by recognising their limitations in steelmaking capacity. They decided to adopt the technique of electroslag welding of two or three large blooms to form an assembly that would be further forged and heat treated to make a large rotor suitable for 1200 - 1300MW turbines. All these projects, although showing promise, were abandoned for the following reasons:-

18. (1) The market for 1200 - 1300MW high speed turbines for AGR and fossil-fired boilers did not materialise.

19. (2) The existing market for 500MW - 900MW turbines had been met by the timely development of monobloc forgings and the use of the conventional welded rotor.

20. (3) The manufacture of LP rotors for the 500MW - 1300MW slow speed turbines operating with light water reactors have been met by the adoption of the shrunk disc rotor (8), the welded rotor using the low carbon 2CrNiMo steel and more recently the large monobloc forging.

21. The use of welded LP rotors with diameters considerably in excess of 2500mm is well established. Steelmaking advances that have been used to aid the development of the monobloc forging have also contributed to significant advances in disc and stub end manufacture for the welded rotor (12). These research programmes have provided a weldable steel with improved toughness, adequate strength and increased resistance to temper embrittlement. Progress is continually being made in improving welding techniques and weld metal and HAZ properties, projects which include narrow gap submerged arc welding and high energy beam welding methods.

Monobloc Construction

22. The inherent mechanical flexibility of rotors with a shrunk on disc construction limits the permissible span between bearing centres. Therefore to improve the design of the steam turbine a more rigid rotor as demonstrated by the monobloc or welded rotor design has always been favoured. The major problem with the production of large monoblocs for LP rotors has been the degree of segregation and axial unsoundness to be found in the large ingots needed to produce them (Fig. 2).

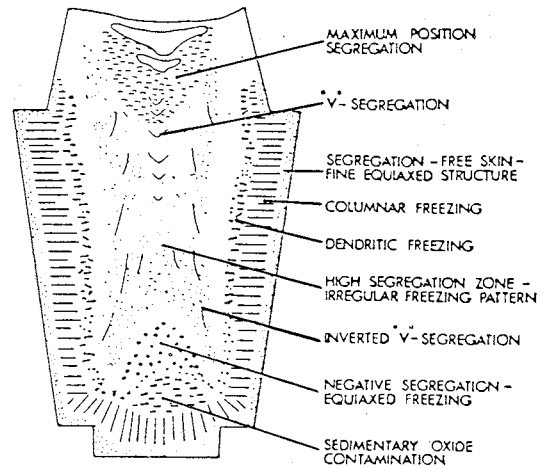


Fig 2 : Zones of solidification and segregation in a forging ingot.

The presence of shrinkage at the top of the ingot and non-metallic inclusions at the bottom has previously required a large proportion of the ingot to be discarded prior to final forging. However, major advances in steelmaking, ingot technology and forging procedures has resulted in the production of larger and larger ingots over the last 20 years (Fig. 3).

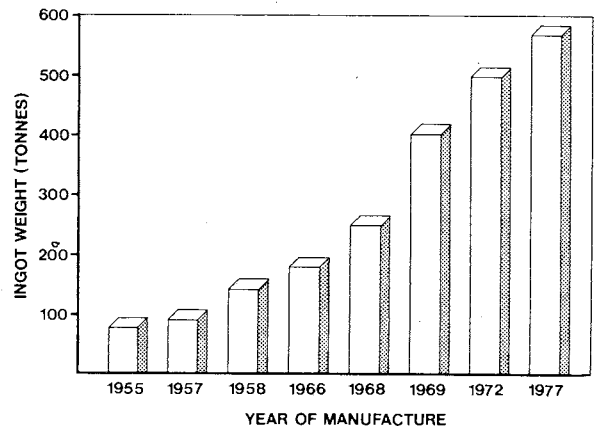


Fig 3 : Ingot development at Japan Steel Works.

23. With the onset of BEA technology, much cleaner steels became available[ however, high hydrogen contents are a feature of this process and in the early stages of development extremely long degassing heat treatment times were necessary to avoid the possibility of 'flaking'. Degassing was facilitated by the introduction of an axial bore prior to heat treatment which also removed any centre line porosity. However, a major breakthrough in steelmaking technology was advanced in the 1950's by the introduction of vacuum degassing pioneered in Europe. This method permitted the removal of hydrogen in the ladle and during pouring into the ingot mould which eliminated the necessity to carry out these long degassing heat treatments.

24. Furthermore, the US developed vacuum ladle installations with steam ejector pumps which resulted in less oxidation of the steel and greatly reduced sizes and numbers of non-metallic inclusions. Until the advent of vacuum degassing, rotor steels were generally killed with silicon to reduce the oxygen content, however, the principle of vacuum carbon deoxidation (VCD) avoided the production of dense oxides such as  $\text{SiO}_2$  and  $\text{MnO}$  and the CO produced was readily emitted from the molten steel. Another benefit of VCD was the greatly reduced silicon contents which increased the toughness of the NiCrMoV steels and decreased the level of segregation in the ingot. Other improvements in ladle refining and slag technology has seen the reduction of sulphur and phosphorus to levels well below 0.01% improving both toughness and ductility (Fig.4). The increase in predictability of properties at the centre of a large rotor coupled with the improvements in segregation has influenced the TG manufacturers' designs of monobloc rotors. This has permitted the removal of through axial bores for high speed turbines thus reducing the stress at the centre of the rotor under the last stage blade row and minimising the risk of brittle fracture.

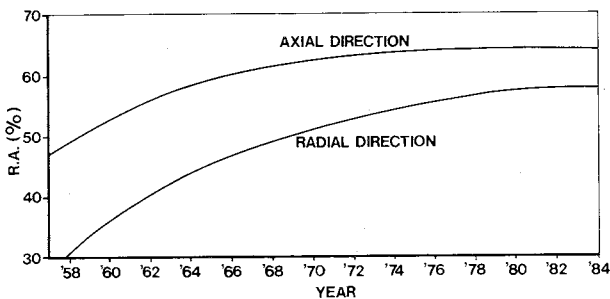


Fig 4 : Improvement in ductility with time.

25. More recent developments in forgemaster technology has seen the introduction of the ESR and Vacuum Arc Remelting (VAR) processes both of which rely on the remelting of existing BEA ingots to further reduce the incidence of non-metallic inclusions. However, the cost to the steelmaker and ultimately the customer of adopting these methods has largely precluded their use in the field of rotor production since conventional BEA vacuum degassing techniques appear adequate to achieve the required quality. The improvement in ingot design has had an influence on yield, with low length to diameter ratios reducing the top end segregation and ultimately the size of the discard. Other methods of reducing segregation have resulted in the implementation of hot topping and electroslag hot topping processes after teeming, the adoption of multifluted ingot geometries as opposed to the earlier hexagonal and octagonal designs and the use of wider but shallower ingot heads.

26. Forging technology has also been investigated to ensure that any porosity present in the ingot is removed and the cast structure is broken up giving fine grained tough material on heat treatment. The introduction of upsetting or double upsetting processes have facilitated these requirements and strict rules have been adopted by the forgemasters to ensure that the ingot receives the optimum forging reduction ratio permitted by their press sizes. Improvement in tool design by the development of V tools and broad flat tools has increased the capability of the forgemaster.

27. There are a few drawbacks in the manufacture of monobloc rotors, especially with large body diameters. After quenching, the coarse bainitic microstructure at the centre can result in toughness values well below those found in their equivalent disc or welded rotor counterparts. Furthermore, the large grained core makes ultrasonic inspection more difficult due to the attenuation of the ultrasonic beam although improvements in forging technology and heat treatments has minimised these effects (Fig. 5). Due to the complex geometry of a monobloc rotor, ultrasonic inspection can be more difficult than with discs and special attention has to be paid to its design to ensure maximum ultrasonic coverage. The elimination of the necessity to gash prior to quenching (a process introduced to improve the toughness at the centre) has facilitated ultrasonic inspection.

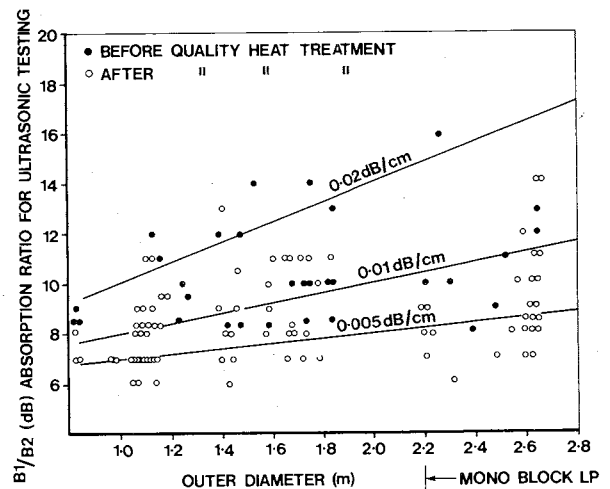


Fig 5 : The effect of diameter and heat treatment on the detectability of defects.

## ANCILLARY PLANT AND MATERIALS OF CONSTRUCTION

28. The total commitment of the suppliers of monobloc rotors to advancing large forging technology has allowed the TG manufacturers to design for units well in excess of 1000MW. In the mid 1970's, a major research programme was undertaken by KWU, NEI Parsons and Japan Steel Works on the development of a large ingot for monobloc rotor forgings. Two full scale trials using 400 tonne ingots, with mean body diameters of 3550mm, were made but the forging route was modified for each to investigate the optimum sequence. It was concluded that double upsetting was necessary and a final forging ratio of approximately 3:1 from the upset diameter was a prerequisite for a fully consolidated rotor forging. Production of a generator rotor from one of these experimental forgings gave excellent mechanical properties and NDT results. More recently Japan Steel Works (13) presented data on a 570 tonne ingot which produced a rotor forging with a diameter of 2600mm, more than adequate for the needs of current designs of steam turbine both in fossil fired and nuclear power plants.

### CONCLUSIONS

29. The shrunk on disc LP turbine is no longer a preferred design because of its complexity of manufacture and the problems associated with stress corrosion cracking at disc bores. The monobloc forging is now well established for both 1800 rpm and high speed turbines up to approximately 1300MW, although some turbine makers have shown a preference for a welded disc construction. Should there be a demand for a larger slow speed turbine then it is possible that this can only be met by the adoption of a welded LP rotor as currently being used in France for their 1500MW PWR units (14).

### ACKNOWLEDGEMENTS

30. The authors would like to express their thanks to Japan Steel Works for the data on large monobloc rotor forgings.

### REFERENCES

- (1) Advanced Steelmaking Processes for Rotor Forgings, EPRI Report No. RD-3336, 1983.
- (2) Reid E.A. Forging Methods and Tooling for Production of Large Forgings, Bethlehem Steel Corporation, International Forging Conference, 1967.

- (3) Manufacturers Purchase Specification No. 2, Steel for Disc Forgings for the Manufacture of Land Turbines, British Electrical and Allied Manufacturers Association, 1920.
- (4) Hodge J.M. and Mogford I.L. U.K. Experience of Stress Corrosion Cracking in Steam Turbine Discs, Proc. Instn. Mech. Engrs., 193, 93 1979.
- (5) Eason E.D., Nelson E.E., and Patterson S.D., Stress Corrosion Cracking in Steam Turbine Discs ; Analysis of Field and Laboratory Data, EPRI Report No. NP4056, 1985.
- (6) Discussion on Hodge and Mogford Paper, U.K. Experience of Stress Corrosion Cracking in Steam Turbine Discs, Proc. Instn. Mech. Engrs. 193, S23, 1979.
- (7) Discussion on Build-up Vs Monobloc Rotors, Workshop Proceedings ; Rotor Forgings for Turbine and Generators, EPRI Report No. WS-79-235, 5-182, 1981.
- (8) Bolter J.R., Development and Operating Experience with Inlet Steam Turbines, *ibid.*
- (9) Luthy A., Some Advantages of Welding Turbine Rotors, Weld J., 47 (No. 6), 461, June 1968.
- (10) Davies H.E., Large Turbine Rotors Fabricated by Welding, Engineering, 204, (No. 5288), 293, August 1967.
- (11) McGill B., and Murphy M.C. A 5% NiCrMoV Steel for Welded Low Pressure Steam Turbine Rotors (Parts 1 and 2), Metal Construction 10, 63 Ind 172, February and April 1978,
- (12) Pisseloup J., Bocquet P., Poitroult I. and De Badereau A., Manufacture of Welded Polyblock Turbine Rotors for PWR Plants, 10th International Forging Conference, Sheffield, 1985.
- (13) Yanagimoto R., Kanno N., Jin T., Ikeda Y., Tanaka M. and Tanaka Y., Manufacturing of Large Monobloc LP Turbine Rotor-Shaft Forging, Proceedings of Advances in Material Technology for Fossil Power Plants 71, Chicago, September 1987.
- (14) Riollet G. and Brunar H.R., New Generation Arabelle 1500MWe Steam Turbines use Major Design Advances, Modern Power Systems, (No. 10), 3, 32, November 1983.

## 18. French experience of corrosion in nuclear turbines

P. AUBRY and D. DUCHATEAU, Alsthom, Le Bourget

After considering the very good availability of nuclear turbines in operation in France, an analysis of a certain number of problems due to corrosion is made. The main components with problems are: moisture-separator reheater/HP exhaust connecting pipes, HP casing bolts, LP blades, and shrunk-on discs. A solution was founded for all cases. The solutions are described here.

### INTRODUCTION

1. Industrial units and especially steam turbines can undergo heavy damage because of corrosion. Actions carried out in the design field can minimize these problems. Yet the cost of corrosion is still high. Steam turbines associated with PWR reactors are obviously concerned in a significant way considering steam quality both in the HP and LP sections.

2. Alsthom Company constructed the whole nuclear turbine park for Electricité de France (EDF) and therefore acquired a large experience in that field. The first turbine associated with a PWR reactor was commissioned in 1967 in Chooz and at the present time it has more than 110,000 operating hours.

3. Since the beginning of the 1970s' the nuclear programme in France has developed a lot, which led to the commissioning of a great number of large rating turbines, operating at half speed. Two 500 MW steam turbines, forty 900/1000 MW steam turbines (CPO, CP1, CP2 programmes and export), twelve 1350 MW steam turbines (P4 and P'4 programmes) are today in operation. In addition eight 1350 MW steam turbines (P'4) and two 1500 MW steam turbines (N4 programme) are currently being erected or produced.

4. At the present time, the whole park accounts for more than 1.5 million operating hours, more than 2/3 of them have been performed with turbines provided with shrunk-on disc LP rotors (CPO and CP1). All units reveal a very good availability coefficient, which is due to both equipment quality and quality of operation. Thus in 1987 CPO/CP1 units revealed an availability coefficient  $K_d$  of 78.8%:

$$(K_d = \frac{\text{available net energy} \times 100}{\text{CNR} \times \text{PH}})$$

During the same period, the availability coefficient of the turbines alone was:

$$* k_d = \frac{\text{PH} - \text{MOH} - \text{FOH} - \text{POH}}{\text{PH}} \times 100$$

\*  $k_d$  = 87.8 %.  
with:

PH = Period Hours, MOH = Maintenance Outage Hours, FOH = Forced Outage Hours, POH = Planned Outage Hours, CNR = Continuous Nominal Rating.

5. In spite of the very good results reached in operation, a certain number of problems due to corrosion occurred on turbines. The main problems encountered are explained in the following paragraphs. A solution was found for all cases. The most serious problem deals with the cracks which were noted at the bore of some shrunk-on discs of LP rotors. All manufacturers using this technology have faced this problem.

6. Up to now, most interventions have been carried out during the planned outages for the reactor refuelling. This could only be achieved thanks to the maintenance policy jointly drawn up by Alsthom and EDF.

### EROSION-CORROSION OF MOISTURE-SEPARATOR REHEATERS/HP EXHAUST CONNECTING PIPES

7. A phenomenon of deterioration of turbines and their auxiliaries appeared with the commissioning of light water nuclear plants. This phenomenon had never been noted in the turbines of reheat fossil-fired plants. This difference in behaviour is due to the early occurrence of moisture in the expansion line of nuclear turbines. Thus, steam with a high degree of moisture passes through the pipes which ensure the connections between HP exhaust and moisture-separator reheaters.

8. Originally these pipes were to be made of unalloyed carbon steel; losses of thickness were noticed from the very first outages. The analysis of this phenomenon revealed both mechanical and chemical effects to explain these thickness losses. The name of erosion-corrosion was given to this kind of attack. This phenomenon was subject to several studies and its process can be shortly explained:

- first an incubation period during which loss of metal remains low,
- then an acceleration of metal loss is noted,

## ANCILLARY PLANT AND MATERIALS OF CONSTRUCTION

- finally the phenomenon stabilizes and the loss of metal becomes linear as a function of time.

9. In addition, the intensity of erosion-corrosion phenomenon is at a maximum for a temperature of about 180°C, which corresponds to the temperature of the wet steam in pipes. In order to find a remedy to fight against this phenomenon, Alsthom performed systematic studies as well as measurements of the pipe wall thickness during planned outages. Steel specimens of various types were arranged in the pipes in order to assess the behaviour of different grades with regard to erosion-corrosion (ref. 1).

At the same time, the use of morpholine conditioning with a more favourable steam-water partition coefficient than the one of ammonia solution was recommended.

10. The main conclusions of this experiment were the following:

- the change of conditioning (from ammonia solution to morpholine) slows the phenomenon down but it doesn't stop it,
- the presence of chromium in steel improves resistance to erosion-corrosion a great deal. Therefore a grade at 2.25 Cr could be recommended for these pipes. This change of grade is totally satisfactory.

11. As regards the French nuclear plants originally built with pipes made of unalloyed carbon steel and therefore requiring a replacement, stainless steel 304L, which allows easy on-site utilization was chosen. This solution adopted for the French power plants also proves fully satisfactory.

### INCIDENT ON HP CASING BOLTS

12. The first incident occurred on a CPl turbine (900 MW) in September 1983, about 1,000 hours after a planned overhaul operation with HP casing opening. At that time, the turbine had 16,000 operating hours and was in steady operation at 900 MW: a stud enabling the closing of HP casing was found near the turbine after it had broken through the thermal insulation. A small steam leakage was noticed at the location of the stud. Other similar breaks took place on other sites and as well on units close to the one where the first incident occurred. The stud is composed of two threaded parts separated by a barrel. It is bored to allow the passage of a heating rod during tightening.

13. The metallurgical analyses reveal that the cracks generally initiate in the stud bore. Some cases of initiation at the root of threads are also noticed. The micrographic sections reveal that the cracks are transcrystalline and largely branched and oxidized (see Fig. 1). So the aspect of these cracks is characteristic of a stress-corrosion phenomenon.

14. The microprobe analysis reveals the presence of a high quantity of chloride in the cracks. As the mechanical characteristics of material and tightening were satisfactory, a study was carried out dealing with different cleaning products which were used during the

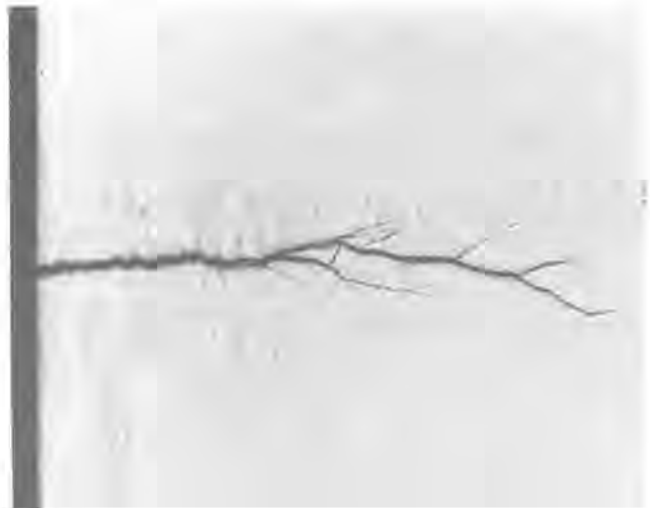


Fig. 1. Transcrystalline and branched crack of a HP bolt.

overhauls prior to the incidents. In the same way, Alsthom researched the nature of chemical contaminating agents which are present in the stud bore and surfaces of fracture.

### The analyses were carried out as follows:

15. Control bore. For three hours the stud bore was filled with demineralized water provided with known characteristics. The solution obtained was then analysed (pH, conductivity, ionic chromatography). The results reveal the significant presence of chlorides, fluorides and sulphates on the bore walls. By applying the results to the quantities of water used and to the relevant surface, the quantity of ions present in the analysed stud section (15 cm) is determined as follows:

$$\text{Cl}^- = 1.32 \text{ mg}, \text{F}^- = 0.08 \text{ mg}, \text{SO}_4^{=} = 0.57 \text{ mg}.$$

16. Fracture surface. The fracture was washed by dipping and by spraying with demineralized water. And in this case also, the results showed the significant presence of the three ions:  $\text{Cl}^-$ ,  $\text{F}^-$  and  $\text{SO}_4^{=}$ . The quantities present on the fracture were approximately as follows:

$$\text{Cl}^- = 0.073 \text{ mg}, \text{F}^- = 0.035 \text{ mg}, \text{SO}_4^{=} = 0.225 \text{ mg}.$$

These results indeed confirm the analysis carried out with the microprobe.

17. Concurrently, the hydrolysis behaviour of the cleaning product used for overhauls has been studied. The evolution of the characteristics of the aqueous phase of a solution composed of 500 ml of cleaning product and of 500 ml of demineralized water boiled for twenty hours has been followed. The results are presented in the form of a graph (see Fig. 2). They show a very rapid hydrolysis of the cleaning product, resulting in an acidification of the medium and in the release of chlorides and fluorides in the form of hydrochloric and hydrofluoric acids.

18. One notes in particular that:

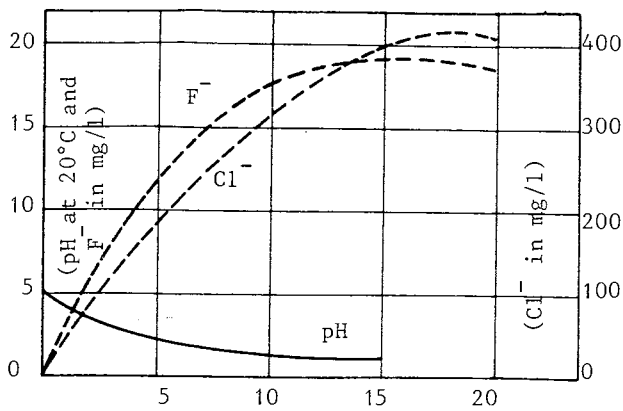


Fig. 2. Chemical characteristics versus time of aqueous solution (500 ml of cleaning agent and 500 ml of de-ionized water).

- the pH of the aqueous phase rapidly falls below 2,
- the respective proportions of chlorides and fluorides formed during the hydrolysis test are comparable with those found in the bore of a broken stud.

Hydrolysis test ( $\text{Cl}^-/\text{F}^-$ ) = 20

Bore of the broken stud ( $\text{Cl}^-/\text{F}^-$ ) = 17

19. Thus, the origin of the stud pollution which led to ruptures in operation has been determined unambiguously (it is a cleaning product, clearly identified, which releases a high quantity of chlorine while decomposing at service temperature); the presence of a slight leakage at the joint plane allows the presence of an aqueous medium necessary for the development of stress corrosion to be explained.

20. In addition, tests carried out by EDF (ref. 2) proved that the other steel grades generally used for studs are also sensitive to the stress-corrosion phenomenon in presence of the cleaning product and of the water heated to 250°C.

21. The actions undertaken to prevent such ruptures are as follows:

- ban on products including halogens,
- cleaning of the studs which were in contact with the polluting product.

22. This incident shows the importance the Utility must attach to the use of any new product. In this case, the consequences were immediate: but a mere check on its halogen content would have led to its ban.

23. It should be noted that since this cleaning product has been banned from EDF power plants, no cracking has been detected on studs.

#### CORROSION FATIGUE OF LP BLADES

24. In 1985, a blade of an LP rotor of a CPl turbine broke in service, after 17,000 operating hours. Blades are provided with forked-root attachments, and the fracture is located at the pin outer line. Cracks initiated on numerous points of the bore of the pin holes and propa-

gated by fatigue. Considering the numerous incipient points, it can be guessed that the fractures developed under a corrosion fatigue mechanism.

25. The microprobe analysis of several cracks showed that chlorine, sulphur and tin were present. The tin comes from a surface treatment, originally scheduled, carried out on the pins to protect them against corrosion. This treatment consists of a tin electroplating followed by a diffusion heat treatment.

26. This treatment leads to the build-up of a deposit composed of three coats:

- a. At the surface - very thin coat of tin,
- b. A thin porous coat composed of compounds defined as follows:  $\text{Fe Sn}$  and  $\text{Fe Sn}_2$ ,
- c. A transition zone ensuring a perfect junction with the support.

The surface treatment is followed by a coating with a product composed of molybdenum disulphide, of epoxy thermo-hardenable at 180°C and of a phenolic binder, the purpose of which is to make the sliding easier.

27. The above mentioned operation accounts for the presence of sulphur coming from the decomposition of molybdenum disulphide; this decomposition occurs when the bladed discs undergo heating-up for the shrinking-on operation.

28. The micrographic examinations of the pins of the damaged blade revealed the presence of numerous corrosion pits under the protective coat. These corrosion pits also contained sulphur and chlorine, which proves that the corrosion process was also developing on pins during operation. These corrosion pits exude iron oxides through the protective coat, which causes a swelling of the pins and therefore different conditions of fitting as regards the blade.

This was confirmed after a test simulating the shrinking-on of a blade root provided with coated pins. This blade root was installed in an enclosure with a humidity rate of 100% at 100°C. After 300 hours, it was noted that the pins were locked in their housing and that a large amount of oxidation had developed.

29. We then carried out the study of the thermal behaviour of the coating in order to determine the aggressivity of the species released during the shrinking-on operation. The coating was then taken to three different temperatures 200, 350 and 500°C, for three hours, and a test sampling of approximately 1 g of the residual matters obtained was carried out. This test sampling was treated in presence of 100 ml of hot water, for 10 minutes, in a ultrasonic tank.

30. After separation of the residual matters by filtering, the aqueous solution was analysed; the conductivity and the pH were determined. These results are represented on Fig. 3a. The same analyses were carried out after passage of the coating at 350°C for 24 and 48 hours. The results are given on Fig. 3b.

31. It can be noted that from 350°C, the

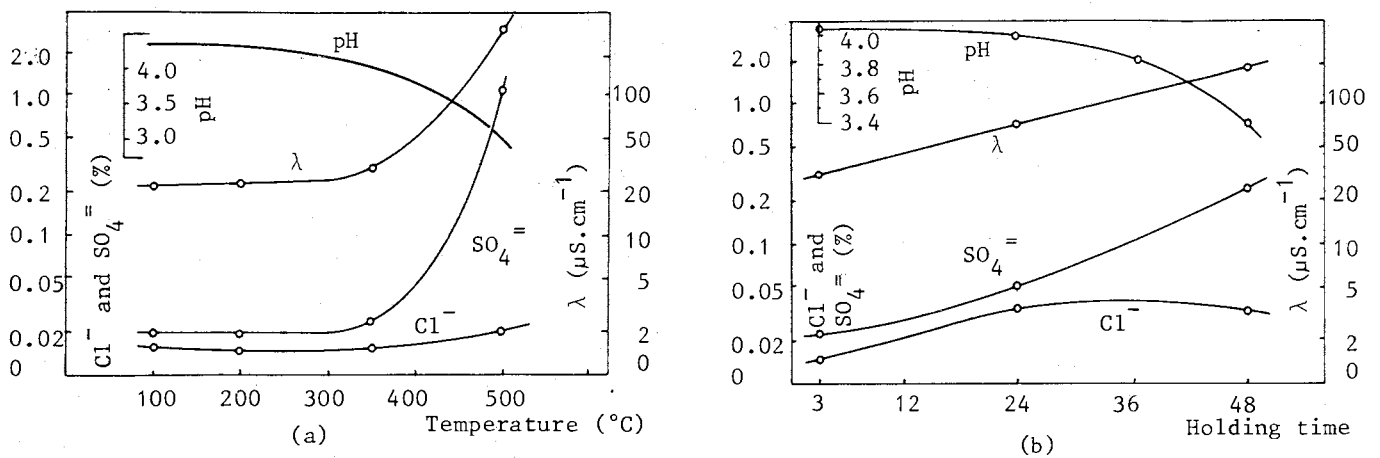


Fig. 3a and b. Chemical characteristics of aqueous solution containing 1 g of enduction residual parts, obtained under the following conditions:  
 (a) Holding time = 3 h, different temperatures  
 (b) Temperature = 350°C, different holding times.

coating mainly releases sulfates. The quantity of sulfates depends on the holding time and on the temperature. This is correlated with an increase of the conductivity and a decrease in the pH. A release of chloride can also be noted.

32. The presence of sulphur in the cracks indeed comes from the decomposition of molybdenum disulphide which occurs during the shrinking-on operation at 350°C. In presence of moisture, the elements released during this decomposition make the ambient medium strongly acid. This results in a significant corrosive activity at the location of the blade root, with a formation of oxides leading to different conditions of fitting and to a decrease in the fatigue limit of the steel the blade is made of. The conditions for cracking to occur are then clearly favoured.

33. Further to this incident, Alsthom developed a method for the ultrasonic analysis of blade roots. This made it possible to find out that many discs identical with the one damaged were affected.

34. The replacement of damaged blades with identical blades is under progress. As regards pins, we decided to use a stainless grade with 13% Cr without surface treatment, in place of 1% C, 1.5% Cr steel.

CORROSION ON SHRUNK-ON DISCS

35. Worldwide experience with shrunk-on LP rotor discs has shown that the risk of stress corrosion was significant. Considering the consequences of such corrosion, the shrink-fit discs on LP rotors as used in CPO and CPL turbines were carefully monitored. Thus during scheduled outages for replacement of fuel, the discs and the rotors are regularly checked. Ultra-sonic testing is used to inspect all the sensitive areas on these parts (ref. 3).

36. Until 1986 no major anomaly was detected. The first alert occurred in September 1986 when indications were revealed on the bore of an LP

turbine disc with 40,000 operating hours. Since then, about twenty rotors have showed indications on the disc bores. In every case the rotors have more than 40,000 running hours. The discs affected are all located at the same position in the steam path, where the steam is at approximately 100°C with a slight humidity rate (at about the Wilson line). It is therefore an area favouring stress corrosion. In order to qualify the hypothesis as to the origin of the indications detected by ultra-sound, a rotor was taken for in-factory testing.

37. Before and during removal of the shrunk-on parts, the rotor was subjected to meticulous inspection. Also many samples were taken from the surfaces of the bores and faces of the discs. All the discs on this rotor and the central shaft showed considerable oxidation, even in the areas where the steam is superheated in normal operation. This oxidation is probably caused during start-up, and especially during prolonged outages, periods during which condensation of the steam can take place on the metal.

38. The inspection revealed cracking on the bore and face of the disc, but there was no direct link between the two types of crack (see Fig. 4) which were not located in the same radial plane. Six cylindrical blocks (ref. 4) act as keys between the discs. The cracks are generally located between the blocks, but the whole of the bore is affected (approximately 20 more or less large-scale cracks were counted). The largest crack was 25 mm long and 12 mm deep, located on the disc face. In the bore the cracks were no deeper than 12 mm. In general it was proven that the ultra-sonic testing had correctly identified the angular position of defects.

39. The discs are made of steel with 2.8% Ni, with tensile properties at 20°C of 856 MPa ultimate strength and 723 MPa yield strength (E 0.2). In the crack area the values of stresses in operation don't exceed 400 MPa, which is a comparatively low value (< 0.6 E 0.2) (in the Alsthom design of LP rotors provided

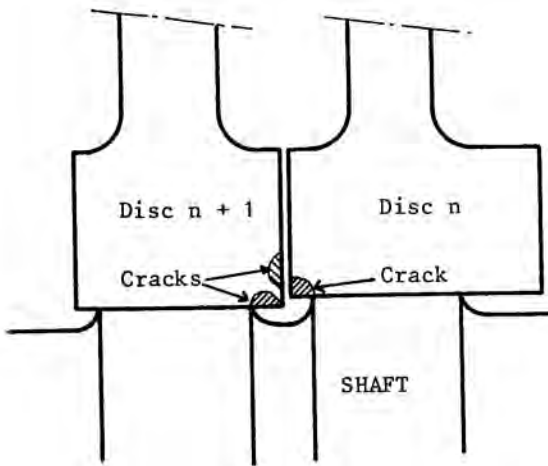


Fig. 4. Position of cracks on LP discs.

with shrunk-on discs, there isn't any axial key between rotor and discs).

40. The tests carried out after crack opening revealed an entirely intergranular propagation (see Fig. 5). However, it couldn't be determined whether cracks initiated in a corrosion pit or not; some small size corrosion pits were seen, especially on the disc face. Searches for products (in the cracks) that might be behind the corrosion were not fruitful: some chlorine and sulphur was found. However there can be no doubt that the cracking was caused by stress corrosion.



Fig. 5. Appearance of one of the cracks of the bore.

41. The face cracks mainly originate in a very oxidated area, just opposite a paint type mark (made on assembly) on the adjacent disc face. Careful examination showed that oxidation had caused the mark to be transferred from one disc to the other. At this point there is very little space between the two discs. Probably, during outages a film of water had formed between the two faces, promoting their oxidation, as the marking was made with a product containing chlorine particles. The problem could no doubt have been avoided by drying these areas when shut-down (ref. 5).

The bore cracks are, however, outside the highly oxidated area. They are located in an area at the end of the bore that is not shrunk on. Together with the rotor this part forms a catchment area that is difficult to dry out both in operation and at standstill.

42. Thus, despite the favourable resilience and mechanical characteristics of the material, and despite the low stress levels for this type of construction, corrosion cracks have appeared (after 40,000 operating hours). Microscopic probe testing only revealed traces of chlorine and sulphur, but it is known that it is always hard to find the products responsible for corrosion. All polluting agents are being actively investigated by establishing case histories for the rotors including details of manufacture, erection and operating conditions.

43. Considering the number of identical machines affected by this problem, on one hand steps are being taken to determine how harmful the defects are (in order to safely schedule the outages for repair work) and on the other hand to perfect the solutions for replacement or repair.

44. Harmfulness of disc defects. On finding a crack of given dimensions in a disc, two factors should be determined:

- the propagation rate of the defect,
- the critical dimensions of the defect, beyond which there is a risk of bursting.

These two parameters can only be exploited if the dimensioning of the crack by ultra-sonic testing is accurate. Important developments have therefore been made in this area both by EDF and by Alsthom.

45. The propagation rate of defects is difficult to establish theoretically with the required precision. Therefore for this parameter on the one hand theoretical values are used and on the other hand successive testing is carried out in order to have a solid experimental basis corresponding exactly to the problem under study.

46. As far as the critical dimensions of defects are concerned, a purely theoretical approach was used, based on calculations of structure by integral equations, and on fracture mechanics. The critical dimensions depend on a number of parameters:

- the characteristics of the material, particularly the  $K_{IC}$ , in operating conditions. For the disc materials  $K_{IC}$  measurements were taken

(ref. 6). The minimum value of this parameter is approximately equal to 220 MPa√m, i.e. a very high value,

- the requirements of the disc, represented by the value of the stress intensity coefficient  $K_I$ . The  $K_I$  is a function of the shape and size of the defect. Comparison of  $K_I$  and  $K_{IC}$  makes it possible to obtain the maximum value for the crack before bursting. Clearly a considerable margin is allowed when determining whether a defect is significant enough to withdraw a rotor from use.

47. The value of  $K_I$  can only be obtained by calculation. Therefore a major study was undertaken to determine this value for several types of defect. The calculations used the integral operations method which is particularly suitable for three-dimensional calculations (ref. 7). From the calculations it was possible to deduce laws in order to calculate the  $K_I$  for all possible defect dimensions (see Fig. 6).

48. The good mechanical characteristics of the disc meant that critical defects have large dimensions, and only a slow propagation rate is observed (low stress level). Discs presenting cracks can continue to be used safely, and the area can be repaired without disturbing the routine of the power plant, considering the number of spare rotors that EDF has available.

Solutions for repair

49. In order to define the type of repair to be carried out for these LP rotors, two main parameters must be considered: the life time of CPO/CP1 turbines and the cost of repairs. Two solutions can be proposed in parallel:

- new rotors with alternative technology for considerable life expectancy: welded type rotors,
- rotor renovation keeping the same technology: the cost being less than for a new rotor, but the guarantees for longer life are also less.

50. The second solution was adopted. However, since EDF needed spare rotors, three welded type

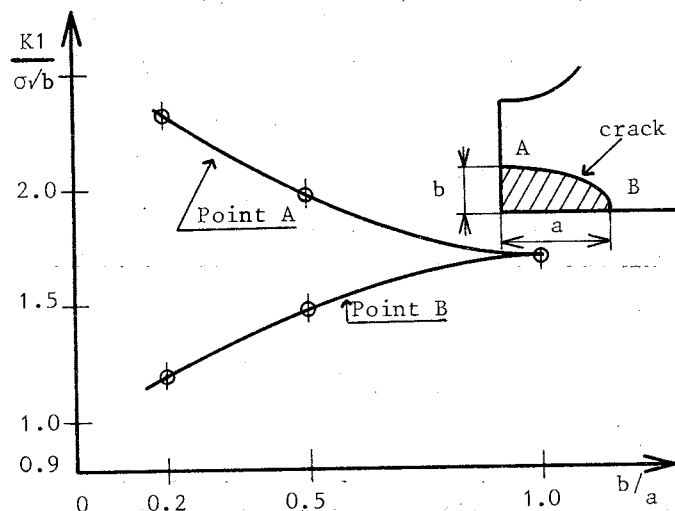


Fig. 6. Stress intensity coefficient: calculation for elliptical crack.

rotors are currently being manufactured: these rotors are interchangeable with the shrunk-on rotors in the same position. These rotors represent a very significant technical improvement in relation to the shrunk-on rotors: in particular they have improved characteristics for stress corrosion (refs. 8-9).

51. The following points were taken into account when defining the renovation to be carried out on the rotors:

- the rotors will continue to be shrunk-on rotors: the objective being to retain the maximum of existing parts,
- the present design, minimizing stresses on the discs is not to be changed (ref. 4). In particular the method of locking by means of blocks between the discs is to be retained.
- as the discs had suffered from stress corrosion, the actions to be taken are intended to protect them from corrosion. This induced us to develop effective surface protections.

52. The surface protections involve all the areas of the discs where cracking was observed and, generally, all locations that might be subject to stress corrosion. As a result, the following actions were decided upon:

- boring of the discs: protection by electrolytic nickel-plating (in bath),
  - discs faces: prestress shot-peening for compression of the face and thus better corrosion resistance,
  - block housing: either shot-peening or electrolytic nickel-plating (with swab).
- The nickel plating must be of the highest quality. Procedures were therefore determined with special regard for the following:
- minimum hardness,
  - total tightness of the coating,
  - total adherence.

53. Actual size tests were carried out on a disc. The main results of these tests are as follows:

- slow bending tests showed that the surface preparation treatment entailed no danger of fragilisation due to hydrogen,
- no trace of unbonding or chipping was observed, even after thermal shock ( $\Delta\theta = 300^\circ\text{C}$ ),
- hardness is approx. 260 HV 100 g,
- the nickel has a column type structure (which does not develop after shrink fitting),
- there is no risk of galvanic corrosion (low potential difference between nickel and steel),
- the plating is perfectly tight, as confirmed by porosopic testing,
- tests showed that the discs could be subjected to eleven successive shrink-fitting and removal operations without degradation.

54. Tests were also carried out to check that the nickel-steel connection could be shot-peened without risking detachment of the nickel plate. Thus all areas of the disc where there is the greatest danger of stress corrosion can be protected. Two main modifications were added to these disc protection methods:

- modification of diaphragm tightness, so that the steam temperature is as low as possible,

preferably less than the disc metal temperature, to promote vaporisation in operation, - increasing the space between neighbouring discs so as to reduce confinement effect and also to prevent films of water developing between the two discs, especially during shut-down.

55. The solution proposed by Alsthom thus enables the repair of the LP rotor in conditions more favourable to operation. By taking special precautions in addition in operation and especially during outages or during start-up (steam quality) the proposed modification should significantly extend the life of the rotor.

#### CONCLUSION

56. We have reviewed the main problems of corrosion encountered by Alsthom on high-rating turbines associated to PWRs. In all cases effective solutions were found. There are still lessons to be learnt from this analysis. Even with techniques of a very high quality, corrosion can still arise due to related causes. This is the case for the HP bolts for which a harmful substance was used during overhaul, or the LP blades whose fastenings were polluted by the hot decomposition of the pin coating. In both cases - for the bolts and the blades - it was not a design fault. This demonstrates the importance of vigilance at all times, and the role of maintenance is to ensure that the work is carried out properly and that adequate checks are carried out to reveal any incipient problems. The co-operation between Alsthom and EDF has made it possible to make great progress in this respect.

#### REFERENCES

1. CERDAN J.P., GREGOIRE J. and LACAILLE L.

Observation des phénomènes d'érosion-corrosion en vapeur humide. Paramètres influents et remèdes possibles. ADERP. EDF. SEILLAC. March 1980.

2. MOUSSET P. and GARNIER F. Ruptures par corrosion sous contrainte de goujons de corps de turbine HP du palier 900 MW CP1. SFEN, Colloque International de Fontevraud, September 1985. p. 366-378.

3. BESANCENEY M., COULON A. and RISACHER R. Les rotors à disques frettés et leurs contrôles par ultra-sons. SFEN, Colloque International de Fontevraud, September 1985. p. 357-365.

4. AUBRY P. Development of rotors with shrunk-on discs. The South African Mechanical Engineers, 1985, vol. 35, October, p. 434-441.

5. LACAILLE L. Protection de la turbine et de ses équipements auxiliaires principaux pendant les périodes d'arrêt. La Technique Moderne, March/April 1986, p. 28-29.

6. COULON A. Essais métallurgiques et de la mécanique de la rupture sur acier pour disques de turbines de grandes dimensions, October, Revue de la Métallurgie, 1977.

7. AUBRY P. Détermination de la taille critique de défauts dans des disques frettés, June, CETIM, Information n° 51, 1977, p. 43-54.

8. AUBRY P. and BAYARD S. Nuclear LP turbine design and operating experience, Proceedings of American Power Conference, April, Vol 48, 1986.

9. BAYARD S., NOUGARET M. and ANIS A. Material developments for large welded steam turbine rotors. American Power Conference, April 1988.



## 19. The flow in last stages of large steam turbines at part load and low load

Professor Dipl.-Ing. W. RIESS and Dipl.-Ing. U. BLÖCKER, Institute for Turbomachines, University of Hanover; Dipl.-Ing. H. NEFT and Dipl.-Ing. H.-G. OTTO, MAN Energie GmbH, Nuremberg

The flow field in turbines with low hub-tip ratio under low and extreme low load conditions was investigated in an experimental air turbine. A measuring technique for determining the flow field in wet steam atmosphere of steam turbines was developed and successfully applied. Flow measurements in the LP-part of a 350 MW steam turbine at part load confirmed the results.

### INTRODUCTION

1. The continuous efforts to increase the operational reliability and safety of modern, high-output steam turbines create, too, an interest in the precise information about their behaviour at part load and "extreme part load". The definition "extreme part load" implies operating points of an LP-turbine at nominal speed with the exhaust steam flow approaching zero. A part of the blading, beginning at the last stage, enters the regime of the power input then, i.e. the rotating blades transmit energy into the flow by local ventilation. The limiting case is pure ventilation operation, where the steam mass flow is zero and the blade movement causes a violent vortex flow of the steam filling the machine, a condition which cannot continue in a larger steam turbine but for a very short time because of overheating.

2. "Extreme part load conditions" occur at several occasions in steam turbines, e.g. at start-up and shut-down, after a load dump and especially in turbines with regulated steam extraction upstream of the LP-part which may result in continuous LP-operation at a very low steam flow. In all these cases the behaviour of the LP-turbine is of a specific interest, because its long blades produce high ventilation losses and the danger of overheating. In most practical cases a sufficient mass flow of "cooling-steam" has to be maintained to avoid this. In turbines for district-heating plants minimizing of the cooling-steam flow is attempted, because it means a heat loss for the system.

3. The flow conditions at low and very low loads have been investigated thoroughly in an experimental multi-stage air turbine at the Institute for Turbomachines.

4. In addition flow measurements for verification of the results have been carried out in the last stage of a 350-MW steam turbine at nominal and part load in cooperation with MAN-GHH (Maschinenfabrik Augsburg Nürnberg-Gutehoffnungshütte GmbH) and

BKB (Braunschweigische Kohlen-Bergwerke AG) in the "Buschhaus" power station.

### THE EXPERIMENTAL AIR TURBINE OF THE INSTITUTE FOR TURBOMACHINES

5. Fig. 1 shows a longitudinal section of the turbine in a four-stage configuration. The design data are:

Power output	$P_i = 703$ kW
Speed	$n = 7500$ rpm
Air flow	$\dot{m} = 7.80$ kg/sec
inlet conditions	$p_E = 2.60$ bar, $T_E = 413$ K
outlet conditions	$p_A = 1.022$ bar, $T_A = 319$ K

6. The turbine is supplied with compressed air from a compressor plant, the power output is transmitted to a DC-generator by a gear train.

7. The blading can be changed to a single-stage or two-stage configuration. The casing contains exchangeable rings which carry the stationary blades. The rotor has axial grooves of the total length, the rotor blades can be shifted and positioned by axial spacers. The stationary blades carry shrouds, the rotor blades are free-ending.

8. The blading has been designed according to the free-vortex-law with a degree of reaction of about 50% at mean height. Form and aerodynamic loading of the blading are not exactly similar to those of a last stage in a steam turbine, since peripheral speed and Mach numbers are considerably lower. Nevertheless, relative blade length, blade twist and distribution of reaction are sufficiently typical and therefore suitable for an investigation of the fundamental nature of flow phenomena at extreme low load. Air instead of steam facilitates the probe measurements in the turbine considerably.

9. Detailed information on the flow field inside the turbine blading at part load operation can be acquired by three-dimensional probe traverses behind each blade row, the

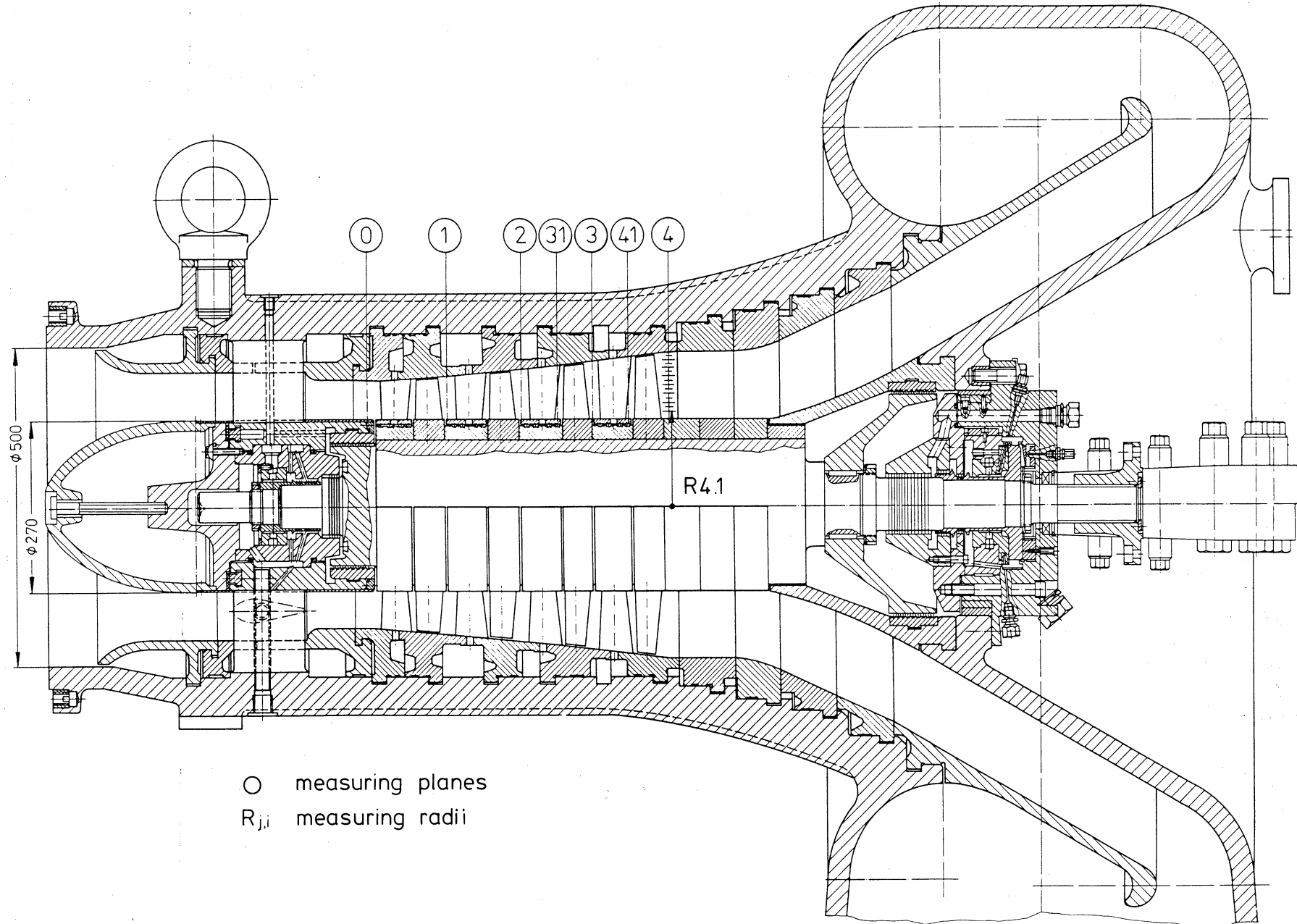


Fig. 1. Experimental air turbine of the Institute for Turbomachines (four-stage configuration)

measuring planes are shown in Fig. 1. The radial distribution of representative values of the flow field is normally determined by a peripheral probe traverse over at least one blade pitch at a sufficient number of measuring radii. In the single-stage and two-stage configuration of the experimental air turbine this can be realized by the rotation of a complete stator blade row with peripherally stationary probes. In the four-stage turbine this method is not applicable because of a possible interference of blades and probe in the planes "31" and "41". Here only radial traverses in suitable representative positions are made.

10. At each measuring plane the flow parameters are determined by 14 equally spaced radii. Two different probes are installed with a sufficient peripheral offset, a temperature probe (see Fig. 3a) and a three-dimensional flow vector probe unit with an additional thermocouple (see Fig. 3b). All the probes can be rotated at 360° to conform to all possible flow conditions.

11. All probes have been calibrated in the high-speed calibration tunnel of the Institute for Turbomachines at Mach numbers up to 0.9.

**Experimental Program and Results**

12. In order to gain an insight into the fundamental phenomena of the ventilation flow regime a broad experimental investigation was necessary. An experimental program according to Table 1 was realized for the single-, two- and four-stage turbine configuration.

Table 1. Experimental program

$\frac{\dot{m}}{\dot{m}_N}$ \ / $\frac{n}{n_N}$	0.05	0.1	0.2	0.3	0.4	0.5	0.6	0.7	0.8	0.9	1.0
0.75	.	.	.	.	.			.			
1.00	.	.	.	.	.	.	.				.

In Fig. 2 the exemplary results are shown for the single- and four-stage blading. A complete documentation of the results is given in (ref. 1). In the two cases shown, the turbine operated with a very low mass flow; in the single-stage case with 5% of the nominal mass flow at nominal speed (see Fig. 2a), in the four-stage case with 4% of nominal mass flow at 75% of nominal speed (see Fig. 2b).

13. The typical flow field which develops at a very low mass flow, can be analysed in Fig. 2a, because it shows very clearly the characteristic ventilation phenomena. The operating parameters had been chosen intentionally for these cases, since they represent the start-up condition of the LP-parts of modern steam turbines where a cooling-steam flow of 3 to 5% of nominal mass flow is necessary and usual at nominal speed.

14. A review of the complete experimental results allows a general description of the changes of the flow field produced by a gradual reduction of the mass flow in a turbine. At about 40% nominal mass flow a local separation starts at the rotor blade tips. At a 30% flow the separation extends to the measuring plane 1 (see Fig. 2a) between stator and rotor in the tip region. At the same time the flow separation begins behind the rotor in the hub region. Two vortices are formed at these two places. A further mass flow reduction renders an extreme extension of the vortices at the 5% nominal flow operating point (see Fig. 2a). The recirculating mass flow within the vortices amounts up to 60% of the passing mass flow. The flow field consists of two large vortices and a narrow band of active flow traversing diagonally the rotor. In addition to the meridional streamline diagrams (see Fig. 2), which give an impression of the axial velocity distribution, the absolute circumferential flow velocities for the different measuring planes are given in the smaller diagrams. In the vortex regions the circumferential velocities are high, the vortices move rapidly around in circumferential direction.

15. The absolute circumferential fluid velocity of the active, non-vortex flow increases - on the contrary to normal flow conditions - during the passage through the rotor which entails at the same time an energy input to the fluid.

16. In addition to the measurements of the flow velocities the fluid temperature distribution was determined. The experiments (ref. 1) proved that the temperatures attain stationary values after a short time in low load flow regimes. The temperature itself depends mainly on the mass flow, very small variations momentarily result in considerable temperature changes. The fluid temperature in the vortices has been increased, but is stable. This points to a continuous fluid exchange between vortex and through-flow.

17. In a multi-stage turbine the flow conditions in each stage at low load operation are quite similar to a single stage configuration. Fig. 2b shows the meridional streamlines at 4% nominal flow and at 75% nominal speed. The active through-flow oscillates between hub and tip in a regular manner, accompanied by the typical vortices. These characteristic features of the flow field are intensified by increasing blade length. Simultaneously the ventilating character of the stage operation increases. In a multi-stage turbine the early stages convey energy to the rotor while the last stages transport energy to the fluid. The fluid exchange between vortex and through-flow transports the hot fluid away.

18. Arising from the experimental results there are some interesting questions concerning the practical steam turbine operation:

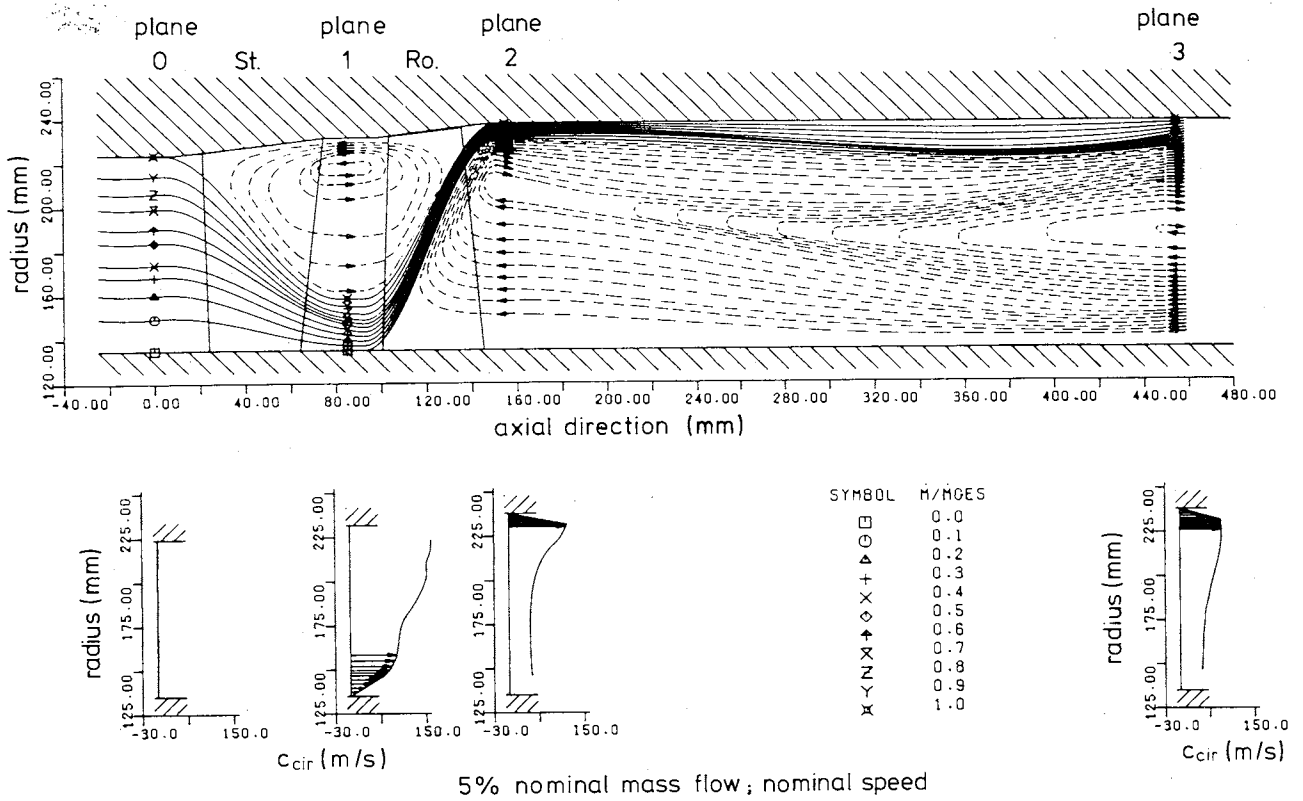


Fig. 2a. Streamline shapes and circumferential velocity components for single-stage turbine

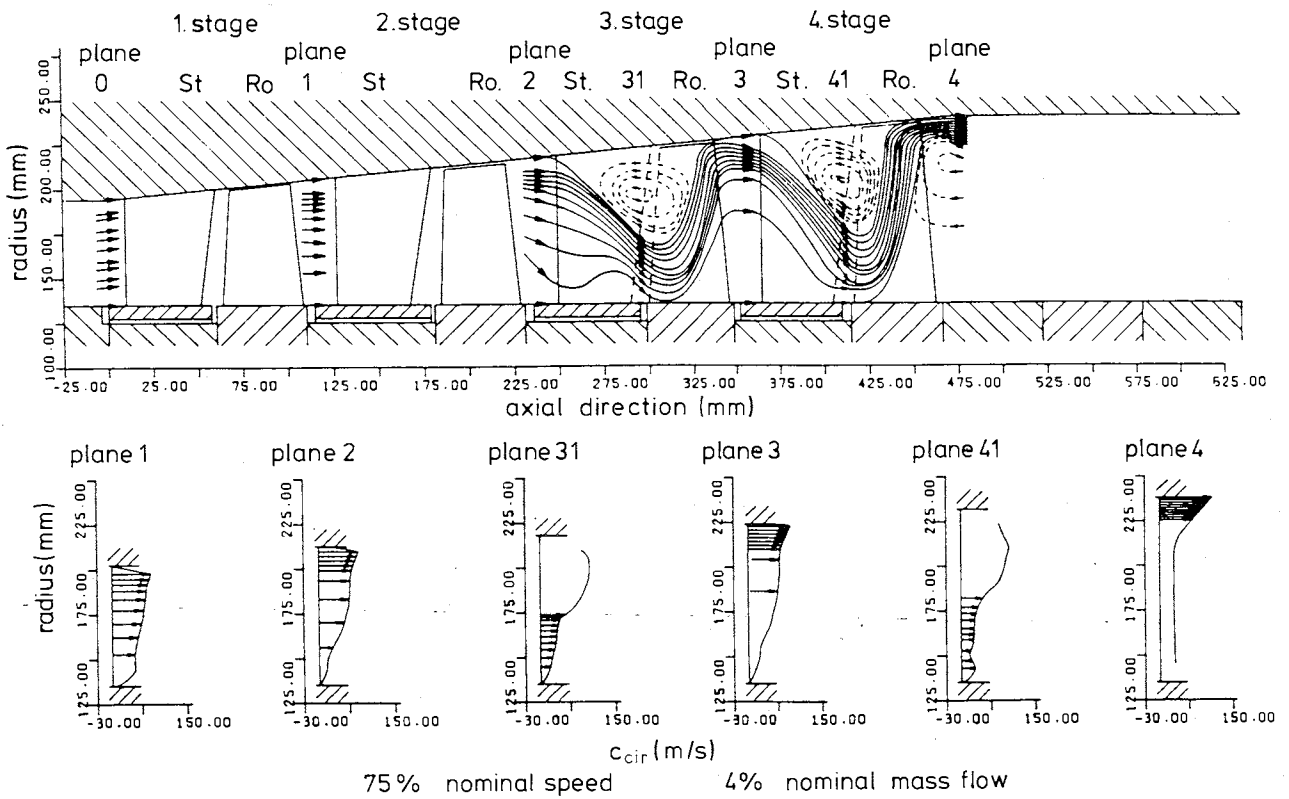


Fig. 2b. Streamline shapes and circumferential velocity components for four-stage turbine

- Can the usual temperature monitoring method of LP-turbines record the highest fluid temperatures in a low load operation?
- Will the usual cooling methods reduce these temperatures?
- What minimum mass flow rates ensure an avoiding of overheating?

At the current state of investigation these questions cannot be solved satisfactorily.

#### MEASUREMENTS IN THE MAN-GHH STEAM TURBINE OF "BUSCHHAUS" POWER STATION

19. In the LP-part of the 350 MW reheat steam turbine in "Buschhaus" power station, which is operated by BKB, extensive measurements have been carried out in cooperation with MAN-GHH in a load range between 360 and 150 MW. The following quantities have been measured in the generator-side exhaust:

- Static pressure and temperature at the hub and the tip of the last stage.
- Distribution of static pressure and stream velocity vector along a radial line behind the last rotor at diffuser inlet.
- Distribution of static pressure at the diffuser outlet.
- Pressure losses down to the condenser inlet.

20. Fig. 4 shows the static pressure wall taps upstream and downstream of the last stator at the hub (P1, P3) and at the tip (P2, P4). Downstream of the last rotor the static pressure has been determined by four evenly distributed wall taps at the tip (P7, P8, P9, P10), at the hub two taps have been available (P5, P6). The static pressure and the flow velocity vector along a radial line behind the last rotor have been determined by the velocity probe (S) (see Fig. 3c). The nearly horizontal position of the traversing line is shown in Fig. 4. The traversing installation was originally developed by the Institute for Thermodynamics (University of Hanover) (ref. 2).

21. We installed a new probe type and measuring system. During the manufacture of the turbine the blank flange (h) for the entry part and the probe guiding (l) already had been properly installed as shown in Fig. 3d. Before starting the measurements the guide tube (k) was installed and positioned with the plate valve (g). The probe has been sealed with elastic rings in the charging valve (r). The traversing mechanism is situated outside the turbine and carries the probe. It can be rotated around the axis with a worm-gear drive (p). The axial movement of the probe is realized in two stages, since the sliding carriage (c) has to be shifted from the front part to the back end of the probe.

22. The diffuser width (j) measures in probe axis (radial) direction 1230 mm, 1180 mm of it could be traversed with the probe (see Fig. 3d).

23. The active part of the pneumatic flow vector probe is a conical five-hole probe with additional static pressure taps (see Fig. 3c). It has been calibrated in our high-speed calibration tunnel for Mach numbers between 0.4 and 0.8. The measured quantities are:

- Radial probe position  $r$ ,
- circumferential probe angle  $\alpha$ ,
- total pressure  $p^{\circ}$ ,
- static pressure  $p$  and
- pressure difference  $\Delta p_{\gamma}$  for radial flow angle  $\gamma$ .

24. The angle  $\alpha$  has been determined by probe rotation and zeroing the pressure difference  $\Delta p_{\alpha}$ . The angle  $\gamma$  has been determined by the pressure difference  $\Delta p_{\gamma}$  by means of the calibration curves.

25. Since the fluid has been wet steam at about ambient temperature, condensation phenomena in the probe and the pressure leads caused considerable difficulties during the measurements. Continuous flushing of all pressure leads and of the probe with ambient air before each measurement has been necessary, so that all condensate has been driven out into the steam flow. After interrupting the air flush, an air over-pressure remained in the measuring leads and during the pressure equalization air flowed continuously out of each probe hole. Detailed experiments have shown that with the given measuring system configuration the pressure equalization took 50 seconds. After another 30 seconds the falsification of the measured pressures by condensation started again.

26. A measuring sequence comprises several steps:

1. Radial positioning of the probe.
2. Air flush of all pressure leads for at least 10 seconds.
3. Closing of the air flush and beginning the measurement of the angle  $\alpha$  by probe rotation after about 35 seconds. After 50 seconds the pressure equalization is completed and within further 30 seconds the angle measurement has to be finished. In total step 3 has to be performed within 80 seconds.
4. Air flush for 10 seconds
5. Pressure equalization for 50 seconds, control of zeroing of the pressure difference for the  $\alpha$ -angle measurement. Carrying out the measurement of  $p$ ,  $p^{\circ}$  and  $\Delta p_{\gamma}$  within 30 seconds.
6. Air flush for 10 seconds.
7. After 50 seconds pressure equalization repetition of all measurements to ensure the reliability of the obtained data.

27. The total measuring time for one radial position with this method was 5.5 minutes. It could be reduced to some extent by optimizing the air flushing with reduced pressure to shorten the equalization period of 50 seconds.

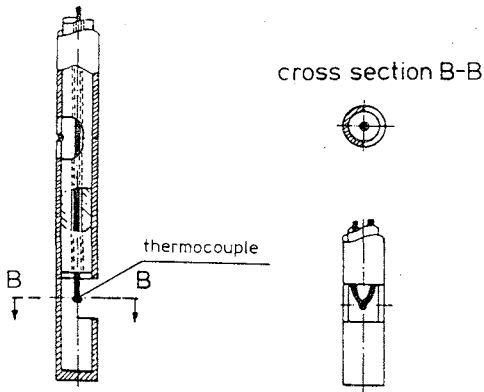


Fig. 3a. Temperature probe

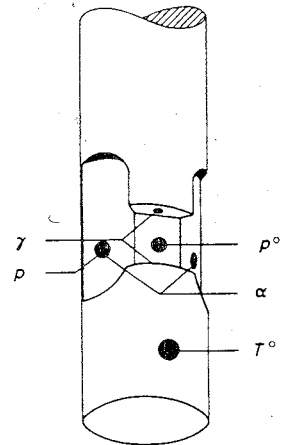


Fig. 3b. Cylindrical five-hole probe

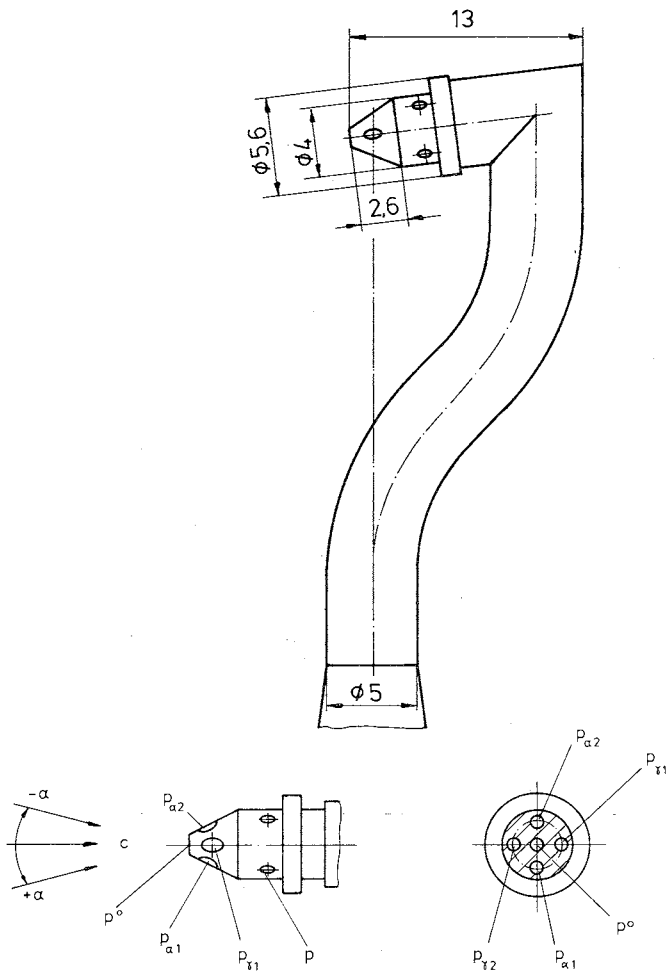


Fig. 3c. Probe head of the pneumatic flow vector probe, conical five-hole type with static taps

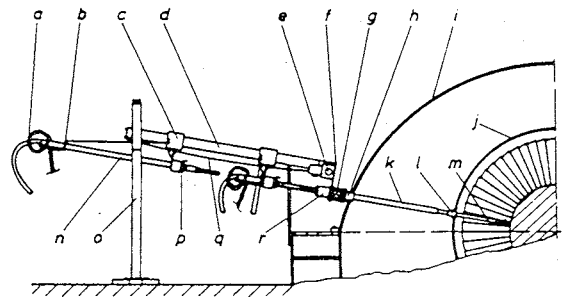


Fig. 3d. Probe-traversing installation:  
 (a) measuring leads; (b) pivot bearing;  
 (c) sliding carriage; (d) guide rail;  
 (e) geared engine; (f) angle plate;  
 (g) plate valve; (h) blank flange;  
 (i) LP-turbine outer casing; (j) diffuser;  
 (k) guide tube; (l) probe guiding;  
 (m) pneumatic probe in measuring position;  
 (n) pneumatic probe in mounting position;  
 (o) frame; (p) worm-gear; (q) chain;  
 (r) charging valve

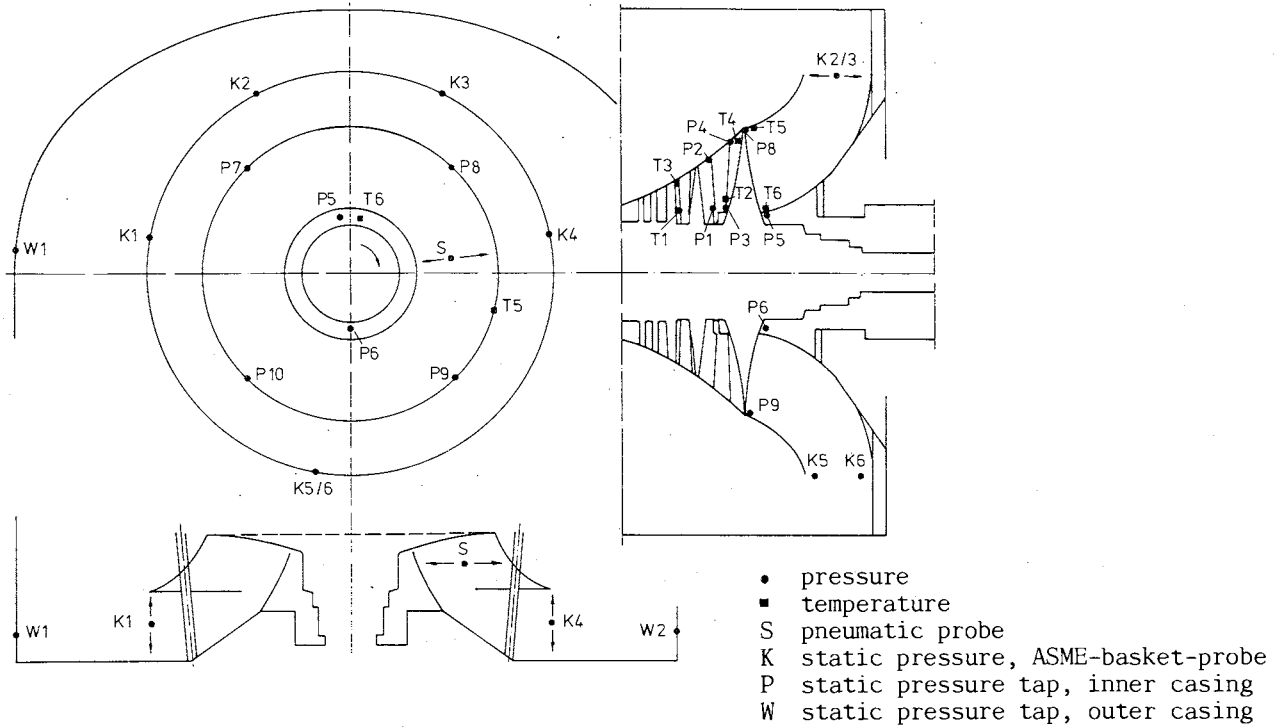


Fig. 4. MAN-GHH LP-turbine (schematic)

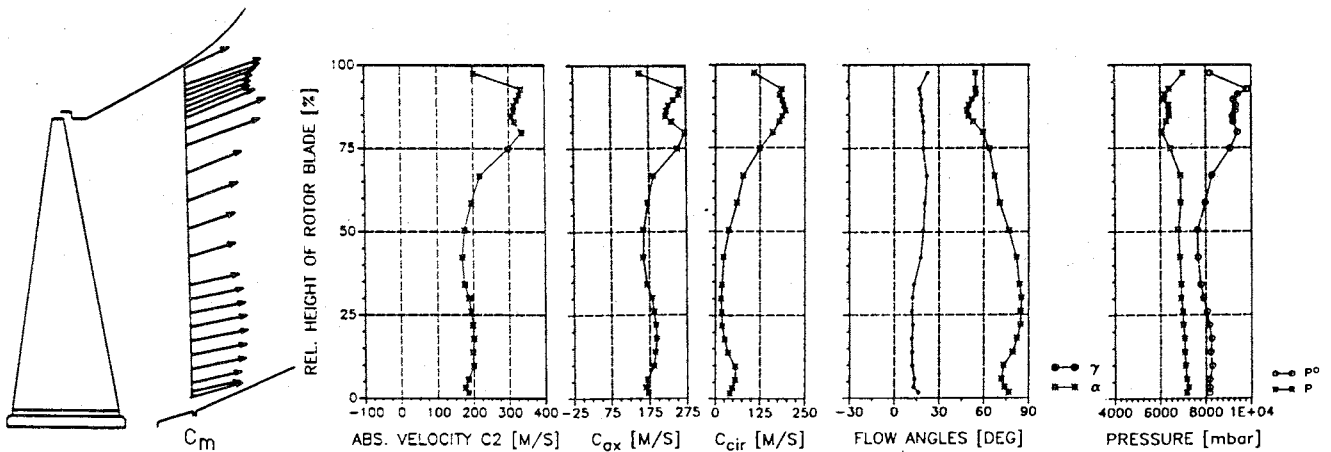


Fig. 5. Measuring data of the MAN-GHH LP-turbine at nominal operating point (366 MW)

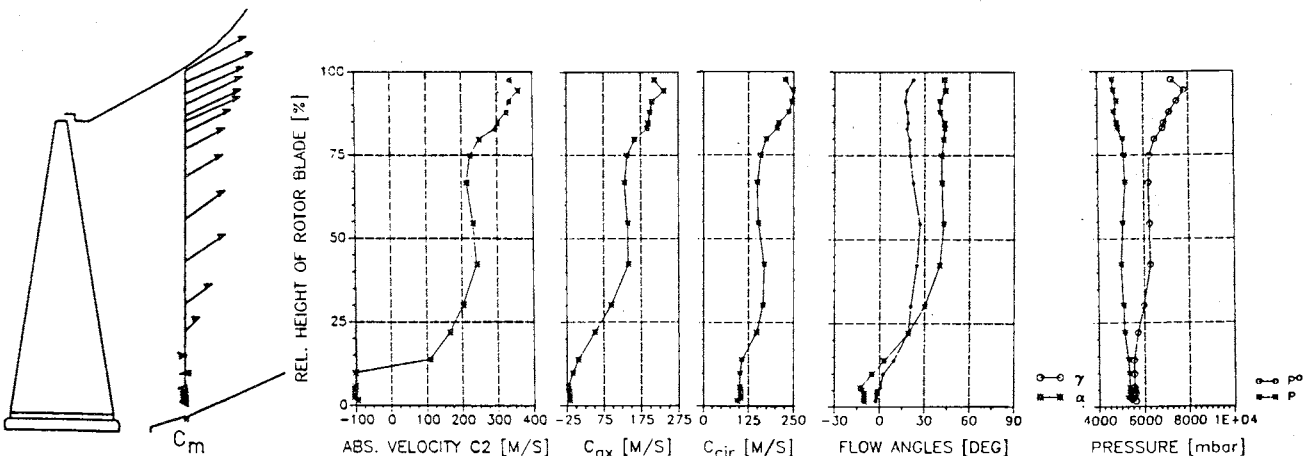


Fig. 6. Measuring data of the MAN-GHH LP-turbine at low load operating point (149 MW)

Similar precautions for probe measurements in wet steam are described by Moore (ref. 3). Heneka (ref. 4) developed a continuous flushing method. Several additional influences, e.g. pressure drop in the pressure leads in function of back pressure and temperature and air flow out of the probe head have to be considered.

28. In the diffuser outlet (see Fig. 4) the static pressure has been measured with ASME basket-tip probes. In the top half four axially movable baskets (K1, K2, K3, K4) have been installed. The two basket probes (K5, K6) in the lower half have been fixed.

29. The static wall-pressure at the outer casing has been measured at two points (W1, W2), the measuring points at the condenser inlet are not visible in Fig. 4.

30. The temperature measurement probes (T1-T6) were installed for control of the pressure measurements. The velocity probe (S) comprised a temperature probe, too (see Fig. 3a).

#### Experimental Results

31. The results of the measurements at full load of 366 MW and low load of 146 MW are shown in Figs 5 and 6. They give the static pressure  $p$ , the total pressure  $p^0$ , the velocity components in meridional ( $c_m$ ), peripheral ( $c_{cir}$ ) and axial ( $c_{ax}$ ) direction, the yaw angle  $\alpha_2$  and the pitch angle  $\gamma_2$  of the flow in function of the relative rotor blade height.

32. All the diagrams in Fig. 5 clearly indicate the influence of the circumferential connecting members - a typical MAN-GHH technique - near the tip region of the last stage rotor blades. The absolute outlet velocity  $c_2$  has been increased in the tip region, mainly because of the circumferential component  $c_{cir}$ . This effect is probably due to the supersonic expansion in the top part of the rotor blades at high load, resulting in a jet deflection, which has been proved by the flow angle. Evidently this causes a decrease of the absolute flow angle  $\alpha_2$ , as to be seen in Fig. 5. The pitch angle  $\gamma$  increases slightly in the lower half of the blade and remains nearly constant in the upper part. This might be due to the fact that the measuring plane is already situated in the diffuser entry with a diagonal flow.

33. The meridional velocity distribution is characterized by a gradual increase from hub to tip, a design technique which somehow diminishes the effect of the low efficiency

region near the hub. The blade connecting members are the cause of the local velocity depression near the tip.

34. Fig. 6 gives the same data for a low load operation. It very clearly points out the begin of a vortex formation near the blade outlet at the hub, where a flow reversal already occurs. The vortex region can also be recognized by the decrease of the pitch angle at about 50% relative blade height and the negative values of the pitch angle in the hub region. The different operating regime results also in a rather high circumferential velocity  $c_{cir}$  over the total blade length.

#### SUMMARY

35. Here only a few results of the extensive investigations of low load and ventilation operation in an experimental air turbine with single- and multi-stage configuration are presented. They show the fundamental differences between the flow fields within a turbine operating at full load and extreme part load.

36. A system for pneumatic velocity measurements in wet steam atmosphere has been developed and successfully applied in a 360 MW steam turbine. The results at about 40% load show - quite similar to the results obtained on the model-turbine test rig - the beginning of vortex formation.

#### REFERENCES

1. EVERS, H. B.: Strömungsformen im Ventilationsbetrieb einer ein- und mehrstufig beschauelten Modellturbine. Dissertation, 1985, Universität Hannover.
2. PUPPICH, P., ROEGENER, H.: Bestimmung des Expansionsendpunktes in Kondensations-turbinen. VDI-Berichte Nr. 487 (1983), S. 151-159.
3. MOORE, M. J.: Instrumentation for wet steam. Von Karman Institute for Fluid Dynamics, Lecture Serie 70 (May 29-31, 1974), p. 29-31.
4. HENEKA, A.: Strömungsmessungen an Niederdruck-Dampfturbinen. VGB-Sonderheft: Forschung in der Kraftwerkstechnik (1977), S. 61-66.

#### ACKNOWLEDGEMENT

We want to express our gratitude to the Braunschweigische Kohlen-Bergwerke AG, Helmstedt, and especially to the director of "Buschhaus" power station, Dipl.-Ing. Pracht, for granting the possibility for the measurements and for the very satisfactory cooperation.

## 20. Wetness measurements in a model multistage low pressure steam turbine

B. R. HALLER, BA, MA, PhD, and R. G. UNSWORTH, GEC Turbine Generators Ltd, P. T. WALTERS, BSc, Central Electricity Research Laboratories, and M. J. LORD, MA, GEC Engineering Research Centre

Comprehensive measurement of wetness losses, exhaust fog droplet diameters, wetness and coarse water content have been taken in a model multistage LP steam turbine over a wide range of flow conditions. It was found that for conventional condensing turbine exhaust wetness fractions of approximately 0.10, the measured wetness loss factor was in reasonable agreement with the Baumann value. Comparison of exhaust wetness fractions derived from dynamometer power and five-hole probe radial traverse measurements, with those found independently from the Central Electricity Research Laboratories optical probe traverses, generally showed agreement to within approximately  $\pm 0.01$ .

NOMENCLATURE (for parameters not defined within the text)

g	extinction or turbidity = $\log_e(f_0/f)$
LE	leaving energy
P, p	pressure
T	temperature
WD	'work done'
y	wetness fraction
$\alpha$	wetness loss factor, also particle size parameter (= $\pi D/\lambda$ )
n	efficiency

### Subscripts

C	coarse water, also condenser
DYN	dynamometer
OP	optical probe
S	static
T	total

### Superscripts

—	mean value
'	isentropic

### 1. INTRODUCTION

In large fossil-fired power stations, despite supplying superheated steam at the turbine inlet and reheating after the high pressure expansion, the latter stages of the low pressure (LP) cylinders still have to operate with wet steam. The exhaust wetness fraction is typically around 0.10. As early as 1912 Baumann (Reference 1) established that expansion of the flow into the wet region produced a loss of thermodynamic efficiency relative to a dry expansion, and his well-known finding from turbine tests was that 'the efficiency will change by 1 per cent for each 1 per cent variation in wetness'. This simple rule has so far stood the test of time and is still used by large steam turbine manufacturers in assessing wetness losses. The development of pressurised water cooled nuclear reactor power stations has provided

added impetus for a better understanding of the physics of wet steam flows, since with this cycle the steam delivery is virtually on the saturation line, and both the entire high pressure turbine cylinder and the last few stages of the low pressure turbine cylinders have to operate with wet steam.

It is found from tests that wetness losses lead to a significant reduction in the efficiency of the last two LP stages (up to 5 per cent loss in efficiency in the wet region with an exhaust wetness fraction of 0.10), and thus the behaviour of wet steam flows in LP cylinders has been the subject of continuous study for many years. Despite this fact many areas of uncertainty still remain, and the availability of good quality experimental data to confirm theoretical calculations is scarce. Flow surveys, including measurement of steam wetness, coarse water flow rates etc., have been carried out in the past on a number of full size machines by various investigators including teams from the Aerodynamics Group of GEC Turbine Generators Limited and CERL. Although such investigations have yielded good quality data, comprehensive measurement of all parameters of interest over a range of flow conditions has inevitably been lacking. Furthermore the scope of such experiments on turbines in service is severely restricted by the inability, due to operational requirements, to systematically vary inlet steam conditions. The study of changes of flow behaviour and cylinder efficiency due to a change in steam wetness is, therefore, correspondingly limited. It is against this background that a series of performance and wetness tests has been planned and executed on a one-fifth scale model LP steam turbine in the Aerodynamics Laboratories of GEC Turbine Generators Limited.

Advantage was taken of the facilities offered by the model turbine rig and the associated steam plant to carry out a controlled set of experiments with varying flow conditions, including direct power output

## FLOW ANALYSIS AND MEASUREMENT

measurement and detailed flow surveys, which overcame the disadvantages of site testing mentioned above and provided more complete data to assist future theoretical studies.

The value of the experimental programme was further enhanced by collaboration with CERL who provided the expertise and apparatus necessary to measure fog droplet sizes and wetness in the turbine exhaust.

### 2. SUMMARY OF WETNESS LOSS GENERATION MECHANISMS IN TURBINES

During the expansion of steam through the LP cylinders in power stations with both fossil-fired boilers and pressurised water cooled nuclear reactors the saturation line is crossed, and the last few LP stages operate with a two-phase mixture of steam and minute water droplets (typically with diameters in the range  $0.1 \mu\text{m}$  to  $2 \mu\text{m}$ ). The expansion is very rapid due to the high velocity of the flow and only a few milliseconds elapse after crossing the saturation line to a state in which, for example, up to 10 per cent water by mass should have been precipitated. It is unlikely that thermodynamic equilibrium would be established in such a short period of time, and a number of important physical processes, as listed below, are considered to take place.

(i) Once the saturation line has been crossed the steam becomes 'supercooled', with its temperature lower than the saturation temperature corresponding to the local steam pressure. As expansion proceeds the supercooling increases to a maximum (at the Wilson point), and then spontaneous condensation occurs suddenly with the steam being transformed into a fog with a very large number of minute water droplets. Internal heat transfer takes place between the water droplets and surrounding supercooled steam across a finite temperature difference, which leads to an increase in entropy (i.e. a reduction in stage efficiency). This mixture of steam and water then flows through a number of successive downstream blade rows, where subsequent supercooling of the steam occurs in areas where the expansion rate is high. Molecules of steam are continuously precipitated on the existing water droplets causing them to gradually grow, and the released latent heat of condensation transferred to the surrounding colder steam gives a further increase in the thermodynamic wetness loss. In areas of very high expansion rate, such as in the root region of the fixed blade and in the tip region of the moving blade of the last LP stage, the supercooling can again reach a point where spontaneous condensation re-occurs. This results in a second cloud of fog droplets of much smaller diameter intermingled with the first generation of droplets ('secondary nucleation').

(ii) Some of the fog droplets due to their mass (inertia) are unable to exactly

follow the vapour streamlines in the blade passages and are deposited on the pressure surfaces. Some water droplets are also transported onto the blade surfaces by turbulent velocity fluctuations in the blade surface boundary layers. The droplets then coagulate into films and rivulets and are drawn to the blade trailing edges by the viscous drag of the steam. Periodically this water is stripped off the trailing edges in the form of coarse droplets (typically with diameters in the range  $2 \mu\text{m}$  to  $200 \mu\text{m}$ ) which are accelerated by the steam until they are hit by the leading edges of the following rotating blades. This leads to erosion damage of the moving blade leading edges towards the tip, where the wheel circumferential velocity is highest and where the concentration of coarse water droplets is also normally higher.

(iii) Apart from the thermodynamic wetness loss mentioned previously there are a number of other sources of entropy increase in the wet steam flow, some of which are described below.

- .. As water is dragged along by the steam flow, frictional energy is imparted to the droplets ('drag loss'). The droplets only acquire part of the energy spent on accelerating them and the remaining energy is dissipated.
- .. A 'braking loss' caused by coarse water from the fixed blades striking the suction surface of the following moving blades, and tending to slow them down.
- .. A 'deposition loss' due to the loss in kinetic energy of all sizes of water droplets when they impact on the blades.
- .. A loss due to centrifuging of water films radially outwards on the moving blade surfaces.
- .. A further family of consequential aerodynamic losses.

### 3. OBJECTIVES

The primary task of the investigation was to obtain performance and flow traverse data, including wet steam measurements with optical and catchpot probes, relating to different operating conditions and duties. Analysis of the experimental data would then yield the detailed information itemised below:

- (a) overall turbine performance with varying pressure ratio, inlet superheat and inlet pressure (mass flow).
- (b) the dry total-to-total efficiency of each stage.
- (c) overall wetness losses.
- (d) velocity vectors and flow distributions at outlet from each stage, giving a detailed picture of the flow behaviour.
- (e) fog droplet sizes, wetness and coarse water flow rates at outlet from the turbine.

A secondary objective of the investigation was to compare the mean exhaust wetness obtained from the optical and catchpot probe measurements over a range of flow conditions with those inferred from the work done by the turbine, as measured with the dynamometers. This would enable a check to be made on the accuracy of the optical probe, albeit only for the model turbine droplet sizes concerned.

4. DESCRIPTION OF MODEL MULTISTAGE LOW PRESSURE STEAM TURBINE

4.1 Turbine Rig

The test turbine, shown in cross-section on Figure 1 is a one-fifth scale model of the last three stages of a five-stage LP cylinder from a standard 600-700 MW reheat machine. The turbine design speed is nominally 15,000 rev/min but higher speeds up to 16,500 rev/min can be safely achieved. Two directly coupled high speed hydraulic dynamometers in tandem can absorb power outputs from the rig up to 2.61 MW, which permits operation up to the maximum output of the existing boilers. The inlet temperature to the turbine is controlled to within approximately  $\pm 1^\circ\text{C}$  in a variable orifice direct contact desuperheater.

4.2 Experimental Technique and Instrumentation

4.2.1 Overall Performance Measurements

The rig is equipped with a modern instrumentation system which includes automatic data recording. A computer controlled data logger accepts calibrated signals from numerous electrical transducers and sensors which provide the actual test measurements. Such measurements include brake loads, turbine speed, steam temperatures and pressures etc. The instrumentation also includes an automatic purge valve system, which maintains all pressure connections free of condensation. Static pressure tapings are installed in the root and tip end walls at turbine inlet and outlet, and also at the interspace and interstage positions (see Figure 1). Further static pressure tapings are located in the inlet plenum chamber, for measurement of the turbine inlet stagnation pressure, and at entry to the condenser.

Guide tubes and access stub pipes are installed in the model turbine to allow traversing with probe instruments at outlet from each moving blade row in Stations 3, 4 and 5 as shown in Figure 1. To enable

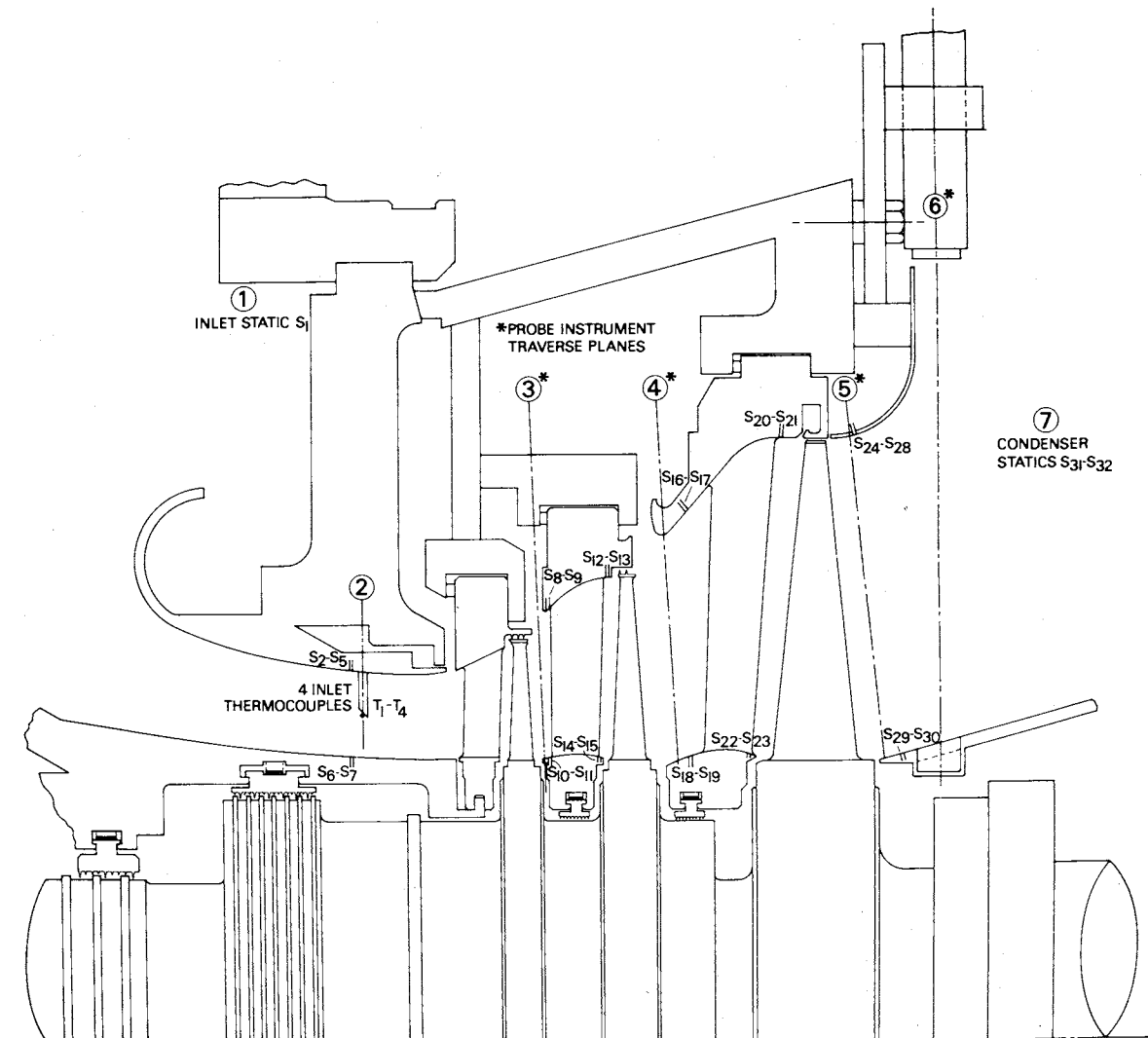


Fig. 1. Cross-sectional view of the model three-stage low pressure steam turbine, showing the instrumentation and location of probe traverse planes.

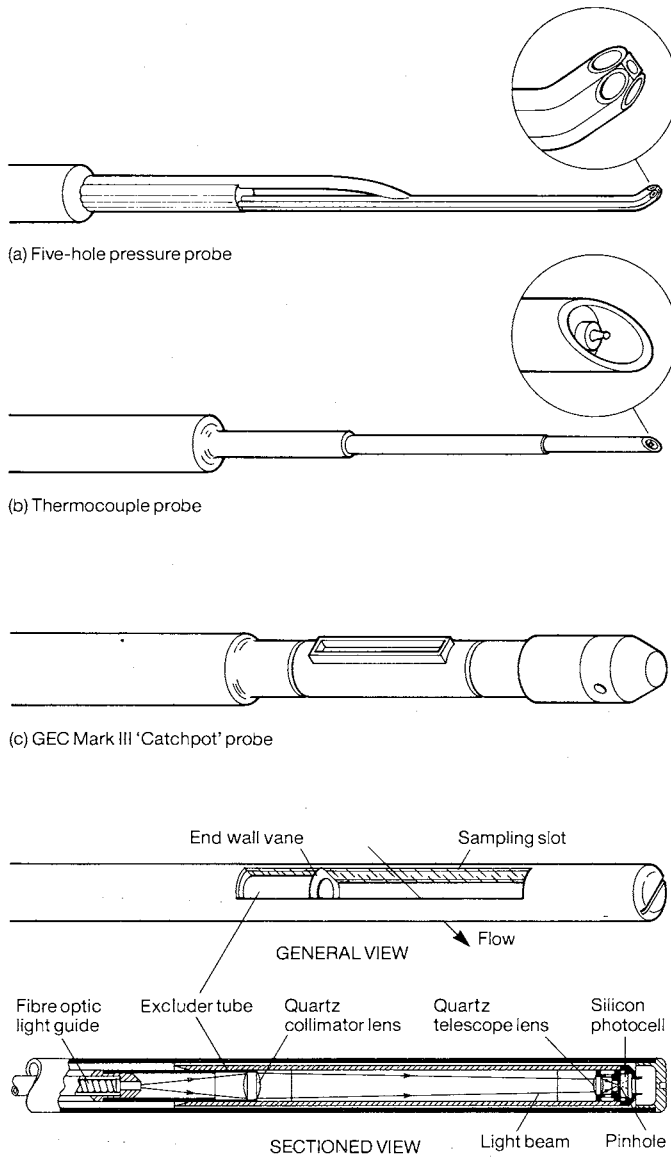
## FLOW ANALYSIS AND MEASUREMENT

traverses to be performed with the 25.4 mm diameter CERL optical probe in the turbine exhaust, three extra traverse planes were located slightly downstream of the exhaust diffuser outer lip in Plane 6. One of these planes was radial with a 'well' located in the exhaust hub casing to improve measurement definition near the endwall, whilst the other two traverse planes were tangentially inclined to the hub casing to obtain extra measurement points across the annulus.

### 4.2.2 Flow Traverse Measurements

Probe instruments used for flow traversing are illustrated on Figure 2. They comprise:

- a miniaturised five-hole pressure probe for basic aerodynamic flow measurements at outlet from Stages 3, 4 and 5.
- an exposed copper-constantan thermocouple probe for stagnation temperature measurements where dry steam conditions exist.
- a 'catchpot' probe for measurement of coarse water flow rates at outlet from the turbine (described in more detail in



(d) C.E.R.L. optical wetness probe

Fig. 2. Probes used for the wetness investigations.

Section 7).

- an optical light extinction probe for droplet size and wetness measurements at outlet from the turbine (described in more detail in Section 6).

## 5. OVERALL WETNESS LOSSES

The wetness losses on the model turbine were accurately established over a range of exhaust wetness fractions, by performing a series of efficiency measurements with varying inlet superheat whilst maintaining constant inlet stagnation pressure and outlet condenser vacuum pressure. These measurements were taken at a number of overall pressure ratios and inlet pressures, which covered the range of operating duties for these stages in service.

Figure 3 shows the location of the turbine inlet conditions on the Mollier chart for an overall pressure ratio of 21 to 1, and with an inlet pressure of  $151 \text{ kN/m}^2$ . During all tests the shaft speed was kept constant at 15,000 rev/min. The first measurement point at the maximum level of inlet superheat established the dry total-to-total efficiency of each stage. Progressively lower levels of inlet superheat were then obtained by injecting more water into the desuperheater, and the measurement sequence repeated. Figure 4 shows the typical measured progressive reduction in overall total-to-total efficiency for the model turbine with increasing exhaust wetness (decreasing inlet superheat), relative to a datum condition. The accuracy of the efficiency measurements is  $\pm 0.5$  percentage points. It should be remembered that the

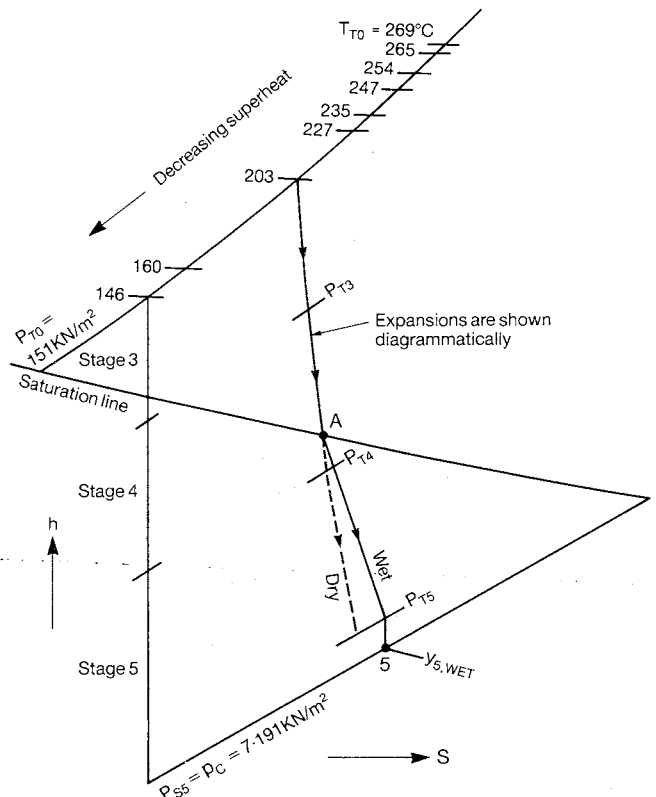


Fig. 3. Overall efficiency measurement points for the model three-stage LP turbine showing varying amounts of inlet superheat.

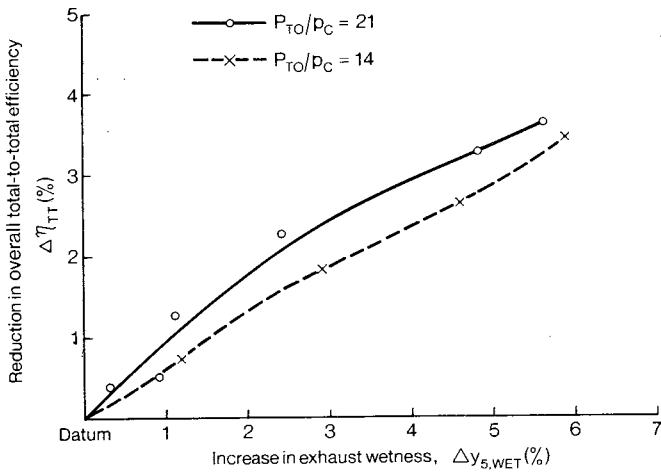


Fig. 4. The reduction in overall total-to-total efficiency for the three-stage LP model turbine with increasing exhaust wetness for overall pressure ratios of 21 and 14 to 1 (with  $P_{T0} = 151 \text{ KN/m}^2$ ,  $N = 15,000 \text{ rev/min}$ ).

wetness losses as measured in the model turbine may not directly apply to the full size unit, due to changes in expansion rates, and droplet sizes etc. Initially the slope of the curve is near unity, but decreases slightly as the exhaust wetness increases.

For the results shown on Figure 4 the first part of the expansion takes place above the saturation line, and as the turbine inlet temperature is reduced the proportion of work done in the wet region to the overall work done gradually increases. Therefore, to enable comparisons to be made on a consistent basis, wetness losses were established for the wet part of the expansion only below the saturation line, for each level of inlet superheat. This was achieved by using individual dry stage total-to-total efficiencies measured at the maximum inlet temperature, and applying a small efficiency correction calculated from the Company's standard performance prediction methods, for each lower level of inlet superheat. Figure 5 illustrates how the wetness loss factors were derived. For the proportion of the turbine expansion below the saturation line only, the dry and wet efficiencies are given by

$$\eta_{A-5,DRY} = \frac{W_{D,DRY}}{\Delta H'} \quad (1)$$

$$\eta_{A-5,WET} = \frac{W_{D,WET}}{\Delta H'} \quad (2)$$

where  $\Delta H'$  is the isentropic total-to-static specific enthalpy drop. If we now employ the concept of a wetness loss factor, which was first introduced by Baumann, then the wet and dry efficiencies are related by:

$$\eta_{A-5,WET} = \eta_{A-5,DRY} \left( 1 - \alpha \frac{y_{5,WET}}{2} \right) \quad (3)$$

and thus

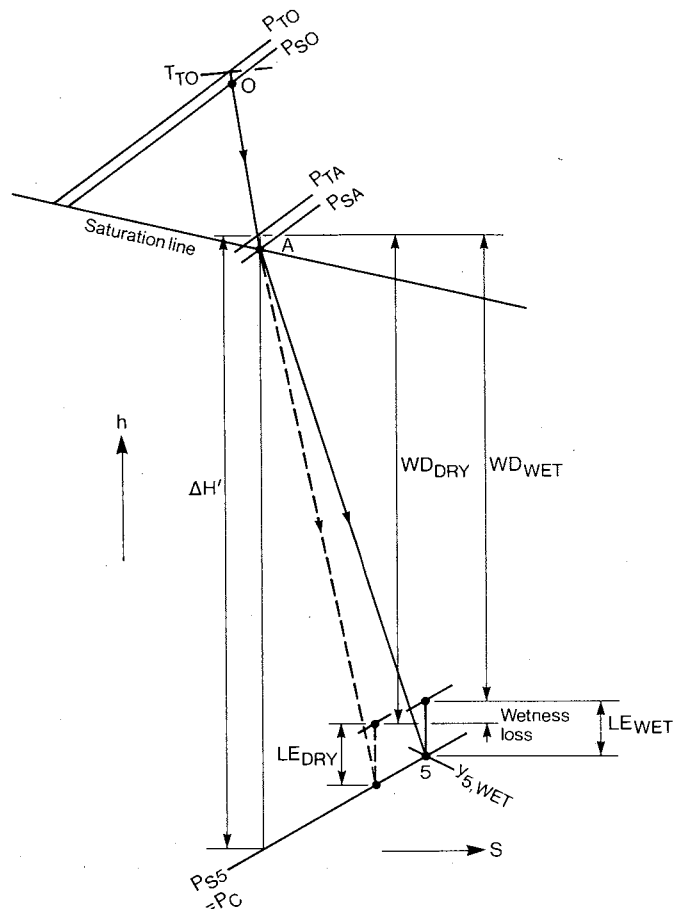


Fig. 5. A typical wet expansion drawn on the Mollier chart showing how the wetness loss factor  $\alpha$  was calculated from the model turbine wet and dry efficiency measurements. The broken line shows the expansion in the homogeneous ideal 'dry' case, whilst the full line illustrates the actual expansion.

$$\alpha = \frac{W_{D,DRY} - W_{D,WET}}{W_{D,DRY}} \cdot \frac{2}{y_{5,WET}} \quad (4)$$

The Baumann rule is that  $\alpha = 1.0$ .

For conventional condensing turbine exhaust wetness fractions of around 0.10, it was found that the measured wetness loss factor agreed reasonably well with the Baumann value.

Present work is concerned with comparison of the measured wetness losses for the model turbine, against results from a number of non-equilibrium wet steam calculations, with the aim of formulating improved design methods to allow for wetness effects in last LP stages.

## 6. WETNESS MEASUREMENTS IN THE MODEL TURBINE WITH THE OPTICAL PROBE

### 6.1 Description of the Optical Probe

The current version of the CERN optical wetness probe is described in published literature by Walters (Reference 2), but a brief description of the instrument is included here for completeness. As indicated in Figure 2(d) the probe is used to illuminate the wet steam which flows transversely through a slot in the probe body with light at a

series of fixed wavelengths. The incident light is scattered in all directions by the minute fog droplets in the flow but some light remains travelling in the original forward direction. The droplet size and concentration can then be determined from the Mie Theory, which is an exact mathematical description of the process of electromagnetic scattering that occurs when a collimated beam of light is incident on small droplets.

To operate the probe a tubular shutter is first extended along the full length of the sampling slot to exclude the wet steam, and the light path cleared with an air purge. The light flux then measured with the photocell is the reference level  $f_o$ . When the air purging is switched off and the shutter quickly withdrawn this incident light flux is attenuated in the forward direction to the level  $f$  by the wet steam flow. This measurement procedure provides an accurate data value at each wavelength, by eliminating errors resulting from drift in the response of the system or from contamination of optical surfaces.

The optical system is optimised for operation with ultra violet (UV) light using quartz components since transmittance data from this end of the spectrum contains most droplet size information for the submicron diameters encountered in steam turbines. 'Monochromatic' light is generated in an external unit by inserting a sequence of interference filters into the output beam of a 300 Watt Xenon Arc lamp. The light is then conducted to the probe by a flexible UV light guide. For diagnostic measurements in full size machines twelve filters are used to cover the wavelength range  $346 \text{ nm} < \lambda < 1050 \text{ nm}$ . Smaller droplets were anticipated in the model turbine however, and the UV end of the spectrum was extended down to  $\lambda = 280 \text{ nm}$  by using triple cavity interference filters in pairs.

6.2 Model Turbine Optical Data and the Calculation of Wetness

The optical transmittance  $f/f_o$  measured by the probe is related to the size and number of droplets in the wet flow by:

$$g(\nu) = \log_e \left( \frac{f_o}{f} \right) = \frac{\pi c_n t}{4} \int_0^\infty Q_{\text{ext}}(\lambda, D) N_r(D) D^2 dD \quad (5)$$

where  $N_r(D)dD$  is the number of droplets occurring per unit volume in the diameter range  $D$  to  $D+dD$ ,  $Q_{\text{ext}}$  is the Mie Extinction Coefficient and  $t$  is the length of the sampling slot. For measurements in the model turbine the maximum slot length of 124 mm was used.

The recovery of a wetness value from equation (5) for a measured  $g(\nu)$  is described in Reference 2. It involves replacing the integral with a numerical quadrature and then applying a standard Matrix Inversion technique. This was found to be unsuccessful however when applied to the model turbine data because the droplet size involved at around  $D = 0.1 \mu\text{m}$  is too small to provide a well

resolved inverse. However an alternative approach, described in Reference 3, proved to be more successful. Essentially as described in Reference 3 the effect of the particle size distribution function  $N_r(D)$  on the measured extinction reduces with droplet size, and for very fine droplets the assumption of a uniform size becomes a reasonable approximation. Under these conditions equation (5) reduces to

$$g = c_n t \frac{\pi D^2}{4} Q_{\text{ext}} \quad (6)$$

The mass of water suspended per unit volume of the wet flow  $c_m$  is then simply

$$c_m = \frac{\pi c_n D^3}{6v_f} = \frac{2gD}{3tv_f Q_{\text{ext}}} \quad (7)$$

giving the wetness as

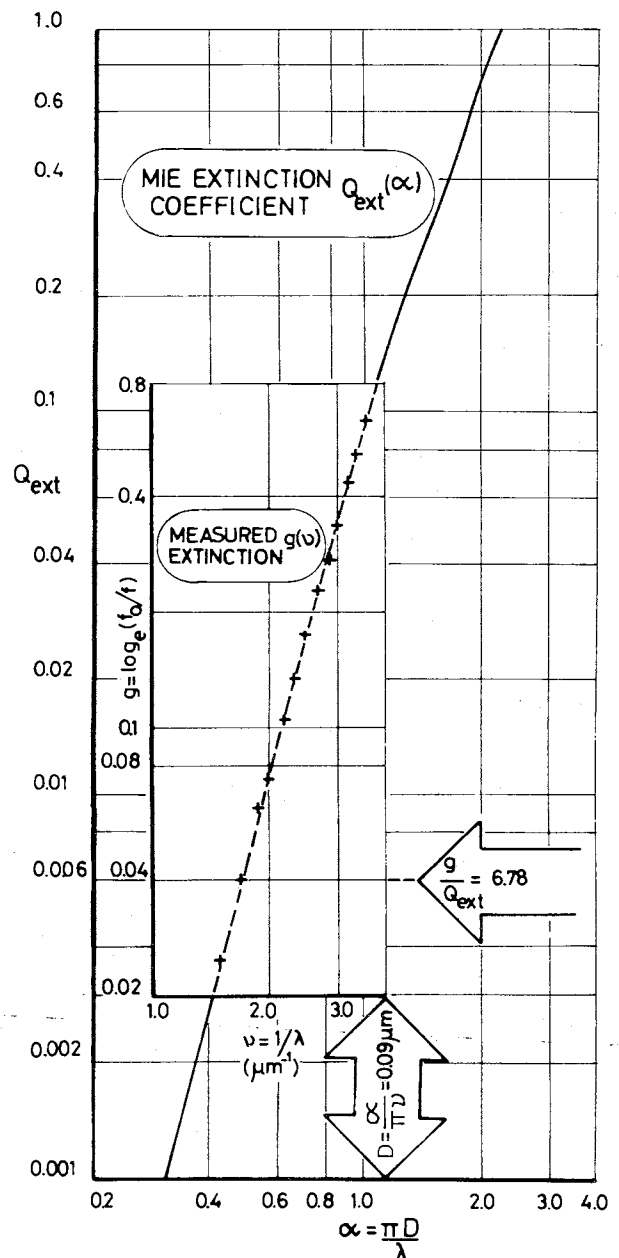


Fig. 6. Model turbine optical data located on the Mie extinction curve.

$$y = \frac{c_m v_g}{1 + c_m v_g} \quad (8)$$

where  $v_f$  and  $v_g$  are the saturation specific volumes of the liquid and vapour phases at the local static pressure.

It is clear from equation (6) that for a given location in a wet steam flow, where the droplet diameter  $D$  although unknown is constant,  $g$  is simply part of  $Q_{ext}$  scaled by the total droplet cross section. The relation between  $g$  and  $Q_{ext}$  may then be established as shown on Figure 6 by locating  $g(v)$  measured in the model turbine on  $Q_{ext}(\pi D/\lambda)$  plotted to the same logarithmic scale. Values of the ratio  $g/Q_{ext}$  and the droplet diameter  $D = \alpha\lambda/\pi$  can be simply read from corresponding points on the logarithmic axes as indicated, providing a wetness value directly from (7) and (8) if the local static pressure is known to provide the vapour specific volume  $v_g$ . As shown by Figure 6 the curve fitting process is rather tenuous since  $Q_{ext}$  tends to become a straight line on logarithmic axes as the Rayleigh scattering regime is approached at  $\alpha \leq 0.3$ . For the model turbine data however there was just sufficient residual curvature to define a droplet size, and in this case a diameter of  $D = 0.09 \mu m$  was obtained, at the mean position in the range  $0.08 < D < 0.1 \mu m$ , that offered a close fit between  $g$  and  $Q_{ext}$ .

For a number of other test points a reversal in the curvature of the measured extinction indicated that up to 7% of the fog droplet wetness consisted of a separate larger group of droplets with  $D \approx 1 \mu m$ . These measurements were processed as bidispersions in a similar manner to that described above, and also as detailed in Reference 3.

The difference in wetness fractions obtained from the optical probe traverses with those derived independently by GEC from dynamometer power and five-hole probe measurements are shown on Figure 7. Apart from two cases where the difference was approximately 0.02 in wetness fraction, agreement was generally within  $\pm 0.01$ , which may be regarded as reasonably close consistency, considering the very small size of the predominant droplet group and the

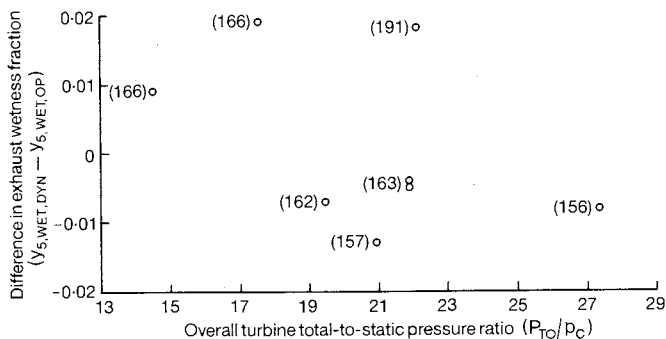


Fig. 7. Difference in exhaust wetness fractions derived from dynamometer power measurements/five-hole probe traverses and the CERL optical probe (figures in parentheses signify turbine inlet stagnation temperature in °C).

complex size distribution effects that were encountered.

7. COARSE WATER MEASUREMENTS AT OUTLET FROM THE TURBINE USING A CATCHPOT PROBE

A series of coarse water radial traverse measurements were taken downstream of the last stage of the model LP turbine in Plane 6 using a GEC Mark III catchpot probe, previously developed by Williams and Lord (Reference 4). The probe incorporates a fence around the rectangular orifice slot to exclude splashing water (see Figure 2c), and a calibration in an air/water tunnel showed that this design of probe has a good cosine response in yaw for pitch angles of  $0^\circ$  and  $+20^\circ$ . Droplet trajectory calculations showed that in the model turbine the probe would accept the majority of coarse water drops and reject virtually all the fog droplets. Therefore corrections have not been made to the coarse water measurements for fog collection.

The coarse water traverses were made under five different turbine flow conditions as shown on Figure 8. In some cases these measurements were accompanied by complementary optical probe and five-hole probe measurements in the same traverse plane.

The experimental technique employed with the catchpot probe was identical to that described in Reference 4, using absorbent samples of tightly rolled filter paper exposed for a sampling period of typically one minute. Exposures were such that the sample was not saturated, and there was always sufficient weight gain to be well above evaporation

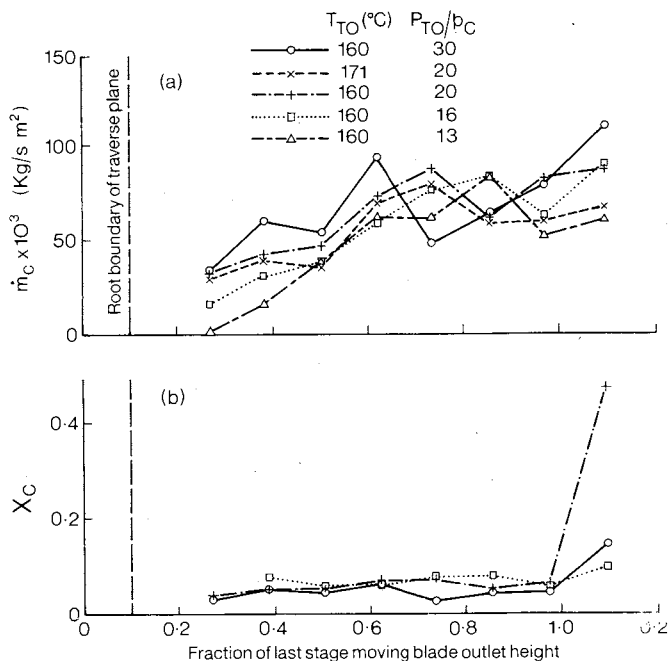


Fig. 8. The radial distribution of coarse water at outlet from the turbine (in traverse plane 6):

- (a) coarse water specific mass flow rate in the axial direction.
- (b) coarse water fraction of total wetness (using the wetness fraction inferred from the dynamometer power measurements).

## FLOW ANALYSIS AND MEASUREMENT

levels during weighing. The sample was weighed immediately after retracting from the turbine. Each traverse consisted of measurements of mass flow collection ( $M_c$ ) at eight radial positions with the probe set at the local mainstream swirl angle  $\theta$ . In analysing the data it was assumed that the coarse water was aligned with the local mainstream absolute flow direction. If  $A_s$  is the orifice slot area then the coarse water specific mass flow rate in the axial direction  $\dot{m}_c$  is given by the following simple expression:

$$\dot{m}_c = \frac{M_c \cos \theta}{t_c A_s} \quad (9)$$

where  $t_c$  = sampling period in seconds.

The coarse water specific mass flow rate in the axial direction has been plotted against fraction of last stage moving blade outlet height for all five test conditions on Figure 8(a). At each condition there is a general rise in the amount of coarse water from root to tip which may be due to a combination of centrifuging effects in the moving blade, and tip leakage effects.

The coarse water fraction of total wetness is given by

$$X_c = \frac{\dot{m}_c}{\dot{m}_c + \dot{m}_F} \quad (10)$$

where  $\dot{m}_F$  = specific mass flow rate of the 'fog' (small water droplets whose diameter is less than approximately  $2 \mu\text{m}$ ).

The five-hole probe was calibrated in wet steam and therefore measures the vapour and fog phases of the total wet steam flow (i.e.

$\dot{m}_v + \dot{m}_F$  is measured by the five-hole probe). A mean wetness fraction can be inferred from the dynamometer power measurements and turbine outlet five-hole probe traverse measurements. Thus we obtain

$$\bar{y}_{\text{DYN}} = \frac{\dot{m}_c + \dot{m}_F}{\dot{m}_c + \dot{m}_v + \dot{m}_F} = \frac{\dot{m}_c + \dot{m}_F}{\dot{m}_c + \dot{m}_{5\text{-HOLE}}} \quad (11)$$

hence the specific mass flow rate of the fog is found from

$$\dot{m}_F = \bar{y}_{\text{DYN}}(\dot{m}_c + \dot{m}_{5\text{-HOLE}}) - \dot{m}_c$$

and

$$X_c = \frac{\dot{m}_c}{\bar{y}_{\text{DYN}}(\dot{m}_c + \dot{m}_{5\text{-HOLE}})} \quad (12)$$

The coarse water fractions of total wetness have been derived using the approach described above, and are plotted against fraction of last stage moving blade outlet height in Figure 8(b). The distribution of coarse water fraction was virtually uniform over the central part of the annulus, but increased towards the tip. The mean coarse water

fractions of total wetness for the various test points, found by integrating over the annulus height, were as follows:

$T_{To} (^{\circ}\text{C})$	$P_{To}/p_c$	$X_c$
160	30	0.056
160	20	0.072
160	16	0.075

## 8. ONE-DIMENSIONAL PREDICTIONS USING GYARMATHY'S METHOD

One-dimensional non-equilibrium wet steam calculations were performed along the root, mean and tip streamlines of the model turbine using Gyarmathy's method. Details regarding the calculation procedure are fully described in Reference 5 and need not be repeated here. The predictions were performed near the turbine design point ( $P_{To}/p_c = 20$ ,  $P_{To} = 150 \text{ KN/m}^2$ ,  $T_{To} = 160^{\circ}\text{C}$ ), using homogeneous ideal dry conditions taken from a corresponding equilibrium streamline curvature throughflow calculation.

The Gyarmathy calculation commences by calculating the build up of supercooling to the point of nucleation, the resultant wetness and fog droplet diameter. The next part of the calculation follows the growth of the fog and any subsequent build up of supercooling. Next the quantity of water deposited is predicted and the coarse water flow rates and their droplet diameters. Lastly the wetness losses are predicted for each stage and combined to give a value for the wetness loss factor for the whole wet region. Figure 9 shows the predicted local wetness fractions relative to unit mass flow of dry steam at inlet to the turbine, fog and coarse water droplet diameters, and deposited plus centrifuged water. Comparison of the turbine experimental measurements with the theory yielded the following conclusions:

(a) The predicted fog droplet diameters of  $0.066 \mu\text{m}$ ,  $0.131 \mu\text{m}$  and  $0.139 \mu\text{m}$  at root, mean and tip respectively at outlet from the turbine were in reasonable agreement with the CERL optical probe data for the first droplet group ( $D = 0.1 \mu\text{m}$ ). However the measurements at this turbine operating condition showed that a small proportion of the fog consisted of larger drops with diameter approximately equal to  $1 \mu\text{m}$ , but this second group of droplets was not predicted.

(b) The predicted coarse water fractions of total wetness at outlet from the turbine ( $0.026$ ,  $0.013$  and  $0.016$  at root, mean and tip respectively) were considerably lower than the measured value of approximately  $0.07$ . Possible reasons for this discrepancy are:

- the amount of coarse water formed by the second larger group of droplets was not calculated;
- Gyarmathy's method does not calculate

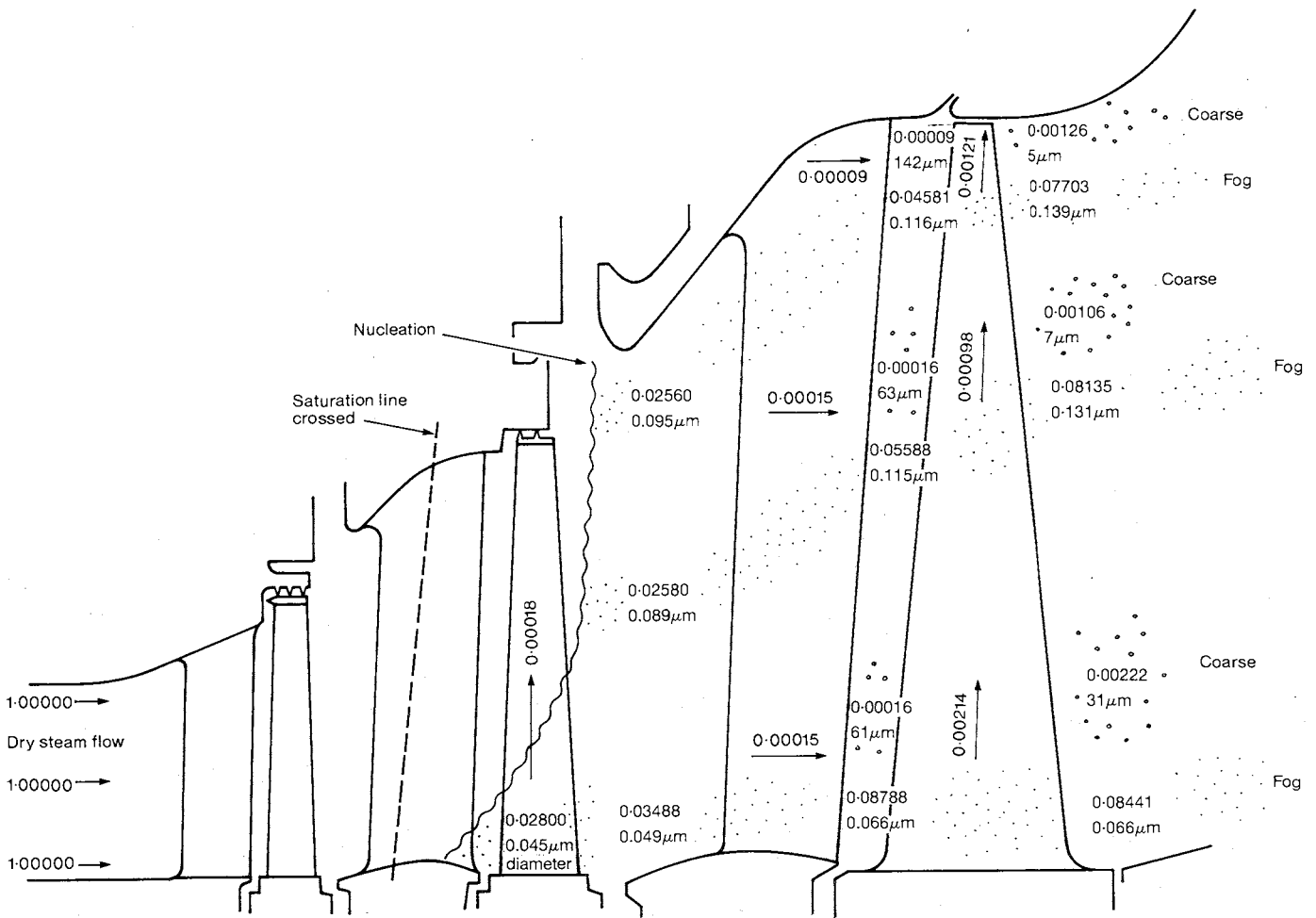


Fig. 9. The predicted distribution of moisture in the model three-stage LP turbine, found from Gyarmathy's one-dimensional method.

the amount of coarse water formed by turbulent diffusion of the fog through the boundary layers;

- no allowance was made for 'scavenging' effects occurring between the coarse water shed from the blades, and the fog.

CONCLUSIONS

For conventional condensing turbine exhaust wetness fractions of around 0.10, it was found that the measured wetness loss factor was in reasonable agreement with the Baumann value.

Traverses in the turbine exhaust with the CERL optical probe showed that there was just sufficient residual curvature in the extinction data to define the very small droplet diameter of approximately 0.1 μm. For a number of other test points the data indicated that up to 7% of the fog by mass consisted of a second larger group of droplets, with diameter approximately equal to 1 μm. Comparison of exhaust wetness fractions derived from dynamometer power and five-hole probe measurements, with those found completely independently from the optical probe traverses, generally showed agreement to be within ±0.01. This is thought to be a reasonable level of consistency, considering the very small size of the main droplet group, and the complex size distribution effects that were encountered in the model turbine.

The measured coarse water fraction of total wetness at outlet from the turbine was approximately 0.07. This was considerably higher than the value predicted from Gyarmathy's method.

REFERENCES

1. BAUMANN, K. "Recent Developments in Steam Turbine Practice". Journal of the Institute of Electrical Engineers, Vol.48, p.830, 1912.
2. WALTERS, P.T. "Wetness and Efficiency Measurements in LP Turbines With an Optical Probe as an Aid to Improving Performance". Transactions of the ASME Journal of Engineering for Gas Turbines and Power, January 1987, Vol.109, 185.
3. WALTERS, P.T. "Optical Measurement of Water Droplets in Wet Steam Flows". I.Mech.E. Conference on Heat and Fluid Flow in Steam and Gas Turbine Plant, University of Warwick, Paper C32/73, pp.32-40, April 1973.
4. WILLIAMS, G.J. and LORD, M.J. "Measurement of Coarse Water Distribution in the LP Cylinders of Operating Steam Turbines". Proc. Instn. Mech. Engrs., Vol.190 4/76, pp.59-69, 1976.
5. GYARMATHY, G. "Bases for a Theory for Wet Steam Turbines". Bulletin No. 6 of the Institute of Thermal Turbo-machines in the Federal University (also CEGB Translation T.781), Zurich 1963.



## 21. A reconsideration of wetness loss in LP steam turbines

S. A. SKILLINGS, BA, M. J. MOORE, MSc, PhD, MIMechE, P. T. WALTERS, BSc, and  
R. JACKSON, BSc, PhD, Central Electricity Research Laboratories

Modern design methods for wet steam turbines invariably assume an unavoidable wetness loss component which is included empirically. A programme of work undertaken by the Research Division of the CEBG has indicated that this premiss is somewhat misleading and considerably improved turbine efficiency is a realistic expectation. Low pressure turbine measurements have identified areas in which performance is poor and theoretical analyses and laboratory experiments have been able to provide possible explanations for the observed behaviour. It is suggested that transport and thermodynamic losses resulting directly from the presence of water droplets in the flow are small; however, adverse aerodynamic consequences of the condensation process are more serious and could potentially be dramatically reduced.

### 1. INTRODUCTION

Since the early days of steam turbine development it has been recognised that the presence of water drops in the steam causes a reduction in turbine efficiency. An empirical rule to quantify this efficiency penalty was proposed by Baumann in 1921 (1) - each 1% mean stage wetness fraction produces a 1% additional loss. Since that time turbine unit output has increased from the order of a few hundred KWs to over a thousand MW. However, despite dramatic advances in aerodynamic design methods, the simplistic Baumann rule has yet to be superseded by a physically based model of the loss processes in wet steam. As a consequence, there exists a tendency to consider this loss component as unavoidable,

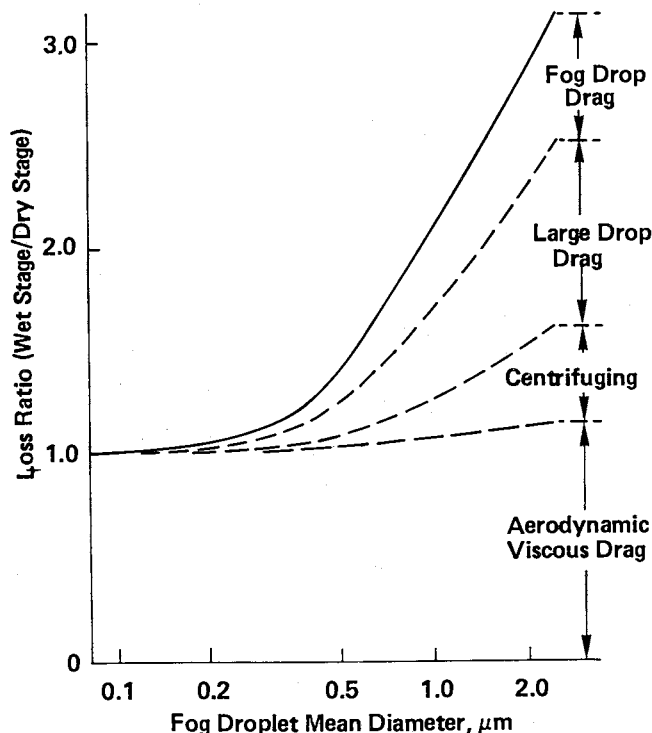


FIG. 1 CALACULATED LP TURBINE FINAL STAGE WETNESS LOSS COMPONENTS (FOR AN ASSUMED 7% STAGE MEAN WETNESS FRACTION) (reproduced from ref. 3)

even though it represents a major operating cost. For example, on the basis of the Baumann rule, the continuous power output lost by the CEBG due to adverse wet steam effects is approximately 500-700MW, equivalent to the fuel costs for a coal fired plant of £50 million per annum.

The lack of progress in understanding and reducing wet steam losses arises principally from the complexity of the processes involved and the difficulty of making measurements in such flows. A programme of research has been underway for several years at the Central Electricity Research Laboratories of the CEBG and this paper reviews progress and describes some recent findings which shed new light on the applicability of the Baumann rule.

### 2. WETNESS LOSS MECHANISMS

Whilst the Baumann rule is still widely used in turbine design methods, various efforts have been made to develop a theoretical analysis of the condensation and flow of wet steam. One of the first attempts to compile a theory to describe behaviour in a wet steam turbine was made by Gyarmathy (2). This work was extended by Moore (3) and similar models are discussed in several Russian texts (e.g. 4).

Such analyses predict that wetness losses increase with both wetness fraction and with the size of the fog droplets produced in the condensing steam flow. Moore calculated the approximate magnitude of the wetness loss across a typical LP turbine final stage, at blade mid-height, as a function of fog droplet diameter, Fig. 1. The major components of loss in the stage are shown as a ratio of the conventional (dry) aerodynamic loss of the blading (\*). Results indicate wet steam losses which are of similar magnitude to aerodynamic losses at fog droplet diameters of  $1\mu\text{m}$ . Since aerodynamic losses for dry steam would be equivalent to a 6-7% reduction in stage efficiency (at mid-height), the wetness loss is predicted to be of the same order as the mean wetness fraction ( $\approx 7\%$ ), thus endorsing the Baumann rule.

\* - The calculations were performed for a final stage in which it was assumed that no further droplet nucleation was occurring and that losses due to subcooling are negligible. In the earlier stage, where condensation first occurs, a thermodynamic loss from subcooling was considered. However, evidence presented later in this paper (Appendix and Fig. 2) suggests that secondary nucleations are not uncommon.

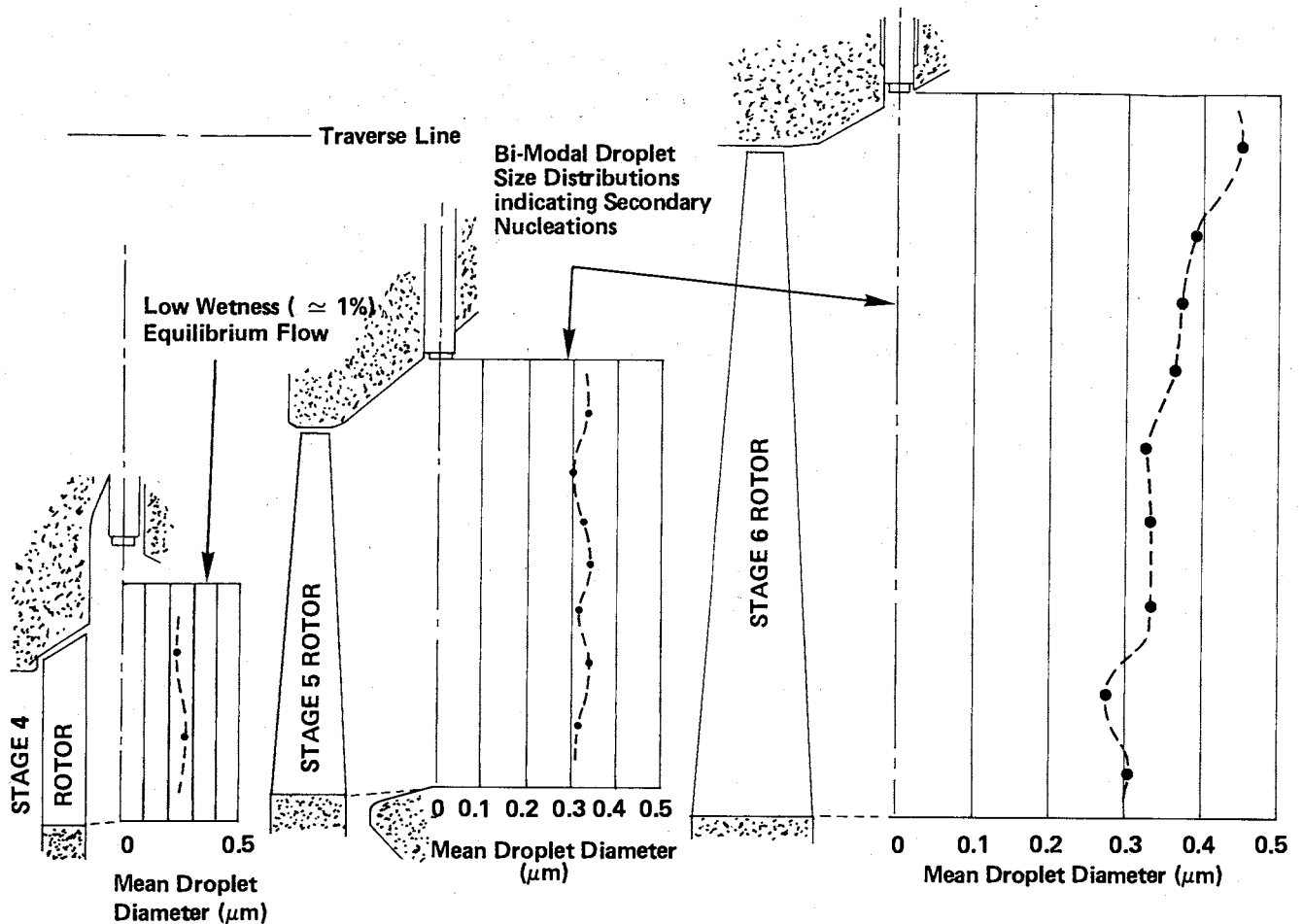


FIG. 2 TYPICAL MEASURED TURBINE DROPLET SIZE DISTRIBUTIONS

However, when this calculation was first performed, reliable measurements of fog droplet sizes in the final stages of steam turbines were not available. Pioneering work by Walters (5,6) has produced an optical probe capable of making radial traverses in operating turbines. The probe can be used to measure wetness fraction and mean droplet size, a typical result for the latter being shown in Fig. 2. It can be seen that the fog droplets are small, in the example shown they average around  $0.3\mu\text{m}$  in Sauter mean diameter. At such droplet sizes the predictions of Fig. 1 show a very small wetness loss which is much smaller than the Baumann prediction. It may either be concluded that the wetness loss models are unrealistic, or that the wetness loss in such a stage is actually quite small.

The optical probe and aerodynamic probes have now been used to provide data from many turbines; the former giving wetness fractions, the latter providing corresponding steam pressures and velocities. Integrating the results provides mean inter-stage enthalpies and consequently separate stage efficiencies can be determined (values for overall cylinder efficiencies calculated using this technique have usually been corroborated by independent heat rate measurements when available). The condition lines for several typical turbines are shown in Fig. 3 and a considerable range of measured stage efficiencies is evident. Conventionally it is anticipated that increasing wetness towards the exhaust will result in a progressive reduction in stage efficiency. This is not the pattern observed; in many cases the final stage is more efficient than earlier wet stages. It is therefore concluded that the so-called 'wetness loss' is not necessarily a continuously increasing function of wetness fraction and the conventional aerodynamic (viscous) losses may vary substantially from stage to stage. An examination of Fig. 3 reveals that one stage in the region of the steam saturation line - the 'nucleating' stage - tends to have the lowest efficiency.

It is apparent that additional aerodynamic losses may be induced by the presence of moisture and consequently cannot be measured separately from so-called wetness losses. It is therefore the aim of the research programme to develop an improved theoretical model to predict the wetness loss component and to investigate the interaction between moisture and flow aerodynamics. The initial objective was to develop a one-dimensional theory which could be validated using laboratory experiments.

### 3. CONDENSATION IN STRAIGHT NOZZLE FLOWS

The straight convergent-divergent nozzle has proved a convenient laboratory experiment for many researchers investigating spontaneous condensation (e.g. 7,8,9) since the earliest experiments recorded by Stodola (10) in 1922. The principal measurement in these experiments has been the steady pressure distribution along the nozzle but the facility to measure fog droplet size by light extinction (11) enabled Moore *et al.* (12) to provide a more detailed validation of condensation theory. Building on early work by Oswatitsch (13), many theories to predict one-dimensional nucleating steam flows have emerged (e.g. 14,15) and a code developed by Skillings and Jackson (16) now gives good agreement with both pressure distribution and Sauter mean droplet diameter, as shown in Fig. 4(a).

Such one-dimensional methods have been applied by various workers (e.g. 3,17) to provide an approximate representation of wet steam flow development along streamtubes in a multi-stage turbine. The calculation code developed by Skillings and Jackson (16) has also been used in such an

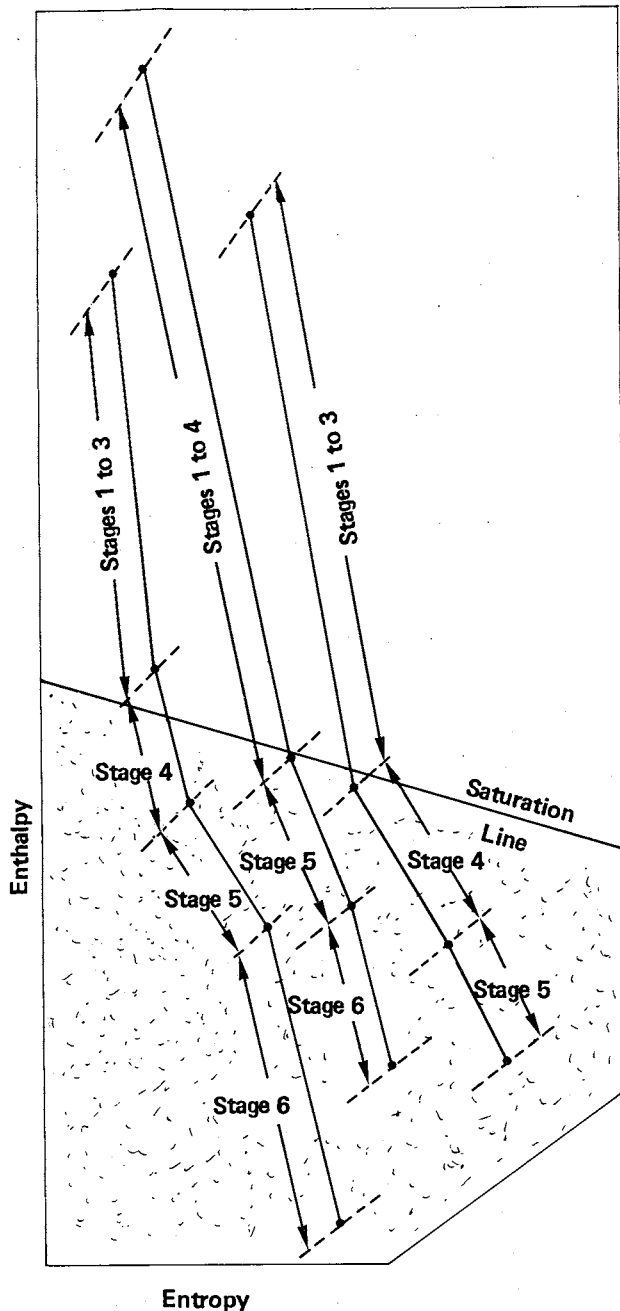


**FIG. 3 TYPICAL TURBINE CONDITION LINES SHOWING VARIATION IN MEASURED STAGE EFFICIENCIES**

exercise where the equivalent one-dimensional geometries were obtained by combining measured traverse data with the blade profiles and the predictions of an axisymmetric through-flow program (a detailed description is beyond the scope of this paper). It was found that spontaneous nucleation invariably occurred near the position where the flow became sonic and consequently in the throats of either moving or fixed blades. Fig. 5 illustrates schematically the locations in an LP turbine at which water droplets are expected to appear (the concept of a 'pre-nucleation' has been introduced and this is explained in the Appendix).

The heat release following spontaneous condensation in a one-dimensional nozzle flow is known to give rise to several flow regimes as discussed in detail by Barschdorff (18):

1. Steady, shock free expansion (subcritical)
2. Steady expansion with an embedded aerodynamic shock wave (steady supercritical)

3. Unsteady expansion with an embedded aerodynamic shock wave (unsteady supercritical)

The supercritical regimes are particularly relevant for cases in which nucleation occurs near the nozzle throat and therefore, in order to calculate flow within the transonic blading, a computational technique capable of predicting unsteadiness is required. The code developed by Skillings and Jackson possesses this property and has been validated for both supercritical regimes using nozzle experiments performed in the CERL steam tunnel (19). A typical unsteady result is shown in Fig. 4(b) and shows excellent agreement with the measured pressure fluctuation amplitude ( $\approx 6\%$  of the inlet total pressure) and with the mean droplet size. The oscillatory regime produces fog droplet diameters which are considerably larger ( $\approx \times 2$ ) than would be predicted by steady flow solvers. Of particular significance is the result that measured turbine droplet sizes could only be predicted with reasonable accuracy using the streamtube analysis mentioned above when the unsteady supercritical regime prevailed in the transonic passages.

The significance of the one-dimensional analysis is therefore that it enables the flow regimes arising in nucleating flows to be described and, in particular, has indicated that it is necessary to account for unsteadiness in the calculation of such flows. As a prelude to explaining 'wetness loss' in turbines however and before any firm conclusions can be drawn, evidence from a more representative two-dimensional flow field, generated in blade cascades, is an important requirement.

#### 4. CONDENSATION IN A CASCADE OF TURBINE BLADES

In contrast to studies of (one-dimensional) nozzle flow, publications concerning condensation in a turbine blade passage are relatively scarce (20,21,22 being some of the few examples). These studies provide little detailed information on the phenomena which arise as a result of the condensation process and, in particular, do not indicate whether the oscillatory regime identified in straight nozzles can occur in this two-dimensional flow. A few two-dimensional condensing flow predictors have also been reported (e.g. 23,24,25) but these are in an early stage of development and validation has been prevented by the dearth of detailed experimental data. Consequently, neither experimental nor theoretical studies have yet been able to confirm whether distinct regimes occur when a nucleating steam flow is deflected by turbine blades.

In order to provide more comprehensive information a cascade of turbine blades was installed in the CERL steam tunnel (26). In addition to the conventional instrumentation - Schlieren optics, blade surface pressure tapings, downstream pressure probe traverse - fast response pressure transducers were mounted in the test section to record unsteady pressure fluctuations and the steam tunnel optical system (described in 19) was included to measure fog droplet size. Two sample shock wave structures, which have been reproduced from Schlieren photographs, are shown in Fig. 6. Of initial interest was the observation that the flow patterns were relatively insensitive towards the level of superheat at inlet to the cascade. Over the range of inlet conditions investigated ( $0^\circ\text{C} \leq \Delta T \leq 15^\circ\text{C}$ ) the condensation shock position, shown in Fig. 6(a), remained virtually unaltered. Compared with conventional single phase flow, Fig. 6(a) shows an additional aerodynamic shock embedded in the condensation zone, corresponding to the steady supercritical shock observed in nozzles. However, as outlet Mach number decreases, this shock merges with the conventional trailing edge shock pattern and it becomes difficult to form an analogy with the one-dimensional case. On further reduction in outlet Mach number to high subsonic values (when velocities at the blade throat will still be sonic) an oscillatory regime was

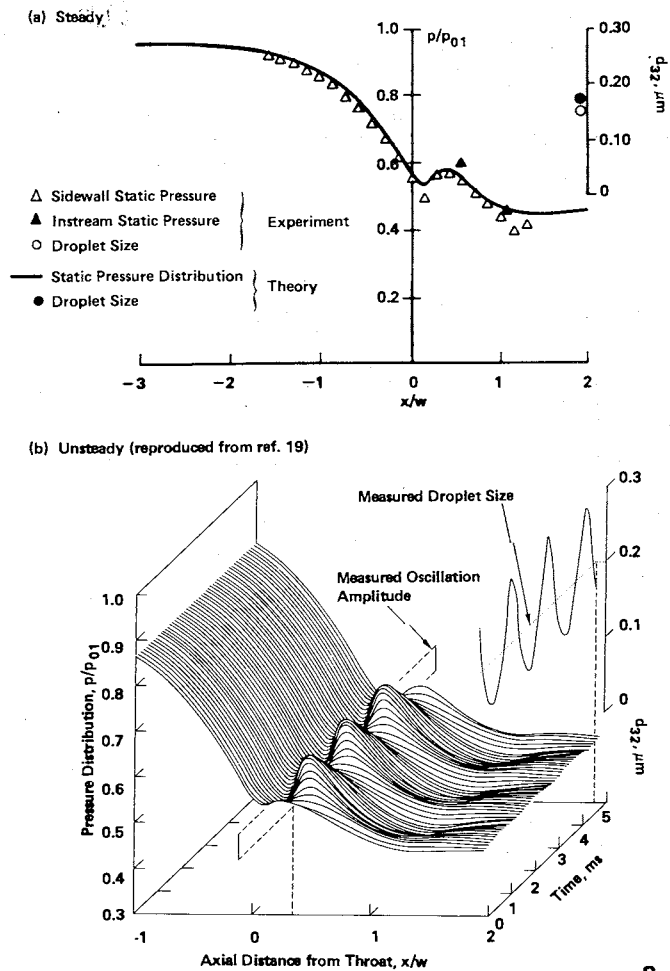


FIG. 4 COMPARISON BETWEEN EXPERIMENT AND THEORY FOR SUPERCRITICAL NOZZLE TESTS

encountered, Fig. 6(b). Strong periodic pressure fluctuations were measured with frequencies in the range  $1.8\text{KHz} < \nu < 3.2\text{KHz}$  and with amplitudes  $\approx 6\%$  of inlet total pressure.

It is possible that such instabilities are exacerbated by interactions with the turbulent shear boundary (no tailboards having been fitted to the cascade), however Deich *et al.* (27) describe a similar effect in a cascade flow which they attribute to shock wave/boundary layer interaction. Of particular interest is the fact that the optical droplet sizing measurements performed in the CERL steam tunnel experiment indicated that the shock system was interacting strongly with the nucleation process. The fog droplet sizes formed when these fluctuations were present was more than double that recorded at steady but otherwise similar conditions and this suggests that the condensation process is being modified by periodic quenching of nucleation. It is a distinct possibility that such flows will also arise within steam turbine blade passages, not only having an important influence on the immediate blade row performance but also on subsequent blade rows in the turbine.

### 5. IMPLICATIONS FOR TURBINE PERFORMANCE

Increased understanding of the condensation processes now suggests that the basic approach implied by the Baumann correction - that wetness introduces an unavoidable separate loss - is misleading. Attempts to calculate the total transport losses (droplet drag, centrifuging of coarse water, etc.) have invariably predicted very small reductions in efficiency. This

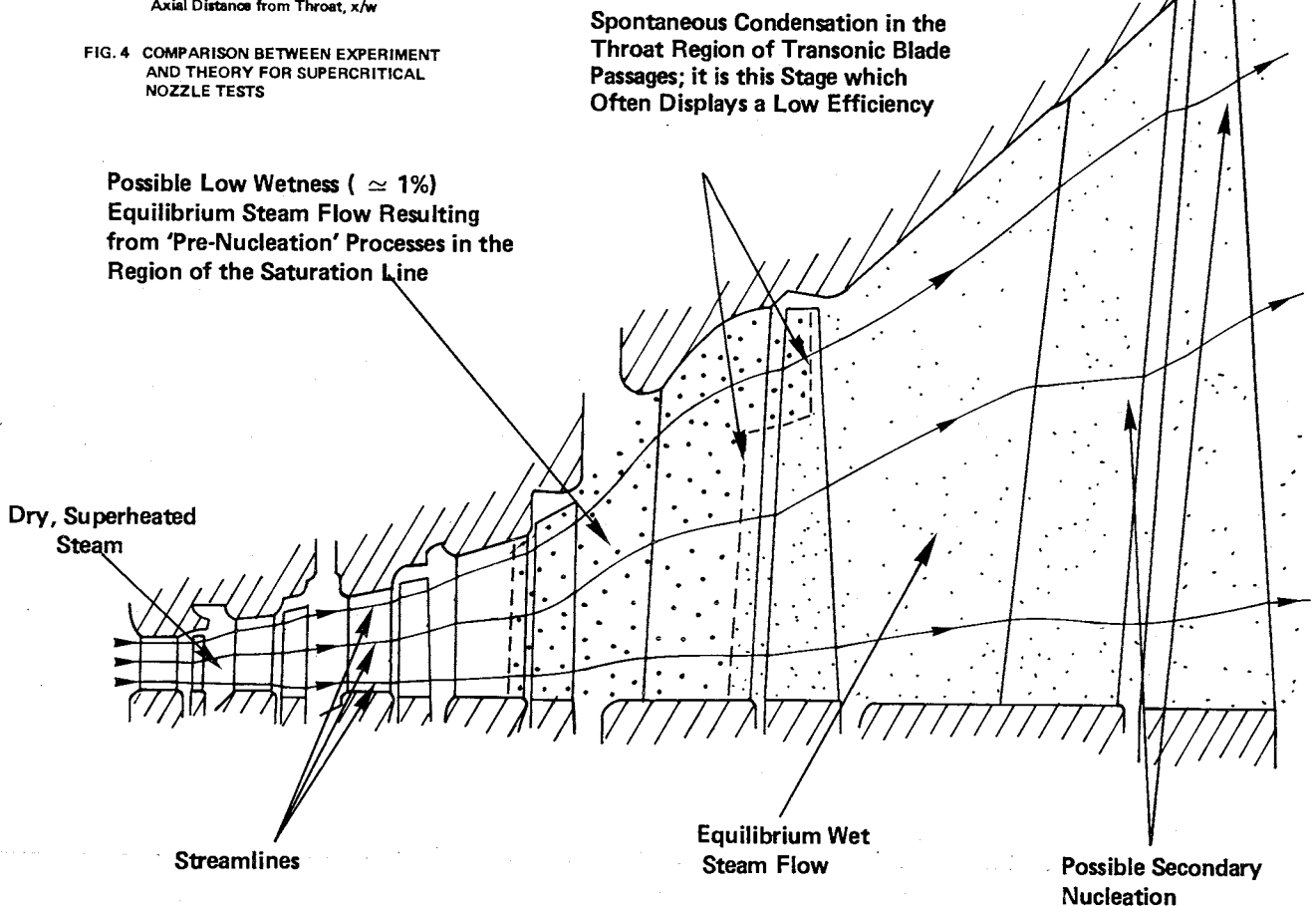
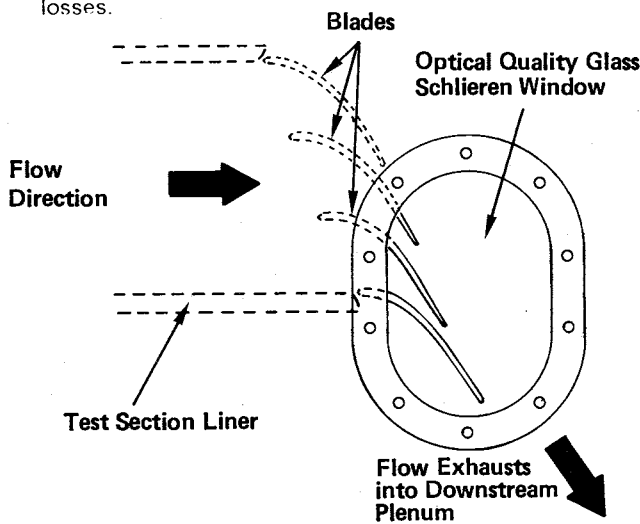


FIG. 5 LOCATION OF CONDENSATION PROCESSES IN A LOW PRESSURE STEAM TURBINE

may be partly attributed to the extremely small fog drop sizes predicted using steady flow condensation theories, although the inclusion of typical turbine fog drop sizes in the transport loss calculations still fails to account for more than a small fraction of the Baumann loss. Similarly, calculations of the thermodynamic loss which arises from irreversible transfer processes when the steam surrounding the droplets is subcooled, suggest a rather modest contribution to the loss, even for cases involving an embedded supercritical shock.

In the past, it has been common practice to attribute any reduction in the efficiency of wet steam stages to an unavoidable wetness loss mechanism. It is, however, likely that high losses occurring over wet stages are the result of adverse aerodynamics induced by the condensation process. For example, if the turbine is designed on the assumption of equilibrium wet steam flow (plus Baumann correction) the actual flow field may be operating at an off-design condition because:

1. Blading outlet flow angles and velocities differ from design, leading to high flow incidence angles onto the following row with a consequent increase in viscous losses.



(a) Distinct 'Three-Shock-System' Observed at High Mean Outlet Mach Numbers ( $M_2 \approx 1.4$ )

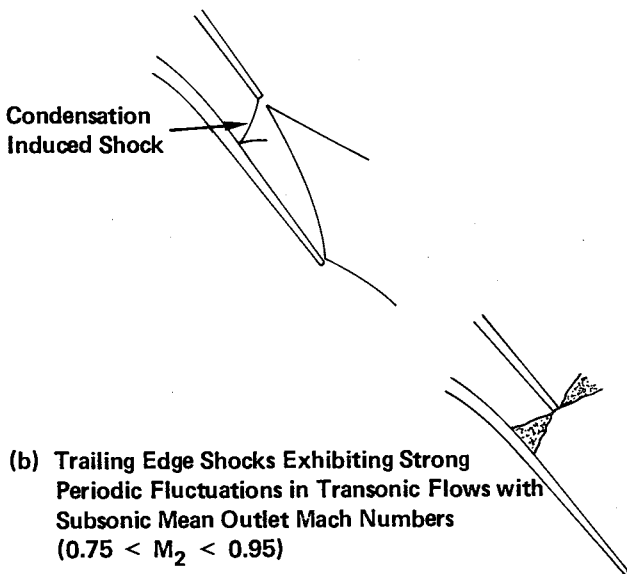


**FIG. 6 OBSERVATION OF TRAILING EDGE SHOCK STRUCTURE IN A CONDENSING STEAM CASCADE EXPERIMENT**

2. Erroneous prediction of the blade throat to outlet pressure ratio in transonic nucleating stage passages, may result in an oscillating flow of the type described in Section 4. Incidence angles which are both high and fluctuating would increase viscous losses in the downstream blade row.
3. The appearance of an additional shock wave in the throat region of the nucleating blade passage might, through boundary layer interaction and subsequent flow separation, diminish the aerodynamic efficiency of the blade.

Further evidence of possible interaction between condensation and flow aerodynamics was obtained from a turbine condition line, measured by the aerodynamic and optical wetness probes, at differing cylinder inlet conditions, Fig. 7 (5). At the design condition, the nucleating (5th) stage showed a noticeably lower efficiency than other stages. Decreasing the inlet superheat moved nucleation to the 4th stage and the efficiency of stage 5 increased markedly. Unfortunately, independent heat rate tests were not available to confirm these efficiencies although the results reveal a gross effect which is large enough to be immune from small measurement error. The location of the condensation process is, therefore, obviously important. Spontaneous condensation is expected to occur near the first sonic position in a machine, which is most likely to lie within a stator blade row. Nucleation in the fixed blading is potentially more harmful since the performance of the stage is sensitive to the flow direction onto the rotor. Nucleation in the rotor is probably less important since the following fixed blades can accept off-design inlet flows with less adverse loss.

## 6. CONCLUSIONS

The principal conclusions from a programme of laboratory and turbine measurements and complimentary theoretical analyses undertaken at CERL is that the concept of a superimposed additional loss to account for wetness effects (such as the Baumann correction) may be misleading. The actual parasitic losses due to the transport of the liquid phase and the internal thermodynamic losses associated with subcooling are thought to be relatively small. Most of the 'extra' loss generated over the wet stages in LP turbines is likely to be aerodynamic in origin, resulting from the off-design conditions introduced by the condensation process in a turbine designed for equilibrium flow.

Further research is required to consolidate these conclusions, but this encouraging result suggests that the adoption of appropriate design procedures should enable the manufacturers to produce more efficient wet steam turbines.

## 7. ACKNOWLEDGEMENTS

The work was carried out at the Central Electricity Research Laboratories of the Research Division and the paper is published with permission of the Central Electricity Generating Board.

## 8. REFERENCES

1. Baumann, K., Some Recent Developments in Large Steam Turbine Practice. J. Instn. Elec. Engrs., 1921, 59, 565
2. Gyarmathy, G., Bases for a Theory for Wet Steam Turbines, Bull. 6. Inst. for Thermal Turbomachines, Federal Technical University, Zurich, 1962
3. Moore, M.J., Chapter 2, Two-Phase Steam Flow in Turbines and Separators, Eds. Moore M.J. and Sieverding C.H., Hemisphere Pub. Corp., 1976

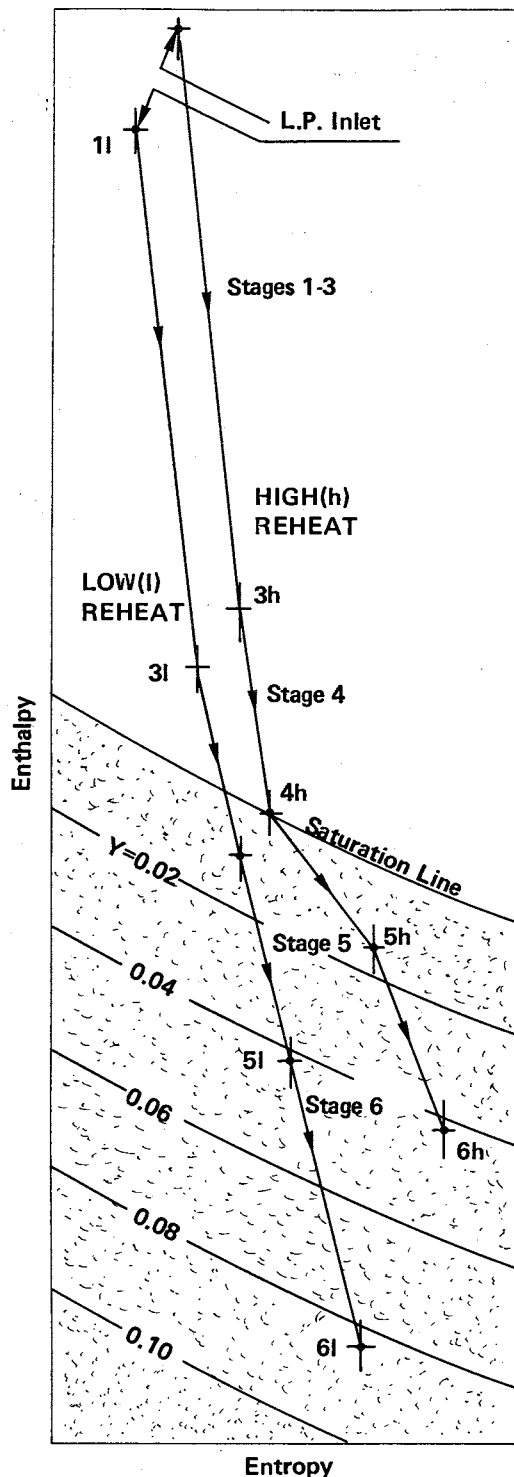


**FIG. 7 CONDITION LINES FOR AN L.P. TURBINE AT HIGH AND LOW REHEAT TEMPERATURES (reproduced from ref. 6)**

4. Deich, M.E. and Filippov, G.A., Two Phase Flow in Basic Heat and Power Machinery, MEI, 1987
5. Walters, P.T. and Skingley, P.C., An Optical Instrument for Measuring The Wetness Fraction and Droplet Size of Wet Steam Flows in LP Turbines, Inst. Mech. Eng., Conf. on Steam Turbines for the 1980's, Paper C141/79, London, 1979
6. Walters, P.T., Wetness and Efficiency Measurements in LP Turbines with an Optical Probe as an Aid to Improving Performance, ASME, 85-JPGC-GT-9, 1985

7. Binnie, A.M. and Woods, M.W., The pressure Distribution in a Convergent- Divergent Steam Nozzle, Proc. Instn. Mech. Engrs., 1938, Vol. 138, 229
8. Binnie, A.M. and Green, J.R., An Electrical Detector of Condensation in High Velocity Steam, Proc. Roy. Soc. A, 1943, Vol. 181, 134
9. Gyarmathy, G. and Meyer, H., Spontaneous Condensation Phenomena, V.D.I. Forschungsheft 508, 1965, (C.E. Trans. 4160)
10. Stodola, A., Dampf-und Gasturbinen, 5th edition, Springer, Berlin, 1922
11. Walters, P.T., Optical Measurement of Water Droplets in Wet Steam Flows, I. Mech. Eng. Conf., Wet Steam 4, Paper C32/73, Warwick, 1973
12. Moore, M.J., Walters, P.T., Crane, R.I. and Davidson, B.J., Predicting the Fog Drop Size in Wet-Steam Turbines, I. Mech. Eng. Conf., Wet Steam 4, Paper C37/73, Warwick, 1973
13. Oswatitsch, K., Kondensationserscheinungen in Ueberschallduesen, Z. Angew. Math. Mech., 1942, Vol. 22, No. 1, 1-14
14. Campbell, B.A. and Bakhtar, F., Condensation Phenomena in High Speed Flow of Steam, Proc. Instn. Mech. Engrs., 1970-71, Vol. 185, 25/71, 395-405
15. Young, J.B., The Spontaneous Condensation of Steam in Supersonic Nozzles, PCH, 1982, Vol. 3, No. 1, 57-82
16. Skillings, S.A. and Jackson, R., A Robust Time-Marching Solver for One-Dimensional Nucleating Steam Flows, 1987, Int. J. of Heat and Fluid Flow, Vol. 8, No. 2, 139-144
17. Bakhtar, F., Young, J.B. and Ghoniem, Z., A Study of Nucleating and Wet Steam Flows in Turbines, Heat and Fluid Flow, 1976, Vol 6, No 2, 119-133
18. Barschdorff, D., Droplet Formation, Influence of Shock Waves and Instationary Flow Patterns by Condensation Phenomena at Supersonic Speeds, Brd. int. conf. of Rain Erosion and Associated Phenomena, Farnborough, 1970
19. Skillings, S.A., Walters, P.T. and Moore, M.J., A Study of Supercritical Heat Addition as a Potential Loss Mechanism in Condensing Steam Turbines, Instn. of Mech. Eng., Int. Conf. on Turbomachinery, Paper C259/87, Cambridge, 1987
20. Ikeda, T. and Suzuki, A., Some Findings on the Flow Behaviour of Last-Stage Turbine Buckets by Linear Cascade Tests in Steam, I. Mech. Eng. Conf., Wet Steam 4, Paper C26/73, Warwick, 1973
21. Jackson, R. and Walters, P.T., Design Considerations for the CERL Wet Steam Tip Section Cascade and First Test Results, Proc. of 5th Symp. 'Measuring Techniques for Transonic and Supersonic Flow in Cascades and Turbomachines', Leatherhead, 1979
22. Trucco Martinengo, A., Benvenuto, G. and Campor'a, U., Observation of Condensation Shock in a High Deviation Blade Cascade by Means of the Schlieren Technique, Proc. of 8th Symp. 'Measuring Techniques for Transonic and Supersonic Flow in Cascades and Turbomachines', Genoa, Italy, 1985
23. Bakhtar, F. and Mohammadi Tochai, M.T., An Investigation of Two- Dimensional Flows of Nucleating and Wet Steam by the Time-Marching Method, Int. J. Heat and Fluid Flow, 1980, Vol. 2, No. 1, 5-19
24. Moheban, M. and Young, J.B., A Time-Marching Method for the Calculation of Blade-to-Blade non-equilibrium Wet-Steam Flows in Turbine Cascades, Inst. Mech. Eng., Conference Publications, Computational Methods for Turbomachinery, Paper C76/84, Birmingham, 1984

25. Snoeck, J., Chapter 4, *Aerothermodynamics of LP Turbines and Condensers*, Eds. Moore M.J. and Sieverding C.H., Hemisphere Pub. Corp., 1987
26. Skillings, S.A., *An Analysis of the Condensation Phenomena Occurring in Wet Steam Turbines*, PhD Thesis, CNAA, CERL, 1987
27. Deich, M.E., Laukhin, Yu.A., Saltanov, G.A., *Investigation of Unsteady Wave Structure in Turbine Nozzle Blade Cascades*, Thermal Eng., 1975, Vol. 22, No. 8, 30-32

## APPENDIX - The Mechanism of Condensation in Turbines

The condensation mechanism investigated in fast nozzle expansions is that initiated by homogeneous nucleation of water droplets in which embryo drops are generated spontaneously from within the gas phase under non-equilibrium conditions. Any impurity nucleation centres present will not prevent significant departures from equilibrium due to the rate of the nozzle expansion. However, the expansion encountered in turbines is very different from that produced in straight nozzles. Fast expansions within blade rows are followed by slow expansions in inter-row gaps, the centres of blade wake vortex filaments are created by very fast expansions whilst the expansion rate encountered in the boundary layers attached to the blades is comparatively slow, and superimposed upon these variations is the high degree of unsteadiness which prevails within a machine. Given the non-uniform nature of the expansion in a turbine it has often been suggested that spontaneous condensation in the flow core does not occur and alternative mechanisms govern the appearance of water droplets.

1. *Heterogeneous nucleation onto impurity centres*: This will become the dominant competitive rate process in regions where expansion rates are low.

2. *Localised spontaneous condensation*: This may result from over-expansion within vortex filaments or on the blade suction surface where the velocity distribution exhibits a pronounced peak. Alternatively, significant localised variations in the thermodynamic state of the steam are certain to arise and this may produce pockets of gas which prematurely attain the conditions required to initiate spontaneous condensation. The droplets formed by these processes would be able to 'seed' the entire flow field and prevent the development of further subcooling.

It is sometimes proposed that the averaged steam conditions within a turbine will follow an equilibrium path between dry and wet steam. However, this is probably a false conclusion as is demonstrated by examining the data from optical turbine traverses, an example set of results being plotted in Fig. 2. Droplets are first detected at very low wetness equilibrium conditions ( $\approx 1\%$ ). It is extremely difficult to envisage spontaneous condensation in the flow core producing this situation and it must be attributed to one or both of the alternative mechanisms mentioned above. We shall denominate this process the 'pre-nucleation'. In passing through the next stage the mean droplet size does not increase significantly and a bimodal size distribution is detected. It is over this stage that a particularly high loss is often observed and it is likely that the fast expansion within the blade passage has produced sufficient levels of subcooling for spontaneous condensation in the flow core, despite the conditions being wet at inlet. It is this stage which is considered to be the 'nucleating' stage and the one to which the work described in this paper is most relevant. It is worth noting that the measured mean droplet sizes also indicate the possibility of a secondary nucleation within the final stage.

It appears that several mechanisms will be involved in the turbine condensation process. However, it is probable that spontaneous condensation in the flow core will occur and turbine measurements suggest that a high loss is potentially associated with this phenomenon.



## 22. A calculation and measurement of the flow field in a steam condenser external to the tube nest

Dr M. ŠŤASTNÝ, ŠKODA Concern Enterprises, Plzeň, and M. FEISTAUER, Charles University, Prague

The suggested physical and mathematical model is used to solve the flow of steam normal to the cooling tubes of condenser cross-sections in the region external to the nests. Numerical calculations are carried out by means of a multipurpose system of programmes for the finite element method and of the programme for the boundary layer calculation. The results of the calculations are compared with measurements on the condenser of a 500MW steam turbine. The calculations of the flow field in a double pass condenser for the 1000 MW saturated steam turbine are described.

### INTRODUCTION

Condensers of steam turbines of great power output are very large and expensive. This is especially so for condensers of saturated steam turbines used in nuclear power stations, as they have about 1.6 time the steam flow rate per unit of output as in thermal power stations. Therefore it is necessary to intensify the processes connected with the condensation of steam, and one of the possibilities is to study the improvement of steam flow to the tube nests by means of a suitable physical and mathematical model. Various authors have developed different detailed calculation models enabling the determination of steam flow normal to the cooling tubes of the condenser cross-section, including the flow in the region of the tube nests. Some authors (ref. 1-3) based their models on the solution of the equations of continuity and momentum and air concentration, with the consideration of auxiliary relations especially for heat transfer and drag of the tube nests. A similar model was worked out by Palagin et al. (ref.4). Further, the explanation of the physical and mathematical model of the flow in a condenser, based on the self-contained calculation of the processes in tube nests, dealing with the steam flow past the tube nests, will be given in greater detail.

### Physical and mathematical model

The physical and mathematical model which is described is used for the solution of saturated steam flow normal to cooling tubes of cross-sections of the condenser external to the tube nests. It is assumed that the steam flow in this region is principally the potential subsonic stationary flow, and the equation of continuity and the momentum equation are solved by means of a general programme for the calculation of two-dimensional flow of a single-phase fluid. At the condenser wall, the parameters of the turbulent boundary layer are taken into account.

The processes in the tube nests are solved separately, out of the framework of the model of the introduced steam flow, by means of the so-called zonal calculation, performed for the whole condenser simultaneously (ref.5). The tube

nests are for this purpose suitably divided into separate regions in the cross-section, and into areas along the tubes. Each of these parts of tube nests is taken to be the elementary zone of condenser. The zonal calculation is performed with the assumption that the total pressure, or the total enthalpy of steam, at the entrance to the tube nests is constant.

In this supposed mathematical treatment, the symmetry of the flow field is used for the delimitation of a region of calculation. The actual solution is made with the aid of the stream function. For the inlet and outlet of potential flow from the region of calculation, the Dirichlet's boundary condition is used. For the outlet from the region of calculation (the inlet to the tube nests) the boundary conditions are fixed through the normal components of velocity defined from the zonal calculation of the tube nests. The numerical calculation uses the finite element method.

Two different condensers will be dealt with.

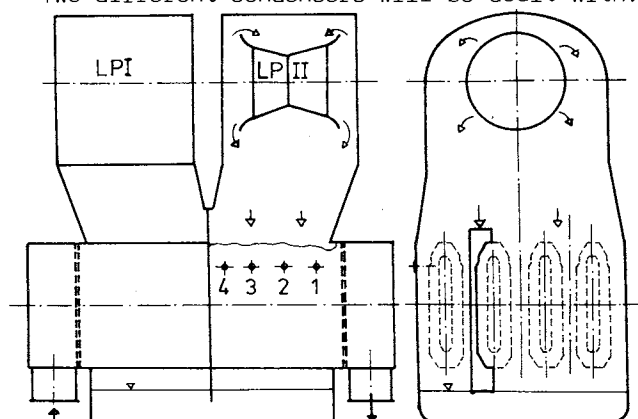


Fig.1: Diagram of the condenser for a 500 MW steam turbine (LPI, LPII - low pressure sections of the turbine)

Fig.1 shows schematically the single-pass two-pressure condenser of a 500 MW steam turbine, with four tube nests.

In the condenser cross-section there is then a region for which it is sufficient to solve the flow field with regard to the configuration of

the tube nests. Measurements of velocity profiles between the condenser wall and the tube nest at points (1) to (4) have been made on this condenser.

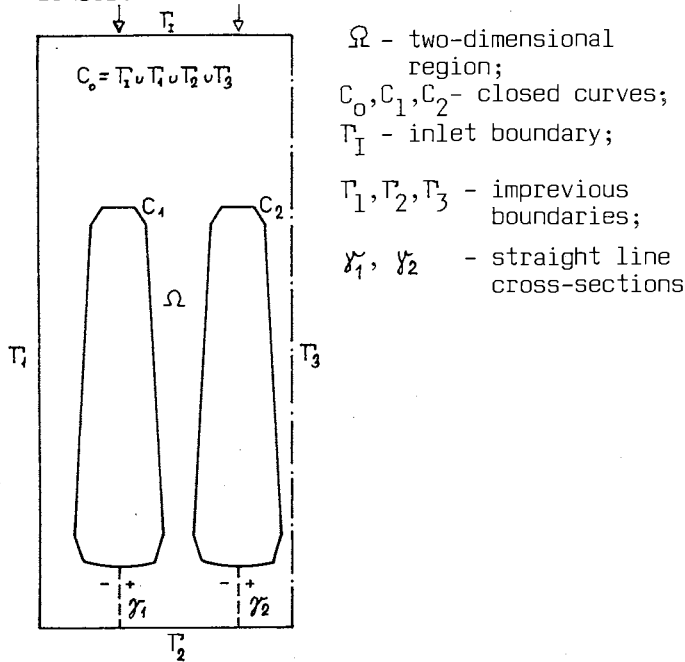


Fig.2: The calculation region of the double-pass condenser for a 1000MW saturated steam turbine. Fig.2 shows the region of calculation for the more complicated case of the double-pass condenser for a 1000 MW saturated steam turbine.

Calculation of the flow field by the finite element method

The use of the finite element method is described for the more general case of a double-pass condenser.

The condenser cross-section is represented by a two-dimensional region ( $\Omega$ ) with the boundary ( $\partial\Omega$ ) formed by three simple closed curves ( $C_0$ ) (outer component) and ( $C_1, C_2$ ) (inner components). ( $C_0$ ) consists of the inlet ( $T_1$ ) and the impervious boundaries ( $T_2, T_3$ ); ( $C_1$ ) and ( $C_2$ ) represent the outlet from the solved region into the tube nests (Fig.2). The circulation of velocity along ( $C_1$ ) and ( $C_2$ ) is considered zero. On ( $T_1, C_1, C_2$ ) the quantity ( $\rho v_n$ ) is given. Here ( $\rho$ ) is the density and ( $v_n$ ) the normal component of velocity. It is obvious that  $\rho v_n = 0$  at the impervious parts of ( $\partial\Omega$ ) (as  $T_2, T_3$ ). The total mass flow through ( $\partial\Omega$ ) is zero.

The stream function ( $\psi$ ) is defined as follows:

$$\frac{\partial\psi}{\partial x_1} = -\rho v_2, \quad \frac{\partial\psi}{\partial x_2} = \rho v_1, \quad (1)$$

where ( $v_1, v_2$ ) are the velocity components in the ( $x_1, x_2$ ) directions respectively. Since the mass flows through ( $C_1$ ) and ( $C_2$ ) are not generally equal to zero, ( $\psi$ ) does not exist in the whole region ( $\Omega$ ). Therefore the stream function problem in a simply continuous region ( $\Omega_m = \Omega - (\gamma_1 \cup \gamma_2)$ ) is considered, where ( $\gamma_i, i = 1, 2$ ) are suitable straight line cross-sections connecting ( $C_i$ ) with ( $T_2$ ) (Fig.2). On ( $\gamma_i$ ) the function ( $\psi$ ) has a discontinuity, which is given by the total mass flow ( $q_i$ ) through ( $C_i$ ). Also the boundary conditions for ( $\psi$ ), calculated from ( $\rho v_n | \partial\Omega$ ) present the same discontinuities at the points ( $C_1 \cap \gamma_i$ )

and ( $T_2 \cap \gamma_i, i = 1, 2$ ). The coherent problem can be formulated as follows: Find ( $\psi$ ) defined in ( $\Omega_m$ ) satisfying the equation:

$$\sum_{i=1}^2 \frac{\partial}{\partial x_i} \left( \frac{1}{\rho} \frac{\partial \psi}{\partial x_i} \right) = 0 \text{ in } \Omega_m \quad (2)$$

and the boundary conditions:

$$\psi | C_i = \tilde{\psi}_i + k_i, \quad i = 0, 1, 2, \quad k_0 = 0, \quad (3)$$

$$\psi(x_+) = \psi(x_-) + q_i \text{ for } x \in \gamma_i, \quad i = 1, 2, \quad (4)$$

$$\frac{\partial \psi}{\partial n}(x_+) = \frac{\partial \psi}{\partial n}(x_-) \text{ for } x \in \gamma_i, \quad i = 1, 2, \quad (5)$$

$$\int_{C_i} \frac{1}{\rho} \frac{\partial \psi}{\partial n} ds = 0, \quad i = 1, 2. \quad (6)$$

Here, the density ( $\rho$ ) is either constant, if the fluid is incompressible, or ( $\rho = \rho(\nabla\psi)^2$ ) if it is compressible. ( $\tilde{\psi}_i$ ) are given functions, ( $q_i$ ) given constants, ( $k_1, k_2$ ) are unknown constants. ( $\psi(x_+)$ ) and ( $\psi(x_-)$ ) denote the limits of ( $\psi$ ) on ( $\gamma_i$ ) taken from the right- and left-hand sides respectively. ( $\frac{\partial \psi}{\partial n}(x_+)$ ) and ( $\frac{\partial \psi}{\partial n}(x_-)$ ) have similar meanings. ( $\frac{\partial \psi}{\partial n}$ ) denotes the derivative in the direction of the normal to ( $\gamma_i$ ) and ( $C_1, C_2$ ).

With the aid of Green's Theorem we come to the variational formulation formally equivalent to (2) - (6): find ( $\psi$ ) defined in ( $\Omega_m$ ) satisfying conditions (3), (4) and the identity:

$$\int_{\Omega} \frac{1}{\rho} \nabla \psi \nabla v dx = 0 \quad (7)$$

for all ( $v \in V$ ), where:

$$V = \{v \text{ is sufficiently smooth in } \Omega; v | C_0 = 0, v | C_i = \text{const}, i = 1, 2\}. \quad (8)$$

It is possible to prove that this problem has only one weak solution.

The integral identity (7) is the starting point for the application of the finite element method. The region ( $\Omega_m$ ) is approximated by a polygonal region ( $\Omega_h$ ). Let ( $T_h$ ) be a triangulation of ( $\Omega_h$ ) with the usual properties. ( $\Omega_h$ ) can also be considered as a polygonal approximation to ( $\Omega$ ). Each vertex ( $P$ ) from ( $\gamma_i$ ) is nevertheless considered twice - as ( $P^-$ ) on the left hand side ( $\gamma_i$ ) and ( $P^+$ ) on its right hand side.

The approximate solution can be found in the space of planar triangular elements:

$$X_h = \{v_h \in C(\Omega_h \cup \partial\Omega_h); \quad (9)$$

$$v_h | T \text{ is linear for each } T \in T_h\}.$$

In general, ( $v_h(P^-) \neq v_h(P^+)$ ) for ( $P \in \gamma_i$ ) and ( $v_h \in X_h$ ).

The space ( $V$ ) is approximated by:

$$V_h = \{v_h \in X_h; v_h | C_0 = 0, v_h | C_i = \text{const for } i = 1, 2, v_h(P^-) = v_h(P^+) \text{ for } P \in \gamma_i, i = 1, 2\}. \quad (10)$$

Now the discrete problem for (3), (4), (7) reads as follows:

Find ( $\psi_h \in X_h$ ) and constants ( $k_1, k_2$ ) such that:

$$\psi_h(P^+) = \psi_h(P^-) + q_i \text{ for } P \in \gamma_i, \quad i = 1, 2, \quad (11)$$

$$\psi_h(P_j) = \tilde{\psi}_i(P_j) + k_i \text{ for all vertices } P_j \in C_i, \quad (12)$$

$$i = 0, 1, 2 \text{ with } k_0 = 0,$$

$$\int_{\Omega_h} \frac{1}{\rho} (\nabla \psi)^2 \nabla \psi_h \nabla v_h dx = 0 \text{ for all } v_h \in V_h. \quad (13)$$

This Problem has a unique solution in both incompressible and compressible cases. If the fluid is incompressible and the problem represents a system of linear algebraic equations, the solution can be calculated by the well-known SOR method. The method of conjugate gradients with preconditioning by the SSOR method proves to be faster. The algorithmization and programming of these both methods is very simple. In the non-linear compressible case the steepest descent method with preconditioning is applied.

Numerical computation have been realized with the aid of the multipurpose system of finite element programmes.

Comparison of the results of computation with measurements

The comparison of the results of computation with the results of measurements has been performed for the case of the single-pass double-pressure condenser of a 500 MW turbine.

The calculations have been made for a region representing one-eighth of the condenser cross-section (Fig.1) The inlet steam velocity was 51 m/s. For the zonal calculation the cross-section of the tube nest has been divided into 12 separate parts and the tube nest into 4 longitudinal parts, for each pressure used. The normal components of velocity at the inlet to the tube nest are in the range from 8 m/s up to 12,5 m/s.

The calculated velocity distribution in the region studied is shown in Fig.3a.

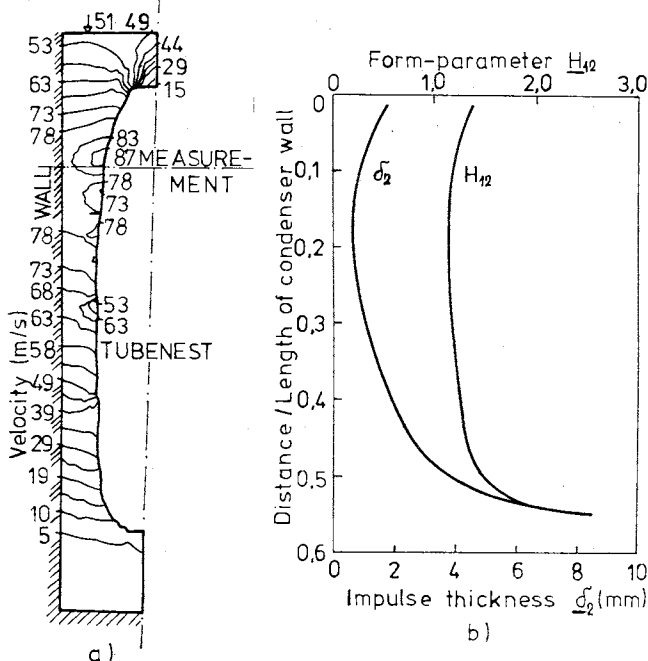


Fig.3: Results of calculations of the condenser for a 500 MW turbine:  
(a) Field of velocities,  
(b) Parameters of boundary layer at the wall

The maximum local velocity near the tube nest is over 87 m/s. This rather high velocity causes concern with respect to the possibility of excessive vibration of the tubes.

The results of turbulent boundary layer calculations for the smooth condenser wall are

given in Fig.3b. The starting point of the boundary layer is assumed to be at the wall opposite the turbine axis. The variations of the impulse-thickness ( $\delta_2$ ) and the form-parameter ( $H_{1,2}$ ) show that there is a separation of the boundary layer at the bottom part of the condenser wall.

The calculation of the velocity field was checked by the method of electro-hydrodynamic analogy (ref.6). The measured results are practically identical with calculation with the exception of areas of large velocity gradients, where the finite element method reduces the local increases of velocity a little by comparison with the electro-hydrodynamic analogy.

The results of steam velocity measurements at the turbine power output of 450 MW are shown in Figs.4a and 4b. The probes and measuring techniques have been used as developed for the wet steam measurements (ref.7).

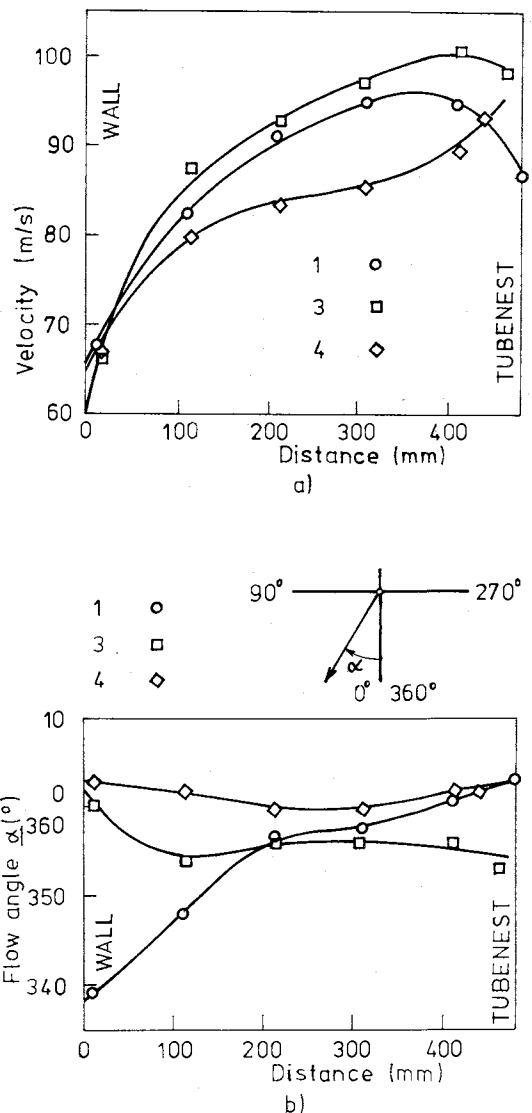


Fig.4: Steam velocities in the condenser of a 500MW turbine as obtained by measurements:  
(a) Magnitudes of velocities,  
(b) Directions of flow.

Fig.4a shows the magnitudes of velocities ( $v$ ) between the condenser wall and the tube nest at the points (1) - (4), situated in the vicinity

of maximum velocities (Fig.1 and Fig.3a). It is evident that the velocities in the tube nest reach high values, and at the same time it can be seen that, differently from the potential flow calculation, the wall boundary layers affect the flow to a great extent and cause a decrease in velocities near the condenser wall and a further increase in velocities near the tube nest.

The directions of the flow, expressed by the angle  $\alpha$ , can be seen in Fig.4b.

It is evident that, with some exceptions, they differ relatively only a little from the normal direction towards the tubes, so that the assumption of the two-dimensional flow in the planes normal to the tube nests can be taken as approximately correct.

Results of calculations of the flow field in a double-pass condenser

Calculations have also been performed for a double-pass single-pressure condenser for a 1000 MW saturated steam turbine. The region of calculation, as seen in Fig.2, represents half of the cross-section of one of the three identical condensers which are used. The inlet velocity was 68 m/s. For the zonal calculation each tube bank was cross-sectionally divided into 8 separate parts and longitudinally into 2 parts. The calculation of the steam flow is carried out for the transverse plane, by with cold cooling water entering the left tube nest and the heated cooling leaving through the right tube nest. The normal components of velocity at the inlet to the tube nest with cold water are about 17 m/s, and at the inlet to the tube nest with heated water are about 4 m/s.

In the region of calculation a grid of 5161 finite elements has been generated by the method of automation, as shown in Fig.5.

The main results of the calculations are clear from Fig.6. The lines of  $\psi = \text{const.}$  are drawn in Fig.6a, and can be denoted as streamlines. The very small angles at which the steam enters the tube nests should to be noticed. Fig.6b shows the distribution of velocities in the region of calculation. Near the tube nest with cold water the local steam velocity from the left side reaches the maximum value of 130 m/s, and from the right side 118 m/s. In the tube nest with heated water, the local steam velocity on the left side is 130 m/s, whereas on the right side it is only 50 m/s.

The physical and mathematical model described can be used for the optimisation of the shape of the region investigated, in order to achieve a velocity distribution more suitable with regard to the possibility of condenser tube vibration and due to the boundary layer separation from the condenser wall.

The authors express their gratitude to all their co-workers at Charles University, Prague and the ŠKODA Concern, Enterprise, Plzen for their help with calculations and measurements.

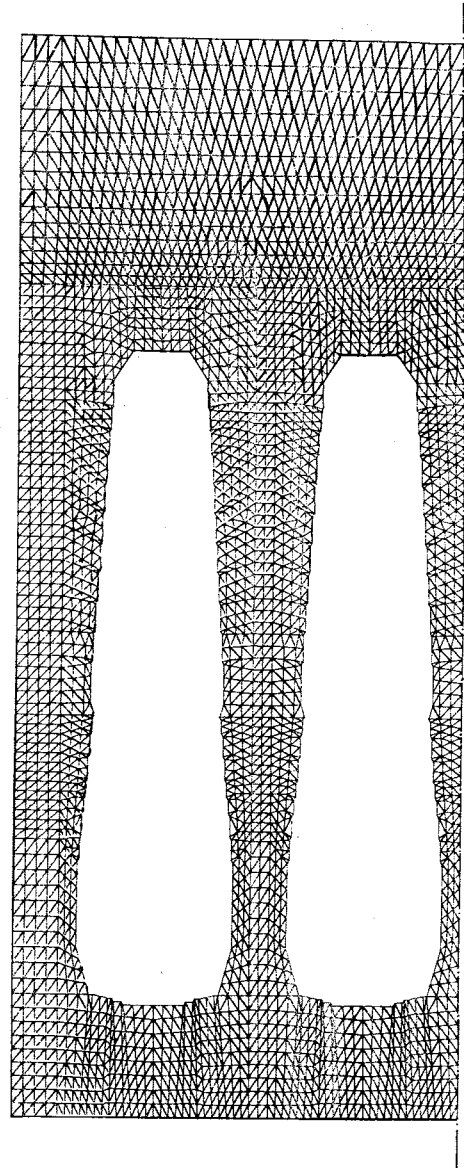


Fig.5: The grid of finite elements of the double-pass condenser for a 1000 MW turbine.

REFERENCES

1. AL-SANEA S., RHODES N., TATCHELL D.G., WILKINSON T.S.  
A Computer Model for Detailed Calculation of the Flow in Power Station Condensers, Condensers: Theory and Practice, EFCE Publication Series No.30, 1983, 70 - 88.
2. CAREMOLI C.  
Numerical Computation of Steam Flow in Power Plant Condensers, Condensers: Theory and Practice, EFCE Publication Series No.30, 1983, 89 - 96.
3. DAVIDSON B.J. Condensers for Large Steam Turbines: Thermal Design, Chap.8, Hemisphere Pub.corp.1987
4. PALAGIN A.A., ZEVIN L.I., DOROCHOV V.A.  
Computation of velocity field in condensers for steam turbines (in Russian). Problemy mashinostrojenija, 1983, Vyp.18, 63-66, Moscow, U.S.S.R.

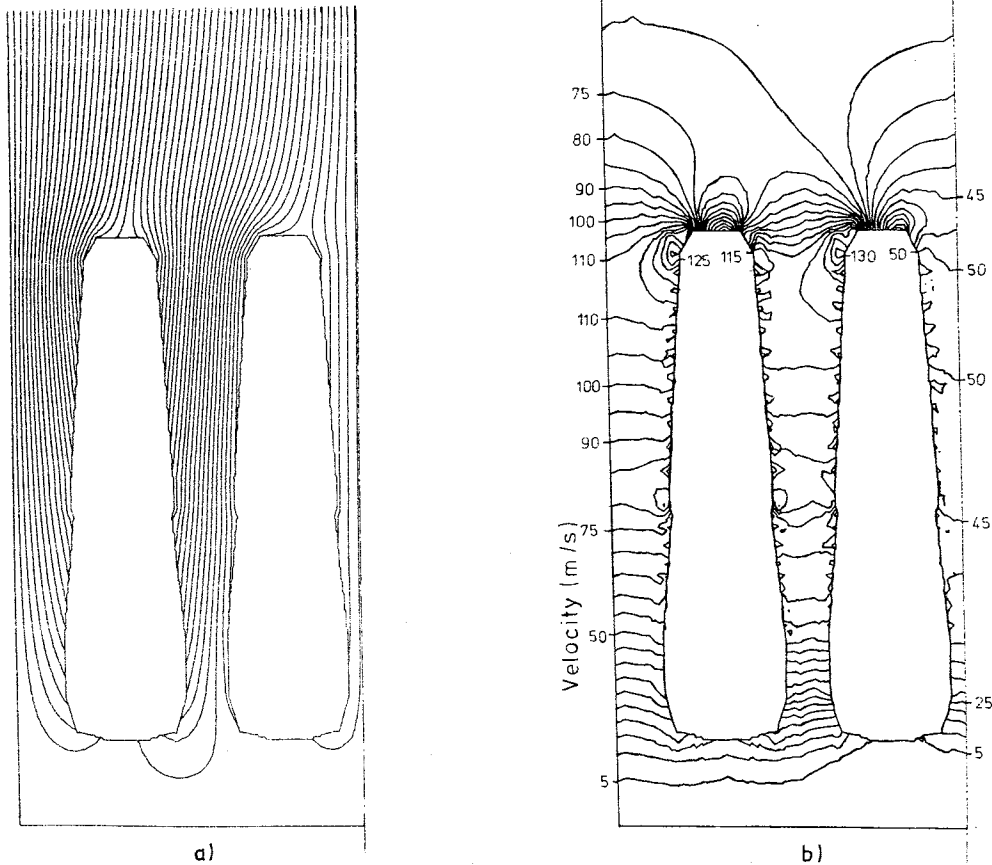


Fig.6.: Results of calculations of the double-pass condenser for a 1000MW turbine:  
 a) Streamlines; b) Field of velocities.

5. ROTH Z. Zonal calculation of condensers (in Czech), Proceedings of the Conference: Heat Exchanging Equipment of Steam Turbines, 1982, 27-34, ČSVTS, ŠKODA CONCERN, ZES, Plzen, Czechoslovakia
6. NOŽIČKA J. Analog Methods in Fluid Flow (in Czech) Academia, Prague, Czechoslovakia, 1967.

7. ŠTASTNÝ M. An Experimental Research into Flow of Wet Steam through the Last Stage of a Full-Scale Turbine. Sixth Thermodynamics and Fluid Mechanics Conference, IME Conference, 1976, 29-37. Durham, England.



## 23. On-line measurement methods of single component velocities in two-phase flow systems

Professor Dr-Ing. D. BARSCHDORFF and Dr-Ing. D. WETZLAR, Institute for Electrical Measurement Techniques, University of Paderborn

An on-line correlation method for separate velocity measurement in two phase water-droplet or -bubble flow systems is discussed, which is implemented on a signal processor. Suitable sensors are presented in an overview. An off-line application analysing reactor blowdown data is discussed. The real time behaviour of the new system for typical applications is under investigation.

### INTRODUCTION

1. In highly accelerated multi phase flow systems with different mass inertia a velocity difference in form of a slip between the different phases is observed. The knowledge of the individual component velocities is important not only in wet steam turbine sections, but also in chemical reactors, electrostatic dust collectors, cyclone separators, liquid atomizers and others. So far, applications of measurement techniques for single component velocity determination in the form of the radioactive tracer method (ref. 1) the Laser-Doppler-anemometer (LDA) (ref. 2), correlation methods (refs 3, 4) and a combined color-tracer- and correlation method (ref. 4) have been reported.

2. Applying the LDA, the presence of particles within the fluid is necessary. Smaller particles are assumed to move with the fluid velocity. Actually, the particle velocity is measured with such an instrument. The tracer methods mostly are characterized by a disturbance of the fluid due to the injected tracer material. This does not apply, however, for special temperature tracer applications.

3. Utilizing correlation methods, stochastic disturbances within the fluid phases have to be detected at two different locations in flow direction. Here, the characteristic flow patterns are assumed to move with flow velocity as well.

4. The latter method is the base for this investigation. The sensors should be chosen to measure the velocity inhomogenities without interacting and without direct flow contact. In the following, suitable sensors and measuring methods are described.

### SENSORS FOR VELOCITY DETERMINATION IN TWO PHASE FLOW SYSTEMS

5. Sensors can be divided in those measuring local flow speeds (LDA, L2F), those detecting an averaged velocity in a limited flow cross section (ultrasonic flow meters or optical sensors) and sensors measuring an averaged total flow velocity (turbine flow meters).

6. Table 1 shows sensors yielding an electrical signal proportional to the flow velocity. The application of statistical methods like cross correlation, rehocence or cepstrum (ref.

5) require the detection of stochastic disturbances within the fluid. Table 2 shows suitable sensors.

7. For the determination of single component velocities, suitable signals have to be modulated by the specific flow patterns of the different phases. In all known two phase liquid-gas flow applications, however, the sensor signals are always influenced by the liquid and gaseous phases, yielding summation signals. As an example optical transmission measurement techniques with infrared absorption in the fluid phase and simultaneous scattering on particles are mentioned.

$$I_1 = I_{o1} \exp[-N\pi r^2 Q_{\text{ext}}(\lambda_1, m, r) l] \quad (1)$$

$$I_2 = I_{o2} \exp[-N\pi r^2 Q_{\text{ext}}(\lambda_2, m, r) (1 - \epsilon(\lambda_2) \rho_D) l] \quad (2)$$

$I_i$	intensity at wavelenth $\lambda_i$
$I_{oi}$	incident intensity at wavelenth $\lambda_i$
$N$	particle number density
$r$	radius of particle
$Q_{\text{ext}}(\lambda_i, m, r)$	cross-section for scattering at wavelenth $\lambda_i$
$m$	refractiv index
$l$	measuring length
$\epsilon(\lambda_i)$	extinction coefficient
$\rho_D$	density

8. These equations can be derived combining Lambert-Beer's absorption law and Mie's scattering theory with respect to a given measuring volume (ref. 3). The measuring volume, defined by the optical beam, causes a spatial filtering.

9. Optical techniques have the advantage of measuring the distinct phase disturbances with a single sensor system. However, in principal, two or more sensors can be used in combination. Fig. 1a shows a signal model for a transmission measuring system.

10. In (refs 3, 4) a method for the separation of additively superposed signals is developed. It yields results under the assumption, that the stochastic signals due to flow disturbances are uncorrelated. From the measurable summation signal, a suitably adapted signal, which must be correlated with one of the single component disturbances, has to be subtracted. The method was applied off line using a process computer. Fig. 1b shows, how this method can be utilized

FLOW ANALYSIS AND MEASUREMENT

Table 1: Pick up's for velocity measurement

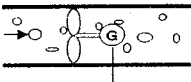
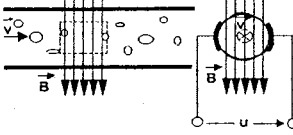
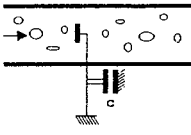
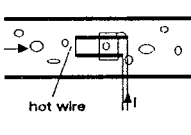
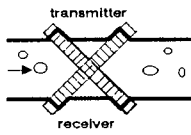
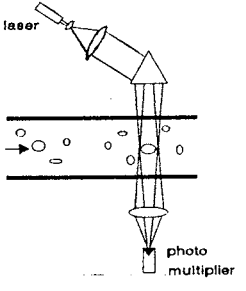
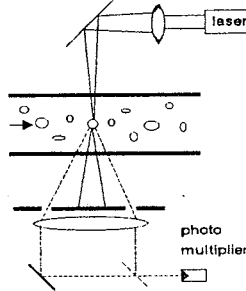
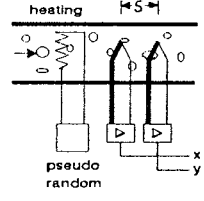
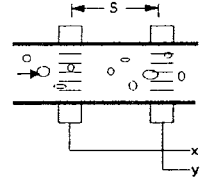
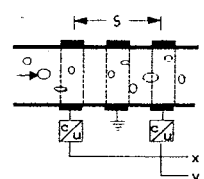
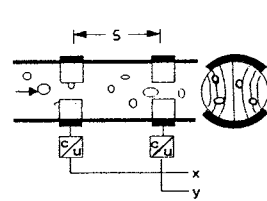
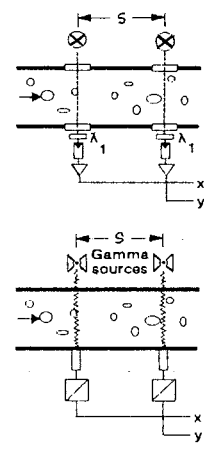
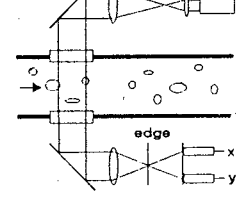
Scheme	<ul style="list-style-type: none"> <li>Name</li> <li>local resolution</li> <li>detected phase</li> </ul>
	<ul style="list-style-type: none"> <li>turbine flow meter (true turbine mass flow meter)</li> <li>area</li> <li>both phases</li> </ul>
	<ul style="list-style-type: none"> <li>electromagnetic flow meter</li> <li>area</li> <li>fluid</li> </ul>
	<ul style="list-style-type: none"> <li>drag body transducer</li> <li>area/point</li> <li>both phases</li> </ul>
	<ul style="list-style-type: none"> <li>hot wire probe</li> <li>point</li> <li>fluid/ both phases</li> </ul>
	<ul style="list-style-type: none"> <li>ultrasonic Doppler effect flow meter</li> <li>line</li> <li>particle</li> </ul>
	<ul style="list-style-type: none"> <li>laser two focus anemometer (L2F)</li> <li>point</li> <li>particle</li> </ul>
	<ul style="list-style-type: none"> <li>laser Doppler anemometer (LDA)</li> <li>point</li> <li>particle (very low concentrations)</li> </ul>

Table 2: Detection of stochastic disturbances for application of correlation methods

measuring equipment	<ul style="list-style-type: none"> <li>stochastic fluctuations</li> <li>local resolution</li> <li>detected phase</li> <li>two phase flow (particle/fluid)</li> </ul>
	<ul style="list-style-type: none"> <li>temperature</li> <li>point</li> <li>both or fluid</li> <li>gas/liquid (buble flow)</li> <li>liquid/gas (fog flow)</li> <li>solid/liquid</li> <li>solid/gas</li> </ul>
	<ul style="list-style-type: none"> <li>ultrasonic intensity</li> <li>line</li> <li>particle</li> <li>gas/liquid/solid</li> </ul>
	<ul style="list-style-type: none"> <li>dielectric coefficient</li> <li>ring area</li> <li>particle</li> <li>solid/liquid</li> <li>solid/gas</li> </ul>
	<ul style="list-style-type: none"> <li>dielectric coefficient</li> <li>area</li> <li>particle</li> <li>solid/liquid</li> <li>solid/gas</li> </ul>
	<ul style="list-style-type: none"> <li>fluid density (absorption) and particle number density (scattering)</li> <li>line</li> <li>particle or both</li> </ul>
	<ul style="list-style-type: none"> <li>gas/liquid</li> <li>liquid/gas</li> <li>solid/liquid</li> <li>solid/gas</li> </ul>

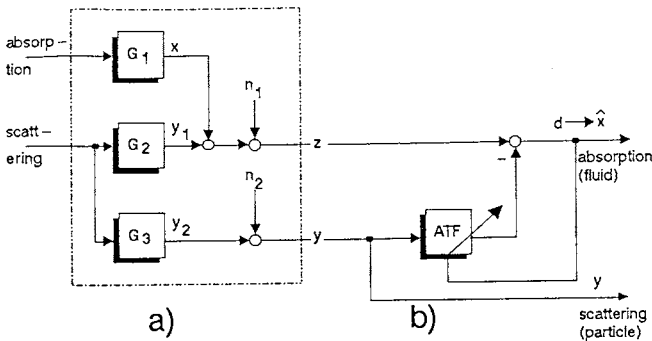


Fig. 1 Model of signal generation in two phase flows by optical transmission techniques (a) and separation in single signals (b)

using an adaptive transversal filter (ATF). The differential signal  $d$  represents an estimation of the signal  $x$ , which cannot be measured separately. The theoretical value of the transfer function of the ATF is given by

$$V_{opt}(f) = G_2(f)/G_3(f), \quad (3)$$

however,  $G_2(f)$  and  $G_3(f)$  are unknown.

11. Using the optical transmission technique, the two transfer functions  $G_2(f)$  and  $G_3(f)$  only differ by an amplification factor, so that an ATF can be substituted by a variable gain amplifier. The optimum gain factor is determined from (ref. 3)

$$V = C_{zy}(\tau=0)/C_{yy}(\tau=0). \quad (4)$$

The value of  $V$  can be computed from the known measurable values  $y$  and  $z$ .

12. For an on-line application, a feedback method, Fig. 1b, is of advantage, because a result is obtained after every scanning cycle. The amplification factor  $V[k]$  at time  $kT$  is controlled in such a way that a differential signal  $d$  is obtained which is uncorrelated with the measurable single signal  $y$ . It can be computed by the LMS (least mean square) algorithm with constant step size  $\eta$ .

$$V[k] = V[k-1] + \eta d[k] y[k] \quad (5)$$

### OFF-LINE ANALYSIS AT REACTOR BLOWDOWN EXPERIMENTS

13. The application of usual correlation techniques requires the simultaneous signal acquisition at two locations. In this case, however, four signals have to be digitized in parallel. Fig. 2 shows the procedure for the determination of the single component velocities.

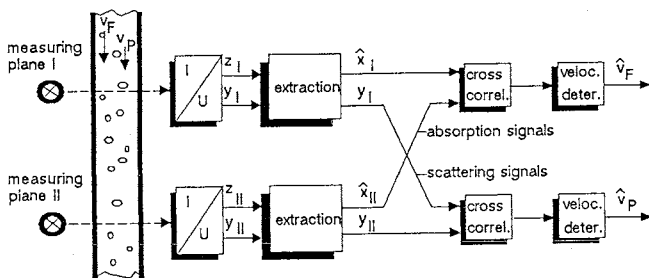


Fig. 2 Determination of individual velocities

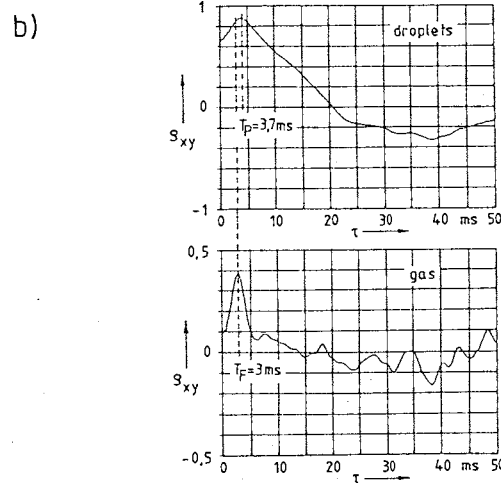
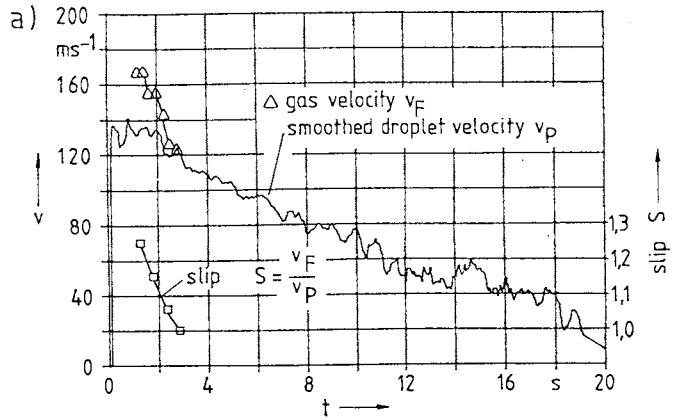


Fig. 3 Slip, droplet and gas velocities in an accelerated fog flow (a), typical cross correlation functions of scattering and estimated absorption signals (b) (ref. 7)

14. This method was investigated at blowdown experiments in a reactor containment, where highly accelerated air-water vapour-droplet flows had been induced by a simulated rupture of a pipe in the primary circulation of a pressurized water reactor (ref. 6). A result in form of time dependent slip between the droplet and gas velocities is given in Fig. 3a. Fig. 3b shows typical cross correlation functions.

### ON-LINE MEASUREMENT

15. To-day's signal processing techniques can be highly improved by utilizing signal processors in combination with personal computers, yielding very efficient on-line processing methods for a great variety of applications. In this investigation the TMS 320C25 signal processor on a PC-board was used.

16. In Fig. 4a block scheme of the necessary computational steps using a signal processor are given. While Fig. 4a shows the overview scheme of the arrangement, Fig. 4b gives the more detailed scheme for determination of the running averaged cross correlation function.  $\alpha$  is an exponential averaging factor, which takes into consideration the degree of flow turbulence (Reynolds number) and the separation between the measuring planes  $s$ . Only one matching factor is therefore necessary for the averaging process.

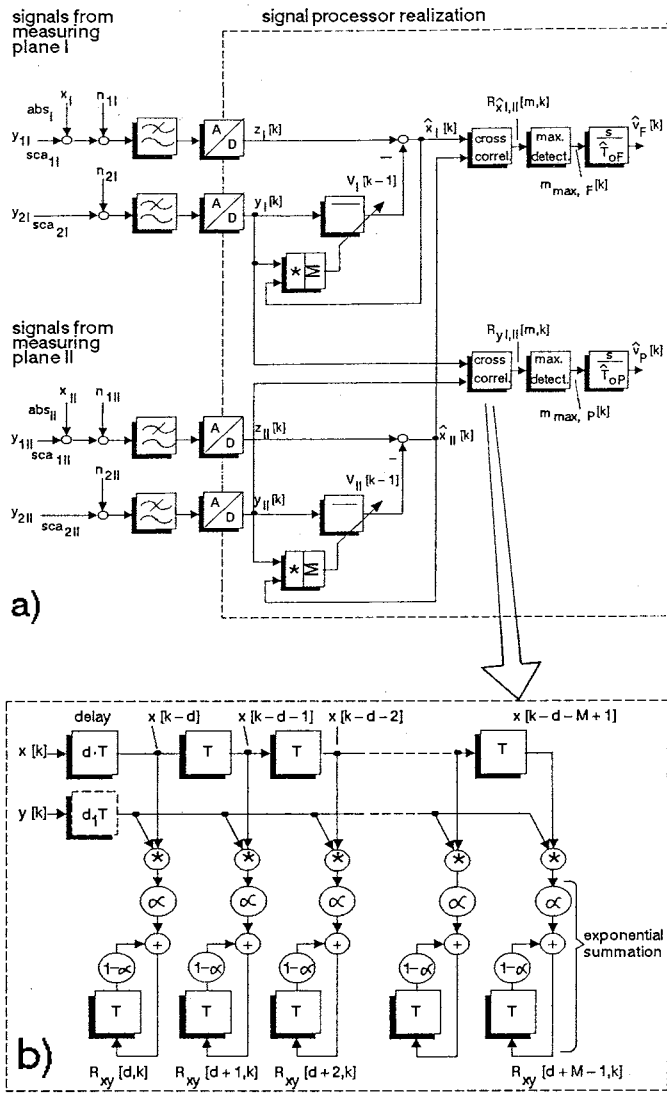


Fig. 4 Block diagram of signal processor arrangement (a) and detail of the determination of the cross correlation function (b)

$$R_{xy}[m,k] = (1-\alpha) R_{xy}[m,k-1] + \alpha x[k-m] y[k] \quad (6)$$

$R_{xy}[m,k]$  cross correlation function at delay time  $mT$  and time  $kT$   
 $\alpha$  exponentially averaging factor  
 $x[k] y[k]$  signals at time  $kT$

17. An individual pre-delay of the measured time series  $x$  and  $y$  can be maintained by  $dT$  and  $d_1T$ , so that the maximum of the cross correlation function appears within the center of the time window.

18. The typical sampling frequency of 1 kHz corresponds to a delay time increment of the cross correlation function of 1 ms. Especially at high fluid velocities and small transit time intervals, this leads to an insufficient time resolution. Therefore, the slope of the cross correlation function is interpolated for three computed correlation values.

19. As the signals under consideration are of limited bandwidth, it is suitable to compute the cross correlation function within the time do-

main. The sampling period is about 1 ms. Using FFT-analysis, computation could begin after digitizing a complete data sample, however, three complete FFT computations are necessary. The "running computational" technique, carrying out the complete necessary computational steps within every sampling interval requires efficient algorithms and computational power. The contribution of every data sample to the total time shift interval of the cross correlation function is taken into account and errors by cyclic correlation by FFT analysis are avoided.

20. The sensor signals are digitized in the order  $y_{I1}$ ,  $y_{II1}$ ,  $z_{I1}$  and  $z_{II1}$ . Already during the data acquisition time of the sample and hold circuits and the conversion time of the ADC's previous sampled data can be processed. Instead of four ADC's in Fig. 4 an ADC - multiplexer configuration can be used. To avoid a time delay due to multiplexing, four sample and hold circuits must be applied.

21. The numerical determination of the single component velocities is maintained in two steps: First the cross correlation function of the scattering signals  $y_I$  and  $y_{II}$  is computed in a search run over a large time delay ( $0 \leq m \leq M-1$ ). If the resulting maximum exceeds a predefined threshold, a tracking mode is activated, in which the correlation functions of the scattering and the absorption signals are processed within a limited scan range  $S$  in the neighbourhood of the maxima ( $m_{op,F}-S/2 \leq m \leq m_{op,F}+S/2$ ). In case of a missing maximum of the cross correlation function of the absorption signals, the system computes the particle velocity. This incorrect condition is identified by a certain flag (digital output). If the maximum of the scattering signal cross correlation function does not exceed the threshold, the program starts with a new search run, indicated by another flag.

22. The normalized cross covariance function yields a measure for the degree of correlation,

$$\rho_{xy}(\tau) = \frac{R_{xy}(\tau) - \mu_x \mu_y}{\sigma_x \sigma_y} \quad (7)$$

$\rho_{xy}(\tau)$  normalized cross covariance function  
 $R_{xy}(\tau)$  cross correlation function  
 $\mu_x, \mu_y$  mean  
 $\sigma_x, \sigma_y$  standard deviation

The range of  $\rho_{xy}$  is between  $\pm 1$ . The threshold for the estimation of the scattering signal cross correlation function depends on the flow velocity, the degree of flow turbulence, and the sensor separation distance  $s$ . Signals should be amplified in order to utilize the given amplitude range of the ADC's. Therefore, the threshold can be regarded as constant within a certain velocity range. However, the threshold can be deduced from the determined absorption signals using the variance of the signals, which must correspond approximately in their rms values.

23. The signal processor realisation computes the phase velocities at sampling frequencies of 1 kHz and a total delay time of 200 ms (search mode) or 100 ms (tracking mode) in real time. A computer flow chart is given in the appendix.

CONCLUSIONS

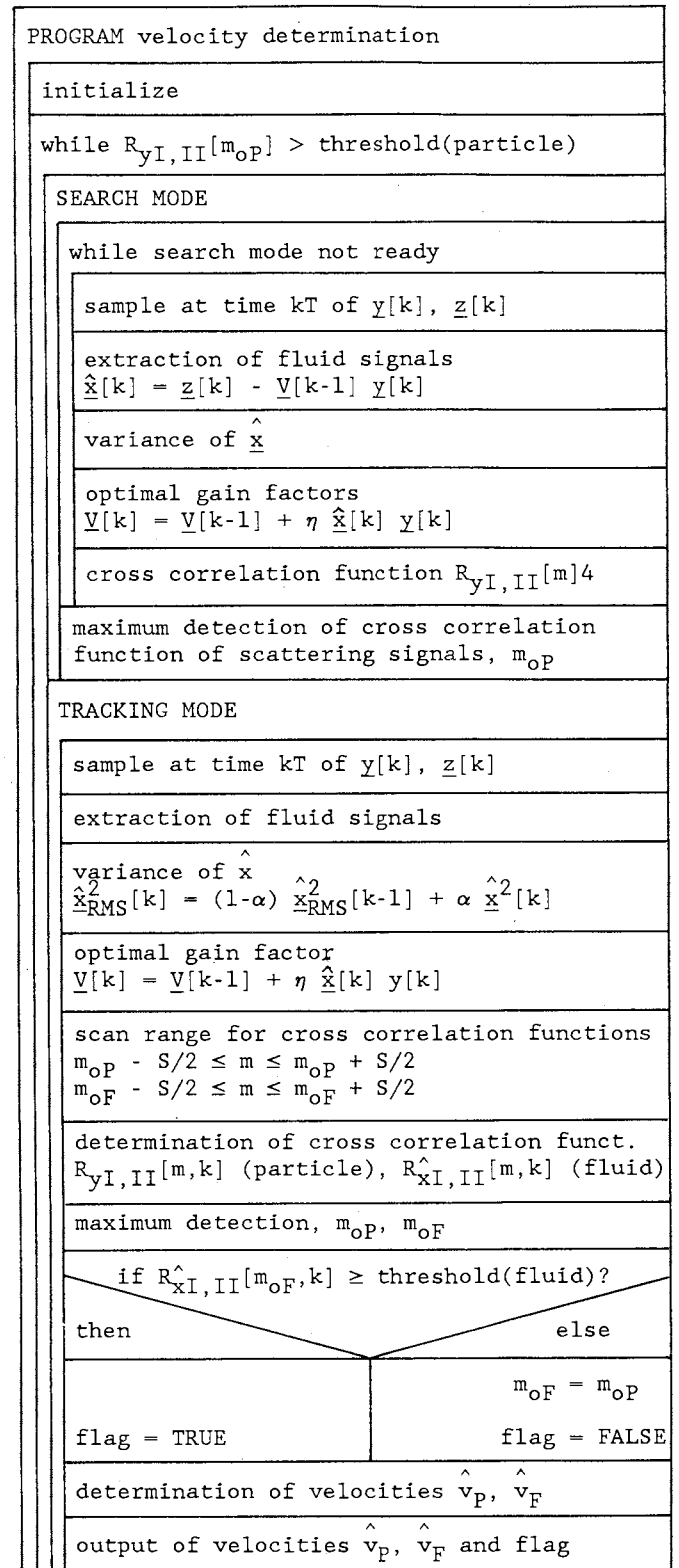
24. Several sensor arrangements suitable for the velocity measurement in two phase flow applications have been discussed. They yield summation signals as well as signals, which are proportional to stochastic fluctuations of one of the individual phases of a two phase flow system. In the case of optical transmission techniques, signals are influenced by absorption in the fluid phase and additional by scattering at particles. The availability of a second correlated scattering signal allows separation into single signals. By use of correlation techniques, the determination of single phase velocities is possible. The technique was applied successfully in off-line applications in high accelerated fog flows at reactor blowdown experiments. Gas velocities of 170 m/s and a slip of 1.25 were measured. In the present investigation an on-line signal processor arrangement is introduced. At a water air bubble flow both liquid and gas velocities from 0.1 m/s up to 1 m/s were measured separately 1000 times per second. It could be shown, that slip increases with decreasing flow velocity.

REFERENCES

1. LÖFFEL, R: Massenstrommessungen an Ein- und Mehrphasenströmungen. In: Atomkernenergie / Kerntechnik 33 (1979), 139-143
2. STOCK, D. E. ; JUREWICZ, J. T. ; CROWE, C. T. and ESCHBACK, J. E.: Measurement of Both Gas and Partikle Velocity in Turbulent Two-Phase Flow (Fourth Biennial Symposium on Turbulence in Liquids University of Missouri-Rolla USA Sept. 1975, Zakin, J. L. ; Patterson, G. K. (Ed.)). In: turbulence in liquids, 91- 102 Princeton, New Jersey : Science Press 1977 - Proceedings
3. BARSCHDORFF, D. and WETZLAR, D.: Determination of Single Component Velocities in Two-Phase Flow Systems using Correlation Methods. In: J. Nucl. Techn. Vol. 58 (1982), July, 107-112
4. WETZLAR, D.: Ein Verfahren zur getrennten Geschwindigkeitsbestimmung in Zweiphasenströmungen auf der Grundlage stochastischer Summenprozesse, Paderborn, Universität-GH-Paderborn, Fachbereich Elektrotechnik, Thesis, 1986, Fortschritt - Berichte VDI, Reihe 8, Nr. 106, Düsseldorf : VDI-Verlag GmbH 1986
5. BARSCHDORFF, D. and WETZLAR, D.: Comparison of Statistical Methods for Single Component Velocity Determination in a Bubble Flow. Measurement, Vol. 2, No. 4, 1984, 180-186
6. NEUMANN, M.: Ein Infrarotmeßverfahren zur Bestimmung von Strömungsparametern einer instationären H<sub>2</sub>O-Zweiphasenströmung bei simulierten Kühlmittelverlustunfällen. Karlsruhe, Universität Karlsruhe (TH), Fakultät für Maschinenbau, Thesis, 1980
7. BARSCHDORFF, D. ; JANSEN, K. and WETZLAR, D.: Bestimmung von Tropfen- und Dampfgeschwindigkeit in einer Zweiphasen-Nebelströmung bei HDR-CONT-Dampf-Versuchen. Kernforschungszentrum Karlsruhe (PHDR-Arbeitsbericht Nr. 3.407/84)

APPENDIX

Computer flow chart





## 24. Effects of steam inlet conditions on behaviour of non-equilibrium flow in the primary wet steam turbine stage

M. Z. YU, B. SUN and W. S. WANG, Department of Energy and Power Engineering, Xi'an Jiaotong University, Xi'an, China

In order to understand the effects of steam inlet conditions on the performance of the primary wet steam stage of low pressure turbine, the non-equilibrium flow in a typical stage has been studied by means of the numerical analysis of governing equations for one-dimensional nucleating steam flow in blade passage. The computational results obtained show that variations of the inlet condition do have some significant effects on the non-equilibrium flow pattern in the stage. When the steam inlet state is close to Wilson zone, the flow pattern is particularly sensitive to the fluctuation of steam inlet condition. The resulting influences on the operation performance of the wet steam turbine are discussed.

### NOMENCLATURE

c	Absolute velocity
E	$E = \sin \alpha_0 / \sin \alpha_1$ or $\sin \beta_2 / \sin \beta_3$
H	Local equivalent width of blade passage
h	Dimensionless width of blade passage, $h = H/0$
$h_s$	Isentropic heat drop
$I^s$	Nucleation rate
i	Specific enthalpy
L	Length of stream line from the blade inlet to the blade exit
M	Mach number
O	Width of blade passage at throat
p	Pressure
$\dot{P}$	Expansion rate
r	Mean droplet radius
S	Specific entropy
T	Temperature
w	Relative velocity
x	Dryness fraction
y	Wetness fraction
Z	Distance from blade inlet along stream line
$\bar{Z}$	Dimensionless distance, $\bar{Z} = Z/L$
$\Delta T$	Supercooling
$\xi_T$	Thermodynamic loss coefficient at blade exit
$\xi_{Tx}$	Local thermodynamic loss coefficient
$\alpha$	Absolute outlet flow angle with respect to peripheral direction
$\beta$	Relative outlet flow angle with respect to peripheral direction
$\phi$	Mass flow coefficient
$\varepsilon$	Overall pressure ratio
Subscripts	
e	Equilibrium
ne	Non-equilibrium
x	Local value
s	Saturation value
0	Stage inlet
1	Stator blade exit
2	Rotor blade inlet
3	Rotor blade exit

### INTRODUCTION

1. The non-equilibrium steam flow pattern and the distribution structure of liquid phase in primary wet steam turbine stage play an important role for the operation performance of low pressure steam turbine, because these factors strongly influence the magnitude of departure from thermal equilibrium, the discharge capacity and thermodynamic wetness losses of the turbine stage. It is well known that steam inlet conditions of a primary wet steam stage affect significantly the non-equilibrium flow pattern and the droplet sizes. Therefore, it is interesting for turbine designer and engineer to know whether the resulting changes in flow pattern mean any importance for turbine design and operation. Up to now, there is lack of experimental data to determine the effects of inlet conditions on the performance of low pressure turbine, although a number of theoretical calculations of nucleating steam flow in turbine stages have been performed by different authors using numerical analysis of governing equations for one-dimensional nucleating steam flow in conjunction with throughflow calculation of stages (refs 1-4). Recently, the suspicion about the validity of one-dimensional method to determine the non-equilibrium pattern of wet steam flow in turbine has been aroused. The reason for the argument is the fact that condensation in turbine stages may begin earlier than in one-dimensional nozzles. Some possible factors, such as the nucleation in the blade wake, two-dimensionality of cascade flow and static temperature fluctuations etc., have been put forward to explain the difference found between the condensation processes in Laval nozzle and turbine flow. Hitherto the problem remains unsolved and more investigations are required to obtain a complete understanding. But it would be still interesting to know whether the one-dimensional method could provide some insight into the basic phenomena of the non-equilibrium flow pattern in stages. Recently, a comparison between the experimental data of mass flow coefficient of a wet steam cascade

## FLOW ANALYSIS AND MEASUREMENT

reported by Filippov etc. (ref.5). and the theoretical results assuming one-dimensional flow at cascade exit has been made by young (ref.6). Although the approximation of passage shape for determining the rate of expansion to actual blade passage shape is rather poor, the overall agreement between computational results and experimental data is excellent. These comparisons give support to the application of one dimensional method and imply that the calculation results using one-dimensional theory in conjunction with throughflow calculation can demonstrate at least the overall effects of different flow parameters on the non-equilibrium flow pattern of stage and provide some physical insight and usefull quantitative informations for turbine designer and engineer.

2. In this paper some applications of one-dimensional method to analysing the effects of steam inlet conditions on the performance of primary wet steam stage are described. The method is by no means perfect but with the hope that the results will reveal how the inlet conditions can affect the magnitude of departures from thermal equilibrium and their subsequent influences on turbine performance.

### COMPUTATION PROCEDURES

3. The results presented in the next section are computed using a program for calculating one-dimensional non-equilibrium wet steam flow in blade passages of a turbine stage. The numerical solution method of the governing equations for nucleating flow is similar to those in many literatures so the equations will not be given. In the following some descriptions to procedures will be given briefly.

4.1) The basic conservation equations of continuity, momentum and energy for one-dimensional nucleating flow are solved with the nucleation and droplet growth equations by the Runge-Kutta method. In calculating the nucleation and droplet growth rates, classical theory with non-isothermal correction has been adopted as described in Ref.7.

5.2) The calculation is carried out for the flow in frictionless flow passage. The aerodynamic losses due to friction etc. are considered using a velocity coefficient at the exit of cascade.

6.3) The equivalent width along the flow path in stator and rotor passages are determined by the following equations:

$$h=1 - E^{0.012\frac{-}{z}} + E^{0.48\frac{-}{z^2}}$$

$$h = H/0 , E = \sin \alpha_0 / \sin \alpha_1 , \bar{z} = z/L$$

Rotor passage:-

$$h = 1 - E^{-2.4\frac{-}{z}} + E^{0.25\frac{-}{z^2}} + E^{-0.5\frac{-}{z^3}}$$

$$E = \sin \beta_2 / \sin \beta_3$$

7. These equations are obtained according to the equivalent passage shapes of five sets of blade sections of a turbine stage in different heights.

8.4) The flow calculation in the gap between stator blade and rotor blade is performed as that in the duct of constant section. The inter-

row pressure for the stage has been determined on the base of throughflow calculation. 9.5) The local thermodynamic wetness loss coefficient  $\xi_{TX}$  and the thermodynamic wetness loss coefficient  $\xi_T$  of the blade are calculated by following equation

$$\xi_{TX} = \frac{T_{sx} \cdot \Delta S_x}{h_s}$$

where  $\Delta S_x$  is thermodynamic entropy increase from the blade inlet to the calculation point and  $T_{sx}$  the saturation temperature at the calculation point and  $h_s$  is the isentropic heat drop over the stage.

10. The outlet flow angles of non-equilibrium flow are determined using the continuity condition as follows:

$$\frac{\sin \alpha_{1ne}}{\sin \alpha_{1e}} = \frac{\rho_{1e} c_{1e}}{\rho_{1ne} c_{1ne}}$$

$$\frac{\sin \beta_{3ne}}{\sin \beta_{3e}} = \frac{\rho_{3e} w_{3e}}{\rho_{3ne} w_{3ne}}$$

11. Moreover, the mass flow coefficient  $\phi$  is defined by the ratio of actual mass flow rate to equilibrium mass flow rate.

### DISCUSSION OF RESULTS

12. Calculations are related to the primary wet steam stage of a 125 MW turbine set. For convenience, only the results for the mid-height section of the stage are selected for analysis. The expansion path is obtained on the base of design data and is plotted on the Mollier diagram in Fig.1. In order to reveal the effects

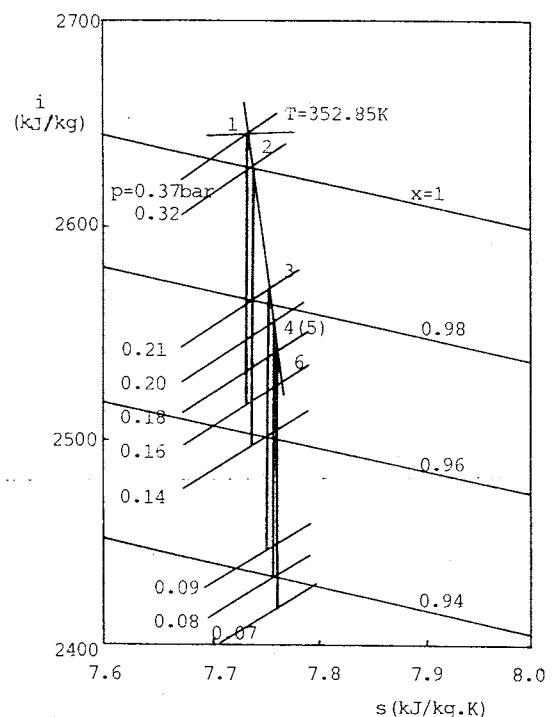


Fig.1. Steam inlet conditions and isentropic expansion lines

of steam inlet conditions on the non-equilibrium flow pattern, a range of different upstream stagnation pressures is chosen, while the overall pressure ratio of stage keeps nearly constant. In Fig. 1 the isentropic expansion lines related to these conditions are also given.

13. Table 1 presents the input data of steam inlet conditions and the overall results for supercooling, thermodynamic loss, wetness fraction and outlet flow angle etc..

14. Fig.2 shows the distribution of different flow parameters along the flow path in the stator and rotor passages. The numbers of lines in Fig.2 correspond to the numbers of expansion lines in Fig. 1.

15. Fig.2.(a) shows the Mach number distribution along the flow path for two limiting steam inlet conditions 1 and 6. They differ only slightly from each other. This fact implies that the effects of steam inlet conditions on the pressure ratio distributions are also small.

16. When the inlet steam flow is superheated or slightly supercooled (corresponding to the inlet conditions 1 and 2), it is clear from figs 2.(d) and 2.(e) that the steam remains dry and supercooled in the most part of blade passages. In this case, the influences of departures from equilibrium reflect mainly in the increase in mass flow coefficient and the decrease in outlet flow angle. Moreover, the differences between the non-equilibrium and equilibrium computational results increases with decreasing pressure at stage inlet.

Table 1 Input data and results

	No.1	No.2	No.3	No.4	No.5	No.6
$p_o$ (bar)	0.37	0.32	0.21	0.20	0.20	0.18
$T_o$ (K)	352.85	341.65	307.92	304.06	332.65	297.22
$y_o$ (%)	0.0	0.0	0.0	0.0	2.377	0.0
$\Delta T_o$ (K)		0.0	26.14	28.74	0.033	33.34
$r_o$ ( $\mu\text{m}$ )	0.0	0.0	0.0	0.0	0.588	0.0
$p_1$ (bar)	0.21	0.18	0.12	0.11	0.11	0.10
$\Delta T_1$ (K)	23.00	29.37	47.86	45.54	19.27	14.43
$y_{1e}$ (%)	2.173	2.751	4.543	4.701	4.701	5.048
$y_{1ne}$ (%)	0.0	0.0	0.286	0.725	3.777	3.569
$\phi_1$	1.021	1.03	1.058	1.047	0.97	0.978
$\alpha_{1e}$ (deg)	14.03	14.03	14.03	14.03	14.03	14.03
$\alpha_{1ne}$ (deg)	13.23	13.14	12.76	12.92	12.74	13.83
$\xi_{T1}$ (%)	0.0	0.0	0.762	1.618	0.328	2.389
$\Delta T_2$ (K)	23.00	29.35	2.40	2.10	19.27	14.43
$p_3$ (bar)	0.16	0.14	0.09	0.08	0.08	0.07
$\Delta T_3$ (K)	34.16	34.07	0.73	0.42	3.31	10.73
$y_{3e}$ (%)	3.196	3.848	5.595	5.795	5.795	6.114
$y_{3ne}$ (%)	0.001	0.587	4.855	4.710	5.792	4.799
$\phi_3$	1.012	0.999	0.949	0.949	0.948	0.953
$\beta_{3e}$ (deg)	23.59	23.59	23.59	23.59	23.59	23.59
$\beta_{3ne}$ (deg)	22.15	22.94	25.50	25.85	23.24	24.58
$\xi_{T3}$ (%)	0.0	2.145	0.965	0.296	1.066	0.977

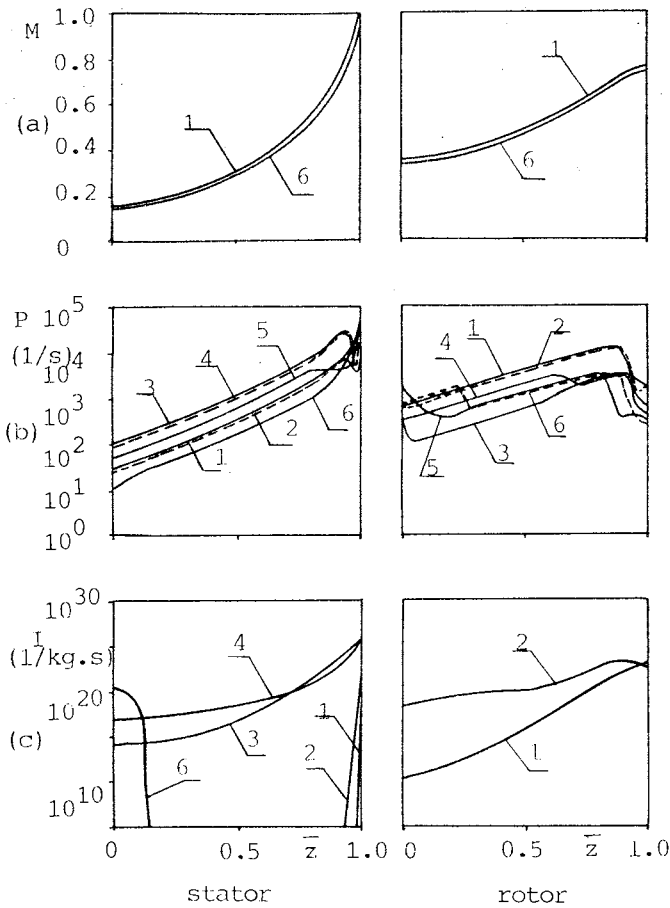


Fig.2 a-c. Distributions of flow parameters

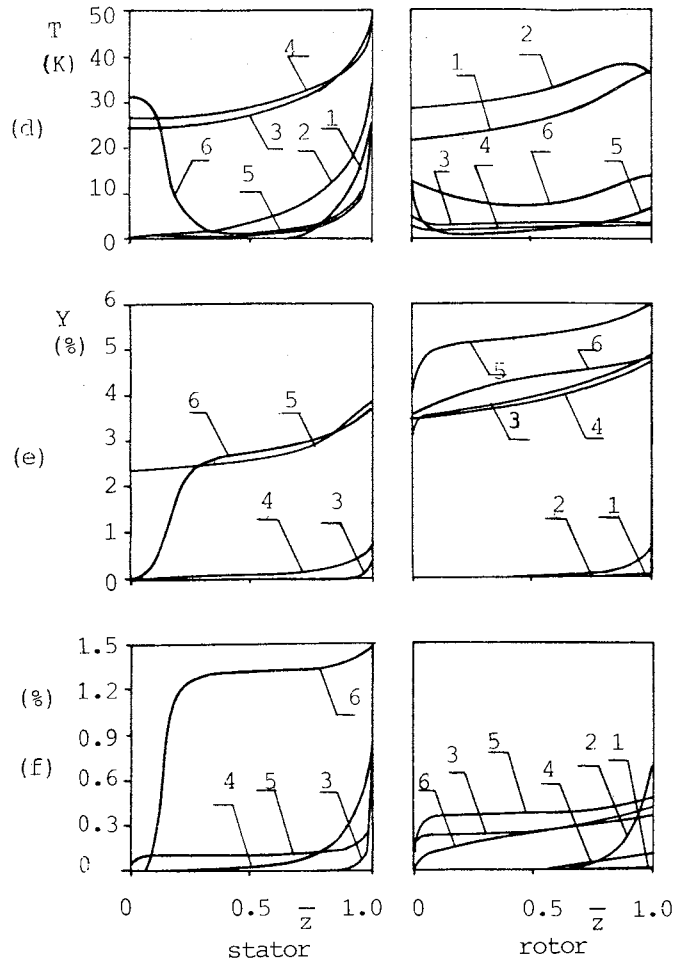


Fig. 2 d-f. Distributions of flow parameters

17. When the inlet steam is dry supercooled by 26.14 K and 28.74 K (corresponding to a wetness fraction 1.9% and 2.4% in equilibrium condition), the rapid nucleation zone occurs near the trailing edge of the stator blade and the supercooling rises to about 47.86 K and 45.54°C at the blade exit, but the wetness fraction is still negligible (see lines 3,4 in Figs 2.(c), 2.(d) and 2.(e)). Therefore, the steam stream in the stator blade passage remains fast dry supercooled. The mass flow coefficient of the stator blade passage rises to 1.058 and 1.047. In this case, the strong condensation occurs in the gap between stator and rotor blades. At the inlet of the rotor blade passage the steam state is close to equilibrium state with a residual supercooling of 2.4 K and 2.1 K. The steam flowing in the rotor blade passage remains nearly equilibrium, and the mass flow coefficient of the rotor blade passage is less than 1 due to the assumed aerodynamic losses.

18. In order to investigate the effect of departures from equilibrium at the stage inlet on the flow pattern, a wet equilibrium inlet steam flow at the upstream total pressure (0.2 bar) of calculation 4 is also assumed. The results are presented in Fig.2 by line 5. In contrast to the results of calculation 4, condensation occurs in stator blade passage, and the subcooling at stator blade exit is much smaller than that under the non-equilibrium

steam inlet condition. It will result in a significant decrease in mass flow coefficient of the stator blade passage. The difference between the mass flow coefficients of calculations 4 and 5 equals to 0.077. This comparison suggests that the magnitude of departures from equilibrium at the stage inlet is also an important factor for the stage performance. The fluctuation of subcooling of the inlet steam might induce a significant fluctuation of the discharge capacity of the stage, and this might result in the fluctuations of other stage performances, for example, the load and stress of the rotor blade.

19. In fact, the subcooling of the inlet steam depends on both the flow pattern in the preceding stage and the condensation process in the gap before stages, therefore, any fluctuation of supercooling due to the variation of operation conditions of turbine is possible.

20. When the inlet stream is dry supercooled by 33.34 K (corresponding to a wetness fraction 2.7% in equilibrium condition), strong condensation occurs immediately behind the stator blade inlet and result in a significant decrease in subcooling (see line 6 in Fig.2.(d)). The pattern of non-equilibrium flow downstream is then similar to that of calculation 5.

21. Fig 2.(f) shows the distribution of local thermodynamic loss along the flow path. It can be seen that there is a significant difference between the results under different steam inlet

conditions. When the strong condensation occurs at any position, the thermodynamic loss increases rapidly, for example, in the front part of the stator blade passage under the inlet condition 6. It is interesting to note that the main part of thermodynamic loss can be induced in the gap between the stator and rotor blade passage, for instance, in calculation 3 and 4. Therefore, the determination of velocity coefficient of the steam flow for the engineering calculation of a turbine involves complexity because of these facts.

22. It is worth noting that the variation of another flow parameters of inlet steam flow, for example, droplet size etc., can also affect the non-equilibrium flow pattern in stage. In this paper only a few examples for the variation of steam inlet conditions have been artificially chosen to reveal the complexity and multiplicity of the problem.

#### CONCLUSIONS

23.1) If the inlet steam is superheated or slightly supercooled and the overall pressure ratio of stage is moderate, the steam flow in the entire stage passage remains nearly dry supercooled. In this case, the influences of non-equilibrium character reflect mainly in the change of mass flow coefficient, the thermodynamic loss and the outlet flow angle. The differences between the results obtained from non-equilibrium and equilibrium calculations increase with decreasing inlet stagnation pressure.

24.2) If the steam inlet conditions are near to the Wilson zone a slight fluctuation of supercooling or stagnation parameters of inlet steam can produce a radical change of non-equilibrium flow pattern in the stator and rotor blade passage, and may result in significant fluctuation of the discharge capacity of stage, working temperature of blade, load and stress of blade etc. These effects might be responsible for the damage of blades working in the Wilson zone and also for the difference between the operation performances of the same type of turbines.

25.3) The condensation processes in the gap between the blade passages may play an important role for the reversion to thermodynamic equilibrium, and then result in the variation of non-equilibrium flow pattern in the following blade passages.

26.4) More theoretical and experimental investigations of non-equilibrium flow pattern in primary wet steam stage operating near the Wilson zone are required to further demonstrate the effects of steam inlet conditions on the turbine performance.

#### REFERENCES

1. YEOH C.C. and YOUNG J.B. Non-equilibrium curvature throughflow calculations in wet steam turbines. ASME Trans., Series A: Journal of Engineering for Power, 1982, vol. 104, no.2, April, 489-496.
2. YEOH C.C. and YOUNG J.B. Non-equilibrium throughflow analyses of low pressure wet steam turbines. AMSE Trans., Series A: Journal for Gas Turbines and Power, 1984, vol. 106, no.4, October, 716-727.
3. YOUNG J.B. and BAKTAR F. Non-equilibrium effects in wet steam turbines. Steam Turbines for Large Power Outputs, VKI LS 1980-06.
4. MOORE M.J. and SIEVERDING C.H. Aero-thermodynamics of low pressure steam turbines and condensers, McGraw-Hill, New York., 1987.
5. FILIPPOV G.A.; POVAROV O.A. and NICKOLSKY A.J. The steam flow discharge coefficient and losses in nozzles of a steam turbine stage operating in the low steam wetness zone. Aero-thermodynamics of Steam Turbines, ASME, 1981, 37-46.
6. YOUNG J.B. Critical conditions and the choking mass flowrate in non-equilibrium wet steam flows. ASME Trans., Series 1: Journal of Fluids Engineering, 1984, vol.106, no.4, December, 452-458.
7. MOORE K.J. and SIEVERDING C.H. Two-phase steam flow in turbines and separators, McGraw-Hill, New York., 1976.



## 25. An examination of the effect of 'wake chopping' on droplet sizes in steam turbines

F. BAKHTAR, PhD, DSc, FIMechE, Mechanical Engineering Department, University of Birmingham, and  
A. V. HEATON, BSc, PhD, The Electricity Council Research Centre (formerly of the University of Birmingham)

The paper presents an order of magnitude examination of the influence of "wake chopping" on the distribution of water droplets formed by homogeneous nucleation in steam turbines. It is shown that the fluctuations caused by the wakes can contribute substantially to the polydisperse nature of the droplet sizes and account for the coarse water observed in turbines.

### Introduction

1. The incidence of the vapour/liquid phase boundary in the operating range of steam turbines necessitates that some of the stages operate on wet steam. The wetness consists of a large number of minute droplets which are initially nucleated within and are generally carried by the flow. The formation and subsequent behaviour of these droplets lower the performance of the wet stages of the turbines and their effects on the efficiency are collectively known as wetness losses. Any realistic evaluation of the behaviour of the liquid phase or the flow requires information about the size of the droplets and this is an aspect which is still subject to considerable uncertainty. As a very major proportion of the power consumed by society is developed in steam turbine driven power stations, any progress in the understanding of these effects leading to an increase in the efficiency will yield handsome economic dividends.

2. With the availability of the nucleation theory and of large computers, theoretical treatments of two and three dimensional condensing flows in turbines are becoming available. Although the state of progress can be regarded as satisfactory, nevertheless these developments are still at an early stage. It is generally assumed that the coarse water present in the steam is a consequence of the deposition and re-entrainment of the fine droplets and the degree of agreement between the calculated droplet sizes and the deposition rates necessary to yield the observed coarse water is poor. The reason is partly that the theoretical treatments are based on idealized assumptions. For example, the steam used in turbines is assumed to be a pure vapour and its condition is regarded as uniform, whereas it is known that steam carries impurities resulting from water treatment and its temperature is subject to fluctuations caused by the effect of the wakes. This latter aspect is considered in this paper.

3. The wakes generated by one row of blades are disrupted by a succeeding row. The temperature fluctuations caused by this effect in aircraft axial compressors and turbines have been studied amongst others by (ref.1-5).

Similar fluctuations in temperature in the dry stages of axial flow steam turbines have been observed by Wood (ref.6) and studied by Suter and Gyarmathy (ref.7). In the case of a multi-stage turbine, temperature fluctuations resulting from this effect are comparable in magnitude with the temperature change associated with the stage heat drop. To examine the influence of these fluctuations on the distribution of droplet sizes formed due to nucleation, an order of magnitude analysis has been carried out which forms the subject of the present paper.

### Physical Model

#### 4.a. Case of the First Blade Row in Dry Vapour

The process of "wake-chopping" in an axial flow turbine may be illustrated with reference to the stator/rotor arrangement shown diagrammatically in Fig. 1. The shaded area represents the fluid contained in the wakes. On reaching the rotor, the tangential velocity component of the fluid contained in the wake will be less than the rotor velocity. Consequently the wake will be cut by the rotor. Because the fluid contained in the wake has suffered viscous dissipation its temperature will be higher than that of the fluid in the core of the flow which has expanded isentropically. Thus packets of fluid of higher temperature will exist within the flow giving rise to fluctuations in its temperature.

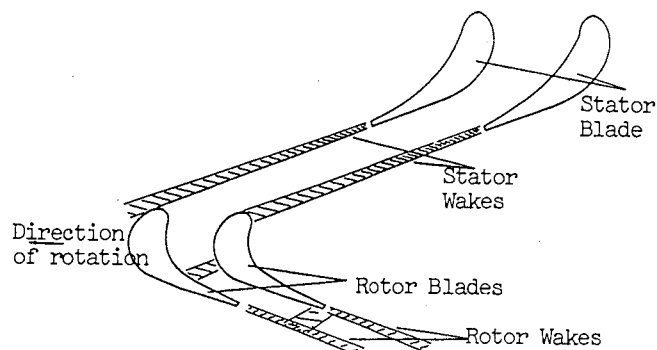


Figure 1. Wake Interaction in Turbomachines

5. The order of magnitude of the temperature changes associated with the formation of wakes in the first row of blades can be estimated by considering the velocity profile across the

pitch of the blade passage downstream of the row. In the ideal case the velocity is regarded as uniform everywhere and a packet of fluid entering the blade would have the same outlet velocity wherever it entered the row. In the real situation the outlet velocity of the packet (and hence its temperature) will depend on its inlet position. Assuming the expansion to be adiabatic, once the velocity profile is known the enthalpy profile follows directly.

6. In the present case it has been more convenient to work in terms of the dissipation. The local loss coefficient  $X_f$  is defined as

$$X_f = \frac{\Delta h_s - \Delta h_a}{\Delta h_s}$$

Where  $\Delta h_s$  and  $\Delta h_a$  are the isentropic and actual enthalpy drops for the fluid packet over the blade row respectively. If precise predictions were required, it would be necessary to obtain actual velocity traverses across the blade pitch and from them to construct the variations of the loss coefficient as a function of the inlet position of the packet. However, as only the order of magnitude of the changes is of interest a simple form can be assumed for the velocity distribution. The calculations have been carried out in relation to mid height blade sections where the flow is assumed to experience profile losses only and the efficiency of the expansion has been estimated to be in 94-95% range. To investigate the influence of the effect of the wake width, two separate dissipation profiles shown in Fig. 2 have been examined. Thus providing the position of each packet of fluid at inlet to the blade is known its probable outlet velocity and temperature can be estimated.

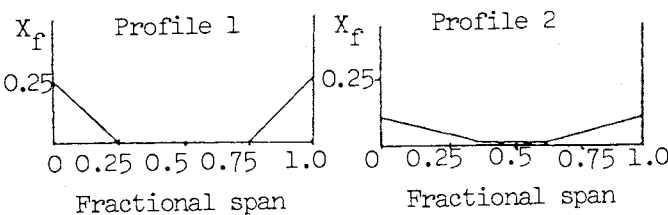


Figure 2 - Dissipation Profiles

**7. b. Case of Flow over the succeeding rows of blades**

In the case of the second and succeeding rows of blades the process of dissipation in the packets of fluids entering the row is similar but the temperatures of the individual packets will vary depending on whether or not they have been affected by the wake in the preceding row (or rows). Making assumptions about the blade efficiency the dissipation probability is similarly established. For each incoming packet its velocity relative to the rotor is calculated from the known outlet angle and velocity from the previous row and the rotor linear speed. The fluid stagnation enthalpy relative to the rotor is calculated from its known inlet static temperature and relative inlet velocity.

8. It is also assumed that for all the packets of fluid irrespective of their previous history the location at which they enter a row of blades is completely random.

9. With the dissipation profiles for the succeeding rows established the effect of the wakes in a multi-stage turbine can be

considered. Adopting the fractional pitch  $y/s$  as a measure of the location where a packet enters a blade row and using a random number generator to assign a value to  $y/s$  at entrance to the row each time, its probable outlet properties can be estimated. Consequently, by starting at inlet to the first row and working through the machine the probable inlet and outlet temperatures of the packet through the succeeding rows can be determined. By repeating the procedure for a large number of fluid packets, the pattern of the temperature changes within the machine can be established.

10. The above procedure is essentially the same as that used by Suter and Gyarmathy, who in particular applied the treatment to the conditions studied experimentally by Wood. Suter and Gyarmathy carried out their analysis with and without some allowance for the equalisation of the temperatures of the packets due to internal heat transfer within the flow. The results of the calculations without heat transfer were in better agreement with the experimental observations.

**Application to Nucleating Steam Flows**

11. If the state path of steam crosses the saturation line, the fluid is expected to supercool and then to nucleate. To investigate the influence of "wake-chopping" on the nucleation characteristics of the flow the behaviour of a large number of individual packets can be examined. The examination of the rate of expansion of steam in typical turbine blading indicates that the rate is not uniform. The expansion is slow in the entrance region but then accelerates very rapidly as the throat is approached. Thus, unless there is some good reason to the contrary, it would be reasonable to assume that if steam is not nucleating substantially at inlet to a row of blades it will continue to expand in a supercooled state until it reaches the throat. In the present investigation as the pressure drops over the individual blade rows have been sub-critical, and consistent with the simple physical model adopted, it has been assumed that the throat is at the blade outlet pressure. It also follows that the subsequent flow and mixing in the gaps between the blade rows is at constant pressure. Under these conditions the nucleation characteristics of the packets can be evaluated by using tabulated data on the reversion of steam. The tables have been calculated for steam flowing in a duct where because of the low flow velocity the pressure changes have been negligible (ref. 8). It has then been assumed that at inlet to the duct specified amounts of supercooling have been imposed on the steam and its subsequent reversion to thermodynamic equilibrium tabulated. Of particular interest are the eventual size and the number of water droplets formed and the time taken by the fluid to progress through particular stages of reversion.

12. To examine the influence of wake chopping on the reversion characteristics of the packets the dissipation probabilities are established for the individual blade rows in a similar manner to that for the dry stages. Then taking any fluid packet of known pressure and

temperature at inlet to a row, its degree of supercooling is evaluated. If the packet is not nucleating substantially, it is assumed that it will continue to expand in a supercooled state until it reaches the end of the row. With the packet inlet position and hence the outlet conditions known, the degrees of supercooling at the outlet from the blade are estimated. With the known gap axial distance and the flow axial velocity, the time taken by the fluid to traverse the gap and reach the next blade row is determined. This would be the time available for the packet to regain thermodynamic equilibrium. Having already established the pressure and temperature of the fluid at inlet to the gap, reference to the tabulated results will provide a ready estimate of whether or not the available time is sufficient to revert the flow. If the nucleation rate is not substantial the procedure is continued through the next row. Once the supercooling is sufficient to revert the flow the tabulated results give the droplet size and the corresponding wetness fraction directly. The number of droplets per unit mass and droplet sizes at other wetness fractions can be calculated directly from this information. The procedure is then repeated for a large number of fluid packets.

**Results of the Analysis**

**13. a. Analysis of a Dry Test** The calculations have been carried out in relation to a four stage 50% reaction turbine originally described by Smith (ref. 9). Initially a test has been considered in which the fluid has been superheated throughout the expansion and the analysis performed for 10,000 fluid packets. The overall pressures are given in Table (1). The inlet stagnation temperature has been 312.8°C. The probability distribution of the enthalpy changes of the packets expressed as a fraction of the overall machine enthalpy drop associated with the two dissipation profiles considered are shown in Fig. 3. The mean conditions for the rows are indicated by dotted lines. The fluctuations represent temperature variations of  $\pm 15K$  from the mean values.

**14. b. Analysis of the nucleating flow** Conditions were next considered of the inlet temperature lowered to 148°C whilst maintaining the same pressure levels. Starting with the first row of blades and using the procedure outlined above once again the reversion characteristics of 10,000 fluid packets were examined. The flow was found to revert after two stages. The probability distribution of nucleation currents for the packets are plotted in Fig. 4 and the final distributions of the droplet sizes for each of the dissipation profiles adopted are given in Fig. 5.

**Table 1 Overall Pressures**

Location	Pressure bar
Machine inlet total	1.2
Stage 2 inlet static	.66
Stage 3 inlet static	.32
Stage 4 inlet static	.15
Machine outlet static	.044

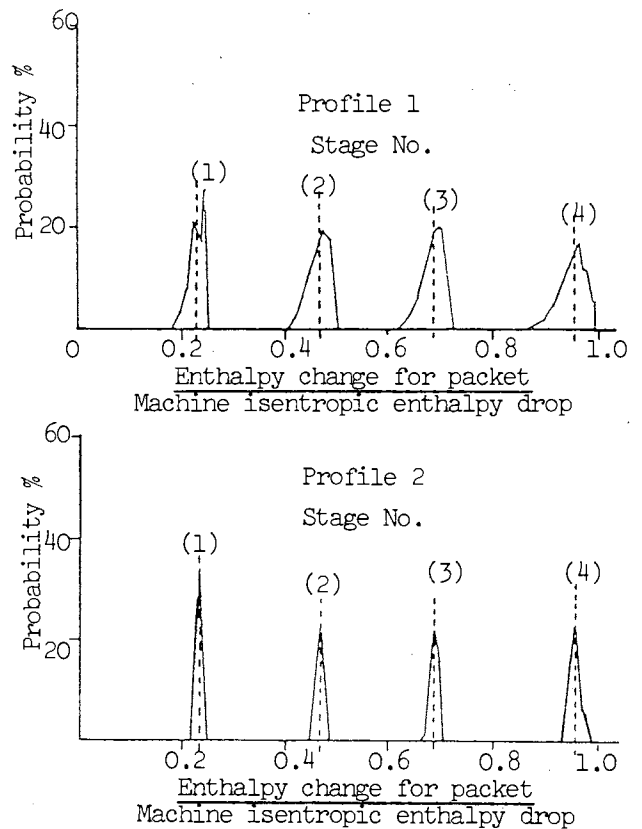


Fig. 3. Probability Distribution of Normalised Enthalpy changes of packets.

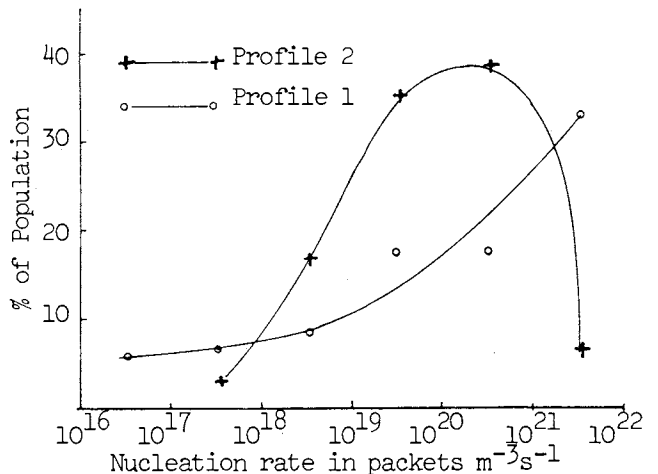


Figure 4. Probability Distribution of Nucleation Rate in Packets

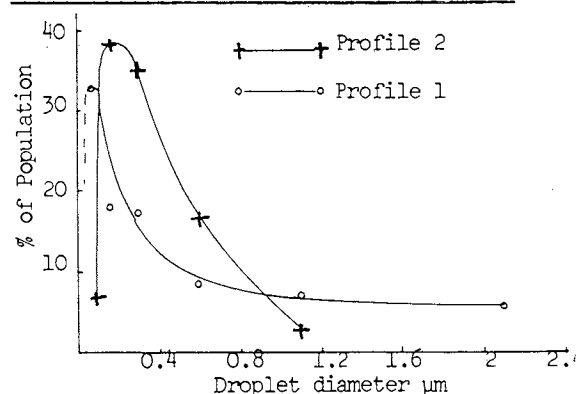


Figure 5. Probability Distribution of

Discussion and Conclusions

15. It is accepted that the method is approximate but the number of fluid packets examined was sufficiently large for the general effect of wake chopping on condensing flows to be correctly indicated. For example the polydisperse nature of the distribution is well produced.

16. Of particular interest is the deposition rate of nucleated droplets in steam turbines. Deposition of water droplets on turbine blading has been studied in the literature by Crane (ref.10) and by Parker and Lee (ref.11) amongst others. The measurements by Parker and Lee are concerned with droplets of  $0.2\mu\text{m}$  and smaller diameters where the deposition rates are small. The calculations by Crane indicate negligible deposition rates for droplets smaller than  $0.7\mu\text{m}$  diameter above which the rate increases drastically. Theoretical solutions of condensing flows in turbines (refs.12-14) generally indicate the resulting droplets to be fractions of a micron in diameter with low expected deposition rates. The measurements of coarse water distribution in operating steam turbines by Williams and Lord (ref.15) indicate 5-7% of the moisture to be in the form of coarse droplets. If it is accepted that the coarse water present in turbines results from the re-entrainment of the deposited droplets, it would appear that the degree of agreement between the droplet sizes predicted by the theoretical solutions and those necessary to produce the observed coarse water is unsatisfactory.

17. Now considering the distribution curves predicted by the present order of magnitude analysis, it will be seen that the peaks of the distribution curves shown in Fig.5 occur at droplet diameters of  $0.1$  and  $0.2\mu\text{m}$  for profiles 1 and 2 respectively. The disparity indicates the sensitivity of the detailed results to the assumptions employed. Nevertheless both these values are in the size range which would be expected to have a low collection efficiency and are comparable with the sizes predicted by the more rigorous theoretical solutions. On the other hand, particularly in the case of the distribution curve for profile 1, over 12% of the liquid will be in the form of droplets with diameters larger than  $1\mu\text{m}$  which have a substantial collection efficiency. Because of the approximate nature of the present method no detailed calculations of deposition rates for the resulting droplets have been carried out. It can, however, be seen that the deposition of the larger droplets in the spectrum caused by wake chopping can account for some of the observed coarse water.

18. It is also of interest to note that despite the simple nature of the treatment, the bulk of the nucleated droplets are in a size range which corresponds with those predicted by the more rigorous treatments. Remembering that the larger droplets are prone to deposition on the blade surfaces it would be reasonable to expect them to have a small influence on the overall behaviour of the flow. The bulk of the fluid must be, therefore, dominated by the vast majority of the droplets which are in the small size range.

Acknowledgements

The investigation described in the paper was carried out in the Department of Mechanical Engineering, University of Birmingham and supported by a grant from the Science and Engineering Research Council.

References

1. Kerrebrock, J.L. and Mikolajczak, A.A. "Intra-stator Transport of Rotor Wakes and Its Effect on Compressor Performance", *Jl. of Engineering for Power*, ASME, October 1970, 359.
2. Gallus, H.E. Bohn, D. Broichhansen, K.D., "Measurements of Quasi-steady and Unsteady Flow Effects in a Supersonic Compressor Stage", *Jl. of Engineering for Power*, ASME, October 1977, 537.
3. AGARD Conf. Proc. "Unsteady Phenomena in Turbomachinery" Monterey, Calif, September 1975.
4. Binder, A., Forster, W., Kruse, H. and Rogge, H., "An Experimental Investigation Into the Effects of Wakes in the Unsteady Turbine Rotor Flow". *Jl. Engg. for Gas Turbines and Power*, ASME, 1985, 107, 458.
5. Ashworth, D.A., La Graff, J.E., Schultz, D.L. and Grindrod, K.J., "Unsteady Aerodynamic and Heat Transfer Processes in a Transonic Turbine Stage", *Jl. Engg. for Gas Turbines and Power*, ASME, 1985, 107, 1022.
6. Wood, N.B. "Flow Unsteadiness and Turbulence Measurements in the Low Pressure Cylinder of a 500 MW Steam Turbine", *Inst. Mech. Engrs.*, London, Conf. Pub. 3, 1973.
7. Gyarmathy, G. and Spengler, P., "Flow Fluctuations in Multi-Stage Thermal Turbomachines" Traupel-Festschrift, Juris-Verlag, Zurich, 1974.
8. Bakhtar, F. and Webb, R.A. "A Tabular Method of Estimating Nucleating Steam Flows", *Int. Jl. Ht. and Fluid Flow*, Vol. 4, No. 4, 1983.
9. Smith, A., "The Influence of Moisture on the Efficiency of One-Third Scale Model Low Pressure Steam Turbine", *Proc. Inst. Mech. Engrs.* 180, Pt.31, 1965-66.
10. Crane, R.I., "Deposition of Fog Drops on Low Pressure Steam Turbine Blades" *Int.J.Mech.Sci.*, 1973, Vol.15.
11. Parker, G.J. and Lee, P. "Studies of the Deposition of Submicron Particles on Turbine Blades" *Proc. Inst. Mech. Engrs.* Vol. 186 38/72 1972 pp 519-526.
12. Bakhtar, F. and Mohammadi Tochai, M.T. "An Investigation of Two-Dimensional Flows of Nucleating and Wet Steam by the Time Marching Method". *Int. Jnl. Ht & Fluid Flow* Vol.2. No.1, 1980.
13. Bakhtar, F. and Heaton, A.V., "On the Dissimilarities in Wet Steam Behaviour in Model and Full Scale Turbines, Proc. BNES Conference "Technology of Turbine Plant Operating with Wet Steam, London 1988.
14. Haller, B.R., Unsworth, R.G., Walters, P.T. and Lord, M.J. "Wetness Measurements in a Model Multistage Low Pressure Steam Turbine", *Ibid.*
15. Williams, G.J. and Lord, M.J. "Measurement of Coarse Water Distribution in the L.P. Cylinders of Operating Steam Turbines", *Proc. Instn. Mech. Engrs.* Vol. 190, 4/76, 1976.

# 26. Fog droplet size measurement and calculation in wet steam turbines

A. KLEITZ, A. R. LAALI, MSc, PhD, and J. J. COURANT, BSc, Electricité de France

## 1 - INTRODUCTION

Despite of improvements in the design of large modern turbines to reduce harmful wetness, the problem of erosion especially on the last LP blades has not yet been solved. Moreover, the feedback of experience is still not sufficient to be able to predict the trend of erosion over the entire lifetime of the power stations.

It is a well known fact that progress in this field necessitates the use of a reliable model of the trend of wetness inside the turbine, especially for primary fog formation.

Many complex phenomena act in the formation and growth of droplets during steam expansion in a turbine. Some of these phenomena are still not well known. The recent measurement of fog droplet size carried out at the exhaust of EDF LP turbines reveals the existence of a bidispersed fog drop size distribution. The first ranges from 0.1 to 0.5  $\mu\text{m}$  and the second from 1 to 2  $\mu\text{m}$ . The mass flow rate corresponding to each dispersion is strongly dependent on admission thermodynamic conditions and to some extent on water treatment in power station.

The improvement in internal water extraction devices such as draining belts and suction slots requires knowledge of the deposition of fog droplets. The rates of deposition corresponding to each of the dispersions mentioned differ to a considerable extent. It is therefore of particular interest to secure knowledge of the origin of these fog dispersions.

This paper presents the results of droplet size measurements and calculations, carried out on a 5 MW test and a 900 MW PWR low pressure turbine. The calculations performed by a computer program based on the classical condensation theory grafted on the mean expansion line, justify the presence of the first dispersion (0.1 to 0.5  $\mu\text{m}$ ). These computations could also prove the existence of the second dispersion created only by truncated shock, but the measurements does not always confirm this hypothesis.

## 2 - SUMMARY OF THE THEORETICAL APPROACH

Based on the classical spontaneous condensation theory, a numerical code has been developed to

compute the wet steam flow in a turbine (ref. [1]).

The method consists of grafting the nucleation theory and the droplet growth model on pressure and velocity field of a stream tube resulting from a turbine throughflow calculation. Prior throughflow calculation, based on a streamline curvature method is performed with the assumption of equilibrium wet steam (ref. [2] and [3]).

It is assumed that the delay in wetness formation does not modify both pressure and velocity but only temperature change. The slip between steam and droplets is supposed to be negligible.

### 2.1 Basic equations

The three conservation equations are developed to compute the steady adiabatic flow of condensing steam through a stream tube.

Mass conservation

$$Q_0 = Q'' + Q' \\ dQ'' + dQ' = 0 \quad (1)$$

Momentum conservation :

$$\rho V \cdot dV + dP = 0 \quad (2)$$

Energy conservation :

$$dh + VdV = 0 \quad (3)$$

The equation of state for equilibrium and non-equilibrium wet steam is derived from a computer program [4]. The specific enthalpy and specific volume for wet steam are given by :

$$h = \eta h'' + (1-\eta)h' \quad (4)$$

$$v = \frac{1}{\rho} = \eta v'' + (1-\eta)v' \quad (5)$$

The differential form of equation (4) is :

$$dh = \eta dh'' + (1-\eta) dh' + (h''-h') d\eta \quad (6)$$

Rearranging the equations leads to :

$$dh'' = \frac{[v - (1-\eta) dh'/dp]dp - (h''-h') d\eta}{\eta} \quad (7)$$

## FLOW ANALYSIS AND MEASUREMENT

The created water  $dQ'$  consists of two components:  $q_1$ , the water formed by nucleation of drops of critical radius ( $r_c$ ) and  $q_2$ , the water condensing on existing drops:

$$dQ' = (q_1 + q_2) dx$$

$$dn = \frac{dQ''}{Q_0} = - \frac{(q_1 + q_2)}{Q_0} dx$$

$$q_1 = A J \rho' \frac{4\pi}{3} r_c^3$$

The critical radius is given by the Kelvin formula:

$$r_c = \frac{2\sigma}{\rho' R T L_n(p/p_S)}$$

The nucleation rate can be calculated using the Wolmer and Frenkl formula:

$$J = \sqrt{2\sigma N^3/\pi} \frac{\rho''}{\rho'} \exp. (-4\pi \sigma r_c^2 N/3RT)$$

The droplet growth or the rate of condensation on a drop is governed by the rate at which the latent heat can be transferred from the surface to the cooler steam. This is given by the Gyermathy formula:

$$\dot{m} = \frac{dm}{dt} = 4\pi r^2 \cdot \frac{\lambda}{L} \frac{(1 - r_c/r)}{r+1,59 \bar{l}} \cdot \Delta T$$

with:

$$\Delta T = T_S(p) - T_{\text{steam}} \quad T_{\text{steam}} = f(h', \rho)$$

$L$ : latent heat

$$\bar{l} = 1,5 \mu \frac{\sqrt{RT}}{\rho} \quad (\text{mean free path length})$$

The water condensing on existing drops is then:

$$q_2 = \frac{1}{V} \int dx \dot{m}(x, x_0 - J(x_0)) A(x) dx$$

All parameters of the differential equation (7) could then be calculated. A fourth order Runge-Kutta method is used to solve the equation.

The main advantage of this method is to calculate the droplet formation and growth on any pre-calculated stream tube without a numerical wet steam flow choking problem.

### 3 - MEASUREMENT OF FOG DROPLET SIZE

The fog droplet size is measured using a probe based on a classical extinction technique. A brief description of the method and the probe is given below.

#### 3.1 Summary of the extinction technique

A monochromatic light beam crosses polydispersed droplet suspension. The transmittance ( $I/I_0$ ) is a function of droplet size and concentration given by the following relation:

$$C(\lambda_j) = \text{Log} \left( \frac{I_0}{I} \right)_j = \pi L \sum_i r_i^2 n(r_i) K(r_i, \lambda_j) \quad (8)$$

where:  $I$  and  $I_0$  are the light intensities before and after crossing a droplets suspension for different wavelengths.

$n(r_i)$  is the number of droplets of radius  $r_i$ .

$K(r_i, \lambda_j)$  is the extinction coefficient given by Pendorff calculations based on the Mie theory.

$L$  is the crossing length.

An inversion method [5] similar to the one used by Walters [6] has been developed to obtain the droplet size from the measured data.

The summary of this method is given in Appendix 1. A less sophisticated method has also been used (see Appendix 2). All these methods have shown, in contrast to previous investigations, that primary fog in steam turbines could be determined with a good degree of approximation by a bi-dispersed distributions ( $N_1$

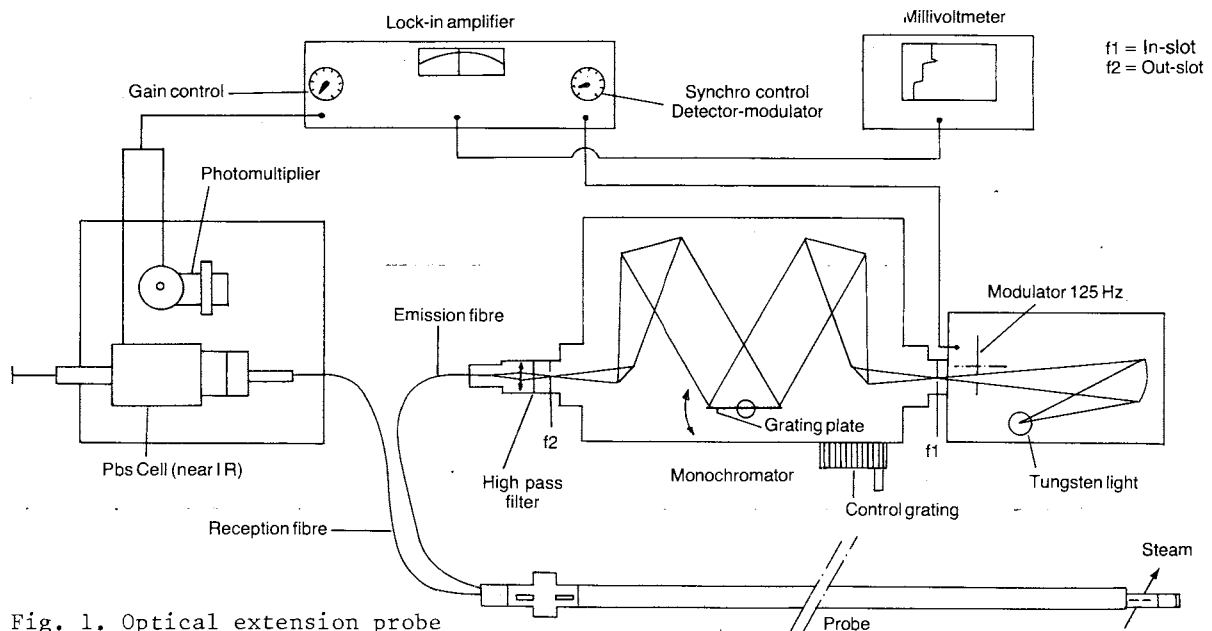


Fig. 1. Optical extension probe

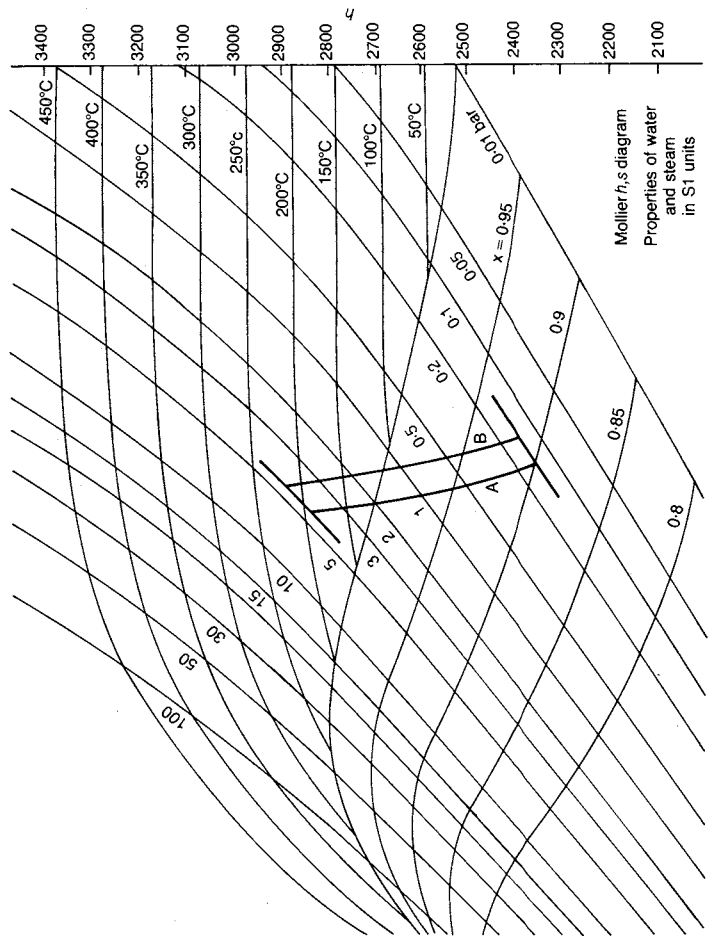
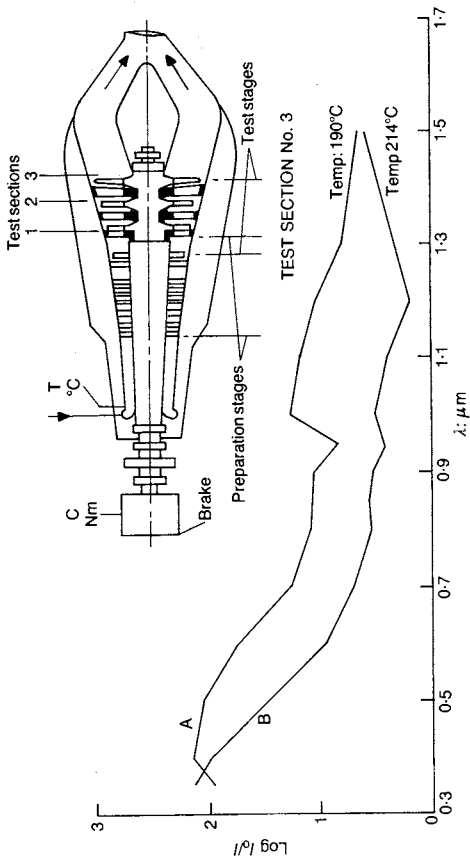
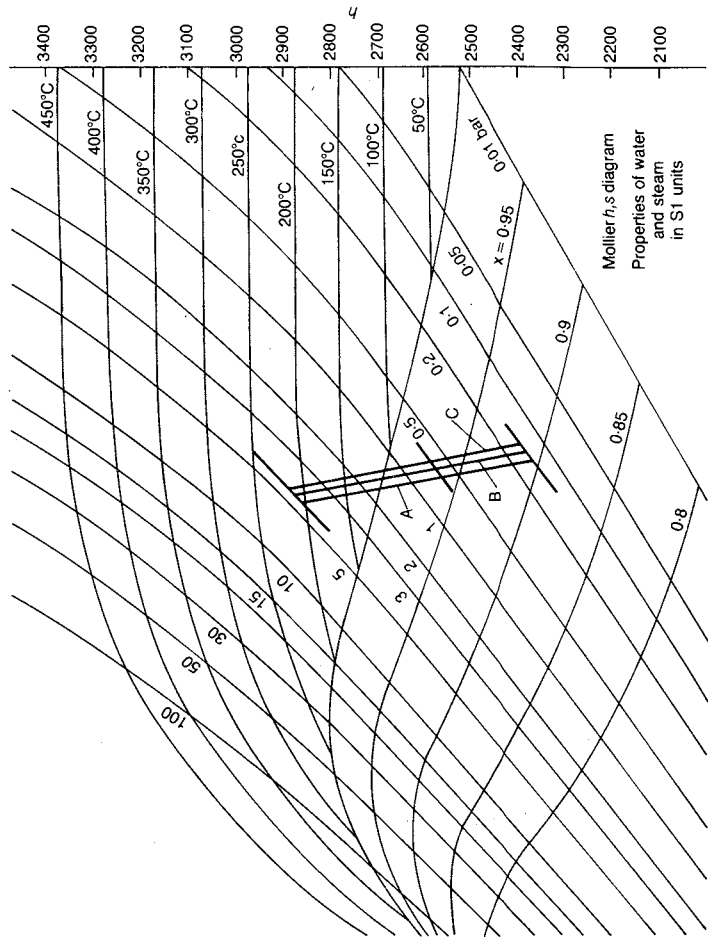
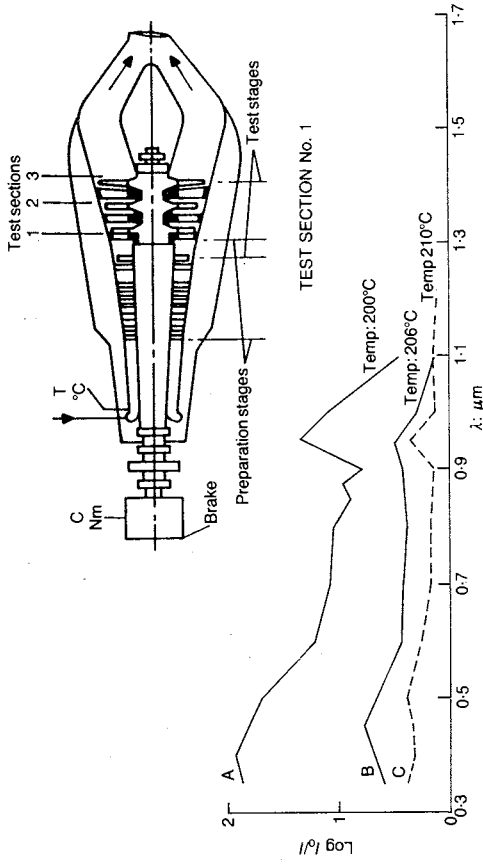


Fig. 3. Temperature influence

Fig. 2. Condensation shock appearance

## FLOW ANALYSIS AND MEASUREMENT

droplets of mean radius  $r_1 = 0.1$  to  $0.5$  and  $N_2$  droplets of mean radius  $r_2 = 1$  to  $2 \mu\text{m}$ ). This is essentially due to the large width of the spectral band.

### 3.2 Description of the optical probe

The optical probe developed for the application of the steam turbines is shown in Figure 1. The special feature of this probe is the width of the spectral band. The measurements could be performed within a wavelength range of  $0.35$  to  $1.8 \mu\text{m}$ . It is hoped that this range will be increased to  $5 \mu\text{m}$  in I.R. in the near future.

The optical system has been incorporated in a  $25 \text{ mm}$  diameter probe. The wet steam flows through a slot whose length varies between zero and  $200 \text{ mm}$ . Purge air is blown on both ends of the slot to prevent the deposition of droplets on the sapphire windows. The light source is obtained from a tungsten lamp via a monochromating system of interchangeable grating plates.

It is then channelled through the probe by a flexible  $1 \text{ mm}$  silica optical fiber. The detection component is a photomultiplier for the visible light ( $0.4$  to  $0.7 \mu\text{m}$ ) or a Pb S cell for I.R. ( $0.8$  to  $2 \mu\text{m}$ ).

## 4 - RESULTS

The measurements are carried out on a  $5 \text{ MW}$  wet steam test turbine (TEVH) and a low pressure  $900 \text{ MW}$  nuclear turbine (Fessenheim). The measurements are compared with the computed results.

### 4.1 The TEVH test turbine

The TEVH is a low pressure eight stage turbine fed with superheated steam. The first five stages prepare the steam for the last three wet stages which are used to conduct experiments. The full load thermodynamic conditions are :

Inlet pressure	: 4,3 bar
Inlet temperature	: $200^\circ\text{C}$
Mass flow rate	: $12,5 \text{ K/s}$
Outlet pressure	: $150 \text{ mbar}$

The first set of experiments is carried out in test section number 1 located upstream of the sixth fixed wheel. The results are shown in Figure 2. The turbine admission temperature varies from  $200$  to  $210^\circ\text{C}$ . There is a slight extinction at the admission temperature  $210^\circ\text{C}$  in this section. When the temperature is reduced, the thermodynamic conditions of the section are below the Wilson line. The increase in extinction shows the appearance of the condensation in this section at the Wilson line.

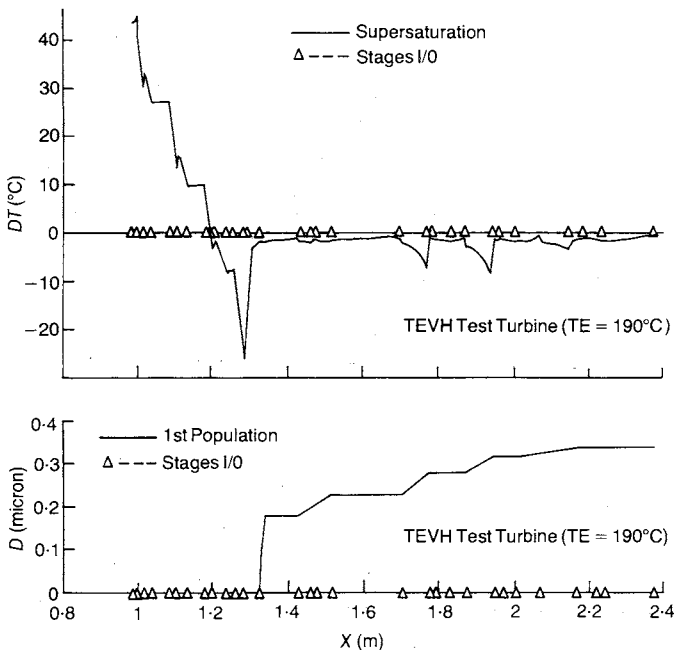


Fig. 4. (a) Supersaturation variation; and (b) droplet radius variation

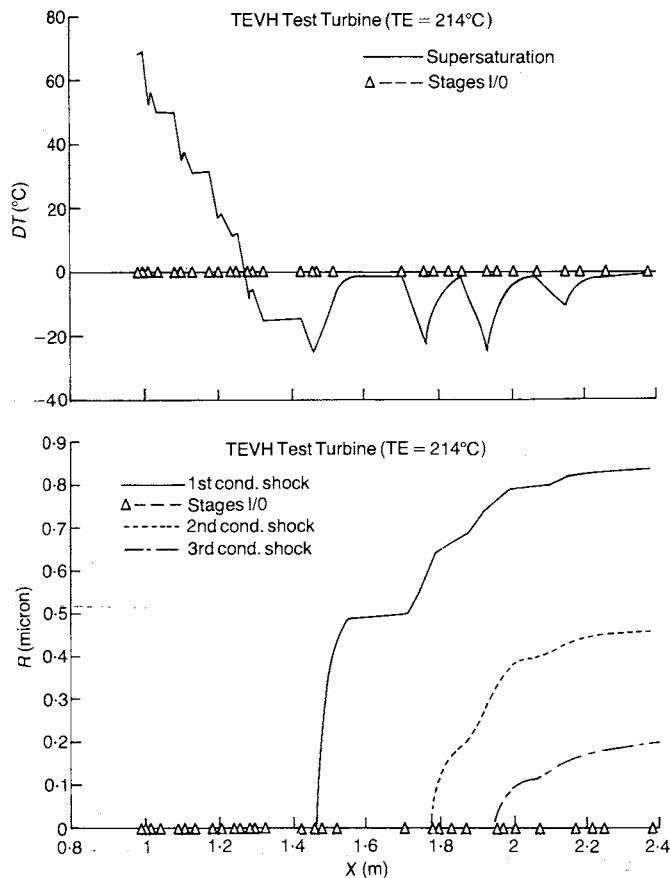


Fig. 5. (a) Supersaturation variation; and (b) droplet radius variation

Figure 3 shows the influence of admission temperature on the size of fog droplets at turbine exhaust (curves A, B). The results are shown in the table below :

	Droplet radius $\mu\text{m}$	Wetness distributions
A	0,20	33 %
	0,85	67 %
B	0,25	75 %
	1,10	25 %

An attempt has been made to show the existence of the bi-dispersions by calculating the condensation on the mean expansion line of the turbine. For an admission temperature 190°C one condensation shock is substantial enough to create fog droplets. Figure 4 shows supersaturation and droplet growth in the turbine. A droplet radius of 0,34  $\mu\text{m}$  is found at turbine exhaust. The calculation carried out on other stream tubes provide the same results.

If the admission temperature is increased to 214°C in the computation (Figure 5), three condensation shocks will appear in the turbine. The first one is truncated and the resulting droplets are relatively large (0,84  $\mu\text{m}$  at turbine exhaust). The second and third condensation shocks create smaller droplets with a radius of 0,2 to 0,46  $\mu\text{m}$ .

4.2 Fessenheim nuclear 900 MW LP turbine

Some measurements have been taken upstream of the rotor blades of the last stage of the LP turbine at the Fessenheim power plant. The position of the probe varies from the top to the middle of the blade. The results are shown in the table below :

Position	Droplet radius $\mu\text{m}$	Wetness distributions
1 (top)	0.2 to 0.5	40 %
	1 to 2	60 %
2	0.4	55 %
	1.5 to 2	45 %
3	0.3 to 0.5	90 %
	2	10 %
4	0.3 to 0.5	65 %
	2	35 %
5 (middle)	0.18 to 0.5	90 %
	1.3	10 %

The result of calculations for the middle stream tube taken are shown in Figure 6. The fog droplet radius at the exhaust of the turbine reaches 0,5  $\mu\text{m}$ . At the normal thermodynamic conditions at full load it is not possible to compute the second dispersion with a radius of 1 to 2  $\mu\text{m}$ .

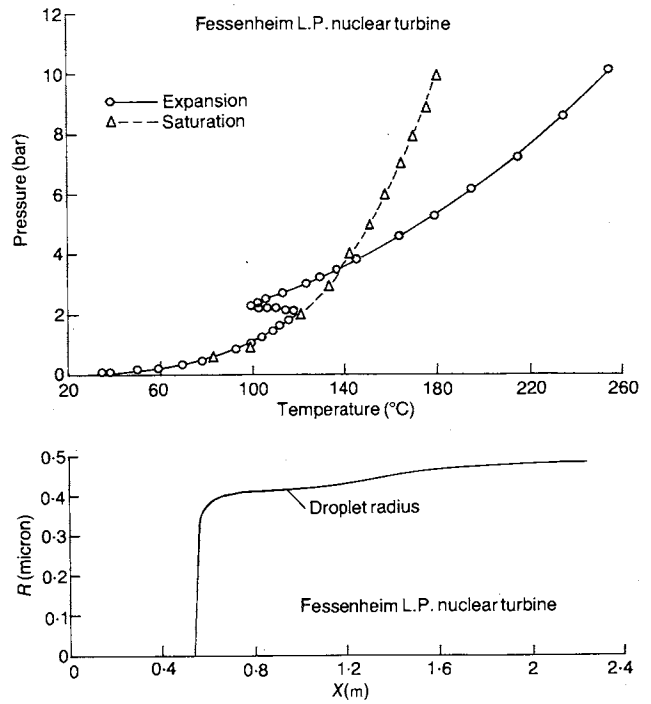


Fig. 6. (a) Pressure - temperature variation; and (b) droplet radius variation

5 - CONCLUSION

Measurements fog droplet size in turbines have clearly shown the existence of two distinct dispersions of variable quantity depending on the steam supply characteristics.

By comparing these experiments and the results of computations it is found that the first dispersion, and sometimes the second, could be predicted with accuracy by the classical nucleation theory. In fact, many parameters contribute to create this second dispersion whose deposition rate is much more substantial than the first.

To study the origin of different fog droplet dispersions, the authors propose a new test facility. It consists of cylindrical two stage rotating cascades simulating a stream tube of an actual LP steam turbine. The observation windows installed on the cylindrical casing allows measurements to be performed between the blades.

APPENDIX 1 : INVERSION METHOD

The integral form of the extinction equation is :

$$C(\lambda) + \epsilon = \pi \int_0^\infty r^2 K(r, \lambda) n(r) dr \tag{1}$$

The distribution function  $n(r)$  has to be determined using a set of measurements of transmittance  $C(\lambda)$ . This is a Fredholm first degree equation and  $\epsilon$  is the measurement error.

This equation is badly conditioned. Very little change in  $\epsilon$  could lead to a major variation of the distribution function. There is no precise solution to this problem. Only approximate solutions can be provided.

## FLOW ANALYSIS AND MEASUREMENT

The integral equation (1) has been discretized using a Gaussian quadrature with a large number of points. It can then be written :

$$C(\lambda_i) + \epsilon_i = \sum_j w_j K(\xi_j, \lambda_i) N(\xi_j)$$

where  $w$  and  $\xi$  are respectively the weights and abscissa of the Gaussian quadrature. The linear system to be solved is :

$$AZ = B + \epsilon \quad (\text{matrix form})$$

$$\text{with : } A = \sum_i \sum_j A_{ij} = W_j K(\xi_j, \lambda_i)$$

The problem is solved using the Tikhonov (or Phillips - Twomey) inversion formula :

$$A^t A Z + \gamma Z = A^t B$$

where  $\gamma$  is a parameter which controls the amount of smoothing required to eliminate the unwanted oscillations.

To calculate a bi-dispersion distribution (see also Appendix 2) it is assumed that the small size droplets dominate the extinction at short wavelengths. The half of the measured values are therefore inverted separately to provide the first dispersion. The extinction is then calculated for this dispersion over the whole spectral range. This calculated extinction is then deduced from the measured one and the result is inverted to provide the seconde dispersion.

### APPENDIX 2 : SIZE DISTRIBUTION - FIRST APPROXIMATION

The first approximation of size distribution has been obtained by minimizing the error function :

$$S = \sum_{\lambda} [C(\lambda) - \sum_j n(r_j) r_j^2 K(r_j, \lambda)]^2$$

assuming the general form of size distribution. Physical limitations have been introduced to accelerate the convergence of the program:

The droplet size ranges from 0.1  $\mu\text{m}$  (due to spontaneous condensation calculations) to 2  $\mu\text{m}$  (limited growth of any condensation droplets inside the turbine). The total wetness must be roughly the same as the equilibrium wetness determined by the turbine expansion line.

Several distributions have been tested (Nukyama, Log-normal, ...). The most suitable feature was provided by a bi-distribution (or sometimes a three-distribution) even represented by a discrete distribution ( $N_1$  droplets of radius  $r_1$  and  $N_2$  droplets of radius  $r_2$ ).

## NOTATION

A	cross section
h	specific enthalpy
I	light intensity
J	number of droplets per unit mass of wet steam
N	number of molecules per unit mass of vapour
m	mass flow rate
P	pressure
$P_S$	saturated pressure
$Q_0$	total mass flow rate
$Q'$	water mass flow rate
$Q''$	steam mass flow rate
r	droplet radius
R	gas constant
T	temperature
V	velocity
v	specific volume of wet steam
$v'$	specific volume of water
$v''$	specific volume of steam
x	coordinate
$\alpha = \frac{2\pi r}{\lambda}$	particle size parameter
$\eta$	dryness fraction
$\rho$	density
$\mu$	dynamic viscosity
$\sigma$	surface tension

## REFERENCES

1. KLEITZ A. - LAALI A.R. - MARTY C. Rapporteur LAALI A.R. Programme de calcul de condensation spontanée à partir d'une loi de détente. EDF Report P44/D01/86/1.1, July 1986
2. BIRR-MEZA C. - HUVET P. Calcul des turbines transsoniques. Comparaison analytique des méthodes matricielle et de courbure de la ligne de courant. EDF report HP316/H01/82.01, February 1982.
3. BIRR-MEZA G. - GRISON P. Through flow analysis in large low pressure turbine at off design condition. Institution of Mechanical Engineers, September 1987.
4. LUX F. - PERRIN M. Programme de calcul des propriétés de l'eau et de la vapeur d'eau (états stables et métastables). Programme PROMEE.
5. LALLEMAND M. Détermination de la distribution de taille de gouttes par inversion des mesures spectrales de coefficients d'extinction. EDF-ENSMA Contract. Final report, June 1987.
6. WALTERS P.T. Wetness and Efficiency Measurements in L.P. turbines with an optical probe as an aid to improving performance. ASME/IEEE Power Generation Conference Milwaukee, October 20-24, 1985.
7. PEREZ G. - TALLEU P. Evaluation de la taille des gouttes d'eau dans une vapeur humide. EDF Report P32/D07/85/1.2

# 27. Improving the accuracy of wetness measurements in generating turbines by using a new procedure for analysing optical transmission data

P. T. WALTERS, BSc, Central Electricity Research Laboratories

The calculation of the wetness in steam flows from spectral transmissions measured in LP turbines with an optical probe is described. It is shown however that the linear inversion process used underestimates the wetness when the distribution of droplet size is bimodal. A new procedure is then described which detects bimodality in the optical data and when this occurs calculates the wetness contributed separately by each mode. Examples of measurements in operational generating turbines are presented finally to demonstrate the improved accuracy of performance diagnostics based on wetness levels calculated by the new process.

## INTRODUCTION

1. Although steam turbines have been operating with wet flows for about 80 years relatively little is known in detail about the effect of wetness on stage performance. At a time when computer programs of ever increasing sophistication are being developed to model the aerodynamics of turbomachinery, the wetness input to steam turbine design codes has not progressed beyond the simple Baumann Rule loss correlation dating from 1912 (ref. 1).

2. Essentially this is because no real progress could be made in this field when neither the efficiency of the stages in the wet zone of the turbine nor the wetness level of the flow could be measured directly.

3. Recently however this situation has been potentially improved by the development of the CERL optical wetness probe (ref. 2). This instrument is traversed between the stages of LP turbines to provide radial distributions of wetness, and hence enthalpy flux, at a series of axial stations within the machine leading up to and including the exhaust plane. In principle therefore the efficiency of any wet stage within a large steam turbine is now accessible to measurement. From the results obtained to date some surprising departures from the conventional view of wetness loss have been observed; the most significant being the reduced efficiency of the stage, where spontaneous condensation begins, that has been detected in many units (ref. 3).

4. The optical measurement of wetness is a classical example of indirect sensing in that the spectral transmission detected by the probe represents the known light scattering power of small droplets integrated over an unknown distribution of droplet size. Obtaining a wetness value, essentially the sum total of the numbers of droplets of known sizes occurring per unit volume of the flow, therefore requires the extraction of the size distribution from underneath the integral.

5. Currently this is achieved by applying the Phillips-Twomey matrix inversion technique, which as described by the author

(ref. 2), usually provides reliable performance data for LP cylinders and stages. In some cases however there is evidence to suggest that the distribution of droplet size contains two distinct modal sizes. In these cases the smoothing constraint that must be applied to obtain a stable inverse of the central matrix of light scattering coefficients appears to reject the second mode which results in a slight underestimate for the wetness.

6. This paper describes how the presence of a secondary mode is clearly indicated by the spectral extinction curve measured by the optical probe. Results from a particular LP turbine measured at different operating conditions are then presented to show how the effect of the second mode emerges in the data and how this provides a basis for inverting the data in two parts to obtain the contribution of each mode to the total wetness. Finally comparisons are made between some LP turbine exhaust conditions measured optically and the corresponding values derived from heat rate tests that demonstrate how the bimodal treatment of optical probe data increases the accuracy of the wetness fractions they provide and hence their diagnostic value.

## THE THEORY OF OPTICAL WETNESS MEASUREMENT IN STEAM FLOWS

7. The wetness of steam flows in LP turbines may be measured optically because these flows are optically dense fogs and the amount of light they transmit provides an indication of how much liquid water they contain. As a light beam traverses a wet flow its intensity reduces according to the exponential law

$$\frac{I}{I_0} = e^{-gt} \quad (1)$$

as radiant power is scattered out of the beam by the water droplets. The ratio  $I/I_0$  is the attenuation of an incident intensity  $I_0$  after a distance  $t$ , and  $g$  (the extinction) is the Mie total scattering or extinction coefficient  $E$

integrated over the total droplet cross section as

$$g = \frac{\pi}{4} \int_0^{D_\infty} E N_r(D) D^2 dD \quad (2)$$

where  $N_r(D)dD$  is the number of droplets per unit volume with a diameter between  $D$  and  $D + dD$  and  $D_\infty$  is the largest droplet diameter present in significant numbers. Expressing the distribution of droplet cross section as:

$$f(D) = \frac{\pi}{4} N_r(D) D^2 \quad (3)$$

gives finally the first kind Fredholm Integral Equation

$$g(v) = \int_0^{D_\infty} E(v, D) f(D) dD \quad (4)$$

where  $g = \frac{1}{t} \log_e I_0/I$  is measured over a range of inverse wavelength  $v = 1/\lambda$  by the optical probe and  $t$  is the length of the light transmission path of the probe head. Hence in order to relate the amount of liquid water suspended by the flow, the volumetric fraction

$$C_v = \frac{\pi}{6} \int_0^{D_\infty} N_r(D) D^3 dD = \frac{2}{3} \int_0^{D_\infty} f(D) D dD \quad (5)$$

to the measured optical transmittance  $I/I_0$  the function  $f(D)$  must be extracted from underneath the integral of equation (4).

8. As posed in this form however the problem is not very tractable since Mie Theory does not specify the total scattering coefficient  $E$  in a convenient analytical form. The integral is therefore replaced by the numerical quadrature:-

$$g(v) = E(v, D_1) f(D_1) \frac{\Delta D}{2} + E(v, D_2) f(D_2) \Delta D + \dots + E(v, D_m) f(D_m) \frac{\Delta D}{2} \quad (6)$$

where  $\Delta D$  is the interval between  $D_n$  and  $D_{n+1}$ . Hence  $g$  measured at  $n$  wavenumbers ( $v_1 = 1/\lambda_1, \dots, v_n = 1/\lambda_n$ ) generates the systems of linear equations

$$g(v_1) = E(v_1, D_1) f_1 \frac{\Delta D}{2} + E(v_1, D_2) f_2 \Delta D + \dots + E(v_1, D_m) f_m \frac{\Delta D}{2}$$

$$g(v_n) = E(v_n, D_1) f_1 \frac{\Delta D}{2} + E(v_n, D_2) f_2 \Delta D + \dots + E(v_n, D_m) f_m \frac{\Delta D}{2} \quad (7)$$

9. Each term in the RHS of these equations is the product of a scattering coefficient  $E$  the cross section  $f$  of a group of droplets of diameter  $D$  and the weighting factor of the quadrature formula which in this case is simple trapezoidal integration since  $E$  and  $f$  are inherently smooth functions. The general term for the  $i$ th droplet diameter  $D_i$  and the  $j$ th wavenumber  $v_j$  therefore defines the matrix

$$A_{ij} = w_i E_{ij} \quad (8)$$

hence (7) may be written

$$\underline{g} = \underline{A} \underline{f} \quad (9)$$

for which the direct solution is:

$$\underline{f} = \underline{A}^{-1} \underline{g} \quad (10)$$

In practice however any attempt at such a direct inversion would fail because equation (9) is ill conditioned which means that the inverse  $\underline{f}$  would be dominated by high frequency oscillations of large amplitude as demonstrated for wet steam measurements by the author in reference (4). Oscillations in the inverse are physically unacceptable for steam flow data since the function  $f$  that is being sought is the distribution of droplet cross section of a condensation aerosol which is inherently smooth. A smoothed inverse is therefore required and this is obtained by minimising the squared curvature of  $f$

$$\sum_{i=1}^n (f_{i+1} - 2f_i + f_{i-1})^2 \quad (11)$$

subject to the constraint on the residual

$$\sum_{i=1}^n (A f_i - g_i)^2 = \sum_{i=1}^n \epsilon_i^2 \leq \epsilon^2 \text{ a constant} \quad (12)$$

Hence differentiating the expression

$$\sum_{i=1}^n (f_{i+1} - 2f_i + f_{i-1})^2 + \gamma^{-1} \sum_{i=1}^n (A f_i - g_i)^2 \quad (13)$$

with respect to the  $f_i$  and equating to zero provides the Phillips-Twomey inversion formula (ref. 5)

$$\underline{f}^S = (\underline{A}^T \underline{A} + \gamma \underline{H})^{-1} \underline{A}^T \underline{g} \quad (14)$$

where  $f^S$  is a smoothed approximation to the solution to equation (9), H is a smoothing matrix composed of fourth difference coefficients 1,-4,6,-4,1 centred on the diagonal  $H_{jj} = 6$  and  $\gamma$  is an arbitrary constant that controls the amount of smoothing applied. In principle a smoothed inverse is obtained by gradually increasing  $\gamma$  until the oscillations are just removed from  $f^S$ .

10. The application of equation (14) to the spectral extinction of wet flows measured in turbine cylinders with the optical probe is described in detail in reference 2, but once a stable inverse  $f^S$  has been obtained for a set of data  $g$  the route to a wetness value is straightforward. The suspended liquid volume fraction is calculated from the elements of  $f^S$  using equation 5 in the form,

$$C_v = \frac{2}{3} \sum_{i=1}^n f_i D_i \Delta D \quad (15)$$

providing the wetness fraction,

$$Y = C_v \frac{v_g}{v_f} / (1 + C_v \frac{v_g}{v_f}) \quad (16)$$

where  $v_g$  and  $v_f$  are the saturation specific volumes of the liquid and vapour phases at the local static pressure which is measured in the turbine with a pitot static probe.

THE MIE TOTAL SCATTERING COEFFICIENT AND THE SPECTRAL EXTINCTION OF LIGHT BY WET FLOWS CONTAINING BIMODAL DISTRIBUTIONS OF DROPLET SIZE

11. The function E in a Fredholm integral equation such as equation (4) is known as the kernel but in a wider sense E the Mie total scattering coefficient is the essential kernel of the optical measurement of wetness. It is the known fundamental physical property of small droplets that ultimately provides an absolute relation between the wetness of the flow and the transmission of light.

12. Values of E are obtained from Mie Theory by integrating the scattered intensity functions for a droplet of diameter D illuminated by plane light waves of wavelength  $\lambda$  at a series of increasing values of the particle size parameter  $\alpha = \pi D/\lambda$ . Hence at a given position in a steady wet flow, where the droplet size distribution  $N_r(D)$  although unknown is constant, it is the spectral ( $1/\lambda$ ) variation of  $E(\pi D/\lambda)$  [the columnar variation in (7)] that is being scanned in the measurement of  $g(v)$ . A relation between transmittance and wetness can therefore only be established when the spectral variation of E, for the droplet population involved, enables a non trivial solution to be found for the set of simultaneous equations (7).

13.  $E(\alpha)$  for small water droplets (refractive index  $m = 1.33$ ) is shown in Fig. 1 plotted from Penndorfs Mie tabulations (ref. 6). To illustrate the spectral variation in E

encountered in practice the part of the  $\alpha$  scale scanned by the optical probe for a typical turbine droplet size of  $D = 0.4 \mu m$  is indicated. It is clear from this illustration that for droplets of this order of size a set of discrete values of  $E(\alpha)$  over the spectral range of the probe will provide linearly independent coefficients for the unknown  $f$  of (7) and hence for the matrix A of (14). In principle therefore a valid inverse  $f^S$  should be obtained from (14) for a measurement  $g(v)$  when the droplets involved are in this region of size.

14. In order to examine how the extinction of a real polydispersion will differ from the  $E(\alpha)$  curve which describes the extinction of a uniform droplet size a mean extinction coefficient  $\bar{E}$  can be calculated for a postulated distribution function  $N_r(D)$  using

$$\bar{E} = \int_0^{D_\infty} E(v,D) N_r(D) D^2 dD / \int_0^{D_\infty} N_r(D) D^2 dD \quad (17)$$

or numerically from equations (4)-(10)

$$E_j(\alpha_{32}) = A f_i / \sum_{i=1}^n f_i \Delta D \quad (18)$$

where  $\alpha_{32}$  is the Particle size parameter based on the Sauter Mean diameter

$$D_{32} = \frac{\sum_{i=1}^n f_i D_i \Delta D}{\sum_{i=1}^n f_i \Delta D} \quad (19)$$

15. Equally a set of measurements  $g$  can be expressed as a normalised extinction coefficient using the inverse  $f^S$  as:-

$$\bar{G}_j = g_j / \sum_{i=1}^n f_i^S \Delta D \quad (20)$$

Equations (4) to (10) show that the extinction of a polydispersion consists of a linear combination of extinction kernels (Sections of  $E(\alpha)$ ), one for each of the  $D_i$  produced by the spectral scan  $v_1 \dots$  to  $\dots v_n$ , and weighted by the concentration of cross section  $f$ .

16. Two mean polydispersed extinction coefficients are compared, on this basis, with  $E(\alpha)$  in Fig. (1); one for the broad distribution of droplet size shown inset and the other for a set of data measured in an LP turbine where the underlying distribution of droplet diameter was thought to be bimodal. In the case of the prescribed polydispersion the  $\bar{E}$  curve is clearly derived from  $E(\alpha)$  but combining parts of the basic curve that relate to the different droplet sizes in  $N_r(D)$  (as in equations (7)) has slightly damped the amplitude of the spectral variation. In contrast however the measured extinction coefficient  $\bar{G}$  presents something of a paradox. The gross structure, a steeply rising curve,

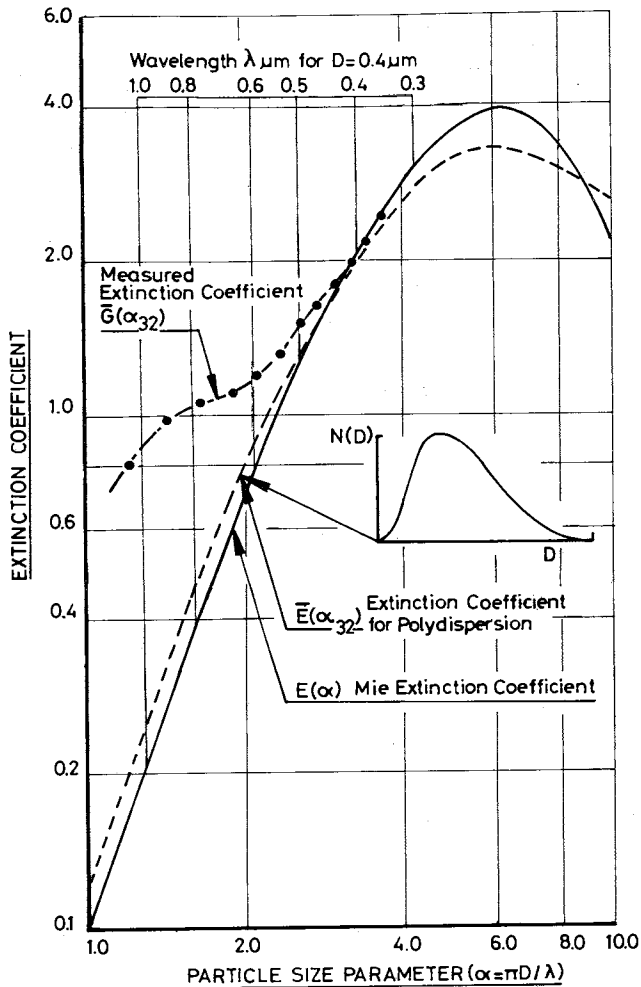


Fig. 1. Light extinction by a wet steam flow in an L.P. turbine showing bimodality

is clearly related to the rising section of  $E(\alpha)$  but  $\bar{G}$  and  $E$  differ fundamentally in this region in that they have opposing curvatures. The way in which  $\bar{G}$  is constructed from a linear combinations of sections of  $E(\alpha)$  is not therefore immediately apparent.

17. It is possible however to explain the observed spectral variation in  $\bar{G}$  in terms of two separate droplet groups which combined form a bimodal distribution. If the flow under consideration, for example, contained two polydispersed groups of droplets with mean diameters of 0.4 and 1.0  $\mu\text{m}$  the overall extinction coefficient would contain two components each having a very different spectral character. The small droplet group would contribute the steeply rising component of  $\bar{E}$  between  $1.0 \lesssim \alpha_{32} \lesssim 4.0$  and the large group would contribute the much flatter curve from the peak in  $E$  between  $3.0 \lesssim \alpha_{32} \lesssim 10.0$ . Hence if the smaller droplet group contributed the predominant cross section the spectral character of the overall extinction would be a rising curve. At longer wavelengths (low  $\alpha$  and  $v$ ) however where the extinction contributed by the small droplets falls away sharply the total extinction would be sustained by the small but more spectrally even contribution from the

larger droplets producing the observed reversal in curvature. This hypothesis is based on steam tunnel experiments where a bimodal distribution is generated by expanding a wet flow in a Laval nozzle and nucleating a secondary population of droplets which produces the essential characteristic of  $\bar{G}$  in Fig. 1 as described by the author in reference (7). The following sections of the paper discuss the error in wetness that arises from inverting 'bimodal' data directly and the experimental basis for separating the contribution from each mode to provide a more accurate result.

THE ERROR IN WETNESS RESULTING FROM THE DIRECT INVERSION OF BIMODAL EXTINCTION DATA

18. An alternative approach to calculating aerosol mass loadings from spectral extinction data is suggested by Box and McKellar (ref. 8) who transform the basic equations:

$$g\left(\frac{1}{\lambda}\right) = \frac{\pi}{4} \int_0^{\infty} E(D, 1/\lambda) N_r(D) D^2 dD \quad (20)$$

into

$$\int_0^{\infty} g\left(\frac{\lambda}{2\pi}\right) d\lambda = \frac{\pi}{6} \int_0^{\infty} N_r(D) D^3 dD \int_0^{\infty} \frac{3}{4} E(\alpha) \alpha^{-2} d\alpha \quad (21)$$

Of the two integrals on the RHS of the transformed equation the first is the required suspended volume fraction  $C_v$  (equation 5) and the second, the weighted integral over the Mie Coefficient  $E(\alpha)$  may be calculated from the simple empirical relation given in reference (8)

$$I_E = \int_0^{\infty} \frac{2}{3} E(\alpha) \alpha^{-2} d\alpha \approx \frac{3}{2} \pi(m^2-1)/(m^2+1) \quad (22)$$

where  $m$  is the refractive index of the particulate material. For the water droplets of present concern ( $m = 1.33$ )  $I_E = 0.9614$  and the suspended volume fraction:

$$C_v = 1.04 T \quad (23)$$

is simply proportional to the area under the measured extinction curve:

$$T = \int_0^{\infty} g\left(\frac{\lambda}{2\pi}\right) d\lambda \quad (24)$$

19. In practice, however, this simple and direct route from the measured light extinction to a wetness value (via equation 16) cannot be exploited since in general  $g$  cannot be specified over  $0 < \lambda < \infty$  from the measured data with sufficient accuracy. As indicated by the example shown in Fig. 2 regions providing major contributions to the area under  $g(\lambda)$ , such as the peak that is known to occur at  $\lambda = D/2$  [ $\alpha \approx 6$ , see Fig. 1] and the asymptotic behaviour of  $g$ , simply cannot be inferred from the part

of  $g$  measured over the spectral range of the instrument.

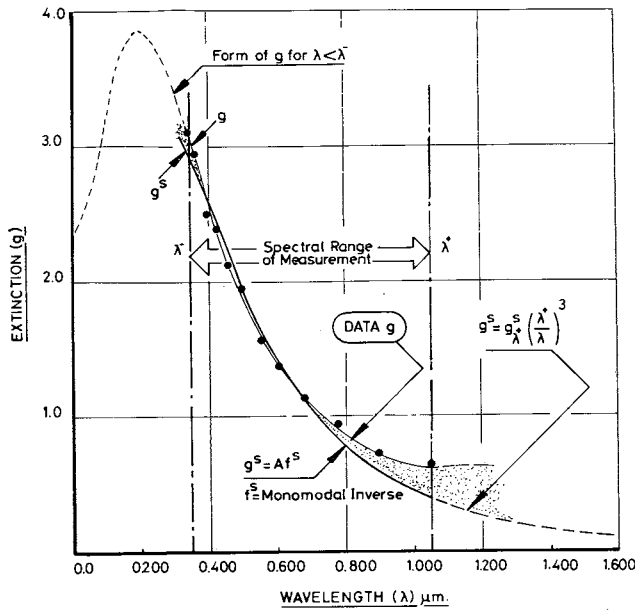


Fig. 2. The error in monomodal inversion of extinction data

20. The alternative procedure described in Section 2 is therefore adopted whereby an inverse  $f^S$  is calculated for the data  $g$  using equation (14) and  $C_V$  is obtained from (15) as the integral of  $f^S$ . In principle this is an equally valid approach provided that the inverse  $f^S$  satisfies the basic equation  $Af = g$  to within fairly close limits. As discussed in Section 2 however  $f^S$  is not an exact solution to  $Af = g$  but only an approximation obtained subject to applied constraints such as smoothness. The original system  $Af = g$  has therefore been replaced by the approximate system  $Af^S = g^S$  and the volumetric fraction that is calculated from  $f^S$  will therefore be proportional to the area under  $g^S(\lambda)$  rather than that under the true  $g(\lambda)$ . There is therefore a risk of error in calculating wetness from the inverse  $f^S$  if the corresponding  $g^S$  departs significantly from  $g$ .

21. Although Box and McKellar's transformed equation cannot be used to calculate wetness directly from extinction the underlying strategy can usefully indicate the error in a wetness value that is based on an inaccurate inverse  $f^S$ . When the smoothed inverse of the data in Fig. 2 is back substituted to generate  $g^S = Af^S$  it is clear that  $g^S$  does not fit the measured data at all well. It is shown in Fig. 2 that the area under  $g^S$  is seriously deficient and a wetness calculated from  $f^S$  will therefore be an underestimate. The exact shape of the peak in  $g$  is unknown but it is clear that  $g^S$  is tending to fall short of  $g$  for  $\lambda < \lambda^-$ , but at the other end of the spectral range  $\lambda > \lambda^+$  the shortfall is more serious since  $g$  and  $g^S$  are diverging quite strongly.

22. Box and McKellar suggest that the asymptotic part of  $g$ , beyond the upper wavelength limit  $\lambda^+$  of the measured spectral range, can be estimated from:

$$g = g_{\lambda}^+ \left(\frac{\lambda^+}{\lambda}\right)^4 \quad (25)$$

on the basis that the extinction at long wavelengths ( $\lambda \rightarrow \infty, \alpha \rightarrow 0$ ) can be characterised by Rayleigh Scattering. In the case of  $g^S$  this appears to be so, although for the droplet size involved ( $D \approx 0.4 \mu\text{m}$ ) Mie Theory indicates an exponent of 3 at  $\lambda^+ = 1.05 \mu\text{m}$ . In contrast however the real extinction  $g$  cannot be extended for  $\lambda > \lambda^+$  using (25) since it would be discontinuous at  $\lambda^+$ . As discussed in paragraphs (15-16) this is consistent with the presence of separate population of larger droplets that is sustaining the extinction into the infra red, since the extinction of a continuous distribution of droplet size would in common with  $E(\alpha)$  merge continuously into a  $\lambda^{-b}$  ( $3 < b < 4$ ) asymptote as shown in Fig. 1.

23. The rejection of the second mode by the inversion process based on equation (14) cannot be simply ascribed to the application of the smoothing constraint since the author demonstrates a successful retrieval of a smoothed bimodal inverse in reference 4. It is more probable that the smooth extinction kernels, of the very fine droplets encountered in the wet steam flows of LP turbines, impose an inherent limitation on the amount of fine structure that can be retrieved by inversion as discussed by Twomey (ref. 9). Nevertheless a great deal of data exhibiting bimodality had been obtained from traverse tests on generating plant with the optical probe and a method of inversion was therefore required urgently. The following section describes how the existing inversion process was adapted in a very simple way that forced it to take the second mode into account thereby improving the accuracy of the wetness fractions obtained.

THE INVERSION OF BIMODAL EXTINCTION DATA  
The Basic Strategy

24. As discussed in paragraph (20) a direct inversion of a spectral extinction generally fails to recognise the presence of a second mode when it occurs and consequently provides an underestimated wetness in these cases. It was necessary therefore to build a test for bimodality into the inversion process and to devise a method for calculating a bimodal inverse to improve the accuracy of the wetness value obtained.

25. A strategy for approaching this problem was suggested by the extinction curves presented in Fig. 3. These two results were measured with the optical probe at the same position in the exhaust plane of a 660 MW turbine at slightly different back pressures. The results differ markedly in that only the result for the lower back pressure shows pronounced bimodality. In this case the influence of the second mode in sustaining the

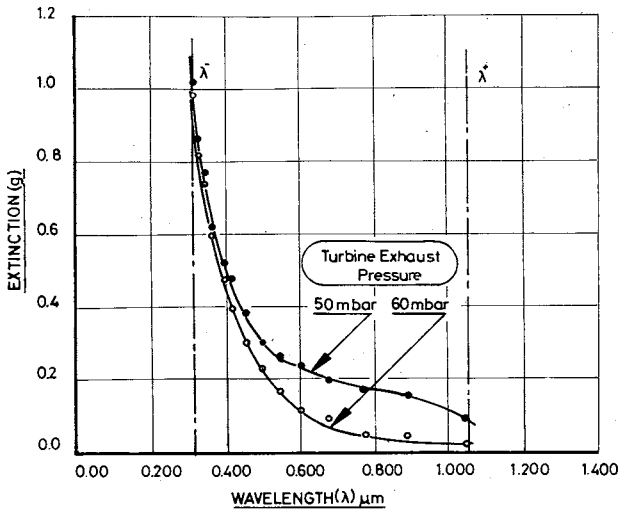


Fig. 3. Extinction curves measured in an L.P. turbine at different back pressures

extinction at long wavelengths suddenly emerges at about the mid point of the spectral range (based on  $\nu = 1/\lambda$ ). In the ultra violet however the two curves tend to merge and rise steeply together indicating the same predominantly small droplet size for both cases which may be expected for flows that were subjected to essentially the same pressure history over the same flow path. It is not known why these two results should differ so much at long wavelengths under similar flow conditions but optically these results represent basically the same flow with and without the second mode. On this basis these results suggest the possibility of isolating the contribution of the predominant first mode from the UV section alone.

26. The basis of the bimodal inversion process therefore is to assume that the measured extinction  $g$  can be separated into two components  $g_1$  and  $g_2$  (contributed by each of the two modes). As indicated by Fig. 3 an approximation for  $g_1$  alone can be obtained by inverting the UV end of the extinction to provide the partial inverse  $f_1^S$ . The extinction contributed by the secondary mode may then be calculated from,

$$g_2 = g - g_1 = g - Af_1^S \quad (26)$$

Equation 14 may then be applied to  $g_2$  to generate the inverse  $f_2^S$  of the second mode. Then if  $Af_1^S + Af_2^S$  is closer to  $g$  than  $Af_1^S$  where  $f_1^S$  is the smoothed inverse of the whole of  $g$  a more accurate value of wetness can be calculated from the two components  $f_1$  and  $f_2$  using equations (15 and 16).

Example of Bimodal Inversion

27. To illustrate how the preceding strategy is used in practice to process the spectral extinction curves of wet flows measured in LP turbines the procedural steps involved are described here using the data shown in Fig. 2 as an example.

28. A smoothed approximate inverse  $f_1^S$  for the first mode is obtained first by inverting the data measured over the lower half of the spectral range  $\lambda^- < \lambda < \Lambda$  (where  $\Lambda$  is the wavelength of the mean  $\nu = 1/\lambda$ ) using equation (14) as described in reference (2).

29. Back substitution of the first mode inverse  $f_1^S$  into the basic equation  $Af = g$  with the matrix  $A$  extended to cover the full spectral range then provides an estimate for the overall extinction of the first mode  $g_1^S = Af_1^S$  over  $\lambda^- < \lambda < \lambda^+$ . This is shown compared with the source curve  $g$  in Fig. 4 and visibly provides a better fit to the data for  $\lambda \rightarrow \lambda^-$  than did the original monomodal inverse  $f_1^S$  as shown by  $g_1^S$  in Fig. 2.

30. The extinction of the second mode is then obtained by subtracting  $g_1^S$  from  $g$  over  $\Lambda < \lambda < \lambda^+$  and again a smoothed inverse of the partial data set is obtained by applying equation (14).

The result of this process  $g_2^S = Af_2^S$  is shown in Fig. 4 at the bottom of the diagram as a slowly rising curve.

31. Finally however when the extinction of the composite inverse:

$$f_{12}^S = Af_1^S + Af_2^S \quad (27)$$

is assembled and compared with the original extinction curve  $g(\lambda)$  it is immediately clear that the bimodal inverse

$$f_{12}^S = f_1^S + f_2^S \quad (28)$$

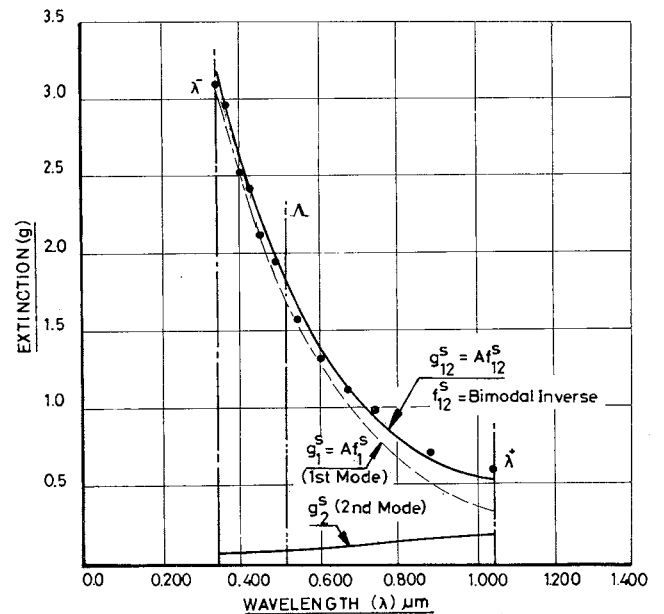


Fig. 4. Result of applying bimodal inversion

comes much closer to satisfying  $Af = g$  than the monomodal or direct smoothed inverse  $f_1^S$  as shown by  $g_1^S$  in Fig. 2. It is also clear from Fig. 2 that most of the deficit in the area under  $g^S$  occurs outside the measured spectral range whereas  $g_{12}^S$  in addition to being much closer to  $g$  over  $\lambda^- < \lambda < \lambda^+$  has similar derivatives at  $\lambda^+$  and  $\lambda^-$ . Therefore since both

$g$  and  $g_{12}^S$  consist of a linear combination of Mie extinction kernels it is probable that  $g_{12}^S$  will also be fairly close to  $g$  in the spectral regions that are not accessible to measurement,  $\lambda^+ < \lambda < \lambda^-$ . A wetness based on  $f_{12}^S$  will be proportional to the area under  $g_{12}^S$  and Figs. 2 and 4 together with the preceding argument demonstrate clearly that this will provide a much more accurate value than the wetness calculated from the direct inverse  $f^S$ .

32. In practice a direct or monomodal inverse of the whole of  $g(v)$  as described in reference 2 precedes the application of the bimodal process to provide initial values for the range of  $D$  and the smoothing parameter  $\gamma$  for inverting the first mode. Then if the data does not show bimodality which is immediately indicated by zero and negative values in  $g_2$  the wetness based on the monomodal inverse may be retained as being a reasonably accurate value. BIMODAL INVERSION APPLIED TO TURBINE TRAVERSE TESTS

33. In order to provide a clear illustration of the symptoms of bimodality in spectral extinction measurements and the way in which this is detected and compensated for in the modified inversion process rather extreme cases have been selected as examples. For the case considered in Section 5 for instance monomodal inversion gave a wetness and droplet size of

$$Y = 0.07 \text{ and } D_{32} = 0.45 \mu\text{m}$$

respectively whereas bimodal analysis gave

$$\begin{aligned} Y_1 &= 0.071 & D_{132} &= 0.41 \mu\text{m} \\ Y_2 &= 0.020 & D_{232} &= 2.8 \mu\text{m} \end{aligned}$$

for the two modes it detected. Bimodal analysis has therefore found 30% more wetness in this case. This example however is simply based on one wetness measurement on one traverse and to provide a more balanced impression of how bimodal analysis improves the accuracy of overall turbine performance diagnostics and some complete results are given in Fig. 5.

34. Each of the curves A, B and C shows the radial distribution of wetness measured in the exhaust annulus of the LP cylinder of a 500 MW turbine. The wetness is measured as shown as a series of mean levels on the discrete intervals of the flow sampled by the optical probe along the radial traverse line as described in reference (2). At positions where bimodality was detected the additional wetness is shown by a shaded area and the illustration shows how this effect ranges from being scarcely detectable to providing a major contribution to the overall exhaust wetness level. The effect on the LP turbine performance parameters is given in Table I and shows changes, in the LP cylinder efficiency indicated by optical measurements, ranging from 0.7 to nearly 4 percentage points.

35. Currently it is not clear why such a large variation in apparent bimodality is found in optical transmission data measured in LP turbines where the expansion rates and pressure drops are broadly similar. It can only be concluded for turbine A, where most of the  $g(\lambda)$  curves merged continuously into a Rayleigh asymptote, that the two sizes were close enough together to be adequately approximated by a continuous or monomodal inverse. In cases B

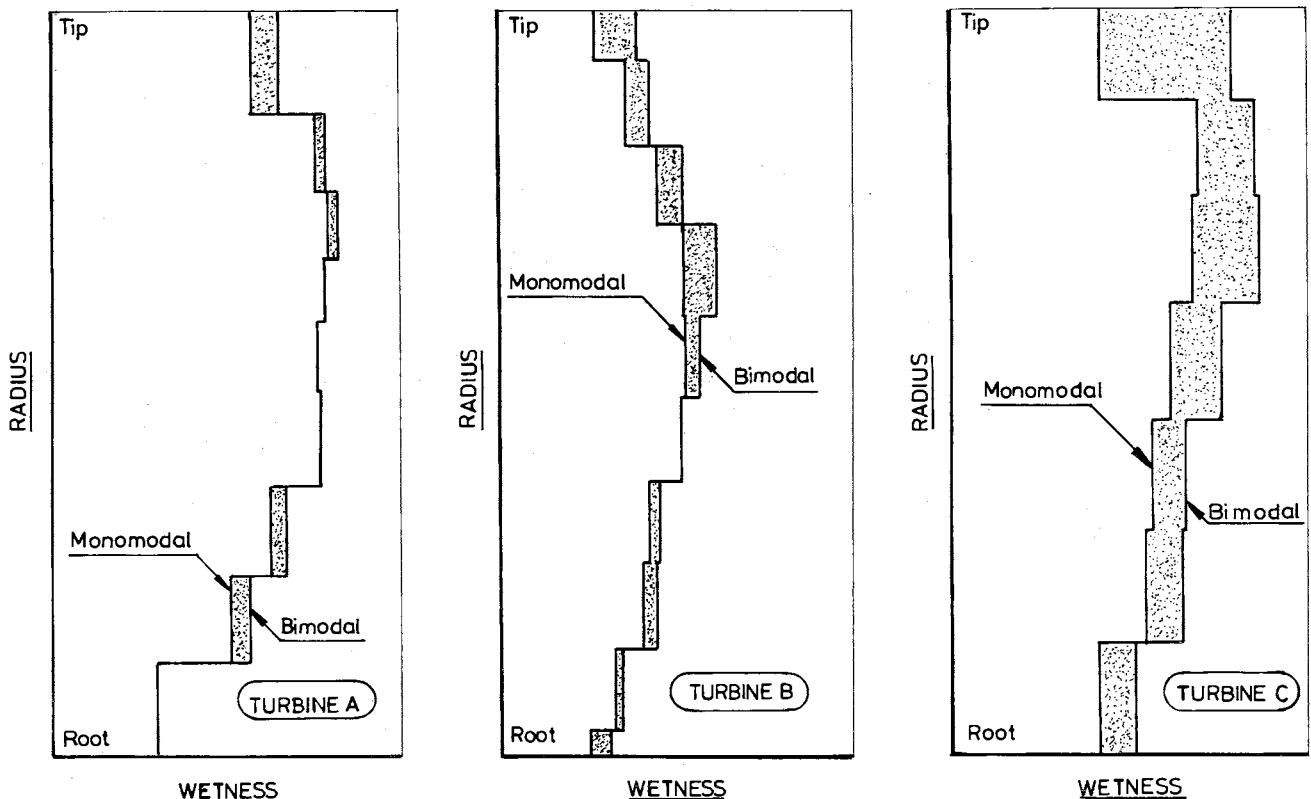


Fig. 5. Wetness profiles at exhaust from 3 L.P. turbines showing effect of bimodality

## FLOW ANALYSIS AND MEASUREMENT

and C however a reversed curvature in the extinction, as shown in Fig. 1, was general over the entire annulus and bimodal inversion was required to find an inverse  $f_{12}^S$  that reflected this. As shown in Table 1 this

Table 1. The Effect of Applying Bimodal Analysis on LP Turbine Performance Parameters Indicated by Optical Wetness Measurements for the Cases Illustrated in Fig. 5

Turbine	Change in Indicated Mean Exhaust Wetness $\delta\bar{Y}$	Change in LP Turbine Total Enthalpy Drop $\delta(\bar{h}_{o1} - \bar{h}_{o2})$	Charges in Indicated LP Cylinder Efficiency $\delta\eta_{TS}$ (% Points)
A	+0.0023	+5.52	+0.69
B	+0.0084	+20.0	+2.7
C	+0.0126	+30.24	+3.8

produced considerable changes in the mean exhaust wetness levels and hence LP cylinder efficiencies indicated by optical measurement. Incidentally in each of the three cases A, B and C a full heat rate test was run on the unit simultaneously with the optical probe traverse. In each case the LP cylinder efficiency derived by heat balance and from direct exhaust wetness measurement, following the application of bimodal analysis, agree to within a single percentage point. The improvement in accuracy of the wetness values indicated in detail by the improved fit to the data provided by the bimodal inverse as  $Af_{12}^S$  shown in Figs. 2 and 4 is therefore confirmed more generally by consistent agreement with the only performance parameter that can be derived independently.

36. Prior to the introduction of bimodal analysis the agreement between Heat Rate Test and Probe derived turbine efficiencies was also fairly close as shown in Reference 2. The wetness in these cases however was subject to a correction of 1.08 to compensate for the coarse water component of the wetness which the optical probe does not detect. Concurrently with the introduction of Bimodal Analysis however the coarse water correction was reduced to 1.04 following the more recent study of Young Yau and Walters (ref. 10) where for the first time measurements of coarse water flow could be related to simultaneous direct measurements of bulk wetness. For the cases listed in reference (2) therefore some of the wetness deficit incurred by inverting optical data directly was being compensated for by an over estimate for coarse water. For turbine A in Table (1), for example this would be almost exactly the case. It is noticeable however that even in reference 2 the probe derived efficiencies although close to the Heat Rate values were all slightly lower. Bimodal analysis was introduced in response to a series

of more recent measurements where this deficit was consistently larger and it was becoming increasingly clear from the inversion test shown in Fig. 2 that the direct application of the Phillips-Twomey inversion formula to optical probe data was systematically underestimating the wetness. From the corrections indicated in Fig. 5 and Table (1) it is clear that the introduction of this process has considerably improved the accuracy of optical wetness measurements in LP turbines thereby enhancing the diagnostic value of cylinder and stage efficiencies based on probe measurements alone.

### CONCLUDING DISCUSSION

37. Although the underlying strategy of the bimodal inversion process described in this paper represents a fairly gross approximation it is clear from the example given in Figs. 2 and 4 that a bimodal inverse  $f_{12}^S$  will be generally much closer to the true solution  $f$  than the smoothed direct inverse  $f^S$ . The area under the curve  $g_{12}^S = Af_{12}^S$  is consequently much closer to that under the source curve  $g$ , and Box and McKellar's transformed integral equation (equation 21) shows that the wetness calculated from the bimodal inverse  $f_{12}^S$  will therefore be the more accurate value.

38. In addition to usefully indicating the potential error in calculating wetness from light extinction data Box and McKellar's approach to this problem enables another important conclusion to be drawn about optically derived wetness namely: that the absolute accuracy of the measurement cannot be determined.

39. Outside of the spectral range of measurement, which will always be confined by the limits of real optical systems  $g(\lambda)$  cannot be specified exactly. Hence even if an inverse  $f'$  could be obtained such that  $|Af' - g| < \epsilon$  over  $\lambda^- < \lambda < \lambda^+$ , where  $\epsilon$  is the experimental error in  $g$ , there is no way of establishing that  $Af'$  and  $g$  will be in such close agreement at longer or shorter wavelengths. Hence although it can be safely concluded that bimodal analysis has improved the accuracy of optically measured wetness it is not possible to say exactly to within what limits.

40. The only independent validation of the wetness levels measured optically in turbines therefore remains the end point enthalpies derived by Heat Balance from Heat Rate Tests conducted on the whole turbine system. These values however can scarcely be regarded as a calibration reference since LP cylinder efficiencies derived in this way are inherently subject to an error of up to  $\pm 2$  percentage points which represents a fractional error in exhaust wetness of about 6%. Since the introduction of bimodal analysis however LP cylinder efficiencies derived from Heat Rate Tests and Optical wetness measurement have generally agreed to within about  $\pm 1$  efficiency percentage points.

41. This supports the claim for improved accuracy of the wetness measurement obtained by using the bimodal inverse and confirms the consequently enhanced value of optical probe measurements for providing performance diagnostics for the wet zone of LP turbines.

## ACKNOWLEDGEMENTS

42. This work was carried out at the Central Electricity Research Laboratories and the paper is published by permission of the Central Electricity Generating Board.

## REFERENCES

1. Baumann, K. Recent Developments in Steam Turbine Practice. Journal of the Institution of Electrical Engineers, Vol. 48, p 830, 1912.
2. Walters, P.T. Wetness and Efficiency Measurements in LP Turbines with an Optical Probe as an Aid to Improving Performance. Transactions of the ASME Journal of Engineering for Gas Turbines and Power, Vol. 109, 85, January 1987.
3. Skillings, S.A., Walters, P.T. and Jackson, R. "A Theoretical Analysis of Flow Through the Nucleating Stage in a Low Pressure Steam Turbine". Paper submitted to ASME Journal of Turbomachinery.
4. Walters, P.T. "Practical Applications of Inverting Spectral Turbidity Data to Provide Aerosol Size Distributions", Applied Optics, Vol. 19, p 2383, July 1980.
5. Twomey, S. "On the Numerical Solution of Fredholm Integral Equations of the First Kind by Inversion of the Linear System Produced by Quadrature". J. Assoc. Comput. Mach., 10, 97 (1963).
6. Pemdorf, R.B. "New Tables of Mie Scattering Functions for Spherical Particles", Geophysical Research Paper No. 45, Part 6 (1956).
7. Walters, P.T. Optical Measurements of Water Droplets in Wet Steam Flows Conference Proceedings (Instn. Mech. Engrs.) Vol. 3, London (1973).
8. Box, M.A. and McKellar, B.H.J. Direct Evaluation of Aerosol Mass Loadings from Multi-Spectral Extinction Data, Quart. J. Royal Met. Soc., Vol. 104, No. 441, July (1978).
9. Twomey, S. Introduction to the Mathematics of Inversion in Remote Sensing and Indirect Measurements (Chapter 5), Elsevier Publishing Company, Amsterdam (1977).
10. Young, J.B., Yau, K.K. and Walters, P.T. Fog Droplet Deposition and Coarse Water Formation in Low Pressure Steam Turbines: A Combined Experimental and Theoretical Analysis. ASME Journal of Turbomachinery, Vol. 110, 181, April 1988.



## 28. Calculations of the nozzle coefficient of discharge of wet steam turbine stages

Z. JINLING and C. YINIAN, Department of Energy and Power Engineering, Xi'an Jiaotong University, Xi'an, China

This paper seeks to give a full account of the problem of the nozzle coefficient of discharge of wet steam turbine stages. The fundamental logic of the treatment of the problem is believed to be sound and the theoretical formulation of the problem is rigorously in accordance with the theory of two-phase wet steam expansion flow through steam turbine nozzles. The computational values are plotted into sets of curves in accordance with orthogonality test principles. They check satisfactorily both with traditional empirical data and most recent experimental data obtained in the wet steam two-phase flow laboratory of Xian Jiaotong University.

### NOMENCLATURE

A	cross-sectional area of nozzle
c	steam velocity
h	specific enthalpy
Kn	Knudsen number
l	free path of molecule
m	mass of a droplet
n	number of droplets
Nu	Nusselt number
P	Pressure
Pr	Prandtl number
r	droplet radius
Re <sub>r</sub>	relative Reynolds number
D <sub>r</sub>	drag force
G	mass of discharge
T	temperature
u	liquid velocity
V	specific volume
x	dryness fraction, distance along nozzle axis
y	wetness fraction
$\mu$	coefficient of discharge, viscosity of vapor
$\varphi$	velocity coefficient
$\sigma$	surface tension
$\lambda$	conductivity of vapor
$\rho$	density
$\epsilon$	pressure ratio
$\xi$	correction factor of the coefficient

### SUBSCRIPT

*	critical
o	stagnant
s	isentropic, saturation
f	liquid
g	steam
w	equilibrium
1	outlet

### INTRODUCTION

1. The coefficient of discharge of a nozzle is defined as the ratio of the actual mass discharge per unit time through a nozzle to its theoretical mass discharge as calculated for an isentropic expansion in equilibrium state when both of expansive pressure ratios are the same. As wet steam expands through a nozzle, the phenomenon of supersaturation may occur and the actual discharge of the nozzle may be greater than its equilibrium isentropic discharge causing the coefficient of discharge of the nozzle to exceed unity. It seems that this particular phenomenon of wet steam nozzles, although quite familiar to steam turbine technologists (refs 1-3), has not been studied very closely by all of them. For a long enough time, people had apparently been satisfied with the empirical curves and formulas for design, until the 1980's when steam turbine researchers' interest in wet steam nozzle discharge problems were revived (ref.4), but this time with a possibility of solving these problems in the light of the theory of wet steam two-phase flows (refs 5-9).

2. The aim of this paper is to give a brief account of the theoretical and computational study of wet steam nozzles conducted recently by the wet steam group of the division of thermal turbines of Xian Jiaotong University. The results of the research project embodying sufficient experimental data are applicable to nozzle discharge problems of conventional and nuclear steam turbines.

### THEORETICAL FORMULATION OF THE PROBLEM

3. A physical model of stable wet steam expansion flow through a convergent nozzle may be established on the following simple assumptions:

a. For nozzle flows of wet steam initially in equilibrium or not in equilibrium, the number of water droplets after initial nucleation, are assumed to be constant throughout the expansion, but for non-equilibrium flow an additional assumption is also provided that the undercooling is not great so that no secondary condensation is likely to occur.

b. The liquid phase water droplets appear in the flow as homogeneous dispersed substance.

c. At nozzle entrance all droplets are greater than 0.05µm in diameter.

4. Proceeding from the above assumptions, the following system of basic equations may be derived as was done by the first author in her MS thesis of 1987 (ref.8).

Continuity equation:

$$\frac{d\rho_g}{\rho_g} + \frac{dA}{A} + \frac{dc}{c} + \frac{u}{c} \frac{dy}{1-y} = 0 \quad (1)$$

Momentum equation:

$$\text{Vapour phase: } \varphi^2 \frac{dp}{\rho_g} + nDdx + \frac{c}{1-y} dc = 0 \quad (2)$$

$$\text{Liquid phase: } D = \mu u \frac{du}{dx} - (c-u)u \frac{dm}{dx} \quad (3)$$

Energy equation:

$$\text{Assumption } dh_f = 0: \quad c^2 dc + yu^2 du + cdh_g - (uh_{fg} + u \frac{c^2 - u^2}{2}) dy = 0 \quad (4)$$

$$\text{Equation of state: } \frac{dp}{p} = \frac{2B+V_g}{B+V_g} \frac{dV_g}{V_g} - (1 + \frac{T_g dB/dT_g}{B+V_g}) \frac{dT_g}{T_g} = 0 \quad (5)$$

5. In these equations, the various variables involved are calculated by the following equations:

For the surface tension of plane water  $\sigma_w$ :

$$\sigma_w = 0.2358(1-Tr)^{1.256} [1 - 0.625(1-Tr)] \quad (6)$$

Heat conductivity of steam  $\lambda$ :

$$\lambda = -0.2045 + 1.1370Tr - 1.9390Tr^2 + 1.1418Tr^3 \quad (7)$$

For dynamic viscosity of steam  $\mu$ :

$$\mu = (-15.371 + 99.871Tr - 133.993Tr^2 + 75.8226Tr^3) * 10^{-6} \quad (8)$$

where  $Tr = T/T_c$ .

For steam pressure  $p_s$ :

$$\ln p_s = 18.3036 - \frac{3816.44}{T - 46.13} \quad (9)$$

For droplet growth rate  $dr/dt$ :

$$\frac{dr}{dt} = \frac{(1-r_c/r)(T_s - T_g)V_f}{h_{fg}r(1 - \sqrt{8\pi}/(1.5Pr) * k/(k+1) * 1)}$$

without droplet slippage (10)

$$\frac{dr}{dt} = \frac{Nu(T_s - T_g)(1-r_c/r)}{2h_{fg}r\rho_f}$$

with droplet slippage (11)

where  $Nu = Nu_0 / (1 + \sqrt{8\pi}/1.5 * k / (k+1) * kn / p_r * Nu_0)$ ;

$Kn = 1/2r$ , and

$$Nu_0 = 2 + 0.03Pr^{0.33} Re_r^{0.54} + 0.35Pr^{0.356} Re_r^{0.58}$$

6. The nozzle discharge is obtained with reference to the exit section of the nozzle by the following equation:

$$G = A_g c \rho_g + A_f u \rho_f \quad (12)$$

7. The ratio of the measured (or calculated) discharge  $G$  to the theoretical discharge  $G_w$  isentropic equilibrium flow gives the coefficient of discharge:

$$\mu = G/G_w \quad (13)$$

8. The solution of the above system of differential equations is obtained by means of standard 4th order Runge-Kutta method on a electronic computer. A block diagram of the computer program is shown in the accompanying sketch.

9. It is known that the critical pressure ratio of non-equilibrium expansion is smaller than that of equilibrium expansion. With both expansive pressure ratios being the same, the calculations in the paper cover only subcritical and critical pressure ratios of equilibrium expansion, and not deal with the non-equilibrium choked conditions.

PLOTTING OF COMPUTATIONAL RESULTS

10. Careful considerations have to be given to the plotting of the large volumes of computational results obtained from the theoretical equations describing the wet steam two-phase flow through a nozzle before one can hope to get useful curves for design purposes.

11. It is judged that at least two sets of curves are required for complete representation of the results. The first set of curves, called the main curves, represent the basic relationship between the coefficient of discharge and several known quantities or easily measured quantities. The second set may be called the correction curves which reflect the individual influences of the various factors such as droplet diameter at nozzle entrance, expansion rate of the nozzle, etc. on the value of discharge as well as the cross influences that these factors have on the main curves.

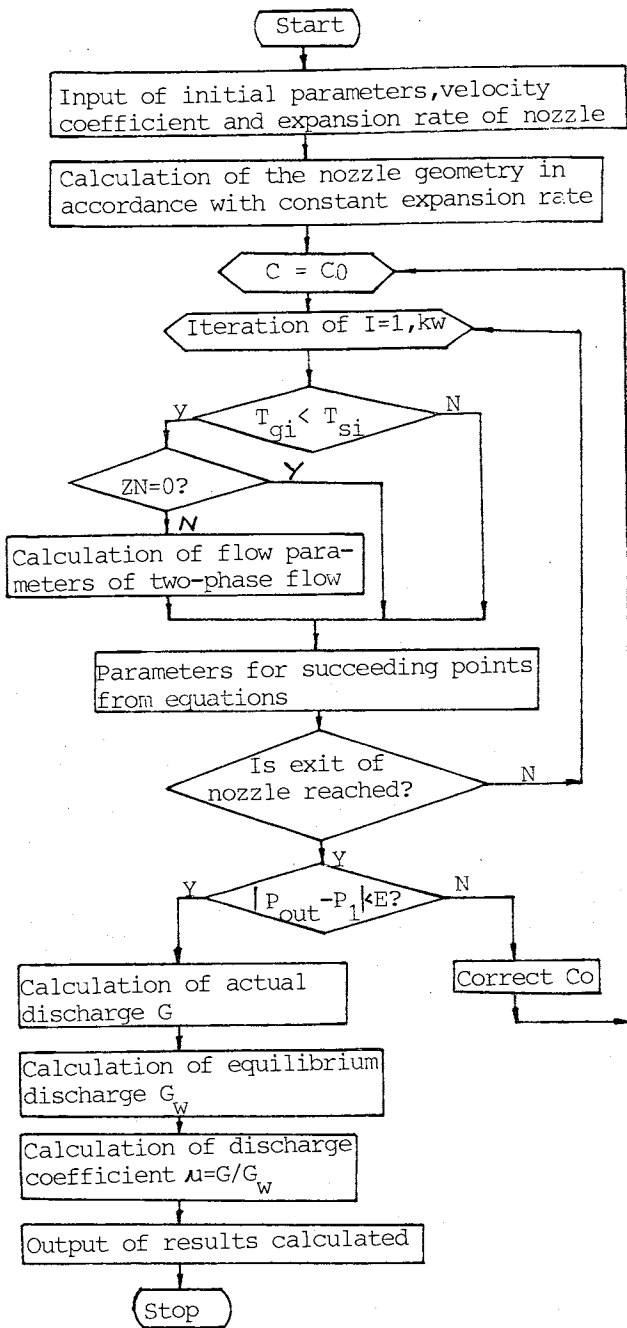


Fig.1 The block diagram of the computer program

12. The design of the main curves is somewhat straight forward. 11 sets of main curves have been plotted to cover the whole range of pressures usually met with in nuclear steam turbines associated with light-water reactors. An example of these 11 sets is shown in Fig.2. The nozzle geometry for calculating the main curves can be seen in Fig.3.

13. As can be seen, Fig. 2 is divided into three regions, the superheat, two-phase, and undercooled regions, respectively with degree of superheat  $\Delta T$ , inlet wetness  $y_0$ , and degree of undercooling  $\Delta T$  as well  $y_0$  as parameters. These parameters are all easily measured or determined and have the greatest

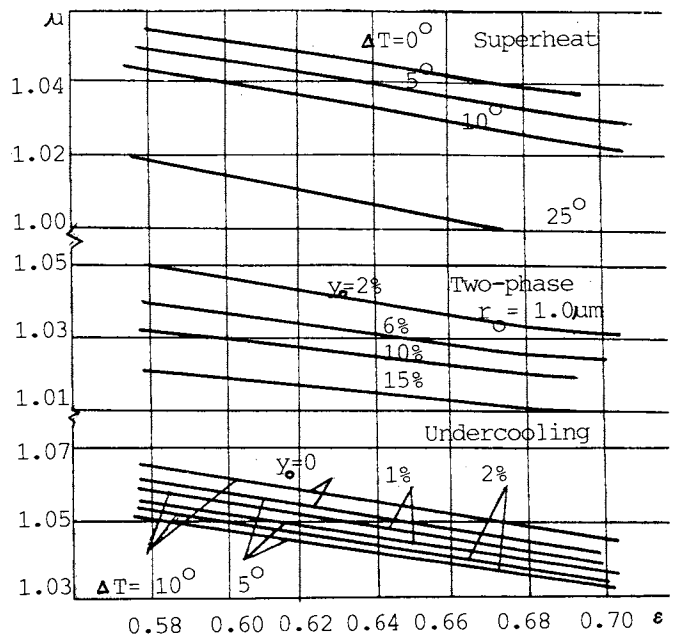


Fig.2 The main curves of the coefficient  $p_0 = 1.0 \text{ bar}$

effects on the  $\mu - p_1/p_0$  curves. In the first region, the actual expansive process is the process of dry steam, and no condensation occurs. The states in the third region may be found at entrance of blades of wet steam turbine stages.

14. But since the value of coefficient of discharge depends on far more factors than on  $p_1/p_0$  alone, the effect of each of these factors must be taken care of. Orthogonal test is one of methods applied in mathematical statistics. To obtain some information, smallest cost of testing needs to be expended by using the method. The authors have applied the theory of orthogonal tests to determine the relative importance of these factors and have come to the conclusion that for the superheat region the most important factor is the degree of superheat  $\Delta T$ , for the two-phase region, the factor is droplet diameter  $r$ , and for the undercooled region, it is the inlet pressure  $p_0$ .

15. Using  $\xi$  to represent the correction factor to be applied to the  $\mu$  values from Fig. 2, then  $\xi$  may be defined as

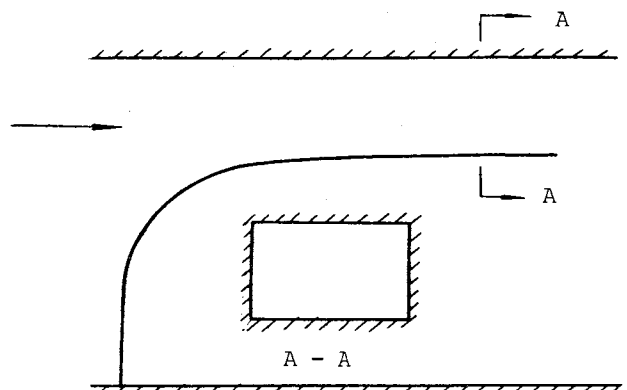


Fig.3 The nozzle geometry for calculating the  $\mu$  curves (scale 1:1)

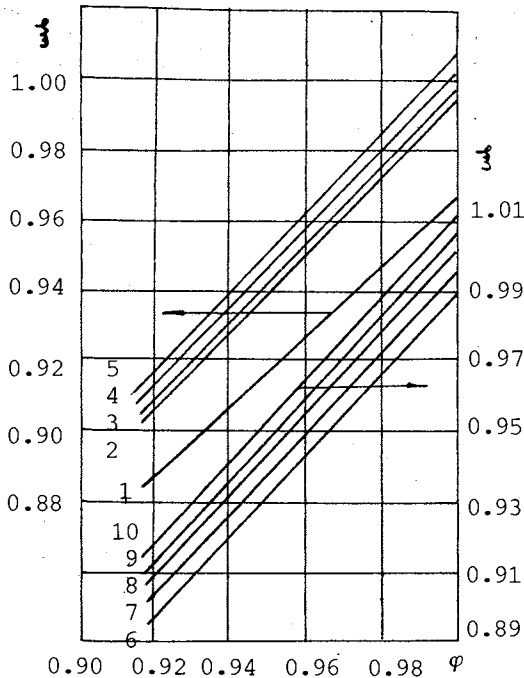


Fig.4 The correct curves

1,2,3,4 and 5 correct the two-phase region;  
6,7,8,9 and 10 correct the undercooling region;  
and 10 also correct the superheat.

- 1:  $r_o = 0.1\mu m$ ; 2:  $r_o = 0.5\mu m$ ;
- 3:  $r_o = 1.0\mu m$ ; 4:  $r_o = 2.0\mu m$ ;
- 5:  $r_o = 5.0\mu m$ ; 6:  $p_o = 10.0 bar$ ;
- 7:  $p_o = 1.0, 2.0, 5.0 bar$ ;
- 8:  $p_o = 0.5 bar$ ;
- 9:  $p_o = 0.08, 0.1, 0.2 bar$ ;
- 10:  $p_o = 20.0, 40.0, 60.0 bar$ .

$$\xi = \frac{\text{Actual coefficient of discharge}}{\text{Value from Fig.2}}$$

Fig.4 gives the values of  $\xi$ . In Fig.4, the expansion rates of the nozzle are not shown as a parameter because the theory of orthogonal tests finally shows that their effect on the value of coefficient of discharge is small. In fact, the expansion rates of steam in a convergent nozzle mainly depend on its expansion pressure ratios, and have a little to do with the rates of the nozzle. Therefore, the effect of the expansion rates of steam on the coefficient has been reflected by the pressure ratios in the main curves.

ACCURACY OF THEORETICAL CALCULATIONS

16. Our theoretical calculations of the coefficient of discharge may be examined with respect both to the empirical values commonly in use in steam turbine practice and to those provided by M.Moheban and J.B.Young in ref.6.

17. Generally speaking, the empirical values of nozzle discharge coefficient show good agreement with our computational curves. This agreement sufficiently proves the reliability of our curves. Table 1 presents a summary of the comparison.

Table 1 The comparison between the calculational values and the empirical values

stage parameters; $\mu$	HP 200 MW turbine		HP 50 MW turbine			
	stage 31	stage 32	stage 14	stage 15	stage 16	stage 17
$p_o$ bar	0.35	0.127	2.18	0.97	0.365	0.122
$t_o(x_o)$ °C (%)	92	0.976	0.997	0.963	0.930	0.897
$\xi = p_1/p_o$	0.609	0.606	0.577	0.577	0.577	0.577
$\phi$	0.968	0.955	0.97	0.975	0.975	0.975
$\mu$ in ref.2	0.99	1.01	0.99	1.01	1.02	1.02
$\mu$ in the paper	0.990	1.000	1.016	1.015	1.016	1.016

18. A comparison with the results given by Moheban and Young is summarized in Table 2. The data in column 7 of Table 2 are taken from the non-equilibrium calculation of a low pressure wet steam turbine using a blade-to-blade time-marching technique. In ref.6, the same parameters are used as those in our curves. Therefore the computational curves like those given in Fig. 2 would certainly embody the range of application of ref.6. In their second paper (ref. 7), Moheban and Young give further experimental results to illustrate the reliability of their calculations.

Table 2 The comparison between the coefficients of discharge of this paper and the coefficients of discharge of ref.6

$p_o$ bar	$T_o$ °K	$p_1/p_o$	$r_o^m$	$y_o$	$\phi$	$\mu$ in ref.6	$\mu$ in the paper
0.671	378	0.564			1.00	1.03	1.034
0.16	327	0.58	0.01	0.055	0.998	1.00	1.00
0.16	327	0.58	0.05	0.055	0.997	1.007	1.002
0.16	327	0.58	0.10	0.055	0.995	1.014	1.012
0.16	327	0.588	0.30	0.055	0.990	1.022	1.022
0.16	327	0.58	0.50	0.055	0.986	1.032	1.028

CONCLUSIONS

1. Based on the general theory of wet steam two-phase flow, this paper attempts to make a thorough study of the problem of the coefficient of discharge of wet steam turbine nozzles and to present a complete set of design curves that could ultimately be applied to steam turbine low pressure flow path design. We intend that, with this paper, the historical issue of nozzle discharge coefficient may come to an end.

2. The computational program offered in the present paper may be easily incorporated into a general computational procedure for wet steam turbine design when such a need arises.

3. The method of orthogonal tests has been successfully applied to determine the relative importance of the numerous factors that affect the values of the coefficient of discharge of the nozzle. The resulting sets of design curves are believed to be original and useful in the art of modern steam turbine design.

## REFERENCES

1. RYLEY, D.J.: Supersaturation in steam expanding from a low initial quality. *The Engineer*, 1957, vol. 203, 708.
- 2.
3. EDITOR of *POWER ENGINEERING*: Normogram determines correction factor for flow of wet steam in nozzles. *Power Engineering*, 1973, vol. 77, no.3, 65.
4. FAN, J.R. and GUAN, Y.: A study of the discharge coefficient of a supersaturated steam flow through nozzle. *Journal of Xi'an Jiaotong University*, 1984, vol.18, no.4, 67-76.
5. FILIPPOV, G.A., et.al.: The steam flow discharge coefficient and losses in nozzle of a steam turbine stage operating in the low steam wetness zone. *Aero-thermodynamics of steam Turbines*, ASME, 1981.
6. MOHEBAN, M. and YOUNG, J.B.: A study of thermal non-equilibrium effects on low-pressure wet-steam turbines using blade-to-blade time-marching technique. *Int. J. Heat and Fluid Flow*, 1985, vol.6, no.4, 269.
7. MOHEBAN, M. and YOUNG, J.B.: Experimental results for nucleating steam flow in a two-dimensional supersonic duct and comparison with theory. *Int. J. Heat and Fluid Flow*, 1985, vol. 6, no.4, 223.
8. ZHANG, J.L.: A study of the discharge coefficient of supersaturated steam flow through steam turbine in the presence of various effects on the flow. MS Thesis, 1987.
9. JACKSON, R.: SLIPFLO-A computer program for one dimensional wet steam flow with distinct phase velocities. Central Electricity Generating Board, 1977.
10. MOORE, M.J. and SIEVERDING (ed.), *Two-phase flow in turbines and separators*, McGraw-Hill, 1976.
11. HUANG, Y.: Numerical solution of the theoretical equations of wet steam expansion flow in a Laval nozzle with condensation of flow friction and Virial correction for the equation of state. MS Thesis, 1984.



## 29. Water drop sizing and the development of an off-line automatic drop image analysis system

M. JINGRU and P. SHAOMIN, Department of Energy and Power Engineering, Xi'an Jiaotong University, Xi'an, China

The knowledge about water drop sizes and distribution, within a turbine stage is essential to people attempting to understand the phenomena in a wet steam turbine flow path as well as the cause for blade erosion due to the impinging action of coarse water drops. Accordingly, the Department of Energy and Power Engineering and the Department of Information and Control Engineering of Xi'an Jiaotong University have worked closely together for a period of two years in developing an automatic image analysis system which composes of a drop image recognition and sizing component. The reliability of recognition of the system for drop images is roughly above 90%. The sampling apparatus of water drop can capture drops of  $10\mu\text{m}$  in diameter and above. This paper gives a full account of the work. A typical analysis is presented and compared with a manual sizing.

### INTRODUCTION

1. Drop size is one of the important parameters in many science researches and engineering practices. An accurate knowledge of drop size and distribution as a function of a system is a prerequisite for fundamental analysis of the transport of mass or heat, motion trajectory of the drops in a dispersed system, and so on. For example, the different sizes and distributions of coarse water drop determine the erosion position and extent on the blade of wet steam turbine. Again, in many combustion and atomization mechanism studies, here a knowledge of the drop size is also important.

2. Despite the importance of drop size distribution in evaluating most dispersed systems and in fundamental analysis, little is known about the actual drop size range in these units. This is due to the difficulties in measuring drop size within these types of systems. Thus it can be seen that the development of suitable instrumentation is an important part of the study of wet steam, determining to a large extent the rate at which new knowledge is obtained.

3. This paper discusses a measurement system for drop sizes and their distributions in two-phase flow. It is composed of sampling apparatus and automatic image analysis system.

### CHOICE OF METHOD

4. In present, the measuring methods used for drop size and distribution in two-phase flow are mainly several optical methods. However, it is known that optical systems are often more complex and their prices are also more expensive. But, they may provide only an intergrated value of whole light beam path, for example, MALVERN PARTICLE SIZER utilizes the principle of Fraunhofer Diffraction. As particles enter and leave the illuminated area the diffraction pattern "evolves" always reflecting the instantaneous size distribution in this area. Having measured the diffraction pattern, the computer uses the method of non-linear least squares analysis to find the size distribution that gives the close-

set fitting diffraction pattern, thus only accumulated value is provided. MALVERN PARTICLE SIZER provides three kinds of distribution functions, Rosin-Rammler; Lognormal; Normal. It can supply perfect particle system with better measurement. In practice, various physical processes taken place within different devices have certain extent effect on normal distribution law. Then, it is very difficult to determine the distribution function about multimodal distribution encountered in imperfect conditions (ref.1). Besides, it is not reliable that Rosin-Rammler function is used to calculate mean drop diameter (ref.2). In short, photography is probably the simplest, most reliable technique for obtaining droplet-sizing spectra, but can be time consuming (ref.3). Recently, due to the development of high speed photography and laser hologram the measuring range of the method has further been extended. Its advantages are that the flow is not disturbed and no calibration. But, it suffers from two grave disadvantages: first is to require for focus depth of photography lens being quite short, second is that probability of drops being visible to the camera at all in the zone which can be sharply focussed is remote because there are many other drops in the intervening space. Besides, the light source producing a flash of very short duration is necessary in flow field of high speed and photograph sizing has been the tedious, error-prone and subjective task of manual analysing the photographs (ref. 4).

5. In order to overcome these problems and produce consistent, repeatable results, the acquirement of drop picture is sampling from wet steam/gas, and then, the specimens are photomicrographed and processed by the automatic image analysis system.

6. In present, several types of the systems are in use, however, for reasons of commercial confidentiality published details of many purposebuilt systems are spare. This paper introduces a off-line automatic drop image analysis system with application to drop sizing in oper-

ating turbine of wet steam and in two-phase flows.

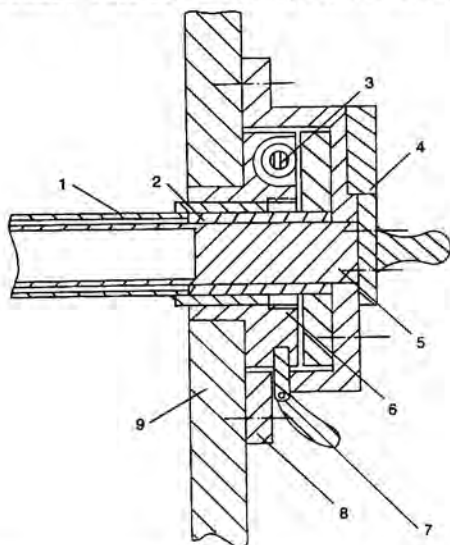
INTRODUCTION OF THE MEASURING METHOD

Sampling method

7. The exposure time in sampling must be suitable to the velocity and drop density of wet-steam flow. The compound of sampling film for the immersion method so called (ref.5) is also very important. The film must fulfill the requirements: it must be transparent, possess the same specific gravity as the drops to be sampled, have a low surface tension, high viscosity, a different refractive index from the drops and it must not dissolve the drop. For example, a mixture of mineral oil (silicone oil) and vaseline according to certain proportion from different temperature is quite suitable for sampling water drop.

8. The specimens of drop are obtained by the method that a glass slide with one surface coated with a thin layer of immersion fluid faces the stream of the medium containing drops. so that the drops impinge the treated surface and are captured. It is remarkable that the thickness of immersion fluid film must be matchable for the size of the drop to be sampled, otherwise, the drops either are not well focused in a focusing plane at all if the film is too thick or quickly disappear if it is too thin.

9. The elevation of the sampling apparatus is shown in Fig.1. According to the density and size range of drop to be measured, the spring 3 must properly be setted and slide 5 laying the glass slide with a thin layer of immersion fluid is inserted into the shell of the sampler before sampling. No sooner the spring has been released than the shell was rotated, and the drops in wet-steam/gas are captured on the glass slide. Finally, the specimes either are



- 1. shell
- 2. cover supporting slide
- 3. spring
- 4. slide cover
- 5. slide
- 6. ring setting
- 7. handle
- 8. sealed cowling
- 9. measured body

Fig.1 Simpling apparatus

photomicrographed or are directly input television camera after enlarged under microscope.

10. The advantages of the method above mentioned are simple and reliable, meantime, no calibration because the drops retain their spherical shape in the immersion fluid. Its disadvantages is that the exact maintenance and control of the same temperature of sampling slide as the steam during the exposure is very difficult when wet steam is the flow medium. Moreover, owing to the sampling slide perpendicular to the direction of flow, drops are deflected from their original direction, hence some droplets do not impinge on the slide at all. To evaluate the sampling efficiency an investigation of drop trajectories approaching an orifice slot in a cylindrical probe head has been carried out. On the basis of these calculations it was indicated that the majority of coarse water drops should be collected and the collection efficiency for drops more than 10μm in diameter will be at least 95% (ref.6).

11. Fig.2 shows a drop photograph taken with the mentioned method in test of water separator.

12. However, it must be emphasized that not only drop photographs should be clear, but also its background noise should be as less as possible to suit for a machine vision system recognizing the drop images. For this reason, the combination back lighting with reflection lighting is preferable.

Automatic analysis system for the drop images

13. The system hardware is shown in Fig.3. A conventional television camera (NSX-20A) scans the selected region of the image and transmitted video signal, T.V. scanning lines, and then the digitalizer divides each TV line into certain picture elements and assigns each of them to a grey level and coordinate value. Finally, they are inputted APPLE II computer with the support software of the image and two 128K RAM extensive cards. A TV image A/D digitalizer was designed by our research group. The image resolution is 256 x 25 x 8 bits. Management software is based on Dos 3.3, calling subrou-



Fig.2 Drop photograph (enlarged 57.74 times)

tine in the form of menu. The processes, access, input, output, processing, display, calculation and the result output of the images are controlled by different level orders. All of applied software is written in ASSEMBLY Language. It is an utility system due to the low cost and high performance.

14. In processing the drop images, the following simplify algorithms are put forward: the whole image is segmented into certain subimages regarding to the convexo-concave characteristic of its gray level, numbering the subimage order, and then the Generalized Hough Transform (refs 7-8) is used to measure the radius of each drop

Finally, the various representation form for statistical results is printed or displayed. The flow diagram of the algorithm is given in Table 1

15. The segmentation algorithm of drop image is given: where,  $f$  is the gray level function of an original drop image and  $(x,y)$  is a picture element coordination;  $g$  is a two-valued image. A  $3 \times 3$  window is used to smooth the images. The average value of its gray level is expressed as:

$$\bar{f} = 1/9 \left[ \sum_{i=-1}^1 \sum_{j=-1}^1 f(x+i, y+j) \right]$$

if  $f(x,y) - \bar{f}(x,y) < \Delta$  then  $g(x,y) = 1$ , else  $g(x,y) = 0$ . Now the two-valued image is obtained. Its algorithm can be described as:

$$g(x,y) = f(x,y) * \begin{bmatrix} 1 & 1 & 1 \\ 1 & -8 & 1 \\ 1 & 1 & 1 \end{bmatrix} \quad (1)$$

here  $\Delta$  is a threshold. The noises can be decreased if the  $\Delta$  is properly chosen. But the connectivity of each part must be ensured.

16. On the baiss of four connected standard, the points of  $g=1$  are the interested object, and the points of  $g=0$  are background. The numbering process is divided into two steps:

17. Step 1 (first scan):  
The two-valued images of each line are scanned from left to right. If the  $g$  value of  $P$  point is "0" its number is "0" when it is scanned (see Table 2.), but if its  $g$  value is "1", the  $g$  values of  $A$  and  $B$  must be considered according to the following:

(1) If  $A$  or  $B$  is "0".  $P$  number is the same one as  $A$  or  $B$  which of them has been numbered



Fig. 3 Automatic image analysis system

Table 1. Flow diagram of algorithm

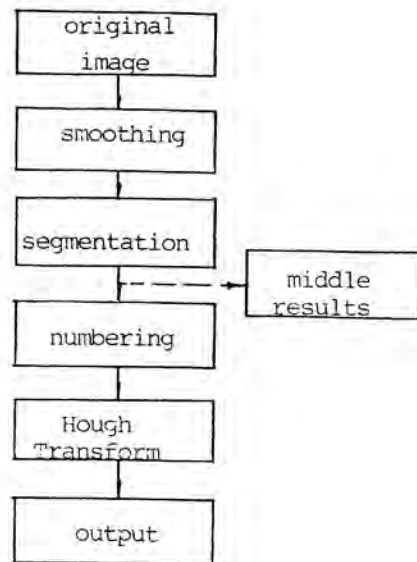


Table 2.

	A
B	P

into no zero. (2) If  $A$  and  $B$  are all "1" and  $A$  and  $B$  are a equal number, then  $P$ 's number is same as them, else,  $P$  is equal to  $B$ , however the equality of  $A$  and  $B$  must be recorded in a special form. (3) If  $A$  and  $B$  are all "0",  $P$  is given a new number.

18. Step 2(second scan):

The equality numbers are setted same a number, and then all of number is put in order and arranged again. Thus, all picture element in one connective area would have same a number and every unconnective areas would have different number each other.

19. After the two steps, the whole image is segmented into certain areas. As shown in Fig.4, the four coordinates of each connective area, above; below; left; right are its angle top points. If the area is too small, it is given up as a noise.

20. Now, the Generatized Hough Transform is used to measure drop radius.

21. The edge points of the drop image within same a connective area are first defined as the turn points of their gray level change and the following conditions must also be met:

$$f''(x,y) = 0 \quad \text{and} \quad f'(x,y) \neq 0$$

Here Pseudo-Laplacian operator can express the bidifferential  $f''(x,y)$ . Its form is the same as expression (1). hence,  $f''(x,y)$  can use the convolution result  $g(x,y)$  in segmentation. Thus the edge points of drop image must meet the conditions:

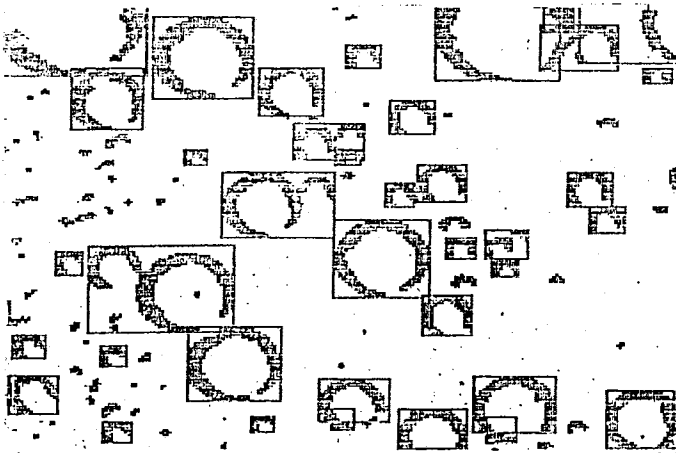


Fig.4 Segmenting a frame of T.V image into a certain subimages

$$g=0 \quad \text{and} \quad f' \neq 0$$

The integer coordinate values meeting  $g(x,y)=0$  is not often found, so the approximate zero-crossing points are also considered as the edge points.

22. The Generalized Hough Transform is defined as follows:

Now let  $r$  be drop radius,  $(x_i, y_i)$  be its edge point set and  $\phi_i$  be its direction angle of the greatest gray gradient. Then we can get:

$$\begin{aligned} a_i &= x_i - r \sin \phi_i \\ b_i &= y_i - r \cos \phi_i \end{aligned} \quad (2)$$

So the point  $(x_i, y_i)$  can be converted in the  $\phi_i$  direction into  $(a_i, b_i)$  in parameter plane where  $r$  is as a reference. If the radius of the circle which is joined by  $(x_i, y_i)$  point set is  $r_0$ , the converted points could all concentrate to same a point in the  $(a, b)$  plane when  $r=r_0$ . This point is just the  $(x_i, y_i)$  circle center and  $r_0$  is its radius. But this point will not be found if  $r \neq r_0$ . Therefore, a matrix accumulator is set up to examine the concentrated process of  $(a_i, b_i)$  with  $r$  change. The point which is corresponding to the concentrated value of the matrix in  $(a_i, b_i)$  plane is the circle center when the value is equal to or greater than a threshold and the reference  $r_0$  is its radius.

23. The correct detection can not be influenced by some of light spots within the drop images because the direction of their edge gray gradient is inward, but the direction of light spot gradient is outwardly divergent. In practice, by means of a small window instead of the point in the matrix, this method is still effective to those drop images which have some

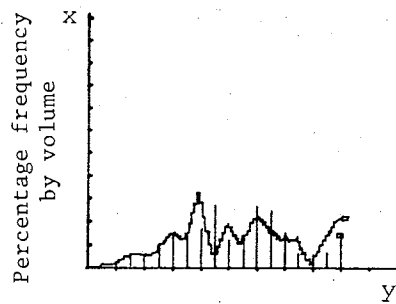


Fig.5 Drop histogram  
X=25 $\mu$ m/w ; Y=0.1/w

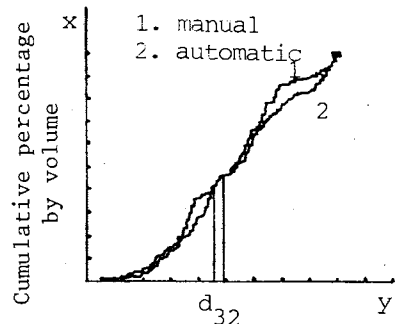


Fig.6 Cumulative curve  
X=25 $\mu$ m ; Y= 0.1/w

edge loses so long as the threshold is properly selected and the drop images of irregular circle could be automatically given up as a noise.

24. However, there still are some errors in the detecting processes above mentioned:

1. The quantity error is one picture element because the digital circle replaces continuous serial circle.

2. Due to matrixing radius into diameter in Hough Transform one picture element of error may also be produced when the picture elements of some drop images are even numbers. The smaller circle size is, the larger relative error is.

25. If you want to improve the analysis precision, the higher resolution computer can be selected.

#### A TYPICAL EXAMPLE APPLICATION FOR SEPARATOR

26. Fig. 5,6 show the statistical results by manual and the automatic image analysis system in test of water separator. The drop number by manual analysis is 593, more 154 than automatic because of the difference from measuring area range. In Fig.5. The extent covering on the results of the automatic analysis expres-

sed by all of vertical line indicates the difference between them. As shown in Fig.6, two kinds of cumulative curves are in good agreement. The Sauter mean diameters are  $(d_{32})_{\text{man}} = 113 \mu\text{m}$  and  $(d_{32})_{\text{auto}} = 120 \mu\text{m}$  respectively. The error between them is 5.8%.

#### CONCLUSION

27. (1) The method above discussion is simple and reliable to size the drops more than  $10 \mu\text{m}$  in diameter. It is no calibration, hence, is a absolute method.

(2) Dividing a frame of T.V. image into certain number subimages, the automatic image analysis system has successfully detected circle (drop image) radius with Generatized Hough Transform.

#### ACKNOWLEDGEMENTS

28. The automatic image analysis system was developed in Information and Control Engineering Dept. under Prof. Yuanlong Cai and the contributions of his staff and students are gratefully acknowledged. Prof. Yinian Cai is especially thanked for his funding the work.

#### REFERENCES

1. DALLVALLE J.M., ORR C., JR., and BLOCKER H. G. Fitting bimodal particle size distribution curves comparison of methods, *Industrial and engineering chemistry*, 1951, vol. 43, June, 1377-1380.
2. MUGGLE R.A. and EVANS H.D. Droplet size distribution in spray, *Industrial and engineering chemistry*, 1951, vol.43, June, 1317-1324.
3. MOORE M.J. Two-phase steam flow in turbines and separators, p.235. McGraw-Hill, New York, 1976.
4. OW C.S. and CRANE R.I. A simple off-line automatic image analysis system with application to drop sizing in two-phase flows, *Int.J. heat & fluid flow*, 1980, vol.2, 47-53.
5. Measuring the size of droplets in wet-steam turbines. *Brown boveri review*, vol.49 no. 7/8, p.350-359.
6. WILLIAMS G.J., *EL Instrumentation for wet steam measurements*, IMech E, 1976, C67/76.
7. CAROLYN KIMME, DANA BALLARD and JACK SKLANSKY Finding circles by an array of accumulators, *Communication of the ACM*, 1975, vol.18, Feb., 120-125.
8. JACK SKLANSKY On the hough technique for curve detection, *IEEE Trans*, 1978, vol. c-27, Oct., no.10.



## 30. On the dissimilarities in wet steam behaviour in model and full-scale turbines

F. BAKHTAR, PhD, DSc, FIMechE, Department of Mechanical Engineering, University of Birmingham, and  
A. V. HEATON, BSc, PhD, The Electricity Council Research Centre (formerly of the University of Birmingham)

The paper describes the results of an investigation in which nucleation theory has been applied to one-dimensional equivalents of flow in a model low pressure steam turbine and a geometrically similar full size machine.

In an earlier investigation one-dimensional programs have been applied to representations of a superheated and a nucleating run on a model turbine. The calculations were then repeated for a scaled up version. The overall conditions thus obtained have been used as the basis for the analysis reported, in which the procedure has been applied to the root and tip sections of the nucleating stage.

### NOTATION

d	equivalent diameter of passage
f <sup>e</sup>	friction factor
h	specific enthalpy
I	nucleation rate      1/(m <sup>3</sup> s)
Ma	Mach number
p	pressure                      bar
r	droplet radius
ΔT	degrees of supercooling
x	distance along flow path
y	wetness fraction

### INTRODUCTION

1. As estimated by Taupel (ref.1) some 80% of the world power consumption is supplied electrically and with very few exceptions the electrical generators are driven by steam turbines, the only machines capable of operating on any fuel and generating power on a large scale. It is, therefore, important that the expansion in steam turbines be made as efficient as possible.

2. During the expansion of steam through a turbine, the state path crosses the saturation line and the fluid becomes a two-phase mixture, consisting of a large number of minute droplets carried by the vapour phase. The formation and subsequent behaviour of the liquid create problems which lead to reductions in the machine output and are collectively known as wetness losses but the detailed processes which give rise to them are insufficiently understood. The development of the nucleation theory has been of help to the study of wetness problems in steam turbines as in combination with the gas dynamic equations it allows nucleating and wet steam flows to be described analytically (refs.2-4). The earlier treatments were concerned with one-dimensional flows and have reached a high degree of sophistication. More recently the technique is being extended to two- and three- dimensional fields (refs.5-6). but these are still in early stages of development. Despite its limitations the one-dimensional method of

treatment remains a useful tool because of its simplicity. A number of cases of its careful application to one-dimensional representations of flow through turbines have yielded interesting results (refs.7-8).

3. Experimental investigations of wetness problems are hindered by the difficulties of reproducing turbine flows under controlled conditions in the laboratory. Model turbines are often used in the development of turbomachines. In view of the large number of parameters which have to be matched between model and full size turbines, originally an investigation was undertaken to examine how realistically wetness problems could be scaled in model turbines. To this end, the one-dimensional programs were first applied to the representation of an overall expansion in a model turbine and then repeated for a scaled up version (ref.9). Adopting the overall conditions thus obtained, this has been followed up by the present study in which the procedure has been repeated for the root and tip sections of the nucleating stage.

### Outline of the method of treatment

4. The method of treating the flows of nucleating and wet steam used in the investigation has already been described (ref.10). As stated, the treatment is one-dimensional but differs from others available in the literature in two important respects:-

a. The properties of steam are calculated from equations which are mutually consistent and there are no approximations in the energy equation. This allows the isentropic efficiencies of different expansions to be calculated and compared.

b. The aerodynamic losses are introduced into the equations by friction factors; allowing the aerodynamic and thermodynamic losses incurred by the flow to be separated.

5. Before applying the treatment to the

## FLOW ANALYSIS AND MEASUREMENT

flow in a turbine it is necessary to construct a one-dimensional equivalent for the region under scrutiny. Furthermore in view of the sensitivity of nucleating flows to frictional reheat, it is important that the losses be distributed along the flow path realistically. For this reason the calculations are best carried out for specific expansions in given machines.

### Test Results

6. The analysis is based on the results of two tests carried out on a scale model of the last two stages of a full size turbine run at the correspondingly higher speed. The tests were run at the same pressure levels and velocity ratios but different inlet temperatures. In the first run, called the dry test the inlet temperature was kept sufficiently high to inhibit nucleation while in the second experiment, termed the wet run the temperature was lowered and the steam allowed to nucleate. The measurements of the pressure ratio, overall efficiency and the mass flow rate taken in the dry test were used for the estimation of the friction coefficients which were then used for the analysis of the wet test. In the case of the full scale machine, the calculations were repeated using a combination of design data and the measurements on the model to assess the effects of wetness at full size.

### Method of Analysis

7. Analysis of the dry test The flow passage in a turbine stage is shown diagrammatically in Fig. 1. Taking the stator blades as an example, from the point of view of its behaviour the flow over this part of the stage may be divided into three sections, blade inlet to throat, throat to the end of blade and the end of the blade to the end of gap, referred to as sections A, B and gap respectively. The method of determining the one-dimensional equivalents for the passage shapes is given in Appendix 1.

8. Evaluation of Aerodynamic Losses The losses suffered by dry steam passing through a turbine stage are commonly divided into two groups. Group (1) includes the profile, secondary and annulus losses while those associated with lacing wire, disc windage, partial admission and any leakages through guide glands, balancing holes and rotor tip are regarded as group (2) losses.

9. Group (1) losses were calculated for both the model and full scale machines from the data published by Craig and Cox (ref.11). In the case of group (2) losses, for the model, as the total of the losses was known they were inferred as the difference. Group (2) losses were also estimated from data available in the literature with reasonable agreement. The full size group (2) losses were then assumed to be the same as those for the model.

10. Distribution of Aerodynamic Losses Along the Flow Paths With the magnitude of the aerodynamic losses determined their distribution over the flow path was by

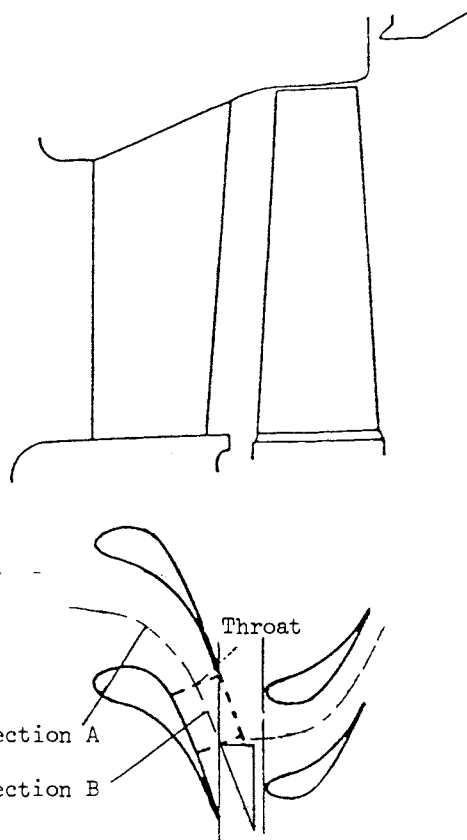


Fig. 1. Representation of Flow Passage selection of suitable friction factors to give

$$\int_{x_1}^{x_2} \frac{f u^2}{2 d_e} dx = \Delta h_{loss}$$

where  $f$  is the friction factor  $h$  the specific enthalpy of the fluid,  $u$  the velocity  $x$  the distance along flow path and  $d_e$  the equivalent passage diameter.

11. In the analysis of the overall machine performance 90% of the profile and the whole of the secondary losses were distributed over sections A and B of blade passage. 10% of the profile, the whole of the annulus and group (2) losses were distributed in the gaps.

12. In practice the distributions were achieved by iterating the solutions and the arrangement adopted gave reasonable consistency in mass flow rate between blade rows as well as agreement with design degrees of reaction.

13. Analysis of the Wet Test. The equivalent shapes and friction factors thus estimated were then used for the analysis of the wet test. The interstage and inter row pressures were iterated until mass flow consistency was achieved. Following this the loss coefficients were finally checked using Craig's and Cox's data and only a small adjustment was found necessary in the last blade row.

14. As already stated the above procedure was initially applied to the overall conditions for the machine. The solutions thus obtained were designated as the main

solutions and have been given elsewhere (ref.9). It was then reasoned that since these refer to gross averages for the machine they do not necessarily represent any particular part of the flow but they can be used as the basis for further investigations of the problem. One of the specific solutions already described and relevant to the present study are those of the flow at mid-height. In these the flare of the casing was neglected and it was assumed that the flow experiences the profile losses only. For the ease of comparison with the root and tip solutions Tables (A1) and (A2) in Appendix 2 have been extracted from Tables (2) and (3) of Reference (9).

#### Root and Tip Solution

15. Analysis of Dry Test The group (1) losses for the flow over these sections were estimated by using the data of Craig and Cox and group (2) losses were taken from the main solutions. 90% of the profile losses were distributed in sections A and B of the blade and the remaining 10% in the gap as in the main solutions but two separate schemes for distributing the group (2) losses were tried. The arrangement adopted was to divide the group (2) losses equally between the root and tip sections for the flow following the stator and to distribute them completely at the tip section following the rotor. The analysis of the dry flow was then carried out according to the procedure established for the main solution. The resulting expansion paths for the root and tip solutions for the model turbine are given diagrammatically in Fig. (2). The general features of the flow over the root section are shown by the full line in the figure. The flow accelerates rapidly to the stator throat. Further expansion is caused by the deflection of the supersonic flow in section B of the blade and there is a slight pressure drop on the stator gap caused by friction. The flow then accelerates to the throat of the impulse rotor blading followed by diffusion in the rest of the blade.

16. The features are somewhat different for the flow over the tip section as shown by the dotted line in Fig. 2. The flow accelerated to the stator throat but there is then some diffusion in section B of the blade caused by the flare of the casing. There is a small further acceleration in the stator gap which is a consequence of introducing the losses into the flow by a friction factor. Acceleration is similarly rapid up to the rotor throat where sonic velocity is attained but there is further acceleration in section B of the blade due to the deflection of the supersonic stream. In the gap following the rotor there is some diffusion caused by the flare of the casing.

17. Analysis of the Wet Tests. The specific conditions associated with each of the root and tip solutions for the model and full size machines led to a different problem. For this reason they will be discussed individually.

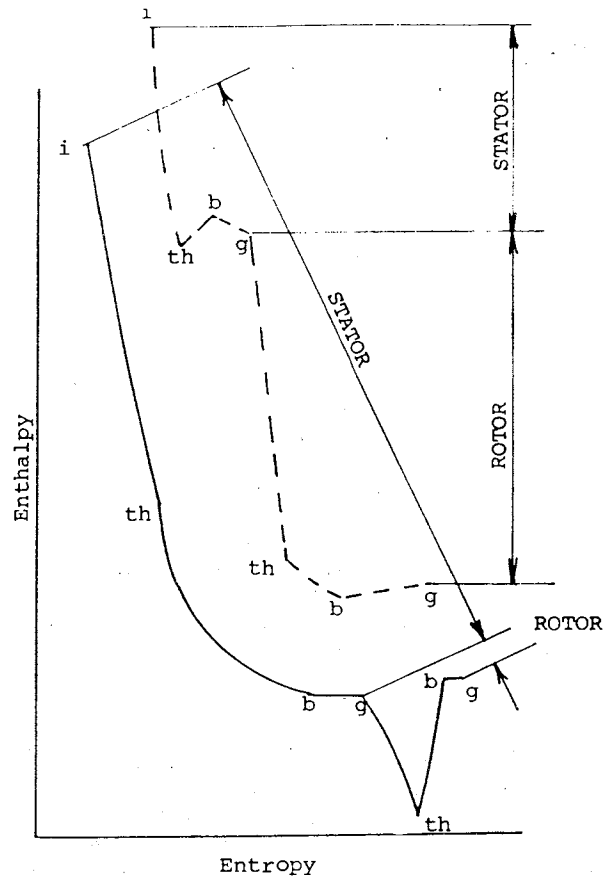


Fig. 2. Typical Expansion Paths Dry Solutions

#### The model root solutions

18. There is a very small degree of reaction at this section and the stage supercritical heat drop occurs almost entirely over the stator. With the blade section being convergent, the flow angle was assumed to change at the trailing edge of the stator for both the dry and wet solutions. But the adoption of the outlet angles from the dry solution in the case of the wet flow led to thermal choking and unstable conditions as described in (ref.12). To achieve an acceptable solution the outlet angle for the wet solution had to be increased by  $4^\circ$  above that for the dry flow.

19. An abridged version of the computed results for the flow over the stator and rotor is given in Table (1). It will be seen that the flow continues dry in section A of stator blades but attains 32.9K of supercooling on reaching the throat by which point it has already begun to nucleate. There is a drastic increase in the nucleation rate with further expansion in section B which returns the flow to near equilibrium. The release of latent heat to the supersonic flow causes a pressure rise starting in section B of the blade and continuing into the gap. This may have possible implications for boundary layer stability and flow distribution near the root. Reversion is completed by the end of the stator gap and the fluid remains near equilibrium through the rotor. It is interesting to note that

TABLE 1

Model Root Wet Solution

For Legend see Fig. 2  
Mach numbers with \* are in the relative frame

Loca- tion	x cm	$\rho$ bar	Ma	$\Delta T$ K	I 1/(m <sup>3</sup> s)	$r$ $\mu\text{m}$	$y$ %
i	0	0.375	0.15	-	-	-	-
th	3.81	0.197	1.00	32.9	$1.87 \times 10^{18}$	-	-
	4.32	0.118	1.33	51.4	$1.2 \times 10^{24}$	.002	0.261
b	4.75	0.122	1.21	10.7	-	.005	3.27
g	7.19	0.135	1.11	3.5	-	.005	3.22
	1.02	0.125	0.75*	4.2	-	.005	3.47
th	2.21	0.103	0.88*	4.9	-	.0052	4.02
	2.54	0.103	0.89*	2.7	-	.0058	4.22
b	3.05	0.127	0.69*	1.9	-	.005	3.35
g	7.62	0.126	0.36	3.8	-	.0048	3.18

the slight change in the flow area in the rotor blade causes the fluid to accelerate considerably in the rotor and the Mach number of 0.899 in the throat section is very close to the choking condition. At exit from the rotor the droplets are estimated to have a mean diameter of 0.01  $\mu\text{m}$  at a steam wetness fraction of 3.18%.

**Model Tip Solution**

20. The blading at this section is of a relatively high reaction and the heat drop over the stator blades is well below the critical while that for the rotor exceeds it. Despite this the flow passage over the rotor blades is convergent. Thus to allow for further expansion of the flow downstream of rotor throat the outlet angle was assumed to deflect.

21. In the case of the dry solution the inter row pressure selected gave good agreement with the design degree of reaction and adequate agreement in mass flow rates between the stator and rotor rows. In the wet solutions, however, selection of an inter row pressure to match the degree of reaction caused discrepancy in mass flow rates between the stator and rotor. In order to bring the mass flow rates to an agreement similar to that obtained for the dry solution the inter row pressure and with it the degree of reaction had to be altered.

22. With the inter row pressure thus determined, the solution of the wet flow over the rotor blades presented some further points of interest arising from choking conditions in two-phase mixtures. The speed of sound in a two-phase mixture has been examined by a number of investigators e.g. (ref.13-14). It has been shown that the propagation velocity can vary from the equilibrium to frozen speeds of sound depending on the wave frequency. The parallel situation in the flow of a two-phase mixture through a convergent-divergent nozzle is the choking at the throat. It can vary between the equilibrium and frozen speeds of sound depending on the conditions (ref.10). In cases where the flow chokes at a velocity below the frozen speed, the mathematical singularity associated with it shifts into the diverging section where this condition is attained. The angle of

divergence is one of the important factors influencing the choking speed at the throat. In the case of convergent blades the tilt in the outlet angle, being itself a function of flow conditions allows for the possibility that the overall parameters may be satisfied by more than one solution. Indeed with a throat Mach number just below unity many different solutions downstream of the throat were possible but non in fact matched the outlet pressure. To obtain the given outlet pressure it had to be assumed that the flow chokes at the frozen speed of sound at the throat. An abridged version of the solution is given in Table 2.

TABLE 2

Model Tip Wet Solution

For Legend see Fig 2

Mach numbers with \* are in the relative frame

Loca- tion	x cm	$\rho$ bar	Ma	$\Delta T$ K	I 1/(m <sup>3</sup> s)	$r$ $\mu\text{m}$	$y$ %
i	0.0	0.375	0.18	-	-	-	-
th	4.92	0.249	0.81	22.4	-	-	-
b	6.27	0.262	0.73	18.0	-	-	-
g	8.89	0.247	0.77	19.7	-	-	-
th	1.80	0.139	1.00*	42.7	$4.2 \times 10^{23}$	.0006	.0003
	1.90	0.127	1.06*	52.2	$1 \times 10^{24}$	.0005	.0005
	2.05	0.123	1.08*	53.6	$1.4 \times 10^{24}$	.0005	.0045
	2.16	0.121	1.09*	54.1	$1.6 \times 10^{24}$	.0007	.017
b	2.36	0.128	1.04*	47.8	$2.5 \times 10^{23}$	.0018	0.324
g	9.98	0.123	0.33	4.4	-	.0041	3.59

23. The fluid supercools on passing through the stator but not sufficiently to cause appreciable nucleation. At entry to the rotor the supercooling attained is 19.7K. Expansion through section A of the rotor increases the supercooling and nucleation rate drastically, the rapid rise in the nucleation rate occurs near the throat and in the time available does not yield any significant water at the throat. With the tilt in the outlet angle, the supercooling increases with the further expansion of the fluid for a short distance but then the release of heat resulting from condensation retards the flow and causes a slight pressure rise. On reaching the end of section B the fluid is still substantially supercooled and the Mach number just above unity. At this stage on entering the rotor gap the relevant fluid velocity becomes its absolute value which is well below the sonic speed and the flow can accommodate the release of the latent heat as the fluid returns to thermodynamic equilibrium. It will be appreciated that the choking Mach number at the throat and the tilt in the flow outlet angle were dependent on the degrees of supercooling at inlet and the overall pressure ratio. A small change in either parameter can yield a different flow pattern in section B of the blade.

**Full Scale Root Solution**

24. The general features of the solution over the full scale stator were similar to those obtained for the model. Once again to avoid problems of thermal choking the outlet angle had to be increased. But the slower

expansion partly compensated for the larger dimensions of the full scale machine and only a small increase in the outlet angle over that used for the model wet flow was sufficient to yield a stable solution. The situation was different with the flow over the rotor blades. With the slower expansion the rotor was also found to choke and in fact carried a lower mass flow than was passed by the stator. It will be remembered that the supercritical stage pressure drop occurs almost entirely over the stator. It is therefore necessary that the stator throat be choked. It was, therefore, argued that the practical consequence could be either one or the combination of two possibilities.

a. As the zone of rapid condensation occurs in the supersonic part of the flow downstream of stator throat, the release of the latent heat causes the pressure to rise. This may in turn increase the boundary layer losses raising the inlet pressure to the rotor. The consequent rise in the general pressure level in the rotor would increase the mass flow rate through it. To investigate this possibility a series of calculations were carried out.

Increasing the friction factor in the stator gap from .014 to .0317 increased the inlet pressure to the rotor sufficiently to pass the flow.

b. The flow will tilt in the radial direction. In this case the inter row pressure and with it the pressure distribution would be accepted and the discrepancy in mass flow rate assumed to be accommodated by flow re-distribution. The advice available suggested this to be the more likely possibility, although clearly many solutions intermediate between the two are possible.

25. An abridged version of the computed results adopting approach 2 is given in Table 3. The general features of the solution are similar to those for the model. The maximum supercooling experienced by the flow is 45.7k in comparison with 51.4k for the model which is a consequence of the slower expansion in the full scale machine. The predicted pressure rise in the gap between the stator and rotor is higher but occurs over a larger distance. The choking Mach number in the rotor throat is 0.86.

**Full Scale Tip Solution**

26. The inter-row pressure was taken to be the same as that adopted for the model. The solution for the flow over the full-scale stator was very similar to that for the model, the fluid remaining in dry supercooled state throughout the expansion in both cases. The only difference was in the degrees of supercooling attained by the flow at inlet to the rotor which was slightly higher for the full scale machine reflecting the lower profile losses caused by the higher Reynolds number of the flow.

27. The position was different in the case of the rotor. This was because with the larger dimensions of the full scale machine, the time intervals available for the flow to

TABLE 3  
Full Size Machine Root Wet Solution  
For Legend see Fig. 2

Mach numbers with * are in the relative frame							
Loca- tion	x cm	p bar	Ma	$\Delta T$ K	$I_3$ 1/(m <sup>3</sup> s)	r $\mu$ m	y %
i	0.0	0.375	0.15	-	-	-	-
th	17.78	0.196	1.00	32.8	1.8x10 <sup>18</sup>	-	-
	18.41	0.148	1.22	45.7	1.9x10 <sup>23</sup>	0.0018	.02
	19.05	0.168	1.06	14.8	-	0.0077	1.92
b	22.10	0.112	1.27	3.3	-	0.0103	4.36
	30.48	0.131	1.1	1.3	-	0.0093	3.24
g	33.5	0.142	1.03	1.3	-	0.0087	2.7
	5.08	0.131	0.75*	2.2	-	0.0091	2.9
th	10.16	0.113	0.86*	2.4	-	0.0095	3.42
b	14.22	0.133	0.69*	1.6	-	0.0087	2.66
g	35.56	0.131	0.36	2.1	-	0.0087	2.61

traverse corresponding points were greater and the droplets nucleated before the throat affected the fluid significantly. The flow choked at the physical throat at a velocity well below the frozen speed of sound which was then attained downstream of this location. Under the given conditions the outlet pressure could be matched without tilting the outlet angle. An abridged version of the computed results is given in Table 4. The flow behaviour for the rotor is totally different from that observed for the model.

TABLE 4  
Full Size Machine Tip Wet Solution  
For Legend see Fig. 2

Mach numbers with * are in the relative frame							
Loca- tion	x cm	p bar	Ma	$\Delta T$ K	$I_3$ 1/(m <sup>3</sup> s)	r $\mu$ m	y %
i	0.0	0.375	0.183	-	-	-	-
th	22.86	0.243	0.84	23.7	4.3x10 <sup>10</sup>	-	-
b	29.21	0.26	0.75	18.8	0.72	-	-
g	38.9	0.247	0.79	20.4	1.4x10 <sup>4</sup>	-	-
	7.62	0.189	0.68*	33.9	3.5x10 <sup>19</sup>	0.005	.0001
th	8.38	0.18	0.72*	35.9	3.9x10 <sup>20</sup>	0.009	.0046
	9.14	0.176	0.75*	34.1	3.5x10 <sup>19</sup>	0.024	0.2755
	9.9	0.167	0.77*	30.7	3.6x10 <sup>15</sup>	0.036	.936
	10.67	.152	0.84*	23.3	3.5x10 <sup>9</sup>	0.045	1.74
b	11.05	.133	0.98*	25.5	1.1x10 <sup>12</sup>	0.048	2.14
	12.32	0.13	0.43	4.4	-	0.059	3.84
g	37.74	0.128	0.29	0.2	-	0.059	3.8

28. This is because to match the imposed outlet pressure it was necessary to assume that the flow outlet angle remained constant downstream of the throat. Under these conditions the flow attains a maximum supercooling of 35.9k and then rapid condensation occurs in the still subsonic flow in section B of the blades.

**General Remarks**

29. It is accepted that representation of three-dimensional flows in a turbomachine by a series of streamtubes is crude. But the actual calculations of the one-dimensional flows are accurate and the assumptions regarding overall pressures and positions and dimensions of blade throats and spacings are correct. Thus within the validity of the assumptions about changes in the thickness of stream tubes in the radial direction the

FLOW ANALYSIS AND MEASUREMENT

calculations provide valuable indications of the likely behaviour of the flow.

30. The resulting droplet sizes normalised to a wetness fraction of 4%, the maximum degrees of supercooling, the locations where they occur and some estimates of the thermodynamic losses associated with the nucleation process are summarised in Table 5.

TABLE 5

Extracted Nucleation Data

Key for Location of  $\Delta T^*$

R=rotor, S=stator, B=Section B, th=throat.

	MODEL			FULL SIZE		
	Mid		Mid		Tip	
	Root	Height	Root	Height	Root	Tip
Max super-cooling $\Delta T^*/K$	51	43	54	46	37	36
Location of $\Delta T^*$	S	R	R	S	R	R
	B	th	B	B	th	th
Droplet radius $\mu m$ $y = .04$	.0054	.017	.004	.010	.04	.06
Nucleation loss kJ/kg	8.4	5.6	9.4	6.5	4.2	3.9

31. It will be seen that within each machine, there are wide variations in the maximum degrees of supercooling and a general shift in the location where it occurs. In both machines the pressure ratio over the stator root section is higher than the critical and the Wilson point occurs downstream of the throat but still within the passage. At mid-height it has moved to the rotor throat. As already discussed the nucleation behaviour has been completely different between the model and full scale machines at the rotor tip. With the slower expansion in the full scale machine, the limiting degrees of supercooling are lower and the resulting droplets larger. But in both cases the droplets are predicted to be extremely small. However, the existence of any non-uniformities within the flow will cause the droplet distributions to be polydisperse (ref.16). The reversion losses are calculated by an approximate procedure but the values quoted are mutually consistent. As expected the higher the maximum degrees of supercooling, the higher are the nucleation losses and the smaller the droplets.

32. The thermodynamic losses are only one aspect of two-phase effects in steam turbines. A further and perhaps more important aspect brought out by the analysis is the aerodynamic consequences.

33. Considering the flow over the root section of the stator blades first and leaving aside the choking problems of the full scale rotor at this section, there was a small degree of reaction and the supercritical stage heat drop had to occur over the stator. It was therefore necessary to assume that the stator blades were choked and the flow became supersonic downstream of the throats. With the steam temperatures adopted the zone of rapid condensation occurred in the supersonic streams and it was predicted that this would cause the pressure

to rise. This may in turn cause the boundary layer losses to increase.

34. A further effect is the influence of the variations in the speed of sound on choking mass flow rates in turbine blading. It has been known from the early days that the choking mass flow rate through the throat of a nozzle is higher when the fluid supercools than when it can be assumed to be in equilibrium. Thus when considering a turbine stage the fluid passing through the stator must flow through the rotor, the pressure ratio over each row necessary to pass a given flow rate must depend on the steam condition. This will vary depending on whether the fluid is supercooled or wet. It will also depend on the rate of expansion. Thus for a given stage pressure drop the inter row pressure must depend on whether the flow through both the rows is dry, wet or whether it is supercooled in one and wet in the other.

35. The very complex problem of flow in a turbine with twisted blading cannot be adequately represented by a one-dimensional treatment but indications of problems caused by this effect may be sought by comparing the solutions. The presented results for the flows over both the hub and tip sections provide examples of this effect. The flow over the mid-height section provides a further illustration. For the given overall stage pressure drop, the necessary inter row pressure to achieve mass flow consistency between the stator and rotor rows has been 0.197 bar for the model which has resulted in an exit Mach number of 0.96 from the stator gap. Thus it can be said that the stator blades have choked and the rotor has taken the mass flow without choking. This may be contrasted with the inter row pressure of 0.215 bar for the full scale machine. With a lower overall pressure drop the stator blades are not choked but the associated lower mass flow rate is sufficient to choke the rotor blades which have needed the larger pressure drop.

36. The variations of pressure at strategic locations at root, mid-height and tip for the model and full size wet solutions expressed as a fraction of inlet stagnation pressure are given in Table 6.

TABLE 6

Pressure distributions in model and full scale wet solutions given as fraction of inlet stagnation pressure

Locations	Stator		Inter-row	Rotor		
	Inlet	Throat		Throat	Outlet	
Model	Tip	0.973	.646	.641	.361	.319
	Mid-height	0.973	.656	.511	.389	.324
	Root	0.973	.511	.350	.267	.327
Full size	Tip	0.973	.631	.641	.467	.332
	Mid-height	0.973	.656	.558	.428	.324
	Root	0.973	.509	.368	.293	.340

37. Excepting the stator outlet pressure at mid height, the pressure distributions in the stators of both machines are very similar. Large differences in the distribution are apparent at the throat sections of the rotors. The present distributions have resulted from the assumption of uniform variations of stream tube thickness with radius through the machines and only reflect the changes brought about by the differences in scale. Important differences were also apparent between the wet and dry solutions for the model. But the wet and dry tests on the model had been carried out at slightly different pressure ratios and the rotor speeds had been adjusted to keep the velocity ratios the same. It is therefore not easy to see the differences caused by choking at a glance. For this reason the results of the dry solution have not been given.

38. Returning to the results of the mid-height solutions in Table 6. If the calculated inter row pressures are accepted there will be a noticeable difference in the degree of reaction at mid height between the model and full scale machines. This will, in turn, affect the outlet velocity from the stator and the incidence to the rotor. Apart from the differences in flow behaviour discussed in connection with the individual root and tip solution, the question arises as to the effect of the different pressure distributions in model and full scale rotors on the radial equilibrium of flow in these machines.

#### Summary of Conclusions

39. The conclusions drawn may be summarised as follows:-

a. The complexities of three dimensional flows through steam turbines are aggravated by the problems of nucleation and two-phase effects in the working fluid. The nucleation process is extremely sensitive to frictional reheat, dissipation and operating conditions whilst the heat release due to phase change can have potentially serious aerodynamic repercussions. A complete theoretical solution allowing for all relevant parameters is not available at present but much valuable insight into the wetness problems may be obtained by the judicious application of the one-dimensional method.

b. An important aerodynamic consequence of heat release by condensation in a turbine stage is its effect on the choking mass flow rate. For otherwise similar conditions the swallowing capacity depends on the thermodynamic state of the fluid as well as the rate of expansion. For a given stage overall pressure ratio, the inter row pressure necessary to give mass flow consistency between the rows depends on the choking conditions. This in turn can affect the degree of reaction of the nucleating stage between model and full scale turbines.

c. The processes of nucleation and droplet growth in flowing steam are time dependent but the initial degrees of supercooling necessary to yield substantial nucleation is relatively high. Thus the difference in the

time available for the flow over the rotor tip sections of the model and full scale turbines considered have been sufficient to yield totally different characteristics.

d. To obtain similar wetness behaviour in model and full scale turbines it is necessary that the rates of expansion in the two machines be matched. In the absence of such matched conditions the use of nucleation behaviour obtained in model turbines for application to full scale machines requires considerable care.

#### Acknowledgements

40. The theoretical investigations described in the paper have been carried out in the Department of Mechanical Engineering, University of Birmingham and supported by a grant from the Science and Engineering Research Council. The authors are extremely grateful to Dr. R A Webb and R A Savage for assistance in the computation of some of the results presented.

#### Appendix 1

##### Evaluation of Equivalent One-Dimensional Shapes

This has consisted of the determination of the equivalent width, height and length of each of the sections comprising a stage.

Equivalent width The equivalent width and length of Section A were determined by the procedure of fitting with circles. The length of the arc perpendicular to both sides of the passage is taken as the equivalent width and the distance along the mid point of the paths is taken as the passage length. When the flow is subsonic the width of Section B is taken as constant and equal to the throat width. For supersonic outlets, the flow is assumed to choke at the throat and to become supersonic in section B. To allow for this effect with reference to Fig. 1, the imaginary wall after the trailing edge on the pressure side is tilted. The gaps following the stator are treated similarly. For gaps following the rotor the width is regarded as constant and equal to that at exit from the rotor and adjusted to allow for the velocity triangles.

Passage height This is taken as equal to stream tube height.

Passage length The procedure for determining the length of section A has just been described. That for section B is taken to be from the throat to the point of intersection of mid streamline and one joining trailing edges of blades. The length of the gap following the stator is calculated from a knowledge of the gap axial length and the flow outlet angle. That for the rotor gap is calculated from the axial length and the absolute angle.

The equivalent shapes thus determined are fitted by cubic polynomials which are then adopted.

APPENDIX 2  
Mid-height Wet Solutions

TABLE A1  
Wet Test, Model Mid-height Solution  
For Legend see Fig. 2

Mach numbers with \* are in the relative frame

Loca- tion	x cm	p bar	Ma	$\Delta T$ K	$I$ $m^{-3}s^{-1}$	r $\mu m$	y %
i	0.0	0.375	0.17	-	-	-	-
th	4.32	0.253	0.76	19.9	$3.0 \times 10^2$	-	-
b	5.79	0.225	0.86	24.0	$1.7 \times 10^8$	-	-
g	8.33	0.197	0.96	29.6	$6.0 \times 10^{16}$	-	-
th	1.42	0.150	0.60*	42.6	$3.9 \times 10^{22}$	0.003	0.02
	1.88	0.141	0.73*	32.6	$3.6 \times 10^{13}$	0.011	1.11
b	2.18	0.126	0.82*	22.1	-	0.015	2.40
	2.79	0.125	0.37	1.7	-	0.017	4.06
g	7.29	0.125	0.38	1.1	-	0.017	4.11

TABLE A2  
Full Size Machine Mid-height Solution  
For Legend See Fig. 2

Mach numbers with \* are in the relative frame

Loca- tion	x cm	p bar	Ma	$\Delta T$ K	$I$ $m^{-3}s^{-1}$	r $\mu m$	y %
i	0.0	0.375	0.18	-	-	-	-
th	20.16	0.253	0.79	21.2	$7 \times 10^5$	-	-
b	26.92	0.224	0.88	25.5	$3.3 \times 10^{12}$	-	-
g	38.86	0.215	0.91	27.4	$7.1 \times 10^{14}$	-	-
th	6.53	0.165	0.67*	35.8	$2.0 \times 10^{20}$	0.017	0.42
	8.13	0.148	0.76*	12.8	-	0.036	2.39
	9.65	0.133	0.84*	4.9	-	0.040	3.84
b	10.16	0.126	0.89*	4.4	-	0.041	4.11
	11.43	0.126	0.39	0.8	-	0.042	4.39
g	34.04	0.125	0.40	0.4	-	0.042	4.43

References

1. Traupel, W. "Steam Turbines, Yesterday, Today and Tomorrow", Proc. Inst. Mech. Engrs. Vol. 193, 1979, 391.
2. Wegener, P.P. "Gas Dynamics of Expansion Flows with Condensation and Homogeneous Nucleation of Water Vapour", in Gas Dynamics Vol.1. Pt.1. Ed.P.P. Wegener, 1969, Marcel Dekker, N.Y.
3. Moore, M.J. and Sieverding, C.H. "Two-Phase Steam Flow in Steam Turbines and Separators" 1976, Hemisphere Publishing.
4. Bakhtar, F. and Piran, M. "Thermodynamic Properties of Supercooled Steam", Int.Jnl. Ht. and Fl. Flow, 1, 2, 1979.

5. Bakhtar, F. and Mohammadi Tochai, M.T. "An Investigation of Two-Dimensional Flows of Nucleating and Wet Steam by the Time Machining Method", Int. Jnl. Ht. and Fl. Flow 2,1, 1980.
6. Yeoh, C. C. and Young, J.B. "Non-Equilibrium Streamline Curvature Through flow Calculations in Wet Steam Turbines", Proc. ASME, J. Engineering for Power, April 1982, p.489.
7. Bakhtar, F. Ghoneim, Z. and Young, J.B. "A Study of Nucleating and Wet Steam Flows in Turbines", Proc. Instn. Mech. Engrs., Vol. 190, 44/76, 1976, pp 545-559.
8. Bakhtar, F. and Ghassemi, B. "A Study of Nucleating and Wet Steam Flows in High Pressure Steam Turbines", Proc. Inst. Mech. Engrs. Conference Steam Turbines for the 1980's, London, October 79, pp 327-335.
9. Bakhtar, F. and Heaton, A.V. "A Theoretical Comparative Study of Wetness Problems in A Model and Full Scale Turbine in Aerothermodynamics of Steam Turbines" Ed. Steltz and Donaldson, Winter Annual Meeting, ASME, Washington DC, 1981.
10. Bakhtar, F. Ryley, D.J. Tubman, K.A. and Young, J.B. "Nucleation Studies in Flowing High Pressure Steam", Proc. Inst. Mech. Engrs, 189, 41/75, 1975, pp 427-436.
11. Craig, H.R.M. and Cox, H.J.A. "Performance Estimation of Axial Flow Turbines", Proc. Instn. Mech. Engrs. 185, 32/71, 1970-71 pp 407-425.
12. Yousif, F.H. Campbell, B.A. and Bakhtar, F. "Instability in Condensing Flow of Steam" Proc. Instn. Mech Engrs. 186, 37/72, 1972, p439.
13. Baum, M.R. and Horn, G. "The Propagation Velocity of a Small Rarefaction Wave in a Non-Equilibrium Vapour Liquid Bubble Flow - a Prediction of the Onset of Choked Flow", J.M.E.S., 13, 4, 1971, 243.
14. Petr, V. "Variation of Sound Velocity in Wet Steam Heat & Fluid Flow in Steam and Gas Turbine Plant, 1973, Conf. Pub. No.3, Instn. Mech. Engrs. London.
15. Bakhtar, F. and Young, J.B. "A Study of Choking Conditions in the Flow of Wet Steam", Proc. Instn. Mech. Engrs. 192, 21, 1978, 237.
16. Bakhtar, F. and Heaton, A.V. "An Examination of the Effect of "Wake-Chopping" on Droplet Sizes in Steam Turbines", Proc. BNES Conference Technology of Turbine Plant Operating with Wet Steam, London, 1988.